



Durham E-Theses

Processes of granite emplacement: NW Ireland and SE Brazil

Molyneux, Simon J.

How to cite:

Molyneux, Simon J. (1997) *Processes of granite emplacement: NW Ireland and SE Brazil*, Durham theses, Durham University. Available at Durham E-Theses Online: <http://etheses.dur.ac.uk/4774/>

Use policy

The full-text may be used and/or reproduced, and given to third parties in any format or medium, without prior permission or charge, for personal research or study, educational, or not-for-profit purposes provided that:

- a full bibliographic reference is made to the original source
- a [link](#) is made to the metadata record in Durham E-Theses
- the full-text is not changed in any way

The full-text must not be sold in any format or medium without the formal permission of the copyright holders.

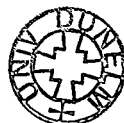
Please consult the [full Durham E-Theses policy](#) for further details.

PROCESSES OF GRANITE EMPLACEMENT: NW IRELAND AND SE BRAZIL

by

Simon J. Molyneux

The copyright of this thesis rests
with the author. No quotation
from it should be published
without the written consent of the
author and information derived
from it should be acknowledged.



A thesis submitted in partial fulfillment of the degree of Doctor of Philosophy at
the Department of Geological Sciences, University of Durham.

October 1997

12 MAY 1998

For Mum & Dad,

Copyright

The copyright of this thesis rests with the author. No quotation from it should be published without prior written consent and any information derived from it should be acknowledged.

No part of this thesis has been previously submitted for a degree at this university. The work described in this thesis is entirely that of the author except where reference is made to collaborative research or to previous unpublished or published work.



Simon J. Molyneux

University of Durham

Department of Geological Sciences

October, 1997

Acknowledgments

There are so many people to thank for help over the last few years that I'm bound to miss someone out so I apologise for that. Many thanks to all:

- Firstly to my parents, to whom I have dedicated this thesis, and my sister for supporting and helping me in so many ways to get through both the good times and the bad times of the last 25 years.
- Then to Donny Hutton, my supervisor, motivator and mentor over the past three years who was responsible for first introducing me to this subject, by leaving me in a field in Donegal to get on with it.
- To Hans Ebert my Brazilian supervisor, friend and general 'Mr Fix-It' without whom fieldwork would have been a far more difficult undertaking
- Secondly to all other people in the Department in Durham, particularly to Graham Pearson for supervising me towards the end, to Bob H. for his help, sarcasm and friendly advice, and to all the other staff members.
- Thanks to all the other postgrads Zoe, Wayne, Alun, Johnny, Roberto, Jo, Gail, Adam, Toby, Andy, Jon, Lorraine and Alfonso who have all managed to put up with me over the last few years.
- To all the behind the scenes people in the Department in particular Julie and Ron for the thin sections, Karen for her helpful advice, the secretaries for always being helpful and polite and to Dave for sorting every problem out with a smile and a cheery word.
- To Julian Baldry at NERC and Dave Asberry in the Department who have always reacted favourably to my demands for money.
- To the TSG & VSG boys, particularly Petford and Reavy for long nights, heavy heads and stimulating discussion.
- To my field assistants Marcello, Alexandre, Marcel and Johnson without whom fieldwork would have been impossible and a lot less fun; also to everyone I know at UNESP, Rio Claro (especially Paulo and Claudiozone) who made my stay in Brazil fun; and to the DPM in particular who allowed me to use all their facilities without question.
- To the Prefecture of Atibaia, particularly everyone at the Tourist Office, for giving me so much assistance; the Prefecture of Igarata, for putting the word about; the Suzano paper company for allowing me to stay on their logging camp; the Grande Hotel in Atibaia for being the most surreal place I have ever stayed in; to Localiza RentACar for never asking what I did with their vehicle; and everyone at the chalets in Igarata for a few beers and BBQ's.
- And finally to Louise, who has made me very happy over the last year and a half. She has performed duties well above and beyond the call of duty, corrected my tortuous grammar and put up with my moods, snapping and general unpleasantness. Without her I don't think this thesis would have been completed nearly so quickly !

Abstract

This thesis is a study of some of the processes which operate at mid crustal levels (10-20km) during the emplacement of granitoid magmas, with particular reference to the process of in-situ expansion and the association between magma emplacement and orogen evolution. A number of plutons were studied to assess this the Ardara pluton from Donegal, NW Ireland, together with the Atibaia, Morro Azul, Imbiricu and Itapeti plutons from the Rio Paraiba do Sul shear belt (RPSSB), Sao Paulo state, SE Brazil.

The emplacement of the Ardara pluton has been the subject of studies by many authors since the 1950's. It has been interpreted as a diapir ascending along a thrust, a granite balloon which forcefully created more than 60% of its space and, most recently, as a set of nested diapirs which forcefully created only 30% of their own space. Field mapping together with the determination of finite strain within the pluton, shortening estimates, shear sense determinations, petrographic deformation fabrics and computer modelling indicates that: i) the pluton displays a concentrically increasing finite strain and it expanded in-situ from a central 'injection point', having possibly ascended along a shear zone-related conduit; ii) the country rocks partitioned intense strains into the 500m closest to the pluton, a deformation feature which is shown to be consistent with a power-law wallrock rheology; iii) earlier granite pulses and the country rock were 'shouldered aside' to the east and west, expansion of the pluton, which was preferentially in a northwards direction; iv) that the intrusion related shortening preserved within the wallrocks was approximately equivalent to the strain preserved within pluton and the space requirements for the pluton are essentially met by preserved forceful emplacement-related strains; and v) if the pluton magma is considered as having ascended through dyke-like conduits emplacement could occur in a minimum of ~4000yrs, whereas magma ascent as a Hot Stokes diapir would require hundreds of thousands to millions of years for complete emplacement. Finally, the Ardara pluton does not conform to any of the established criteria for diapir-like ascent of a magma body and the data demonstrate it to be a testable example of a pluton which expanded entirely in-situ.

The Rio Paraiba do Sul shear belt (RPSSB) is a dextral transpressional segment of the Late Precambrian Brasiliano-Pan African orogenic belt. The studied plutons were emplaced in the latter stages of this orogen in close spatial association with one of the many northeast-southwest trending, sub-vertical, continental-scale shear zones. All the granites show a similar emplacement and deformation history despite their different petrographic features and isotopic ages. This history consists of an early shallowly dipping, low angle fabric, in the country rocks, associated with crustal thickening, the later development of

dominantly dextral sub-vertical shear zones, followed by the emplacement of the studied plutons and finally overprinting by a pervasive dextral plane strain and late-stage discrete mylonitic shears.

Field examination demonstrates that: i) each of the plutons preserves an internally homogeneous emplacement-related finite strain, weak magmatic fabric, magma sheets and weakly deformed wallrocks; ii) magmatic shear sense determinations and wallrock deformation fabrics indicate that, during emplacement, the RPSSB was extending (at least at the emplacement level) in an east-west direction creating sinistral dilatational pull-aparts along the major shear zones, into which granitic magma was preferentially emplaced; and iii) within this generally extensional context there was a component of long axis perpendicular in-situ forceful expansion, this created no more than 20% of the width of any one granite. Applying a simple pull-apart extension model suggests that pluton emplacement was associated with approximately 40% regional extension sub-parallel to the former orogenic convergence direction. This emplacement, as a result of sheeting through dyke-like conduits, requires thousands of years, rather than the millions of years required for ascent and emplacement of a Hot Stokes diapir. Interpreting these results suggests that the intruded granitoids are associated with a mid-crustal component of orogen perpendicular extension/collapse during the latter stages of the Brasiliano orogeny. Such extension/collapse could have been initiated by: a cessation in continental convergence or; by the delamination of a thickened thermal boundary layer, a process which has been suggested to be the driving force behind orogenic collapse in younger orogenic belts.

These examples demonstrate that: i) 'forceful' balloon-like emplacement of granitic magma can occur; ii) there are very close inter-relationships between granite emplacement and orogenic dynamics; and iii) that 'space' for granitoid magma can be created by a combination of forceful and dilatational and fault-related mechanisms.

“ It may be safely be asserted that, as matters now stand the advancement of Geology could not be carried on without the aid of an efficient body of post-graduate students, occupying a position duly subordinate to that of Supervisors, who directly responsible to the Establishment, yet possessing sufficient independence, character, ability and experience to be able to advise, assist and to some extent influence those who are from time to time set over them.”

- extensively modified from Northcote & Trevelayan (1853)

Contents

Copyright	iii
Acknowledgements	iv
Abstract	v
Contents	viii
Figure list	xiv
Plate list	xix
Table list	xxii

Section 1 Introduction

Chapter 1	Granitoid ascent, emplacement, deformation and analysis	1
1.1	Introduction	2
1.1.1	Preamble	2
1.1.2	Definition of key terms	2
1.1.3	Objectives	6
1.1.4	Conventions	6
1.2	Rheology	8
1.2.1	Elastic behaviour	8
1.2.2	Viscous behaviour	9
1.2.3	More complex rheologies	9
1.2.4	Granite rheology	10
1.3	Tectonic structures related to granite emplacement	12
1.3.1	Magmatic state structures	12
1.3.2	Transition state/lock-up fabrics	12
1.3.3	Sub-magmatic fabrics	13
1.3.4	Solid state fabrics	13
1.3.5	The validity of a Cloosian approach	13
1.4	Shear sense	15
1.4.1	Magmatic state	15
1.4.2	Transition state/lock-up fabrics	16
1.4.3	Solid state	16
1.5	Strain analysis	18
1.5.1	Strain markers - microgranitoid enclaves	19
1.5.2	Fabric strain - Fry (1979) method	21
1.5.3	Solid state strain indicators	23
1.6	Magma ascent and pluton emplacement mechanisms	24
1.6.1	Magma ascent	24
1.6.2	Magma emplacement	26
1.6.3	Tectonic setting	29
1.6.4	Siting mechanisms	30
1.7	Orogenic evolution	32
1.7.1	The Wilson cycle	32
1.7.2	Transpression and transtension	32
1.7.3	Extensional collapse	32
1.8	Regional Introductions	35
1.8.1	The Donegal Batholith, N.W. Ireland	35
1.8.2	The Rio Paraiba do Sul shear belt, S.E. Brazil	35

Section 2 Emplacement of an in-situ expanding pluton

Chapter 2	The Ardara pluton, Co Donegal, NW Ireland	
2.1	Introduction	38
2.1.1	Preamble	38
2.1.2	The Caledonian orogeny and its imprint in Donegal	38
2.1.3	The Dalradian country rock	39
2.1.4	The country rocks surrounding the Ardara pluton	41
2.1.5	Structural evolution	43
2.1.6	The granites of the Donegal batholith	44
2.1.7	The Ardara pluton: previous work	46
2.2	The Ardara pluton: the plutonic phases	51
2.2.1	Nature of the contact	51
2.2.2	Outer unit, G1	51
2.2.3	G2	54
2.2.4	Central unit, G3	56
2.2.5	The Moolagh townlands, GR 734949	57
2.2.6	Conclusion and discussion	57
2.3	Strain measurement	59

	4.4.5	Conclusion and discussion	154
4.5		Shear sense	156
	4.5.1	Introduction	156
	4.5.2	Country rock	156
	4.5.3	Granite	158
	4.5.4	Conclusion and discussion	159
4.6		Emplacement kinematics of the microgranitoid dykes/sheets	161
	4.6.1	Introduction	161
	4.6.2	Methodology	161
	4.6.3	Results	163
	4.6.4	Conclusion and discussion	164
4.7		Overprinting discrete mylonitic shear zones	167
	4.7.1	Introduction	167
	4.7.2	Methodology	167
	4.7.3	Results	169
	4.7.4	Conclusion and discussion	171
4.8		Dykes or diapir ?	174
4.9		Emplacement and deformation	175
	4.9.1	A sequence of events	175
	4.9.2	Pluton shape	176
4.10		Conclusions	178

Chapter 5 The Imbiricu and Morro Azul plutons

5.1		Introduction	179
	5.1.1	Preamble	179
	5.1.2	Previous work	179
5.2		Mapping: the Imbiricu pluton	181
	5.2.1	Country rock	181
	5.2.2	Nature of the contact	183
	5.2.3	Granite	186
	5.2.4	Microgranitoid stocks, dykes, enclaves and country rock xenoliths	192
	5.2.5	Conclusion and discussion	197
5.3		Deformation: the Imbiricu pluton	198
	5.3.1	Country rock	198
	5.3.2	Granite	199
	5.3.3	Conclusion and discussion	203
5.4		Strain measurement: the Imbiricu pluton	204
	5.4.1	Introduction	204
	5.4.2	Microgranitoid enclaves	204
	5.4.3	Fry Strain	205
	5.4.4	Other strain indicators	207
	5.4.5	Country rock strain	208
	5.4.6	Conclusion and discussion	208
5.5		Shear sense: the Imbiricu pluton	210
	5.5.1	Introduction	210
	5.5.2	Country rock	210
	5.5.3	Granite	211
	5.5.4	Conclusion and discussion	214
5.6		Emplacement kinematics of the microgranitoid dykes/sheets: the Imbiricu pluton	216
	5.6.1	Introduction and methodology	216
	5.6.2	Results and conclusions	216
5.7		Overprinting discrete mylonitic shear zones: the Imbiricu pluton	218
	5.7.1	Introduction	218
	5.7.2	Methodology	218
	5.7.3	Results	218
	5.7.4	Conclusion and discussion	220
	5.8	Mapping: the Morro Azul pluton	221
	5.8.1	Country rock	221
	5.8.2	Nature of the contact	226
	5.8.3	Granite	227
	5.8.4	Microgranitoid stocks, dykes, enclaves and country rock xenoliths	237
	5.8.5	Conclusion and discussion	239
5.9		Deformation: the Morro Azul pluton	240
	5.9.1	Country rock	240
	5.9.2	Granite	242
	5.9.3	Conclusion and discussion	249
5.10		Strain measurement: the Morro Azul pluton	251
	5.10.1	Introduction	251
	5.10.2	Microgranitoid enclaves	251

5.10.3	Fry Strain	254
5.10.4	Country rock strain	257
5.10.5	Qualitative estimates of strain	261
5.10.6	Conclusions and discussion	262
5.11	Shear sense: the Morro Azul pluton	264
5.11.1	Introduction	264
5.11.2	Country rock	264
5.11.3	Granite	265
5.11.4	Other shear sense indicators	268
5.11.5	Conclusion and discussion	269
5.12	Emplacement kinematics of the microgranitoid dykes/sheets: the Morro Azul pluton	270
5.12.1	Introduction and methodology	270
5.12.2	Results	270
5.12.3	Conclusion and discussion	271
5.13	Overprinting discrete mylonitic shear zones: the Morro Azul pluton	272
5.13.1	Introduction and methodology	272
5.13.2	Results	272
5.13.3	Conclusion and discussion	273
5.14	Dykes or diapir ?	275
5.14.1	The Imbiricu pluton	275
5.14.2	The Morro Azul pluton	275
5.14.3	General conclusions	275
5.15	Emplacement and deformation	277
5.15.1	A sequence of events	277
5.15.2	Pluton shape	278
5.16	Conclusions	280
5.16.1	The Imbiricu pluton	280
5.16.2	The Morro Azul pluton	280
5.16.3	General conclusions	281

Chapter 6 The Itapeti pluton

6.1	Introduction	282
6.1.1	Preamble	282
6.1.2	Previous work	282
6.2	Mapping and deformation	286
6.2.1	Introduction	286
6.2.2	Country rock	286
6.2.3	Granite	288
6.2.4	Conclusions	292
6.3	Strain measurement	293
6.3.1	Introduction	293
6.3.2	Granite	293
6.3.3	Country rock	296
6.3.4	Conclusions	296
6.4	Shear senses	297
6.4.1	Introduction	297
6.4.2	Country rock	297
6.4.3	Granite	297
6.4.4	Conclusions	299
6.5	Overprinting discrete mylonitic shear zones	300
6.5.1	Introduction	300
6.5.2	Results	300
6.5.3	Conclusion and discussion	301
6.6	Emplacement and deformation	303
6.6.1	A sequence of events	303
6.6.2	The shape of the pluton	304
6.7	Conclusions	306

Chapter 7 Evolution of the RPPSSB

7.1	Introduction	307
7.1.1	Preamble	307
7.1.2	Background	307
7.2	Intrusion of the studied granites	309
7.2.1	Genesis of the magma	309
7.2.2	Tectonics associated with emplacement	312
7.2.3	Reasons for ascent	318
7.2.4	Siting of the pluton	319
7.3	The creation of space for the pluton	321

	7.3.1	Strain preserved within the plutons	321
	7.3.2	Strain in the country rocks	321
	7.3.3	External space creation mechanisms	321
7.4		Emplacement of other granitoids from the RPSSB	323
	7.4.1	Introduction	323
	7.4.2	The Jambeiro pluton	323
	7.4.3	The Piracaia pluton	324
	7.4.4	The Itaqui and Sao Roque plutons	325
	7.4.5	The Sindacta pluton	326
	7.4.6	Conclusions	326
7.5		Conclusions	327
<hr/>			
Section 4 Simple models and emplacement studies			
Chapter 8 Modelling emplacement			
	8.1	Preamble	329
	8.2	Modelling mafic enclave shape during deformation	330
		8.2.1 Introduction	330
		8.2.2 Methodology	330
		8.2.3 Results	335
		8.2.4 Conclusions and discussion	346
		8.2.5 Further work	347
	8.3	Modelling aureole deformation	348
		8.3.1 Introduction	348
		8.3.2 Methodology	349
		8.3.3 Results	351
		8.3.4 Conclusions and discussion	358
	8.4	Speed of emplacement	360
		8.4.1 Introduction	360
		8.4.2 Methodology	360
		8.4.3 Results	363
		8.4.4 Conclusions and discussion	370
	8.5	Using the Fry (1979) method to measure fabric strain in granitoid rocks	372
		8.5.1 Introduction	372
		8.5.2 Results	372
		8.5.3 Conclusions	372
		8.5.4 Discussion	373
	8.6	Conclusions	375
<hr/>			
Chapter 9 Conclusions			
	9.1	Conclusions from Section 2: The emplacement of an in-situ expanding pluton	
	376		
	9.2	Conclusions from Section 3: Granitoid pluton emplacement in the Rio Paraiba do Sul shear belt, SE Brazil	
	378		
	9.3	Conclusions from Section 4: Analytical considerations	380
<hr/>			
References			381
<hr/>			
Appendices			391
Appendix 1	Locality grid references from the Ardara pluton		
Appendix 2	Mafic enclave axial ratio raw data from the Atibaia pluton		
Appendix 3	Fry fabric strain raw data from the Atibaia pluton		
Appendix 4	Fold and cleavage related shortening data collected by D.Hutton		
Appendix 5	Locality grid references from the Atibaia pluton		
Appendix 6	Mafic enclave axial ratio raw data from the Atibaia pluton		
Appendix 7	Fry fabric strain raw data from the Atibaia pluton		
Appendix 8	Locality grid references from the Imbiricu and Morro Azul plutons		
Appendix 9	Mafic enclave axial ratio raw data from the Imbiricu and Morro Azul plutons		
Appendix 10	Fry fabric strain raw data from the Imbiricu and Morro Azul plutons		
Appendix 11	Folded pegmatite raw strain data, Santa Isabel gneisses		
Appendix 12	Locality grid references from the Itapeti pluton		
Appendix 13	Mafic enclave axial ratio raw data from the Itapeti pluton		
Appendix 14	Fortran program to model Power Law rheology deformation of a expanding pluton contact		
Appendix 15	Critical dyke width and pluton filling times for the Ardara pluton		
Appendix 16	Critical dyke width and pluton filling times for plutons from the Rio Paraiba do Sul shear belt		

	7.3.1	Strain preserved within the plutons	321
	7.3.2	Strain in the country rocks	321
	7.3.3	External space creation mechanisms	321
7.4		Emplacement of other granitoids from the RPSSB	323
	7.4.1	Introduction	323
	7.4.2	The Jambreiro pluton	323
	7.4.3	The Piracaia pluton	324
	7.4.4	The Itaqui and Sao Roque plutons	325
	7.4.5	The Sindacta pluton	326
	7.4.6	Conclusions	326
7.5		Conclusions	327
<hr/>			
Section 4 Simple models and emplacement studies			
Chapter 8 Modelling emplacement			
	8.1	Preamble	329
	8.2	Modelling mafic enclave shape during deformation	330
		8.2.1 Introduction	330
		8.2.2 Methodology	330
		8.2.3 Results	335
		8.2.4 Conclusions and discussion	346
		8.2.5 Further work	347
	8.3	Modelling aureole deformation	348
		8.3.1 Introduction	348
		8.3.2 Methodology	349
		8.3.3 Results	351
		8.3.4 Conclusions and discussion	358
	8.4	Speed of emplacement	360
		8.4.1 Introduction	360
		8.4.2 Methodology	360
		8.4.3 Results	363
		8.4.4 Conclusions and discussion	370
	8.5	Using the Fry (1979) method to measure fabric strain in granitoid rocks	372
		8.5.1 Introduction	372
		8.5.2 Results	372
		8.5.3 Conclusions	372
		8.5.4 Discussion	373
	8.6	Conclusions	375
<hr/>			
Chapter 9 Conclusions			
	9.1	Conclusions from Section 2: The emplacement of an in-situ expanding pluton	
	376		
	9.2	Conclusions from Section 3: Granitoid pluton emplacement in the Rio Paraiba do Sul shear belt, SE Brazil	
	378		
	9.3	Conclusions from Section 4: Analytical considerations	380
<hr/>			
References			381
<hr/>			
Appendices			391
Appendix 1	Locality grid references from the Ardara pluton		
Appendix 2	Mafic enclave axial ratio raw data from the Atibaia pluton		
Appendix 3	Fry fabric strain raw data from the Atibaia pluton		
Appendix 4	Fold and cleavage related shortening data collected by D.Hutton		
Appendix 5	Locality grid references from the Atibaia pluton		
Appendix 6	Mafic enclave axial ratio raw data from the Atibaia pluton		
Appendix 7	Fry fabric strain raw data from the Atibaia pluton		
Appendix 8	Locality grid references from the Imbiricu and Morro Azul plutons		
Appendix 9	Mafic enclave axial ratio raw data from the Imbiricu and Morro Azul plutons		
Appendix 10	Fry fabric strain raw data from the Imbiricu and Morro Azul plutons		
Appendix 11	Folded pegmatite raw strain data, Santa Isabel gneisses		
Appendix 12	Locality grid references from the Itapeti pluton		
Appendix 13	Mafic enclave axial ratio raw data from the Itapeti pluton		
Appendix 14	Fortran program to model Power Law rheology deformation of a expanding pluton contact		
Appendix 15	Critical dyke width and pluton filling times for the Ardara pluton		
Appendix 16	Critical dyke width and pluton filling times for plutons from the Rio Paraiba do Sul shear belt		

Inclusions

Map 1	The Ardara pluton
Map 2	The Atibaia pluton
Map 3	The Morro Azul pluton
Map 4	The Imbiricu pluton
Map 5	The Itapeti pluton
Map 6	1:50,000 scale Atibaia regional map sheet modified after Oliveira <i>et al</i> (1983)
Map 7	1:50,000 scale Piracaia regional map sheet modified after Campos Neto <i>et al</i> (1983)
Map 8	1:50,000 scale Igarata regional map sheet modified after Campos Neto <i>et al</i> (1983)
Map 9	1:100,000 scale Sao Jose dos Campos regional map sheet modified after Hasui <i>et al</i> (1978)

Figure list

Figure	Caption	Page
1.1	<i>Methods of magma ascent</i>	3
a	<i>A diapir ascending through the crust</i>	
b	<i>Assembly of a pluton as a result of sheeting</i>	
1.2	<i>Shear stress vs strain rate for a number of theoretical and ideal rheologies</i>	10
1.3	<i>Compilation graph of relative viscosity against melt fraction after van der Molen & Paterson (1979) and Rutter & Neumann (1995)</i>	11
1.4	<i>Magmatic structure produced during progressive deformation and reduced melt fraction</i>	14
a	<i>Magmatic state structure</i>	
b	<i>Lockup structures</i>	
c	<i>Solid state structure</i>	
1.5	<i>Magmatic state shear sense</i>	15
a	<i>Obliquity of bi-modal fabrics</i>	
b	<i>dominant tiling orientation</i>	
1.6	<i>Solid state shear sense indicators</i>	17
a	<i>S-C fabrics</i>	
b	<i>delta-porphyroclast</i>	
c	<i>sigma porphyroclast</i>	
d	<i>stack of cards' brittle rotation</i>	
e	<i>mica 'fish'</i>	
1.7	<i>The strain ellipsoid</i>	19
b	<i>A log Flinn (1962) diagram, detailing the types of fabrics which can be produced</i>	
1.8	<i>Mafic enclaves their measurement and processing</i>	21
a	<i>axial ratio</i>	
b	<i>the principle planes of measurement</i>	
c	<i>Population spread</i>	
1.9	<i>Rigid markers before and after an homogenous deformation</i>	22
1.10	<i>The method of Fry analysis for non-circular grains</i>	23
a	<i>Grain shape tracings</i>	
b	<i>digitisation</i>	
c	<i>the Fry strain ellipse</i>	
1.11	<i>Structures associated with diapiric uprise through the crust</i>	26
1.12	<i>Transpressional deformation, after Sanderson & Marchini (1984)</i>	33
1.13	<i>Extensional collapse, principle stress re-orientation</i>	34
2.1	<i>A geological map of N.W. Ireland, from Hutton & Alsop (1996)</i>	40
2.2	<i>The main sedimentary units of NW Ireland from Pitcher & Berger (1972)</i>	40
2.3	<i>The Cresslough succession from Pitcher & Berger (1972), from the work of Akaad, Mithal, Iyengar and Cheesman.</i>	41
2.4	<i>The distribution of sedimentary rocks around the Ardara pluton, from Akaad (1956a)</i>	42
2.5.	<i>Schematic of S2 and S3 relationships across the study area, from Meneilly (1982)</i>	43
2.6	<i>The Donegal Batholith</i>	45
2.7	<i>Chronology of the Donegal Batholith from field relationships, after Pitcher & Berger (1972)</i>	46
2.8	<i>Geological Map of the Ardara pluton</i>	47
2.9	<i>Bouguer gravity anomaly map of Donegal from Riddihough & Young (1969)</i>	48
2.10	<i>D4 and D5 structures around Gweebarra Bay, from Meneilly (1982)</i>	50
2.11	<i>Tertiary QAPF type plot for rocks of a granitic composition</i>	52
2.12	<i>Field sketch of G2 intruding into G1 during emplacement (GR 72719844)</i>	55
a		
b	<i>Sketch of G1 xenolith in G2 granite (GR 72939847)</i>	
2.13	<i>Field sketch of the Moolagh townlands outcrops showing abundant small microgranitoid enclaves (GR 734949)</i>	58
2.14	<i>Enclave axial ratio data from the Ardara pluton</i>	63
2.15	<i>Fry fabric strains from the Ardara pluton</i>	65
2.16	<i>Interpreted cross-section across the northwest aureole of the Ardara pluton GR 764980 to GR 800805 (after country rock mapping by Meneilly (1981)</i>	68
2.17	<i>Principle foliation map</i>	70
a		
b	<i>Measuring strain associated with line deflection during pluton emplacement</i>	
2.18	<i>Wallrock strain induced by granite emplacement</i>	72
a		
b	<i>Wallrock shortening induced by granite emplacement</i>	
2.19	<i>Granitic and country rock shear sense from horizontal outcrop plane</i>	75
a		
b	<i>North-south cross-section through the pluton showing representative, vertical plane granitic and country rock shear senses</i>	
c	<i>Resolving shear sense data into apparent material movement directions</i>	76
d	<i>Sketch of apparent minimum compressive stresses during emplacement, deduced from shear sense data</i>	

2.20		<i>Contoured stereonet of poles to planes of sinistral intrusive dykes</i>	77
2.21		<i>Contoured stereonet of poles to planar country rock sinistral shear sense indicators from the Western area, Ardara pluton</i>	78
2.22	a	<i>Contoured stereonet of poles to minor thrust planes from around the northern part of the Ardara pluton</i>	79
	b	<i>Contoured stereonet of stretching lineations associated with Figure 2.22a</i>	
2.23		<i>Contoured stereonet of poles to planar dextral fabrics from the eastern area, Ardara pluton</i>	80
2.24		<i>Contoured stereonet of mineral stretching lineations from the Southern contact area, country rocks and granite, Ardara pluton</i>	82
2.25		<i>Oblique fabric development during non-coaxial shear</i>	84
	a	<i>Pure shear</i>	
	b	<i>Non-coaxial dextral and sinistral shear</i>	
	c	<i>Combination pure shear, with a non-coaxial component</i>	
2.26		<i>Migration of strain measurements to their incorporation point</i>	88
2.27		<i>Migrated strain measurement, interpolated to display original pluton shape</i>	89
	a	<i>Mafic enclave strains</i>	
	b	<i>Fry strains</i>	
2.28		<i>Block diagrams showing the intrusive sequence of the Ardara pluton</i>	95
	a	<i>Initial scenario, country rocks cut by sinistrally transpressive shear zone</i>	
	b	<i>Initiation of ascent / emplacement</i>	
3.1		<i>Position of the field area</i>	99
	a	<i>within Brazil</i>	
	b	<i>within Sao Paulo state</i>	
3.2	a	<i>Brazilian structural provinces</i>	101
	b	<i>the Ribeira belt and the Rio Paraiba do Sul shear belt</i>	
3.3		<i>Comparison of South American and African structural provinces, restored to their pre-Atlantic opening positions (modified from Porada 1989)</i>	104
3.4	a	<i>The Rio Paraiba do Sul shear belt (after Ebert et al 1996)</i>	107
	b	<i>The study area</i>	
3.5		<i>Stratigraphic domains recognised in the study area (after Tassinari 1988)</i>	108
3.6		<i>An inferred P-T-t plot for the study area, using the data of Tassinari (1988), Ribeiro et al (1996) and Procher & Fernandes (1997)</i>	109
3.7		<i>D_{n+1} fabric stereonets</i>	111
	a	<i>Poles to planes of low angle foliation</i>	
	b	<i>Orientations of associated lineations</i>	
3.8		<i>Contoured D_{n+2} fabric stereonets</i>	113
	a	<i>Poles to planes of high angle fabric orientations S_{n+2}</i>	
	b	<i>Associated lineations L_{n+2}</i>	
3.9		<i>Contoured stereonet of L_{n+4} lineations</i>	114
4.1		<i>Map of the Atibaia pluton</i>	125
4.2	a	<i>Contoured stereonet of poles to foliation, western side of the Atibaia pluton</i>	127
	b	<i>Stretching lineations from the western side of the Atibaia pluton</i>	
4.3		<i>A summary log through the western contact rocks of the Atibaia pluton (GR 42503867 to GR 43123820)</i>	128
4.4	a	<i>Contoured stereonet of poles to foliation, eastern side of the Atibaia pluton</i>	129
	b	<i>Stretching lineations from the eastern side of the Atibaia pluton</i>	
4.5		<i>Summary log through the eastern contact rocks of the Atibaia pluton (GR47273593 to GR 48053600)</i>	129
4.6		<i>Tertiary QAPF type plot for rocks of a granitic composition, the Atibaia pluton (stars=individual analyses, filled square = average composition)</i>	133
4.7	a	<i>Contoured stereonet of poles to foliation for the whole of the Atibaia pluton</i>	134
	b	<i>Stereonet of stretching lineations from the whole of the Atibaia pluton</i>	
4.8		<i>Map showing the division of the pluton and country rocks used in the text</i>	142
4.9		<i>Spatial plot of horizontal plane average mafic enclave axial ratios from the Atibaia pluton</i>	151
4.10	a	<i>Spatial plot of Fry strains from the horizontal outcrop plane</i>	153
	b	<i>Spatial plot of Fry strains from the vertical outcrop plane</i>	
	c	<i>A log Flinn type plot for Fry strain data</i>	
4.11	a	<i>Solid state shear senses recorded in the horizontal plane within and around the Atibaia pluton</i>	160
	b	<i>Magmatic state shear senses recorded within the Atibaia pluton</i>	
4.12	a	<i>Contoured stereonet of pole to S-type fabrics from the whole of the Atibaia pluton</i>	160
	b	<i>Contoured stereonet of poles to C-type fabrics from the whole of the Atibaia pluton</i>	
4.13	a	<i>Type 1</i>	162
	b	<i>Type 2</i>	
	c	<i>Type 3</i>	
4.14		<i>0-180° rose diagrams of the orientation of microgranitoid sheets from across the Atibaia pluton</i>	165

4.15		<i>Microgranitoid dyke orientations from around the Atibaia pluton</i>	166
	a	<i>Principle dyke orientations</i>	
	b	<i>Minimum compressive stress orientations assuming purely coaxial deformation</i>	
	c	<i>Preserved average shear fabrics associated with microgranitoid dykes</i>	
	d	<i>Maximum and minimum compressive stress orientation assuming non-coaxial deformation</i>	
4.16		<i>Diagram of interpreted principle stress orientations from conjugate mylonite arrays</i>	169
4.17		<i>0-180° rose diagrams of mylonite orientations from the Atibaia pluton</i>	172
4.18		<i>Discrete mylonite orientations from around the Atibaia pluton</i>	173
	a	<i>Principle mylonite orientations</i>	
	b	<i>Minimum compressive stress orientations</i>	
4.19	a	<i>Possible structural architecture of pure transpression in the Atibaia area.</i>	177
	b	<i>East-west directed extension and the creation of space for the Atibaia pluton</i>	
5.1		<i>Geological map of the Morro Azul and Imbiricu plutons</i>	180
5.2		<i>Geological map of the Imbiricu pluton</i>	181
5.3	a	<i>Contoured stereonet poles to country rock foliation from around the Imbiricu pluton</i>	183
	b	<i>Contoured stereonet of stretching lineations from around the Imbiricu pluton</i>	
5.4		<i>A summary log through the northwestern contact of the Imbiricu pluton (GR 89584781 to GR 89754798)</i>	185
5.5		<i>Interpretation of structural fabrics along the southwest contact of the Imbiricu pluton</i>	185
5.6	a	<i>Contoured stereonet of pole to foliation from the northeast G1, Imbiricu pluton.</i>	188
	b	<i>Contoured stereonet of mineral stretching lineations from the northeast G1, Imbiricu pluton</i>	
5.7	a	<i>Contoured stereonet of poles to foliation from the southwest G1, Imbiricu pluton</i>	189
	b	<i>Contoured stereonet of mineral stretching lineations from the southwest G1, Imbiricu pluton</i>	
5.8	a	<i>Contoured stereonet of poles to foliation from G2, Imbiricu pluton</i>	191
5.9	a	<i>Point counting results from G1, Imbiricu pluton</i>	191
	b	<i>Point counting results from G2, Imbiricu pluton</i>	
5.10		<i>Summary log through the G1/G2 contact GR 92664710, Imbiricu pluton</i>	192
5.11		<i>Horizontal plane mafic enclave axial ratios from the Imbiricu pluton</i>	205
5.12		<i>Horizontal plane Fry fabric strains from the Imbiricu pluton</i>	207
5.13	a	<i>Contoured stereonet of poles to C-planes from across the Imbiricu pluton.</i>	212
	b	<i>Plot of observations of solid state shear senses from across the Imbiricu pluton</i>	
5.14	a	<i>Block diagram explaining the formation of magmatic state rotated fabric within the Imbiricu pluton</i>	214
	b	<i>Block diagram explaining the formation of a coincident solid state fabric during deformation of the Imbiricu pluton</i>	
5.15	a	<i>A rose diagram of microgranitoid dyke orientations from across the whole of the Imbiricu pluton</i>	217
	b	<i>A sketch map of average microgranitoid dyke orientations within the Imbiricu pluton</i>	
5.16	a	<i>Rose diagram from G1</i>	220
	b	<i>Rose diagram from G2</i>	
	c	<i>Map of average orientations</i>	
	d	<i>Inferred principle compressive stress</i>	
5.17		<i>Geological map of the Morro Azul pluton</i>	222
5.18	a	<i>Contoured stereonet of poles to foliation from the country rock southeast of the Morro Azul pluton</i>	223
	b	<i>Contoured stereonet of mineral stretching lineations from the country rock southeast of the Morro Azul pluton</i>	
5.19	a	<i>Contoured stereonet of poles to foliation from the country rock northwest of the Morro Azul pluton, showing a best-fit great circle, which demonstrates an upright average axial plane trending at 040°.</i>	225
	b	<i>Stereonet of mineral stretching lineations from the country rock northwest of the Morro Azul pluton</i>	
	c	<i>A cross-section through the Morro Azul pluton and surrounding country rocks (GR 87003425 to GR 80803940)</i>	
5.20	a	<i>Contoured stereonet of poles to foliation from the northwestern and southern G1, Morro Azul pluton.</i>	229
	b	<i>Contoured stereonet of mineral stretching lineations from northwestern and southern G1, Morro Azul pluton.</i>	
	c	<i>Contoured stereonet of poles to foliation from southeastern G1, Morro Azul pluton.</i>	
	d	<i>Contoured stereonet of mineral stretching lineations from southeastern G1, Morro Azul pluton</i>	
5.21	a	<i>Contoured stereonet of poles to foliation from G2, Morro Azul pluton</i>	231
	b	<i>Contoured stereonet of mineral stretching lineations from G2, Morro Azul pluton</i>	
5.22		<i>QAPF modal composition diagram for coarse grained igneous rocks, Morro Azul pluton (stars=individual analyses, filled square=average composition)</i>	231
	a	<i>G1</i>	

	b	G2	
5.23		Summary log through the contact between G1 and G2 around GR 83053790.	233
5.24		Summary log through the southeastern contact between G1 and G2 around GR 84758780	235
5.25		Stereonet showing recorded magmatic state lineations from the northwestern area G1, Morro Azul pluton	245
5.26	a	Average mafic enclave axial ratios from the horizontal outcrop plane of the Morro Azul pluton	253
	b	Average mafic enclave axial ratios from the vertical outcrop plane of the Morro Azul pluton	
	c	A Flinn-type plot for mafic enclave data from the Morro Azul pluton	
5.27	a	Average Fry strains from the horizontal outcrop plane of the Morro Azul pluton	256
	b	Average Fry strains from the vertical outcrop plane of the Morro Azul pluton	
	c	A Flinn-type plot for the Fry strain data from the Morro Azul pluton	
5.28		Sketch diagram showing the measurement required for strain determinations from a flattened layer parallel fold (after Ramsay 1967)	257
5.29		Ramsay (1967) t - α for folded pegmatites from the Santa Isabel gneisses	259
	a	Horizontal plane	
	b	Vertical plane	
5.30		Sketch block diagram of the distribution and sense of magmatic state shear fabrics from the Morro Azul pluton	266
5.31		Contoured stereonet of poles to C-planes from the Morro Azul pluton (compare with poles to foliation planes in Figure 5.20a,c)	267
5.32		Stereonet of minor fold axes (compare with pole to foliation planes in Figure 5.20a,c)	268
5.33	a	Microgranitoid dyke orientations from the Central area Morro Azul pluton	271
	b	Microgranitoid dyke orientations from the Southern area Morro Azul pluton	
	c	Sketch map of principle microgranitoid dyke orientations and inferred extensional stresses during their emplacement within the Morro Azul pluton	
5.34		Rose diagrams of discrete mylonite orientations from the Morro Azul pluton	273
	a	Southern area	
	b	Central area	
	c	Northern area	
5.35	a	Average discrete mylonite orientations from the Morro Azul pluton	274
	b	Inferred principle compressive stress orientations for discrete mylonite orientations from the Morro Azul pluton	
5.36		East-west directed extension inducing sinistral shear during the intrusion of the Morro Azul and Imbiricu plutons	279
6.1		Map of the Itapeti pluton (modified after Morais 1996)	284
6.2		Tertiary QAPF-type plot for rocks of a granitic composition for the Itapeti pluton	285
6.3		Subdivision of the pluton and country rocks used in this study	286
6.4		Country rock to the north of the Itapeti pluton	287
	a	Contoured stereonet of poles to country rock foliation (filled circles) and poles to fold axes (boxes)	
	b	Stereonet of country rock mineral stretching lineations	
6.5	a	Contoured stereonet of poles to foliation from the Itapeti pluton	289
	b	Contoured stereonet of stretching lineations from the Itapeti pluton	
6.6		Horizontal planes microgranitoid enclave axial ratios from the Itapeti pluton	294
6.7		Average Fry strains from the Itapeti pluton	295
6.8		Contoured stereonet of poles to the C-planes of S-C fabrics	298
6.9		Composite map of solid state and magmatic state shear senses of the Itapeti pluton	299
6.10		Rose diagrams showing mylonite orientations from the Itapeti pluton	300
	a	West area	
	b	Central area	
	c	East area	
6.11	a	Average principle mylonite orientations within the Itapeti pluton	302
	b	Inferred principle compressive stress orientation within the Itapeti pluton	
6.12		A model for the emplacement of the Itapeti pluton	304
6.13		Production of sinistral shear fabrics during intrusion of the Itapeti pluton	305
7.1	a	Double thickness continental lithosphere produced during continental collision	311
	b	Convective removal of the lithospheric root producing extension and uplift	
7.2		Early evolution of the RPSSB	313
7.3		Dynamics associated with the evolution of the RPSSB	316
7.4		Ascent of magma sheets along a conduit penetrating a melt zone at depth	317
7.5		Restoring continents to their pre-rift positions after Unterrnher et al (1988)	318
	a	No intra-continent deformation	
	b	Intra-continent dextral simple shear	
7.6		Applying the principle of effective stress to pluton emplacement	320
	a	Positive minimum stress	
	b	Negative minimum stress	

7.7	a	<i>Geological map of the Jambeiro pluton (modified after Hasui et al 1978)</i>	323
	b	<i>Possible tectonics associated with emplacement</i>	
7.8	a	<i>Summary map of the Piracaia pluton</i>	324
	b	<i>Possible tectonics associated with emplacement</i>	
7.9	a	<i>Summary map of the Sao Roque and Itaquí plutons</i>	325
	b	<i>Possible tectonics associated with emplacement</i>	
7.10		<i>Summary map and tectonic interpretations of the Sindacta pluton (after Spanner & Kruhl in press)</i>	326
8.1		<i>Characteristics of an ellipsoid / mafic enclave population</i>	331
8.2		<i>Orientations of the principle vectors before and after deformation</i>	332
8.3		<i>Projection, apparent axial ratios, axis transforamtion and orientation</i>	334
8.4		<i>Correlation between imposed strain and recorded mafic ellipsoid axial ratio for uniform population</i>	336
8.5		<i>Correlation between imposed strain and recorded mafic ellipsoid axial ratio for Normal population 1</i>	338
8.6		<i>Correlation between imposed strain and recorded mafic ellipsoid axial ratio for Normal population 2</i>	340
8.7		<i>Correlation between imposed strain and recorded mafic ellipsoid axial ratio for Elongate population 1</i>	342
8.8		<i>Correlation between imposed strain and recorded mafic ellipsoid axial ratio for Elongate population 2</i>	344
8.9		<i>Log K-values for predicted and modelled datasets</i>	345
8.10		<i>Histograms of outcrop and modelled ellipsoid / enclave axial ratio populations</i>	345
	a	<i>Mafic enclave axial ratio measurements, X/Z plane Ardara plutonlocality O2.</i>	
	b	<i>Modelled distribution Uniform distribution, flattening imposed strain X/Z = 5</i>	
	c	<i>Modelled distribution Normal population 1, flattening imposed strain Y/Z = 5</i>	
	d	<i>Modelled distribution Normal population 2, flattening imposed strain X/Z = 5</i>	
	e	<i>Modelled distribution Elongate population 1, flattening imposed strain X/Z = 5</i>	
	f	<i>Modelled distribution Elongate population 2, flattening imposed strain X/Z = 3</i>	
8.11		<i>Elemental approach to aureole deformation</i>	349
8.12		<i>Temperature variation across the aureole of the Ardara pluto, from Kerrick (1987)</i>	349
8.13	a	<i>Differential stress due to pluton emplacement</i>	350
	b	<i>Strain accumulation through shortening</i>	
8.14		<i>Variation in the power law exponential during deformation</i>	353
8.15		<i>Variation in activation energy and its effect on deformation</i>	355
8.16		<i>Variation in magma supply rate and its influence upon deformation preserved</i>	357
17	a	<i>Parameters affecting diapiric ascent</i>	361
	b	<i>Parameters affecting dyking ascent</i>	
8.18		<i>Ardara pluton, emplacement time against critical fracture size</i>	367
8.19		<i>Plutons from the Rio Paraiba do Sul shear belt, emplacement tiem against critical fracture size</i>	369
8.20	a	<i>Two dimensional particle flow lines during pure shear (after Ramsay & Huber 1983)</i>	374
	b	<i>Three dimensional particle flow lines during pure shear</i>	

Plates list

Objects used for scale: lens cap = 5cm, pencil = 14cm, notebook = 16x11cm, folder 35x25cm, hammer = 30cm

Plate	Caption	Page
2.1	Solid state deformation of G1, Ardara pluton	53
a	in outcrop (GR 72759279)	
b	in thin section (GR 74639874)	
2.2	Photomicrograph of magmatic state deformation of G1, Ardara pluton (GR 72629846)	54
2.3	a Photomicrograph of mafic blebs within G2, Ardara pluton (GR 70429637)	56
b	Photograph of G2, Ardara pluton showing magmatic state deformation (GR 72629846)	
2.4	Photograph of G3, Ardara pluton (GR 81849580)	57
2.5	Photomicrograph of sinistral shear fabric from the Ardara pluton (GR 70329569)	77
2.6	Photograph of a sinistral shear senses recorded by lamprophyric dykes (GR 70519394)	78
2.7	Sinistral country rock shear sense indicator from the Western area, Ardara pluton (GR 70019653)	78
2.8	Top to the north directed minor thrust from the northern part of the Ardara pluton (GR 72910055)	79
2.9	a Photomicrograph of dextral shear fabric from the Eastern area, Ardara pluton (GR 74639874)	81
b	Dextral country rock fabric from the Eastern area, Ardara pluton (GR 75789906)	
2.10	Sinistral solid state deformation from the Southern area, Ardara pluton (GR 79539223)	82
2.11	Steep folds verging weakly northwards from the Southern area, Ardara pluton (GR 75439081)	83
3.1	Pre Brasiliano structures from the Atibaia area (GR 463437)	110
3.2	Low angle S_{n+1} fabric, Nazare paulista region (GR 578369)	110
3.3	Highly deformed sheeted granites (GR 843297)	111
3.4	Nazare Paulista migmatites (GR 578369)	111
3.5	Development of a crenulation cleavage (GR 715366)	112
3.6	Subvertical shear zone, the Jundiuvira shear zone (GR 619345)	112
3.7	Subhorizontal stretching lineation (GR 41103058)	113
3.8	D_{n+3} fabric in the Atibaia pluton (GR 48093108)	114
3.9	Brittle-ductile mylonite from the Atibaia pluton (GR 46783525)	115
3.10	Type 1, Thin migmatite slivers intruding along the foliation (GR 48913121)	117
3.11	Type 2, Massive migmatites intruding along or obliquely to the foliation (GR 516382)	117
3.12	Low-angle sheeted Santa Luzia complex (GR 837310)	118
3.13	Low-angle sheeted Buquira complex (GR 855291)	118
4.1	Migmatites at a distance from the pluton (GR 380344)	126
4.2	Migmatites close to the pluton contact (GR 44484078)	127
4.3	Atibaia granite sheet intruding gneissic gneissic foliation (GR 47653583)	129
4.4	Symmetric boudinage of granitoid sheet (GR 47653583)	130
4.5	Contact country rock gneisses on the western side of the Atibaia pluton (GR 380344)	131
4.6	Contact granite on the western side of the Atibaia pluton (GR 43103818)	131
4.7	Contact country rocks gneisses on the eastern side of the Atibaia pluton (GR 47653583)	131
4.8	Contact granite on the eastern side of the Atibaia pluton (GR 46903503)	132
4.9	Photograph of the Atibaia pluton granite (GR 43833215)	133
4.10	The Atibaia pluton granite in thin section (GR 45403795)	133
4.11	Microgranitoid stock intruded into the country rock around the Atibaia pluton (GR 42843030)	135
4.12	Microgranitoid dyke intruded into the Atibaia pluton (GR 44303948)	135
4.13	Photomicrograph of microgranitoid dykes from the Atibaia pluton (GR 44433904)	136
4.14	Microgranitoid enclave preserved in the pluton (GR 41103058)	136
4.15	Photomicrograph of microgranitoid enclave (GR 44043673)	137
4.16	Country rock xenolith from the Atibaia pluton (GR 44233998)	138
4.17	Shear related fabric from the western side of the Atibaia pluton (GR 47553933)	140
4.18	D_{n+3} fabric close to the eastern pluton contact (GR 47653584)	140
4.19	$D_{n+1/2}$ fabric on the eastern side of the Atibaia pluton (GR 484392)	140
4.20	Granite fabric from the Northern area Atibaia pluton (GR 45504131)	142
4.21	Granite gneiss texture close to the pluton contact Pedra Grande area, Atibaia pluton (GR 43703968)	143
4.22	Solid state fabric preserved in the majority of Pedra Grande outcrops (GR 43583723)	144
4.23	Photomicrograph of the granite gneiss texture, Pedra Grande area, Atibaia pluton (GR 43703968)	144
4.24	Photomicrograph of the solid state fabric, Pedra Grande area, Atibaia pluton (GR 43583723)	144
4.25	Solid state fabric from the North east part of the Atibaia pluton (GR 47063916)	145
4.26	Fabric from the Centre east area, Atibaia pluton (GR 46133453)	146

4.27	<i>Solid state fabric from the South west area, Atibaia pluton (GR 42532923)</i>	146
4.28	<i>Photomicrograph of the solid state fabric South east area, Atibaia pluton (GR 47253086)</i>	147
4.29	<i>Magmatic fabric in outcrop from the Central area, Atibaia pluton (GR 44433648)</i>	148
4.30	<i>Photomicrograph of magmatic fabric from the Central area, Atibaia pluton (GR 44363693)</i>	148
4.31	<i>Dextral fabric from the western side of the Atibaia pluton (GR 42483851)</i>	156
4.32	<i>Dextral asymmetric porphyroclasts from the western side of the Atibaia pluton (GR 43634008)</i>	157
4.33	<i>Dextral shear sense from orthern contact area, Atibaia pluton (GR 47553933)</i>	157
4.34	<i>Sinistral magmatic fabric from the Atibaia pluton (GR 45003600)</i>	158
4.35	<i>S-C fabrics from the Atibaia pluton (GR 44153568)</i>	159
4.36	<i>Asymmetric porphyroclast from the Atibaia pluton (GR 44303591)</i>	159
4.37	<i>Dextral shear fabrics on a microgranitoid dyke from the Pedra Grande area, Atibaia pluton (GR 43002938)</i>	162
4.38	<i>A single discrete mylonitic shear zone (GR 46783525)</i>	168
4.39	<i>Multiple discrete shear zones (GR 47053878)</i>	168
5.1	<i>Contact rocks from the southeastern side of the Imbiricu pluton (GR 95004500)</i>	182
5.2	<i>Sheeting of granite along the country rock foliation, northwestern side of the Imbiricu pluton (GR 92734765)</i>	183
5.3	<i>Gneissic solid state from close to the southeasternmost contact, Imbiricu pluton (GR 96554775)</i>	184
5.4	<i>Imbiricu pluton, G1 in outcrop (GR 92754733)</i>	187
5.5	<i>Solid state fabric northeast G1, Imbiricu pluton (GR 92754733)</i>	187
5.6	<i>Photomicrograph of solid state deformation within G1, Imbiricu pluton (GR 93284780)</i>	188
5.7	<i>Sheeting within the Imbiricu pluton (GR 92384789)</i>	188
5.8	<i>Southwest G1, Imbiricu pluton (GR 94684600)</i>	190
5.9	<i>G2, Imbiricu pluton in outcrop (GR 90384433)</i>	190
5.10	<i>Photomicrograph of fabric preserved in G2, Imbiricu pluton (GR 94534695)</i>	190
5.11	<i>Microgranitoid stock northwest of the Imbiricu pluton (GR 92105235)</i>	193
5.12	<i>Microgranitoid dyke from within the Imbiricu pluton (GR 91404708)</i>	194
5.13	<i>Ellipsoidal enclave from within the Imbiricu pluton (GR 92474778)</i>	195
5.14	<i>Blocky enclave from within the Imbiricu pluton (GR 90384433)</i>	195
5.15	<i>Annulus of basic material preserved within G2 of the Imbiricu pluton (GR 89654618)</i>	195
5.16	<i>Country rock xenoliths within the Imbiricu pluton (GR 89734805)</i>	196
5.17	<i>Solid state fabric within G1, Imbiricu pluton (GR 90634798)</i>	200
5.18	<i>Magmatic fabric within G1, Imbiricu pluton (GR 93584770)</i>	200
5.19	<i>Photomicrograph of solid state deformation from G1, Imbiricu pluton (GR 92484778)</i>	200
5.20	<i>Photomicrograph of magmatic state deformation from G1, Imbiricu pluton (GR 90754513)</i>	201
5.21	<i>Solid state fabric within G2, Imbiricu pluton, showing randomly orientated K-feldspar phenocrysts (GR 94734633)</i>	202
5.22	<i>Photomicrograph of the fabric within G2, Imbiricu pluton (GR 94484750)</i>	202
5.23	<i>Elongate feldspar phenocrysts along the southeastern contact of the Imbiricu pluton (GR 96554775)</i>	208
5.24	<i>Dextral shear fabrics within the southeasternmost part of the Imbiricu pluton (GR 96554775)</i>	210
5.25	<i>Solid state fabrics from the Imbiricu pluton (GR 90684850)</i>	212
5.26	<i>Discrete mylonite from the Imbiricu pluton (GR 90684388)</i>	219
5.27	<i>Photomicrograph of the sharp boundary zone of a mylonite to the surrounding deformed granite (GR 93134680)</i>	219
5.28	<i>Photomontage of the vertical plane from the principle outcrop of the Santa Isabel gneisses (GR 81563308)</i>	223
5.29	<i>Country rocks northwest of the Morro Azul pluton (GR 74232980)</i>	224
5.30	<i>Fractured portion of G1 granite incorporated in the country rocks southeast of the Morro Azul pluton (GR 82283405)</i>	226
5.31	<i>Morro Azul, G1 in outcrop (GR 79943384)</i>	228
5.32	<i>Photomicrograph of fabric preserved in G1, Morro Azul pluton (GR 82103675)</i>	228
5.33	<i>Outcrop photograph of G2, Morro Azul (GR 83103583)</i>	230
5.34	<i>Photomicrograph of the fabric preserved within G2, Morro Azul pluton (GR 83603628)</i>	230
5.35	<i>Homogenous G1 granite (GR 82633530)</i>	233
5.36	<i>Outcrop of G1 preserving intruded sheets of G2 (GR 82763674)</i>	233
5.37	<i>Raft of G1 present within homogenous G2 (GR 82853700)</i>	234
5.38	<i>Homogenous G2 granite (GR 82633616)</i>	234
5.39	<i>Country rock screens preserved within southeastern G1 (GR 84803675)</i>	235
5.40	<i>Intense gneissose fabric preserved within G1 close to its southeastern contact with G2 (GR 8403675)</i>	236
5.41	<i>Band of basic material defining the southeastern G1-G2 contact (GR 8403675)</i>	236
5.42	<i>Microgranitoid enclave present in the quarry at GR 81003428</i>	238
5.43	<i>Incorporated country rock within the Morro Azul pluton (GR 81003428)</i>	238

5.44	<i>Close up of $D_{n+2/4}$ fabric at the southeastern contact of the Morro Azul pluton (GR 82883548)</i>	240
5.45	<i>Photomicrograph of $D_{n+2/4}$ fabric from the southeastern contact of the Morro Azul pluton (GR 77952943)</i>	241
5.46	<i>Close-up of ductile fabric within the Santa Isabel gneisses (GR 81563308)</i>	241
5.47	<i>Sub-vertical country rock fabric northwest of the Morro Azul pluton (GR 80983224)</i>	242
5.48	<i>Northwestern area G1, poorly aligned feldspar phenocrysts (GR 84734059)</i>	243
5.49	<i>Northwestern area G1, aligned feldspar phenocrysts (GR 82103675)</i>	243
5.50	<i>Northwestern area G1, magmatic state feldspar lineation (GR 82333661)</i>	244
5.51	<i>Photomicrograph of strong solid state deformation fabrics from the northwestern area G1, Morro Azul pluton (GR 80683353)</i>	244
5.52	<i>Photomicrograph of weakest solid state deformation fabrics from the northwestern area G1, Morro Azul pluton (GR 84734059)</i>	244
5.53	<i>Southeastern area G1, showing intense solid state fabric (GR 82983453)</i>	245
5.54	<i>Photomicrograph of solid state fabric from the southeastern area G1, Morro Azul pluton (GR 84803685)</i>	246
5.55	<i>Horizontal plane solid state fabric from the southern area G1, Morro Azul pluton (GR 74582904)</i>	246
5.56	<i>Vertical plane solid state fabric from the southern area G1, Morro Azul pluton (GR 74582904)</i>	247
5.57	<i>Weak solid state fabric from the southern area G1, Morro Azul pluton (GR 77233015)</i>	247
5.58	<i>Magmatic fabric from G2, Morro Azul pluton (GR 85033863)</i>	248
5.59	<i>Photomicrograph of preserved magmatic fabric from G2, Morro Azul pluton (GR 84633630)</i>	248
5.60	<i>Pervasive solid state fabric from G2, Morro Azul pluton (GR 83953650)</i>	249
5.61	<i>Intense solid state fabric from G2, Morro Azul pluton (GR 84733855)</i>	250
5.62	<i>Horizontal plane exposure of deformed pegmatites within the Santa Isabel gneisses (GR 81563308)</i>	258
5.63	<i>Vertical plane exposure of deformed pegmatites within the Santa Isabel gneisses (GR 81563308)</i>	258
5.64	<i>Boundinage of feldspar phenocrysts during dextral solid state deformation (GR 79963224)</i>	262
5.65	<i>Intense solid state shear induced fabric along G1-G2 contact (GR 81033399)</i>	262
5.66	<i>Sinistral quartz filled tension gashes at the northernmost extremity of the Morro Azul pluton (GR 85434085)</i>	264
5.67	<i>Crenulating fabric forming dextral S-C fabrics southeast of the Morro Azul pluton (GR 83303481)</i>	265
5.68	<i>Sinistral bimodal magmatic state fabric from the Morro Azul pluton (GR 85033902)</i>	266
5.69	<i>Dextral solid state shear sense fabric from the Morro Azul pluton (GR 84103573)</i>	267
5.70	<i>Photomicrograph of dextral solid state shear sense fabrics from the Morro Azul pluton (GR 75482904)</i>	267
5.71	<i>Discrete mylonite from the Morro Azul pluton (GR 82983453)</i>	272
6.1	<i>Stretching lineation in finely divided country rock gneiss close to the northern contact of the Itapeti pluton (GR 375774039)</i>	287
6.2	<i>Solid state fabric close to the northern contact of the Itapeti pluton (GR 385974059)</i>	288
6.3	<i>Sheeting of similar granite types along the northern contact (GR 389374063)</i>	289
6.4	<i>Solid state fabric from close to the northern contact of the Itapeti pluton (GR 385974059)</i>	290
6.5	<i>Sub-horizontal mineral stretching lineation from close to the northern contact of the Itapeti pluton (GR 375674032)</i>	290
6.6	<i>Photomicrograph of solid state fabric close to the northern contact of the Itapeti pluton (GR 376074029)</i>	291
6.7	<i>Magmatic fabric from close to the southern contact of the Itapeti pluton (GR 378074006)</i>	291
6.8	<i>Photomicrograph of magmatic fabric from close to the southern contact of the Itapeti pluton (GR 378074006)</i>	292
6.9	<i>Asymmetric porphyroblasts and S-C fabrics associated with the solid state deformation of the Itapeti pluton (GR 387274062)</i>	297
6.10	<i>Magmatic state shear fabric from the Itapeti pluton (GR 378074006)</i>	298

Tables list

Table	Caption	Page
2.1	<i>The Ardara pluton.</i>	39
2.2	<i>Deformation chronology of the area adjoining the Ardara pluton</i>	44
2.3	<i>Average mafic enclave axial ratios from the Ardara pluton</i>	60
2.4	<i>Average Fry strains from the Ardara pluton</i>	66
2.5	<i>Line deflection data for the wallrocks surrounding the Ardara pluton</i>	71
2.6	<i>Migrated strain measurements for the Atibaia pluton</i>	88
3.1	<i>Brazilian Precambrian geochronotectonic cycles (after Pinheiro 1997)</i>	102
4.1	<i>Average mafic enclave axial ratios from the Atibaia pluton</i>	151
4.2	<i>Average Fry strains from the Atibaia pluton</i>	152
5.1	<i>Average mafic enclave axial ratios from the Imbiricu pluton</i>	205
5.2	<i>Average Fry strains from the Imbiricu pluton</i>	206
5.3	<i>Average mafic enclave axial ratios from the Morro Azul pluton</i>	254
5.4	<i>Average Fry strains from the Morro Azul pluton</i>	255
5.5	<i>Mean strain ellipsoid axial ratios from the Santa Isabel gneisses</i>	259
5.6	<i>Estimates of contact strain associated with country rock deflection around the northwestern contact of the Morro Azul pluton</i>	261
6.1	<i>Summary table of microgranitoid enclave axial ratios from across the Itapeti pluton</i>	293
6.2	<i>Summary table of Fry strain measurements from the Itapeti pluton</i>	295
8.1	<i>Initial characteristics of the Uniform population ellipsoid population</i>	335
8.2	<i>Imposed strains and recorded ellipsoid axial ratios for the Uniform population</i>	337
8.3	<i>Initial characteristics of Normal population 1, mean axial length = 10, standard deviation = 1</i>	337
8.4	<i>Imposed strains and recorded ellipsoid axial ratios for Normal population 1</i>	338
8.5	<i>Initial characteristics of Normal population 2, mean axial length = 10, standard distribution = 2</i>	339
8.6	<i>Imposed strains and recorded ellipsoid axial ratios for Normal population 2</i>	339
8.7	<i>Initial characteristics of Elongate population 1, one mean axial length = 10, standard deviation = 2, two mean axial lengths = 5, standard deviation = 2</i>	341
8.8	<i>Imposed strains and recorded ellipsoid axial ratios for Elongate population 1</i>	341
8.9	<i>Initial characteristics of Elongate population 2, one mean axial length = 30, standard deviation = 2, two mean axial lengths = 5, standard deviation = 2</i>	343
8.10	<i>Imposed strains and recorded ellipsoid axial ratios for Elongate population 2</i>	343
8.11	<i>Correlation coefficients for each individual dataset</i>	346
8.12	<i>Physical properties of granite and metamorphosed country rocks.</i>	364
8.13	<i>Optimised diapiric ascent characteristics for the Ardara pluton</i>	365
8.14	<i>Ascent data for far-field Peclet number and variable contact wallrock viscosity, Ardara pluton</i>	365
8.15	<i>Ascent rates of multiple diapirs along a single conduit</i>	366
8.16	<i>Optimized diapiric ascent data for the plutons of the Rio Paraíba do Sul shear belt</i>	368
8.17	<i>Ascent data for far-field Peclet number for plutons from the Rio Paraíba do Sul shear belt</i>	368

SECTION 1

Introduction

“The geological record may extend over Earth history but geologists are notoriously poor at inferring tectonic processes from the crust.....The problem is (as always) to ask the useful questions” - Dr Mike Bickle

Chapter 1

Granitoid ascent, emplacement, deformation and analysis

1.1 Introduction

1.1.1 Preamble

Granite is a rock type that is probably unique to the planet Earth in the Solar System, forming as a result of the interaction of water with tectonics and magma. Granitoid rocks form approximately 20% of the continental basement and occur in all tectonic environments, acting as an important method of adding material to the continental crust. *Sensu lato* Granite encompasses a wide range of compositionally diverse rocks, which reflect the variable origin and source of the magma, but can be generally defined as *coarse grained acid igneous rocks*. The vast majority of granite rock outcrops in zones of ancient orogenesis and can be simplistically subdivided into the following categories: i) subduction related, due to melting initiated by a down going subducting slab; ii) orogenic continental margins, as a result of mantle melt facilitated crustal anatexis; iii) continent-continent orogenic belts, as a result of crustal anatexis (melt) during burial and metamorphism; and iv) extension related, as a result of orogenic extension or adiabatic decompression. The methods of focusing and transporting this magma from the place of formation to its position of emplacement are widely debated (Petford *et al* 1993, Cruden 1990), but the influence of large inter-continental shear zones (Sylvester 1988, Hutton & Reavy 1992) and lineamental structures in the lower crust (Pitcher & Bussell 1977, Jacques & Reavy 1994, Hutton & Alsop 1996) appears to be critical. In summary, granites and their associated rocks are formed in large quantities whenever continental crust is heated by rising mantle heat, extended and thinned, or thickened by collision (Fyfe 1988).

1.1.2 Definition of key terms

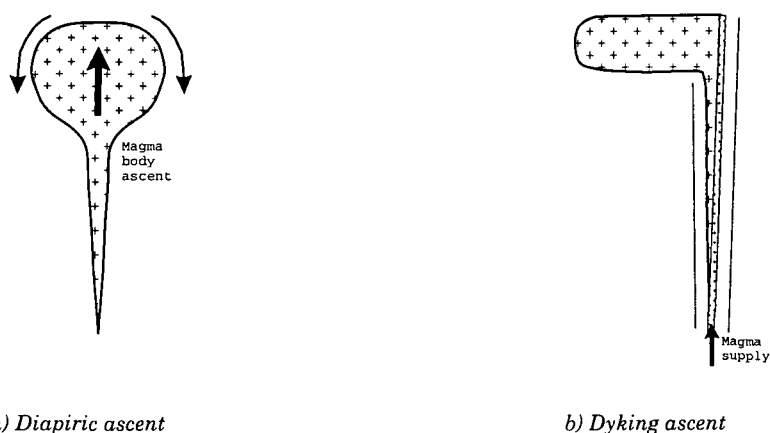
Ascent

The ascent of granite magma is the process by which it travels from a zone of magma genesis to the level of emplacement. It has been a subject of great controversy: historically between the ‘transformists’ who maintain that magma is formed in-situ by the ‘granitization’ of the crust, and the ‘magmatists’ who suggest that magma formed elsewhere and travelled to the emplacement level. With the growing realisation that ‘granitization’ is unlikely to be a crustal scale process for granite formation, the debate now focuses on the methods for magmatic ascent. There are two end-member perspectives,

that of pluton formation through diapiric ascent, and that of piecemeal sheeting/dyking to assemble a pluton.

The concept of diapiric ascent, stems from observations of sub-spherical granites e.g. Criffel pluton, Southern Scotland (Courrioux 1987) and analogies made with other sub-spherical bodies such as salt diapirs, in combination with analogue modelling (Ramberg 1967, 1970, Schmeling *et al* 1988, Cruden 1988, 1990). These authors attempt to demonstrate that large volumes of material, can move 'en masse' through the crust (Figure 1.1a). However dimensionally consistent theoretical models have shown that granite diapirs are likely to move very slowly through the crust and experience 'thermal death' (Marsh 1982), i.e. freezing, unless they experience particular crustal conditions (Weinberg 1995).

The alternative view is, that granitoid magmas ascend as sheets along dyke-like conduits, such as faults or fractures (Leake 1978, Pitcher 1979). Currently there are two models for such ascent: that of Clemens & Mawer (1992), who proposed ascent by magma fracture; and that of Petford *et al* (1993) who propose ascent through existing fault-initiated conduits. In either model thin sheets of magma (Figure, 1.1b) travel rapidly through the crust assembling a granitoid pluton in stages at a higher crustal level.



a) Diapiric ascent

b) Dyking ascent

Figure 1.1 Methods of magma ascent

Emplacement

This is the process by which granitoid magma is added to the crust. It is independent of the mode of ascent and was first tackled comprehensively by Read (1957) and Buddington (1959) who developed the concept of the 'Granite series' (Figure, 1.2). In this approach Cordilleran type plutons or batholiths were interpreted to have formed at relatively high levels in the crust and named 'magmatic intrusive' or 'epizonal'. At intermediate crustal depths 'parautochthonous' or 'mesozonal' plutons formed and, at low levels within the crust, plutons with strong anatectic affinities were termed 'autochthonous' or 'catazonal'. However, Pitcher & Berger (1972) in their study of the Donegal Batholith

observed that each of these plutonic sub-divisions could be observed at approximately the same crustal depth.

Later, following the acceptance of Plate Tectonic theory and its application to continental deformation, Pitcher (1978,1979) showed that emplacement style could be related to the tectonic regime dominant during emplacement. As a result of this work, research has become focused onto a more tectonically based approach to the problem of emplacement. Following on from this Hutton (1982) demonstrated that pluton emplacement can take place syn-tectonically during regional deformation. The application of this hypothesis to other plutons has shown that pluton emplacement can take place syn-tectonically, using a combination of the following end-member environments; transcurrent shear, extensional shear and reverse contractional shear (Hutton 1988, Hutton & Reavy 1992, Hutton & Ingram 1992, Ingram & Hutton 1994).

In addition, if a pluton is emplaced into an area which is relatively tectonically inactive, or has a strong component of internal magma fluid pressure, the magma has the ability to change the local effective stress regime and may; rise diapirically (Courrioux 1987, England 1990); or expand in-situ as a simple balloon (Holder 1979, Molyneux & Hutton *in press*), adding a local co-axial component to the regional deformation field. The form of a pluton being dictated by the interaction of external tectonic and internal body forces.

Genesis

It is widely accepted that granites must have formed as a result, of extensive melting followed by fractionation and other contamination processes of crustal and mantle protoliths. The exact processes by which this occurs continue to be widely debated, but a useful method of classifying the possible origin of granitic rocks was developed from work on the Caledonide, Lachlan Fold Belt of S.E. Australia (Chapell & White 1974, 1984, White & Chappell 1988, Chappell & Stephens 1988), where it was demonstrated that there are two contrasting geochemical suites of granites. This concept has been developed subsequently in an attempt to classify plutonic rocks from every tectonic environment (see Pitcher 1993 for review), and is simplistically summarised below:

I-type granites

'Igneous' granites derived from a purely or dominantly igneous source, e.g. Cordilleran I-type granites, which are subduction related and are interpreted to have formed by the partial melting of a basaltic to andesitic source, or Caledonian I-type granites which are understood to have formed from the melting of older igneous rocks in any environment.

S-type granites

'Sedimentary' granites derived from a predominantly sedimentary source e.g. Himalayan leucogranites which are collision related S-type granites formed from the partial anatexis of meta-sedimentary gneisses.

A-type granites

'Anorogenic' alkali granites of strongly variable composition, they are most common in anorogenic cratons, and their genesis appears to require high temperature, volatile-rich melting in a continental environment, and could be related to adiabatic melt during lithospheric extension.

The process by which melt forms and segregates is known to be complex. It requires a suitable protolith, a heat source and a method of extraction. The supply of heat necessary to start melt could occur as a result of either a) regional metamorphism or b) the injection of hot mafic melts (Petford *pers comm*), both of which can be shown to result in temperatures sufficient to produce significant quantities of crustal melt. In addition, the injection of water or other volatile phases into metamorphic rocks can induce extensive melting. It is generally believed that these processes should be preserved in exhumed rocks. Migmatite terrains, long been cited as examples of areas where granite melt has 'frozen-in' having been formed as result of water-saturated, in-situ partial melting. However, recent experimental work has shown that water-saturated melting of an amphibolite rock produces an actual volume decrease. This would tend to result in local 'under-pressuring' of the rock and the retention of the melt (Brown *et al* 1995). Melting of a dry-granulite facies assemblages results in volume increase (up to 18%) (Clemens & Mawer 1992), with the overpressuring of the regional melt zone enhancing the feasibility of melt extraction and migration.

Extraction of the melt could occur because of the transfer of 'solitary waves' through the melt zone (McKenzie 1984) at high melt fractions. A more feasible process is the tectonic squeezing (filter pressing) of the partially molten country rock. This has been modelled and shown to efficiently extract melt fractions of less than 1% (see Sawyer 1996 for review).

Lineaments

A lineament has been defined as "...an alignment of geological and often geophysical features which is frequently interpreted as a higher crustal expression of an essentially older fault (structure) in the lower lithosphere."- Hutton & Alsop (1996). There have been a number of applications of this concept to magma emplacement. Pitcher & Bussell (1977) demonstrated lineamental control in the siting of granites along the Coastal Batholith of Peru, more recently Jacques & Reavy (1994) and Hutton & Alsop (1996) have demonstrated the interaction of upper crustal faults and shear zones with lower crustal

lineaments in the focusing of magmatism, over long periods of time, across the Caledonian Highland and Donegal granites of the British Isles.

1.1.3 Objectives

In this work granitoids from two classic geological provinces have been studied. The first of these, the Caledonian age, Ardara pluton from the Donegal Batholith, NW Ireland is an upper crustal, sub-circular pluton, emplaced into greenschist facies country rocks. The Donegal area, and the Ardara area in particular, has received extensive previous study and both the distribution of plutonic phases, the stratigraphic sequence and the structural history are particularly well constrained. As a consequence this area was chosen to undertake a detailed study of the country rock and magma dynamics (shear senses, fabric development, preserved finite strain) which existed during the pluton emplacement process.

Whereas the Rio Paraíba do Sul shear belt in southeast Brazil is less well known, nor has it been studied in such detail, but it shows an unequivocal relationship between inter-continental strike-slip shear zones formed in the mid-crust during the Brasiliano orogeny and comparatively undeformed granitic plutons. By studying a number of plutons from this area it has been possible to determine the relationship between the shear zones and the plutons, the dynamics of intrusion, and elements of the structural evolution of the area pre-, syn- and post-intrusion of the granitoids.

Then drawing together these diverse study areas it has been possible to remark upon the general viability and structural features required for various intrusion mechanisms and the possible relationship between orogenic evolution and the emplacement of granitoid plutons.

1.1.4 Conventions

A number of conventions have been used in this thesis, these are outlined below:

Strike/Dip

Planar strikes and dips are given using a strike between 0° and 360°, dip which is 90° clockwise of the strike between 0° and 90° and the dip direction e.g. SE, NW.

Azimuth/Plunge

The orientation of lines is given using the azimuth (the direction of plunge) between 0° and 360° and the plunge between 0° and 90°.

Planes of outcrop

Because of the lack of lineation in many of the studied exposures the principal planes of the strain ellipse cannot be easily identified, and have been approximated to:

The horizontal plane - the horizontal plane orthogonal to the generally sub-vertical foliation plane.

The vertical plane - the vertical plane orthogonal to both the foliation plane and the *horizontal plane*.

Foliation plane

Within the studied plutons the identifiable planar fabric is always referred to as the foliation plane. Additionally in strongly weathered or intensely deformed country rock, the most prominent planar fabric is referred to as the foliation, irrespective of its dynamic context.

Grid references

Locality grid references are given to at least three figure and where possible more accurately using the local grid square markings which have been reproduced on the larger maps. In the case of the Jambeiro pluton a GPS machine was used during mapping and positions are given in latitude and longitude.

Space/volume

It is common in pluton emplacement studies to refer to the 'space' created for a magma body. In most studies authors are non-specific about the way in this term is used, for example, does "30% of pluton space was created by in-situ expansion" refer to a linear, areal or volumetric space. This distinction is important because a 30% increase in spherical volume implies only a 9% increase in radius, or a 20% increase in cross-sectional area. The possibilities for misunderstanding are immense. Throughout this work the term 'space', when describing the emplacement of a granite body is always used in a volumetric sense for example, "the pluton created 30% space by in-situ expansion" would be referring to an approximate estimate of the pluton volume and the 'space' created in the country rocks.

1.2 Rheology

Rheology is the science of deformation and flow, the study of elasticity, viscosity and plasticity; and the relationship between stress (Equation 1.1) and strain rate (Equation 1.3).

Equation 1.1, Stress,

$$\sigma = \text{Force applied / Area} \quad \text{units, N/m}^2$$

Equation 1.2, Strain,

$$\epsilon = \text{Change in length / Original length} \quad \text{dimensionless}$$

Equation 1.3, Strain rate,

$$\dot{\epsilon} = \text{Strain / Time} \quad \text{units, s}^{-1}$$

The rheology of a magma is controlled by a number of factors: the amount of melt, viscosity (both a strong function of temperature and water content), crystal content, the degree of interaction of these crystals, pressure, temperature and the nature of any volatiles phases i.e. water, halogens and other elements. This interaction often results in behaviour which is in detail complex. For simplicity an approximation to an ideal rheology is often made, some of these are outlined below.

1.2.1 Elastic behaviour

For an ideal elastic material deformation is non-permanent and the applied stress is proportional to the strain in accordance with Hooke's Law, the constant of proportionality being the Young's modulus, E , the resistance of a material to elastic distortion

Equation 1.4, Stress,

$$\sigma = E \cdot \epsilon$$

where E = Young's modulus

When the stress is released all the strain is recovered, and the material returns to its original shape, a mechanical analogue to this is the stretching of a spring. In a real material stress cannot be accommodated infinitely by a strain and a point, the Yield Stress (Yield Point) σ_0 , is reached, beyond which the material begins to flow and all deformation will be accommodated plastically i.e. permanently. The characteristics of this plasticity are controlled by the viscous behaviour (Figure 1.2). In addition when the material is in tension the material may fail, i.e. fracture, resulting in permanent deformation. Rocks generally have a very low Yield Stress and behave very poorly as elastic materials, and show an elastic behaviour dependant upon stress vector orientation and strain rate, e.g. at high strain rates deforming elastically, but at geological strain rates a degree of the deformation may be permanently accommodated by creep (grain scale dislocations) (McBirney & Murase 1984)

1.2.2 Viscous behaviour

The viscosity, η , of a material is a co-efficient which describes the ability of that material to have momentum transferred to it, i.e. its resistance to flow, and hence its deformation above the Yield Point.

Equation 1.5,

$$\tau = \tau_0 + \eta(\delta u/\delta y)^n$$

where, τ is the shear stress along the direction x parallel to the shear plane, τ_0 is the minimum stress required to induce permanent deformation, $\delta u/\delta y$ is the velocity gradient normal to the shear stress and n is a constant with a value of 1 or less.

For a Newtonian fluid $n=1$. The strain rate induced is proportional to the stress applied and the fluid has no yield strength (Figure 1.2), since the strain response is instantaneous and permanent. Many pure fluids e.g. water, exhibit Newtonian behaviour and magma has often been modelled as such for convenience (Shaw 1965). However many fluids are not Newtonian: indeed magma is probably highly non-Newtonian and will exhibit more complex behaviour like for example mud, blood and paste, where the relationship between applied stress and induced strain rate is non-linear.

1.2.3 More complex rheologies

The cases described above are ideal cases and can be used as simple modelling tools, but do not describe the actual behaviour of geological materials, which can be modelled using specific equations or by a combination of the ideal rheologies described above (see also Twiss & Moores 1992).

Bingham - visco-plastic- material

This material response displays an elastic response until the Yield Stress is reached, above which it deforms in a linear viscous manner (Figure 1.2). Pitcher (1987) suggested that magmas, particularly when they have high crystal contents, may deform in this way.

Non-linear rheologies

A number of field observations suggest that geological materials may deform in a way which is strongly non-linear, for example when a sheet of magma is emplaced rapidly into a hot magma body, the high initial strain rate results in fracture of the magma, subsequently local stresses are dissipated and the weaker regional stresses deform both magma components viscously i.e. syn-plutonic dykes. This material behaviour is strongly non-linear, strain rate and temperature dependent, with the different mechanical properties of minerals influencing the behaviour of the material as deformation progresses.

These fluids can be modelled empirically, for example as a 'power-law rheology', where the strain rate has an exponential relationship to the stress applied and the temperature of deformation (Equation 1.6). The non-linear material can never have a specific viscosity and can display properties such as strain/temperature softening, where progressively the stress required to produce a given strain rate reduces in time.

Equation 1.6,

$$\dot{\epsilon} = A \sigma_d^n \exp(-Q/RT)$$

where, σ_d is the differential stress, Q the activation energy, T temperature in Kelvin, R the gas constant, A constant and n the exponential constant (generally between 0 and 10) (Twiss & Moores 1992, Shea & Kronenberg 1992, Rubin 1993)

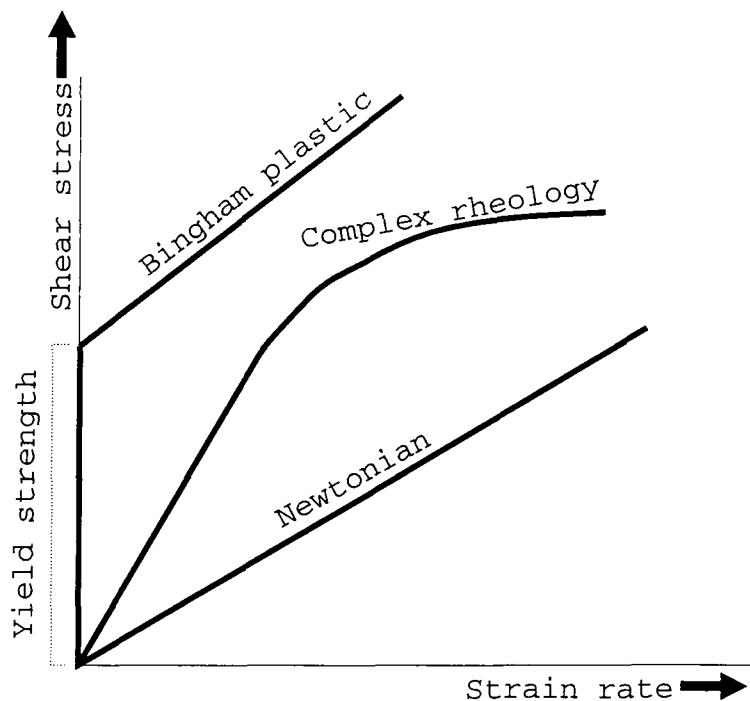


Figure 1.2 Shear stress vs. strain rate for a number of theoretical and ideal rheologies

1.2.4 Granite rheology

Silicate melt has been modelled as having a number of possible rheologies, such as: a Newtonian fluid, where the viscosity is determined from the melt viscosity and the crystal content (Shaw 1965, Arzi 1978); a Bingham material, having a finite Yield Strength which is dependent on the melt fraction (Sparks *et al* 1977 and others); and by experimental work.

The most commonly cited experimental work is that of van der Molen & Paterson (1979) who suggest that granitic magma will illustrate a wide range of rheological properties during crystallisation (Figure 1.3). At high melt percentage (low crystal

contents) the magma will behave as a Newtonian fluid. As the crystal content increases the fluid starts to behave as a Bingham material until it passes through the Rheologically Critical Melt Percentage (RCMP), where the viscosity increases dramatically. Above this point it deforms in a solid-like elastic manner. The melt fraction values for this RCMP quoted by Arzi (1978) are $20 \pm 10\%$ and van der Molen & Paterson (1979) 30-35%.

More recent work by Rutter & Neumann (1995) on samples of dynamically deformed Westerly Granite has shown that there is not a sharp decrease of effective viscosity with increased melt volume, but rather that the strength decreases more or less linearly as a function of increasing melt fraction. They conclude that the concept of a rapid change in viscosity at the RCMP may be mis-leading. In addition Vigneresse (1997) points out the importance of considering both of the possible experimental RCMPs, one that occurs during, melting and the second which occurs during freezing.

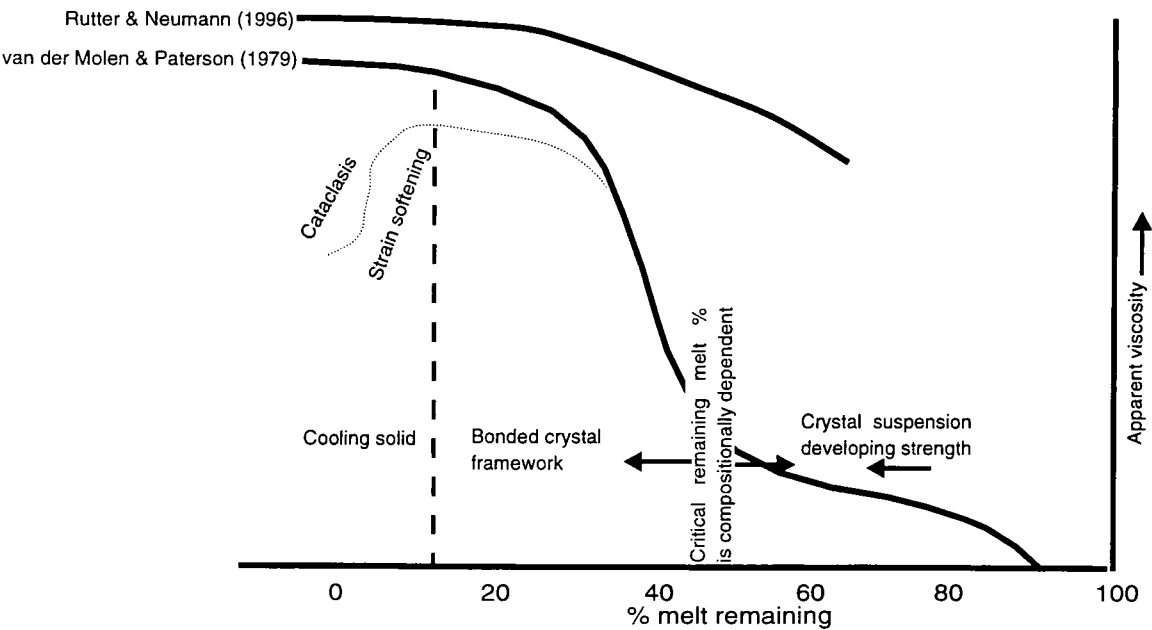


Figure 1.3 Compilation graph of relative viscosity against melt fraction after Jund (1977), Arzi (1978), van der Molen & Paterson (1979), Capais and Barbarin (1986) and Rutter & Neumann (1995)

1.3 Tectonic structures related to granite emplacement

The analysis of the structures present within the wallrock and the granitoid itself are the principal ways by which the tectonic environment and prevalent stress/strain regime pre-, syn-, and post- emplacement can be determined. The rheological models for the interpretation of such structures constitute a framework, in which structures can be viewed relative to the crystallisation state of the original intrusive magma. Research in this area has produced a proliferation of terms and terminology for describing similar features (Blumenfeld & Bouchez 1988, Hutton 1988, Paterson *et al* 1989, Tribe & D'Lemos 1995) an attempt is made to summarise these below.

1.3.1 Magmatic state structures

Magmatic state structures refer to structures formed in the magma when the melt fraction is well in excess of the supposed RCMP, where grains can rotate and move with respect to each other without experiencing internal lattice deformation. They correspond exactly to the PFC 'pre-full crystallisation' structures of Hutton (1988) and the 'magmatic state/flow' structures of Paterson *et al* (1989) and Blumenfeld & Bouchez (1988). In such a situation, the early formed crystal phases and magma enclaves will rotate, interact and align approximately perpendicular to the local principal stress (Figure 1.4a).

The absence of internal deformation of quartz and biotite are often used to identify magmatic fabrics, however it should be noted that high temperature solid-state deformation of quartz, >400°C, (Passchier & Trouw 1996) could result in complete recrystallisation and the absence of any overprinting signature. It must also be assumed that the majority of deformation in the magmatic state takes place at temperatures below the solidus where significant crystal content is present (McCaffrey 1989) and hence the fabric represents most of the strain history.

1.3.2 Transition state/lock-up fabrics

These fabrics are formed close to the supposed RCMP where crystal content is increasing (30-35% melt) and the matrix will become capable of transmitting stress. In such a situation deformation could be partitioned into discrete deformation zones, rather than homogeneously transmitted through the magma. These zones have been termed 'pre-full crystallisation (PFC) lock-up shears' by Ingram & Hutton (1992). A PFC lock-up shear should preserve an undeformed crystal matrix provided there is no deformational overprint.

1.3.3 Sub-magmatic fabrics

Sub-magmatic fabrics (Bouchez *et al* 1992) occur in magmas where there is melt remaining, but insufficient to support magmatic flow. Therefore solid state deformation could occur in the phenocrysts e.g. cracked feldspar grains, dynamic recrystallisation but the matrix e.g. quartz, biotite would continue to display magmatic state fabrics.

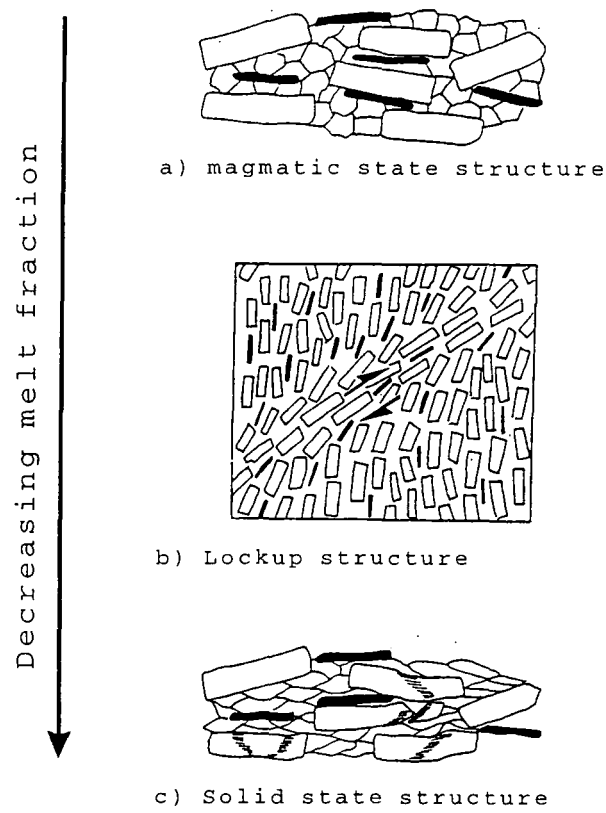
1.3.4 Solid state fabrics

These fabrics represent deformation at or below the solidus temperature of the last crystallising mineral phases, at melt fractions well below the RCMP, and result in strain being taken up inhomogeneously within the mineral phases themselves (Figure 1.4). The exact nature of this deformation process is controlled by the temperature, pressure, volatile (water/halogen) content of the deforming medium. In general quartz and biotite deform before feldspar and any mafic crystals. Solid state fabrics can be recognised by the comminution of grain size, shape changes of crystals, internal lattice deformation, fragment alignment and possible dynamic recrystallisation (polygonal grain fragments, core and mantle structures) of mineral phases (Passchier & Trouw 1996, Tribe & D'Lemos 1996).

1.3.5 The validity of a Cloosian approach

Hans Cloos' (Balk 1937) classification of granitic structures for many years formed the basic analytical approach for igneous rocks (also Marre 1986). Two types of structure occur: i) *Primary structures* - formed in response to flow in the crystallising magma, which align any platy minerals, and imply the operation of magma currents/convecting processes. Joints would also be formed at this time in response to further elongation of the magma; ii) *Secondary structures* - considered as 'tectonic' and formed in the solid state analogously to metamorphic structures i.e. cross-cutting foliations.

Berger & Pitcher (1970), Pitcher & Berger (1972) and Hutton (1988) all criticise this approach, by stating that it is unlikely that magmas flow in currents, but instead as a cohesive viscous magma solid, deforming viscously on the timescale of observation. Hutton (1988) proposed that the Cloosian system be abandoned in favour of a less genetic system, in which the deformation history, modelled in terms of external tectonically deformed strains and internal magma related forces, is related to the changing rheology of the magma. This approach is adopted throughout this work.



After Hutton (1988), Ingram & Hutton (1992),
Blumenfeld & Bouchez (1988)
and Paterson et al (1989)

Figure 1.4 Magmatic structures produced during progressive deformation and reduced melt fraction

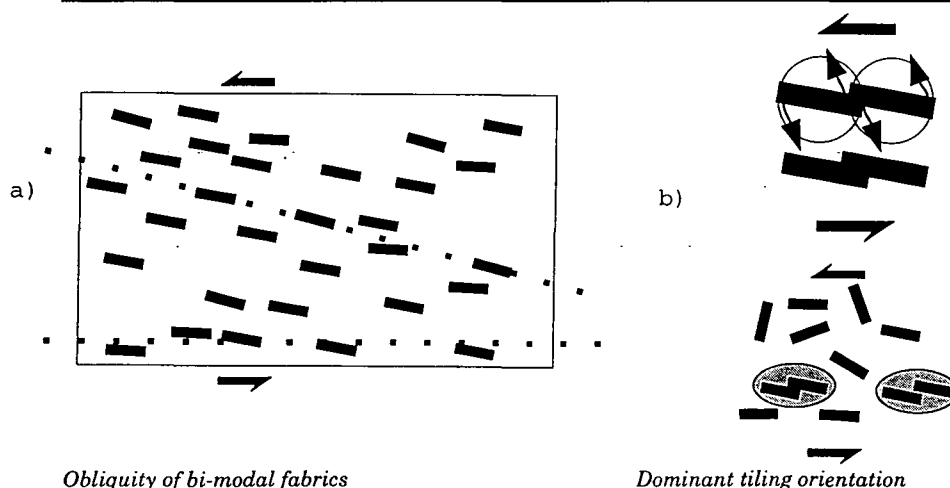
1.4 Shear sense

The recorded shear sense in a rock is a record of non-coaxial deformation, where one mass of rock has moved relative to another and has lead to the development of asymmetries in deformation structures. These asymmetries can occur on all scales, but are most frequently recognised on the meso- to microscopic scale and are termed 'shear sense indicators'. In order to correctly interpret the sense of shear the structures should be viewed in a plane which is perpendicular to the foliation with which they are associated and parallel to the λ_1 lineation (if developed). A number of shear sense indicators have been applied to granitic rocks and a summary of the most commonly cited is supplied below. For a more comprehensive summary (of shear sense indicators in all rocks) see Hanmer & Passchier (1991).

1.4.1 Magmatic state

If a magma contains melt in excess of the supposed RCMP then free rotation of the constituent phenocryst phases will take place during non-coaxial deformation and 'shape-preferred orientation' magmatic state fabrics will be produced (Paterson *et al* 1989, Hutton 1988), due to rotation of crystals into parallelism with the principal flattening plane/shear plane. A sense of shear may be deduced from the interaction of individual rotated crystals to one another, or the relative obliquity of rotated crystals to one another. Blumenfeld & Bouchez (1988) describe a number of possible shear sense indicators for magmatic state deformation, two of which have been used in this thesis:

1. The sense of obliquity of phenocrysts to the shear direction which is produced by interference of many phenocrysts as they rotate in a non-coaxial strain field (Figure 1.5a).
2. The sense of 'tiling' or imbrication of megacrysts which have rotated into contact with each other. The statistical counting of such populations and the determination of the dominant tiling orientation will demonstrate the sense of shear (Figure 1.5b)



Obliquity of bi-modal fabrics

Dominant tiling orientation

Figure 1.5

Magmatic state shear senses

1.4.2 Transition state/lock-up fabrics

When deformation occurs at lower melt fractions, and viscosity is increasing (deformation which could be close to the RCMP of van der Molen & Paterson 1979), deformation is partitioned into discrete zones of magmatic state shear 'PFC lock-up shears' (Ingram & Hutton 1992). In such a situation the shear sense is determined by the sense of obliquity, imbrication or offset sense of the shear with respect to the main fabric.

1.4.3 Solid state

If deformation of the granite continues through the RCMP, into the solid state i.e. when magma is cooled but deformation continues, or is subsequently overprinted by another deformation event, solid state shear sense indicators will be developed, with corresponding structures in the surrounding wallrocks.

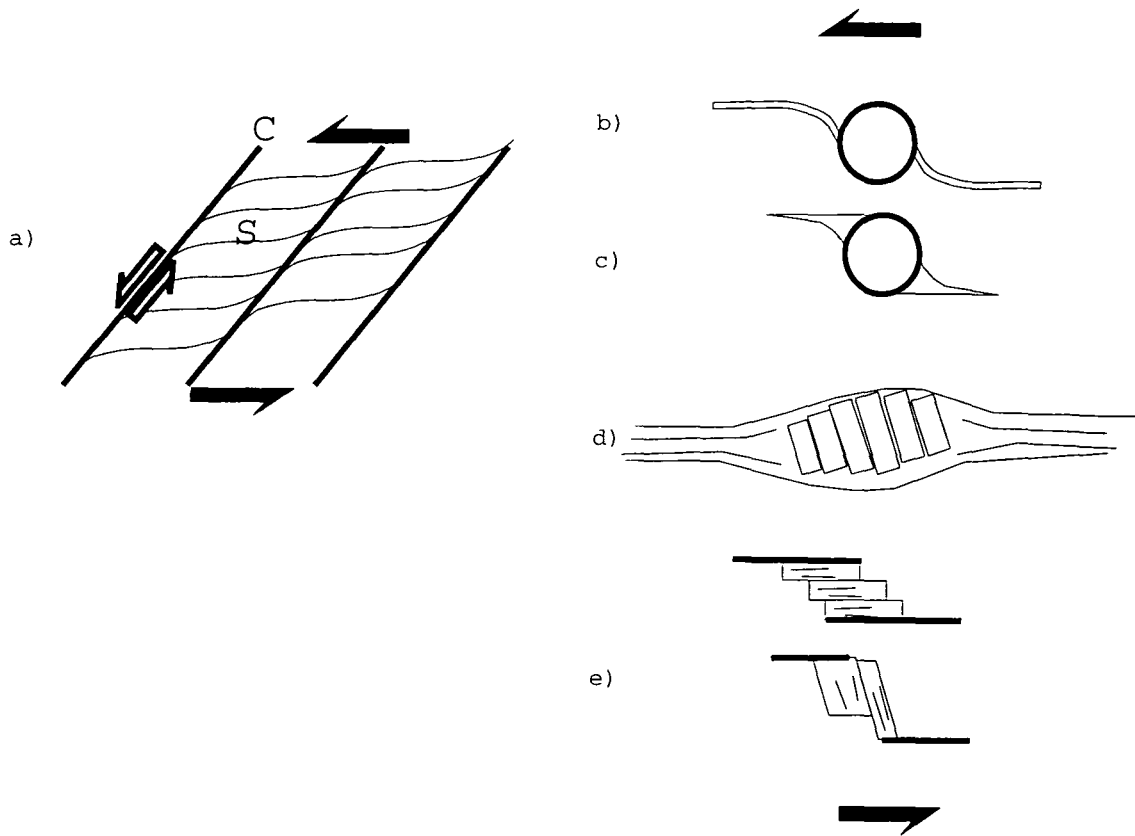
One of the first applications of general shear sense to granitic rocks was made by Berthe *et al* (1979). The term S-C mylonite was applied to the description of the shear sense in an orthogneiss. S refers to the 'schistosity', the principle XY finite strain plane, sub-parallel to the shear zone walls and C refers to the plane of 'cisaillement', the shear surfaces which cross-cut the schistosity. The C-plane initiates at 45° or less to the shear zone walls with a sense of shear synthetic to the wallrock shear sense (Figure 1.6a).

Porphyroclasts, or crystals which have a high ductility contrast to the surrounding material e.g. feldspar cf. quartz, may rotate during deformation with the same shear sense as the surroundings. This rotation can result in preferred patterns of recrystallisation or pressure shadowing. Passchier & Simpson (1986) classified this system in terms of a δ - or σ -type porphyroclast rotation (Figure 1.6b, c).

Grains or crystals which have been broken may also provide good shear sense indicators, such as the 'stack of cards model'. In this situation the fractures within the grains display a sense of shear and rotation, which is dependent upon the shear sense and the initiation angle of the fractures. Figure 1.6d illustrates a case where the sense of slip on the deformed grains is antithetic to the overall sense of shear.

During deformation particular crystallographic deformation mechanisms may be active which, as a result of the ^{non-}co-axial nature of deformation, will be asymmetric with respect to the foliation. A measurement of this asymmetry will reflect the sense of shear.

Large mica grains deformed as part of an S-C mylonite, will result in mica 'fish' (Lister & Snoke 1984), where the shear sense is determined by examination of the internal mica deformation by brittle and crystal plastic processes (Figure 1.6e).



a) S-C fabrics; b) δ -porphyroclast; c) σ -porphyroclast; d) 'stack of cards' brittle rotation; e) mica 'fish'

Figure 1.6 Solid state shear sense indicators

1.5 Strain analysis

Strain analysis requires the determination of the three dimensional change in shape of an object during single or multiple deformation events. It is generally visualised as the change in sphericity of an initially spherical object of unit volume (the strain ellipsoid, Flinn 1962); which in two dimensions is the change from a circle to an ellipse. This change in shape can be visualised graphically (Figure 1.7a), or as a change in the ratio of the lengths of the 3 mutually perpendicular principle axes of the strain ellipsoid (X, Y and Z, where $X > Y > Z$).

Applying such analysis to deformed granitoids and their wall rocks should produce, or aim to produce, a three-dimensional representation of the strain ellipsoid at various points across the study area. Flinn (1962) (Figure 1.7a, b) described the deformation types that could be formed during deformation of the strain ellipse: The X, Y and Z axes correspond to the maximum, intermediate and minimum stretching directions respectively, and are related by the Equations 1.7 and 1.8. When $K < 1$ the ellipsoid is oblate and the fabric produced is a flattening strain (S-tectonite). If $K = 1$, there is shortening along the Z-axis, a constant Y-axis and reciprocal stretching along the X-axis resulting in a plane strain (LS-tectonite). Though when $K > 1$, stretching occurs predominantly along the X-axis and shortening along both the Y- and Z-axes resulting in constrictional strain (L-tectonite) (Figure 1.7).

$$\text{Equation 1.7, } X/Y = (Y/Z)^K$$

$$\text{Equation 1.8, } \log_{10}(X/Y) = K \cdot \log_{10}(Y/Z)$$

where, X, Y, Z are the relative magnitudes of the strain ellipsoid and the k-value is a constant of proportionality used to describe the shape of the ellipsoid and the type of fabric formed.

An alternative scale for measuring strain is to determine the relative shortening or extension during deformation. This is often used for measuring one or two dimensional strain, where the three dimensional deformation environment is less certain (Equation 1.9, 1.10) and can be related to the strain ellipsoid axial ratio using Equation 1.11.

$$\text{Equation 1.9, } \% \text{ shortening} = \frac{(l_0 - l_1)}{l_0} \times 100$$

$$\text{Equation 1.10, } \% \text{ extension} = \frac{(l_1 - l_0)}{l_0} \times 100$$

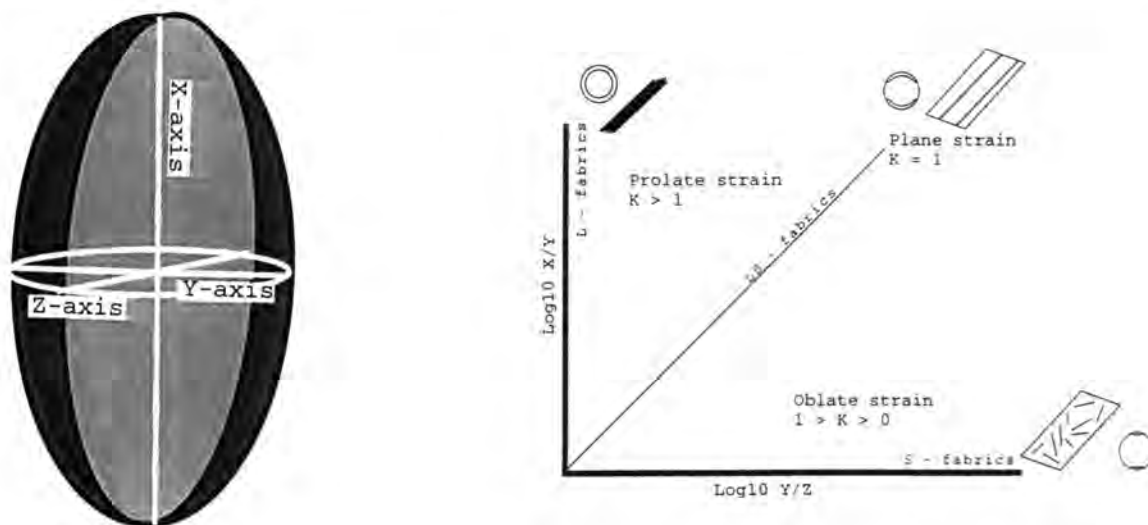
where, l_0 is the initial length and l_1 is the final length

$$\text{Equation 1.11, If the imposed strain is pure flattening strain } (R_{XZ} = R_{YZ})$$

$$\text{Then } R_{XZ} = R_{YZ} = 1/(1 - (\% \text{shortening}/100))^{3/2}$$

Quantitative estimates of the strain in granitoids are often difficult to make due to the paucity of good strain indicators. The methods used in this thesis are detailed below. A

number of estimations of country rock strain have been made, the methods used are detailed at the relevant point in the text.



a) The strain ellipsoid

b) A log-Flinn plot with representative sketches of the possible fabrics types

Figure 1.7

1.5.1 Strain markers - microgranitoid enclaves

This method of strain analysis requires the analysis of mean shapes of populations of microgranitoid enclaves (Vernon 1984, 1990), which are commonly referred to as mafic xenoliths, mafic enclaves or autoliths in the literature, and generally consist of microdiorite, microgranodiorite or microtonalite. Vernon (1984) reviewed much of the literature concerning microgranitoid enclaves and concluded that the existence of the enclaves is best explained by the mingling and quenching of globules of more mafic magma in the host granitoid magma. Some mixing may take place in certain circumstances, but mingling is characteristic of the blob-like appearance and microstructure of the enclaves. The variation of mean shapes in such a population as an estimate of internal strain variation within a pluton has been well documented (Holder 1979, Hutton 1982, Courrioux 1987, Hutton 1988, Molyneux & Hutton *in press*, this work). For the purpose of the strain analysis the enclaves are assumed to have:

1. **A negligible viscosity contrast with respect to their host** - A correct assumption providing that the solidus temperature of the enclave is not greatly in excess of that of the host. This statement has been questioned, most recently by Fowler & Paterson (1997), who suggested that enclaves are injected, instantly frozen and subsequently passive in all deformations. However Vernon (1983) cites microstructural evidence for magmatic fabrics of plagioclase within deformed enclaves and Vernon (1990) remarked that, though enclaves are quenched on injection, resulting in small crystal sizes,

crystallisation and magmatic-high temperature solid state fabrics occur within them. Hence, at the very least microgranitoid enclaves provide an underestimate of the resultant cumulative strain.

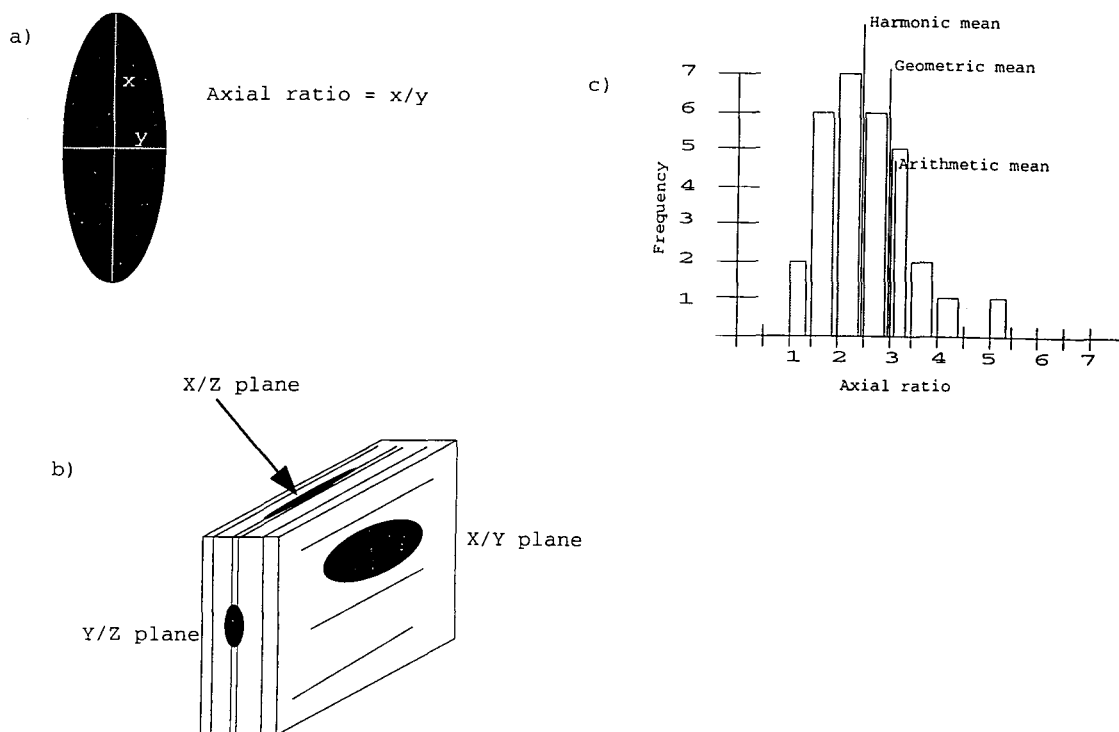
2. An originally subspherical shape - Population measurements from low strain granitoids demonstrate that enclaves are sub-spherical. In addition, Hutton (*unpublished data*) has shown that de-straining of populations of enclaves from a geographically diverse set of plutons show an initially small axial ratio. Furthermore, computer modelling of enclave populations (this work) shows that enclaves can be reliable strain markers.

In order to fulfil these criteria only enclaves which are ellipsoidal, orientated within the foliation plane, preserve a smooth outer contact and have no internal magmatic stratigraphy are used. All other enclaves are identified and subsequently isolated from the strain analysis

Method of strain calculation

A quantitative estimate of the three principal axial ratios of the finite strain ellipsoid can, in principle, be made by measuring the axial ratios (long axis length/short axis length, Figure 1.8a) of a statistically significant sample of mafic enclaves collected in any two planes of known orientation. In practice, it is simpler to measure the axial X, Y and Z lengths of enclaves in the field on exposed principal strain planes where the XY plane is the plane of foliation, the XZ plane is the plane perpendicular to this, containing the lineation (if developed) or the largest axial ratio and the YZ plane is the remaining plane in an orthogonal set (Figure 1.8b). Generally, these correspond to the 3 most commonly exposed outcrop planes.

On each of the exposed surfaces as many enclaves as possible have their axial ratios measured (commonly approximately 30 enclaves, from each of the XZ and YZ planes with rare measurements from the less commonly exposed XY plane). These data are processed to determine using the methods originally set out by Hutton (1982a); i) the true mean of the sample, using the geometric mean (Lisle 1977); ii) the K-value (Flinn 1962); and iii) the deviation and spread of the sample, in order to show the variation of strain estimates (Figure 1.8c). Then the data are plotted on a map of the pluton to estimate the spatial distribution of strain. Techniques may then be applied in an attempt to de-strain the pluton (see later).



a) axial ratio; b) the principal planes of measurement; c) Population spread.

Figure 1.8 Mafic enclaves their measurement and processing

1.5.2 Fabric strain - Fry (1979) method

When applied to deformed magmatic rocks the Fry (1979) method of strain analysis enables a determination of the strain recorded in the fabric to be made, (Figure 1.9) through the auto-correlation of inter-crystal spacing of rigid markers (Ramsay & Huber 1983, Burg & Wilson 1988). This independent method is easily applied and has been used to check that the mafic enclave strain estimates are accurate and reliable.

An assumption is made that the strain markers (magmatic crystal phases for the purpose of granitoid analysis) are initially randomly distributed and do not change their shape significantly during deformation. These assumptions could be invalid if:

- 1. Ascent strain was preserved in the magma fabric** - Field observations suggest that a granite magma fabric is formed when crystal concentrations are high i.e. approaching the RCMP, and hence would not preserve ascent strain.
- 2. Crystallisation occurs during deformation** - It is likely that some crystallisation particularly of late phases e.g. quartz and K-feldspar, would take place during the deformation of a fabric, but it is unlikely that large numbers of entirely new crystals would form or that crystal shape would change significantly during the deformation. However some loss of accuracy is inevitable.

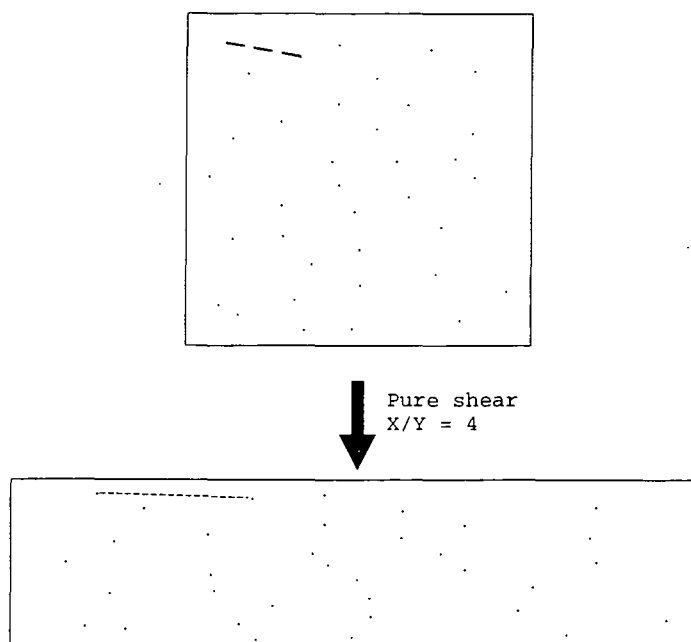


Figure 1.9 Rigid markers before and after an homogenous deformation

Method of strain calculation

In this work the modified grain size normalised Fry (1979) method of Erslev (1988) is used, as implemented in the FRYSTRAIN program developed by DePaor, because it allows the sample to be normalised to allow for non-circular and variably sized grains. Firstly, tracings of a population of individual crystal shapes and distributions are taken e.g. feldspar, biotite, from the principle strain planes (generally XZ and YZ) (Figure 1.10a). These are digitised and approximated to a set of orientated ellipses (Figure 1.10b). This distribution is processed by a grain size normalising algorithm to produce the modified Fry fabric strain ellipse (Figure 1.10c). The value of this 'Fry strain' is recorded, together with its orientation relative to the foliation, and a qualitative estimate of the reliability/reproducibility of the ellipse. The process is then repeated for other crystal phases from the same locality.

Using this method produces a number of 'Fry strain' determinations for each outcrop. These data are then analysed to ascertain a consistent and average result (unreliable or inconsistent data is discarded). The resultant value for a particular locality can then be plotted spatially on the map of the pluton to identify any changes in fabric strain associated with position in the pluton.

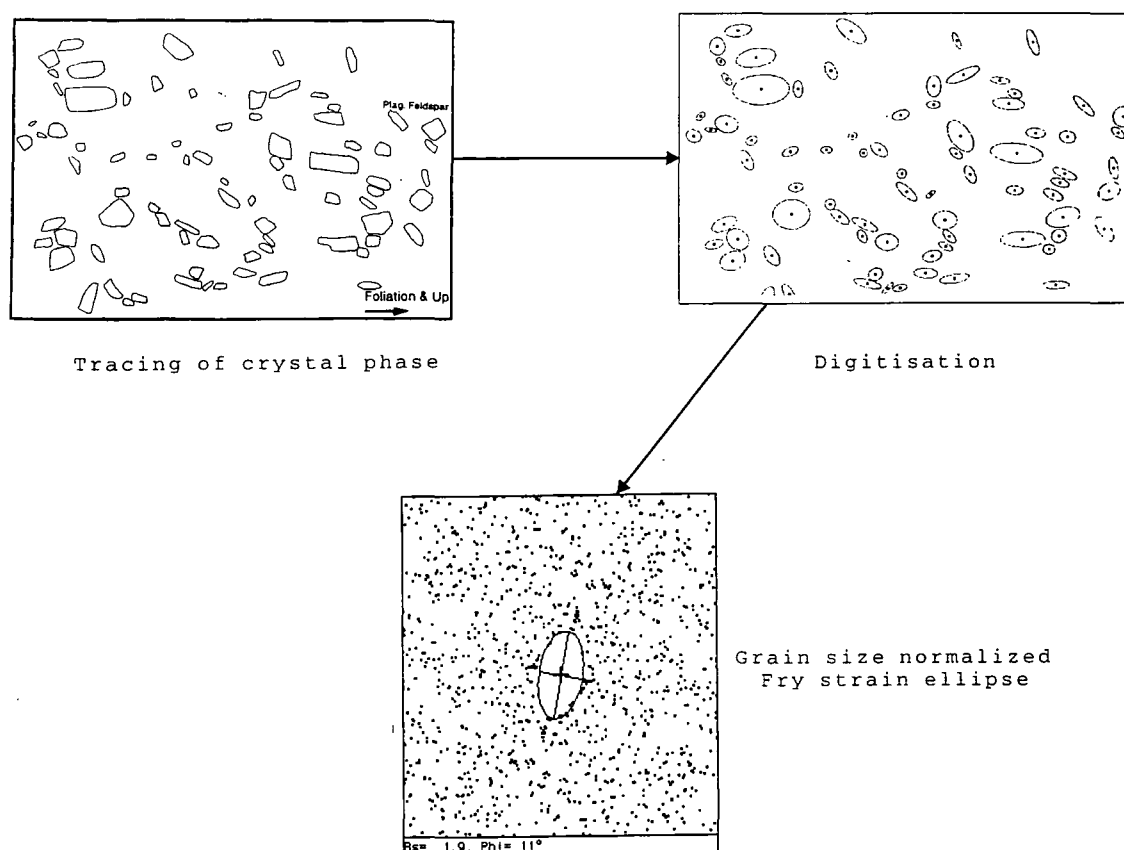


Figure 1.10 The method of Fry analysis for non-circular grains.

1.5.3 Solid state strain indicators

Solid state strain is very difficult to estimate, because generally it is accommodated inhomogeneously by the internal and boundary deformation of individual crystal phases e.g. recrystallisation, grain boundary slip. As a result only qualitative estimates can be made of the intensity of the strain i.e. intense vs weak and of the temperature of deformation using the criteria of Passchier & Trouw (1996). Any strain recorded by strain markers, such as mafic enclaves, which have been heavily overprinted by solid state deformation, are likely to very significantly underestimate the magnitude of the imposed strain.

1.6 Magma ascent and pluton emplacement mechanisms

The emplacement of granite magma and methods for its ascent have been the subject of widespread debate through the history of the science. Simplistically, plutons are referred to as either 'forceful', where granitic magma deforms the surrounding country rocks thus making space for itself, e.g. in the ascent of granite diapirs, England (1988, 1990) Courrioux (1987); or as 'passive', where space is created for the pluton without pushing aside the surrounding wallrocks e.g. stoping, Paterson & Fowler (1996). In detail the problem is more complex requiring an appreciation of the processes of ascent, emplacement and their interaction with regional tectonics.

1.6.1 Magma ascent

Diapirism

The term diapir was introduced by Mrazec in 1927 (Petford 1996) and comes from the Greek verb διαπερῶ "to pierce". It has also been defined as, 'an intrusion which domes the overlying cover after piercing lower layers, which may develop a narrow neck at depth' Whitten & Brooks (1972). It was first introduced to the study of intrusive igneous rocks by Nicolesco (1929) and Wegmann (1930) who made the analogy between circular granitoid intrusives and the circular outcrops produced by salt diapirs, visualising the production of granite material at depth and subsequent ascent driven by 'tectonic squeezing' (Wegmann 1930). The criteria for recognising a diapiric body based on its structure have been defined by Coward (1981), Bateman (1984) and England (1988, 1990):

1. Less dense material should occupy circular to oval shaped complexes enclosed by denser material.
2. Structures such as foliation, cleavage and lineations should be developed parallel to the surface of the less dense material and should be parallel to any foliation developed within the less dense material. The foliation should intensify toward the contact between the dense and less dense material
3. Strain distributions should involve sub-horizontal extension in the crestal region of the less dense material. The long axis of the strain ellipsoid should be tangential to the crestal region. In the trunk of diapirs (by analogy to salt diapirs) the long axes of the strain ellipsoid should be vertical.

These criteria have been observed in the field, notably by England (1988, 1990) and Courrioux (1987), who describe an upper crustal diapir, the North Arran Granite and the obliquely intruding diapir, the Criffel pluton. In addition, diapiric ascent has been cited as a method of ascent, by analogy to the many elegant analogue and finite element models that have been produced for sub-circular plutons (Pitcher 1979, Bateman 1984). Some of the first modelling was carried out by Ramberg (1967, 1970) who used rigorously scaled experiments to model diapiric ascent, showing initial doming of the source region,

through to ascent as a mushroom shaped body with a thin stalk extending down to the source region. More recent experiments (Cruden 1988, 1990) and finite element modelling (Schmeling *et al* 1988) demonstrated overturn within the magma itself and the possible outcrop features that might be produced by ascent of a diapir i.e. weak crestal flattening strains, strong vertical prolate centre strains and centre-margin consistency in zonation (Figure 1.11). An important flaw in these models is the absence of thermal constraints. Marsh (1982) assessed the effect of these factors during the ascent of a magma bleb in an isoviscous material, using a numerical Hot Stokes model (the buoyancy driven ascent of a particle through a viscous medium with heat transfer and thermal softening of the surrounding country rock, see part 8.4). He demonstrated that the lithosphere is too cold to allow ascent of a Hot Stokes diapir to upper crustal levels and that such ascent is only viable in the hot and highly ductile lower crust.

These models assume Newtonian flow in the crust, but it is well known that rocks probably do not generally behave in this way. Indeed Weinberg & Podladchikov (1994, 1995) demonstrated that if the rheology of the crust is considered as non-Newtonian and power-law based with the viscosity of the country rock reduces with increased strain, a granite diapir could rise from the lower crust to within 15km of the surface. However, power-law diapirs are unlikely to reach high crustal levels (<10km). It is important to note that the results of these models are based on the parameters used in the power-law equations (Equation 1.6) and higher crustal levels may be attained if the physical parameters required at different crustal levels, could be better constrained.

In conclusion, there are some convincing analogue and finite element models for granite diapirism, but field evidence is often weak, e.g. there are no field examples of diapir trails/tails, with their supposedly large constrictional strains, or ascent is constrained to a few kilometres of the ascent path (England 1988, 1990). Diapirism could be a common process associated with magma transport in the lower crust (Marsh 1982). These and associated criteria are discussed further in Chapter 2.

Sheeting/dyking

An alternative approach to diapiric ascent is to have piecemeal magma ascent as sheets (dykes), with agglomeration into plutons at a high crustal level. This model was first proposed as a method for granitoid magma ascent by Leake (1978) and Pitcher (1979). Subsequently a number of authors cited field evidence to support this mechanism e.g. Hutton (1982), Bateman (1985), Ingram & Hutton (1992), this work.

The work of Clemens & Mawer (1992) and Petford *et al* (1993) describe this process theoretically, though in slightly different tectonic environments (one fracture controlled, the second fault controlled). Petford (1996) reviews their most important results, in particular the extreme rapidity of dyke magma ascent compared with diapiric rise. Clemens & Mawer (1992), suggested 10^{-2} m/s for dyke ascent velocity compared with 10^{-10}

to 10^{-7} m/s for diapiric ascent velocity. This allows large plutons to^{be} filled in short periods of time e.g. a 5000 km^3 pluton could be filled through a single 5m wide dyke (10km long), with a density difference of 300 kg/m^3 to the country rocks, in only 6 yrs, if the magma viscosity was 10^4 Pa s , or 6000 yrs if the magma viscosity was 10^8 Pa s .

There are some problems with this method for ascent, in particular Rubin (1993,1995) argues that most magma sheets ascending through dykes, where driven by magma pressure in the source (due to volume increase during melting, Clemens & Mawer 1992), would freeze shortly after ejection from the source region. Petford (1996) argues that this is a valid criticism in upper crustal plutons, where fracturing is associated with ejection of aplitic and pegmatitic melts, but does not adequately describe deformation in the hot, weak, 'mushy' lower crust (Bergantz 1989, Petford 1995). In addition the analysis of Petford *et al* (1993) assumes a smooth walled open conduit to achieve the high ascent velocities. Petford (*pers comm*) accepts this point and has demonstrated that the introduction of asperities and anisotropies in the conduit reduces the upward magma velocity.

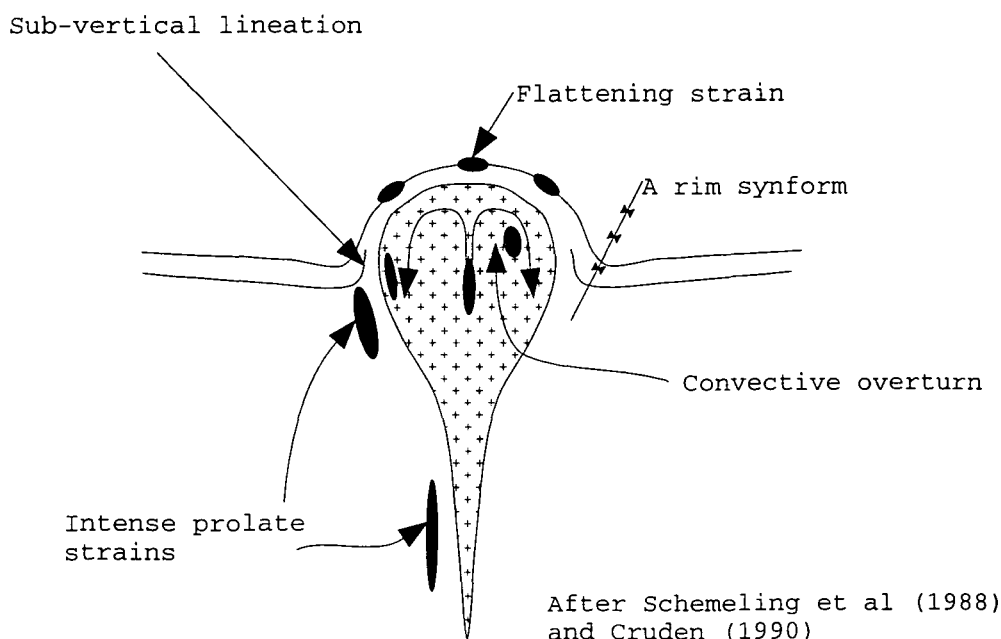


Figure 1.11 Structures associated with diapiric uprise through the crust

1.6.2 Magma emplacement

The emplacement mechanism represents the process by which space is made for magma after, or as a consequence i.e. diapirs, of its ascent. Paterson & Fowler (1993) suggest four processes that could make space in the crust; i) lowering the MOHO; ii) displacement of the Earth's surface; ii) volume loss; and iv) elastic contraction; and that any other processes taking place are 'material-transfer processes', because they move

material within the crust, rather than change the volume of the crust itself. In addition, Paterson & Fowler (1993) divide these 'material-transfer processes' into near-field processes, in the structural aureole of the pluton and far-field processes, operating outside the structural aureole.

Solving the problem of 'space creation' for a pluton in the field is not simple and only by making appropriate assumptions from the two-dimensional outcrop can the best solutions be produced.

Forceful emplacement- in-situ expansion

If the wallrock surrounding the pluton has been at all deformed as a result of the intrusion of the magma itself it can be viewed as a forcefully emplaced pluton. This deformation may have occurred as a result of diapiric ascent or through a component of in-situ expansion. In-situ expansion, or ballooning, assumes that in effect the pluton created its own space. A true balloon should show flattening concentrically increasing $K=0$ strains everywhere. Ramsay (1975 1989) and Holder (1979) first developed this ballooning model to explain the strain patterns observed within and without the Chindamora (Zimbabwe) and Ardara (NW Ireland) plutons. Subsequently, this model has been applied to other plutons where expansion is only a minor component of the space creation mechanism e.g. England (1988, 1992).

The exact processes at work during in-situ expansion are poorly constrained, but can be generally viewed in terms of the ascent of pressurised magma, until a tectonically or rheologically favourable level is reached. The magma then expands, deforming the wallrocks, in a distributed or local manner depending upon the prevailing tectonics and rheology. Indeed it is not necessary that a ballooning pluton be spherical, tectonic anisotropies could produce ballooned plutons with almost any shape.

Forceful emplacement - diapiric ascent

Ascent of a diapir, causes intense deformation within the pluton and surrounding wallrocks. It can be distinguished from an in-situ expanding pluton because it should show all of the following criteria (Molyneux & Hutton *in press*); i) sub-vertical stretching lineations in the wallrocks; ii) pluton-up kinematics everywhere; iii) phases which are petrographically identical between the core and the margins, due to circulation; iv) vertical prolate strains in the centre of the pluton; and v) a crestal zone of weak flattening strains.

In addition the ascent of multiple (nested) diapirs is often cited as a viable method for pluton emplacement (Marsh 1982, Paterson & Vernon 1995), these should show all of the following features; i) a complex strain pattern within each plutonic phase; ii) zones of intense deformation and sub-vertical stretching lineations at the inner and outer edge of each magma phase; and iii) multiple event pluton-up kinematics everywhere.

Magma emplacement can also occur passively with little or no interaction with the surrounding wallrocks.

Passive emplacement - external space creation

If a pluton preserves no internal emplacement fabric i.e. magmatic foliation and the wallrocks appear to have been entirely passive and undeformed during emplacement, then other processes external to the granite itself must have been responsible for space creation. However empty 'space' cannot exist within the crust, the rate of space creation must be less than or equal to the rate of magma supply (Paterson & Fowler 1993) and hence the intruded magma must act as a tectonic filler exploiting tectonic low stress zones. There are a number of ways in which such space might be created:

1. **Lifting the roof / dropping the floor** - Using a reflection seismic profile Evans *et al* (1993) demonstrate that a large pluton, unfoliated in outcrop, from the English Lake District batholith is in fact composed of a large number of thin laccolith-like sheets, which have been emplaced by multiple episodes of minor roof uplift or floor subsidence. Similarly Roman-Berdiel *et al* (*in press*) have shown by analogue modelling that large laccolithic plutons can be emplaced passively in upper crustal settings by lifting the roof off the pluton.
2. **Tectonic opening** - If a pluton is emplaced into a regionally extensional setting stress heterogeneity within this zone, will result in zones of lower stress. Magma from depth will be preferentially injected into these zones, due to the principle of effective stress (Hutton 1997a, b).
3. **Stoping / incorporation of material** - When hot magma comes into contact with cold wallrocks, expansion can result in local deviatoric brittle fracture stresses and the stoping of blocks away from the wallrocks (Marsh 1982). This provides a possible method of magma ascent and emplacement, through continued stoping of blocks from the roof which fall through the magma, and a method of space creation, through roof stoping and incorporation or settling of the blocks. Here lies a major problem with this method, Marsh (1982) examined the thermal effects of block stoping and incorporation and observed that; i) magma would soon choke on the volume of unsorted and poorly packed stoped blocks required for significant ascent or emplacement; and ii) large scale anatexis and incorporation of cold country rocks would quickly result in freezing and thermal death of the pluton. Despite this a number of authors document this process as a significant 'material transfer process' e.g. Vernon & Paterson (1993), Paterson & Vernon (1995), Paterson *et al* (1996). It is perhaps more feasible that stoping is a minor process associated with local space creation.

Passive versus forceful emplacement

In reality these two processes of emplacement, where pluton 'space' is either created entirely passively, by tectonics or other methods, or forcefully, by magma promoting deformation, describe end-members within a continuum. Indeed it is more than likely that plutons with a combination of passive and forceful features will be observed. A comprehensive field study of a granitoid pluton should be able to distinguish the relative importance of the two processes.

1.6.3 Tectonic setting

The importance of local tectonics in the emplacement of granite plutons was first recognised by Pitcher & Read (1970) and Pitcher & Berger (1972). From their examination of the Donegal batholith they demonstrated the broadly coeval nature of deformation in the country rocks and the emplacement of the plutons. Only the detailed structural investigations of Hutton (1977, 1982b) in the same area enabled the determination that emplacement and deformation were more or less synchronous. More recently numerous studies have demonstrated the relationship of plutons to local tectonics (faults and shear zones) e.g. Hutton 1988, Hutton *et al* 1990, McCaffrey 1989 and others. A syn-tectonic pluton which may be recognised by the occurrence of some or all of the following criteria defined by Ingram (1992) and Ingram & Hutton (1994):

1. An elongate shape whose long axis coincides with the local zones of deformation, faults and shear zones.
2. Magmatic and solid state fabrics which are sub-parallel and continuous with those in the shear zones.
3. Magmatic fabrics that are interpreted to be synchronous and consistent with fabrics in the wallrocks
4. The syn-kinematic growth of metamorphic minerals in the wall rocks.
5. The presence of structures related to deformation close to the RCMP.
6. Small scale structures developed at similar times to emplacement e.g. melt-filled shears.

Specific structures may also be preserved in each of the three end-member tectonic environments in which plutons can be emplaced:

Reverse contractional shear

In a convergent setting no 'space' is being created for the magma and hence the magma must reduce the total (tectonic) stress sufficiently to facilitate emplacement (Equation 1.12, Hutton 1997a, b).

Equation 1.8, $\sigma' = \sigma - u$

where σ' is the effective principal stress, σ the total principal stress and u , the fluid pressure.

The pluton should preserve some or all of the following features (modified from Ingram & Hutton 1994):

1. A large number of individual granite sheets, which may or may not be compositionally heterogeneous.
2. Magmatic state and solid state fabrics, with identical shear sense and lineation orientation across the pluton and in the wall rocks.
3. Continuous gradation between magmatic and solid state fabrics.
4. $K \approx 1$ recorded strains, as a result of the tectonically based nature of the strain.

Extensional shear

In an extensional environment granite magma is emplaced at a similar rate to the rate of 'space' creation and should result in plutons with some or all of the following features:

1. Homogeneity in outcrop, and a gradational or cryptic variation in composition across the pluton.
2. Weak magmatic foliation which may be sub-parallel to the regional structural grain, and cross-cut by later overprinting solid-state deformations. The importance of internal "cavity filling" mechanisms may create local variations in emplacement style and hence shear sense indicators and lineations need not have a similar sense or orientation.
3. Generally low magnitude emplacement related strains.

Transcurrent shear

Within this environment the magma must emplace itself along a zone which is deforming during non-coaxial strike-slip shear. With local deflection of such a zone pull aparts (local extension) and positive flower structures (local convergence) will form, thus resulting in plutons displaying both *extensional shear fabrics* and *contractional shear fabrics*. The contemporaneity of such plutons distinguishes them from other tectonic environments.

1.6.4 Siting mechanisms

The processes associated with the siting of granitic plutons are poorly constrained, though it is widely accepted that siting is probably controlled by processes at work in the lower crust. Pitcher (1979) suggested that the siting of plutons along the Andean batholith was controlled by deep crustal lineaments which may not have an expression in the overlying cover. Additionally, Hutton and Reavy (1992) showed that deep crustal shear zones, deforming the lower crust in a ductile manner, could provide a method for focusing magma. More recent work by Jacques & Reavy (1994) on the Scottish Caledonides

suggests that pluton siting is controlled by transcurrent shear zones intersecting with deep crustal lineamental structures in the lower crust to produce 'mega augen' which rotate during deformation focusing magma into the interstices. A similar model has been suggested by Hutton & Alsop (1996) for the siting of magmatism in the Donegal Caledonide batholith. Unfortunately this model though elegant, at present lacks field evidence of such structures from lower crustal terrains. Indeed, Schmidt *et al* (1995) suggest that the geometrical relationship of plutons with shear zones and lineaments is a statistical artefact and pluton siting and ascent are controlled by other processes.

1.7 Orogenic evolution

Defined simply (Press & Siever 1986), orogeny is mountain building by folding and thrusting processes during plate collision. Granite have long been known to be associated with such zones, but what is still poorly understood is the structural role that granites play in the evolution of the orogenic process e.g. why they are emplaced, often in batches, consanguineous with particular tectonic events. The section below illustrates some of the more general issues related to this topic that will be investigated in greater detail later in this work.

1.7.1 The Wilson cycle

With the advent of plate tectonic theory and its general application to oceanic and continental deformation, a cycle (The Wilson cycle) was observed in ancient mountain belts from; i) The rifting of a continent; ii) The opening of an ocean basin by sea-floor spreading; iii) its closing; iv) a continent-continent collision; and v) the formation on an intra-continental mountain belt (see Wilson 1970 for a review). Indeed the whole geological history of the Earth can be viewed as a succession of superimposed Wilson cycles. Granitoid magma has been described as emplacing at every point within this cycle.

1.7.2 Transpression and transtension

Harland (1971) defined transpression as the oblique collision of continental plates and transtension as oblique extension, from observations of Caledonide collision in Spitzbergen. Transpression was later defined more rigorously (Sanderson & Marchini 1984) as being characterised by a combination of a pure shear and strike-slip deformation coincident, or partitioned (temporally and/or spatially), during oblique convergence (Figure 1.12). Subsequent application of these models to zones of orogenesis has shown that orogenic collision rarely occurs along zones at right angles to the convergence vector and transpressional deformation is common. Transtension is the extensional equivalent of transpression and occurs in zones where local or regional oblique extension is taking place.

1.7.3 Extensional collapse

During plate convergence orogenic zones of increased topography are formed due to the rapid rate at which orogenesis occurs, this increased topography is in stress equilibrium as a result of convergence, but only partially compensated isostatically. If this convergence stops or the convergence vector changes in orientation, the orogenic zone enters disequilibrium and will regain equilibrium as rapidly as possible (Dewey 1988). As a result the principal stress is re-orientated; in the case of excess topography it will be vertical with the least principal stress orientated horizontally perpendicular to the grain of the orogenic zone (Figure 1.13). Extension then takes place until the topography is in

equilibrium with its isostatic root or equilibrium is achieved with the regional applied stresses, 'extensional collapse'.

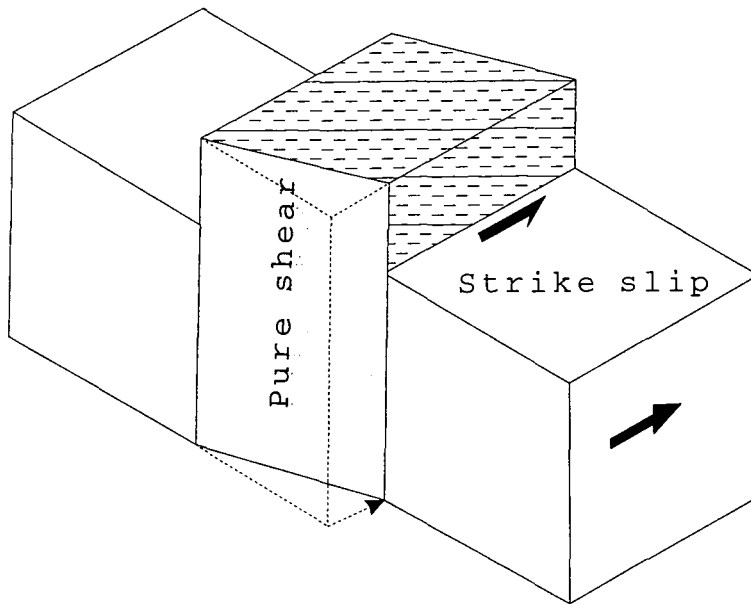
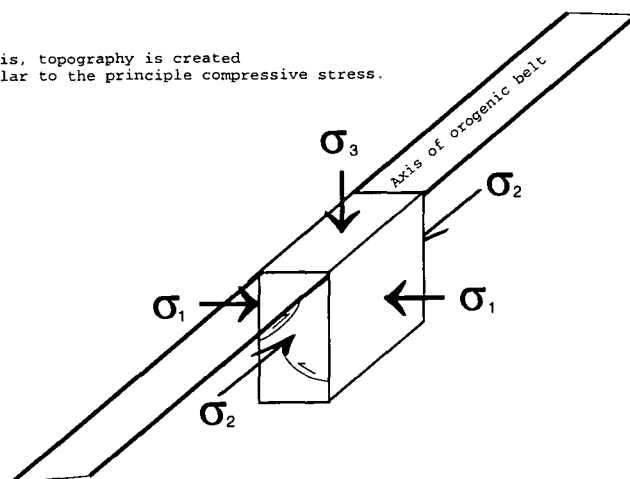
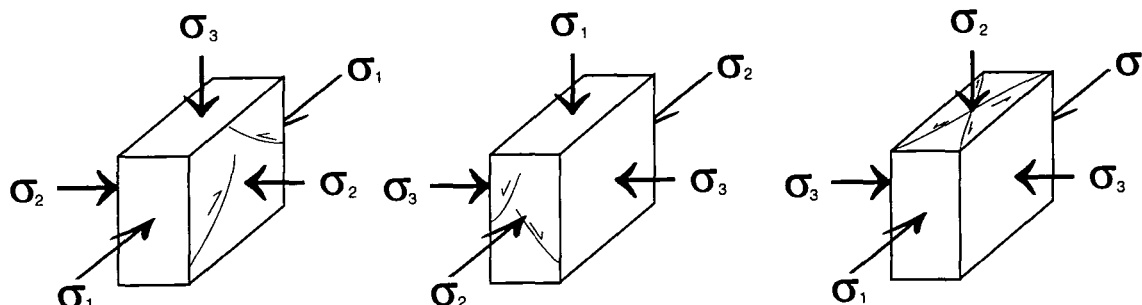


Figure 1.12 Transpressional deformation after Sanderson & Marchini (1984)

During orogenesis, topography is created
sub-perpendicular to the principle compressive stress.



But if the collision process is disturbed
the principal stresses can re-orientate,



Crustal thickening could continue,
with a different orientation

Or extension could take place along,
to perpendicular to the orogenic axis

Figure 1.13 Extensional collapse, principal stress re-orientation associated with orogenic convergence

1.8 Regional Introductions

This thesis describes pluton emplacement from two geographically diverse areas, whose last deformation event occurred during the Caledonian orogeny in Laurentia and Brasiliano-Pan African orogenies in Gondwana.

1.8.1 The Donegal Batholith, NW Ireland

The Donegal batholith is in the north-western corner of the island of Ireland. Geologically it is part of the northeast-southwest trending Caledonian orogeny, which affected eastern North America, the British Isles and Scandinavia during Cambrian to Devonian times. In Donegal the rocks can be divided into two types:

Meta-sedimentary rocks

This sequence is part of the Neoproterozoic Dalradian sequence, which can be correlated across the whole of Donegal and the Southern Highlands of Scotland. It is related to continental shelf sedimentation, associated with approximately coeval tholeiitic magmatism along a continental margin, subsequently deformed during polyphase metamorphism and tectonics to regional greenschist, locally amphibolite, facies along northeast-southwest to east-west trending regional structures (see Pitcher & Berger 1972 and Hutton & Alsop 1996, for references).

Magmatic rocks

In the latter stages of the orogenic episode large volumes of primarily granitic magma, but also of basic (appinitic) magma were emplaced by a variety of mechanisms, spatially associated with the regional structures (see Pitcher & Berger 1972, and Price 1997 for references). The Ardara pluton is one of the earliest plutons of this batholith and the subject of investigation in this work.

1.8.2 The Rio Paraiba do Sul shear belt, SE Brazil

The Rio Paraiba do Sul shear belt is in the southeast of Brazil between the cities of Campinas, Rio de Janeiro and Sao Paulo. Geologically it is part of the Ribeira belt, the Brazilian expression of the Brasiliano-Pan African orogeny (Late Proterozoic to Early Ordovician), which deformed western and southern Africa and South America during the formation of Gondwana. It consists of:

Metamorphic rocks

These are pre-Brasiliano (Archaen-Early Proterozoic) sedimentary and volcano-plutonic sequences which have been metamorphosed to greenschist to granulite grade and undergone intense polyphase deformation during thrusting and strike-slip associated with transpressional east-west directed collision along a northeast-southwest trending structural grain (see Ebert *et al* 1996 for references).

Magmatic rocks

Plutonic rocks emplaced during this and earlier orogenies are exposed throughout the area. Of particular interest are large volumes of granite emplaced, towards the end of the Brasiliano event and spatially related to high angle strike-slip shear zones. These plutons that are the subject of this work.

SECTION 2

Emplacement of an in-situ expanding pluton.

“....for perfect demonstrations in every aspect of structural and plutonic geology this small area (of Donegal) is without equal.” - Iyengar et al (1954)

Chapter 2

The Ardara pluton, Co Donegal, NW Ireland.

2.1 Introduction

2.1.1 Preamble

This small pluton, part of the Caledonian Donegal Batholith of NW Ireland (Figure 2.1, 2.8), has been the object of a large number of investigations which have attempted to elucidate the mechanisms at work during its ascent and emplacement. As a consequence the Ardara pluton and its aureole have attained a great importance in granitoid pluton studies. The pluton itself (Table 2.1) is approximately 55km² in area, sub-circular, 8km in diameter, with a strikingly concordant thermal aureole and a prominent ‘tail’ on the east side (Map 1, Figure 2.1, 2.4) (Akaad 1956a, b, Iyengar *et al* 1954 Meneilly 1981, 1982). It is a normally zoned 3-phase pluton (Akaad, 1956a), which has been dated at 390-405Ma using Rb-Sr whole rock methods (Halliday 1980) and at 451Ma using U-Pb zircon techniques (Vernon & Paterson 1993). It is worthy of note that if this second date is correct it would make the Ardara pluton uniquely ancient among British and Irish Caledonian plutons. The pluton has been characterised isotopically by Dempsey *et al* (1990) who showed the Ardara granite has high ϵ_{Nd} ratios and low initial $^{87}Sr/^{86}Sr$. These data are consistent with magma derivation from either a mantle or very young crustal source. Although Halliday (1980) pointed out the presence of inherited zircons in the Ardara granite suggesting a small degree of crustal contamination.

During this work the pluton has been re-mapped and analysed using strain markers, shear sense indicators and simple modelling, with the aim of presenting a comprehensive study and shedding new light on the emplacement process and likely ascent mechanisms.

2.1.2 The Caledonian orogeny and its imprint in Donegal

The Ardara pluton is emplaced into Neoproterozoic rocks of the Dalradian (Geike 1888, Pitcher & Berger 1972) supergroup, which were deformed and metamorphosed during the early Palaeozoic Caledonian orogeny. The Caledonian orogeny is a linear belt which can be traced from Svalbard, down through Scandinavia, the northern British Isles and across to the east of the North American continent. It is thought to have originated through the closure of the Iapetus ocean (Dewey 1969) during mid-Ordovician to early-Devonian times (Soper *et al* 1992) resulting in the collision of the Gondwanan, Laurentian and Baltica plates. Donegal is understood to have been at the southern margin of the largest of the

colliding landmasses Laurentia (which comprised North America, North Britain and Greenland).

The Caledonian rocks of Donegal (Figure 2.1) are delimited by 2 major structures, the Great Glen fault, offshore to the north, and the Fair Head - Clew Bay Line - 'Highland Boundary fault' (Hutton 1987), to the south. The terrane consists of polyphase deformed Dalradian sediments which are metamorphosed to regional mid-upper greenschist facies (Hutton 1982a, Meneilly 1982) and have a northeast-southwest strike, which swings around what may be an approximately north-south orientated lineamental structure (Hutton & Alsop 1996) situated underneath the Ardara pluton, to become east-west trending towards the western coast. Into these rocks (post-dating most of the regional deformation) a series of magmatic intrusive rocks (granite plutons and mafic sills and dykes), spatially related to the major regional structures were emplaced to form the Donegal batholith (Pitcher & Berger 1972).

Table 2.1 The Ardara pluton

ARDARA	Data	References
Size	8 km diameter ~55km ² area	Akaad (1956a)
Metamorphic environment	Regionally Upper Greenschist to low amphibolite facies. Pluton thermal aureole, andalusite to sillimanite grade pelitic metamorphism.	Akaad (1956a, b) Holder (1979) Meneilly (1982) Kerrick (1987)
Composition	G1, G2 & G3, Quartz diorite - granodiorite	Akaad (1956a) Holder (1979)
Age	Rb-Sr whole rock, 390-405 Ma U-Pb zircon, 451 Ma	Halliday (1980) Vernon & Paterson (1993)
Isotopic characteristics	Ardara, G ₂ , (⁸⁷ Sr/ ⁸⁶ Sr) _i = 0.7062, ε _{Nd} = -1.2	Dempsey <i>et al</i> (1990)

2.1.3 The Dalradian country rock

The country rocks surrounding the Ardara pluton are part of the Dalradian supergroup of meta-sediments, which extends from Donegal through the southern Highlands of Scotland. They were deposited during the Neoproterozoic as shelf sediments, along a subsiding and evolving Laurentian continental margin, during the opening of the Iapetus ocean (Soper *et al* 1992, Soper & England 1995 and references therein). The Donegal sequence is divided into three groups which are broadly similar to the divisions of the Scottish Dalradian (Figure 2.1, 2.2); *The Appin Group* (Creelough Succession), into which the Ardara pluton is emplaced; overlain by *The Argyll Group* (Kilmacrenan Succession); which is in turn overlain by *The Highland Group* (Lough Foyle Succession) (Pitcher & Berger 1972).

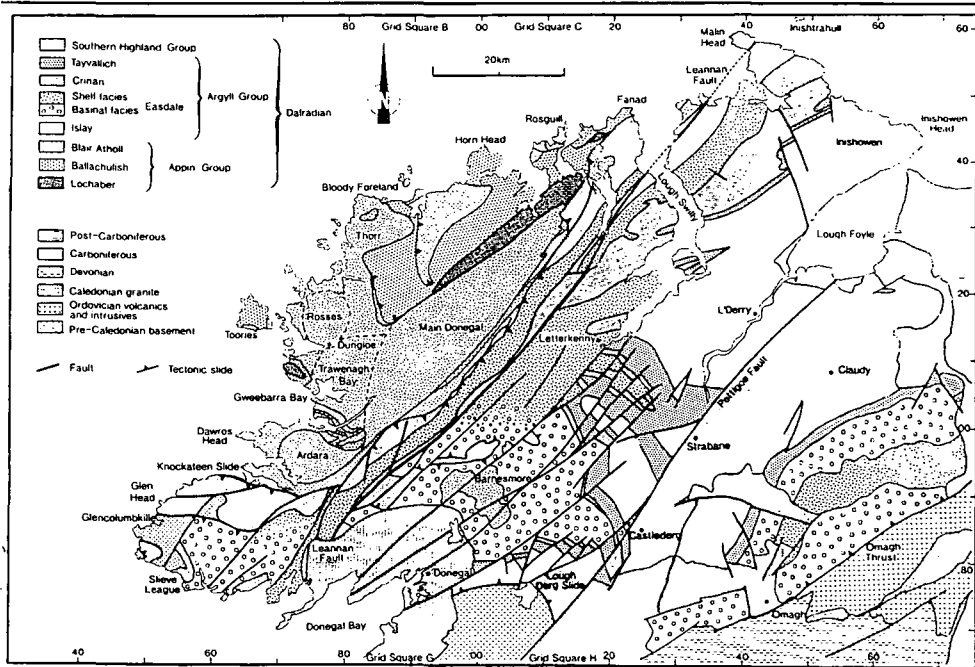


Figure 2.1 A geological map of NW Ireland, from Hutton & Alsop (1996)

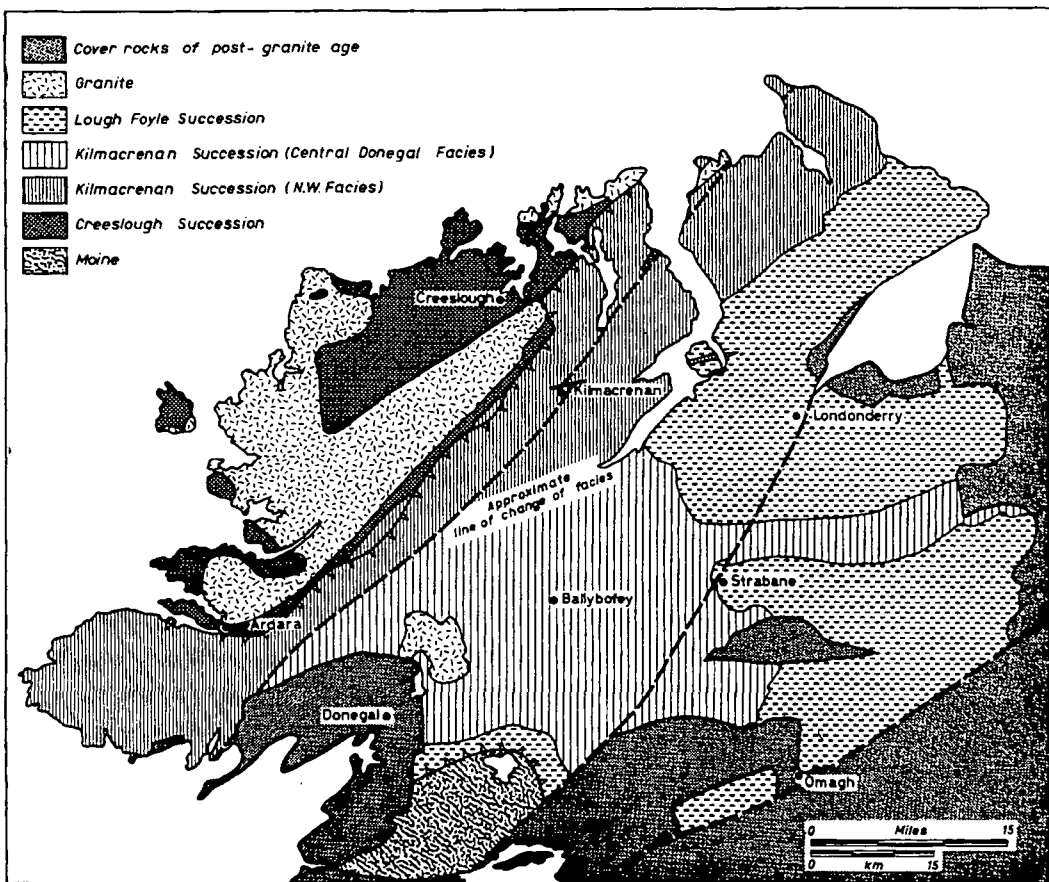


Figure 2.2 The main sedimentary units of NW Ireland from Pitcher & Berger (1972)

2.1.4 The country rocks surrounding the Ardara pluton

The following summary of the stratigraphy around the Ardara pluton (the Maas-Rosbeg sequence) draws heavily on the more detailed account in Pitcher & Berger (1972): A stratigraphic column for the sequence is shown in Figure 2.3. The base of the Maas-Rosbeg sequence is defined by rare outcrops of the Ards Quartzite (Cor quartzite). Above this quartzite there is a stratigraphically diverse unit, the Sessiagh-Clonmass formation (Mulnamin Siliceous and Mulnamin Calc Silicate units) consisting of calcareous lower units grading upwards into a thick sequence of deformed interbedded limestones, marls and shales. Further up sequence the Lower Falcarragh pelites (Maas Semi-Pelites) describe a thick homogenous purplish coloured semipelitic unit with rare calcareous horizons. This unit forms the majority of the wallrock of the Ardara pluton.

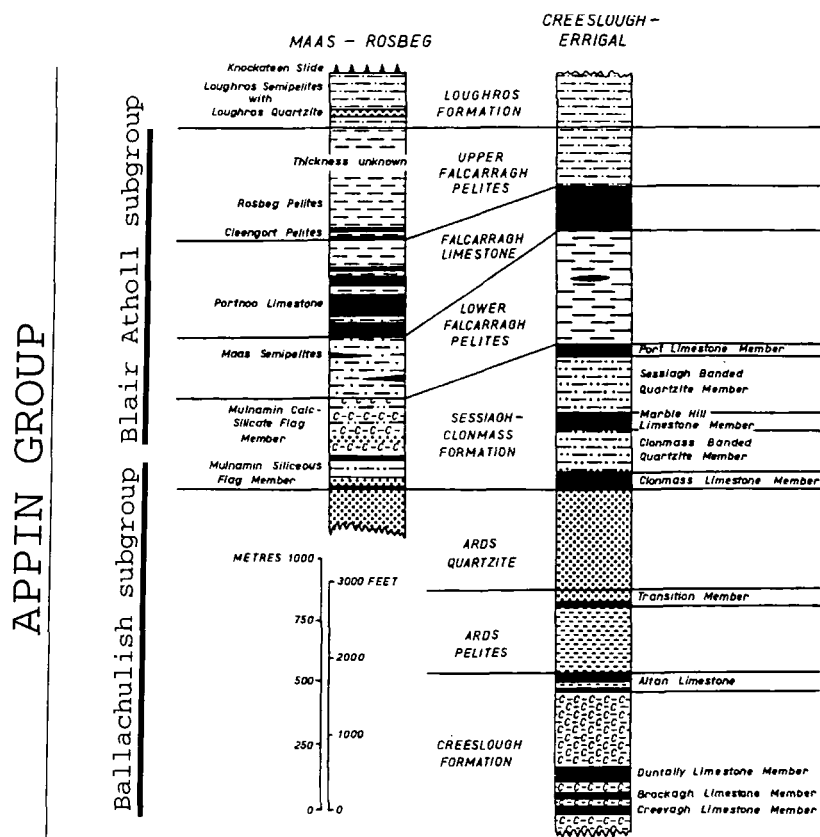


Figure 2.3 The Appin Group (Creelough succession) after Pitcher & Berger (1972), from the work of Akaad, Mithal, Iyengar and Cheesman

At the top of the Falcarragh pelites there is a sharp boundary, above which Falcarragh limestone (Portnoo limestone) is encountered. This is a massive grey deformed and metamorphosed marble, showing gradation into the overlying Upper Falcarragh Pelites (Cleengort, Clooney and Rosbeg pelites). These rocks are dark-grey massive pelites which pass upwards into limestones and semi-pelites with great variation in composition and thickness along strike. At the very top of the sequence are the rocks of the Loughros formation which, in the study area, are composed of semipelites and subordinate impure quartzites.

In subsequent descriptions the local names, as given in brackets above, will be used for consistency with earlier work of Akaad, Pitcher, Berger, Meneilly, Vernon, Paterson and others.

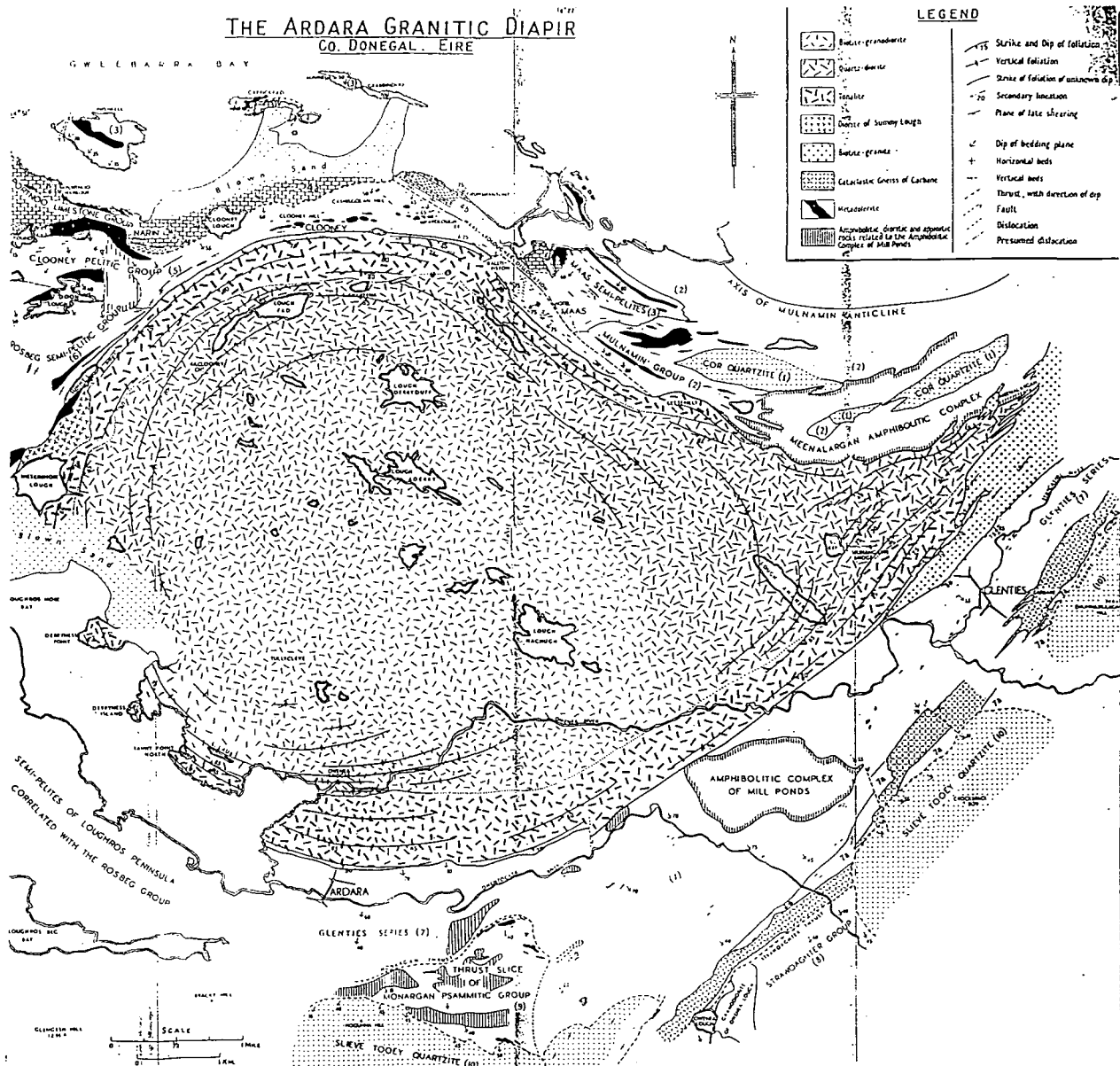


Figure 2.4 The distribution of sedimentary rocks around the Ardara pluton, from Akaad (1956a)

2.1.5 Structural evolution

Donegal has undergone a polyphase metamorphic history, with up to nine phases of deformation being recognised regionally (Pitcher & Berger 1972, Hutton 1977, 1982a, 1987, Hutton & Alsop 1995, Meneilly 1982, Price 1997 and others). Meneilly (1982) established the structural chronology in and around the Ardara pluton. In the following descriptions his nomenclature is used with necessary reference to the regional work of Hutton (1977, 1982a). The structural evolution was first described by Pitcher & Berger (1972), through compilation of the work of a number of earlier workers (Cheesman 1952, Gindy 1953, Mithal 1952, Akaad 1956a, b, Iyengar *et al* 1954). Later work by Meneilly (1981, 1982) comprehensively re-mapped the structures around the northern and western edges of the pluton to elucidate the following sequence (Table 2.1):

D₁ - The 'bedding schistosity' of Pitcher & Berger (1972). In the Ardara area it exists as a weak cleavage forming parallel to bedding (Meneilly 1981, 1982). Although Hutton & Alsop (1996) record the cross-cutting of bedding by S₁ in the Rosbeg area.

D₂ - Regionally this represents widespread long wavelength folding, F₂, the development of tectonic slides and the metamorphic peak (Hutton 1982b, 1987). In the study area S₂ generally dips southwards, moderately in the north but steeply in the south, with associated F₂ north verging folds. This local change in orientation is reflected in S₂ becoming progressively sub-parallel to bedding on travelling northwards (Meneilly 1982) from the southern contact of the pluton (Figure 2.5).

D₃ - Produces a variable relationship with D₂ across the area; in the south it dips *shallowly* southwards crenulating and folding the high angle S₂ and in the northern part of the area S₂ and S₃ are more or less coincident resulting in a composite S_{2/3} fabric (Figure 2.5) Meneilly (1982).

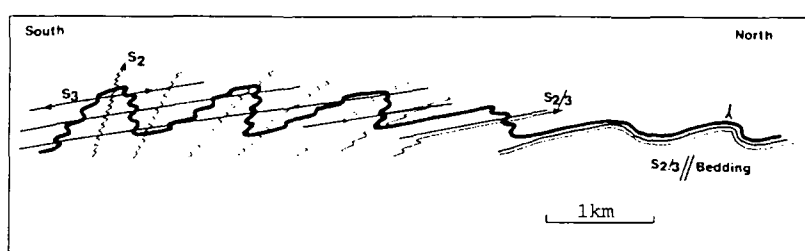


Figure 2.5 Schematic of S₂ and S₃ relationships across study area, from Meneilly (1982)

D₄ - A regional crenulation cleavage S₄ of variable strength, which intensifies on approaching the Ardara pluton margin, to become concordant and pervasive at 500m from the granite contact. Associated with this pervasive cleavage are minor steeply plunging F₄ folds (which verge west-northwestwards on the northeast side of the pluton). Additionally there are km-scale F₄ folds e.g. the Mulnamin anticline and Maas syncline, which become intensified as the contact is approached. Further away from the pluton, to the north of

Gweebarra Bay, S₄ cleavages and F₄ folds are minor weak structures with a north-south orientation (Meneilly 1982) (Figure 2.10)

D₅ - In the study area D₅ is developed as a steep crenulating cleavage with a very constant west-northwest to east-southeast trend. It formed post-Ardara emplacement and resulted in extensive deformation in the 'tail' of the pluton. Meneilly (1982) related this event to regional or local sinistral shearing associated with the emplacement of the Main Donegal Granite.

D₆₋₉ - Hutton (1977, 1982b, 1987) and Price (1997) have observed a number of subsequent events through their work in northern Donegal and the Main Donegal Granite. None of these structures have been conclusively identified in the vicinity of the Ardara pluton.

Table 2.2 Deformation chronology of the area adjoining the Ardara pluton.

Deformation event	Characteristics	Comments	References
D ₁	F ₁ folds ? S ₁ , sub parallel to bedding	Lower greenschist facies metamorphism	Pitcher & Berger (1972) Hutton (1977)
D ₂	Major folding, F ₂ , northwest facing with gently inclined southeast dipping axial planes and tectonic slides	Peak regional metamorphism, syn-late D ₂ , biotite-garnet grade, mid-upper greenschist facies.	Hutton (1977, 1987) Meneilly (1982) Hutton & Alsop (1995)
D ₃	Northwest facing F ₃ and S ₃ facing and dipping moderately to the southeast.	Obviously crenulating in outcrop and thin section	Meneilly (1982) Hutton (1977, 1987)
D ₄	North-south orientated folding with upright attitude and westerly vergence. Around the Ardara pluton it is east-west orientated to concordant with the pluton contact.	Syn-tectonic with the intrusion of Ardara pluton	Pitcher & Berger (1972) Meneilly (1982)
D ₅	Easterly verging, upright, weak intensity	Maybe syn-tectonic to the intrusion of Main Donegal Granite	Pitcher & Berger (1972) Meneilly (1982) Hutton (1977, 1982b)
D ₆	Pervasive shear zones	Maybe syn- to post-tectonic to the intrusion of the Main Donegal Granite	Hutton (1977, 1982b)

also see Price (1997) for an in-depth review

2.1.6 The granites of the Donegal batholith

The Donegal Batholith (Figure 2.6) consists of eight members emplaced between approximately 440Ma and 385Ma (Silurian-Devonian) with a mean age of around 400Ma (Halliday 1980, O'Connor *et al* 1982, 1984, 1987). Since the first geological map (Griffith 1839) showed the presence of metamorphosed sediments between V-shaped areas of granite (Pitcher & Berger 1972) the batholith has been a test-bed for many studies on the processes of granite emplacement and orogenic evolution, e.g. throughout the 1800's the batholith was used to debate whether granites, in general, had a metamorphic or plutonic origin (see McErlean 1993 for references).

Hull *et al* (1891) detailed observations which conclusively demonstrated the multi-stage magmatic-plutonic nature, of the batholith. The subsequent work by Cole (1902, 1905, 1906) made several additional observations, including suggesting emplacement for the Ardara pluton as, "...an igneous boss behaving as a laccolite on its margins". Only with the

establishment of H.H. Read's Imperial College Group during the 1950's and 1960's did the true nature of the batholith become clear as a result of extensive detailed small scale mapping studies of granites and country rocks across Donegal. Their main results are summarised in the seminal work on granite emplacement, '*The Geology of Donegal: A Study of Granite Emplacement and Unroofing*', by Pitcher & Berger (1972). In this book the authors summarised the granites, their country rocks, the regional stratigraphy, dominant regional structure, the state of current knowledge about the emplacement mechanisms of the plutons and their chronology (Figure 2.7).

More recently work has focused on detailed studies of individual plutons; with Hutton (1982b) working on the Main Donegal Granite; McErlean (1993) on the Thorr pluton; Price (1997) demonstrating the piecemeal assembly of the Main Donegal Granite. Others (Holder 1979, Hutton 1982, Vernon & Paterson 1993, Molyneux & Hutton (*in press*), *this work*) have attempted to explain the mechanisms at work in producing the remarkable structural concordance of country rocks and granite fabric observed in and around the Ardara pluton.

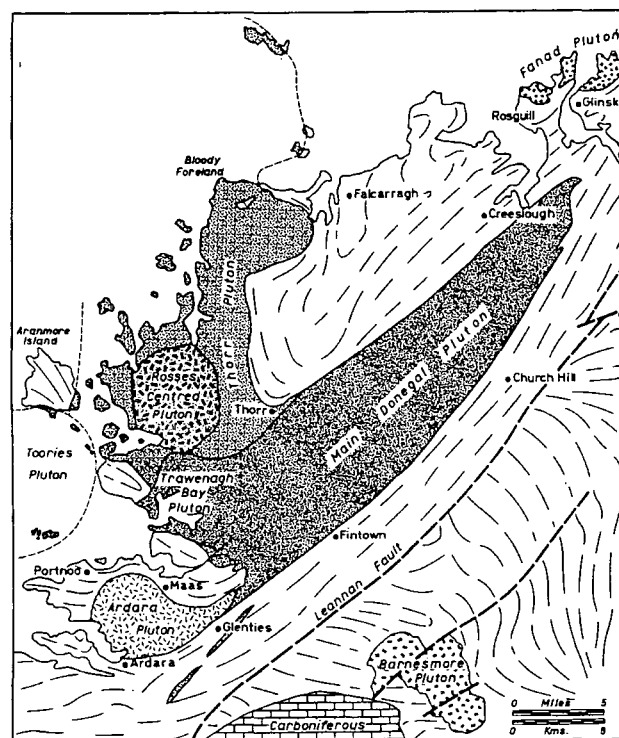


Figure 2.6

The Donegal Batholith after Pitcher & Berger (1972) and others

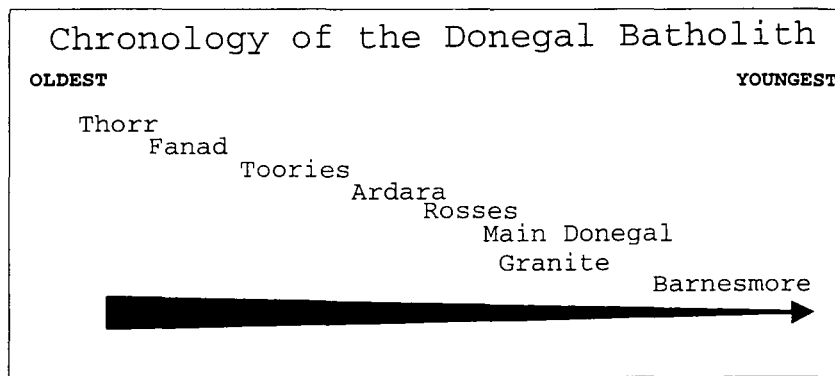


Figure 2.7 Chronology of the Donegal batholith from field relationships, after Pitcher & Berger (1972)

2.1.7 The Ardara pluton: previous work

The first mapping of the Ardara granite was carried out during the Survey mapping of Hull *et al* (1891), but the pluton was not examined in detail until the work of Cole (1902). He remarked upon the striking structural conformity between the foliation in the country rocks adjacent to the granite and the gneissic foliation within the pluton itself. He suggested forceful emplacement of the pluton through laccolithic up-doming of the surrounding schists.

The first comprehensive study of the pluton by Akaad (1956a, b) elucidated the following features:

1. **The concentric internal foliation structure** which is sub-parallel to the country rock foliation at the contact and diminishes in strength towards the pluton centre.
2. **The petrography** of a 3-phase normally zoned (increasing quartz content towards the centre) pluton; classifying, G1, a quartz diorite, G2, granodiorite and G3, the central granodiorite. These have relatively sharp contacts with each other, and contain a large number of microgranitoid enclaves.
3. **The thermal metamorphic aureole** which has an inner narrow sillimanite zone 100m wide followed by an outer andalusite zone, up to 500m wide, within strongly deformed greenschist facies, pelites and limestones.
4. **The deflection of the regional foliation** and bedding traces northwards around the pluton.
5. **Later deformation** along the southern contact, associated with an overprinting movement along a 'thrust plane'.

Iyengar *et al* (1954), working in the Meenalargan area, described the complexities resulting from the intrusion of the Ardara pluton and subsequent overprinting by the Main Donegal Granite. They ascribed the intensification of previously formed structures to be the result of, "...shouldering and pushing aside of the country rocks by a hot plastic body.". The work of Cheesman (1951) on the Loughros peninsula described the inflection of the regional

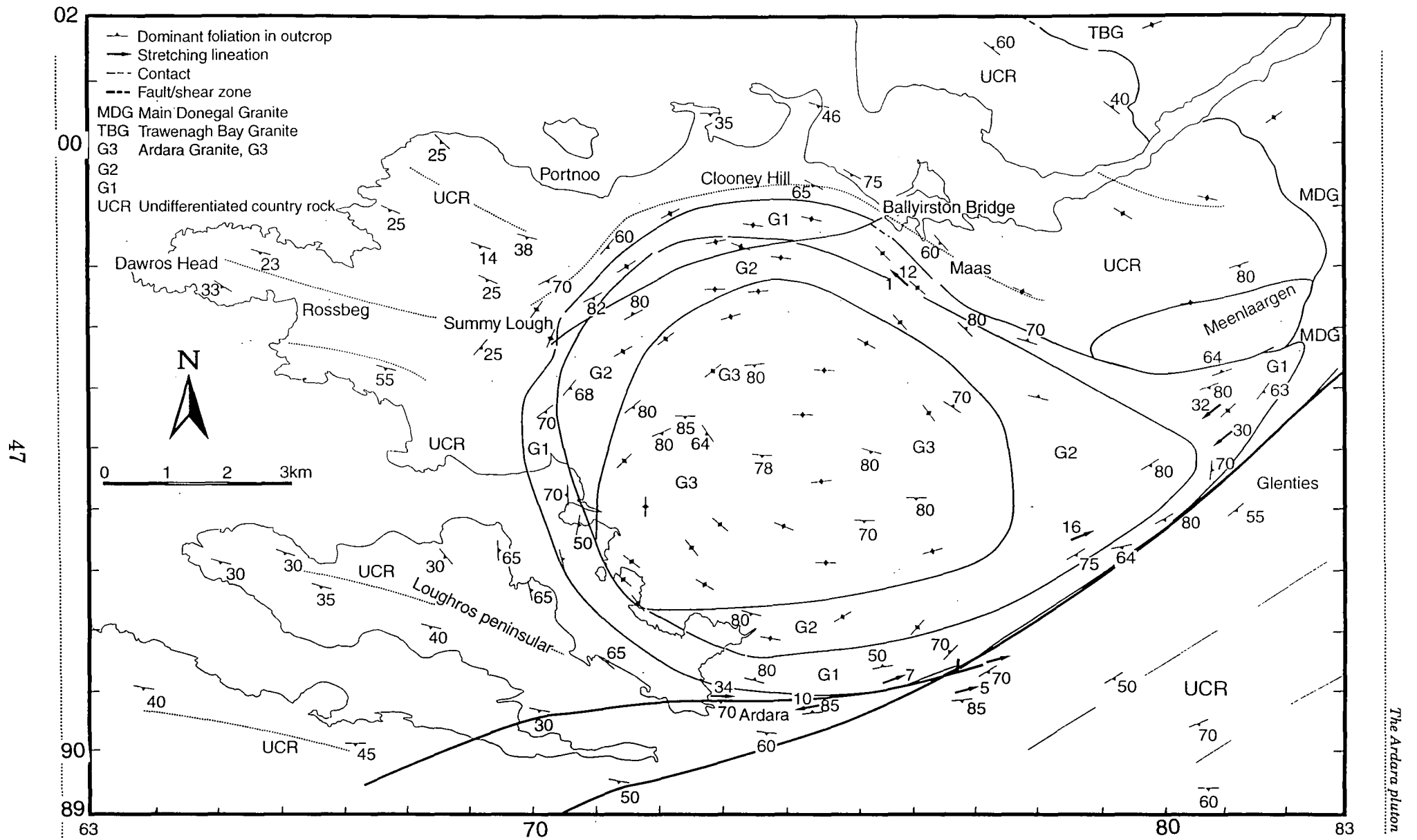


Figure 2.8 Geological Map of the Ardara pluton

country rock and intrusion related thermal metamorphism. This work, together with that of Gindy (1951, 1953) and Mithal (1952), was integrated by Pitcher & Berger (1972) to suggest that the Ardara pluton was emplaced by two stage diapiric uprise which deformed the country rocks around the periphery of the pluton.

A number of additional related regional studies were carried out around this time. Hall (1966), in a simple geochemical study demonstrated what appears to be a simple fractionation trend between G1 and G3. King (1966) in an early application of the measurement of the Magnetic Anisotropy (AMS), demonstrated the possible existence of steep magmatic lineations in the centre of the pluton, except where modified to gentle inclinations around the southern contact. Young (1966) and Riddihough & Young (1969), as part of a regional gravity study of Donegal, showed that the Ardara pluton corresponded to a circular area with a pronounced Bouguer gravity anomaly (Figure 2.9), indicating the presence of a possibly hemispherical zone of lower density (granitic) material at depth (Young 1966).

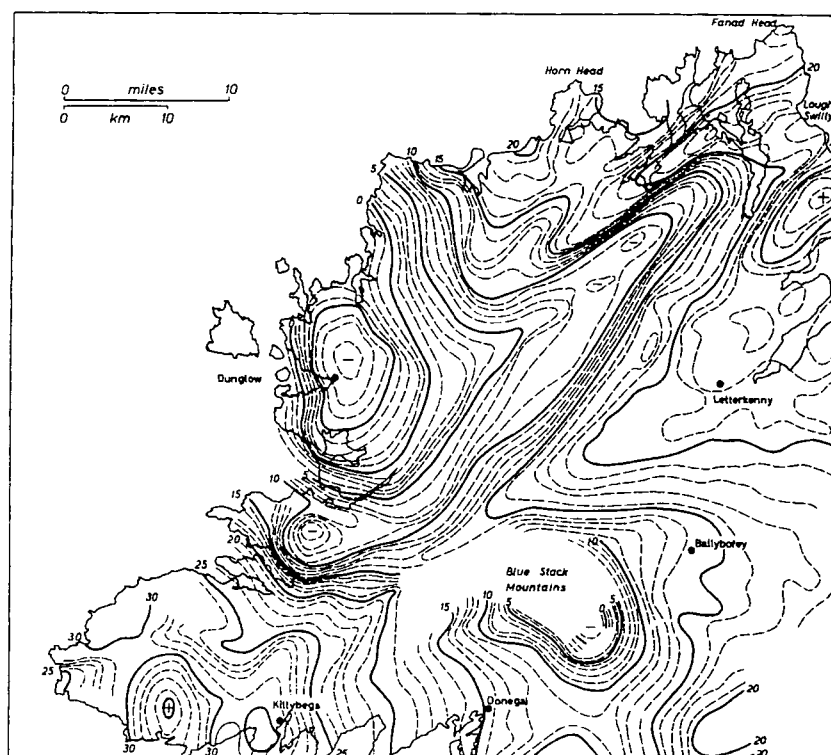


Figure 2.9 Bouguer gravity anomaly map of Donegal from Riddihough & Young (1969)

Research work on the pluton then fell quiet for a number of years until the work of Holder (1979), which may be one of the most significant studies in the investigation of granitic plutons. By measuring the axial ratios of populations of country rock xenoliths incorporated into the pluton magma, and assuming that these xenoliths had been deformed when the viscosity contrast, between xenolith and magma was small, he showed:

1. **Flattening strains** - xenoliths show a $K \sim 0$ flattening strain everywhere (Flinn 1962). Which when taken with the steep concentric fabric, circular granite outline and the presumption that the exposures lie in a non-unique plane, this implies a spherical body which has expanded laterally as a spherical balloon.
2. **Strain gradients** - variations in finite strain intensity, greater axial ratios in the outer units and finite strain discontinuities are consistent with expansion during the emplacement process.
3. **Andalusite growth** - The growth of andalusites within the aureole, show 2/3 phases, which is correlated with the sequential intrusion of the granite phases.

Hence, Holder postulated that the xenoliths began to be deformed as an inwardly migrating 'freezing surface' migrated past them, and modelled this situation to show that some 60% of the volume of the pluton could be accommodated by an in-situ ballooning (expansion) process.

Meneilly (1981, 1982) carefully mapped the structures present around the Ardara pluton in the Gweebarra to Dawros-Rosbeg region. The earlier regional deformations were described in part 2.1.5 above. The specific structures related to granite emplacement (D_4) are below:

1. **Outer zone** - D_4 structures are sporadic in occurrence, forming first 7km from the pluton as minor S_4 cleavages and F_4 folds with a north-northeast south-southwest through to northeast-southwest orientation (Figure 2.10), with occasional zones of remarkably increased intensity. From 750m-2.5km from the pluton contact S_4 cleavages are common. To the north of the pluton in the vicinity of the Trawenagh Bay Granite the structures have a north-south orientation.
2. **Major folds** - The Mulnamin anticline and Maas syncline, form km-scale F_4 folds which become intensified on approaching the northern pluton contact.
3. **Inner zone** - About 500m from the pluton contact there is a zone of ubiquitous F_4 folding, until 100-250m from the contact where the bedding and S_4 become parallel. No further F_4 folding is observed and as the contact is approached bedding and $S_{1/2/3}$ become unrecognisable. Meneilly (1982) suggests that very high strains related to granite emplacement are recorded in this zone, which Sanderson & Meneilly (1981) attempt to quantify through the measurement of andalusite rotation during growth and deformation. Their results show very high flattening strains ($K \sim 0$, $X/Z > 11$) close to the margins decreasing to ($K \sim 0.2$, $X/Z \sim 1.5$) at 500m from the contact.

Interpreting these results Meneilly (1982) suggested that expansion of a granite body resulted in a local stress redistribution, forming D_4 structures with an orientation dependent upon their spatial relationship to the Ardara pluton. In addition thermal softening took place around the pluton concentrating deformation close to the pluton contact.

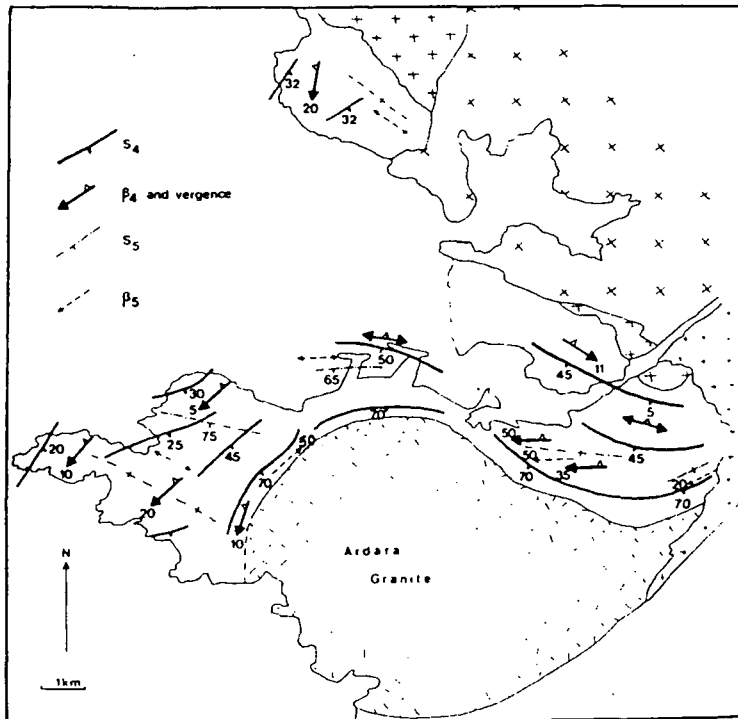


Figure 2.10 D₄ and D₅ structures around Gweebarra Bay, from Meneilly (1982)

Kerrick (1987) carried out a garnet-biotite geothermobarometric analysis of the aureole, suggesting that the andalusites probably grew in two phases; and that for an assumed pressure of emplacement of 2.5 KBar (7-9 km), the maximum attained contact temperature was ~650°C at the contact and ~350°C at 1km.

Most recently the pluton has become the focus of wide-ranging discussion as to the existence or non-existence of diapirs and ballooning plutons, and the validity of using microgranitoid enclaves as strain markers (Vernon & Paterson 1993, Morgan 1995, Paterson & Vernon 1995). The main studies of Vernon & Paterson (1993) and Paterson & Vernon (1995) maintained that:

1. Populations of microgranitoid enclaves show a variation in axial ratio across a single outcrop and therefore a statistical analysis of such enclaves produces an invalid record of the imposed strain.
2. The observed strain path described in the work of Holder (1979) could be produced as a result of convective processes in a diapir or magma chamber.
3. There was significant deformational overprint of the pluton post-emplacement because the igneous foliation cross-cuts certain internal petrological boundaries.
4. The country rocks do not preserve adequate shortening to account for the space occupied by the pluton and therefore space must have been created by mechanisms for which there is little field evidence e.g. stoping.

The following work will attempt to move forward from existing knowledge and, through an analysis of a comprehensive dataset, demonstrate the ballooning nature of pluton emplacement.

2.2 The Ardara pluton: the plutonic phases

The individual outcrop features associated with emplacement are described below:

2.2.1 Nature of the contact

The Ardara pluton has a relatively sharp contact zone (<3 metres) with the surrounding country rock. The contact displays different features depending upon the location.

The southern contact is described by a sharp boundary from vertically foliated, sheared mica schists, the Falcarragh Pelites, into a steeply foliated G1 granite. In places the granite has a gneissic texture, produced during solid state deformation of an earlier magmatic fabric.

Around the eastern and western sides of the pluton the contact is also sharp and well defined (<3m), generally consisting of strongly foliated (S₄) Falcarragh Pelites, with a schistose texture, and granite which displays a gneissose solid state fabric in the 20-30m closest to the contact. This solid state deformation reduces rapidly in intensity away from the contact, becoming indistinguishable from the magmatic foliation (in outcrop) at approximately 50m from the contact.

The contact rock fabric, solid state deformation and magmatic state deformation are everywhere parallel to each other.

2.2.2 Outer unit, G1

The outer plutonic unit has been described as a tonalite (Akaad 1956a) and as a quartz diorite (Holder 1979): Point counting of 23 samples suggests an average plagioclase-rich granodioritic composition (Figure 2.11a). In outcrop the granite appears with obvious phenocryst plagioclase crystals (0.5-1cm) and poorly formed overgrowing K-feldspars (~1cm) in a matrix of small quartz crystals and abundant biotite.

Solid state deformation

Around the outer contact of the pluton (less than 100m from the contact) there is a steep solid state fabric developed which is defined in outcrop by elongate quartz and rounded feldspar, resulting in occasionally developed S-C fabrics and δ - and σ -type fabrics (Plate 2.1). In thin section this deformation is observed to consist of mimetic recrystallised strain-free quartz and weakly developed 'core and mantle' structures around undeformed feldspar cores, indicating a medium-high temperature during fabric development. Using the criteria of Passchier & Trouw (1996), the contact temperature of deformation is estimated at 400-500°C. Away from the immediate contact zone the intensity of this deformation decreases over 100-150m until the fabric is a magmatic state fabric.

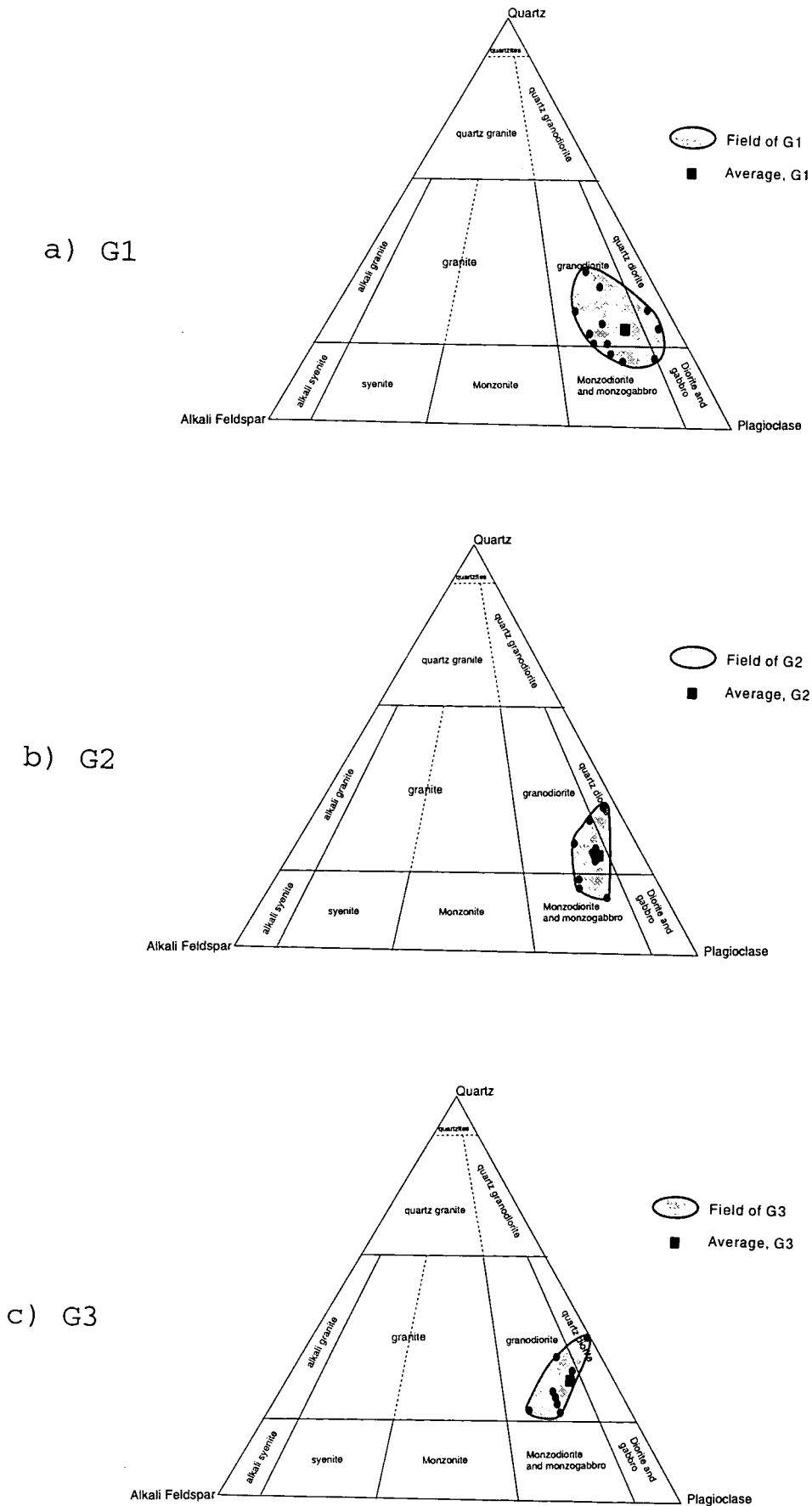
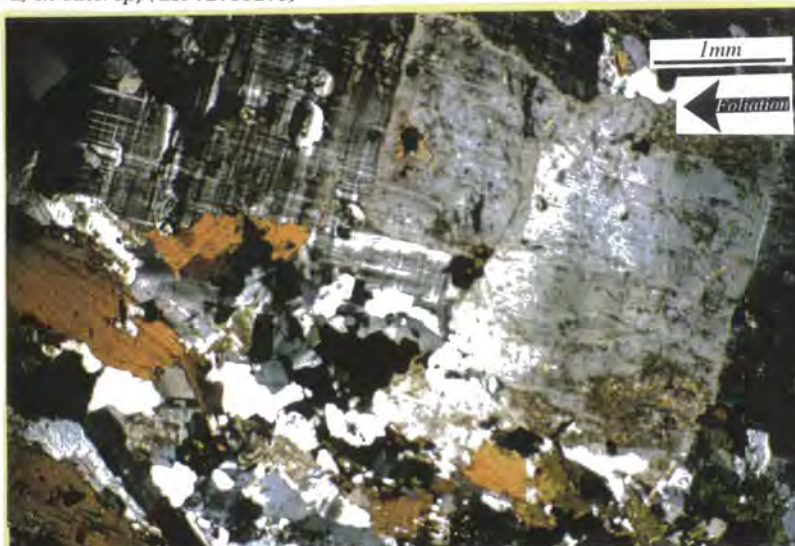


Figure 2.11 Tertiary QAPF-type plot for rocks of a granitic composition for Ardara G1,G2,G3

The solid state fabric is interpreted as being of low intensity because it is non-pervasive, earlier magmatic fabric remnants are preserved, feldspar crystals are generally original in shape and structure and original biotite crystals can be recognised. Traversing away from the contact through G1 towards the centre of the pluton, the solid state fabric diminishes in strength, grades into and is indistinguishable from the magmatic fabric.



a) in outcrop, (GR 72759279)



b) in thin section, (GR 74639874)

Plate 2.1 Solid state deformation of G1, Ardara pluton

Magmatic state deformation

The magmatic state fabric is developed away from the immediate contact zone (greater than 50m from the contact zone) but can often be identified in zones of heterogeneous solid state deformation. This fabric displays feldspar phenocryst interactions, which took place while there was significant melt present, resulting in well developed tilting fabrics, developed by biotite and rare highly retrogressed hornblendes. The later formed phases are quartz and K-feldspar; quartz forms interstitial irregularly shaped

crystals, whereas K-feldspar, forms poorly formed sub-rectangular perthitic crystal which overgrow and incorporate earlier fully crystallised phases (Plate 2.2).

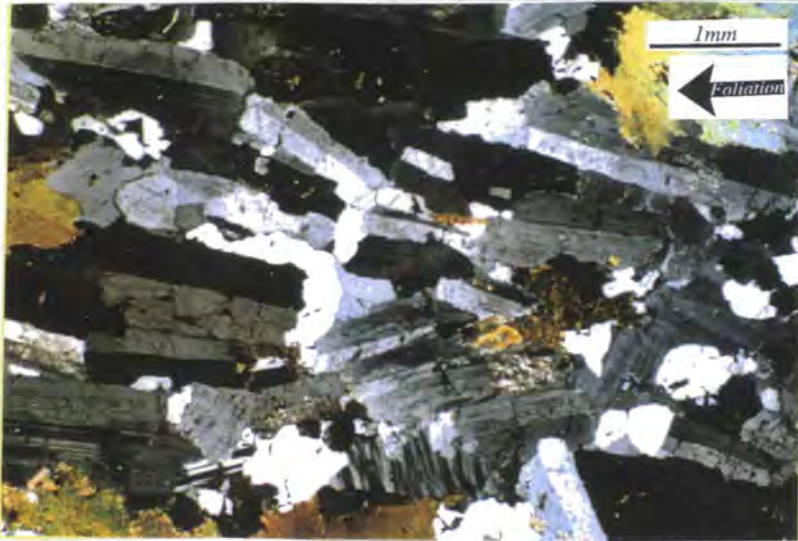


Plate 2.2 Photomicrograph of magmatic state deformation G1, Ardara pluton (GR 72629846)

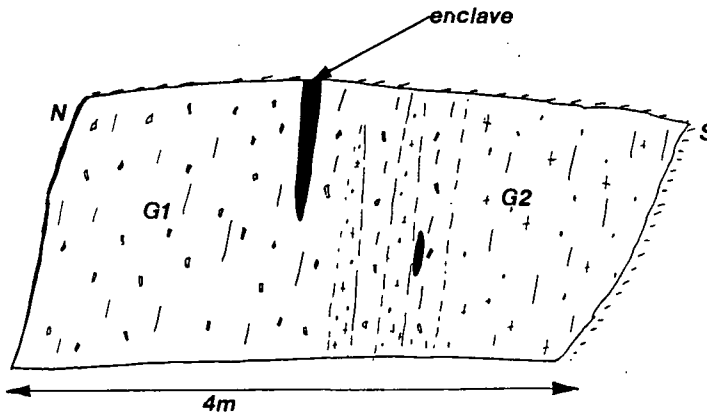
Within G1 there are two dominant types of xenoliths; *amphibolitic xenoliths* - which are blocky, display variable orientation with respect to the foliation and preserve deformed relict sedimentary features; and *microgranitoid enclaves* - that are elliptical in shape, orientated sub-parallel to the foliation and have a fine grain size and a homogenous broadly mafic composition. Their origin may be related to the large number of basic appinitic sills/dykes and complexes in the region around the pluton e.g. Meenalargan complex, Hall (1966).

2.2.3 G2

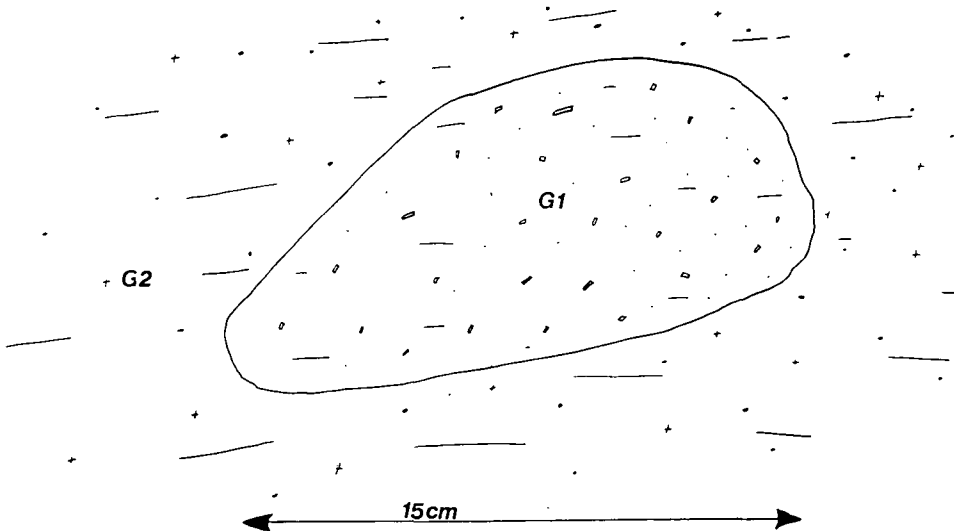
The G2 unit, for which point counting analysis of 24 sections demonstrates a granodioritic composition, has been described as a quartz diorite (Akaad 1956a) and as a granodiorite (Holder 1979) (Figure 2.11b). Its contact with G1 is generally sharp. Of particular remark are the contact zones around GR 730997 on Binwee Hill where minor local xenoliths of G1 can be observed in G2 and the contact zone is defined by very local interfingering and minor dyking of G2 into G1 (Figure 2.12).

This may suggest that G1 had attained a complex semi-solid (perhaps gel-like) rheology before emplacement of G2 took place i.e. on long-medium timescale/low strain rate, the G1 magma flowed producing magmatic structures, whereas on a short timescale/high strain rate the G1 magma could deform brittle fashion. At the south western corner of the pluton (GR 728913), the G1/G2 contact is delimited by a screen of deformed quartzite, ~30m wide (believed to be a fragment of Ards quartzite), which was incorporated during intrusion. This suggests that magma forcefully intruded the country rock, incorporating and translating it during the intrusion process: The closest fragment of Ards quartzite to this locality is incorporated into the Meenalargan complex, over 10km away

(Iyengar *et al* ,1954). This fragment may represent material incorporated from the roof during early emplacement.



a) Field sketch of G2, intruding into G1 during emplacement (GR 72719844)

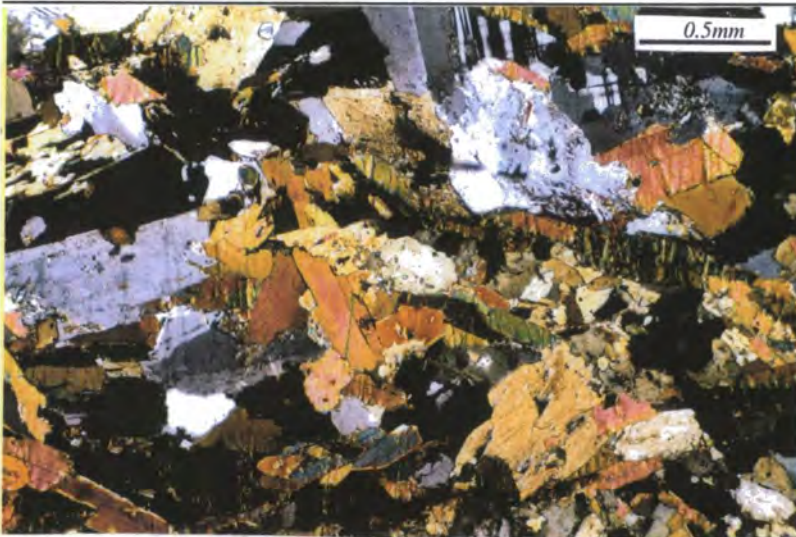


b) Field sketch of G1 xenolith in G2 granite (GR 72939847)

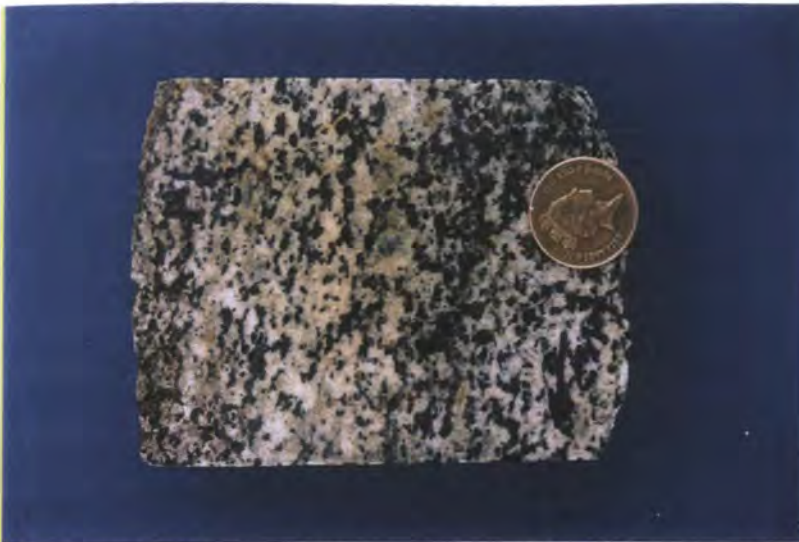
Figure 2.12

In outcrop the most striking features of G2 are its generally small grain size (<0.5cm) and mafic blebs (0.5-1cm), which in thin section can be seen to be made of retrogressed hornblende mantled by biotite and opaques (Plate 2.3a). These inclusions may be related to mixing of mafic and felsic magmas at depth or during ascent, before emplacement. No solid state fabric of any sort is seen in G2, only the well developed magmatic state fabric. This is defined by an often tiled fabric amongst the zoned plagioclase feldspars and magmatic biotites, with original quartz and rare K-feldspar crystallising in the remaining cavities.

Incorporated into G2 there are abundant ellipsoidal microgranitoid enclaves of a mafic composition, which are larger and easily distinguished from the minor blebs in the matrix. Country rock xenoliths are rare to absent in G2.



a) Photomicrograph of mafic blebs within G2, Ardara pluton (GR 70429637)



b) Photograph of G2, Ardara pluton showing magmatic state deformation (GR 72629846)

Plate 2.3

2.2.4 Central unit, G3

The central magmatic phase G3, a granodiorite, is the most evolved of each of the three phases. Both Akaad (1956a) and Holder (1979) also refer to it as a granodiorite. This phase is distinguished in the field through the development of small (<0.5cm) pale pink weathering plagioclase feldspar crystals and prominent, very well formed, dusty grey quartz (Plate 2.4). The fabric itself is weak but recognisable everywhere throughout the pluton. It formed in the magmatic state and is defined through the preferred alignment of feldspar, biotite and quartz.

Across all plutonic phases the foliation forms sub-concentric rings concordant with the outer contact and the country rocks. This fabric diminishes in strength around a point south west of the geographical centre of the pluton, in the vicinity of the Moolagh Townlands (GR 734949).

The contact with G2 is often poorly defined due to the discontinuity of exposure; the available evidence suggests that it is probably gradational over 10-20m. Only in the southwestern area around Trawnacasey (GR 718923) is the contact well defined, where G1 is in contact with a thin country rock screen (similarly to the G1/G2 contact in this area), which is in contact with G3. This country rock screen is estimated to be approximately 7m wide at this point. Throughout G3 microgranitoid enclaves are often small and display a heterogeneous distribution.



Plate 2.4 Photograph of G3, Ardara pluton (GR 81849580)

2.2.5 The Moolagh townlands, GR 734949

The outcrops in this vicinity are noteworthy, with reference to the entire pluton. This area corresponds to a zone of smaller than average crystal size, a fabric which is particularly weak, occasionally unobservable and changes rapidly in orientation, and a remarkable number of very small mafic enclaves (Figure 2.13). In general, the fabric increases qualitatively in intensity outwards from this point and G3 preserves fewer enclaves than are observed here.

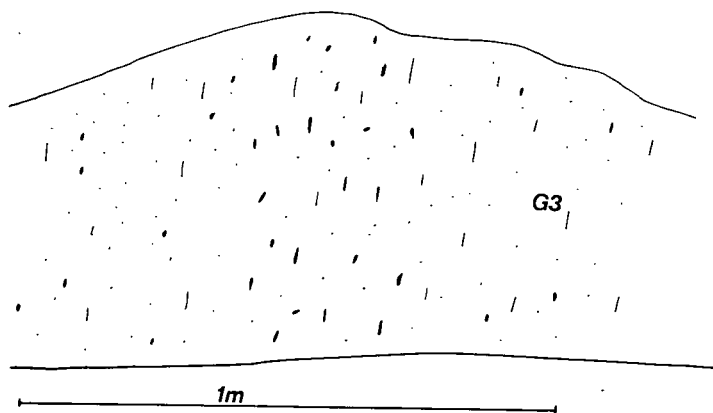
This zone corresponds to the offset centre of the pluton and to the position of latest magma emplacement, the "injection point".

2.2.6 Conclusion and discussion

The Ardara pluton is a three phase normally zoned pluton i.e. it becomes more evolved (quartz rich) with the each additional phase. It is emplaced into deformed pelitic schists which have a concordant narrow contact with the plutonic phases. The outer phase, G1, is strongly coupled to deformation in the country rock: It is deformed in the solid state close to the contact, where the hot granite magma would have been cooled against the surrounding country rocks, and in the magmatic state elsewhere. G2 shows a sharp contact with G1 and locally intrudes into it, which suggests G1 was already partially solidified upon

the intrusion of G2. G3 shows a slightly gradational contact with G2 and appears to deform in a similar manner though they are compositionally quite distinct.

Each plutonic phase displays a recognisable and measurable fabric formed in the magmatic or solid state, which is indistinguishable in orientation across similarly positioned outcrops. The intensity of this fabric diminishes within G3 and is at its weakest at a point south west of the geographical centre of the pluton, around the Moolagh Townlands, where the fabric is conspicuously weak and there are abundant small mafic enclaves.



Field sketch of Moolagh Townlands outcrops showing abundant small microgranitoid enclaves (GR 734949)

Figure 2.13

2.3 Strain measurement

The measurement of finite strain requires the quantification of the degree of shortening/extension that has taken place in three dimensions during deformation. It is commonly represented using the strain ellipse or a percentage extension/shortening. In the following analysis three methods are presented in an attempt to elucidate the preserved strain within and around the Ardara pluton.

2.3.1 Mafic enclaves axial ratio map

The methodology used in the statistical analysis of mafic enclaves to develop statistical population averages was described in Chapter 1. This method was followed at 62 locations across the pluton, measuring nearly 3000 mafic enclaves. At each locality every effort was made to collect a statistical sample (approximately 30 enclaves was used in each analysis) of enclave axial ratios from each of the principal planes (R_{xz} and R_{yz}). Because of the general absence of a lineation and dominance of flattening strain across the pluton R_{xz} and R_{yz} are found to be identical and/or interchangeable; in the analysis the principal planes are referred to as; *the horizontal plane*, which is the horizontal plane of outcrop perpendicular to foliation; and *the vertical plane*, which is the vertical plane of outcrop perpendicular to foliation. In addition to measuring the mean of each population, the following statistical characteristics were determined; *standard deviation*, the statistical variability within a population; *percentage population spread*, (Equation 2.2) statistical percentage variability with a population; *log K-value*, the style of deformation recorded by the population; *population range*, defined by the ω log co-efficient (Equation 2.3). A summary of these principal data are presented in Table 2.3, with a complete listing of all data, localities and grid references in Appendix 2.

Equation 2.2, Percentage population spread = (standard deviation / population mean) x 100

Equation 2.3, Population range, ω log

$$\omega \log = \log_{10} (R_{\max}) - \log_{10}(R_{\min})$$

where R_{\max} is the largest recorded axial ratio, and R_{\min} is the smallest recorded axial ratio.

Table 2.3 Table of average mafic enclave axial ratios from the Ardara pluton

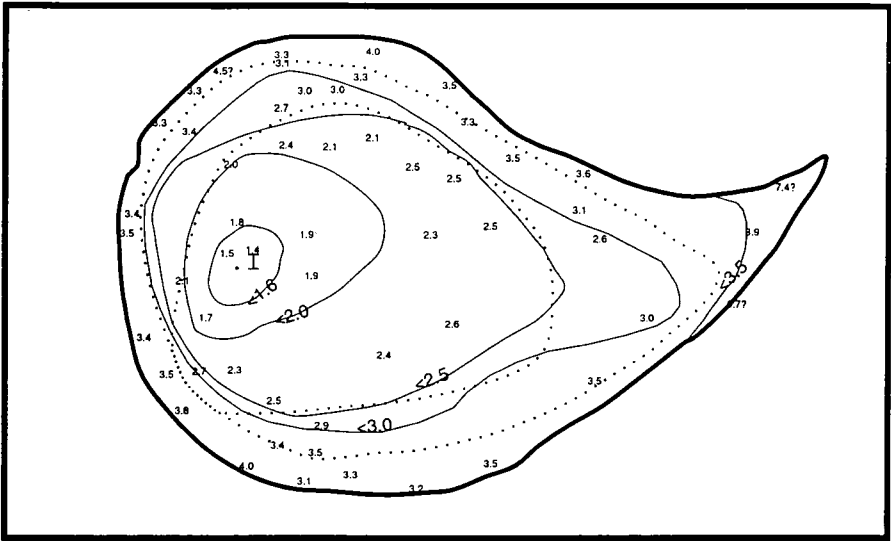
Locality	Grid Ref.	Pluton	Orientation	Mean Axial ratio	Number of analysed enclaves	St. Dev.	Smallest Axial Ratio	Largest Axial Ratio	ω Log	Log K value	% Variation in size
A0	GR 72789221	G2	HORIZ	4.34	30	2.75	1.50	13.50	0.95	0.03	63.36
A0	GR 72789221	G2	VERT	4.51	30	2.97	1.65	14.50	0.94		65.85
A2	GR 72759279	G1	HORIZ	2.51	30	0.94	1.50	6.25	0.62	0.07	37.45
A2	GR 72759279	G1	VERT	2.68	23	0.92	1.27	5.00	0.59		34.33
A4	GR 73269169	G1	HORIZ	4.52	30	1.59	2.50	8.33	0.52	0.10	35.18
A4	GR 73269169	G1	VERT	3.95	17	1.24	2.50	6.67	0.43		31.39
A6	GR 73159211	G2	HORIZ	3.71	29	1.19	1.33	6.50	0.69	0.03	32.08
A6	GR 73159211	G2	VERT	3.89	23	1.62	2.00	7.14	0.55		41.65
B1	GR 71689248	G1	HORIZ	3.82	30	1.35	1.86	6.43	0.54	0.02	35.34
B1	GR 71689248	G1	VERT	3.95	30	1.84	1.36	10.00	0.86		46.58
B5	GR 71269336	G2	HORIZ	3.76	30	1.63	2.00	8.95	0.65	0.04	43.35
B5	GR 71269336	G2	VERT	3.59	30	1.77	1.78	9.38	0.72		49.30
B6	GR 70789380	G1	HORIZ	3.37	30	1.22	1.78	7.25	0.61		36.20
C1	GR 71949842	G1	HORIZ	4.50	30	1.90	2.24	8.67	0.59	0.09	42.22
C1	GR 71949842	G1	VERT	5.26	6	2.83	1.78	9.38	0.72		53.80
C10	GR 73889704	G3	HORIZ	2.07	30	0.83	1.00	4.00	0.60	0.17	40.10
C10	GR 73889704	G3	VERT	1.86	30	0.77	1.00	4.17	0.62		41.40
C4	GR 73089861	G2	HORIZ	3.03	30	1.12	1.37	5.00	0.56	0.09	36.96
C4	GR 73089861	G2	VERT	3.38	23	0.85	2.21	3.38	0.42		25.15
C7	GR 73599793	G2	HORIZ	3.11	30	1.22	1.47	7.33	0.70	0.04	39.23
C7	GR 73599793	G2	VERT	2.99	30	1.07	1.56	5.00	0.50		35.79
D1	GR 70329569	G1	HORIZ	3.57	30	1.20	2.43	8.42	0.54	0.10	33.61
D1	GR 70329569	G1	VERT	3.17	25	1.22	1.17	5.75	0.69		38.49
D2	GR 70619592	G2	HORIZ	3.37	27	1.86	1.88	11.67	0.79		55.19
D4	GR 72119527	G3	HORIZ	1.47	30	0.48	1.00	3.00	0.48		32.65
D4**	GR 72679532	G3	HORIZ	1.40	30	0.28	1.00	2.00	0.30	0.33	20.00
D4**	GR 72679532	G3	VERT	1.65	30	0.63	1.00	3.50	0.54		38.18
E3	GR 80919557	G1	HORIZ	3.89	25	1.91	2.25	8.28	0.57	0.39	49.10
E3	GR 80919557	G1	VERT	2.65	16	0.95	1.36	4.32	0.50		35.85
E7	GR 79639407	G2	HORIZ	3.10	30	1.17	1.26	7.11	0.75		37.74
F1	GR 76789151	G1	HORIZ	3.46	30	1.60	1.93	9.30	0.68	0.00	46.24
F1	GR 76789151	G1	VERT	3.48	30	1.10	1.33	6.80	0.71		31.61
F2	GR 76469325	G3	HORIZ	1.90	30	0.65	1.10	3.35	0.48		34.21
F3	GR 76429342	G3	HORIZ	2.65	30	0.64	1.79	4.50	0.40	0.46	24.15
F3	GR 76429342	G3	VERT	1.95	30	0.57	1.00	3.15	0.50		29.23
G1	GR 71599800	G1	HORIZ	3.32	30	1.29	2.05	7.09	0.54	0.08	38.86
G1	GR 71599800	G1	VERT	3.03	10	1.06	1.19	4.75	0.60		34.98
G2	GR 71009749	G1	HORIZ	3.25	20	0.69	2.21	4.71	0.33		21.23
G4	GR 70429637	G2	HORIZ	2.70	23	0.98	1.42	5.16	0.56	0.04	36.22
G4	GR 70429637	G2	VERT	2.82	15	1.03	1.69	5.23	0.49		36.52
G5	GR 71699720	G2	HORIZ	3.42	30	1.48	1.79	7.82	0.64	0.10	43.27
G5	GR 71699720	G2	VERT	3.05	30	1.44	1.15	8.33	0.86		47.21
H1	GR 73119865	G1	HORIZ	3.26	30	1.39	1.41	6.80	0.68	0.06	42.64
H1	GR 73119865	G1	VERT	3.50	30	1.35	1.92	7.00	0.56		38.57
H3	GR 74639874	G1	HORIZ	4.00	30	1.90	1.49	8.75	0.77	0.06	47.50
H3	GR 74639874	G1	VERT	4.36	30	1.80	1.13	8.75	0.89		41.28
H4	GR 74389821	G2	HORIZ	3.27	25	1.62	1.47	7.33	0.70	0.04	49.54
H4	GR 74389821	G2	VERT	3.13	10	1.82	1.67	7.00	0.62		58.15
H5	GR 74659825	G3	HORIZ	1.91	28	0.69	1.08	3.56	0.52	0.12	36.13
H5	GR 74659825	G3	VERT	2.09	30	0.86	1.10	5.00	0.66		41.15
H6	GR 74029813	G2	HORIZ	2.92	30	2.12	1.13	13.00	1.06	0.02	72.60
H6	GR 74029813	G2	VERT	2.97	30	2.49	1.05	13.30	1.10		83.84
I1	GR 72229674	G3	HORIZ	1.95	30	0.81	1.15	5.06	0.65		41.54
I4	GR 71549484	G2	HORIZ	2.01	30	0.73	1.08	4.54	0.62	0.17	36.37
I4	GR 71549484	G2	VERT	1.82	30	3.18	1.00	18.90	1.27		174.73
I5	GR 71889419	G3	HORIZ	1.68	30	0.55	1.13	3.06	0.43	0.33	32.74
I5	GR 71889419	G3	VERT	2.16	5	0.35	1.89	2.57	0.13		16.20
J1	GR 75789817	G1	HORIZ	2.31	30	0.95	1.57	6.25	0.60	0.20	41.13
J1	GR 75789817	G1	VERT	2.85	30	1.33	1.10	7.08	0.81		46.67

Locality	Grid Ref.	Pluton	Orientation	Mean Axial ratio	Number of analysed enclaves	St. Dev.	Smallest Axial Ratio	Largest Axial Ratio	ω Log	Log K value	% Variation in size
J3	GR 76329753	G1	HORIZ	3.96	30	2.16	2.14	13.18	0.79	0.14	54.55
J3	GR 76329753	G1	VERT	3.33	29	1.36	1.50	7.50	0.70		40.84
J4	GR 77089693	G2	HORIZ	3.48	30	1.81	1.60	10.50	0.81	0.03	52.01
J4	GR 77089693	G2	VERT	3.64	30	1.04	1.08	5.60	0.71		28.57
J5	GR 78149665	G1	HORIZ	2.56	27	1.25	1.25	7.71	0.79	0.10	48.83
J5	GR 78149665	G1	VERT	2.85	16	1.05	1.84	5.88	0.50		36.84
J5*	GR 78409659	G1	HORIZ	3.61	30	1.42	1.50	7.65	0.71		39.34
K2	GR 78299578	G1	HORIZ	3.07	29	1.11	1.33	5.67	0.63	0.15	36.16
K2	GR 78299578	G1	VERT	2.65	30	1.21	1.27	6.00	0.67		45.66
L1	GR 75979704	G2	HORIZ	2.56	30	1.36	1.46	9.06	0.79	0.10	53.13
L1	GR 75979704	G2	VERT	2.85	30	1.17	1.55	5.73	0.57		41.05
L2	GR 75979649	G3	HORIZ	2.55	30	2.50	1.20	14.29	1.07	0.34	98.04
L2	GR 75979649	G3	VERT	2.01	30	0.49	1.04	3.25	0.49		24.38
L3	GR 75789557	G3	HORIZ	2.29	30	0.81	1.13	4.50	0.60	0.08	35.37
L3	GR 75789557	G3	VERT	2.16	30	0.97	1.32	5.67	0.63		44.91
L7	GR 73769186	G2	HORIZ	3.64	30	1.43	1.58	6.50	0.61	0.07	39.29
L7	GR 73769186	G2	VERT	3.36	30	1.59	1.38	7.60	0.74		47.32
M1	GR 74409155	G1	HORIZ	3.39	29	1.07	1.96	6.44	0.52	0.08	31.56
M1	GR 74409155	G1	VERT	3.76	30	1.62	2.00	9.00	0.65		43.09
M2	GR 75619132	G2	HORIZ	3.20	30	1.19	1.84	5.83	0.50	0.15	37.19
M2	GR 75619132	G2	VERT	3.93	30	1.70	2.10	7.80	0.57		43.26
M5	GR 78749311	G2	HORIZ	3.56	15	1.72	1.67	7.50	0.65		48.31
N5	GR 73769492	G3	HORIZ	1.93	30	0.85	1.00	4.67	0.67	0.02	44.04
N5	GR 73769492	G3	VERT	1.91	30	0.55	1.00	3.20	0.51		28.80
O2	GR 71589319	G2	HORIZ	2.65	30	0.93	1.25	5.00	0.60		35.09
O3	GR 72829274	G3	HORIZ	2.56	30	0.79	1.16	4.43	0.58	0.05	30.86
O3	GR 72829274	G3	VERT	2.68	30	0.97	1.41	5.67	0.60		36.19
O4	GR 73469227	G2	HORIZ	2.90	30	0.98	1.38	4.67	0.53	0.17	33.79
O4	GR 73469227	G2	VERT	3.59	30	1.50	2.07	7.14	0.54		41.78
O5	GR 73569113	G3	HORIZ	2.99	30	1.05	1.54	6.67	0.64	0.08	35.12
O5	GR 73569113	G3	VERT	3.28	16	1.03	1.95	5.60	0.46		31.40
P2	GR 73069761	G2	HORIZ	2.68	30	0.90	1.60	5.28	0.52	0.12	33.58
P2	GR 73069761	G2	VERT	3.05	30	1.16	1.50	6.00	0.60		38.03
P3	GR 73219713	G3	HORIZ	2.43	22	0.84	1.44	4.27	0.47	0.16	34.57
P3	GR 73219713	G3	VERT	2.86	3	0.29	2.60	3.17	0.09		10.14
P5	GR 73349560	G3	HORIZ	2.21	4	0.52	1.81	3.00	0.22	0.27	23.53
P5	GR 73349560	G3	VERT	1.87	8	0.40	1.47	2.71	0.26		21.39
P7	GR 72429555	G3	HORIZ	1.77	30	0.67	1.00	3.75	0.57	0.06	37.85
P7	GR 72429555	G3	VERT	1.84	16	1.03	1.18	5.33	0.65		55.98
Q1	GR 81049444	G1	HORIZ	7.38	30	5.00	3.20	22.50	0.84		67.75
Q6	GR 79829553	G2	HORIZ	1.89	30	0.57	1.11	3.33	0.47		30.16
R1	GR 76889563	G2	HORIZ	3.48	30	1.86	1.33	9.00	0.83	0.09	53.45
R1	GR 76889563	G2	VERT	3.14	24	1.16	1.67	6.00	0.56		36.94
R2	GR 76919560	G3	HORIZ	2.45	16	0.83	1.37	4.24	0.49		33.88
R7	GR 75469671	G3	HORIZ	2.81	30	1.01	1.40	5.17	0.57	0.04	35.94
R7	GR 75469671	G3	VERT	2.95	30	0.86	1.76	5.50	0.49		29.15
S2	GR 75429378	G3	HORIZ	3.16	30	1.50	1.83	10.00	0.74	0.12	47.47
S2	GR 75429378	G3	VERT	2.79	14	0.80	2.00	4.50	0.35		28.67
U2	GR 73079378	G3	HORIZ	2.27	30	0.80	1.50	4.40	4.47	0.24	35.24
U2	GR 73079378	G3	VERT	1.94	9	0.45	1.17	2.40	0.31		23.20
U3	GR 73849452	G3	HORIZ	2.59	27	0.51	1.71	3.57	0.32	0.08	19.69
U3	GR 73849452	G3	VERT	2.80	17	1.38	1.35	6.50	0.68		49.29

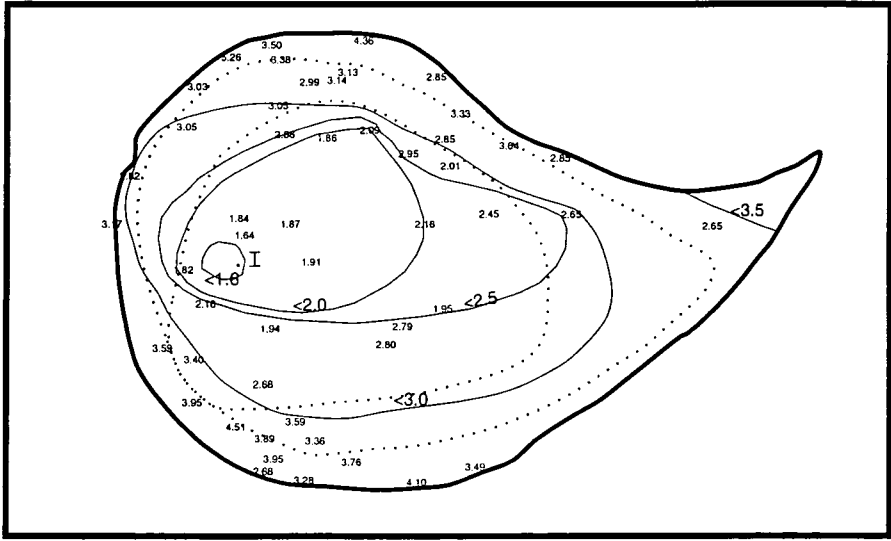
The geometric mean of each of these populations has been plotted spatially on a map of the pluton (Figure 2.14 a, b) and contoured using the nearest neighbour method (Swan & Sandilands 1994). Used in concert with the table above and the Flinn plot (Figure 2.14c) a number of important observations can be about the results:

1. **The enclaves record emplacement finite strain** - The reliability of using mafic/microgranitoid enclave axial ratios as strain markers is widely disputed (Vernon 1984, Vernon & Paterson 1993, Fowler & Paterson 1997 and references therein). These data demonstrate a consistent increase in axial ratio from the interior to the outer contact of the pluton, in both principal planes of foliation. This increase in axial ratio is coincident with a qualitative increase in magmatic and solid state emplacement related foliation intensity. The mafic enclaves across the pluton record this foliation intensity increase quantitatively and therefore are acting as markers of the finite strain. By statistically analysing spatially distinct populations enclave size variability, some of the effects of initial shape obliquity can be diminished. Fowler & Paterson (1997) suggest that differences in freezing temperature of the magmas results in freezing of the mafic enclaves and an underestimate of any finite strain recorded. This criticism of the analysis is accepted and therefore the enclave axial ratio is taken as a lower limit of the possible finite strain during emplacement of the pluton.
2. **Increasing finite strain** - The enclave axial ratio values increase consistently as concentric rings ($R_s \sim 1.6$ in the centre to $R_s \sim 5$ at the contact) in both planes of measurement, from a point displaced south west of the geographic centre of the pluton (Point I, Figure 2.14 a, b). Point 'I', the 'injection point', henceforth describes the area around the Moolagh Townlands (GR 734949), where the magmatic fabric is at its weakest. The low enclave finite strain observed in this area again demonstrates that this area could correspond to a zone where all phases of the magma were injected, before expansion and lateral translation.
3. **Flattening strain** - Because in most of the pluton (except along the southernmost contact) a lineation is not developed and mafic enclave strains are broadly similar in both principal planes of measurement, $X \cong Y$ and the strain is of flattening type (Flinn 1962) (Figure 2.14c). In the overprinted southern area $K \rightarrow 1$.
4. **Low strain enclaves** - The lowest strain enclave populations are preserved around the 'injection point'. If these enclaves represent an initial axial ratio before any deformation could take place, there is a small degree of initial shape obliquity in deformed xenoliths. They were emplaced as weakly elongate ellipsoids not spheres.
5. **Ballooning / in-situ expansion** - Radially increasing strain, flattening $K=0$ type strain and a low strain centre are all features that would be observed if strain were to be measured on the outer surface of a progressively expanding balloon. If the 'inflation point' were known, and a number of intermediate stages during balloon inflation were recorded, it would be possible to inverse model the inflation of the balloon i.e. de-strain the balloon. This type of information is recorded in the granite phases, hence de-straining of the pluton should be possible.

a) Horizontal plane mafic enclave axial ratios



b) Vertical plane, mafic enclave axial ratios



c) Flinn plot for mafic enclave axial ratios

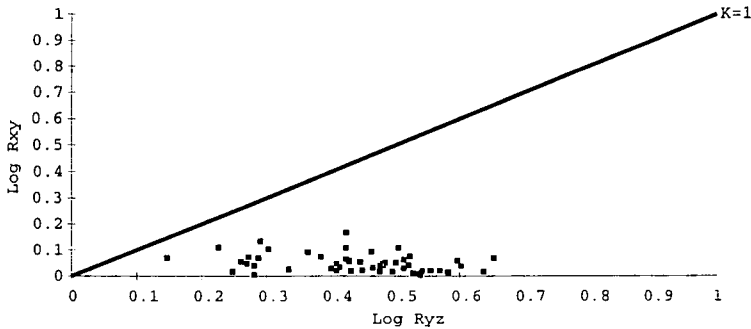


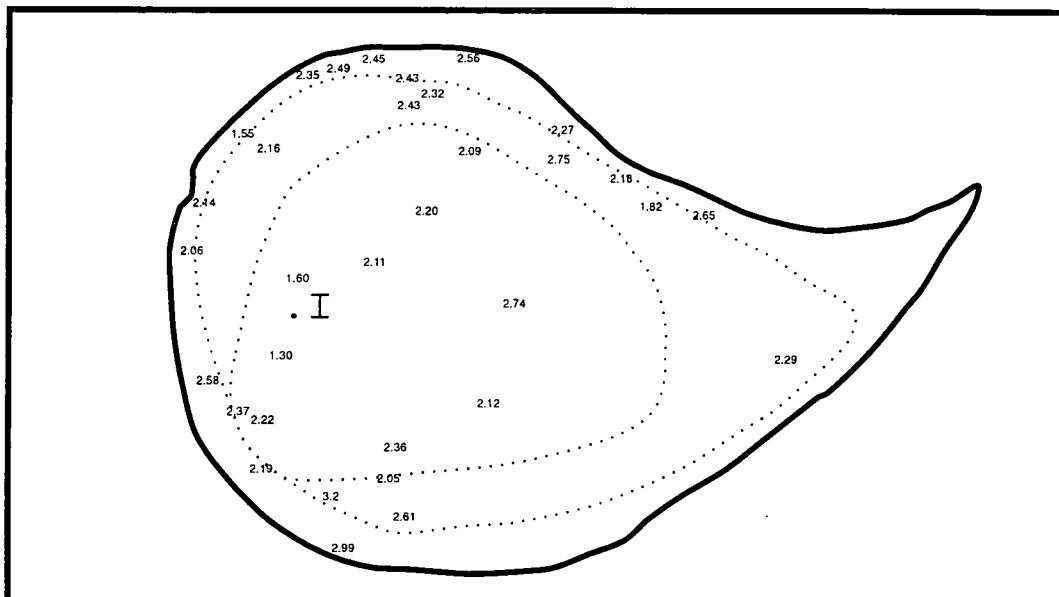
Figure 2.14 Enclave axial ratio data from the Ardara pluton

2.3.2 Fry strain map

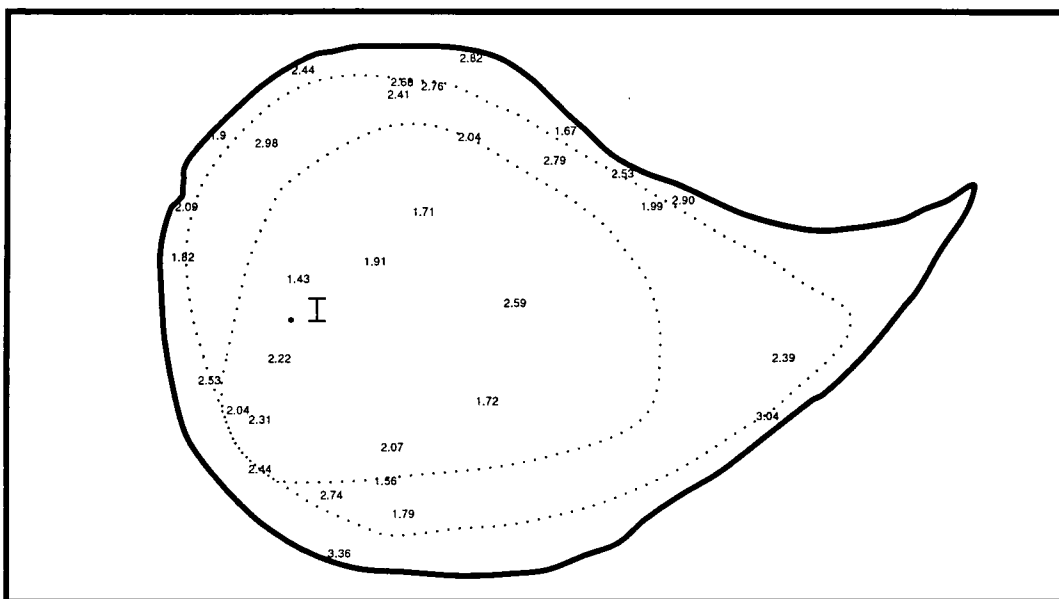
The grain-size normalised Fry strain was measured on the horizontal and vertical principal planes at 36 localities across the pluton. The methods and processes used during the grain-size normalised Fry strain inversion were outlined in Chapter 1. Table 2.5 shows the average Fry strain for each of the principal planes as measured across the pluton: These are plotted, spatially in Figure 2.15 a, b for the vertical and horizontal planes, as a log Flinn plot in Figure 2.15c, and against the corresponding mafic enclave finite strain in Figure 2.15d. Appendix 3 contains more detailed data on the individual number and type of Fry strain inversions carried out. Analysis of the data leads to the following conclusions:

1. **Radial increase** - The Fry strain increases from the centre to the margins of the pluton, similarly to the qualitative increase in fabric intensity and the increase in mafic enclave finite strain. The crystals within the fabric become preferentially spatially dispersed during deformation, which results in a quantifiable 'Fry strain'. In detail it can be seen that the Fry strain data displays a greater variability compared with the mafic enclave data and a consistently lower value.
2. **'Injection point'** - A low Fry strain centre, point 'T' (Figures 2.15 a, b) can be recognised and occurs in a similar position to that of the enclave axial ratio 'injection point' on the Moolagh Townlands.
3. **Low finite strain** - Fry strains measured in a zone around the 'injection point' are close to unity, data which are consistent with the qualitatively weak foliation observed in this area and by corollary mafic enclaves measured in this area are representative of an undeformed state. Hence, the mafic enclave axial ratios in this area may record a component of mafic enclave initial shape obliquity, which they may preserve as a consequence of their formation and injection characteristics.
4. **Lower values** - The Fry strain generally shows lower values compared with mafic enclave axial ratios (Figure 2.15a, b compared with Figure 2.15a, b and Figure 2.15d): This may be a consequence of; i) a degree of enclave initial axial ratio; ii) the mafic enclaves 'seeing' more emplacement related strain, as a result of crystallisation and evolution of the magma fabric i.e. fabric development may occur at some time after initial magma and enclave emplacement; iii) the homogenous outcrop bulk emplacement strain recorded by enclaves is accommodated heterogeneously across the outcrop and not 'seen' at the scale used for Fry strain determination (often less than 10cm); iv) transfer of particles into and out of the strain plane during deformation, inhibiting the anisotropic development of a fabric.
5. **Flattening strain** - The Fry strain values demonstrate flattening strain ($0 < K < 1$) across the pluton, except along the southern contact where the fabric is modified by the overprinting Main Donegal Granite shear zone.

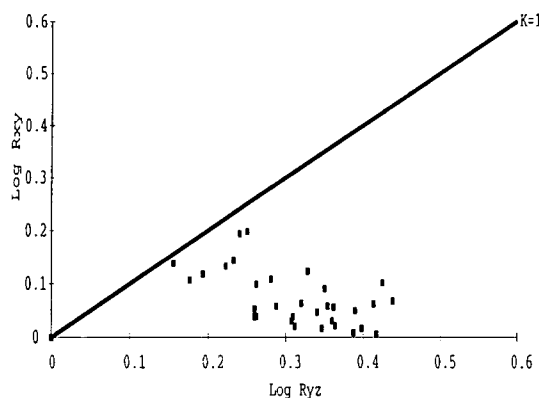
a) Horizontal plane Fry strains



b) Vertical plane Fry strains



c) Log-Flinn plot for Fry strains



d) Enclave axial ratio vs. Fry strain

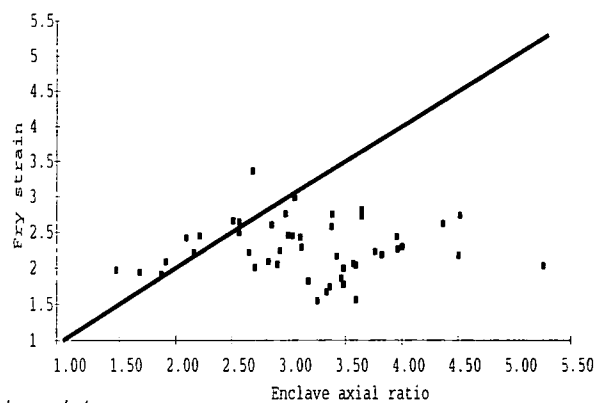


Figure 2.15

Fry fabric strains from the Ardara pluton

6. Correlation with mafic enclave finite strains - Figure 2.15d demonstrates a positive correlation between recorded increases in mafic enclave axial ratio finite strain and Fry strains from across the pluton.

Table 2.5 Table of Fry strains from the Ardara pluton

Locality	Grid Ref.	Pluton	Orientation	Fry strain	Number of analyses	Smallest Fry reading	Largest Fry reading	Log K-value
A0	GR 72789221	G2	HORIZ	3.20	6	2.33	4.48	0.15
A0	GR 72789221	G2	VERT	2.74	5	2.27	3.43	
A2	GR 72759279	G1	HORIZ	2.99	4	2.01	3.13	0.19
A2	GR 72759279	G1	VERT	3.36	4	1.15	3.65	
B1	GR 71689248	G1	HORIZ	2.26	4	1.96	2.46	0.12
B1	GR 71689248	G1	VERT	2.44	4	1.96	2.44	
B5	GR 71269336	G2	HORIZ	2.37	4	2.03	2.39	0.12
B5	GR 71269336	G2	VERT	2.04	4	1.92	2.27	
B6	GR 70789380	G1	HORIZ	2.58	3	2.35	3.00	0.16
B6	GR 70789380	G1	VERT	2.53	4	1.56	2.68	
C1	GR 71949842	G1	HORIZ	2.35	4	1.67	2.49	0.10
C1	GR 71949842	G1	VERT	2.03	4	1.71	2.50	
C3	GR 72629846	G1	HORIZ	2.49	4	2.03	2.93	0.02
C3	GR 72629846	G1	VERT	2.44	4	2.03	2.87	
C4	GR 73089861	G2	HORIZ	2.45	4	1.89	2.85	0.11
C4	GR 73089861	G2	VERT	2.75	4	1.99	3.32	
C7	GR 73599793	G2	HORIZ	2.43	6	1.62	2.86	0.08
C7	GR 73599793	G2	VERT	2.41	6	2.07	3.19	
D1	GR 70329569	G1	HORIZ	2.06	6	1.68	2.64	0.21
D1	GR 70329569	G1	VERT	1.91	7	1.16	2.31	
D4	GR 72119527	G3	HORIZ	1.60	3	1.41	2.91	0.90
D4	GR 72119527	G3	VERT	1.43	4	1.37	1.57	
E1	GR 80789608	G1	VERT	2.23	2	1.50	2.18	
E7	GR 79639407	G2	HORIZ	2.43	4	1.49	3.06	0.06
E7	GR 79639407	G2	VERT	2.31	4	1.85	2.86	
F1	GR 76789151	G1	HORIZ	1.86	3	1.81	1.91	0.10
F1	GR 76789151	G1	VERT	2.00	4	1.96	2.04	
G2	GR 71009749	G1	HORIZ	1.55	2	1.45	1.65	0.44
G2	GR 71009749	G1	VERT	2.19	2	1.90	2.48	
G4	GR 70429637	G2	HORIZ	2.01	4	1.87	2.14	0.05
G4	GR 70429637	G2	VERT	2.09	2	1.84	2.33	
G5	GR 71699720	G2	HORIZ	2.16	2	1.62	2.69	0.29
G5	GR 71699720	G2	VERT	2.98	2	2.74	3.21	
H3	GR 74639874	G1	HORIZ	2.56	7	2.60	1.73	0.14
H3	GR 74639874	G1	VERT	2.82	8	1.95	3.84	
H5	GR 74659825	G3	HORIZ	2.09	4	1.64	2.27	0.17
H5	GR 74659825	G3	VERT	2.04	4	1.79	3.00	
H6	GR 74029813	G2	HORIZ	2.32	6	1.81	2.63	0.21
H6	GR 74029813	G2	VERT	2.80	6	1.94	3.46	
I5	GR 71889419	G3	HORIZ	1.94	4	1.30	2.38	0.17
I5	GR 71889419	G3	VERT	2.22	4	1.00	2.44	
J3	GR 76329753	G1	HORIZ	2.27	3	2.08	2.60	0.60
J3	GR 76329753	G1	VERT	1.67	4	1.43	2.02	
J4	GR 77089693	G2	HORIZ	1.78	4	1.47	2.18	0.44
J4	GR 77089693	G2	VERT	2.53	4	2.54	3.37	
J5	GR 78149665	G1	HORIZ	2.65	8	2.34	3.72	0.02
J5	GR 78149665	G1	VERT	2.90	8	1.79	3.58	
K4	GR 77619632	G1	HORIZ	1.82	6	1.63	2.06	0.13
K4	GR 77619632	G1	VERT	1.99	6	1.64	2.35	
L1	GR 75979704	G2	HORIZ	2.75	5	2.23	2.98	0.04
L1	GR 75979704	G2	VERT	2.79	5	1.70	3.28	
L4	GR 75469499	G3	HORIZ	2.74	4	3.50	2.45	0.15
L4	GR 75469499	G3	VERT	2.59	4	3.30	1.93	

Locality	Grid Ref.	Pluton	Orientation	Fry strain	Number of analyses	Smallest Fry reading	Largest Fry reading	Log K-value
L7	GR 73769186	G2	HORIZ	2.61	4	2.64	3.00	0.81
L7	GR 73769186	G2	VERT	1.79	4	1.76	1.81	
M6	GR 79539323	G2	VERT	3.04	4	2.68	3.57	
N3	GR 74139629	G3	HORIZ	2.38	4	1.97	2.62	0.62
N3	GR 74139629	G3	VERT	1.71	4	1.25	2.30	
O2	GR 71589319	G2	HORIZ	2.29	10	1.60	3.09	0.05
O2	GR 71589319	G2	VERT	2.39	10	1.19	2.76	
O4	GR 73469227	G2	HORIZ	2.05	6	1.31	2.60	0.61
O4	GR 73469227	G2	VERT	1.56	6	1.24	1.82	
P5	GR 73349560	G3	HORIZ	2.11	4	1.51	3.47	0.38
P5	GR 73349560	G3	VERT	1.91	4	1.89	2.02	
Q1	GR 81049444	G1	HORIZ	1.92	4	1.69	2.29	0.61
Q1	GR 81049444	G1	VERT	1.50	4	1.36	1.67	
Q5	GR 81849580	G1	HORIZ	2.05	4	1.11	3.33	0.17
Q5	GR 81849580	G1	VERT	2.15	4	1.74	2.44	
S3	GR 75139359	G3	HORIZ	1.56	2	1.00	2.12	0.18
S3	GR 75139359	G3	VERT	1.72	2	1.72	3.00	
S6	GR 73469230	G3	HORIZ	2.36	2	2.36	3.27	0.18
S6	GR 73469230	G3	VERT	2.07	2	1.81	2.32	

2.3.3 Strain measurement in the country rocks

Making finite strain estimates for deformation recorded in the wallrocks of a pluton is problematic because there are quantification difficulties e.g. nature, type and rheology of any pluton induced, or previous polyphase, deformation. The deformation, stratigraphy and petrography of the Ardara pluton aureole is known in great detail, as a result of the work of Iyengar *et al* (1954), Akaad (1956a, b) and Meneilly (1981,1982) and it is therefore possible to identify and partially quantify the deformation related to intrusion using this comprehensive dataset.

The deformation event D₄, as developed around the pluton (Meneilly 1981, 1982), is regarded as being coeval with the emplacement of the granite. Therefore, by making finite strain estimates based on the degree of deformation associated with the development of D₄ structures (S₄ cleavages and F₄ folding), it should be possible to quantify the wallrock shortening associated with emplacement. The methods used in this process are outlined below:

Restoration of cross sections

Around the northern section of the pluton (Map 1, Figure 2.18, Clooney Hill to Meenalargan area, GR 720980, GR 720010, GR 820010, GR 800960) both Iyengar *et al* (1954) and Meneilly (1981, 1982) detailed the northwards deflection of the country rocks and intensification of the folding associated with intrusion of the pluton. In particular Meneilly (1981, 1982) demonstrates that these structures are dominantly D₄ in age, but preserve remnant earlier D_{2/3} structures.

In an attempt to deduce some of the shortening associated with intrusion, an interpreted cross section drawn across the maps of Meneilly (1981) (from Maas GR 764980 to Letermacaward GR 800805) was made (Figure 2.16). This shows a steeply inclined F₄,

Maas syncline, close to the pluton contact and a northerly facing Mulnamin anticline. Then using a marker horizon across the section of Mulnamin calc-silicates (shown in Meneilly 1982 Figure 5) this section was restored to an original 30° southerly dip. A summary of the data is shown below:

- | |
|--|
| Estimated folded length = 3.3 km |
| Estimated unfolded length = 4.4 km |
| ⇒ 1.1km of space created |
| ⇒ 25 % shortening over 4 km. |
| ⇒ $R_{xz} = R_{yz} = 1.53$ (assuming a constant volume shortening) |

These results show that over the measured section 1 km of shortening for the pluton may have been accommodated by large scale folding. However, there are a number of problems associated with this method: in particular, are the F_4 folds merely amplifying $F_{2/3}$ folds (Pitcher & Berger 1972), did the country rocks initially dip weakly to the south before intrusion of the granite, the effect of S_4 cleavage formation (possible volume loss) in the inner aureole and the effects of granite emplacement to the north e.g. Trawenagh Bay granite, on the development of D_4 structures.

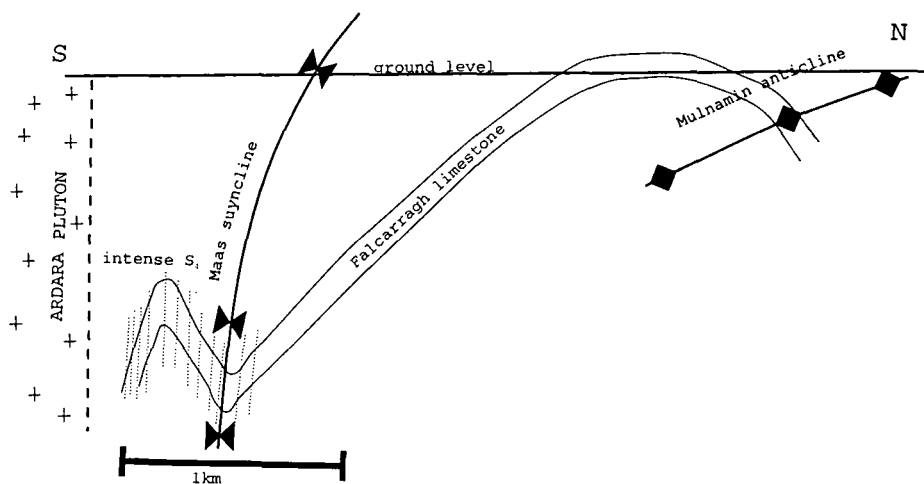


Figure 2.16, Interpreted cross-section across the north- west aureole of the Ardara pluton GR 764980 to GR 800805 (after country rock mapping by Meneilly 1981)

In the light of the problems of quantifying country rock deformation north of the pluton, a study of D_4 features around the west of the pluton (on the Dawros and Loughros peninsulas) was undertaken because this area displays fewer stratigraphical changes than elsewhere around the pluton (country rocks are almost entirely the Falcarragh pelite), no post-Ardara granite emplacement, and no major regional structures. In addition, the early deformation hierarchy is well understood through the work of Cheesman (1952) and Meneilly (1982). Three methods were used to assess how the amount of deformation changes with distance from the pluton contact:

Line rotation

The maps of all workers in the aureole region (primarily Meneilly 1981, 1982, with additional data from Cheesman 1951 and Akaad 1956a, b) were used to produce a principal foliation map (Figure 2.17a). This map corresponds to the S_2 orientation but, close to the pluton these structures are difficult to identify, importantly Pitcher & Berger (1972) demonstrate that earlier structures are deflected to become sub-parallel to the D_4 of Meneilly (1981, 1982) in the 500m closest to the pluton contact. Therefore for the purposes of these calculations bedding is taken to have rotated into parallelism to the granite at and within 500m of the contact. The principle features of the map are; i) a regional strike approximately east-west (around 105°); ii) the development of a foliation 'triple junction', point 'T' (GR 690950, Figure 2.17a) with a northwards deflection around a southerly plunging antiform and a southwards deflection around a northerly plunging antiform.

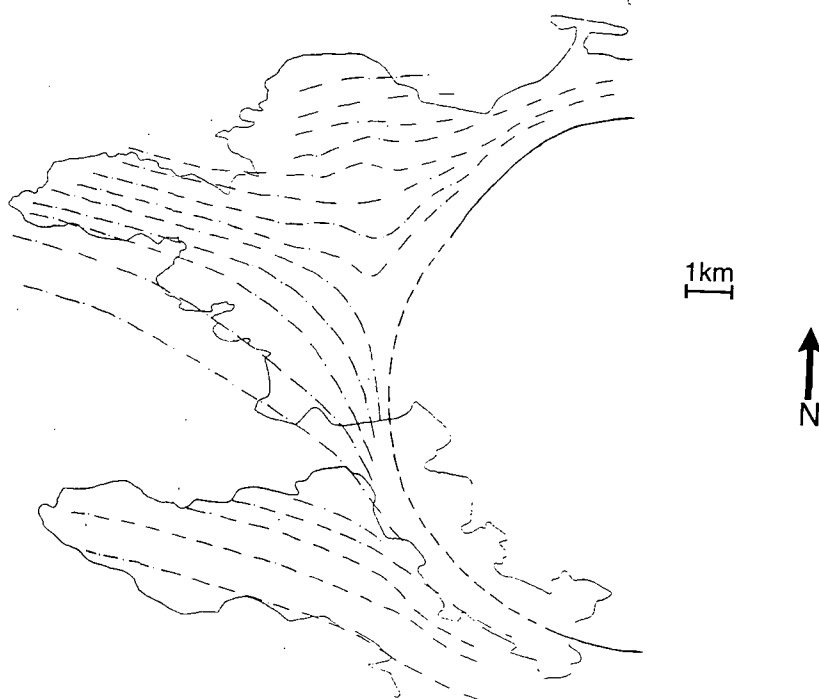
In order to quantify the finite strain associated with deformation it was assumed that any deflection of the regional country rocks occurred as a result of stress applied by the expanding Ardara pluton. This deflection represents a strain which can be quantified using the equation of Ramsay (1967) (Equation 2.4), where the principal shortening plane (X-plane) is defined as a circular projection of the pluton margin (Figure 2.17b). In this calculation an assumption is made that expansion occurred from an initial magma body which had a similar shape to the final pluton.

$$\text{Equation 2.4, } R_1 \cdot \tan \theta' = \tan \theta \cdot R_2$$

where R_1/R_2 is the axial ratio of the strain ellipse, θ the angle made with the x-axis before deformation and $\tan \theta'$ the angle made with the x-axis after deformation.

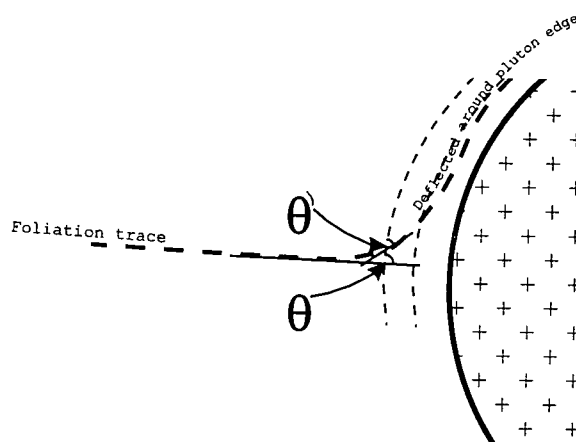
Note: this assumes 2-D deformation, given the entirely flattening nature of strain within the pluton, it is reasonable to assume that deformation transferred outside the pluton will also be flattening.

Using this method a dataset was created which details the emplacement induced finite strain across the western side of the aureole (Figure 2.18a, b, symbol=diamonds, Table 2.3). In particular, note a decrease in shortening from 70-100% ($\infty < R_{xz} < 1.8$) within 500m of the contact (where D_4 is most intense) to about 30% ($R_{xz} \sim 1.2$) at 2 km, where the deflection of the country rocks as a result of emplacement is at its weakest. Note that this dataset shows a high variability in the values recorded. This is a function of the maps used, and local variations in the stress field during emplacement caused by the presence of basic appinites, which have induced heterogeneities into the homogeneously deforming pelitic country rock.



a) Principal foliation map

a1



b) Measuring finite strain associated with line deflection during pluton emplacement

Figure 2.17

Cleavage, folding and thrust development

Between 750m and 2.5km from the pluton contact, a pervasive S_4 cleavage is developed. An examination of these cleavages in thin section suggests that between 20% and 50% shortening may have occurred during their formation. A conservative estimate of 20% is used in all further calculations.

Throughout this same area F_4 folding is developed which results in additional shortening of the wallrocks. The shortening associated with this folding has been estimated

Table 2.5 Line deflection data for wallrocks around the Ardara pluton

Distance from contact / km	Strain	% Shortening	Distance from contact / km	Strain	% Shortening
0.22	13.38	82.26	0.86	2.20	40.88
0.22	15.58	83.97	0.86	3.28	54.70
0.22	14.03	82.81	0.87	15.87	84.17
0.22	>100.00	95.36	0.87	18.60	85.76
0.22	15.58	83.97	0.87	7.00	72.67
0.25	4.40	62.76	0.87	3.78	58.79
0.25	2.91	50.94	1.06	2.06	38.23
0.25	1.44	21.58	1.08	1.22	12.46
0.38	15.31	83.78	1.08	3.21	54.05
0.38	3.55	57.03	1.08	1.97	36.37
0.38	3.27	54.61	1.08	1.89	34.58
0.43	3.26	54.52	1.09	9.30	77.39
0.43	12.93	81.85	1.09	4.04	60.58
0.43	4.29	62.12	1.09	2.22	41.24
0.43	>100.00	95.36	1.09	2.22	41.24
0.43	3.06	52.56	1.09	13.36	82.24
0.43	7.24	73.28	1.29	1.39	19.71
0.44	>100.00	95.36	1.29	1.58	26.28
0.44	9.43	77.60	1.30	6.61	71.61
0.44	8.46	75.91	1.30	5.91	69.41
0.50	5.03	65.94	1.30	4.59	63.79
0.63	4.83	65.00	1.30	2.30	42.61
0.63	4.01	60.38	1.72	2.30	42.61
0.63	2.37	43.74	1.72	2.74	48.93
0.65	9.67	77.97	1.72	1.67	28.96
0.65	1.59	26.59	1.72	1.31	16.47
0.65	2.04	37.83	1.72	1.38	19.32
0.65	2.67	48.04	1.72	1.79	32.17
0.65	6.28	70.62	1.72	5.49	67.87
0.66	7.26	73.33	1.72	8.93	76.77
0.66	9.44	77.61	1.72	2.40	44.21
0.66	7.55	74.01	2.15	1.07	4.41
0.75	2.44	44.83	2.15	1.77	31.66
0.75	3.89	59.57	2.15	2.74	48.93
0.75	4.07	60.77	2.15	4.03	60.51
0.83	8.50	75.99	2.15	2.36	43.59
0.83	4.76	64.66	2.15	2.29	42.44
0.83	4.67	64.21	2.15	2.52	46.00
0.83	4.07	60.77	2.15	13.35	82.23
0.85	10.42	79.04	2.15	2.15	39.97
0.86	1.37	18.77	2.58	1.61	27.20
0.86	2.93	51.16	2.58	1.68	29.24

from data collected between Portnoo Harbour and Dumore Head (GR 702995 to GR 688001) by D. Hutton (Appendix 4). This results in a composite shortening composed of both cleavage development and folding, the resultant shortening was estimated by summing these values and is shown by the crosses in Figure 2.18a, b. Additionally, there are a

number of minor south dipping thrusts which are highly heterogeneous in development, notably around Naran Hill (GR 711985), but their throws and pervasiveness are unknown and any further shortening related to these features is very difficult to quantify and has not been used in this analysis. These data demonstrate shortenings approaching 30% at 1.7km reducing to 20% at 2.5km.

Folding

Further westwards from the pluton margin the S₄ cleavage is not developed, but F₄ folds are still common. These F₄ folds are open, upright buckle-type folding, measurements of the shortening associated with these folds (data from D. Hutton, Appendix 4) along a traverse from Rosbeg Harbour to Dawros Head (GR 664971 to GR 636978) have been made (symbol=closed triangles, Figure 2.18a, b). These show an obvious decrease in the intensity of deformation from 2.7km to 4km from the pluton contact.

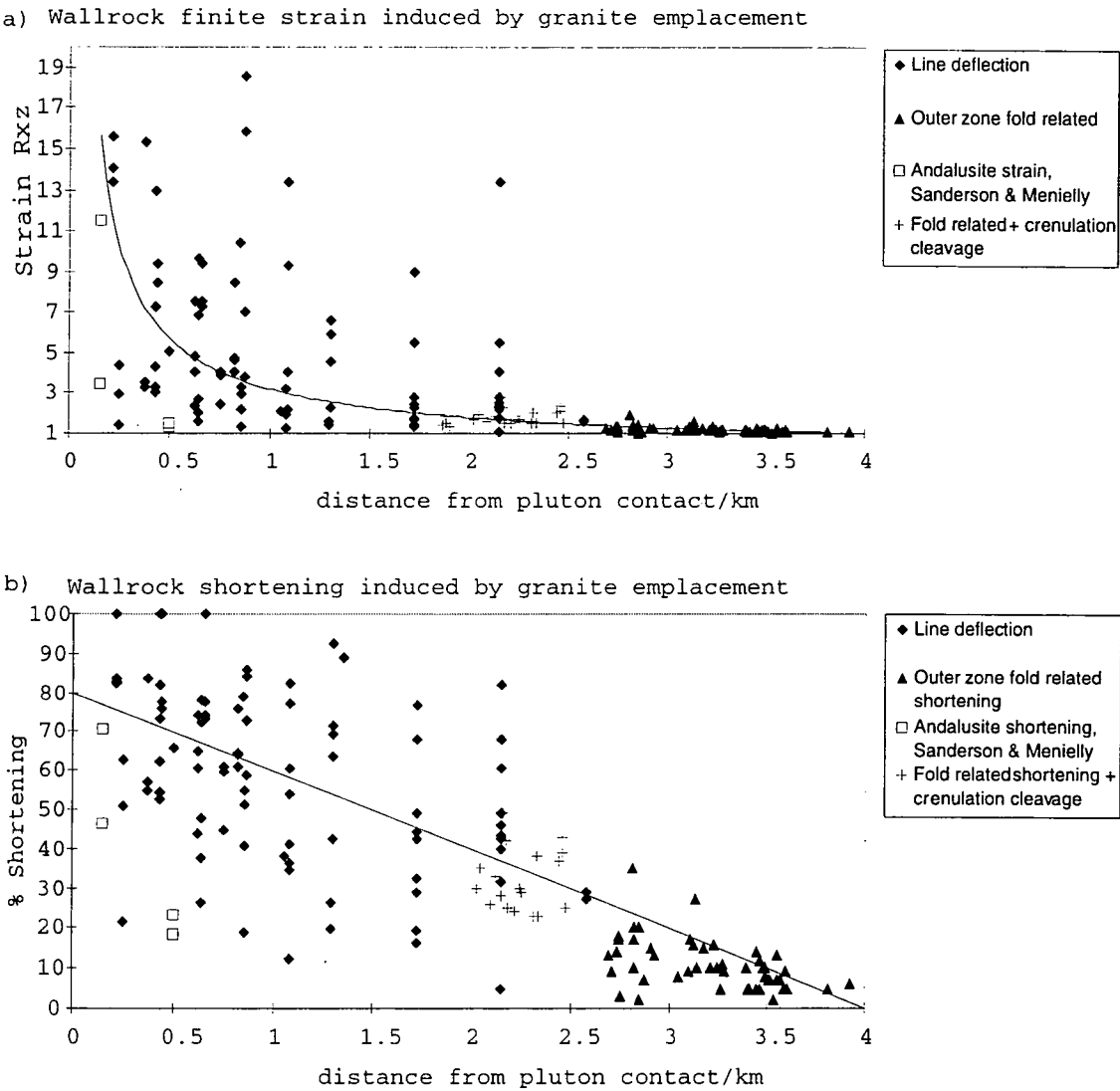


Figure 2.18

Conclusions

Collating the information from all the techniques used to quantify the finite strain in the country rocks shows an almost exponential decrease (Figure 2.18a) from very high finite strains in the inner aureole (less than 750m from contact) through to minor finite strains in the outer rocks 4km from the contact. Examining this data in terms of shortening, similarly shows very high shortening in the inner aureole (70-100%) through to less than 10% at 4km. This decrease in shortening can be approximated to a straight line.

Figures 2.18a, b also show the thermal andalusite finite strain data of Sanderson & Meneilly (1981): These data always plot below the country rock deflection data because; i) thermal andalusites will nucleate slowly, by which time significant deformation may have taken place; and ii) andalusites may not nucleate randomly, homogeneously or rotate freely during deformation. Hence, finite strain estimates using this data underestimate other strain calculations.

2.3.4 Discussion

The finite strain accommodated during emplacement of a pluton is difficult to determine, a number of methods have been used to attempt to reliably quantify the bulk strain/shortening associated with the emplacement of the Ardara granite. A number of these results require additional discussion:

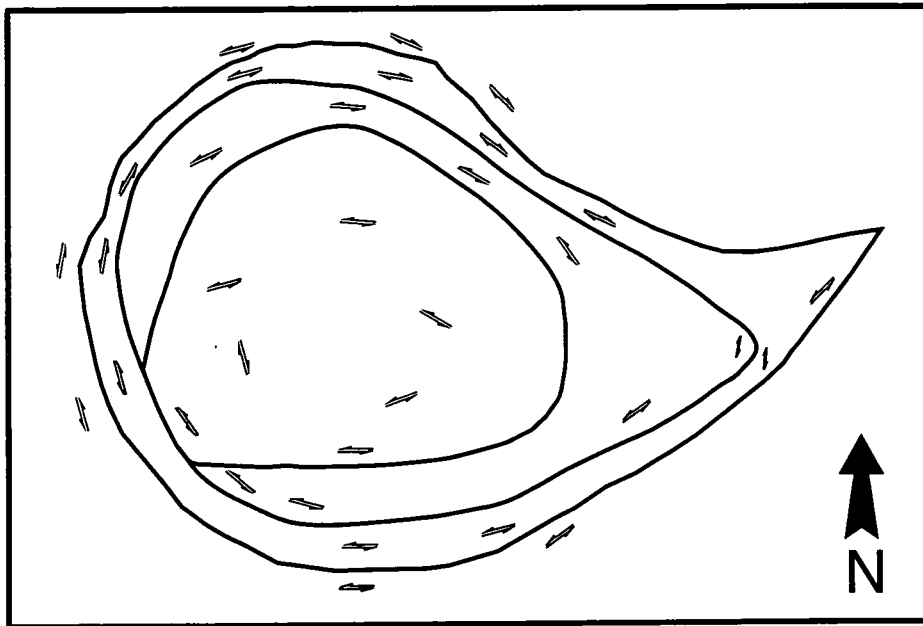
1. **Microgranitoid enclave finite strain** - The axial ratio trends show increases from the 'injection point' to the pluton contacts. This is interpreted to be equivalent to the strain recorded during emplacement, assuming the enclaves were subspherical before and during early stages of emplacement. A number of workers dispute this statement (see Fowler & Paterson 1997 for a review), suggesting that the more mafic enclaves would freeze on contact with the granite and, at the very least show a significant underestimate of the finite strain recorded by the granite. Specifically referencing the Ardara pluton, Vernon & Paterson (1993) suggest that the wide variation in enclave axial ratio across an outcrop suggests different strain paths, a wide variability in initial shape ratio and the general inadequacy of this method of strain measurement. The data detailed above demonstrates that the statistical analysis of such enclave populations leads to useful and consistent results, with widespread applicability, providing the limits of the dataset are well understood (see also Brun *et al* 1990).
2. **The Fry method** - Using the Fry method of quantifying the emplacement strain in the fabric demonstrates that the mafic enclave axial ratios are recording genuine variations in the intensity of the magmatic fabric. However in detail there is a wide variability in the quality of the data produced by this method which may occur for reasons such as fabric heterogeneity during deformation and crystallisation or fabric re-

setting/recrystallisation. Used with appropriate caution the Fry method can demonstrate finite strain variation across a magmatically deformed pluton.

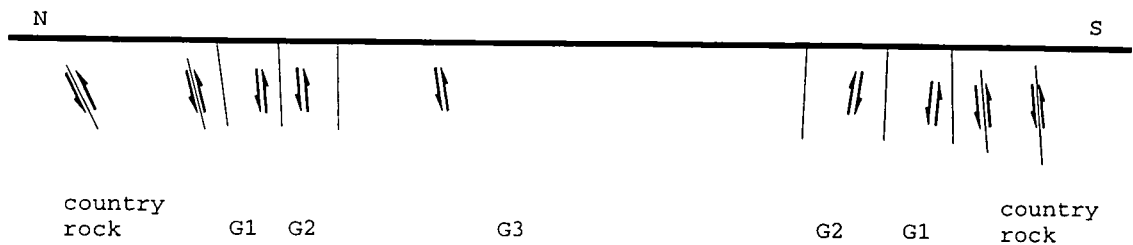
3. **Inner aureole finite strain** - Field observations from the inner aureole suggested very high finite strains in the thermal aureole, the 500m closest to the pluton. This focusing of deformation may have occurred as a result of a non-Newtonian, power-law, type rheology focusing deformation close to the pluton, possibly as a result of thermal, strain or hydrolytic weakening and allows the postulation of extremely high strains in this area.
4. **Remainder of the country rock finite strain** - Meneilly (1982) demonstrated that emplacement related deformation was widely but heterogeneously developed up to 7km from the pluton. Through additional foliation deflection measurements and interpretations of D₄ related shortening fabrics from around the pluton, it has been shown that a large amount of shortening was accommodated across this zone (Figure 2.18a, b). The space creation for the pluton took place over a wide area.
5. **Andalusite strain** - Sanderson & Meneilly (1981) attempted to show the finite strain recorded due to the rotation and alignment of andalusite porphyroblasts. Their results (Figure 2.18a, b symbol = open squares) significantly underestimate the strain recorded by the fabric itself, it is postulated that there may be a number of reasons for this; i) andalusite nucleation requires energetically favourable conditions, which may not have been attained until significant deformation had already taken place; ii) the work of both Holder (1979) and Kerrick (1987) demonstrated that andalusites grew in 2 or 3 stages, each of which probably changed their associated fabric; and iii) andalusites may not have had the initially random alignment as suggested by Sanderson & Meneilly (1981), indeed observations suggest that andalusites may show a preferential original alignment along S_{2/3} (Hutton *pers comm*).

2.4 Shear sense

A compilation of measured shear senses has been made using country rock, magmatic state and solid state granitic shear sense indicators, from coeval deformations. The results divide into three zones, described below. A summary plot of the data is given below where; Figure 2.19a shows the horizontal plane shear sense, Figure 2.19b shows a north-south cross-section through the pluton and Figure 2.19c resolves these shear senses into *material movement direction*. Where the *material movement direction* is a projection of the composite three-dimensional direction that the innermost material would move with respect to the outermost.

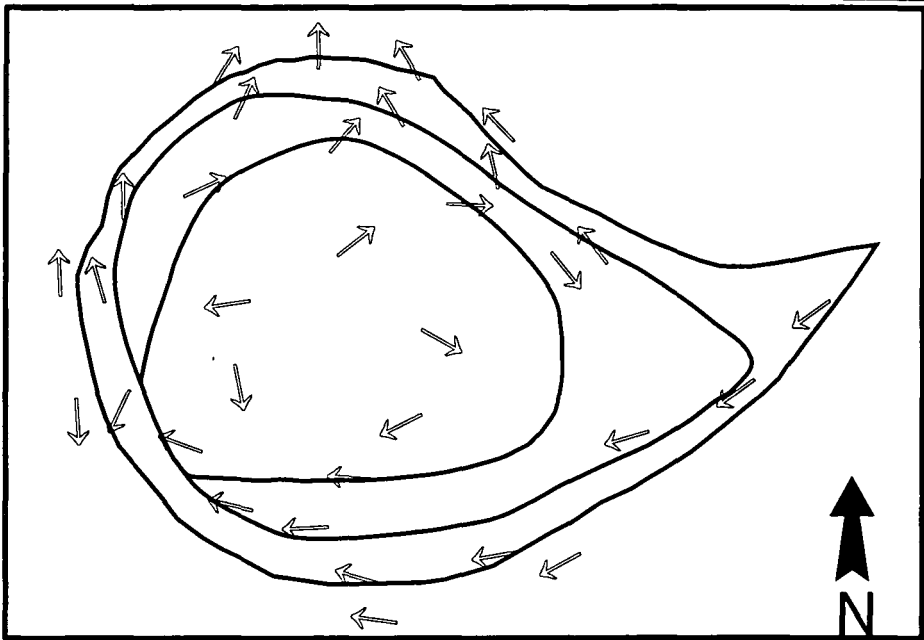


a) Granitic and country rock shear senses from XZ / horizontal outcrop plane.



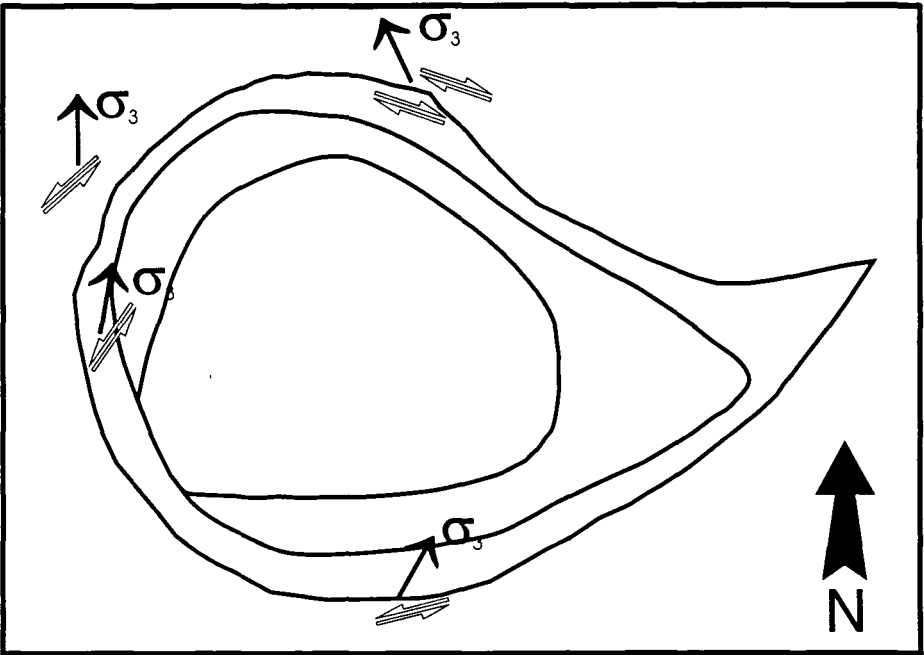
b) North-south cross-section through the pluton showing representative YZ granitic and country rock shear senses.

Figure 2.19



Arrows represent resultant relative material translation vector of the inner material of the outer material.

c) Resolving shear sense data into apparent material movement directions



d) Sketch of average orientations of emplacement related granitic and country rock shear sense indicators

Figure 2.19

2.4.1 Western area

The western area is defined as representing the granite and aureole rock between grid references, GR 735010, GR 690010, GR 750900 and GR 690900.

Granite shear sense

Granitic shear senses have been measured using tiling fabrics and solid state shear sense indicators: These fabrics do not display a lineation, but show a weak sinistral sense of

shear (Plate 2.5) in the horizontal plane of outcrop and a weak top to the outside of the pluton (west through to north) in the vertical plane. In addition, the outer 50-70m of the granite shows intrusion by multiple, later minor appinitic and lamprophyric dykes which preserve a sinistral sense of shear (Plate 2.6) along an average plane of 326°/84°E (Figure 2.20), which suggests an orientation of approximately North, ~010° for σ_3 (Figure 2.19d)

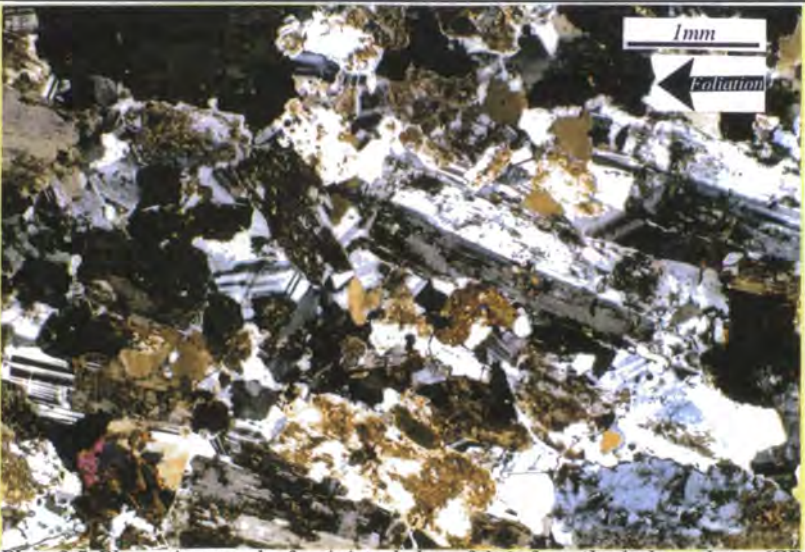


Plate 2.5 Photomicrograph of a sinistral shear fabric from the Ardara pluton (GR 70329569)

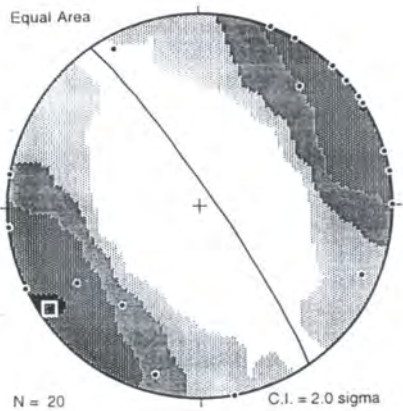


Figure 2.20 Contoured stereonet of poles to planes of sinistral intrusive dykes

Country rock shear sense

The country rock around the pluton, where deformed by the intensive D₄ foliation, records well developed sinistral shear sense indicators all along the western zone (Figures 2.21, Plate 2.7). These show an average plane of 136°/72° E, suggesting a σ_3 orientation of approximately due North, ~000° (Figure 2.19d). In association with these strike slip shear zones are a number minor thrusts with top to the north directed displacements and associated lineations (Figure 2.22a, b, Plate 2.8)



Plate 2.6 Photograph of sinistral shear senses recorded by lamprophyric dykes (GR 70519394)



Plate 2.7 Sinistral country rock shear sense indicator from the Western area, Ardara pluton (GR 70019653)

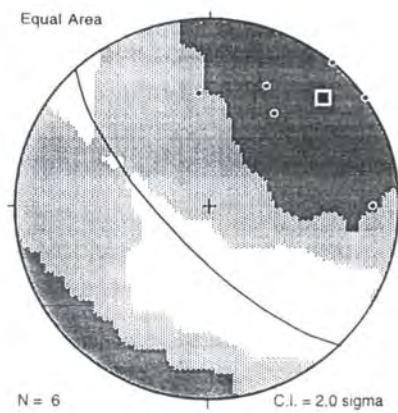
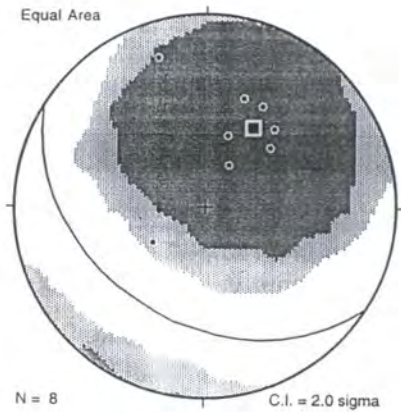


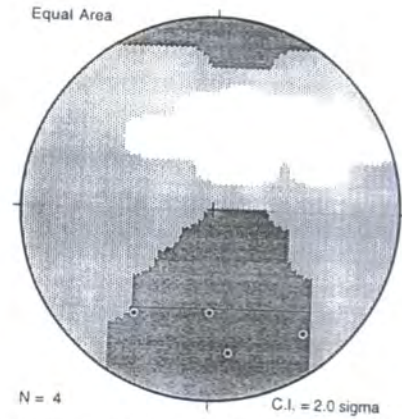
Figure 2.21 Contoured stereonet of poles to planar country rock sinistral shear sense indicators from the Western area, Ardara pluton

Interpretations

This area was intensely deformed during the intrusion of the magma. The non-coaxial shear fabrics show that during emplacement, the material movement direction (Figure 2.19c) on the north and northwest sides of the pluton, was directed northwards. This is recorded as the extension (least compressive stress) orientation in the country rocks and late-emplacement fabrics; around the western side of the pluton the material transport direction is directed southwards, which is consistent with country rock deflection fabrics in this area (Cheesman 1951, Hutton *pers comm*).



a) Contoured stereonet of poles to minor thrust planes from around the northern part of the Ardara pluton.
Figure 2.22



b) Contoured stereonet of mineral stretching lineations associated with Figure 2.22a



Plate 2.8 Top to the north directed minor thrust from the northern part of the Ardara pluton (GR 72910055)

2.4.2 Eastern area

The eastern area is defined as representing the granite and aureole rocks defined by the co-ordinates GR 735010, GR 795980, GR 795940 and GR 735960.

Granite shear sense

The intrusive phases throughout this area develop no lineation, but record weak dextral magmatic state and solid state shear sense fabrics in the horizontal outcrop plane (Plate 2.9) (Figure 2.23). In the vertical plane, perpendicular to foliation, they record top to the north-northeast material transport. There are no syn-magmatic intrusive features (cross-cutting appinite or lamprophyres) in this area.

Country rock shear sense

Country rock fabrics record weak top to the north directed thrusting (Plate 2.8, Figure 2.22a, b) and a dextral shear sense with an average plane orientated $110^{\circ}/78^{\circ}$ S (Plate 2.9, Figure 2.23), which suggests an orientation of approximately $\sim 335^{\circ}$ for σ_3 (Figure 2.19d).

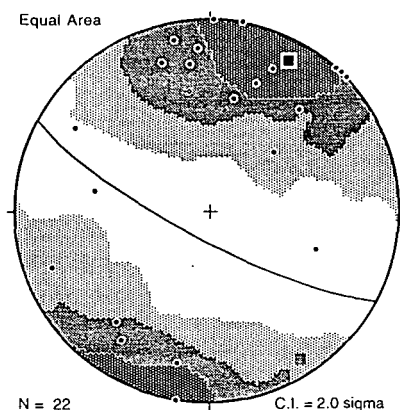
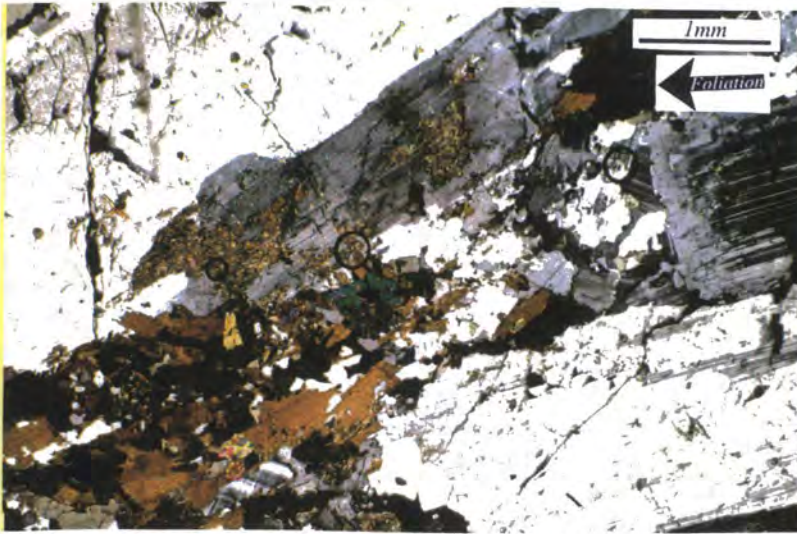


Figure 2.23 Contoured stereonet of poles to planar dextral fabrics from the Eastern area, Ardara pluton

Interpretations

During granite emplacement there was intense non-coaxial deformation which resulted in dextral shear fabrics and top to the north directed thrusting, defining northwards and outwards material movement directions (Figure 2.19c). These define the local extension axis (least compressive stress) as being orientated approximately northwest to north-northwest.



a) Photomicrograph of dextral shear fabric from the Eastern area, Ardara pluton (GR 74639874)



b) Dextral country rock fabric from the Eastern area, Ardara pluton (GR 75879906)

Plate 2.9

2.4.3 Southern area

The southern area is defined as representing the granite and country rocks along the southern contact zone between the co-ordinates GR 730915, GR 810960, GR 830940 and GR 730900.

Granite shear sense

The intrusive phases along this contact preserve a sinistral magmatic sense of shear (Figure 2.19a, b, c), which has been overprinted by a lower temperature (~300°C using the criteria of Passchier & Trouw 1996), solid state sinistral shear, with a sub-horizontal lineation (Figure 2.24) which displays a variable vertical transport direction (Figure 2.19b). This solid state deformation (Plate 2.10) becomes more intense towards the village of Glenties, where a high intensity, gneissic, solid state fabric, with rare highly deformed apophyses and xenoliths of the Main Donegal Granite may be preserved. Deformation in the magmatic state is correlated with intrusion of the pluton, but the lower temperature

solid state deformation is associated with continued movement along the bounding shear zone during intrusion of the later Main Donegal Granite (Hutton 1982a).

Country rock shear sense

The country rock is generally poorly exposed throughout this area, but when structures can be observed, they consist of partitioned zones of either; a) intense sinistral shear with a low angle lineation (Figure 2.24); or b) zones of pure shear with upright, folding verging weakly to the north (Plate 2.11).

Interpretation

These are all features consistent with a local regional sinistrally transpressive shear zone, which was active during and post-emplacement of the Ardara pluton, both within and without the granite itself.



Plate 2.10 Sinistral solid state deformation from the Southern area, Ardara pluton (GR 79539223)

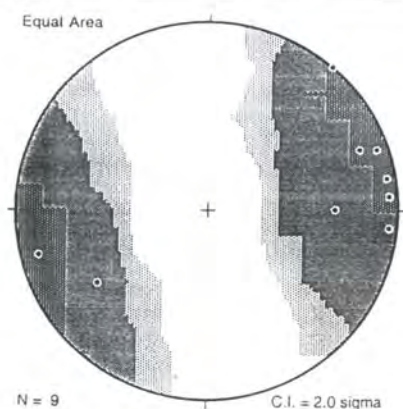


Figure 2.24 Contoured stereonet of mineral stretching lineations from the Southern contact area, country rocks and granite, Ardara pluton.



Plate 2.11 Steep folds verging weakly northwards from the Southern area, Ardara pluton (GR 75439081)

2.4.4 Central area

The central area comprises of the remaining parts of the granite pluton, and is considered to be the phases G2 and G3.

Granite shear sense

The fabric in this area has been formed entirely in the magmatic state, but has a very low intensity and hence shear sense determinations are difficult to obtain (Figure 2.19a, b, c). The results obtained demonstrate weak sinistral shear in the horizontal plane, and occasionally developed very weak top to the north directed transport in the vertical plane.

Interpretations

The material movement directions estimated from these fabrics (Figure 2.19c) demonstrate lateral expulsion of material from a central supply zone during a regional sinistral shear: This deformation of G2 and G3 was partitioned from the outer phase, G1. It is suggested that this partitioning took place because G1 was already partially solidified during the emplacement of G2 and G3 and probably more closely coupled to deformation in the country rocks.

2.4.5 Cross-cutting foliations

The maps (Figure 2.8 and Map 1) show that the granitic fabric often cross-cuts the internal intrusive phase contacts. Vernon & Paterson (1993) and Paterson & Vernon (1995)

suggest that these cross-cutting fabrics are indicative of a post-emplacement overprinting externally originating i.e. regional tectonic, fabric. The shear sense data collected for this thesis across the pluton demonstrates sinistral deformation along the west side, dextral deformation across the east side and the composite nature of deformation during emplacement. During this type of deformation the foliation will form in an orientation which is controlled by the proportion of magma induced pure shear stress and simple shear stress due to the northern directed expansion. In order to induce an obliquity of the magnitude observed ($\sim 10-15^\circ$), the applied ^{simple.} shear stress needs to be 4% of the magnitude of the pure shear stress, assuming an instantaneous applied force.

A pluton whose emplacement is controlled entirely by internal magma forces, which are coaxial in the country rocks should produce a concentric fabric, coincident with the internal phase boundaries. However a pluton which expands preferentially in a single direction i.e. northwards in the case of Ardara, will induce a component of simple shear in the country rocks and will form a fabric which is orientated to reflect this, i.e. perpendicular to σ_3 (Figure 2.25).

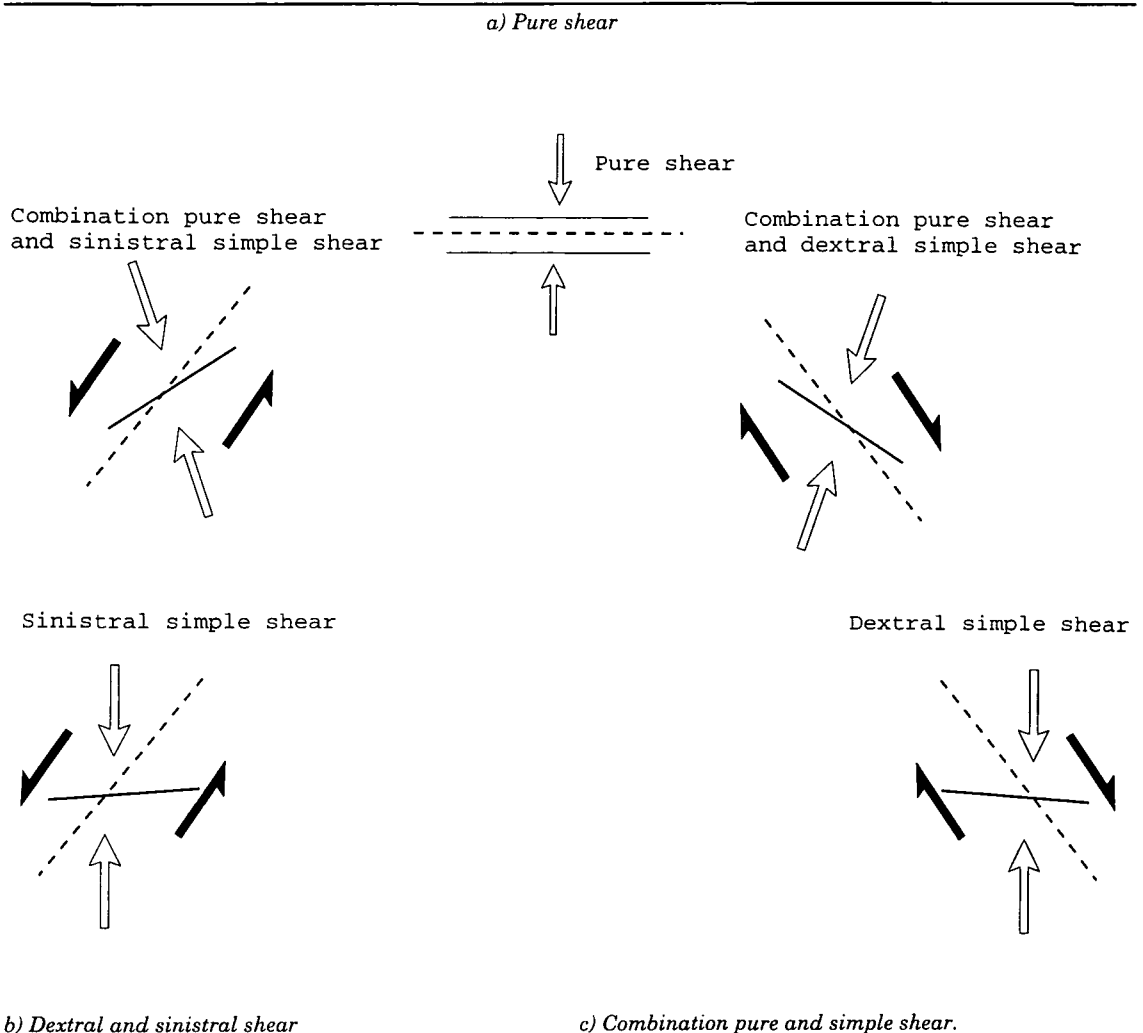


Figure 2.25 Oblique fabric development during non-coaxial shear

2.4.6 Conclusions

The weak shear sense fabrics analysed above record the relative movement of magma and rocks during emplacement. These fabrics describe the lateral transport of magma from the centre of the pluton to the edges and country rock deformation which was strongly coupled with magma transport and expansion. Locally the stress field was determined by the intrusion of magma but the controlling effect of the regional sinistral transpressional shear zone along the southern contact can be seen in many localities deformed in the magmatic state. This demonstrates that this shear zone was active before the intrusion of the younger Main Donegal Granite. In addition the fabrics demonstrate the overprinting nature of deformation related to the emplacement of the Main Donegal Granite.

2.5 Modelling emplacement

The emplacement of the pluton has been modelled using the measured finite strain markers (mafic enclaves, Fry strains) to attempt to constrain the relationship between emplacement volume (volume currently occupied by the pluton) and the space created (volume of pluton which is accounted for through strain measurements). The emplacement volume is modelled as a sphere 8km in diameter (pluton volume = $\sim 265 \text{ km}^3$): a shape estimate which is consistent with the flattening nature of the deformation, and the available geophysical interpretations (Young 1966). This however may not completely reflect the shape of the true pluton because of the influence of the 'tail'.

2.5.1 Country rock finite strain

Part 2.3.3 has already described in detail the strain/shortening accommodated as a result of pluton emplacement within the country rocks. In this section the country rock data will be interpreted in terms of the emplacement of the pluton. Figure 2.18a, b show the shortening/strain across the aureole, with approximately 80% shortening at the contact and negligible finite strain at 4km: the variation in shortening across the aureole can be approximated to a straight line.

The pluton is 4km in radius and therefore assuming a spherical shape for the intrusive body and intrusion from approximately the centre of this body, 4km of shortening in the wallrocks has taken place. The location of the 'injection point', identified in fabric intensity and finite strain determinations is between 3 and 4km from the western pluton contact and therefore, an average of 50% shortening should be accommodated across the whole aureole.

Examination of the line in Figure 2.18b, shows that for approximately 80% shortening at the contact and 0% at 4km, the average would be 40% over the aureole, thereby suggesting that the country rock has accommodated, through quantifiable means the majority of the pluton volume. The error on this determination is significant because of the high variability in the dataset and shortening sufficient to accommodate the entire pluton (average 50%) is within the data distribution identified in Figure 2.18b. A 40% average shortening suggests an initial pluton radius of 1.3km or less.

2.5.2 Granitoid strain

The granitoid strain measurements that were detailed in Part 2.3, have been integrated here in an attempt to quantify the amount of expansion that would be required to induce the observed strains. The Ramsay (1989) balloon model is used which assumes balloon-like inflation of a spheroidal body, a model which is consistent with the nature of finite strain induced (the derivation of the method is outlined below):

When an ideal spherical enclave is incorporated and deformed on the surface of a sphere at constant volume, it will mimic the deformation experienced by the spherical surface. Therefore, if the sphere expands from a radius r to a radius $r+\delta r$, the surface area changes from $4\pi r^2$ to $2\pi(r+\delta r)^2$. The axial lengths of the enclave will change from x to $x+\delta x$, y to $y+\delta y$ and z to $z+\delta z$. Projecting this to the 2 dimensional plane, containing the x and z principle axis of the enclave; the circumference changes from $2\pi r$ to $2\pi(r+\delta r)$ and the axial length from x to $x+\delta x$, hence:

$$(r+\delta r)/r = x+\delta x/x$$

but deformation occurs at constant volume \therefore

$$(x+\delta x)^2.(z+\delta z) = 1 \quad \text{assuming flattening strain}$$

hence the enclave axial ratio becomes :

$$(x+\delta x)/(z+\delta z) = (x.(r+\delta r)/r)^3$$

scaling up shows that :

$$X_f / Z_f = (X_i . (r_f / r_i))^3$$

where X_f / Z_f is the final axial ratio, and r_f is the final radial distance and r_i the initial axial distance and $X_i = 1$, for spherically injected enclaves \therefore

Equation 2.5, $R_f = (r_f / r_i)^3$

where, R_f is the final axial ratio.

This method is similar to that applied by Holder (1979), except in this analysis all enclaves have a magmatic, not meta-sedimentary origin. X_i represents the point at which they were injected/incorporated into the deforming magma, rather than the 'freezing surface' deformation envisaged by Holder.

The contoured finite strain maps for both mafic enclaves and Fry strains (Figures 2.14a, b, 2.15a, b) demonstrate concentrically increasing finite strain from the centre of the pluton to the contacts. The low finite strain centre of the pluton has been identified from fabric and finite strain measurements (Part 2.2, 2.3), and a nominal injection point recognised in the region of the Moolagh townlands. In the analysis this 'injection point' is defined as a point, R_0 where magma is supplied. In order to calculate the incorporation point of each finite strain measurement, R_i , the radial distance, R_f of each population from R_0 is calculated. Then, using equation 2.5, the average incorporation point for this locality can be established, R_i (Figure 2.26). This point is average because it is likely that enclaves within the measured populations will have multiple similar but in detail different strain paths.

The process is repeated for each locality measured, and the point of incorporation is plotted, assuming a radial strain path from the injection point (Figure 2.27a, b). When all localities have been migrated back to their incorporation points, an estimate of the original

shape of the pluton was made using a nearest neighbour interpolation. A geometric mean of the incorporation points and pluton volume estimates based on a spherical pluton are also made at this point.

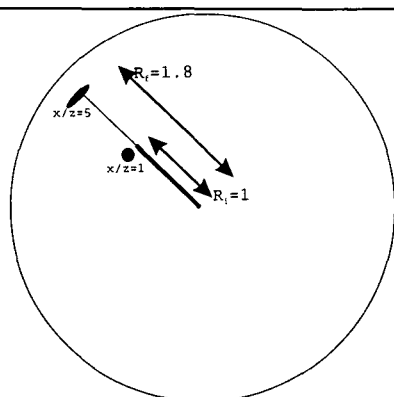


Figure 2.26 Migration of finite strain measurement to their incorporation point

Microgranitoid enclaves

Table 2.6 and Figure 2.27a show that the enclaves were incorporated in a small initial pluton approximately 2km in radius which subsequently expanded its volume by around 90%.

Table 2.6 Migrated finite strain measurements.

Migrated mafic enclave finite strain		Migrated Fry strain	
mean radius / km	1.93	mean radius / km	2.16
St. Dev.	0.82	St. Dev.	0.93
Initial pluton volume / km ³	30	Initial pluton volume / km ³	42
Final pluton volume / km ³	268	Final pluton volume / km ³	268
% ballooning volume	89	% ballooning volume	84

Fry strain

Table 2.6 and Figure 2.27 show that the Fry strain records the formation of a deforming fabric from an initial pluton radius of 2.1km which subsequently expanded resulting in a volume increase through ballooning of 84%.

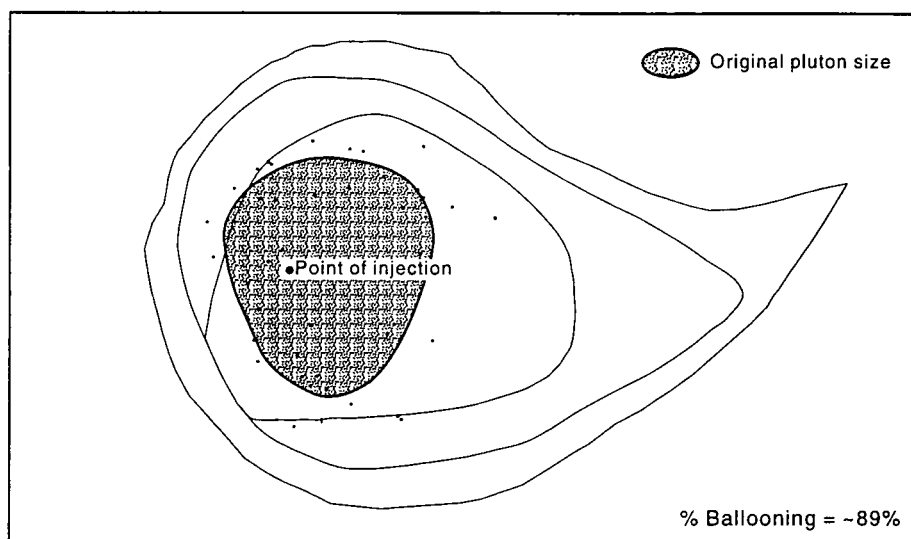
Discussion

This migration process demonstrates the injection of magma into a small central pluton, which subsequently expands in-situ to accommodate the majority of the pluton volume. Some additional points are dealt with in more detail:

1. **Statistical variation** - There is significant variation in the calculated point of incorporation and in the calculated finite strain value, which could result in the initial pluton size being significantly larger, around 3km, or smaller, less than 1km.
2. **Underestimating strain** - Earlier (Part 2.3), the possibility of fabric re-setting and mafic enclaves underestimating the induced strain was discussed. If this were the case, the initial pluton size would be significantly smaller than the estimate made above.

Therefore the estimate above is probably an upper limit for the size of the original pluton.

a) Migrated mafic enclave strains



b) Migrated Fry strains

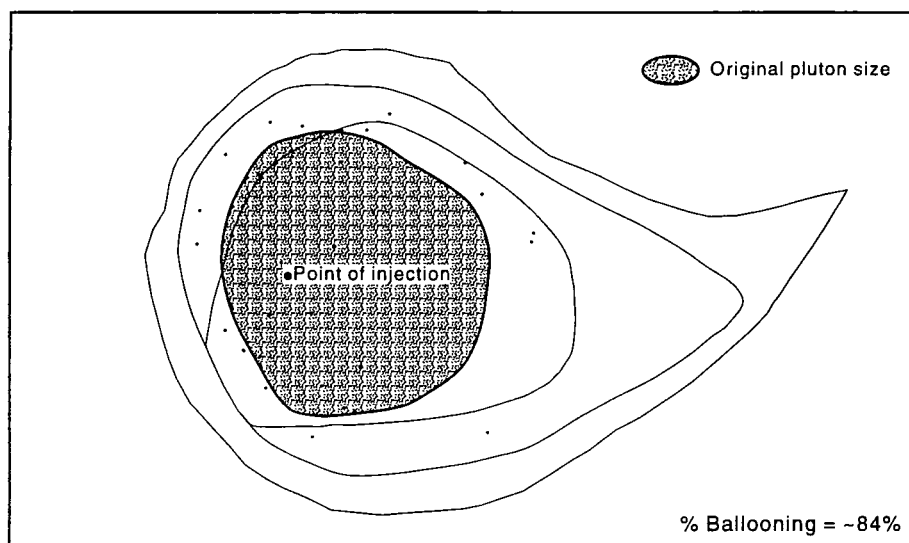


Figure 2.27 Migrated finite strain measurement, interpolated to display original pluton shape

2.5.3 Nature of the early pluton

An initial pluton of less than 2km in radius is still a significant magmatic body, 33km³ in volume. As all relevant country rock structures are heavily overprinted and few magmatic features remain from this time no interpretations can be made. It is important to observe that all plutonic phases, G1, G2 and G3 migrate their finite strain measurements to approximately the same point: This means that the incorporation point represents the point at which the enclaves where either injected or began to deform and the point at which the fabric was coherent enough to deform and register a Fry strain.

On this basis the magma can be envisaged as being injected at or close to the 'injection point' as a homogenous, low viscosity, high melt fraction magma, probably containing sub-spherical mafic enclaves. This magma was translated laterally due to subsequent magma injection, crystallised and cooled, until it was sufficiently viscous to develop a fabric (around 2km from the injection point). Strain is then recorded in the fabric and strain markers.

2.5.4 The 'space problem'?

The analysis above shows that a minimum of 2km of in-situ expansion equivalent to more than 80% of the volume of the pluton, took place within the granite and that at least 3km of shortening took place in the country rocks. These are minimum estimates of the space created and are based on the simple models described above.

Many workers have discussed whether the country rocks around granite plutons preserve adequate deformation to accommodate pluton emplacement. While there is often possible evidence for roof uplift/vertical translation (Morgan 1995b) at high crustal levels, and tectonic space creation (see Section 3), there is no evidence around or within Ardara to support these processes of emplacement. In the case of the Ardara granite the solution presented here is the best possible solution within the constraints of the data accuracy. This pluton is probably not unique and there are other granites where granite and country rock preserve fabrics which can account appropriately for their 'space problem'.

2.6 Diapir or balloon ?

The respective definitions of the terms diapir and balloon were detailed in Chapter 1. The most important distinction being that a diapir must rise as a mass through the crust emplacing itself as a globular body, whereas a balloon must grow or inflate at the emplacement site. While this distinction is conceptually simple, determining whether a pluton is a balloon or a diapir in the field is more complex.

There are a number of obvious similarities between balloons and diapirs; both are sub-circular; contain a concentric fabric; concentrically deform the wallrock; and given an appropriate initial country rock orientation can produce a rim syncline in the surrounding rocks. Since a diapir must move up through the crust, and given that the pluton is magmatic and at least partially coupled to the surroundings, a diapir should show pluton-up kinematics everywhere and steep, well-developed lineations (England 1990). In addition the modelling work of Schmeling *et al* (1988) and Cruden (1988,1990) showed that if a diapir ascended more than one body diameter, a circulation would be induced which produces several distinct features; i) an internal zone of strong vertical prolate finite strains; ii) an overlying crestal zone of weak flattening strains; iii) at the pluton equator $0 < K < 1$ finite strains with sub-horizontal x-axes and pluton up kinematics (vorticity axis = x); and iv) a characteristic circular zonation of marginal granites petrologically identical to the core.

On the other hand a balloon will display concentrically increasing strains, no pluton-up kinematics, no lineations and $K=0$ type strains everywhere. However there exists a grey area between these two end-members, where both diapiric balloons, and ballooning diapirs might occur (Bateman 1984, Brun *et al* 1990, England 1988, 1990). Therefore using the criteria described above and applying them to the Ardara pluton it is possible to say that:

1. There are no macroscopically identifiable stretching lineations in the pluton, nor do the principal strain ratios at any locality indicate the presence of such a predominant elongation axis with K-values very close to zero (except where associated with externally applied tectonic strains).
2. There is no zonation of marginal granites petrologically identical to the core, but rather a simple normal petrological zonation. Notably Paterson & Vernon (1996), suggested the normal zonation was produced by the intrusion of three nested diapirs. But such a scenario implies (from the diapiric criteria), i) an internal petrological zonation within each unit, and ii) the presence of complex finite strain gradients and variable K-values with and without each petrography unit. None of these features are observed.

Nevertheless the Ardara balloon does possess some of the features associated with diapirism. We have identified from syn-magmatic shear sense indicators a slight component of uniaxial movement obliquely upwards to the north. The small magnitude of this

component over the other radial directions can be judged by the fact that there is no measurable or observable lineation associated with this. Therefore the Ardara pluton is predominantly a balloon which has expanded slightly more in one direction than in any other. In terms of the definitions which we have given it lies in the grey area between diapirs and balloons, but very close to the field of true balloons.

2.7 Emplacement and deformation

2.7.1 A sequence of events

Vernon & Paterson (1993) suggest that the pluton was emplaced and subsequently pervasively overprinted by a later deformation. The field observations suggest that the pluton was emplaced in the following sequence:

1. **Initial scenario** - Deformed southerly dipping Dalradian country rocks are cut by a sub-vertical sinistrally transpressive shear zone. This shear zone swings from northeast-southwest trending to east-west trending, where it becomes less defined and bifurcates (Figure 2.28a). This is consistent with the restoration of Donegal before emplacement of the granites (Hutton & Alsop 1996).
2. **Initiation of ascent/emplacement** - This swinging of the shear zone produces local transtensional jogs, low pressure sites which can be preferentially exploited by any crustal fluids i.e. magmas. The influence of a sub-north-south trending deep crustal lineament (Hutton & Alsop 1996) may assist emplacement at this site through the focusing and sheeting of magma along crustal weaknesses (Jaques & Reavy 1994, Petford *et al.* 1993). (Figure 2.28b)
3. **Granitic magma source** - From the outcrop features it is not possible to make many interpretations of what the magma source consisted of, except to remark that there was inhomogeneous mixing of a basic magma with the felsic components on a number of scales; producing the large microgranitoid enclaves and smaller mafic 'clots' of G2. In addition the pluton is known to be a Caledonian I-type pluton, sourced from a mantle of radiogenically young continental crust which was at least weakly contaminated with crustal sources (Demsey *et al.* 1990).
4. **Emplacement of G1** - Once magma ascent has been initiated it travels up a conduit, until it reaches a rheologically or buoyancy favourable structural level and begins to expand laterally. Aureole deformation may be preferentially enhanced by hydrolytic weakening of the country rock through fluid expulsion from crystallising magma and the metamorphosing aureole. Away from the pluton deformation is common but heterogeneous in development. Emplacement and deformation took place in the magmatic state but, where heat was lost to the surrounding cooler country rocks, solid state fabrics were formed.
5. **Emplacement of G2 and G3** - After G1 had achieved a degree of solidity, sufficient to preserve its integrity, but insufficient to prohibit magmatic state deformation or contact dyking, granite phases G2 and G3 were intruded. Contact relations suggest that they were rheologically similar during their emplacement and may have been injected in rapid succession. These phases also had a high magma fluid pressure, sufficient to continue deformation of the country rock in such a way that the country rocks and G1 were deformed in response to a local lateral transport deformation matrix: G2 and G3

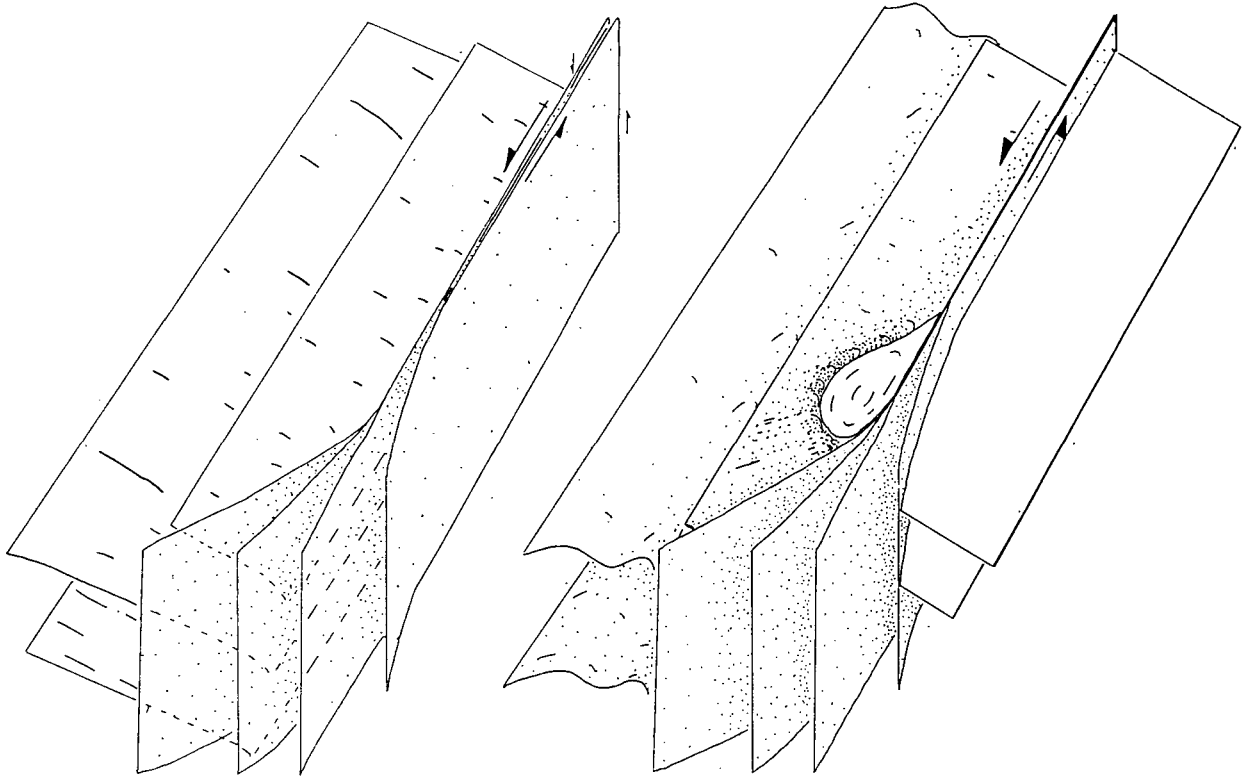
were de-coupled, displaying fabrics and finite strains related to lateral expansion but non-coaxial shear fabrics related to the regional sinistral deformation matrix. Intrusion and deformation of G2 and G3 took place entirely in the magmatic state (Figures 2.28c). Continued sinistral movement of the southern shear zone during the emplacement process resulted in the pluton 'tail'.

6. **Intrusion of the Main Donegal Granite** - After cooling and crystallisation of the Ardara pluton the Main Donegal granite was emplaced, resulting in heterogeneous reactivation of the southern shear zone. This corresponds to a solid state deformational overprint of the 'tail' and southern contact portion of G1.
7. **Subsequent deformations** - Later deformation events in the remainder of Donegal did not significantly affect the Ardara pluton or its surroundings.

2.7.2 Pluton shape

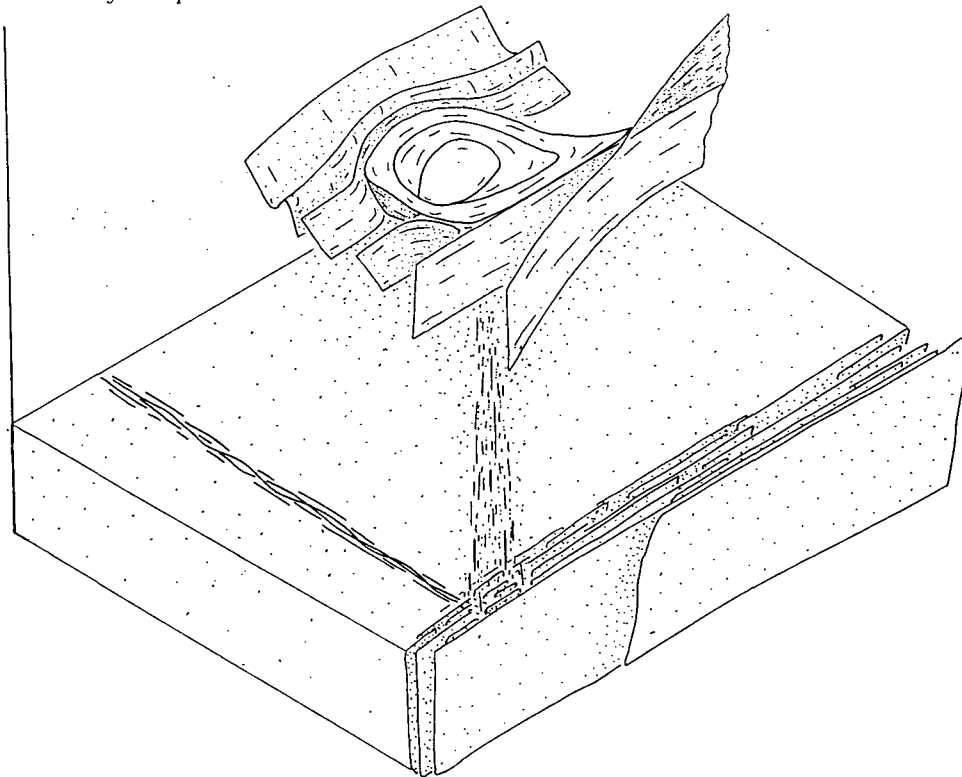
The pluton is sub-circular with a pronounced 'tail'. The circular shape can be accounted for in a number of ways e.g. rise of a spherical diapir, in-situ ballooning, stoping around a major magma conduit. The origin of the 'tail' is less simplistic to explain; Akaad (1956a) described it as part of a 'diapiric stalk', which was overprinted by later deformation, whereas Hutton (1982b) suggested that the 'tail', was formed by deformation of an originally circular diapiric structure during post-emplacement regional sinistral shear. By examining structures around the tail it is possible to see that deformation is much more intense on approach to the contact with the Main Donegal granite and the Meenalargan complex than elsewhere within the pluton. The deformation occurred at a lower temperature (estimated at 300-400°C), producing recrystallised ribbons of quartz, recrystallised biotite and brittle deformation, core and mantle structures in feldspars. In outcrop the fabric in this area has a gneissic to mylonitic texture. This solid state deformation which is at least in part over-printing is correlated with intrusion of the Main Donegal Granite.

Traversing away from the south-southeastern part of the pluton towards Lough Ananima (GR 795945) deformation is magmatic and not overprinted. This part of the pluton is still elongated towards the northeast which suggests that some sort of 'tail' existed before the emplacement and overprinting effects of the Main Donegal Granite. This is consistent with ascent along a bending shear zone related conduit, which would preferentially supply magma along strike into the zone of greatest dilation, but would also inject magma into zones of lesser dilation along strike.



a) Initial scenario, country rocks cut by sinistrally transpressive shear zone.

b) Initiation of ascent / emplacement



c) Intrusion of G2 and G3, magma supply from lineament intersection at depth

Figure 2.28

Block diagrams showing the intrusive sequence of the Ardara pluton

2.8 Conclusions

The Ardara pluton is a 3-phase, 8km diameter, sub-circular pluton, emplaced into Neoproterozoic Dalradian sediments at mid-crustal levels. Emplacement related deformation is recorded in the magmatic and country rocks and shows: a steeply inclined concentric foliation; a country rock fabric sub-parallel to the pluton contact; a shear zone along the southern contact; concentrically flattening magmatic strain fabric which increases in strength towards the contact; non-coaxial northwards directed expansion; and country rock strains which are intense at the contact and extend up to 4km from the contact.

Using this data and applying a simple ballooning model for in-situ expansion (Ramsay 1989), the measured finite strains can be migrated back to their incorporation points. This demonstrates the existence of a small initial pluton which expanded to create more than 80% of the final volume. Quantifying the finite strain recorded in the country rocks demonstrates that at least 3km of shortening has been accommodated across the western side of the pluton, which is consistent with space creation estimates made from strain markers.

These conclusions demonstrate that: i) this pluton was not emplaced by diapirism (Vernon & Paterson 1993, Paterson & Vernon 1995); ii) the feasibility of an in-situ expansion ballooning model; and iii) the importance of an integrated study of pluton and country rocks to understand granite emplacement.

SECTION 3

Granitoid emplacement in the Rio Paraíba do Sul shear belt, SE Brazil

“Within this country of ours there are two nations: between whom there is no intercourse and no sympathy; who are as ignorant of each other’s habits, thoughts, and feelings, as if dwellers in different zones or inhabitants of different planets; who are formed by different breeding, are fed by different food, are ordered by different manners, and are not governed by the same laws” - Disraeli, 1845

Chapter 3

Regional introduction: The Rio Paraiba do Sul shear belt

3.1 Introduction

The purpose of this chapter is to describe the regional background to the granitoid plutons have been studied in south east Brazil. These plutons have been emplaced into the Rio Paraiba do Sul shear belt (RPSSB) (Ebert *et al* 1991) during the Late Precambrian-^{Early Ordovician} Brasiliano-Pan African orogeny (Almeida *et al* 1973, Cordani *et al* 1973). The RPSSB is part of the larger Ribeira orogenic belt (Almeida *et al* 1973), which stretches along the eastern seaboard of Brazil, from Salvador in the north to Curitiba in the south.

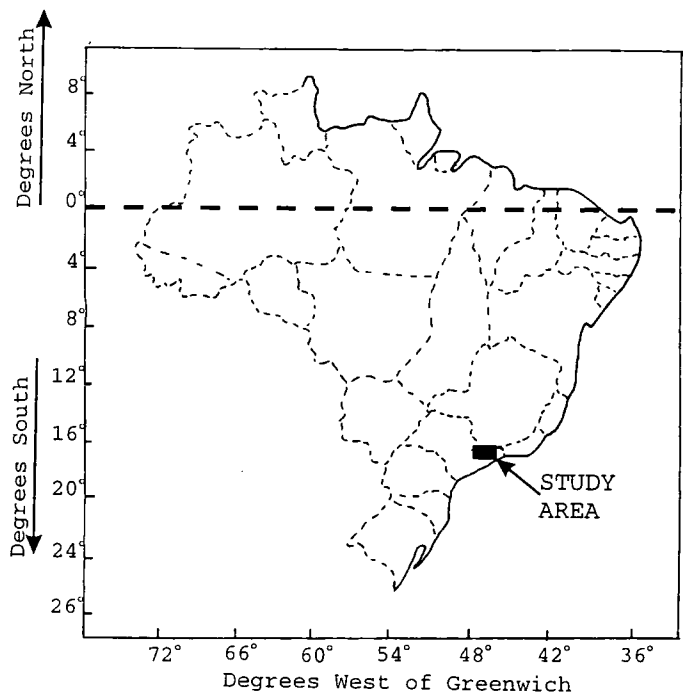
Field analysis of each of the plutons, and integration of this information to gain a regional perspective, facilitates an understanding of; i) the emplacement process; ii) the pre-, syn- and post-emplacement tectonics; and more generally iii) additional information on the dynamic relationship of granitoids in general orogen evolution.

3.1.1 Location

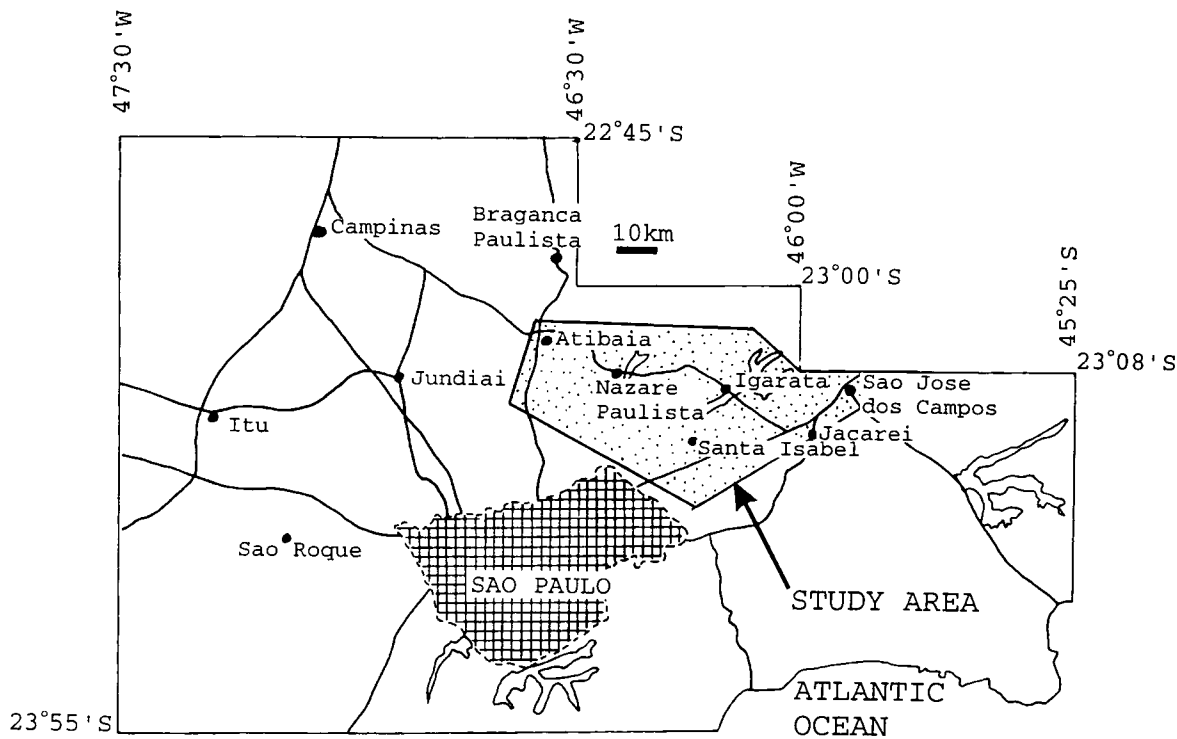
The study area is situated in Sao Paulo state, south east Brazil (Figure 3.1a, b, 3.4b), between 23°S and 23°35'S and 45°30'W and 46°45'W; about 70km north of Sao Paulo City, between Campinas and Sao Jose dos Campos. Sao Paulo state is the most economically developed and populous state in Brazil. It is easily accessible with good quality roads and well-maintained dirt tracks into the hinterland.

Geomorphologically the area is part of the western Serra Mantiqueira, which forms an elevated (400-1200m altitude) region of hills and valleys, from the Atlantic coast in the east to the flank of the Parana basin in the west. In general the vegetation consists of grazing land, scrubland and managed forestry plantations, with occasional pockets of pristine 'Matta Atlantica' rainforest.

Throughout this part of Brazil outcrop is relatively sparse (<10%) consisting of hilltop exposures, large boulders (which are close to in-situ as a result of the absence of glaciation), road cuts and river sections. Most outcrops display strong tropical weathering, making mineralogical and deformational observations usually difficult in the field. Despite this the majority of preserved structural data can be measured.



a) within Brazil



b) within São Paulo state

Figure 3.1 Maps showing the location of the field area

3.1.2 An historical perspective

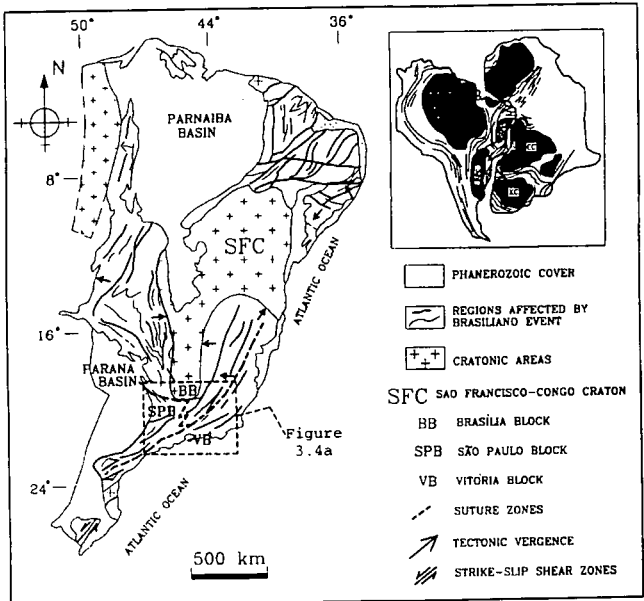
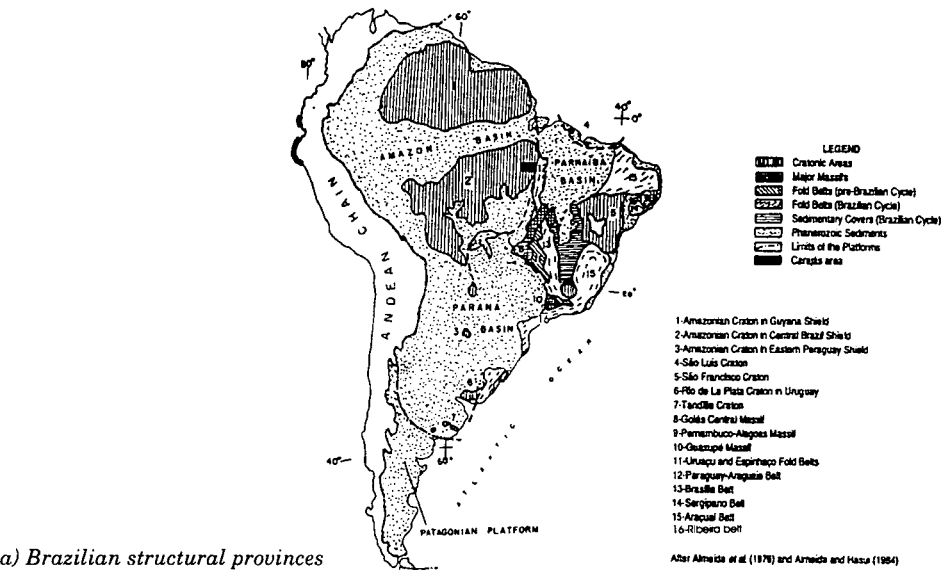
As a result of its relative accessibility and proximity to the largest geological research institutes in Brazil, the Ribeira belt (Figure 3.1, 3.3) has been the object of extensive previous study. Only recently has this work begun to be published in international English language journals. As a result a detailed understanding of the geology of the region can only be gained through the study of conference proceedings, papers and theses, available only in Brazil and written in the Portuguese language.

The first geological observations on the southeast portion of Brazil were made in the nineteenth century during natural history expeditions to South America. The most notable of these was the work of Derby (1878, 1906), who remarked upon the deformed and metamorphosed nature of the Ribeira belt rocks relative to the undeformed older sequences present further north. It was not until the establishment of local geological institutes that the task of mapping and interpreting the whole continent was undertaken. Of particular note was the work of Rosier (1957, 1965) and Ebert (1968), who presented tectonic summaries of the Mantiquera province (the eastern seaboard of Brazil) (see review by Hasui & Oliveira 1984). These early workers suggested that this province consisted of juxtaposed metamorphosed basinal sedimentary terrains and cratonic fragments, incorporated into a northwest verging Alpine-type nappe structure, which was cross-cut by later faults. The work of Almeida *et al* (1973) and Cordani *et al* (1973), who documented the lateral continuation and consanguinity of deformation, led to the suggestion that Brazil consists of ancient continental shields whose margins were deformed during a late Precambrian orogeny, the Brasiliano orogeny.

In recent years the task of mapping the entire region at a scale of 1:50,000 has approached completion. This has elucidated elements of the stratigraphy, deformation and metamorphic history (see Campos Neto *et al* 1983, Oliveira *et al* 1985 and Theodorovicz *et al* 1990 in the study area). This shows that in general the Ribeira belt consists of ancient cratons, or tectonic blocks (the Sao Francisco craton to the north, Rio de la Plata craton to the south and west and the African, Congo and Kalahari cratons to the east) (Figure 3.3). These are surrounded by orogenic belts i.e. the Ribeira belt; of highly deformed metamorphic cratonic fragments and meta-volcano-sedimentary sequences of variable grade, cross-cut by faults and shear zones of various ages.

Using these data, and the results of many more detailed investigations (see Tassinari 1988, Melhem 1995 and Morais 1996 in the study area), a number of tectonic models have been presented for the area (Brito Neves & Cordani 1991, Tommasi *et al* 1994, Campos Neto & Figueredo 1994, Ebert *et al* 1996 and Ebert & Hasui *in press*). Each of these models (which differ in detail and complexity) describes the orogenesis occurring during formation of Gondwana as a result of the late Precambrian collision of cratons (or

tectonic blocks). This collision, the Brasiliano orogeny, was associated with crustal thickening, metamorphism and extensive granite emplacement.



b) The Ribeira belt and the Rio Paraiba do Sul shear belt (after Ebert et al 1996)

Figure 3.2



3.2 The geology of Brazil

This portion aims to describe current understanding of the geological evolution of Brazil, and more generally the South American continent.

3.2.1 The Precambrian

Brazil is composed of: i) Precambrian cratons (granite-gneiss terrains); ii) Late Precambrian 'Brasiliano' orogenic (mobile) belts; which are overlain by iii) Palaeozoic volcano-sedimentary basinal cover sequences (see Almeida & Hasui 1984 and Pinheiro 1997 for a review). There are five major Precambrian cratons: i) the Amazonian craton; ii) the Sao Luis craton; iii) the Sao Francisco craton; iv) the Rio de la Plata craton; and v) the Tandilla and Sierras Australes cratons (Figure 3.2a). As well as a number of smaller areas of exposed basement: i) the Goiás massif; ii) the Pernambuco Alagoas massif; and iii) the Guaxupe massif (Figure 3.2a).

These cratons and associated fragments preserve Archaean and Proterozoic volcanic, sedimentary and orogenic sequences, which help to define geochronotectonic sequences (Table 3.1). The last of these sequences, the Brasiliano sequence, forms the current structural boundary of the older cratons in south and central Brazil.

Table 3.1 Brazilian Precambrian geochronotectonic cycles (after Pinheiro 1997)

Chronometric subdivision used in Brazil (Almeida & Hasui 1984)	Brazilian Tectonic Cycles (Almeida <i>et al</i> 1976)
Late Proterozoic (1000-650/550Ma)	Brasiliano Cycle (1000-500Ma)
Middle Proterozoic (ca. 1800-1000Ma)	Uruacuano Cycle (>1500-1000Ma)
Early Proterozoic (2500/1750Ma)	Transamazonian Cycle (2000±200Ma)
Late Archaean (3000-2500Ma)	Jequie Cycle (2700±100Ma)
Early Archaean (>3000Ma)	Guriense Cycle (>3000Ma)

3.2.2 The Brasiliano orogeny

The Brasiliano orogeny (Almeida *et al* 1973, Cordani *et al* 1973) is generally regarded as the continental collision of cratonic blocks during the Upper Proterozoic and the Cambrian (Almeida 1978, Ebert *et al* 1996). However some authors regard it more broadly as an entire Wilson cycle, which began at 1000-700 Ma with the extension and break-up of an early continent, followed by the deposition of extensive basinal and passive margin sediments, before the onset of subduction at 750-600Ma and collision at 600-450Ma (Hasui *et al* 1978, Fernandes *et al* 1992).

Simplistically, there are four Brasiliano orogenic belts (Figure 3.2a); i) the Araguaia belt in northeast Brazil; ii) the Brasília belt in Central Brazil; iii) the Dom Feliciano belt in southern Brazil and Uruguay; iv) the Aracuai belt in eastern Brazil; and v) the Ribeira belt in southeast Brazil. Within each of these belts there is additional internal complexity for example, Ebert *et al* (1991) subdivided the Ribeira belt to define the Rio Paraíba do Sul

shear belt (RPSSB), in São Paulo, Minas Gerais and Rio de Janeiro states (Figure 3.2b) (Ebert *et al* 1993a, b, 1996, 1997, Ebert & Hasui 1992, Harley & Hasui 1982). Importantly, despite their geographical dispersion, each of these five major orogenic belts, have been described as preserving a similar chronology; i) 1000-900Ma, extension, sedimentation and volcanism associated with continental break-up and possible mantle plume influence (Hasui *et al* 1982, Pedrosa-Soares *et al* 1992, Correa-Gomes & Oliviera 1997); ii) deposition of a volcano-sedimentary passive margin sedimentary sequence (Ebert 1968); iii) onset of subduction, which was west to north-westwards directed at 750Ma (Pedrosa-Soares *et al* 1992, Fernandes *et al* 1992) to 650Ma, (Ebert *et al* 1996); iv) crustal anatexis and peak metamorphism; v) intrusion of late tectonic granites at 600-550 Ma (Hasui & Almeida 1984, Brito Neves & Cordani 1991, Janasi & Ulbrich 1991, Pedrosa-Soares 1992, Pimental *et al* 1996, Ebert *et al* 1996, this work); and vi) post-tectonic/arc collision (?) and granite intrusion at 500-450Ma (Janasi & Ulbrich 1991, Campos Neto & Figueredo 1994).

3.2.3 Relationship to the Pan-African.

The west of the present African continent preserves a cratonic arrangement similar to that described from South America. There are ancient cratons (the Kalahari, Congo and West African) surrounded by late Proterozoic orogenic belts (the Damara-Kaoko, West Congolian and Dahomeyan belts) (Porada 1989) (Figure 3.3).

The similarities to the mobile belts of South America are as follows: i) that the timing and type of metamorphism-igneous intrusion (compare the studies of Tassinari 1988, Campos Neto & Figueredo 1994 to that of Kroner 1982); ii) the foreland sedimentation patterns (Gneisse *et al* 1996) is similar; and iii) the relative positions of these cratons was unchanged from around 1Ga through to the Palaeozoic. These observations have been used to demonstrate that what is now South America and Africa were fused together in Gondwana during the late Proterozoic Brasiliano-Pan African orogeny (see Torquato & Cordani 1981).

3.2.4 Palaeozoic and Mesozoic

The Precambrian and Brasiliano basement is commonly overlain by extensive Palaeozoic and Mesozoic extension-related, volcano-sedimentary sequences: i) the Amazonian basin, overlying the Amazonian craton; ii) the Paraíba basin, in northeast Brazil; and iii) the Parana basin, which covers western Brazil and parts of Paraguay, Uruguay and Argentina (Figure 3.2a). These basins were formed due to late Palaeozoic and Mesozoic extension, associated with the break-up of Gondwana and the opening of the Atlantic ocean (Nurnberg & Muller 1991, Chang *et al* 1992). In addition, there are a few preserved fragments of Early Palaeozoic foreland basin sequences (Gneisse *et al* 1996), whose source was the eroding and uplifting Brasiliano orogenic belt.

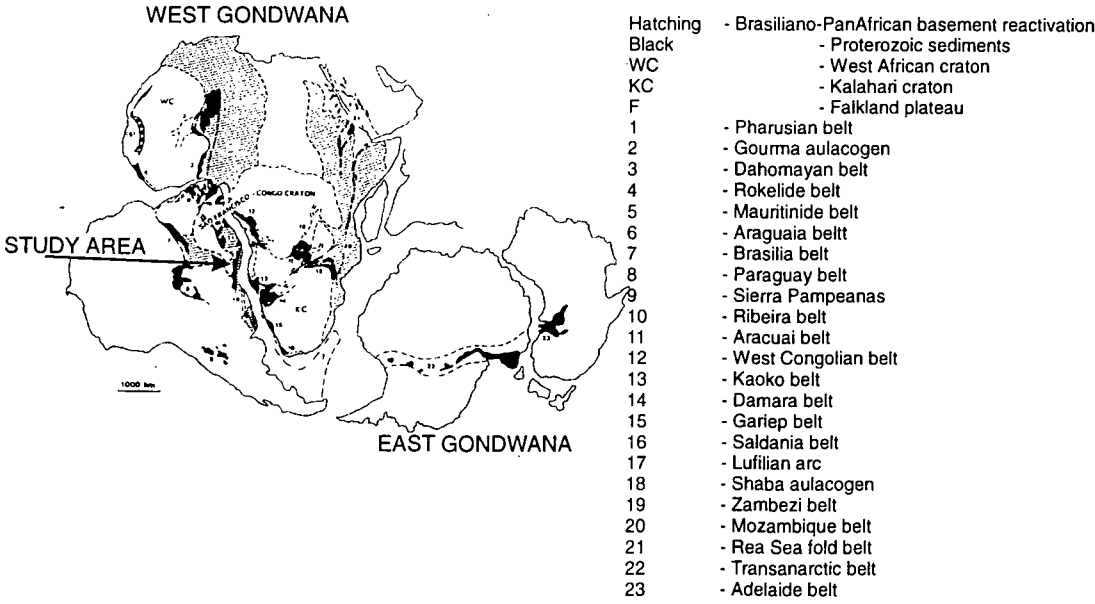


Figure 3.3 Comparison of South American and African structural provinces, restored to their pre-Atlantic opening positions (modified from Porada 1989)

3.3 Geology of the Rio Paraiba do Sul shear belt

3.3.1 Introduction

As described above, the Brasiliano Ribeira Belt has been subdivided to include the Rio Paraiba do Sul shear belt (RPSSB). To the north the Aracuai belt records the approximately orthogonal collision of the Congo and Brasiliano cratons (Pedrosa-Soares 1992, Cunningham *et al* 1996 and references therein). Further south lies the Dom Feliciano belt, which records the transpressional collision between the Kalahari and Rio de la Plata cratons (Fernandes *et al* 1992, Tommasi *et al* 1994) (Figure 3.4).

Between these two belts lies the RPSSB, which records the compressional interaction of three tectonic blocks, the limits of which have been defined geophysically (Haralyi & Hasui 1982): i) the Sao Paulo plate, which comprises part of the Rio de la Plata craton (whose outcrop is overlain by the Palaeozoic Parana basin); ii) the Borborema plate, comprising the southern extension of the Sao Francisco craton; and iii) the Vitoria plate, which consists of the preserved fragments and the rifted-off portions of a larger plate, the Congo craton and its surrounding orogenic belts (Ebert *et al* 1991, 1996, Ebert & Hasui *in press*).

3.3.2 Stratigraphy

As a consequence of the metamorphic grade, the sparsity of outcrop and the tropical weathering, the stratigraphy of this area is difficult to map and interpret. Detailed summaries of the stratigraphy are found in Campos Neto *et al* (1983), Oliveira *et al* (1985) and Theodorovicz *et al* (1990). Generally, the stratigraphy can be summarised in terms of deformed and metamorphosed volcano-sedimentary sequences, divided into *domains* by inter-continental shear zones. These sequences, although highly deformed, have been recognised as being either original Archaean-Proterozoic cratonic fragments or as passive margin-basinal sequences deposited on cratonic margins during Proterozoic times (Hasui & Olivera 1984). In this work the stratigraphic domains set up and described by Tassinari (1988) are used (Figure 3.5) and are summarised below:

Piracaia-Jundiá domain

This domain is exposed between the cities of Piracaia, Jundiá and Itu, north of the Jundiáivira shear zone. It can be summarised as a sequence of predominantly paragneisses, quartzites, and mica-schists intercalated with biotite gneisses, amphibolites and migmatites; thrust onto the Socorro-Guaxuape nappe exposed to the north. It is divided into three groups:

Schists

The basal unit, consisting of mica or quartz mica schists, with occasional garnet or tourmaline, and of a sedimentary or volcano-sedimentary provenance. These schists are normally intercalated with slivers of amphibolites and meta-gabbros.

Gneisses

Banded paragneisses of granitic to tonalitic composition, preserving occasional hornblende and sillimanite. Intercalated within these are orthogneisses preserving massive microcline crystals metamorphosed to high amphibolite facies.

Migmatites

In this area there are two kinds of migmatites palaeosomes of granodioritic to tonalitic composition and leucosomes of white-grey, microcline-oligoclase-quartz-biotite-hornblende granite.

For greater detail see Ebert (1968), Wernick *et al* (1976), Campos Neto *et al* (1983), Campanha *et al* (1983), Vascocelos (1984), Oliveira *et al* (1985), Basei *et al* (1986) and Campos Neto & Vasconcelos (1986).

Sao Roque domain

This domain consists of essentially an homogenous meta-volcano-sedimentary sequence, believed to be of passive margin provenance. It is exposed between the Buquira-Monteiro Lobato and Jundiuvira shear zones.

At its base there is an amphibolite, succeeded by metarenites, quartzites and calc-silicates. Above these are a sequence of metaarkoses, metaarenites and mica-schists, with the top of the domain marked by a phyllite sequence.

Figueiredo *et al* (1982) and Campos Neto *et al* (1983) provide additional descriptions.

Embu domain

These rocks are exposed east of the Monteiro Lobato-Buquira shear zone and west of the Cubatao shear zone, and have previously been described as the Santa Isabel complex. The base of the sequence is defined by the intensely deformed Santa Isabel gneisses which are overlain by a sequence of amphibolite grade gneisses, locally retro-metamorphosed to greenschist facies.

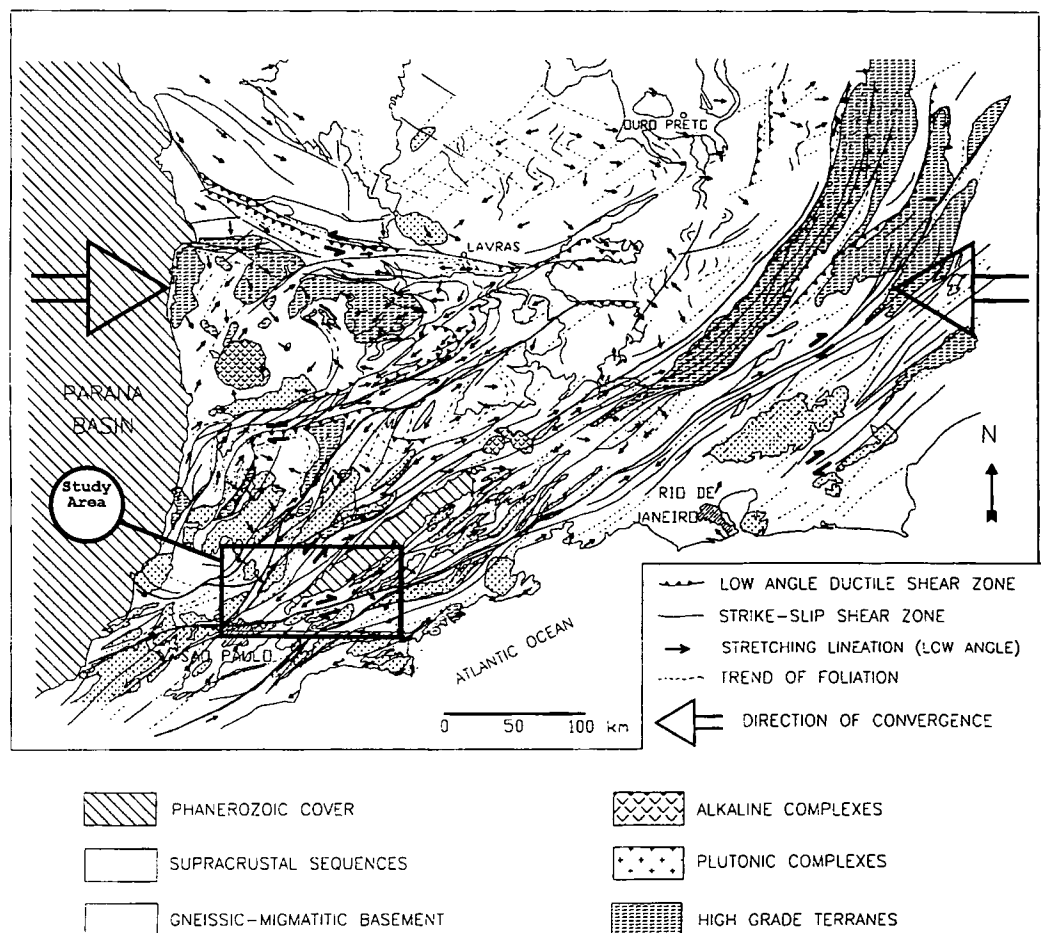
Santa Isabel gneisses

This sequence consists of a blastomylonite gneiss which shows a transition into banded orthogneiss (granodioritic to tonalitic in composition), intercalated with migmatites and quartzite dykes (see part 5.8.1).

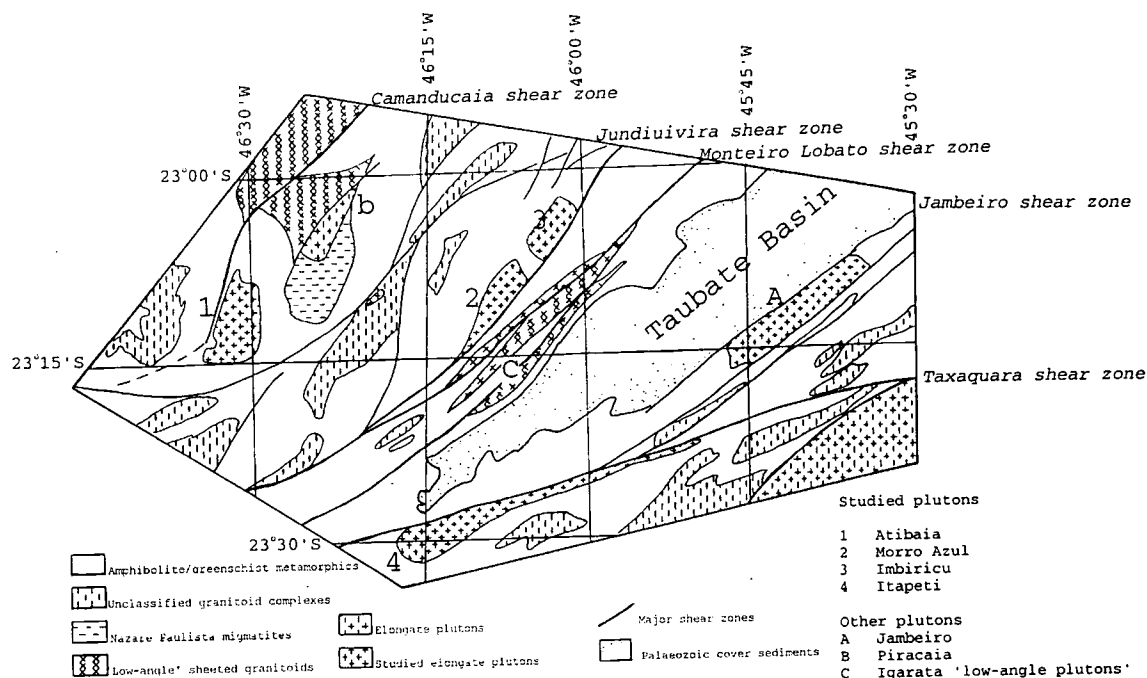
Gneisses

Overlying the Santa Isabel gneisses is a sequence of banded, variably migmatitic, gneisses which were strongly retrometamorphosed to greenschist facies in the vicinity of major faults.

See Campos Neto *et al* (1983) and Theodorovicz *et al* (1990) for additional description.



a) The Rio Paraíba do Sul shear belt (after Ebert et al 1996)



b) The study area

Figure 3.4

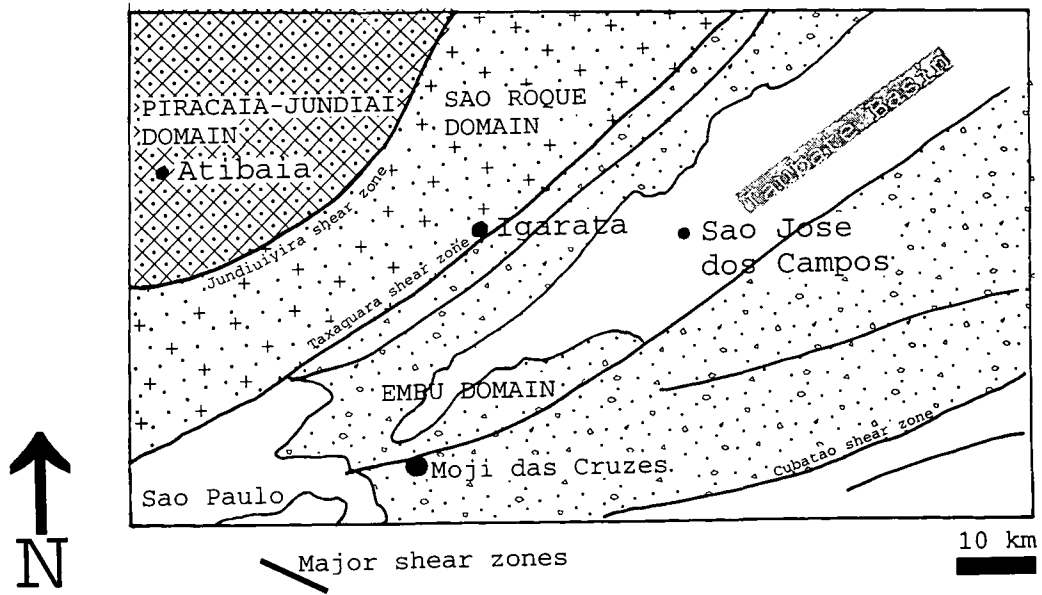


Figure 3.5 Stratigraphic domains recognised in the study area (after Tassinari 1988)

3.3.3 Metamorphism and geochronology

Field studies and, more recently, geothermobarometric and geochronological studies have shown that:

1. The country rocks preserve a polymetamorphic history, Tassinari (1988). Many have very ancient isotopic model ages e.g. 2.7-2.45 Ga, indicating formation during earlier orogenic events.
2. Between 1.3Ga and 0.8Ga there were episodes of granite intrusion e.g. Moinho pluton, which could possibly be related to extension and break-up of an Early-Mid Proterozoic continent (Tassinari 1988).
3. At least two Brasiliano metamorphic events have been recognised, whose metamorphic grade and timing varies along the belt (Hasui *et al* 1975, Ebert *pers comm*). An M_1 event, at amphibolite facies, associated with the low angle fabric, ~650Ma (Tassinari 1988, Brito Neves & Cordani 1991). The temperature and pressure of this event have been estimated at ~700°C, 5-5.6KBar (15-16.5km) (Porcher & Fernandes 1997), and ~650°C and 6KBar (18km) (Iyer *et al* 1996). The second event, M_2 , occurred at greenschist facies, and is associated with intrusion of granites and the high angle shear zones (Tassinari 1988). Temperature and pressure for M_2 have been estimated at 678°C and 5.9KBar (18km) (Porcher & Fernandes 1997).
4. Potassium-Argon ages of between 500 and 450 Ma from across the region indicate cooling to around 400°C by this time.
5. Fission track ages of 100-200Ma indicate a cooling/re-setting through ~200°C, probably associated with Atlantic rifting (Ribeiro *et al* 1996).

Using these data, a P-T-t path has been estimated which records a long period at highest temperatures and pressures, before slow cooling and exhumation (Figure 3.6). The available data suggest that the overall P-T-t path may have been clockwise, consistent with data from other compressional orogenic regions (Yardley 1989).

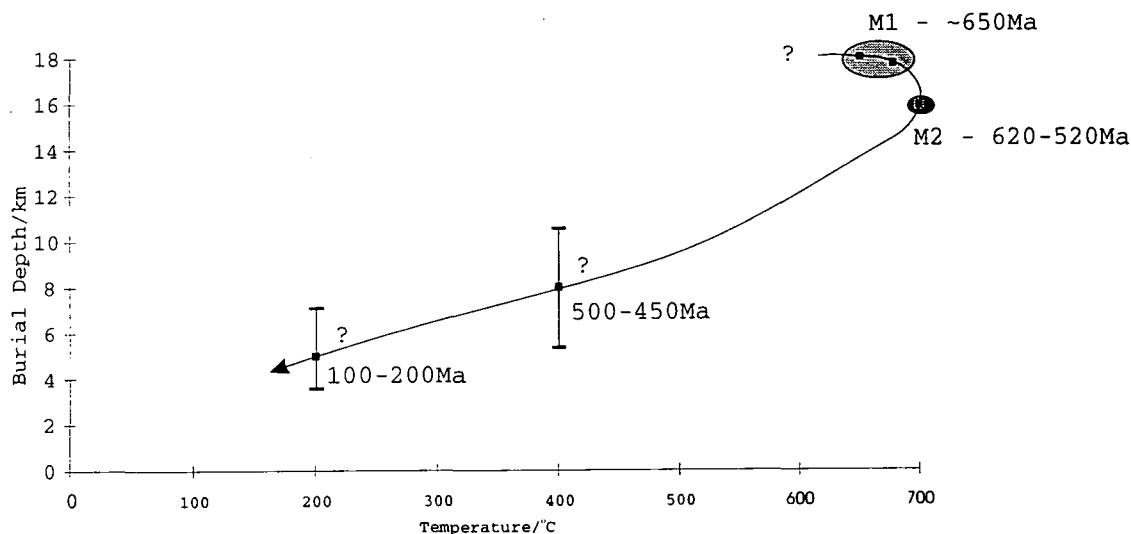


Figure 3.6 An inferred P-T-t plot for the study area, using the data of Tassinari (1988), Ribeiro *et al* (1996) and Porcher & Fernandes (1997)

3.3.4 Structure

The structure of the study area has been the subject of a number of investigations (Campos Neto *et al* 1983, Oliveira *et al* 1985, Hackspacher 1994) and the structural chronology used in this study (set out below) is based on this earlier work. Examining this chronology simplistically there are three components: i) Polyorogenic pre-Brasiliano deformation, D_n ; ii) Syn-Brasiliano deformation, $D_{n+1/2/3}$; and iii) Post Brasiliano deformation, simplistically D_{n+4} . Each of these is described in broad terms below and the utility of this particular sequence of events justified by the fieldwork described in Chapters 4-7:

pre-Brasiliano structures

The gneissose rocks, though they suffered an intense Brasiliano overprint, continue to preserve structures formed as part of earlier deformations. As yet their orientation and exact origins have not yet been determined. Local authors refer to them as D_n structures (Figuereido *et al* 1985) (Plate 3.1).



Plate 3.1 Pre Brasiliano structures from the Atibaia area (GR 463437)

syn-Brasiliano structures

These structures are pervasive across the whole region and understood to be coincident with both of the identified peaks of metamorphism. There are two particular sets of structures, subdivided as follows (after Morales *et al* 1985, Tassinari 1988, Hackspacher 1993 and Ebert *et al* 1993,1996, this work):

D_{n+1} - A northeast-southwest trending, amphibolite facies, pervasive, low-angle, southeast dipping fabric (Figure 3.7a), S_{n+1} . Preserving a down dip stretching lineation, rarely observed in the study area (Figure 3.7b, Plate 3.2). In places these define southeasterly to easterly dipping low angle thrusts, associated with large wavelength, low angle F_{n+1} folds which verge westward-northwestwards, forming nappe structures e.g. Socorro-Guaxupe nappe (Wernick 1978, see Vauchez *et al* 1994 and Cunningham *et al* 1996 for similar structures in southeastern and eastern Brazil). The foliation is intruded by sheeted granitoids of granodiorite to tonalite composition (~650-600Ma), which are often spatially close to the major structures (Plate 3.3), and less deformed anatectic garnet migmatites (~610Ma) (Plate 3.4). The peak recorded metamorphic event, M1, has been interpreted to coincide with the end of this event (Porcher & Fernandes, 1997).



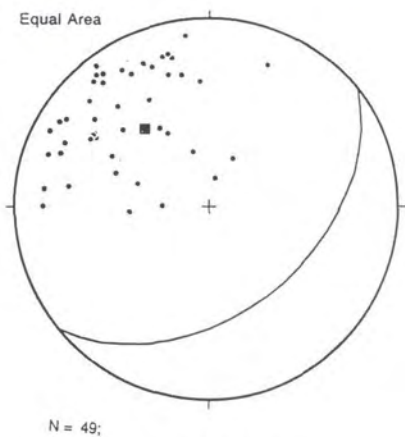
Plate 3.2 Low angle S_{n+1} fabric, Nazare Paulista region (GR 578369)



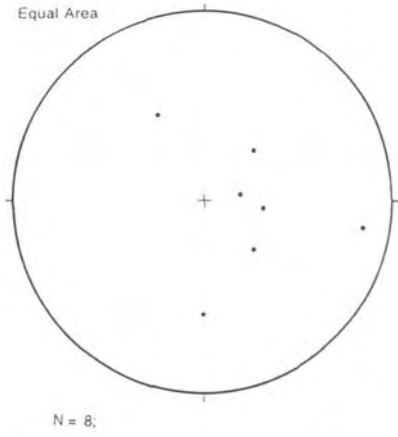
Plate 3.3 Highly deformed sheeted granites (GR 843297)



Plate 3.4 Nazare Paulista migmatites (GR 578369)



a) Stereonet of poles to planes
low angle foliation S_{n+1}



b) Stereonet of associated L_{n+1} stretching of
lineations

Figure 3.7 D_{n+1} fabric stereonets

D_{n+2} - This is a high angle fabric, developed heterogeneously but intensely across the area. At its weakest it is a sub-vertical, northeast-southwest trending, crenulation cleavage, S_{n+2} (Plate 3.5). This is intensified around anastomosing northeast-southwest trending, D_{n+2} sub-vertical, predominantly dextral, brittle-ductile shear zones (Figure 3.8a, Plate 3.6) to become pervasive. S_{n+2} foliations developing an occasional stretching lineation, L_{n+2}, which on average plunges weakly to the northeast (Figure 3.8b, Plate 3.7), and is associated with local sub-vertical isoclinal folds. In addition, larger scale northeast-southwest orientated F_{n+2} upright folds are developed (Map 9). These folds, which have previously been interpreted as F₃ folds forming in response to a northeast-southwest directed collision (Almeida & Hasui 1984). Demonstrating the transpressional nature of D_{n+1} and D_{n+2}, Ebert *et al* (1991) showed that both strike-slip shear zones and upright folds (on all scales) are consanguineous, forming in response to an east-west directed regional transpression.



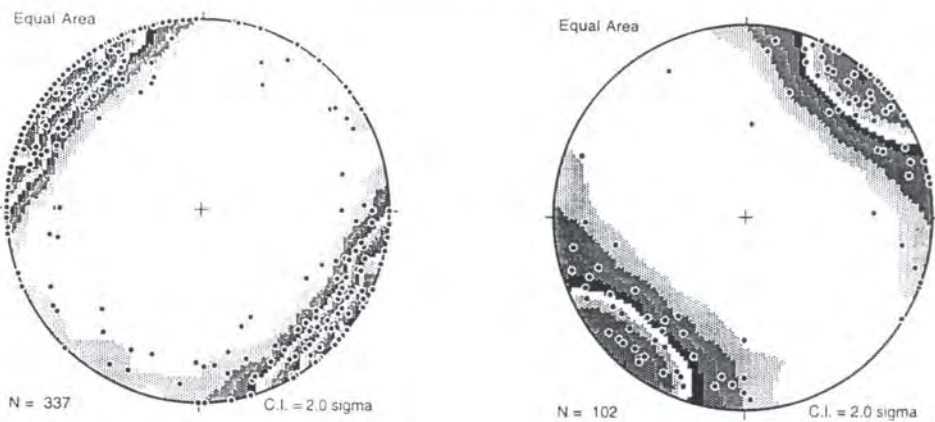
Plate 3.5 Development of crenulation cleavage (GR 715366)



Plate 3.6 Subvertical shear zone, the Jundiuvira shear zone (GR 619345)



Plate 3.7 Sub-horizontal stretching lineation (GR 41103058)



a) Poles to planes of high angle fabric orientations S_{n+2} b) Associated mineral stretching lineations L_{n+2}
Figure 3.8 Contoured D_{n+2} fabric stereonets

D_{n+3} - This event, first postulated by Hackspacher (1993), produces no identifiable country rock deformation. Its existence is inferred from magmatic structures preserved in granites, temporally and spatially associated with D_{n+2} shear zones. This event requires an extensional reversal of movement on these shear zones compared with D_{n+2} (Plate 3.8) and has been correlated with extensional collapse of the orogen (Soares & Rostirolla 1997).

D_{n+4} - After the intrusion of the granitoid plutons associated with D_{n+3} there was a partial reactivation of major D_{n+2} structures. This resulted in solid state, medium-high temperature deformation of the granitoid plutons and greenschist deformation of the country rocks, which led Ebert *et al* 1996 to suggest that the granitoids were hotter than the surrounding country rock during this deformation. There was no additional S_{n+4} fabric developed and the associated weakly northeasterly plunging stretching lineation, L_{n+4} , is indistinguishable, in its orientation from the earlier L_{n+2} fabric (Figure 3.9).

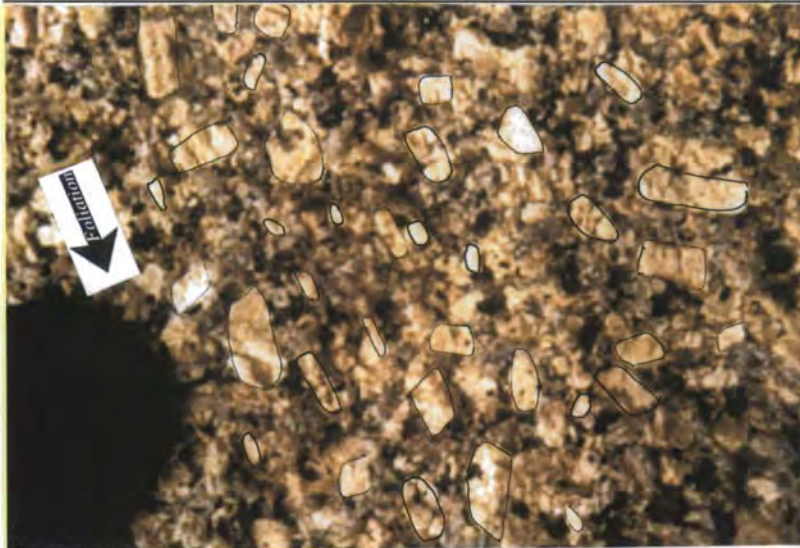


Plate 3.8 D_{n+3} fabric in the Atibaia pluton (GR 48093108)

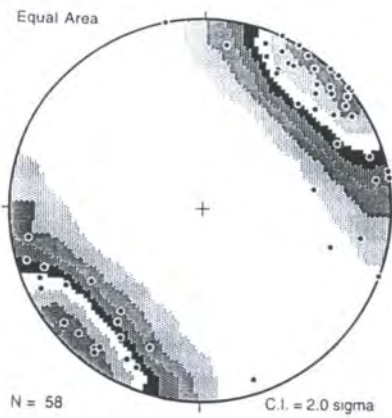


Figure 3.9 Contoured stereonet of L_{n+4} stretching lineation orientations

post-Brasiliano deformation

Post-Brasiliano deformation, is understood to be associated with uplift/extension of the region, in response to Mesozoic continental break-up and the influence of the Trindade mantle plume (Gibson *et al* 1995). In this area discrete brittle-ductile conjugate mylonites (Plate 3.9) and normal faulting have been associated with this event. Almeida & Hasui 1984 and Oliveira *et al* 1985 suggest that many existing faults and shear zones were extensionally reactivated during this event.



Plate 3.9 Brittle-ductile mylonite from the Atibaia pluton (GR 46783525)

3.4 Granite emplacement in the Rio Paraíba do Sul shear belt

An examination of the geological map of the study area (Maps 2- 9) Fig 3.4a, b) shows the existence of a very large quantity and compositional variety of intruded granitoid rocks of various ages. These can be crudely sub-divided as follows:

3.4.1 Precambrian intrusives

Much of the country rock surrounding the better preserved, younger igneous complexes, preserves orthogneisses, with a gabbroic, granodioritic to tonalitic composition. These are often unrecognisable as igneous complexes, elongate and discontinuous along strike, emphasising the intense deformation that they have undergone after intrusion. There are some Precambrian plutons which are at least partially preserved (e.g. Moinho pluton). These show a granodioritic composition, with multiple cross-cutting fabrics, which demonstrate deformation during both D_{n+1} and D_{n+2} .

3.4.2 Migmatites

The migmatites preserved in the region describe two populations; i) minor quantities of migmatites are pervasive across the region, particularly in the poly-orogenic ortho- and paragneisses, they are preserved as thin slivers intruded along or oblique to the foliation (Plate 3.10); or ii) large homogenous bodies intruding the country rock. In general they are understood to have been intruded rather than formed in-situ (Campos Neto *et al* 1983): Melanosomes are rarely observed and the contact between the magma and wallrock is sharp and undeformed (Plate 3.11)

The exact age and age-relationships of these bodies are often difficult and confusing to interpret. A geochronological investigation of the migmatites around the town of Nazare Paulista (Tassinari 1988 and Janasi & Ulbrich 1991) produced a poorly defined Rb-Sr whole rock age of ~800Ma. More recent Sm-Nd whole-rock data (Ragatky *et al* 1997) suggests that an age of 609 ± 7 Ma is more likely. In the Nazare Paulista area the best migmatite exposures can be seen and consist of a garnet, biotite leucocratic granite, intruding and stopping into the gneissic country rock along the low-angle foliation (Plate 3.11).

Structurally the migmatites preserve little fabric, and no examinable magmatic features, though they are overprinted by the regional down-dip lineation, but are not as strongly deformed as the low-angle sheeted granitoid complexes (see Part 3.4.3), this may be because they are not intruded in the proximity of the major high angle shear zones. These observations taken with the geochronological data suggests that these migmatites were probably intruded during or towards the end of the main thrusting/crustal thickening event. Their formation could be linked with anatexis during peak amphibolite facies metamorphism (M1), associated with crustal thickening during the D_{n+1} thrusting event.

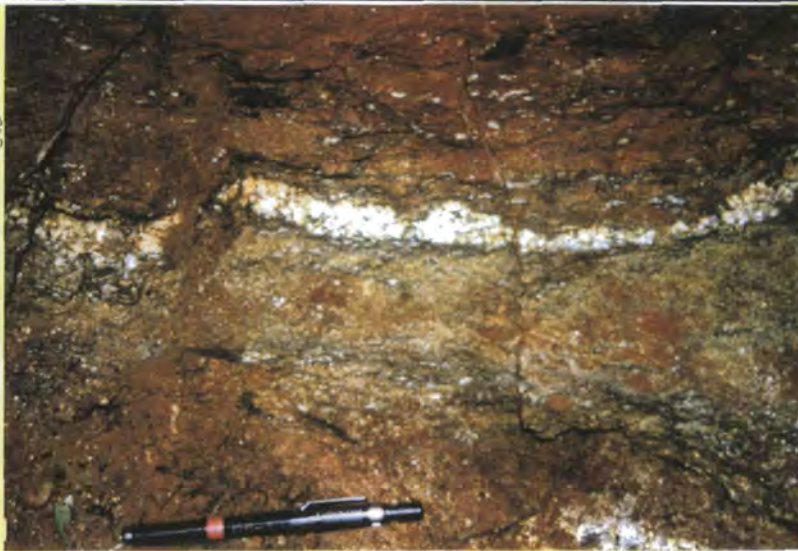


Plate 3.10 Type 1 Thin migmatite slivers intruding along the foliation (GR 48913121)



Plate 3.11 Type 2 Massive migmatites intruding along or obliquely to the foliation (GR 516382)

3.4.3 Low angle sheeted complexes

Throughout this area there are plutons, which are thin, intensely elongated along strike, have a low angle foliation and have experienced extensive deformation e.g. the Braganca Paulista suite of Ebert *et al* 1996. In his analysis lines of evidence were presented to suggest that these plutons were emplaced synchronously to the ductile north-westwards directed thrusting, which occurred around 650Ma.

There are two such plutons in the study area. The first of these is exposed close to the Santa Luzia strike-slip shear zone (GR 837310) showing; i) an easterly dipping low-angle fabric, which is deflected to a high-angle on approaching the shear zone; ii) highly rounded and abraded K-feldspar megacrysts in a fine grained, highly tectonised matrix; iii) a sub-horizontal, along strike stretching lineation. This pluton (Plate 3.12) is interpreted as

being intruded at a low-angle subsequently highly tectonised, by over-printing strike-slip deformation.

The second of these plutons is exposed at GR 855291, close to the Buquira shear zone. This pluton shows; i) a low-angle easterly dipping foliation; ii) both a down dip and a strike-slip related stretching lineation; iii) numerous sheets of granodioritic composition; and iv) westerly verging deformed microgranitoid dykes. This granite is interpreted as being intruded along the low-angle foliation in sheets, during the northwesterly directed thrusting.

Each of these plutons was clearly intruded along the low-angle foliation before being deformed by the later overprinting strike-slip deformation. They are interpreted to belong to a regional granitoid intrusion episode which took place around 650 Ma.



Plate 3.12

Low-angle sheeted Santa Luzia complex (GR 837310)

3.4.4 Elongate plutons

These plutons (which includes the studied granites Figure 3.4b) are the most commonly intruded granitoids. Examination of the regional geological map of southeast Brazil (Hasui *et al* 1981) shows them to have a close spatial coincidence to the sub-vertical strike-slip shear zones: For example the studied plutons Atibaia, Morro Azul, Imbiricu and Itapeti, and plutons described in the literature Serra do Lopo (Ebert *et al* 1996), Itaqui (Wernick *et al* 1993, Hackspacher *et al* 1993,1997, Hackspacher & Godoy 1996), Morungaba (Janasi *et al* 1993), Piracaia (Janasi & Ulbrich 1987, Janasi *et al* 1993), Sindacta (Spanner & Kruhl *in press*). In addition, they show weakly deformed wallrocks, radiometric ages of between 600 and 520Ma, with a median age of approximate 580Ma (Rb-Sr whole rock and Pb-Pb whole rock ages Tassinari, 1988, Janasi & Ulbrich 1991, Melhem 1995, *unpublished data*), Granitic to Alkali Granite composition and isotopic signatures consistent with derivation through anatexis and fractionation of upper continental crust (*unpublished data*).

Structurally the granites generally display a weak sub-vertical intrusion related magmatic foliation and weak deformation of the surrounding country rock (except in the proximity of the major shear zones). The magmatic foliation is heterogeneously over-printed by a later solid-state deformation. Each of the studied plutons has been subjected to a detailed investigation of its intrusion related features in an attempt to understand the regional tectonics pre- syn- and post-emplacement.

3.4.5 Later intrusions

Throughout the RPSSB there are Jurassic-Cretaceous high level potassic-igneous complexes (Gibson *et al* 1995), intruded during Mesozoic extensional magmatism. This magmatism has been associated with decompression melting of highly evolved fractions of continental crust as a result of crustal extension and the impact of the Trinidad hot-spot. Gibson *et al* (1995) explain the focusing of magma in this area to be as a result of the orogenic belt acting as a tectonic weakness or 'thin spot' during extension.

3.5 Tectonic models

A few of the principal tectonic models that have been used to explain the tectonic evolution of this area are outlined below:

3.5.1 Historical perspective

One of the first tectonic models for this area was described by Ebert (1968), who proposed that undeformed passive margin sequences (which are now the gneissose country rocks) have been thrust onto a stable craton to the north during an Alpine-type collisional event. Later following the application of Plate Tectonic theory and the recognition that the Ribeira belt represented part of a Pan-African-Brasiliano orogenic belt (Almeida *et al* 1973, Cordani *et al* 1973), a number of models were formulated which envisaged the orthogonal east-west collision of cratons, associated with continental thickening and later erosion. For example, Porada (1989) envisaged the region as a 'triple junction' collision of three plates (Sao Francisco, Congo and Kalahari cratons), forming the Ribeira belt, in Brazil and the Damara belt in Namibia. While this is broadly the case, in detail the region is of course more complex.

3.5.2 The direction of pre-collision subduction and accretion

Applying Plate Tectonic theory to the evolution of this area requires there to be subduction on one or both sides of the oceanic basin between the colliding continental plates. The evidence for subduction under the present South American continent is outlined as follows:

The African orogenic belts (Kaoko, West Congolian) demonstrate east verging nappe structures whereas the South American belts display north to northwest verging nappes, directions consistent with their post-collision orientation (Figure 3.4a). The tectonic 'set-up' pre-collision is more enigmatic: It is known that at ~1Ga extension took place to form an ocean basin and that by ~650Ma it was probably closed. There is little structural evidence to explain the intermediate 350Ma.

Many workers have demonstrated the existence of geochemical and stratigraphic domains in the Ribeira belt, and have used these in an attempt to elucidate the pre-collisional tectonic arrangement e.g. Tassinari, 1988, Gneisse *et al* 1989, Janasi & Ulbrich 1991 and Campos Neto & Figueredo 1994. These studies suggest that the low-angle sheeted complexes (see part 3.4.3) are Cordilleran I-type granites formed during subduction (Janasi & Ulbrich 1991) and that the Ribeira belt (and the Aracuai belt to the north) is composed of a number of chemically distinct 'arc' terrains (Almeida & Hasui 1984, Campos Neto & Figueredo 1994). Additionally, comparing the foreland basin sequences on each side of the former orogen, Gneisse *et al* (1996) showed there was a greater proportion of arc-

related volcanogenic deposits on the present South American continent than in the corresponding portion of the African continent.

In conclusion, while there is no direct structural evidence for subduction, the preservation of Cordilleran I-type granites (see part 3.4.3), the composite nature of the preserved country rocks and the foreland basin deposits taken together indicate that subduction was more probably under present-day South America i.e. westwards. During subduction the composite terrains along the Ribeira belt were accreted, before final collision took place sometime around 650Ma. The eastward younging direction across the belt (Janasi & Ulbrich 1991, Campos Neto & Figueredo 1994) is related to the progressive accretionary nature of the collision, which migrated westwards and resulted in progressively younger metamorphic ages.

3.5.3 Competing models of orogen evolution

Multiple event: thrusting followed by strike-slip

The use of detailed structural mapping, which recognised top to the northwest thrusting (Ebert 1968, Campos Neto *et al* 1983 and others) and subsequent dominantly dextral strike slip on northeast-southwest trending ductile shear zones (Braun 1972, 1974, Hasui *et al* 1975), resulted in tectonic models which envisage at least two stages of evolution. A first stage of crustal thickening, associated with northwest directed thrusting, followed by a later second stage of dextral strike-slip shear (Braun & Baptista 1977, Cavalcante *et al* 1979).

A number of workers have debated whether these were two distinct processes or part of a continuum. Soares (1988) proposed the collision of continental and arc terrains, before the final collision of continents and evolution to a strike-slip environment. Alternatively, Hasui (1983) proposed that orogenesis took place with crustal thickening along low-angle thrusts, which evolved to strike-slip shear as the orogen matured. He envisaged strike-slip deformation nucleating from lateral ramps.

Partitioned transpression

Harland (1971) recognised that oblique continental collision can result in distinct partitioned zones of pure and simple shear i.e. crustal thickening and strike-slip. A concept which has been developed subsequently by Sanderson & Marchini (1984), Tikoff & Teyssier (1994) and others. Using this concept and applying it to the RPSSB in particular and the entire Ribeira belt in general, Ebert & Hasui (1992, *in press*) showed that it could be modelled as being transpressional.

Their models envisage the orogen as being the result of temporally partitioned oblique transpressional collision between a number of deformable Proterozoic continental blocks, (Figure 3.2b, 3.4a) i.e. initially the orogen was pure shear dominated (low-angle

northwest directed thrusting), producing crustal thickening, before it evolved to be simple shear dominated (high angle dextral strike-slip).

Vaucher *et al* (1994) suggest an alternative model deduced from finite element computer modelling of the Ribeira belt. Their model assumes that a deformable South American continent was more or less assembled in the same form as at present and collided approximately orthogonally with a rigid African continent. The results suggest that deformation would be initially orogen transverse and would switch to orogen parallel as a result of deformation enhanced strain localisation. Notably this model is not accompanied by supporting field data.

3.6 Summary

The Rio Paraiba do Sul shear belt is an anastomosing network of northwesterly verging thrusts and dextral strike-slip shear zones which have a northeast-southwest trend. It preserves evidence of; i) a complex pre-Brasiliano history; ii) crustal anatexis and migmatisation; iii) thrusting, crustal thickening and the intrusion of subduction related sheeted granitoid complexes; iv) overprinting dextral strike-slip followed by granite emplacement and subsequent dextral strike-slip; v) Palaeozoic extension and sedimentation.

In the following chapters the structures associated with a number of intrusive granitoids will be described in order to deduce the tectonic processes at work before, during and subsequent to emplacement of the plutons. Comparing each of these case studies allows general conclusions to be drawn about the evolution of the RPSSB.

Chapter 4

The Atibaia pluton

4.1 Introduction

4.1.1 Preamble

The Atibaia pluton is the westernmost studied pluton within the Rio Paraíba do Sul shear belt (Figure 3.4b). It is situated east and southeast of the town of Atibaia, about 70km north of São Paulo, and comprises parts of the 1:50,000 map sheets named Atibaia and Piracaia. The granite has been mapped previously (Oliveira *et al* 1985, Campos Neto *et al* 1983) and has also been the subject of a simple geochemical study (Melhem 1995). The present work has involved re-mapping the pluton at a 1:25,000 scale and collecting structural and petrological data in an attempt to elucidate the emplacement and deformation processes affecting the pluton.

4.1.2 Previous work

Many of the early references to the geology of the Atibaia region were made solely on the basis of reconnaissance mapping conducted during the compilation of large scale regional maps (reviewed by Oliveira *et al* 1985). The work of Setzer (1953) describes the Atibaia region as consisting of strongly folded and metamorphosed Archaean gneiss, locally containing high grade gneisses and granites. Subsequently Wohlers (1964), who compiled a regional map at 1:100,000 scale, describes the Atibaia granite as underlying (thereby considered older than) the overlying gneisses (then considered to be Archaean in age).

As knowledge of the regional framework became better known the Atibaia region was recognised to consist of ortho- and paragneisses and granites (Ebert 1968), which preserve metamorphic ages (K-Ar) of 553 ± 17 Ma from biotite and 620 ± 19 Ma from amphibole (Ebert & Brochini 1968). The first reference to the tectonics affecting the Atibaia pluton itself was made by Hasui *et al* (1978), who referred to it as being 'syn-tectonic' and part of the regional Cantareira suite.

It was not until the regional mapping projects of Oliveira *et al* (1985) and Campos Neto *et al* (1983) that the structural framework of the Atibaia pluton was recognised (Maps 2, 6 & 7, Figure 4.1). Their mapping shows that the Atibaia area consists of ortho- and paragneissic greenschist to amphibolite facies country rock, which initially had a weak southeasterly dip. Locally this low angle foliation has become steepened into shear zones which have an approximate north-south orientation and a sub-horizontal strike-parallel lineation. These shear zones show a close spatial association with the Atibaia granite itself along the western and southern sides (Camanducaia and Jundiuvira shear zones), but are

not present on the eastern side of the pluton (Figure 4.1). In addition, these authors demonstrate that there are a number of types of intrusive rocks in the area, such as dykes or small, poorly exposed intrusive stocks, but dominated (in areal terms) by the Atibaia pluton, an homogenous body covering 74 km². Oliveira *et al* (1985) describe the pluton as having; i) a north-south alignment; ii) a cataclastic texture; iii) a 3a or 3b granite modal composition; and iv) a zircon topology which characterises it as being deep sub-alkaline in origin.

More recently Melhem (1995) conducted a geochemical study of the granite and was able to demonstrate that the pluton had: i) an approximately alkali granite composition; ii) a highly evolved isotopic source, $(^{87}\text{Sr}/^{86}\text{Sr})_i = 0.7132$; iii) an Rb-Sr whole rock age of $573 \pm 15 \text{ Ma}$; iv) a Caledonian I-type classification; v) crystallised at a high temperature $\sim 860^\circ\text{C}$; and vi) completely homogenised before emplacement in a low water-activity environment. He used these data to suggest that the pluton had been emplaced during subduction related deformation associated with the Brasiliano orogeny.

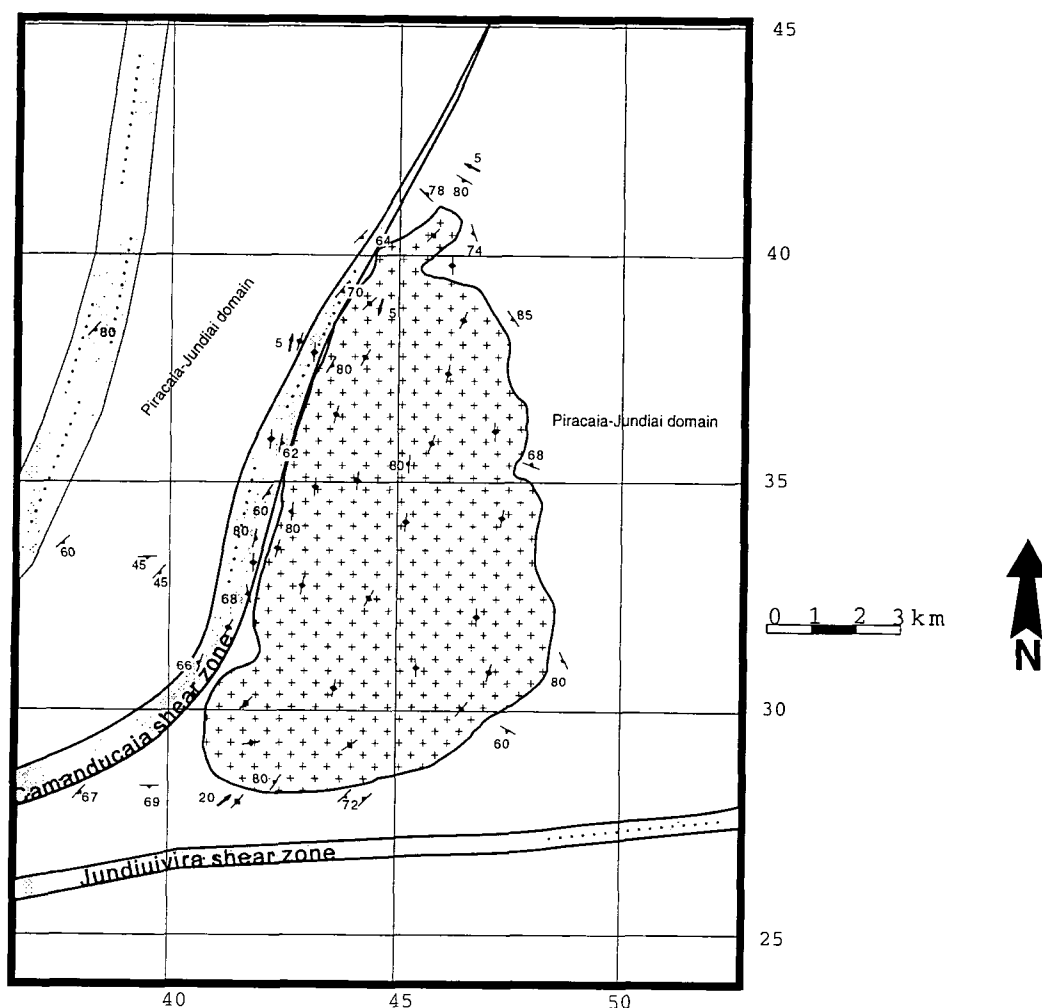


Figure 4.1 Map of the Atibaia pluton

4.2 Mapping

4.2.1 Country rock

The country rock surrounding the pluton is part of the Piracaia-Jundiá domain (Tassinari 1988), a strongly weathered sequence of amphibolite gneisses of volcano-sedimentary derivation (Oliveira *et al* 1985). Mineralogically it consists of quartz, biotite, muscovite, occasional garnet and sillimanite. Sillimanite becomes particularly common along the western side of the Atibaia granite and its formation could possibly be associated with thermal metamorphism during intrusion of the pluton. Intercalated into these gneisses are migmatites, some of which appear to have formed in-situ (Plate 3.10) preserving leucosomes and melanosome. However when larger exposures of migmatite material are observed they are more obviously intruded (Plate 3.11). At distances greater than 500m or so from the pluton the migmatites appear to consist of only 10-20% of the rock (Plate 4.1) but, as the pluton is approached, these become much more common. Examination of localities close to the pluton (<500m) suggests that migmatites (compositionally distinct from the occasionally observed granite dykes) can become up to 50% of the outcrop (Plate 4.2). Granite dykes/sheets are observed within the country rock as rare 10-20cm wide features compositionally similar to the pluton itself, though their exact mineralogy is often difficult to identify as a result of intense weathering.

During this work the country rock exposed around the pluton (1-1.5km from the contact) was mapped as an aid to understanding the dynamics affecting the emplacement and subsequent deformation of the pluton. This mapping has identified two domains which correspond to the eastern and western sides of the pluton.



Plate 4.1 Migmatites at a distance from the pluton (GR 380344).



Plate 4.2 Migmatites close to the pluton contact (GR 44484078).

Western area

The western side of the pluton consists of strongly foliated gneissic rocks which trend north-northeastwards and an associated south-southwestward plunging stretching lineation (Figure 4.2). Close to the pluton the foliation is sub-vertical and very well preserved but, on travelling westward from the contact it becomes much less defined and dips more moderately to the west (Maps 2, 6).

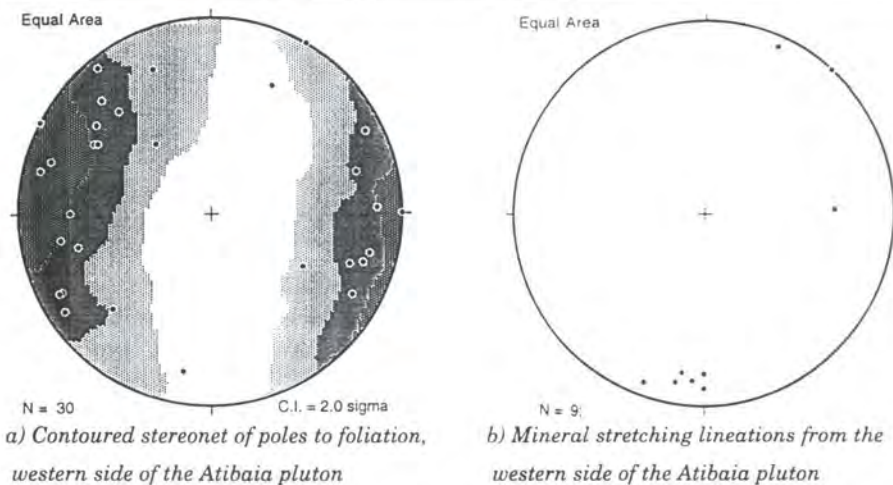
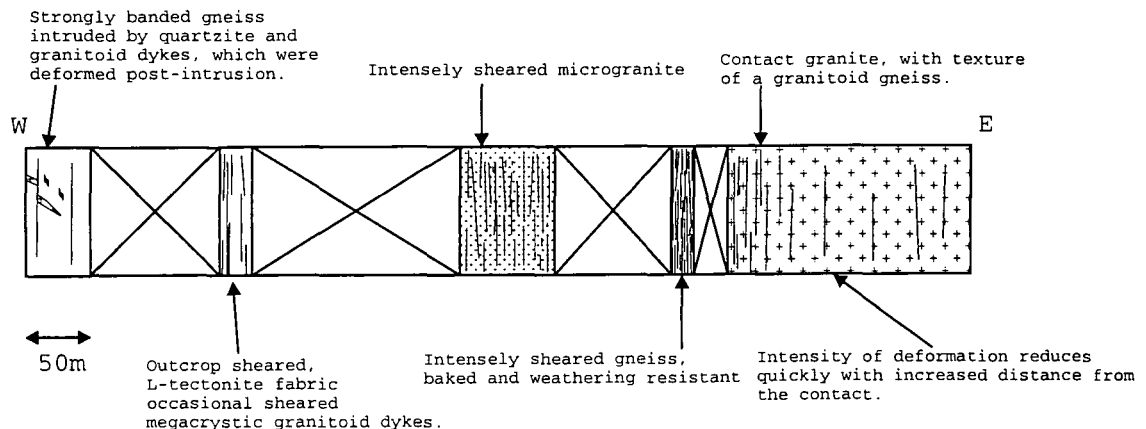


Figure 4.2

In the vicinity of the pluton contact the country rocks show evidence of intense deformation and dextral shearing (see part 4.4.1). In order to describe the nature of the contact and associated deformation a summary log of the contact rocks between GR 42503867 and GR 43123820 is given in Figure 4.3. It shows: i) a strongly foliated gneiss, intruded by granitoid and quartzite dykes, exhibiting non-pervasive shear sense fabrics; ii) 100m closer to the pluton the intensity of deformation increases, the outcrop has a 'rodded', L-tectonite appearance and there are occasional intensely deformed megacrystic granitoid dykes (which may be sourced from the Atibaia pluton itself); iii) 200m closer to the pluton

the gneiss is replaced by microgranite, of indeterminate age, which has developed an intense foliation and a shallowly plunging stretching lineation; iv) the next exposure is situated close to a break of slope, which probably defines the contact with the granite, and shows an intensely deformed gneiss with a sub-horizontal stretching lineation: These gneisses are weathering resistant, which suggests they have been metamorphically altered during intrusion and deformation (their fine-grain size prohibits a mineralogical analysis).



A summary log through the western contact rocks of the Atibaia pluton (GR 42503867 to GR 43123820)

Figure 4.3

Eastern area

The eastern side of the pluton has a similar rock-type to the western side, but there are a number of important differences in the style of deformation observed. In particular the rocks have been only weakly deformed and the foliation is much less intense, showing a greater variability in orientation (Figure 4.1, 4.4, Maps 1, 7). Close to the pluton the average foliation is orientated north-south to northeast-southwest, steep and sub-parallel to the granite contact (Figure 4.4). Stretching lineations are rarely developed and do not show a consistent orientation (Figure 4.4b). Distant from the contact the country rocks show a moderate but variably orientated dip (Map 7), which is locally folded and associated with regional deformation (Campos Neto *et al* 1983).

Examination of a summary log from the pluton itself to the country rock across the contact zone (Figure 4.5) shows: i) homogenous foliated granite with a solid state foliation only weakly overprinting an earlier magmatic foliation; ii) 100m further away from the pluton a fine grained, strongly foliated gneiss which is intruded by metre-scale sheets of Atibaia granite (Plate 4.3) is seen; iii) this zone continues for 20-30m before the sheets become much thinner and have a 'migmatitic' composition; iv) these sheets show symmetric boudinage (Plate 4.4) and continue to develop a strong foliation; v) after 200m of no exposure country rock is again identified and now shows a much weaker foliation with regional structures and fabrics.

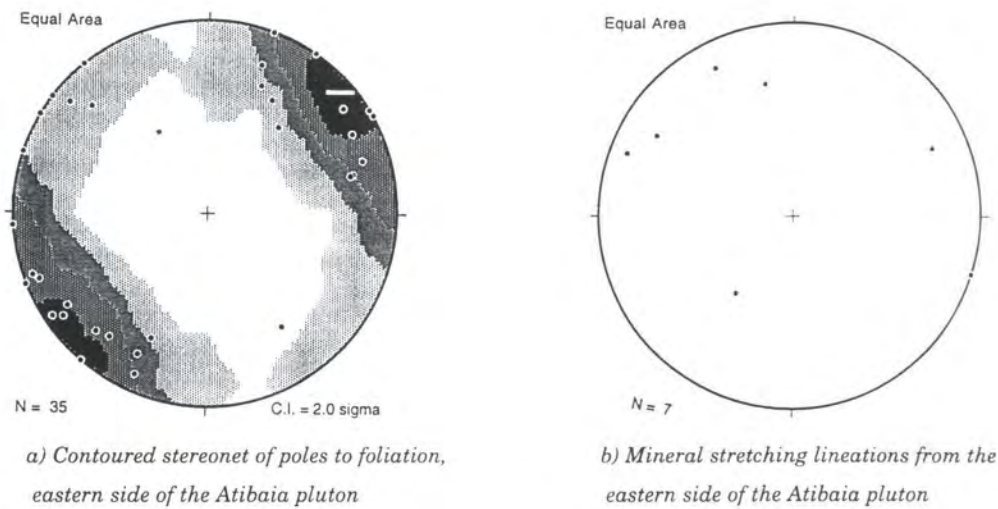
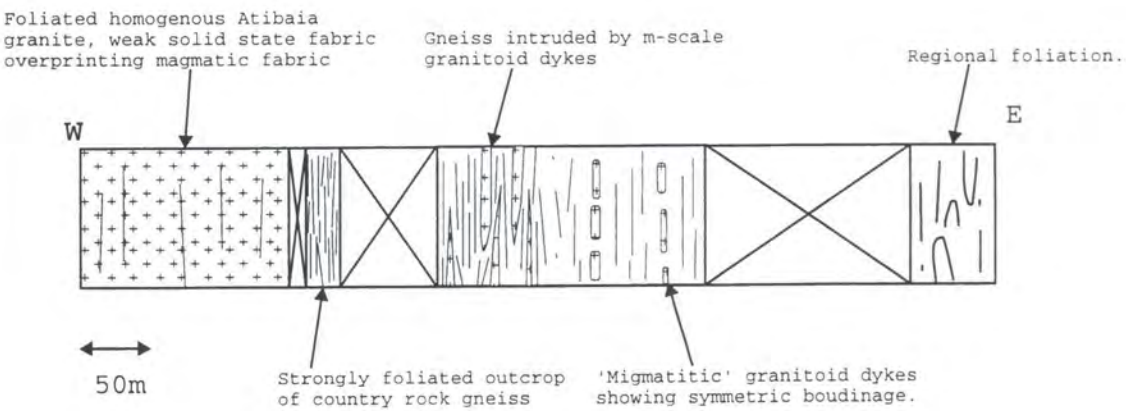


Figure 4.4



Summary log through the eastern contact rocks of the Atibaia pluton (GR 47273593 to GR 48053600)

Figure 4.5

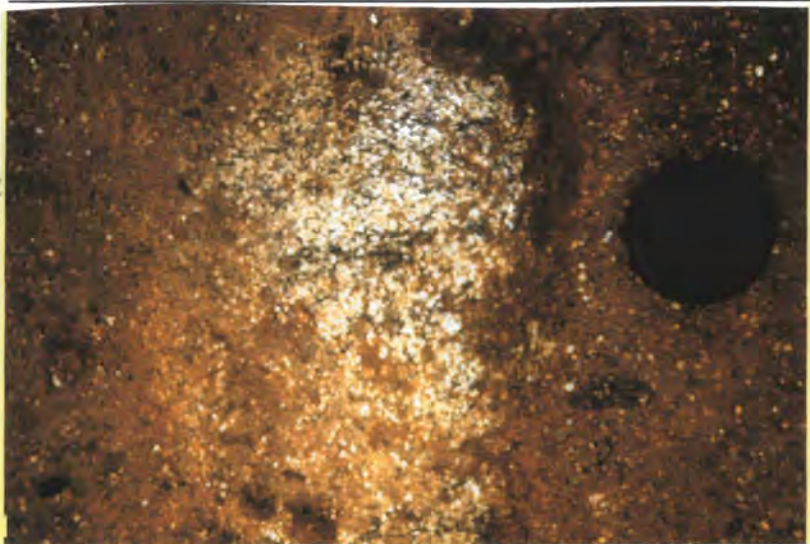


Plate 4.3 Atibaia granite sheet intruding gneissic foliation (GR 44484078)



Plate 4.4 *Symmetric boudinage of granitoid sheet (GR 476 3583)*

Conclusions

These observations suggest that the country rock was intensely deformed and metamorphosed along the western side of the pluton. Along the eastern side deformation was less intense but, importantly, preserves a concordant contact foliation, formed and sheeted into during intrusion of the Atibaia granite.

4.2.2 Nature of the contact

The approach to and deformation surrounding the contact has been described in some detail in the preceding section. The contact itself is generally very sharp and distinct: On the western side of the pluton (Figure 4.3) it is geomorphologically defined by a sharp break in slope and a change in rock type from intensely deformed gneiss (Plate 4.5) into granite, mineralogically identified as the Atibaia granite, but with a granitoid gneiss texture (Plate 4.6). The eastern side of the pluton sees a similar sharp break in slope at the contact (Figure 4.9) and the country rock gneiss shows a fabric sub-parallel to the contact (Plate 4.7), but no intense deformation has been identified. Similarly the granite outcrops close to the pluton contact show a fabric formed in the magmatic state weakly overprinted by a solid-state fabric but not intensified in proximity to the country rocks (Plate 4.8).

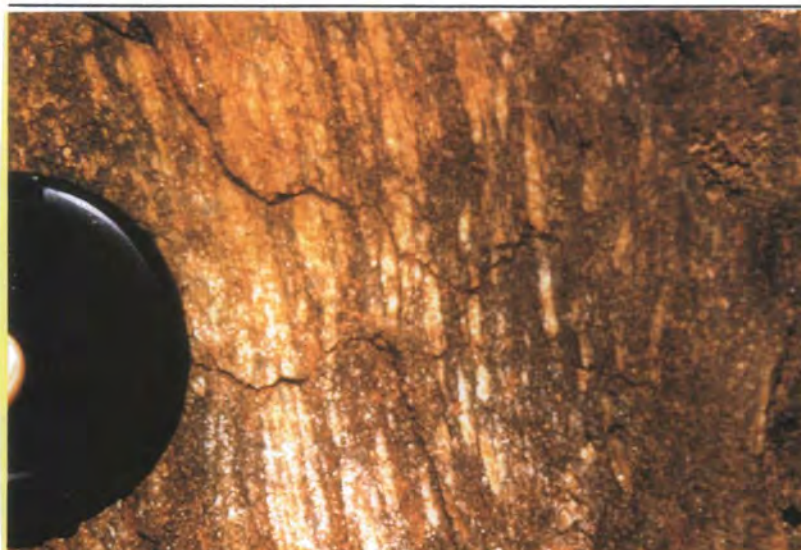


Plate 4.5 *Contact country rocks gneisses on the western side of the Atibaia pluton (GR 380344)*



Plate 4.6 *Contact granite on the western side of the Atibaia pluton (GR 43103818)*



Plate 4.7 *Contact country rock gneisses on the eastern side of the Atibaia pluton (GR 47653583)*

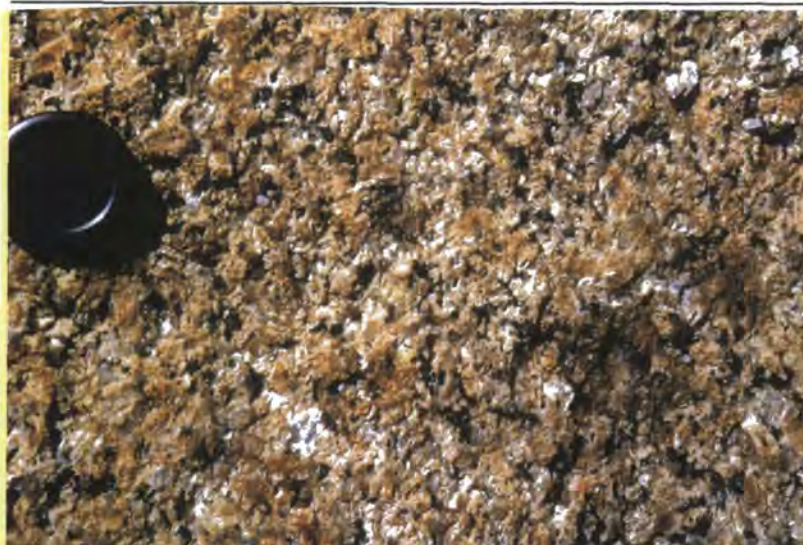


Plate 4.8 *Contact granite on the eastern side of the Atibaia pluton (GR 46903503)*

4.2.3 Granite

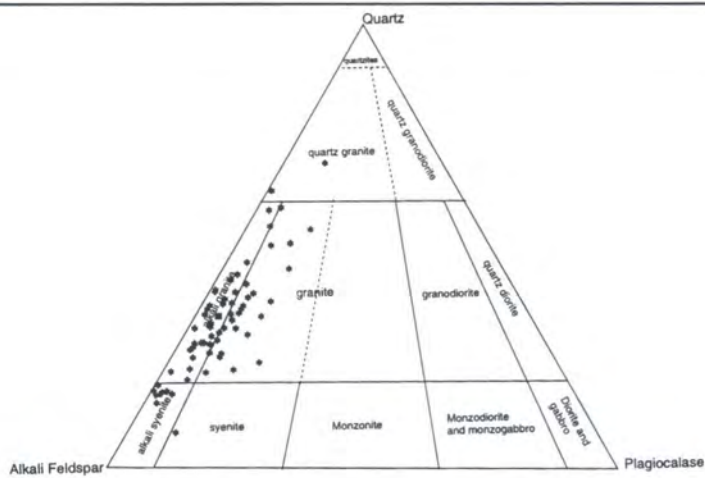
The Atibaia granite itself is a lozenge shaped body which is compositionally homogenous across the whole of its outcrop. In outcrop (Plate 4.9) the granite is coarse grained (crystals ~1cm) and weathers to form a highly abrasive surface texture. It has a pinkish to white colouration as a result of the large percentage of potassium feldspar present. The matrix around these potassium feldspars consists primarily of elongate quartz crystals, blocky biotites and small (1-2mm) plagioclase feldspar lathes. The rock in thin section (Plate 4.10) shows large potassium feldspar crystals (1-2cm), predominantly microcline and perthite, surrounded by a matrix of quartz and biotite, with minor quantities of hornblende, epidote and zircon. Point counting to 500 points of 64 thin sections gives the QAPF diagram modal composition shown in Figure 4.6. This shows the average composition of the Atibaia pluton to be an alkali granite/granite. Structurally the granite shows a strong subvertical composite foliation which has an approximately north-northeast strike (Figure 4.1, 4.7a, Map 1). This fabric has coincident orientations independent of whether it was formed in the magmatic or solid state. In addition there is an occasionally preserved solid state, sub-horizontal stretching lineation (Figure 4.1, 4.7b) defined by the elongation of deformed quartz. No magmatic state lineations have been identified.



Plate 4.9 Photograph of the Atibaia granite (GR 43833215)



Plate 4.10 The Atibaia pluton granite in thin section (GR 45403795)



QAPF modal composition diagram for the Atibaia pluton (stars = Individual analyses, filled square = average composition)

Figure 4.6

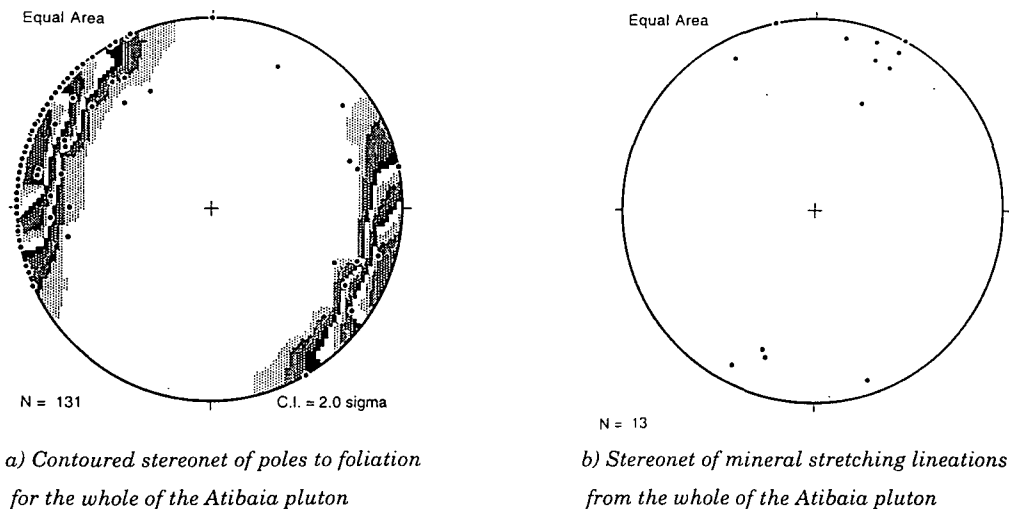


Figure 4.7

4.2.4 Microgranitoid stocks, dykes, enclaves and country rock xenoliths

In and around the pluton there are numerous small microgranitoid stocks, dykes and enclaves. Examining each of these in turn:

Microgranitoid stocks

These are small, very poorly exposed intrusions, often less than 1 km² in size, which intrude into the country rock around the pluton (Plate 4.11). Commonly they show: i) mm-scale grain size; ii) occasional potassium feldspars phenocrysts 1-2cm in size; iii) a matrix of feldspar (plagioclase and microcline), quartz and occasional biotite; and iv) a foliation formed in the solid state which is sub-parallel to the local country rock/pluton fabric. Their contact/age relationships are difficult to determine unequivocally; for example, the intrusion close to the contact around GR 435395 may actually intrude the granite itself, but similar intrusions do not appear to intrude the pluton.

Melhem (1995) interpreted these plutons as contemporary or slightly post-dating the intrusion of the granite itself. The presence of a fabric within the intrusion suggests that they were intruded before the end of tectonism in the area and, if the intrusion at GR 435395 actually intrudes the Atibaia pluton then at least one intrusion occurred post-emplacement of the main granite. In addition their elongate shape suggests that they were deformed by, or the intrusion was strongly controlled by, the regional tectonics. In summary, these bodies have been interpreted to be emplaced post-intrusion of the main pluton but before the end of regional tectonism.

Microgranitoid dykes

Throughout the pluton there are sets of sub-vertically orientated microgranitoid dykes/sheets, commonly less than 50cm in width (Plate 4.12) but continuous along strike for more than 300m. They have sharp contacts with the surrounding granite and have not been conclusively identified in the surrounding wallrocks. They are often unfoliated, but can

preserve an internal shear sense fabric and have a small grain size (1-2mm). Thin section analyses show a modal composition similar to the pluton with the matrix consisting of lathe-shaped potassium feldspars, small plagioclase feldspars, interstitial quartz and biotite (Plate 4.13).

These sheets were intruded after the emplacement of the pluton and non-parallel to the principal granite fabric (see part 4.6 for additional kinematic analysis). Some of them have a shear sense fabric and stretching lineations, but they do not have a planar fabric which is continuous with the plutonic solid state fabric. This suggests that they were intruded either after the development of the final solid state pluton fabric or before this fabric developed, in which case this deformation was not of sufficient intensity to produce a fabric within, or to extensively deform the dykes.



Plate 4.11 Microgranitoid stock intruded into the country rock around the Atibaia pluton (GR 42843030)

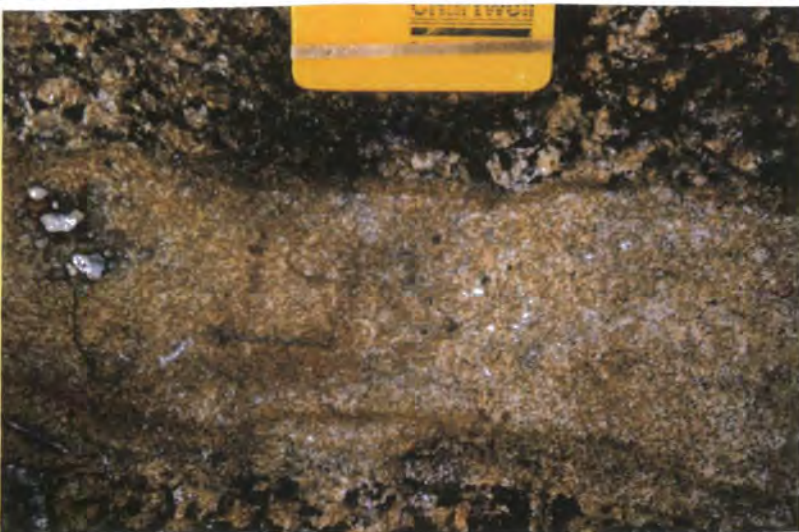


Plate 4.12 Microgranitoid dyke intruded into the Atibaia pluton (GR 44303948)

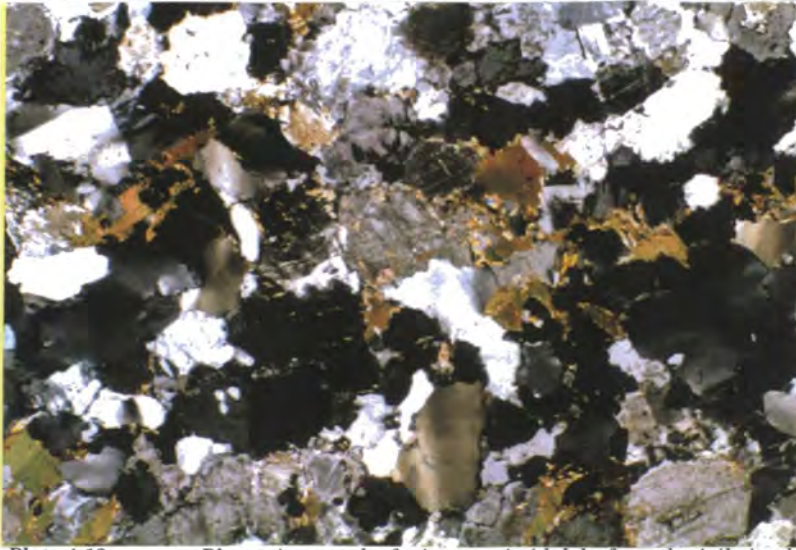


Plate 4.13 Photomicrograph of microgranitoid dyke from the Atibaia pluton (GR 43613690)

Microgranitoid enclaves

This pluton preserves microgranitoid enclaves which are distributed heterogeneously across the intrusion. In general, they are relatively large (average diameter 22cm) and have sharp contacts with the surrounding magma. They are fine grained with an intermediate to felsic, rather than mafic composition (Plate 4.14 and Plate 4.15). In outcrop the enclaves are elliptically elongate along the principal foliation direction and in thin section they preserve a magmatic/solid state fabric sub-parallel to the macroscopic foliation. The axial ratios of the enclaves have been measured and used as indicators of the preserved finite strain using the methods outlined in Chapter 1.



Plate 4.14 Microgranitoid enclave preserved in the pluton (GR 41103058)

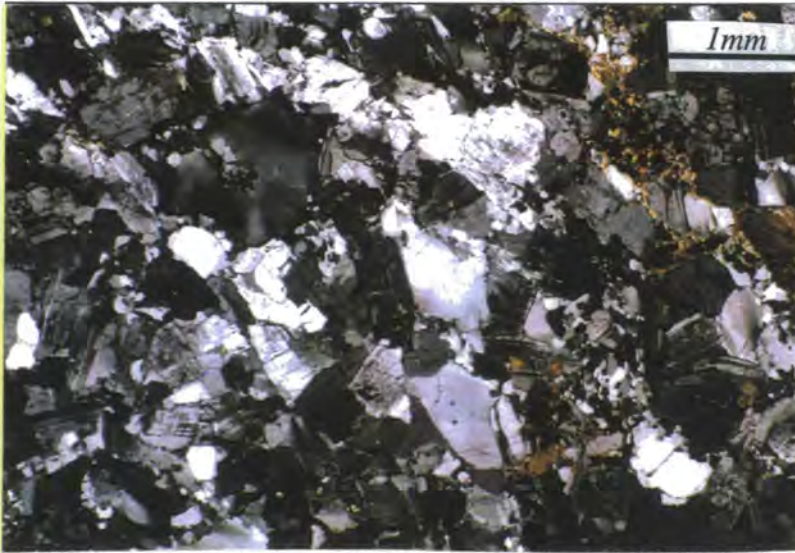


Plate 4.15 Photomicrograph of microgranitoid enclave (GR 43583723)

Country rock xenoliths

Occasionally preserved within the pluton itself are small (dm-scale) angular, dark coloured, foliated fragments of country rock gneiss, aligned sub-parallel to the country rock (Plate 4.16). They are most common in the vicinity of the outer contact and probably represent fragments of wallrock incorporated during intrusion.

4.2.5 Conclusion and discussion

The Atibaia pluton consists of a migmatitic gneissose wallrock which, in the vicinity of the pluton preserves a north-south through to northeast-southwest trending fabric. Close to the pluton this fabric becomes sub-parallel to the contact. The contact between the wallrocks and the granite is generally sharp and defined by a shear zone on the western side and by minor sheeting in the country rocks on the eastern side. The pluton itself is of alkali granite composition and its fabric is steeply dipping, with a north-northeast trend. Subsequent to emplacement of the magma there have been a number of events resulting in an heterogeneous solid state fabric, emplacement of microgranite dykes and the intrusion of a number of small microgranitoid stocks.



Plate 4.16 Country rock xenolith from the Atibaia pluton (GR 44233998)

4.3 Deformation

Examination of the fabrics and deformation preserved within and without the pluton has led to the recognition of discrete events which can be correlated with the regional deformation history as set out in part 3.3.4. These deformations, their features, dispersion and intensity are detailed below using a subdivision of the pluton set out in Figure 4.8.

4.3.1 Country rock

The deformation surrounding the pluton is partitioned into near-field and far-field components, each of which is manifestly different on each side of the pluton. Far from the pluton, particularly on the eastern side of the pluton the regional flat lying or weakly folded D_{n+1} fabric is preserved. Close to the pluton the situation is more complex.

Western side

On the western side of the pluton the fabric is steeply dipping and preserves intense deformation (Plate 4.17) associated with the Camanducaia shear zone, considered to be a regional D_{n+2} feature. This intense deformation has been observed up to 5km from the western contact of the pluton and consists of a fabric defined by deformed quartz, feldspar, and muscovite mica, with or without garnet and sillimanite, which often develops a mineral stretching lineation. It is difficult to estimate the magnitude of this deformation but regional investigations (summarised by Ebert & Hasui *in press*) have suggested that tens of kilometres of offset can occur along similar structures. The scale and intensity of the country rock fabric to the west of the Atibaia pluton suggest that high magnitude deformation has taken place in this area. The ductile deformation and recrystallisation of quartz and possibly feldspar, together with the formation of metamorphic sillimanite, suggests a peak temperature in excess of 500°C. However observations of the Jundiuvira shear zone to the east demonstrate some degree of lower temperature reactivation. It is suggested that since the pluton has only been weakly and heterogeneously deformed (relative to the country rock) by these shear zones (see part 4.3.2) that therefore the shear zones must pre-date the plutons (see Chapter 5 for additional evidence).

Eastern side

The east side of the pluton preserves a similarly steeply dipping fabric, which is concordant with the contact and sheeted into by the granite, but this is seen in only the first 200-300m from the pluton contact. As this fabric was formed in response to the emplacement of the granite it is interpreted as being a D_{n+3} fabric. Further away from this area the country rock fabric is moderately inclined sub-parallel to the regional fabric (composite $D_{n+1/2}$). It is suggested that the intrusion of the pluton formed a D_{n+3} fabric close to the pluton (Plate 4.18), while leaving the remainder of the country rock undeformed (Plate 4.19). Additionally on this eastern side there are no thermal indicators as to the

temperature of deformation. It should simply be noted that the boudinage and sheeting into the country rocks, which make up the contact, occurred in ductile conditions.

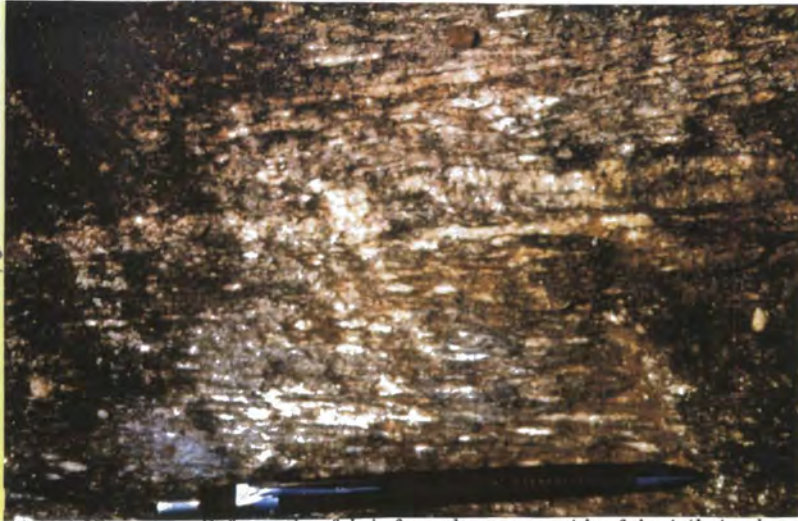


Plate 4.17 *Deformation fabric from the western side of the Atibaia pluton (GR 47553933)*



Plate 4.18 *D_{n+3} fabric close to the eastern pluton contact (GR 47653584)*



Plate 4.19 *$D_{n+1/2}$ fabric on the eastern side of the Atibaia pluton (GR 484392)*

Southern contact zone

The country rocks and granite close to the southern contact are very poorly exposed but, where they can be examined, they show a local concordance with the contact and a rapid return to more regional structure with increasing distance from the pluton itself. Qualitatively the country rock is quite intensely deformed and, as such, is probably related to movement on the Jundiuvira (D_{n+2}) shear zone a few kilometres south of the pluton.

Northern contact zone

The northern contact zone is relatively complex and consists of two zones; the first is related to the contact of the country rocks with the granite of the *North east* area and the second is associated with the contact with the granite of the *northern area* (Figure 4.8). The country rocks associated with the first of these areas show: i) a fabric sub-parallel to the main pluton contact up to 3km from the pluton; ii) a heterogeneous shear-zone related fabric; and iii) intrusion of sheets of strongly deformed Atibaia granite. These features all suggest that this area preserves an intrusion related D_{n+3} fabric which may have been overprinted during later D_{n+4} deformation. The second of these areas shows a fabric sub-parallel to the northern area contact, but with variable dip and few shear sense indicators. This fabric may be a result of the intrusion (D_{n+3}) or a rotation of an earlier regional fabric ($D_{n+1/2}$). Along the eastern side of the *northern area* the fabric shows a greater intensity, which may be the manifestation of a local shear zone in this area (Oliveira *et al* 1985) or a country rock expression of the solid state fabric observed throughout the pluton.

Conclusions

The western side of the pluton preserves the imprint of intense strike-slip deformation, at a peak metamorphic grade of amphibolite facies. These features form part of regional structures which pre-date the intrusion of the pluton. The eastern side of the pluton preserves a regional composite $D_{n+1/2}$ fabric, which is locally deflected within 200-300m of the pluton itself to form a D_{n+3} intrusion related fabric.

4.3.2 Granite

The granite preserves an approximately north-south trending fabric of variable intensity. In order to attempt to describe the observed variation the pluton has been subdivided as detailed in Figure 4.8.

Northern area

The northern part of the pluton comprises the thin northeast trending extension of the main intrusive body. This area preserves granite which has a slightly smaller crystal size than the main body of the pluton and a well-developed foliation. Field observations suggest that this foliation was formed in the magmatic state and that there is only a very weak solid state overprint (Plate 4.20). In addition the country rocks at the western contact

of this area do not show the intense fabric which is characteristic of the area, suggesting that the main shear zone is not sub-parallel to the contact in this area.

The Northern area is interpreted to have formed as a result of local intrusion of Atibaia granite magma, or possible local northwards directed expansion along a tectonic weakness (possibly a shear zone bifurcation). Later deformation, such as the intrusion of microgranite dykes, overprinting foliation and the formation of mylonites, did not affect this area significantly.

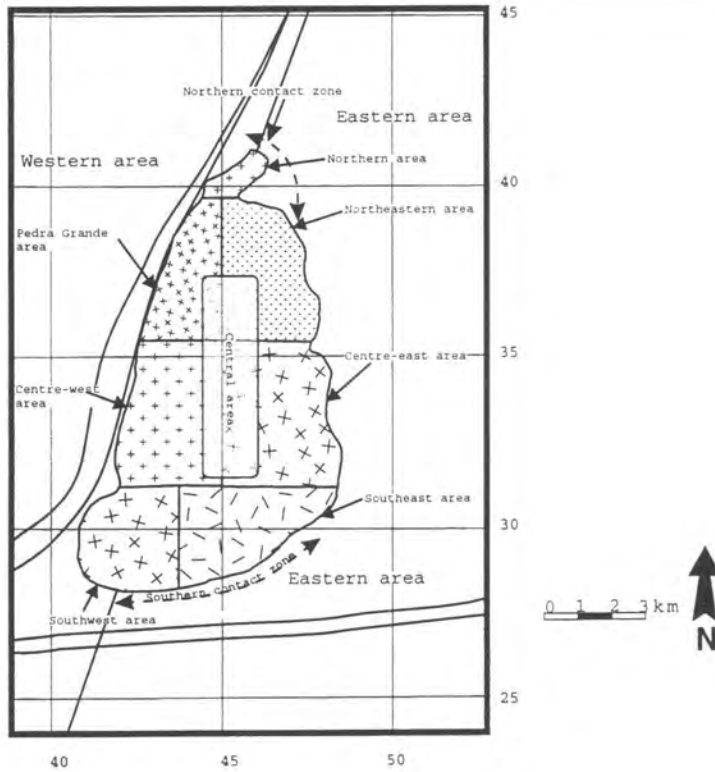


Figure 4.8 Map showing approximate division of the pluton and country rock used in the text



Plate 4.20 Granite fabric from the Northern area Atibaia pluton (GR 45504131)

Pedra Grande area

The Pedra Grande area comprises the northwestern corner of the pluton and is characterised by very large planar hilltop exposures. The deformation in this area is characterised by a solid state fabric of variable intensity. Close to the country rock contact this fabric is locally homogenous and intense, producing a granite gneiss texture defined by ribbon quartz, rounded and abraded feldspars and elongate biotite crystals (Plate 4.21). At distances of more than 100-200m from the contact the intensity of this fabric reduces, and feldspar and biotite retain a rectangular shape, although the fabric continues to be characterised by ribbon quartz (Plate 4.22). Thin section investigation of the Pedra Grande fabric shows that close to the pluton contact the deformation is intense, with strong shear sense fabrics, brittle fabric of feldspar and undulose extinction in quartz (Plate 4.23). In the areas where weaker deformation is recorded, often only quartz is deformed to produce undulose extinction (Plate 4.24). These fabrics indicate deformation took place in this area of the pluton at less than 300°C, using the criteria defined by Passchier & Trouw (1996). The areas of weaker deformation are intruded by microgranite sheets, which are linear along strike and do not appear to be deformed by the solid state overprint, except during the development of occasional ductile shear sense fabrics (see part 4.6). Throughout this area there are occasional thin (~1cm wide) mylonites which criss-cross the outcrops. In the area around GR 4436 they become peculiarly pervasive (see part 4.7 for a kinematic analysis).

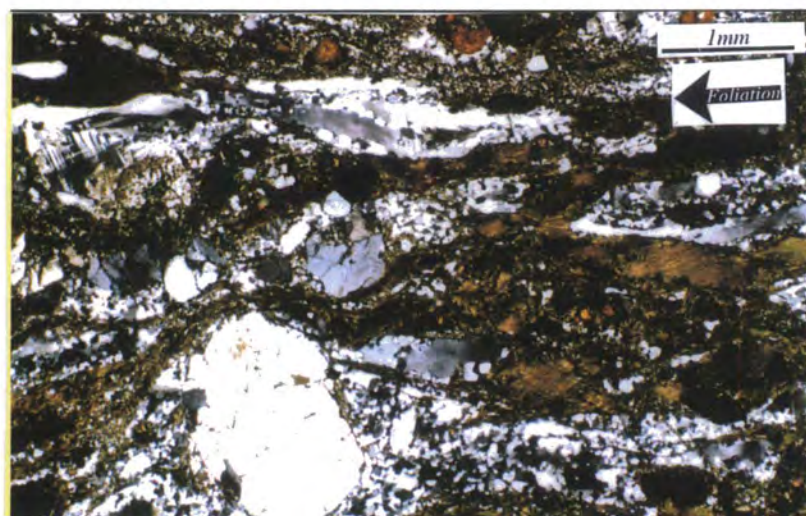


Granite gneiss texture close to the pluton contact, Pedra Grande area, Atibaia pluton (GR 43703968)

Plate 4.21



Plate 4.22 Solid state fabric preserved in the majority of Pedra Grande area outcrops (GR 43583723)



Photomicrograph of the granite gneiss texture, Pedra Grande area, Atibaia pluton (GR 43703968)

Plate 4.23

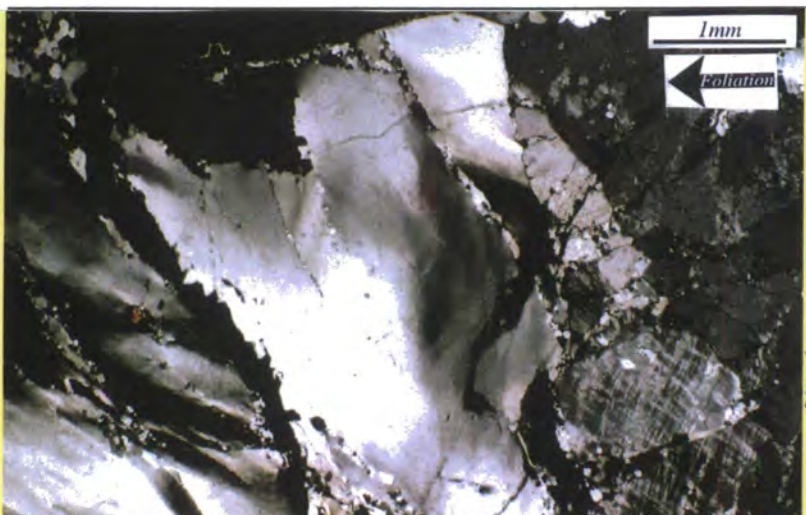


Plate 4.24 Photomicrograph of the solid state fabric, Pedra Grande area, Atibaia pluton (GR 43583723)

North east area

This area comprises the outcrops present in the northeastern corner of the pluton and shows a solid state fabric of variable intensity. In the field it is distinguished by ribbon quartz fabrics, which become more intense as the eastern contact of the pluton is approached (Plate 4.25), but nowhere approaches the intensity developed along the western contact (Pedra Grande area). In thin section quartz exhibits undulose extinction, and feldspar shows cracking, indicating solid state deformation taking place between 300°C and 400°C (Passchier & Trouw 1996). The fabric is approximately north-northeast trending and is not deflected in the vicinity of the northernmost contact of the pluton.



Plate 4.25 Solid state fabric from the North East part of the Atibaia pluton (GR 47063916)

Centre west area

Outcrops from this area along the contact show a similar set of fabrics to those developed in the Pedra Grande area; a strong gneissic fabric which drops rapidly in intensity to preserve a more pervasive solid state fabric. Those outcrops relatively far from the contact (>2km) may additionally preserve original magmatic fabrics, which have suffered only a very minor solid state overprint. Examination of thin sections which display a solid state fabric from this area show minor recrystallisation and undulose extinction quartz and occasional recrystallisation of feldspar. Such features indicate deformation at temperatures between 300°C and 500°C (Passchier & Trouw 1996).

Centre east area

The Centre east area of the pluton is distinguished by having a very low intensity solid state fabric, which is developed relatively homogeneously across the area (Plate 4.26). It is orientated sub-parallel to the long axis of the pluton and is parallel to the earlier magmatic fabric, which can be distinguished in places. The intensity of this fabric does not increase with proximity to the eastern pluton contact. In thin section weakly undulose

quartz crystals and bent feldspars have been observed, indicating formation of the solid state fabric at approximately 300°C (Passchier & Trouw 1996).

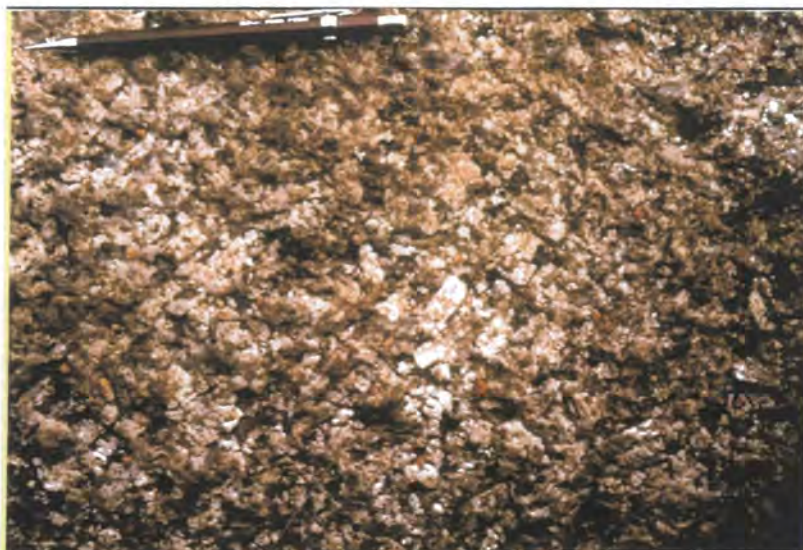


Plate 4.26 Fabric from the Centre East area, Atibaia pluton (GR 46133453)

South west area

The South west area is delimited by the westward bulging of the pluton near its southern contact. This area differs from others in the orientation of its fabric, which trends from northeast-southwest to east northeast-south southwest, but the style of deformation remains the same. The deformation consists of a moderate intensity, relatively homogenous solid state fabric defined in outcrop by ribbon quartz and occasionally by rounded feldspar (Plate 4.27). Contact rocks are poorly exposed in this area but there does not appear to be any intensification of the pluton fabric on approaching either the western or southern pluton contacts. Examination of thin sections from this area shows that the solid state deformation can be locally variable in intensity and consists of quartz which is recrystallised and has undulose extinction as well as bent and occasionally recrystallised feldspars and deformed biotites. These features are consistent with deformation at between 300°C and 500°C. No preserved magmatic fabrics have been observed in the area.

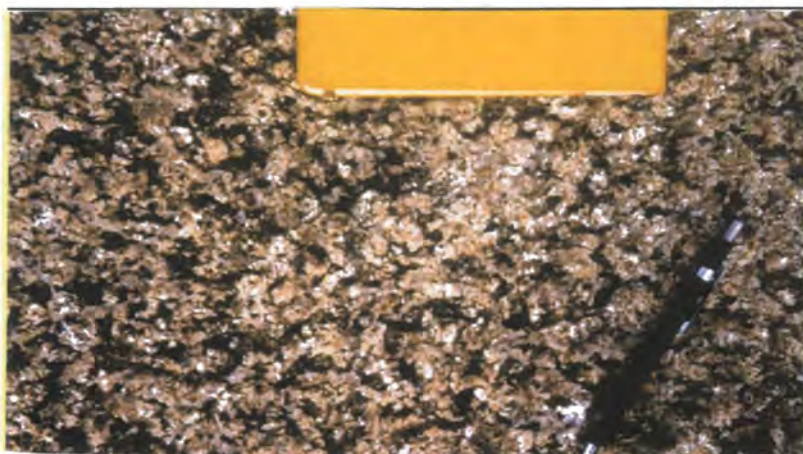


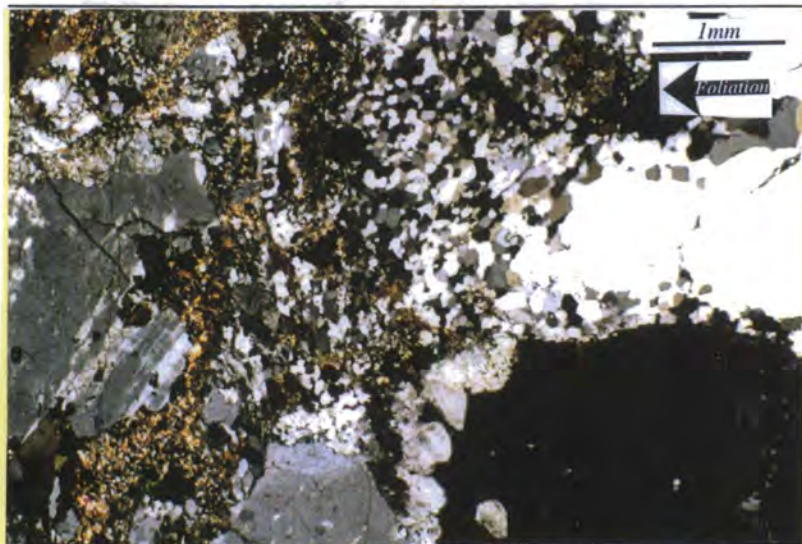
Plate 4.27 Solid state fabric from the south west area of the Atibaia pluton (GR 42532923)

South east area

There are relatively few outcrops in this area, but where they are observed they show a fabric sub-parallel to the pluton axis, which is commonly weak and formed in either the solid or the magmatic state. The solid state fabric is heterogeneously developed and does not appear to show any relationship to the proximity of the pluton contacts. Examination of thin sections of the fabric show that quartz and feldspar recrystallisation are the dominant deformation mechanisms (Plate 4.28) implying a temperature of deformation of 400°C-500°C (Passchier & Trouw 1996)

Central area

The central part of the pluton consists of exposures on the flanks and floor of the central valley which bisects the pluton. The exposures in this area are remarkable because they comprise granite which retains only a magmatic fabric. This fabric is weak, occasionally unidentifiable, sub-parallel to the regional solid state fabric and preserves crystal orientation formed during magmatic flow (Plate 4.29). Examining thin sections from this area shows a set of almost pristine magmatic fabrics in feldspar and biotite, with very weak solid state deformation affecting some of the quartz crystals (Plate 4.30).



Photomicrograph of the solid state fabric from the South East area, Atibaia pluton (GR 47253086)

Plate 4.28

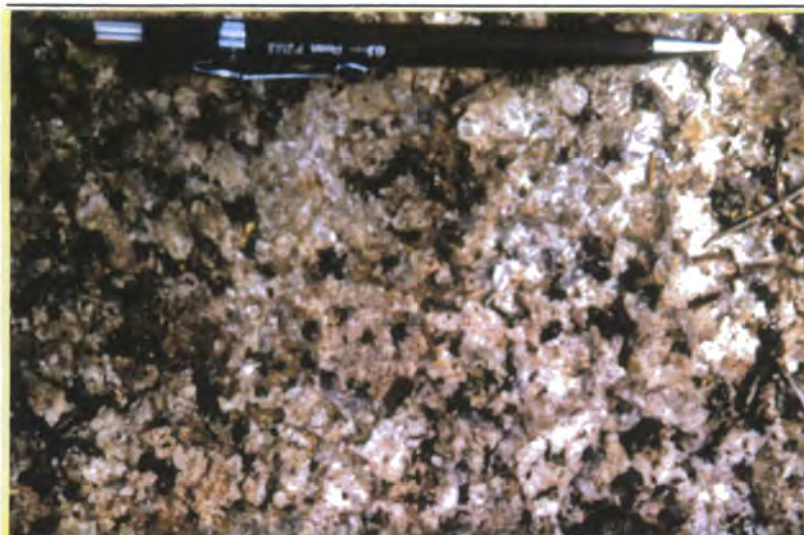


Plate 4.29 Magmatic fabric in outcrop from the Central area, Atibaia pluton (GR 44433648)



Plate 4.30 Magmatic fabric in thin section from the Central area, Atibaia pluton (GR 44363693)

Conclusions

The Atibaia pluton was formed with a D_{n+3} fabric, which trends sub-parallel to the long axis of the pluton. This foliation is best preserved in the central parts of the pluton. After the pluton had cooled it was overprinted by a solid state foliation (orientated sub-parallel to the long axis of the pluton) whose intensity is proportional to the distance of the outcrop from the outer contacts, and particularly by proximity to the Camanducaia shear zone along the western side of the pluton. The Jundiuvira shear zone to the south of the pluton does not appear to have affected the development of this fabric. This solid state overprint formed fabrics which are indicative of deformation between 300°C and 500°C (Passchier & Trouw 1996), the lowest temperature fabrics forming along the western side of the pluton. Both of these fabrics have been overprinted by discrete mylonites, whose density appear to be controlled by proximity to the surrounding shear zones.

4.3.3 Conclusion and discussion

The deformation recorded by the Atibaia pluton and within its surrounding rocks has a number of general features:

1. **Shear zones** - The pluton is bounded on two sides by major D_{n+2} shear zones the Camanducaia shear zone (which controlled deformation along the western contact) and the Jundiuvira shear zone a short distance to the south (this zone does not appear to have controlled fabric formation around the pluton).
2. **Syn-emplacement fabrics** - During emplacement of the pluton a weak D_{n+3} magmatic fabric was formed which trends sub-parallel to the long axis of the pluton. It is now preserved only in the central parts of the pluton.
3. **Solid state overprint** - The magmatic fabric was overprinted by the formation of a D_{n+4} solid state fabric associated with reactivation of the Jundiuvira shear zone. This reactivation controls the fabric preserved in most outcrops, becoming most intense along the western contact and at the northeasternmost corner of the pluton.
4. **Temperature of deformation** - Interpreting the development temperature of the solid state fabric and similar fabrics in the country rocks suggests that, D_{n+4} deformation took place between 300°C and 500°C.
5. **Discrete deformation** - Overprinting all the previous fabrics are discrete mylonites, whose density is controlled by proximity to the outer shear zones.

4.4 Strain measurement

In order to estimate the preserved finite strain within the Atibaia pluton two methods of strain analysis were used; i) the measurement of the axial ratios of incorporated granitoid enclaves; and ii) the measurement of fabric strain using the Fry (1979) method. The methods used in each of these techniques were outlined in part 1.5 and the results are shown below:

4.4.1 Microgranitoid enclaves

Methodology

Microgranitoid enclaves are quite rare within the Atibaia pluton, and consequently there are very few comprehensive datasets. In an effort to produce a dataset which was consistent and accurate enclave populations from discrete localities were combined with others in the vicinity to produce a more statistically robust analysis. Also, exposures rarely display large areas of vertically orientated outcrop, and hence enclave measurements represent axial ratios measured in only the horizontal outcrop plane i.e. the sub-horizontal plane perpendicular to foliation.

Table 4.1, details a summary of the results, which are plotted spatially in Figure 4.9: the full dataset is given in Appendix 6.

Results

Mafic enclave axial ratios from right across the pluton are very consistent (Figure 4.9), recording values from the horizontal plane of $R_s=1.97-3.21$ (pluton average $R_s=2.5$). Indeed across a number of very large single outcrops there is a very remarkable homogeneity. There appears to be no interpretable intra-pluton pattern to these ratios and therefore these axial ratios are taken to represent an average east-southeast directed shortening of 45%, and a stretching sub-parallel to the pluton long axis of 35%, assuming that the enclaves record pure ($K=0$) flattening.

Conclusions

Mafic enclave axial ratio estimates of the finite strain recorded during the emplacement process show a homogeneity of strain right across the pluton. This is interpreted to be the result of an homogenous north-south stretching during and post-emplacement.

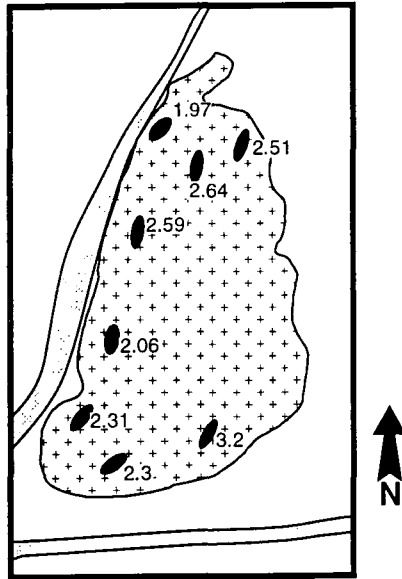


Figure 4.9 Spatial plot of horizontal plane average mafic enclave axial ratios from the Atibaia pluton

Table 4.1 Summary table of mafic enclave axial ratios from across the Atibaia pluton

Localities	Grid Ref.	Mean axial ratio	Number of analysed enclaves	St. Dev	Smallest axial ratio	Largest axial ratio	ω log	% variation in size
BB1	GR 42763494	2.06	38	0.71	1.00	4.26	0.63	34
BG3	GR 46003010	3.21	11	1.56	1.56	6.22	0.60	49
BI	GR 43232810 GR 42532923	2.30	202	0.99	1.00	6.89	0.84	43
BJ	GR 41453028 GR 41283051	2.31	25	0.87	1.33	5.50	0.62	37
BK1 - BK4	GR 43783665 GR 43533670	2.59	57	1.38	1.29	8.82	0.84	53
BQ3, BQ4 & BQ7	GR 44063970 GR 44333904 GR 44303948	1.97	38	0.70	1.00	4.00	0.60	35
BS1 - BS4	GR 45633945 GR 45903868	2.64	58	1.64	1.46	9.61	0.82	62

There is very little vertical plane exposure anywhere across the pluton and therefore all the readings were made in the horizontal plane.

4.4.2 Fry strain

Methodology

During this study 159 individual determinations were made from tracings and photographs of outcrops (each individual tracing consists of an average of 50-70 individual crystals) in the horizontal and vertical planes. Individual Fry determinations were then combined with similar data from the same geographical area to produce a robust and consistent value, for the fabric strain preserved in the horizontal and vertical planes.

These data are listed in full in Appendix 7, plotted spatially in Figure 4.10 and a summary is given in Table 4.2.

Results

These data (Figure 4.10, Table 4.2) show that the Fry strains preserved within the pluton are homogenous, showing axial ratios, R_s , in the horizontal plane of 1.91-2.4, with an average of $R_s=2.14$. In the vertical planes the range of recorded values is 1.81-2.35, with an average of $R_s=2.14$. These results indicate that the entire pluton was subject to an east-southeast directed flattening which resulted in extension in the horizontal and vertical planes of 29% and consequent shortening of approximately 40%.

In addition these results demonstrate that the strain recorded by the fabric was dominantly a flattening strain, with $0 < K < 1$.

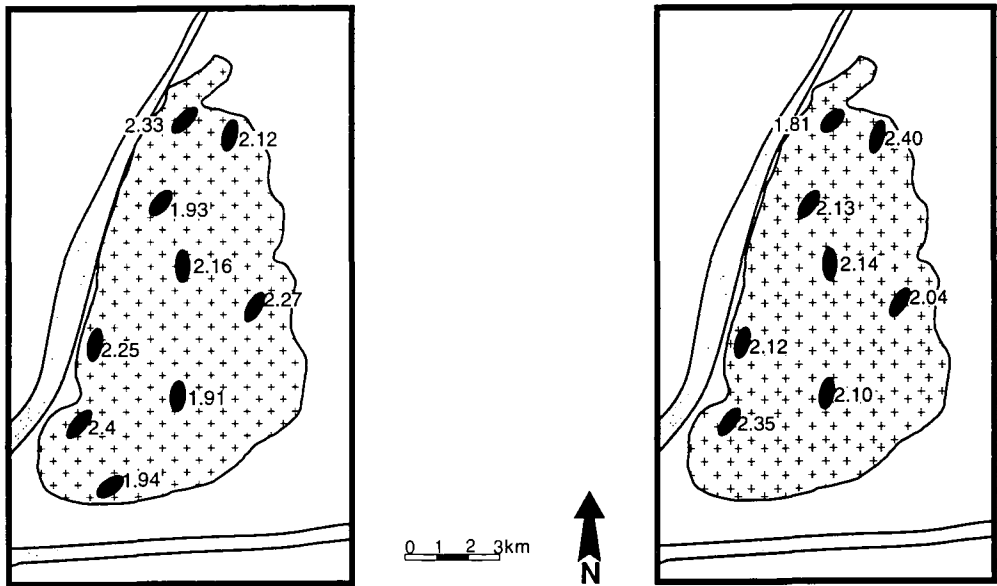
Conclusions

The Fry strain recorded by the Atibaia pluton provide the only dataset which gives a representation of the three-dimensional nature of the finite strain ellipsoid from across the pluton. These data show that the Fry strain is homogenous across the pluton and shows no consistent variation with spatial position within the pluton. In addition, the type of strain recorded is a flattening strain (in general $K < 1$), suggesting that recorded finite strain has not been strongly controlled by the regional shear zones. Similarly to the mafic enclave data, it is concluded that these data represent an homogenous finite strain.

Table 4.2 Summary table of Fry strain data from the Atibaia pluton

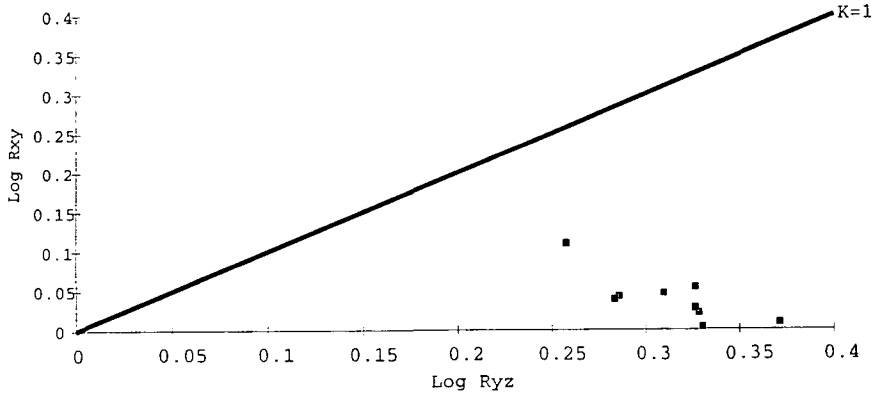
Localities	Grid References	Orientation	Fry strain	Number of analyses	Smallest Fry reading	Largest Fry reading	St. Dev.	K-value
BC5, BX2-5, BQ6-7	GR 43403819, GR 43143843, GR 43333795, GR 43853825, GR 44303948	HORIZ	1.93	8	1.47	2.53	0.35	0.58
BC5, BX2-5, BQ6-7	GR 43403819, GR 43143843, GR 43333795, GR 43853825, GR 44303948	VERT	2.13	5	1.80	2.84	0.42	
BI1-10	GR 43232810, GR 43232923	HORIZ	1.94	8	1.39	2.48	0.41	n/a
BJ1-4	GR 41453028, GR 40503100	HORIZ	2.40	7	1.81	3.50	0.57	0.18
BJ1-4	GR 41453028, GR 40503100	VERT	2.35	2	1.86	2.83	0.69	
BK1-6, BR2-3	GR 43783665, GR 43613698, GR 44043673, GR 44033718	HORIZ	2.24	8	1.54	2.69	0.43	0.06
BK1-6, BR2-3	GR 43783665, GR 43613698, GR 44043673, GR 44033718	VERT	2.13	3	1.94	2.24	0.12	
BL2-7	GR 41743383, GR 42103353	HORIZ	2.26	5	1.94	2.64	0.29	0.09
BL2-7	GR 41743383, GR 42103353	VERT	2.12	3	1.94	2.24	0.16	
BO1-4, BY1-6	GR 43833215, GR 44653262, GR 44353331, GR 42813293	HORIZ	1.92	10	1.47	2.49	0.48	0.14
BO1-4, BY1-6	GR 43833215, GR 44653262, GR 44353331, GR 42813293	VERT	2.10	5	1.74	2.41	0.24	

Localities	Grid References	Orientation	Fry strain	Number of analyses	Smallest Fry reading	Largest Fry reading	St. Dev.	K-value
BP1-2, BE1-3	GR 46783525, GR 46093483	HORIZ	2.27	7	1.77	2.74	0.34	0.15
BP1-2, BE1-3	GR 46783525, GR 46093483	VERT	2.04	2	1.81	2.27	0.13	
BS2-6, CB1	GR 45603909, GR 46703880, GR 47053878	HORIZ	2.12	7	1.78	2.68	0.58	0.17
BS2-6, CB1	GR 45603909, GR 46703880, GR 47053878	VERT	2.40	2	2.00	2.80	0.57	
BV1-8	GR 45783975, GR 46434133	HORIZ	2.33	4	1.70	3.13	0.60	0.43
BV1-8	GR 45783975, GR 46434133	VERT	1.81	2	1.71	1.90	0.13	
BW1-7	GR 45003506, GR 44133439	HORIZ	2.16	6	1.86	2.53	0.24	0.01
BW1-7	GR 45003506, GR 44133439	VERT	2.14	3	1.77	2.59	0.42	



a) horizontal plane

b) vertical plane



c) Log Flinn plot

Figure 4.10 Spatial plot of Fry strains from the Atibaia pluton

4.4.3 Other strain indicators

Close to the western contact of the pluton very high intensity, LS-type, plane strain, solid state deformation fabrics. Examining some of these fabrics shows crystal aspect ratios of up to 10:1 (Plate 4.19) within the country rock gneisses, and up to 4:1 in the granite itself (Plate 4.6). These fabrics suggest sub-horizontal stretching of between 250% and 460%, locally along the contact, during D_{n+4} solid state overprinting. Elsewhere within the pluton this deformation did not induce significant additional finite strain into the measured strain markers.

4.4.4 Country rock strain

Measurements of the strain recorded within the country rock are not easily made because of the often poor exposure and the lack of appropriate strain markers. Qualitative estimates can be made from observations of the intensity of deformation in the country rock, which suggest that:

1. Along the eastern side of the pluton country rock strain is more regionally controlled, but in the vicinity of the eastern pluton contact some emplacement related strain of significant magnitude took place.
2. The rocks along the eastern contact are deflected within 300m of the contact from a moderate westerly dip of approximately 50° to being approximately sub-vertical. Making a calculation based on the deflection of this country rock (Equation 2.4) suggests a strain ellipsoid axial ratio of $R_s \sim 10$, which is equivalent to local shortening (assuming pure flattening, as demonstrated by the fabric in this area) $\sim 80\%$. Therefore it is possible that up to 1km of space for the pluton may have created as a consequence of this deflection.

4.4.5 Conclusion and discussion

The analyses detailed above show that while the fabric of the Atibaia pluton may vary in qualitative intensity both across a single outcrop and the whole pluton, the recorded strain is very homogenous: this is independent of the method used for its determination, though the actual values recorded by each method vary somewhat (see part 8.5 for discussion of this effect). These results suggest a number of general conclusions about the emplacement of the pluton:

1. **Intensity of solid state overprint** - Though the pluton was subject to a pervasive, overprinting, solid state strain (S_{n+4}), which is most intense along the western side of the pluton, it was not sufficiently intense to result in a general increase in the finite strain registered by either the mafic enclaves or the fabric itself. It is known that there are some areas where more intense overprinting deformation has been partitioned e.g. GR 4436, but this is not thought to be a general effect. Therefore, it is concluded that the overprinting D_{n+4} deformation was pervasive but, on the pluton scale, of low magnitude.

- 2. Source of strain homogeneity** - The pluton demonstrates a remarkable degree of homogeneity of strain, despite preserving a pervasive solid state overprint of an earlier magmatic fabric. Therefore it is probable that this finite strain was induced during the initial intrusion of the magma itself. There could be a number of reasons for this initial strain: i) an initially spherical pluton could have been deformed into to a lozenge shape during regional compression. This is considered as being unlikely because; a) the axial ratio of the pluton is approximately $R=1.6$, and the recorded axial ratios are generally greater than $R=2$; and b) a concentric foliation and conjugate shear sense fabrics would be expected within and without the pluton none of which are observed; or ii) individual magma sheets or dykes emplaced through a central conduit underwent a flattening-type strain sufficient to induce strain ellipsoid axial ratios of approximately $R=2.14$ during homogenisation into the body of the pluton. This would suggest, given that the pluton length is approximately 13km, that the conduit length could have been around 10km long; and iii) it is possible that an initial shape obliquity of the microgranitoid enclaves could produce these results but Hutton *et al* (1995) and this work (Chapter 2) have shown that where weakly deformed microgranitoid enclaves have been observed they have small initial shape obliquities of the order of $R\sim 1.4-1.6$.
- 3. Passive emplacement** - These finite strain estimates, from both the mafic enclave axial ratios and the Fry strains, show that the pluton was subject to straining during the emplacement process. Where observed the magmatic fabric has a qualitatively weak intensity but preserves quantifiable finite strain and therefore the pluton did not emplace entirely passively but deformed itself and its surroundings during intrusion.
- 4. Country rock strain** - Estimates of the finite strain recorded by the wallrock around the eastern contact of the pluton suggest that up to 1km of space could have been created in this manner. This is a maximum of 20% of the total width of the pluton, and demonstrates that at least 3km of space may have been created by other processes.

4.5 Shear senses

4.5.1 Introduction

Within both the country rock and granite shear sense fabrics can be recognised and have been recorded as part of this work. They have been determined in a number of ways: i) by qualitative description of outcrop fabrics; ii) examination of thin section microstructures; iii) quantitative analysis of fabrics. These results have then been plotted upon the pluton map and the associated tectonic interpretations discussed in the text.

4.5.2 Country rock

Shear sense fabrics of various types are ubiquitous throughout the country rock around the pluton but vary in intensity and shear sense depending upon their position relative to the Atibaia granite itself. In general country rock fabrics form LS- or L-tectonites as a result of sub-horizontal simple shear (Figure 4.2, 4.4).

Western area

As described in part 4.2.1, the western side of the pluton shows strong ductile deformation consistent with its interpretation as the local expression of the Camanducaia shear zone. All the shear sense fabrics (asymmetric porphyroclasts/boudinage, S-C fabrics etc.) recognised in this area have been interpreted as having a dextral shear sense. Some examples are shown in Plates 4.31 and 4.32, and individual measurements of shear sense in Figure 4.11a.

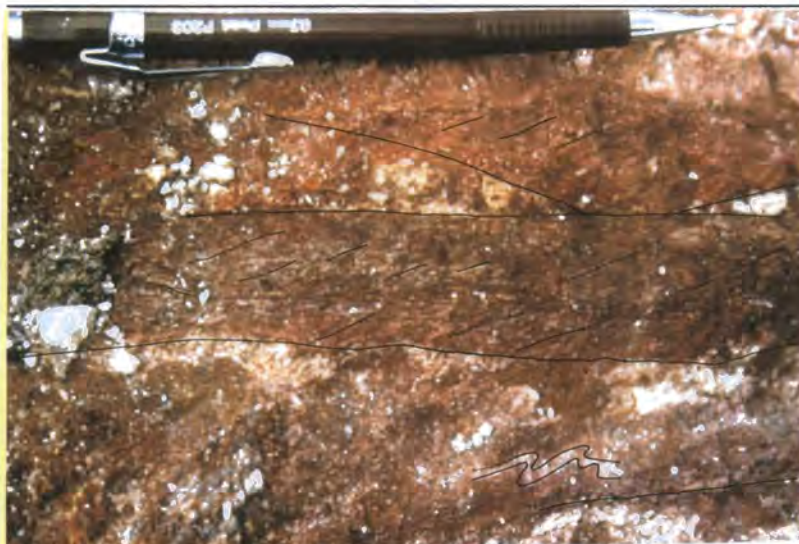


Plate 4.31 Dextral fabric from the western side of the Atibaia pluton (GR 42483851)



Plate 4.32 Dextral asymmetric porphyroclasts from the western side of the Atibaia pluton (GR 43634008)

Eastern area

The eastern side of the pluton often preserves no shear sense fabric at all, indeed the contact at GR 47253590 appears to preserve symmetric boudinage fabrics. The country rocks to the southeast of the granite do not preserve any consistent pluton related shear sense fabrics; whereas around the *Northern contact area* the country rocks which preserve a strong intrusion/deformation related fabric display dextral shear senses (Plate 4.35).



Plate 4.33 Dextral shear sense from the northern contact area Atibaia pluton (GR 47553933)

Southern contact area

The southern contact of the pluton is relatively poorly exposed and it was only possible to identify a few shear sense fabrics in this area, which show a sinistral sense of shear. This shear sense has an identical orientation to that found on the Jundiuvira shear zone which is exposed a few kilometres to the south of the pluton.

4.5.3 Granite

Magmatic state deformation

The magmatic state fabric was the earliest fabric formed within the pluton and is generally overprinted by the solid state deformation. In some places this earlier fabric is preserved and a sense of shear can be determined, either qualitatively in the field or quantitatively using photographs, thin sections or samples in the laboratory. These data are plotted in Figure 4.11b. In general they describe weak sinistral shear senses sub-parallel to the pluton long axis (Plate 4.34) in the horizontal plane and weak centre-up shear in the vertical plane.



Plate 4.34 Sinistral magmatic fabric from the Atibaia pluton (GR 45003600)

Solid state deformation

As described in part 4.3.2 the pluton has been the subject of a heterogeneous solid state deformation. This deformation resulted in a medium temperature solid state LS-type fabric being developed across the pluton, as indicated by the stereonet in Figure 4.7. The shear sense associated with this fabric is predominantly dextral (Figure 4.11a), as indicated by a number of different types of shear sense indicators (S-C fabrics, asymmetric porphyroclasts etc.) (Figure 4.12, Plates 4.35, 4.36). Importantly there are no recognised sinistral shear fabrics along the southern contact of the pluton, possibly indicating that the westernmost shear zone was most active in controlling the development of this deformation.



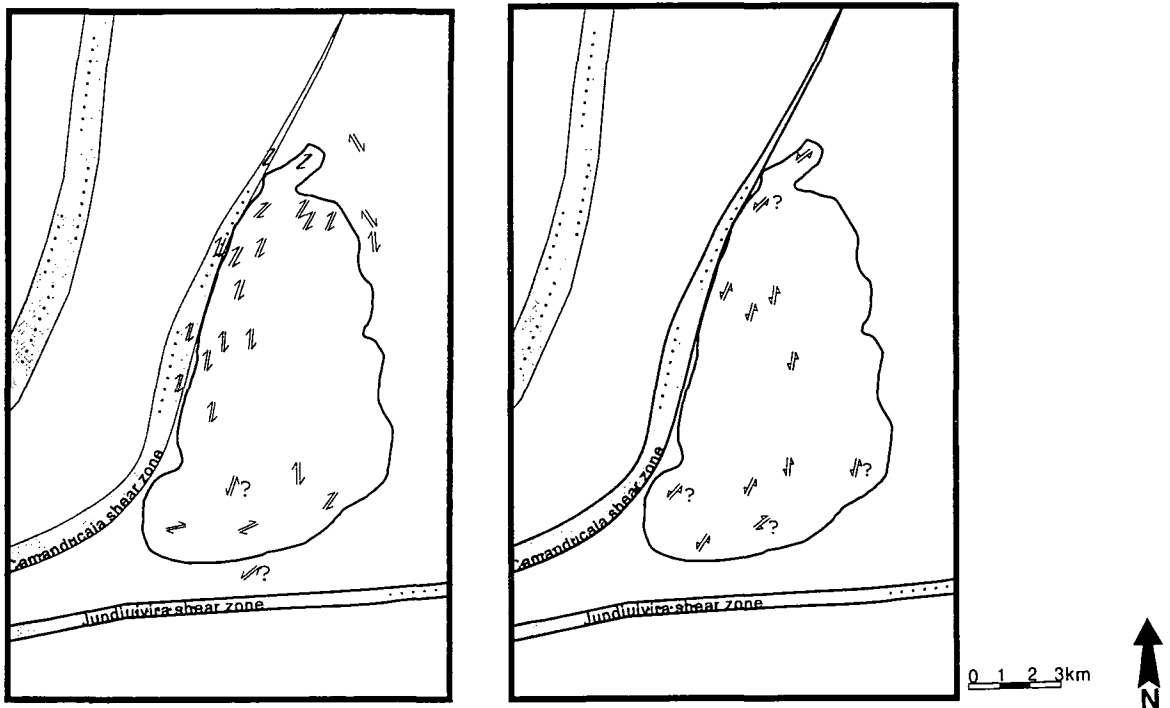
Plate 4.35 *S-C fabrics from the Atibaia pluton (GR 44153568)*



Plate 4.36 *Asymmetric porphyroblast from the Atibaia pluton (GR 44303591)*

4.5.4 Conclusion and discussion

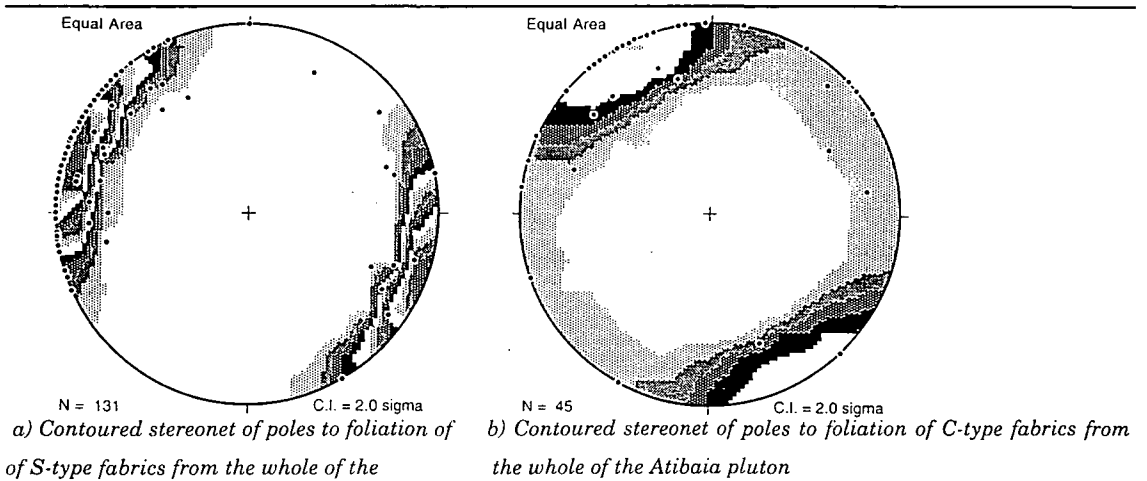
The field evidence demonstrates that during the intrusion of the magma a fabric sub-parallel to the pluton long axis was formed within the body. This fabric contained a weak centre-up and sinistral sense of shear. These shear senses are not preserved within the surrounding the country rock. Such a shear sense demonstrates a reversal of shear sense compared with D_{n+2} transpression, but would be consistent with emplacement into a dilatational environment. After the emplacement and cooling of the magma the pluton was deformed by an heterogeneous planar dextral deformation, which suggests that the Camanducaia shear zone was the dominant structure at this time. The east-west trending sinistral Jundiuvira shear zone only weakly affects the country rock to the south of the pluton and its effects cannot be seen in the pluton itself.



a) Solid state shear senses recorded in the horizontal plane within and around the Atibaia pluton

b) Magmatic state shear sense recorded in the horizontal plane within the Atibaia pluton

Figure 4.11



a) Contoured stereonet of poles to foliation of S-type fabrics from the whole of the Atibaia pluton

b) Contoured stereonet of poles to foliation of C-type fabrics from the whole of the Atibaia pluton

Figure 4.12

4.6 Emplacement kinematics of the microgranitoid dyke/sheets

4.6.1 Introduction

As previously stated microgranitoid dykes have been interpreted as post-dating the emplacement of the magma but pre-dating the development of the solid-state fabric. They are pervasive throughout the pluton, have sharp, sometimes chilled contacts and on average their width is 5-10cm, although occasionally sheets are up to 1m in width. They generally have a sub-vertical dip, but one or two are more moderately inclined. The dykes are commonly unfoliated, but some preserve a ductile shear sense fabric (Plate 4.37), whose exact age with respect to the injection of these sheets and the solid state deformation of the fabric is difficult to determine (see part 4.2.4). However it is observed that ductile fabrics within individual sheets are more common in the vicinity of areas with a more intense solid state fabric. This spatial concordance suggests that the ductile fabrics post-date intrusion and may be syn-tectonic to the overprinting solid state strain.

4.6.2 Methodology

At each locality the orientation (strike and dip), width and associated fabrics (shear sense, lineation etc.) were measured and recorded. These have been amalgamated, using the subdivision of the pluton described earlier (Figure 4.8) and their orientations plotted in rose diagrams in order to visualise the sub-vertical nature of the data (Figure 4.14). These rose diagrams have then been interpreted in order to estimate the possible stress orientations during intrusion, assuming plane stress, instantaneous emplacement and no subsequent bulk rotation of the dykes. Given the sub-vertical orientation, the homogeneous nature and along strike linearity of individual sheets these are probably valid assumptions. Three possible stress relationships of dykes to stress directions have been envisaged:

Type 1 - An environment where the dykes have been formed by the initiation of fractures orthogonal to σ_3 and parallel to σ_1 (Figure 4.13a).

Type 2 - An environment where a single dyke is formed in response to initiation of a fracture oblique to both σ_1 and σ_3 (Figure 4.13b).

Type 3 - An environment where dykes formed in response to the initiation of a fracture set conjugate to σ_1 and σ_3 (Figure 4.13c)

It is important to note that these sheets are exposed primarily on large horizontal planar outcrops, which rarely preserve outcrop from any vertical plane. Where data can be collected from the vertical plane it suggests that ductile deformation associated with the dykes took place almost entirely as a result of two-dimensional horizontal planar deformation i.e. preserved lineations are sub-horizontal and there are no vertical shear sense fabrics.

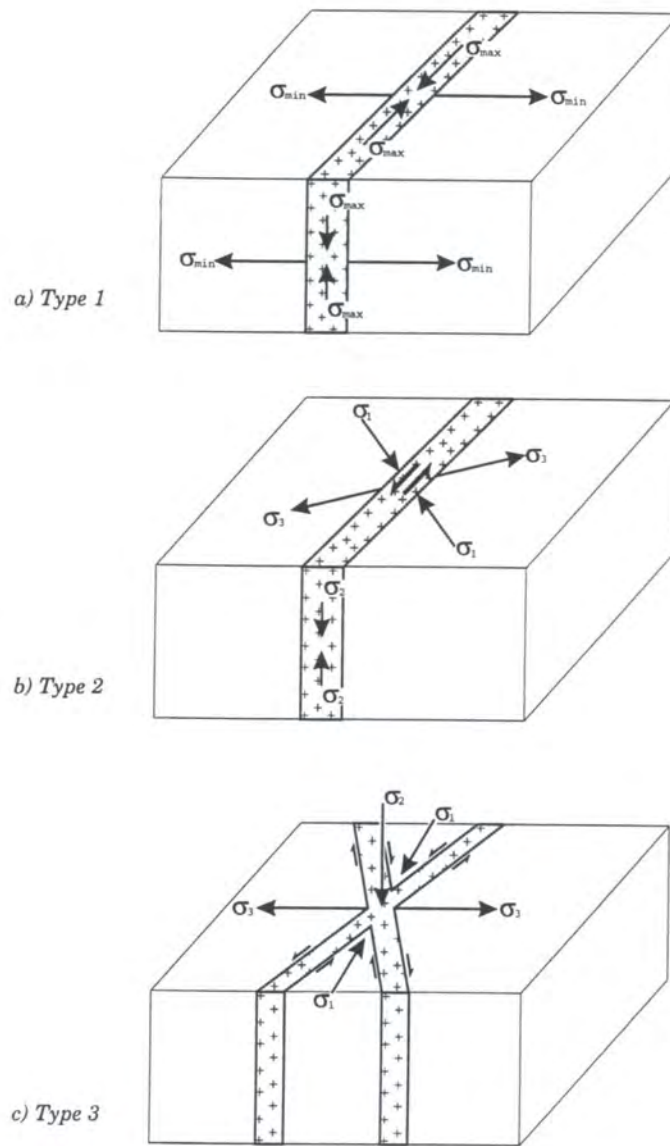
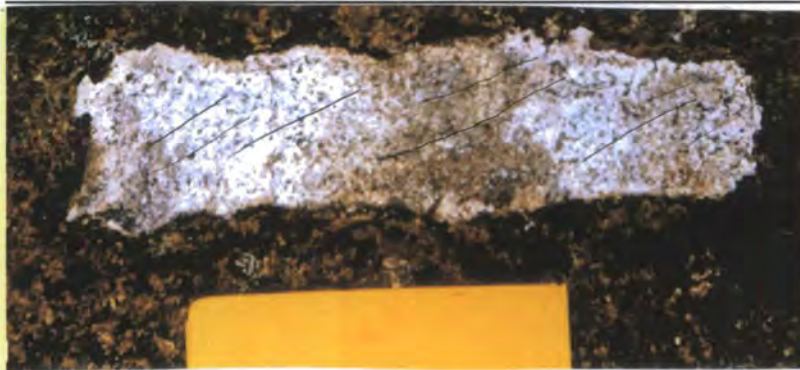


Figure 4.13



Dextral shear sense fabrics on a microgranitoid dyke from the South West area, Atibaia pluton (GR 43002938)
Plate 4.37

4.6.3 Results

Northern area

None of the outcrops in the Northern area are seen to develop microgranitoid dykes of any sort.

Pedra Grande area

This area develops numerous dykes (Figure 4.14a) and a plot of the orientations ($n=57$) shows a single well defined mean of $028^{\circ} \pm 17^{\circ}$. In addition 10 of the dykes preserve dextral shear sense fabrics. Interpreting these data suggests that in Type 1, σ_3 would be orientated sub-horizontally along 118° , with σ_2 and σ_1 orthogonal to this. Alternatively if these dykes were formed during dextral shear (Type 2) then the inferred σ_3 would be sub-horizontally orientated along 153° and σ_1 at 063° , σ_2 would be sub-vertical. Type 3 is not applicable to these data.

North east area

In this area the dominant orientation of the dykes (Figure 4.14b) is between 100° and 110° , but there is a second data peak at 140° to 150° ($n=22$). The ductile fabrics associated with the dominant set of these features (105°) are dextral. These results suggest that in Type 1, σ_3 would be horizontally orientated along 010° , σ_1 and σ_2 being orthogonal to this. Although if these dykes were formed during dextral shear (Type 2) σ_1 would be orientated in the region of 150° and σ_3 at 060° , σ_2 would be vertical. Interpreting the data as a conjugate set (though only a single sinistral fabric has been recognised) and applying Type 3, would suggest σ_1 orientated at 125° and σ_3 orientated at 035° .

Centre west area

In this area there are only a very few measurable dykes ($n=6$). Those that have been measured record a poorly defined peak at between 130° and 140° (Figure 4.14c) and none of the sheets preserve any recognisable shear sense. If this peak can be considered as defining the mean orientation then, assuming a Type 1 stress during emplacement, σ_3 would be orientated at 045° and σ_1 at 135° . Types 2 and 3 are not applicable to these data.

Centre east area

In this area 38 individual sheets were measured and their rose diagram shows a data peak between 010° and 020° , though there are dykes recorded in almost all orientations (Figure 4.14d). The sheets which define the data peak often record no associated shear sense, although 3 sheets have recognisable sinistral fabrics. In addition there are a number of subsidiary sheets which record dextral shear sense in orientations between 056° and 130° . If these data are taken as describing a Type 1 environment producing dykes dominantly orientated along 015° then σ_3 would be orientated at 105° , with σ_2 and σ_1 orthogonal to this. Alternatively if the sheets which display dextral shear with an approximate orientation of 100° are combined with the average orientation of 015°

(sinistral shear sense) then the dykes can be envisaged as a conjugate set (Type 3) where σ_1 and σ_3 are horizontal, orientated at 143° and 048° respectively and σ_2 is vertical.

South west area

In the southwestern area 26 sheets have been identified; their orientations show a well-defined peak between 070° and 080° and an identifiable secondary peak between 040° and 050° (Figure 4.14e). Dextral shear senses ($n=7$) are associated with the principal peak and sinistral shear senses with the subsidiary peak ($n=4$). These data suggest that the sheets in this area define a conjugate set (Type 3) where σ_1 and σ_3 are horizontal and orientated at 150° and 060° , respectively. In such a situation σ_2 would be vertically orientated. Alternatively, the principal peak can be interpreted as defining a Type 1 dataset where σ_3 is orientated at 165° and σ_1 and σ_2 are perpendicular to this.

South east area

Only a small number of dykes have been identified in the southeastern area ($n=9$). These data show two peaks one at 060° - 070° and the second at 150° - 160° . Three of the sheets record dextral deformation between 060° and 070° , whereas dykes associated with the second peak do not appear to record any shear sense. Interpreting these data as being produced in a Type 1 situation suggests an orientation for σ_3 between 070° and 150° , σ_1 and σ_2 being orthogonal to this. Alternatively these dykes can be envisaged as being part of a conjugate set (Type 3) where σ_1 is orientated at 110° and σ_3 at 020° .

4.6.4 Conclusion and discussion

Figures 4.15 a-d summarises the results from the above section and demonstrates that:

1. Wherever the sheets are developed they appear to align approximately sub-parallel to the pluton contact (Figure 4.15a), with easily recognisable average orientations (Figure 4.14a-f). In general they describe single peak values, although minor secondary data peaks can sometimes be recognised. Shear sense fabrics are not widely identifiable within the dykes themselves suggesting, that many were formed perpendicular to σ_3 or had their fabric reset after injection.
2. Interpreting these data in terms of a Type 1 environment suggests that, in general, extension took place perpendicular to the local pluton contact (Figure 4.15b) and that conjugate sets formed in areas where the contact had a variable orientation.
3. Alternatively, interpreting the dykes as being Type 2 and 3 (Figure 4.15c, d) suggests their formation in an environment where the orientation was locally controlled and showed no consistent or interpretable orientation.

In summary, it is suggested that the ductile solid state heterogeneous nature of the developed shear sense fabrics and the complex inferred palaeostress pattern imply that this

was a later deformation imposed on existing features. It was probably induced during the development of the solid state fabric (D_{n+4}). A more consistent model for the nucleation of these dykes suggests that emplacement was linked to margin perpendicular extension after the emplacement and cooling of the magma but while sufficient petrographically and geochemically similar magma (unpublished data, Artur *pers comm.*) remained at depth. Therefore this event can be assigned as the final manifestation of the regional 'extensional' D_{n+3} pluton emplacement event.

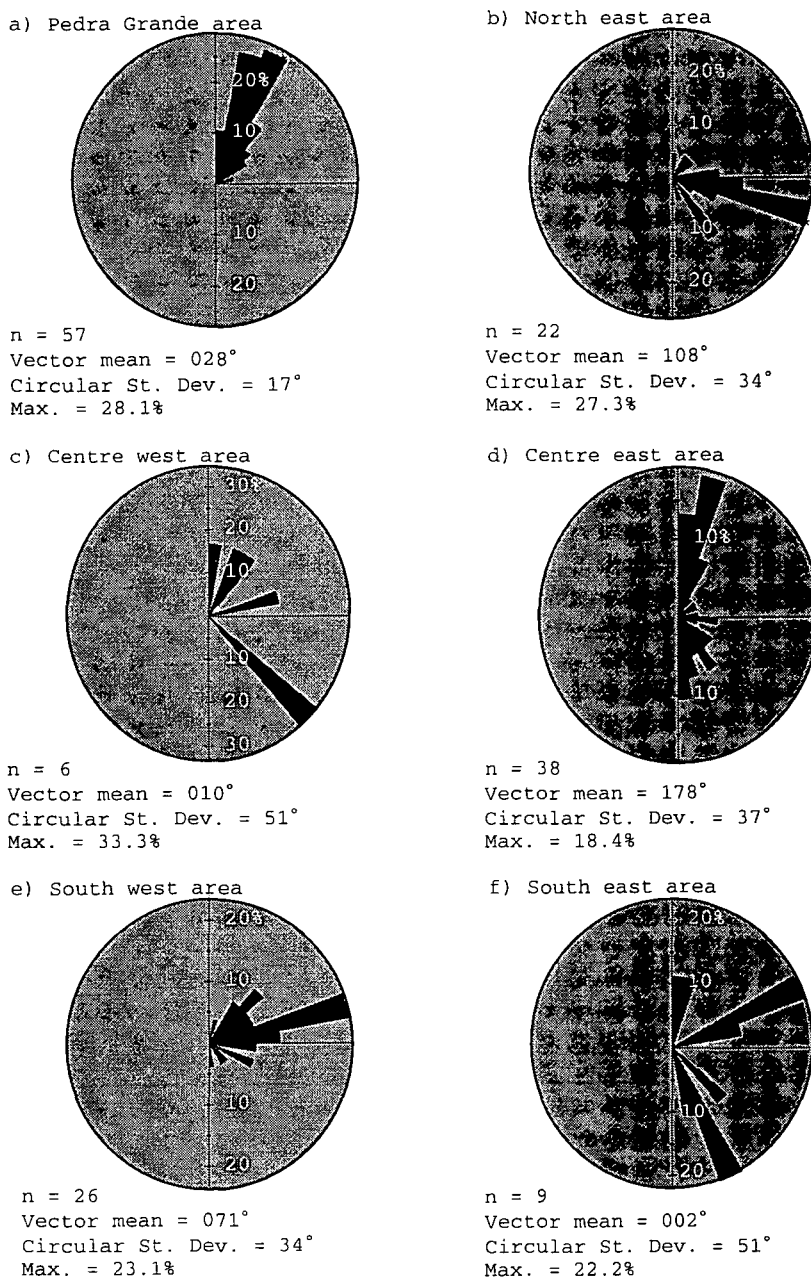
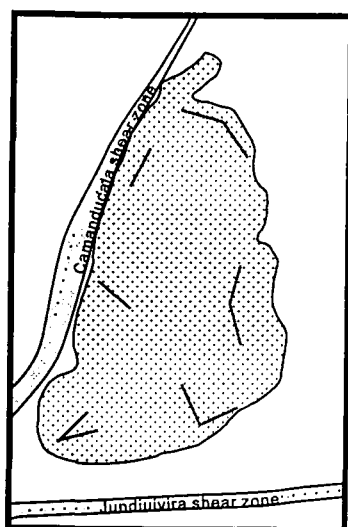
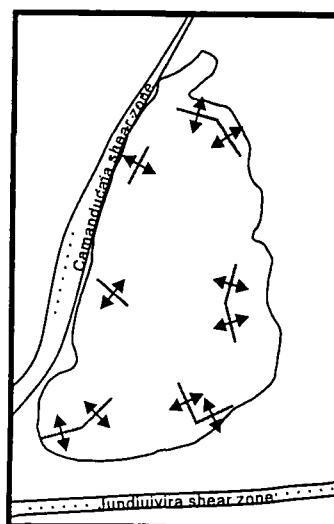


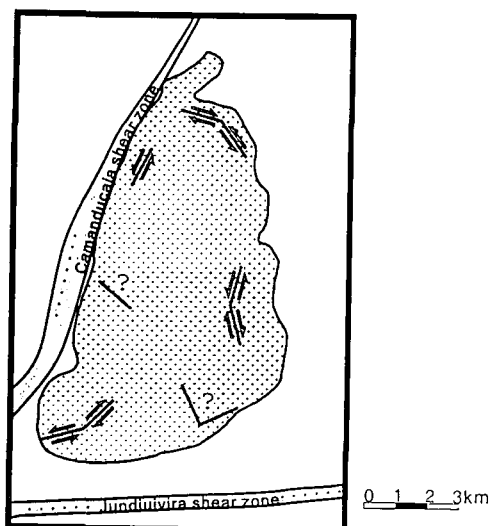
Figure 4.14 0-180° rose diagrams of the orientation of microgranitoid sheets from across the Atibaia pluton



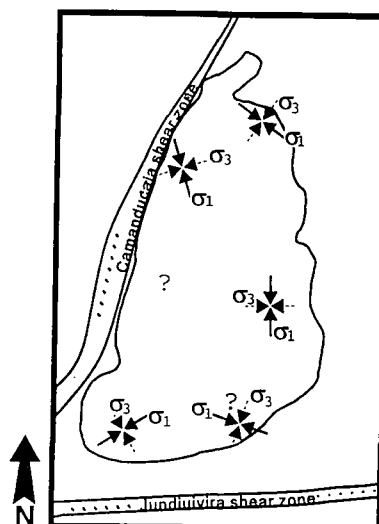
a) Principal dyke orientations



b) Minimum compressive stress orientations, Type 1



c) Preserved average shear senses associated with microgranitoid dykes



d) Maximum and minimum compressive stress orientations assuming Type 2 or 3

Figure 4.15 Microgranitoid dyke orientations from around the Atibaia pluton

4.7 Overprinting discrete mylonitic shear zones

4.7.1 Introduction

Overprinting and cross-cutting the solid state fabric, magmatic state fabric and the microgranitoid dykes of the pluton are discrete mylonitic shear zones with variable orientations (Plate 4.38). These are generally millimetres in width, but can be zones centimetres wide, which have a glassy appearance and are continuous and linear along strike for tens to hundreds of metres. They have a consistently sub-vertical dip (Plate 4.39) and generally a conjugate nature. Although they could represent a discrete continuation of the solid state event. Mineralogically they consist of intensely deformed feldspar and biotite within a matrix of dynamically recrystallised quartz. These features suggest a temperature of up to 400°C during formation, although the influence of a high strain rate and possible fluid interaction in reducing the temperature required to form such fabrics should not be discounted (Knipe 1989, Passchier & Trouw 1996).

The mylonites are preserved heterogeneously across the pluton and are most common in the vicinity of the pluton contact and within zones of more intense solid state deformation. The age and tectonic conditions required for the formation of these features is a subject of debate (Saadi *et al* 1991, Campanha *et al* 1994, Ribeiro *et al* 1995, Riccomini 1995, Salvador & Riccomini 1995), but they are often considered to be Cretaceous to Eocene in age, formed in response to deformation associated with the break-up of Gondwana and the opening of the Atlantic Ocean. Observations from this pluton and others (see parts 3.3.4 and 5.6.2) suggest that they were formed in a single event, for example individual mylonites of different orientations often appear to cross-cut each other in a non-consistent manner i.e. dextral mylonites overprint sinistral mylonites and vice versa. Hence it appears that a regional stress was applied to the pluton in conditions where the body could accommodate deformation along conjugate small discrete features. The presence of large numbers of these mylonites in areas of more intense solid-state deformation and their discrete nature suggests either, formation during reactivation of major structures at a lower temperature or during higher strain rate deformation than had occurred previously, or that there is a genetic relationship between the solid state fabric and the production of the mylonites. If there was a genetic relationship between the solid state fabric and the nucleation of these structures this would imply that these structures are much older than the suggested Cretaceous-Eocene ages.

4.7.2 Methodology

At each outcrop the orientation, width, qualitative intensity of deformation and associated shear sense were recorded. These data have been collated and analysed using the subdivision of the pluton established earlier (Figure 4.8). Their orientations have been plotted on rose diagrams in order to examine the distribution of this sub-vertically

orientated dataset and interpreted using the associated shear sense observations. It was assumed that they formed single or conjugate sets in response to an applied stress i.e. no rotation (Figure 4.16).

As was made clear in the analysis of the microgranitoid dykes the mylonite data has been collected from predominantly sub-horizontal planar exposures, with very little vertically orientated outcrop available. Where examination of the vertical plane has been possible there is often no associated sense of shear and the observed lineations are all sub-horizontal.

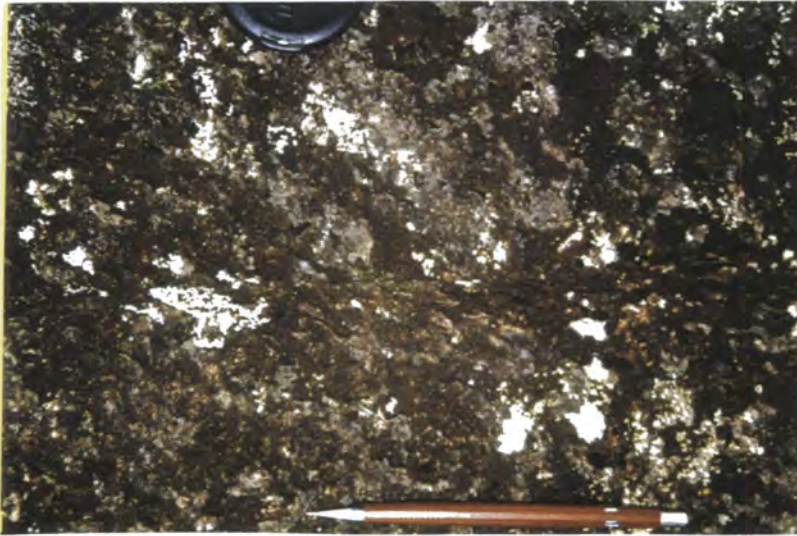


Plate 4.38 *A single discrete mylonitic shear zone (GR 46783525)*



Plate 4.39 *Multiple discrete shear zones (GR 47053878)*

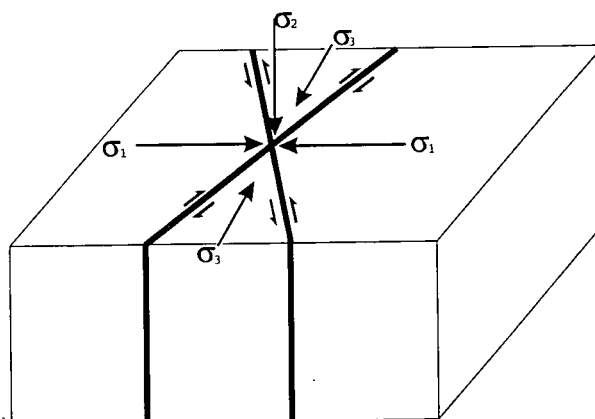


Figure 4.16 Diagram of interpreted principal stress orientations from conjugate mylonite arrays.

4.7.3 Results

Northern area

None of the outcrops examined in the northern part of the pluton preserve any discrete mylonites. This area appears to be undeformed by this deformation event.

Pedra Grande area

A total of 38 individual mylonites have been measured from this area, all of which are continuous along strike, sub-vertical and generally less than 1cm in width (Plate 4.41). Examining the rose diagram (Figure 4.17a) shows that there is a dominant population orientated between 010° and 020° and a second subsidiary population present between 140° and 160° . Mylonites orientated in the first population display a dominantly dextral shear sense whereas, mylonites forming the second population display a sinistral shear sense.

These mylonites define a conjugate set; the shear senses associated with them suggest formation in a stress environment where σ_1 would be orientated at approximately 083° and σ_3 orientated at approximately 173° . Therefore during their formation this area was subject to an approximately east-west orientated compression.

North east area

The northeastern area of the pluton records a very large number of mylonites ($n=80$). Examination of the rose diagram of these features (Figure 4.17b) shows the existence of a dominant population with a peak at between 140° and 150° and a subsidiary population with a peak at between 020° and 030° . Individual mylonites from the principal population show a sinistral sense of shear whereas mylonites from the subsidiary population show a dextral sense of shear.

These results show that in this area mylonites formed in a conjugate set and analysis of the associated shear senses suggests formation in an environment where σ_1 is orientated at approximately 085° and σ_3 at approximately 175° . This is an approximately east-west orientated compression, similar to that recorded in the Pedra Grande area.

Centre west area

Only a relatively small number of mylonites were recorded in this area ($n=9$), the orientations of which define a prominent mean between 120° and 130° (Figure 4.17c). All of the mylonites with orientations around the mean value record sinistral shear. These data suggest (assuming there was no conjugate orientation) σ_1 orientated at approximately 080° and σ_3 at approximately 170° . This is an east-west compression, as has been suggested for each of the previously examined areas.

Centre east area

The centre east area records mylonites with a wide variety of orientations. Nevertheless two distinct populations can be distinguished from these data, one which has a peak value between 120° and 140° and a second with a peak value between 350° and 010° (Figure 4.17d). Shear senses recorded in association with the first of these populations are sinistral, whereas features associated with the second are dextral.

These results suggest that the data forms a conjugate set, which was formed in response to a simple shear where σ_1 is orientated at 065° and σ_3 orientated at 155° i.e. in response to an east-northeast directed compression.

South west area

The data from the southwestern part of the pluton describes two well defined peak values, the first with a mean value between 040° and 050° and the second with a mean value between 130° and 140° (Figure 4.17e). In this area the mylonites were very narrow and as a consequence shear senses were impossible to conclusively identify. No dominant sense of shear or orientation of the major stress axes could be made. Even so the orientation of these data remains consistent with similar readings in the areas to the north, which were formed in apparent response to an approximately east-west directed compression. As a consequence of this consistency with earlier data it is tentatively suggested that σ_1 was orientated at 090° and σ_3 at 000° during the formation of these features.

South east area

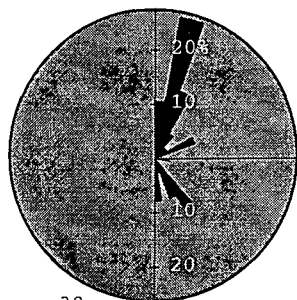
The southeast of the pluton preserves very few mylonites ($n=7$) which do not define any sort of well defined mean or peak value (Figure 4.17f). As a consequence of this lack of consistency no conclusions are drawn about the possible stress conditions existing during formation of these features.

4.7.4 Conclusion and discussion

The Atibaia pluton suffered a number of deformation events after its emplacement the most pervasive of these being the imposition of a solid state foliation. The mylonites appear to have been initiated after the solid state fabric had formed in response to deformation which produced conjugate discrete zones of intense deformation cross-cutting the earlier fabrics. Interpreting the kinematics of these features suggests (Figure 4.18a, b):

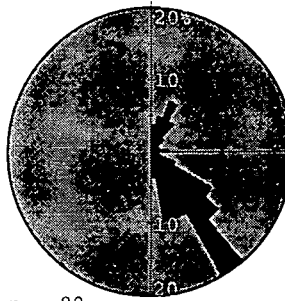
1. That they were all formed in response to an approximately east-west directed compression. The spatial distribution of these features (they are most prevalent near the outer margins and most deformed parts of the pluton) suggests that they were formed in response to deformation associated with the major shear zones.
2. The high angle ($\geq 45^\circ$) between the inferred principal compressive stress and the shear planes (Figure 4.18a, b) indicate a number of possible scenarios for formation, such as: i) the deformation had a strong component of compression (from simple mechanics); ii) that the deformation was strongly confined ($\sigma_3 = \sigma_2$) (Twiss & Moores 1992); iii) the principal compressive stress was at a high angle to the existing foliation (Twiss & Moores 1992). A comparison of the pluton map (Figure 4.1) with the orientation of the inferred principal compressive stress (Figure 4.18b) shows that scenario iii) is possible, as is scenario ii) given that this deformation probably occurred while the pluton remained buried at depth. Although it is the authors opinion that scenario i) was important in forming these fabrics since if an east-west orientated compressional deformation acts upon a body associated with a weak fabric (shear zone) this will be preferentially reactivated before any new structures are formed. Therefore the nucleation of these mylonite fabrics represents the expression of the reactivation of the strike-slip fabric during weak east-west directed compression/transpression, that was of insufficient intensity, in this area, to nucleate new compressional fabrics.

a) Pedra Grande area



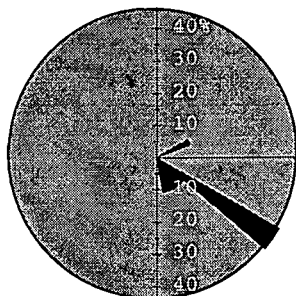
n = 38
 Vector mean = 012°
 Circular St. Dev. = 30°
 Max. = 26.3%

b) North east area



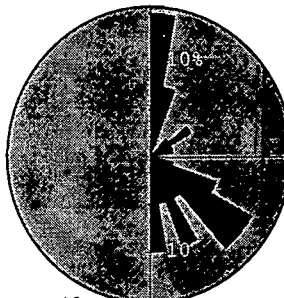
n = 80
 Vector mean = 155°
 Circular St. Dev. = 33°
 Max. = 20%

c) Centre west area



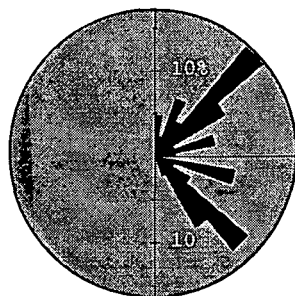
n = 9
 Vector mean = 135°
 Circular St. Dev. = 25°
 Max. = 44.4%

d) Centre east area



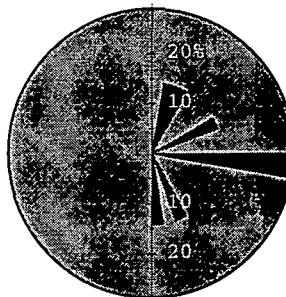
n = 40
 Vector mean = 158°
 Circular St. Dev. = 37°
 Max. = 15%

e) South west area



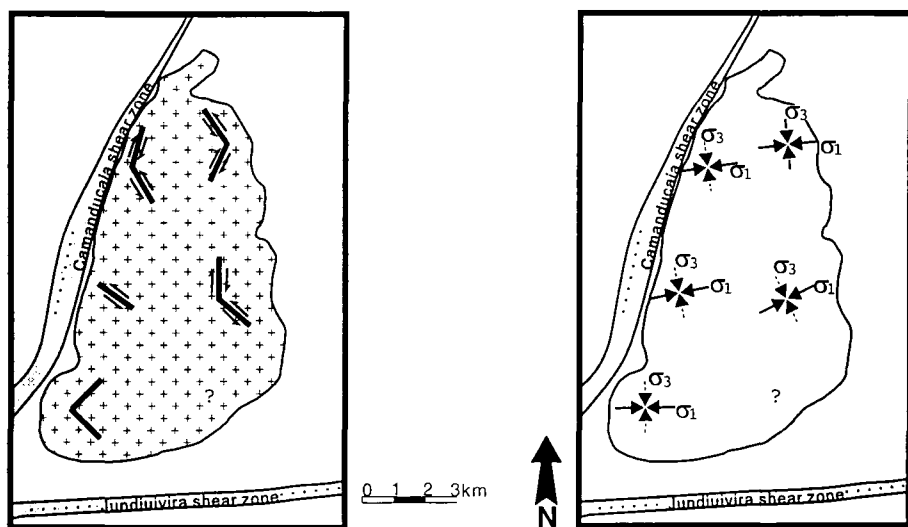
n = 42
 Vector mean = 068°
 Circular St. Dev. = 61°
 Max. = 16.7%

f) South east area



n = 7
 Vector mean = 014°
 Circular St. Dev. = 61°
 Max. = 28.6%

Figure 4.17 0-180° rose diagrams of mylonite orientations from the Atibaia pluton



a) Principle mylonite orientations

b) Inferred compressive stress orientations

Figure 4.18 Discrete mylonite orientations from around the Atibaia pluton

4.8 Dykes or diapir ?

In this section the field evidence will be examined, and conclusions drawn as to the method of ascent and emplacement of the Atibaia pluton. The field criteria associated with each of these ascent and emplacement mechanisms have been extensively discussed in Chapters 1 and 2. Specifically the Atibaia pluton shows:

1. A lozenge shape combined with an along axis, sub-vertical, planar magmatic fabric, which is associated with an homogenous flattening-type strain.
2. Local sheeting of magma into the country rock along the western side of the pluton.
3. Symmetrical boudinage fabrics (where observed) on the western side of the pluton.
4. No pluton-up type kinematics anywhere.
5. No centre-margin petrographic zonation.

These data lead the author to suggest that pluton ascent took place along dykes, which are preserved in the country rock, but were obscured in the granite itself. This obscuring of internal sheet contacts could occur as a consequence of rapid emplacement and thereby the magma had little opportunity to differentiate en route from source to emplacement level, hence dykes contacts are obscured in outcrop. During the emplacement these dykes were shortened by approximately 40% and extended by up to 30%. There is no evidence in this pluton for movement of a bleb/diapir of material up through the crust to its current level of emplacement.

4.9 Emplacement and deformation

4.9.1 A sequence of events

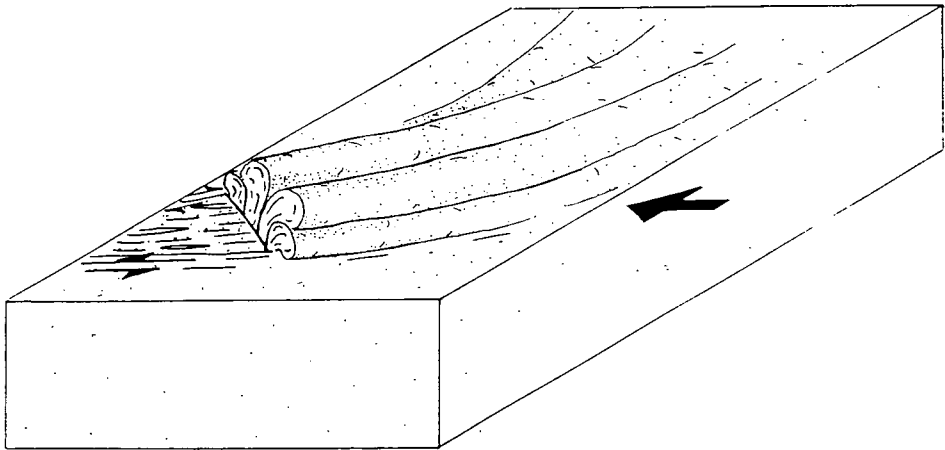
Pluton emplacement throughout this area has been the subject of previous debate and a regional model for magma ascent and deformation will be presented in Chapter 7. Below the sequence of events and suggested ascent and emplacement mechanisms are detailed with specific reference to field evidence collected from the Atibaia pluton:

1. **Initial scenario** - During the Brasiliano orogeny the Atibaia area was deformed during a west through to northwest directed crustal thickening ductile thrusting event, which produced the regional low angle D_{n+1} foliation. This was later overprinted by continental-scale sub-vertical ductile shear zones with an approximately northeasterly trend. The Camanducaia shear zone along the western side of the Atibaia pluton and the Jundiuvira shear zone to the south of the pluton are examples of these D_{n+2} shear zones. It was into this environment that the Atibaia pluton was emplaced.
2. **Initiation of ascent/emplacement** - Preserved regional shear sense indicators suggest that the dominant deformation in this area was a regional dextral transpression (Ebert *et al* 1996) and, given such a deformation, the Atibaia area should preserve a compressional 'flower structure' (Figure 4.19a). In such an environment pluton emplacement can take place and the expected features of such a granitoid are detailed in part 1.6.3. However the Atibaia pluton preserves none of these criteria (outcrop heterogeneity, down dip magmatic lineations etc.) in particular, it is compositionally homogenous, has a weak magmatic fabric and displays magmatic shear criteria which are in opposition to those preserved in the contact rocks. Therefore it is suggested that initiation of the intrusion of the Atibaia pluton required a re-orientation of local applied stresses of sufficient duration and magnitude to facilitate the development of a lower stress point dilation zone (at any level in the crust) in the area and hence the focusing of the sheeted ascent of granitoid magma formed at depth.
3. **Continued magma ascent and emplacement** - The compositional homogeneity, low emplacement strain and the lack of screens of strongly deformed country rock within the pluton, as well as the relatively weak deformation of the eastern wallrocks suggests that: i) magma supply to the pluton was rapid and possibly continuous, especially since there are no internal magma contacts which would be produced by a rheological hiatus (caused by cooling/crystallisation) between magma batches; ii) magma emplacement was not especially 'forceful' and at least some of the 'space' for the was created externally.
4. **Granitic magma source** - Isotopic and geochemical data (Melhem 1995) suggests that this pluton was possibly formed through the fusion of large amounts of evolved continental crust with a smaller more primitive contribution. This is consistent with a lower crustal anatexic source.

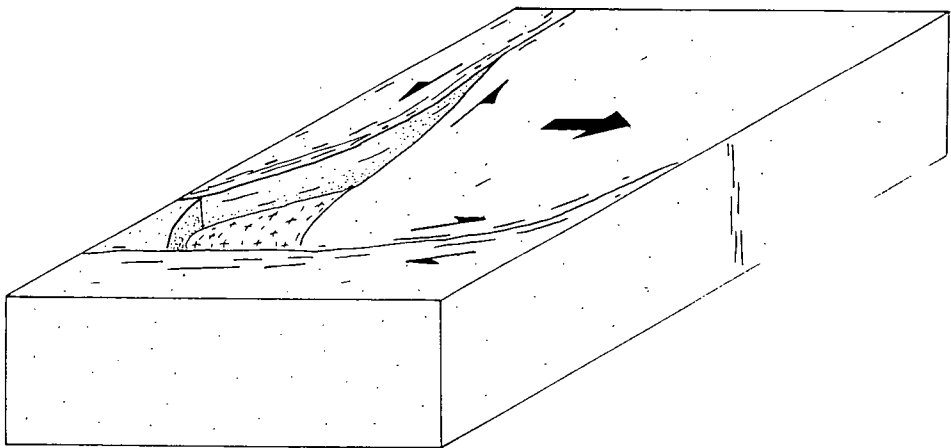
5. **Post-emplacement magmatic activity** - After the intrusion of the main pluton there may have been minor intrusion of microgranitoid stocks into the country rocks. Within the pluton itself sheets of microgranitoid material, with a bulk composition similar to the pluton, were emplaced sub-parallel to the local pluton margin. An orientation which suggests that the minimum principle stress was orientated orthogonally to the pluton contact, facilitating the emplacement of magma as sheets into 'extensional' fractures.
6. **Post-emplacement tectonic activity** - After the intrusion of the microgranite dykes the pluton was overprinted by a lower temperature solid state fabric, which was formed during a dextral reactivation of regional structures. This occurred after the Atibaia pluton had cooled to around 300-400°C.
7. **Formation of discrete mylonites** - Cross-cutting all the previous fabrics there are conjugate or single sets of discrete mylonites which have been kinematically analysed. These features show shear senses and orientations which are consistent with a weak, approximately east-west directed compression associated with movement on the regional shear zones but was of insufficient intensity to produce a new homogeneous compressional fabrics within the pluton itself.

4.8.2 Pluton shape

The Atibaia pluton is lozenge shaped and tapered towards its northern termination. This, taken with the magmatic shear senses recorded within the pluton (sinistral along the pluton axis), weak intrusion related deformation along the eastern contact and regional kinematics (dextral transpression suggests that: i) the magmatic fabrics are at odds with the solid state deformation; and more importantly that ii) the shape of the pluton could be the result of approximately east-west directed extension. Such a deformation would result in a component of sinistral deformation along the western Camanducaia shear zone and dextral deformation along the Jundiuvira shear zone to the south, resulting in a transtensional pull-apart and ultimately a pluton with a similar shape to the observed Atibaia pluton (Figure 4.19b). Such a regional tectonic method of pluton emplacement, would (providing the magma supply rate/pressure was excessive) result in only weakly deformed country rocks and the low, but homogenous strains recorded throughout the pluton.



a) Possible structural architecture of transpression in the Atibaia area



b) East-west directed extension and the creation of space for the Atibaia pluton

Figure 4.19

4.10 Conclusions

- The Atibaia pluton was emplaced as an homogenous magma body as a result of the ascent of sheets from depth.
- The Brasiliano orogeny is interpreted to have been a regional dextral transpression event in this area, but the Atibaia pluton preserves no features that might be expected in such tectonic environment. Indeed the magmatic structures and deformation in the surrounding country rock suggest that the pluton was emplaced during local east-west directed extension into a local pull-apart.
- During such extension the spatial interaction of the Jundiuvira and Camanducaia shear zones probably focused magma ascent into this area.
- After emplacement and cooling (sufficient for the magma to behave as a solid during brittle fracturing) the pluton was injected by microgranitoid dykes of similar bulk composition to the magma itself thereby recording continuing extensional tectonics.
- At some later time the pluton was heterogeneously overprinted by a dextral solid state shear fabric formed in response to continued regional deformation.

Chapter 5

The Imbiricu and Morro Azul plutons

5.1 Introduction

5.1.1 Preamble

The Imbiricu and Morro Azul plutons are linear, elongate granitoid bodies, intruded sub-parallel to the regional foliation. They are both spatially associated with the Monteiro Lobato shear zone, one of the major Brasiliano D_{n+2} continental-scale shear zones which cross-cut this area (Figure 3.4, Maps 3, 4, 8). Geographically, the Imbiricu pluton is 20km north-west of the city of Sao Jose dos Campos and 15km northeast of the town of Igarata. The Morro Azul pluton is south-west of the Imbiricu pluton, exposed on low hills both north and south of the town of Igarata. The field area is part of the 1:50,000 map sheet named Igarata and was previously mapped by Campos Neto *et al* (1983).

5.1.2 Previous work

There has been little previous work on the geology of the area surrounding these two plutons (Figure 5.1). Only in the comparatively recent past, with the regional studies of Hasui *et al* (1978) and Oliveira *et al* (1983), was the distribution of greenschist to amphibolite grade schists and gneisses surrounding inter-continental shear zones and granite plutons of various ages described in detail, although Ebert (1968) makes reference to the existence of major shear zones in this area. Tassinari (1988), during his regional geochronological study attempted to establish the age of the Morro Azul pluton. He recorded a poorly defined Rb-Sr whole rock age of 523 ± 62 Ma, $(^{87}\text{Sr}/^{86}\text{Sr})_i \approx 0.7113$ and a Pb-Pb whole rock age of ~ 580 Ma. This age is similar to that recorded in other granitoid complexes from this area. A more recent unpublished geochemical and isotopic study of the Igarata area has suggested that the Imbiricu and Morro Azul plutons were sourced from the melting of a lower crustal protolith. This interpretation is consistent with the geochemical data of Tassinari (1988).

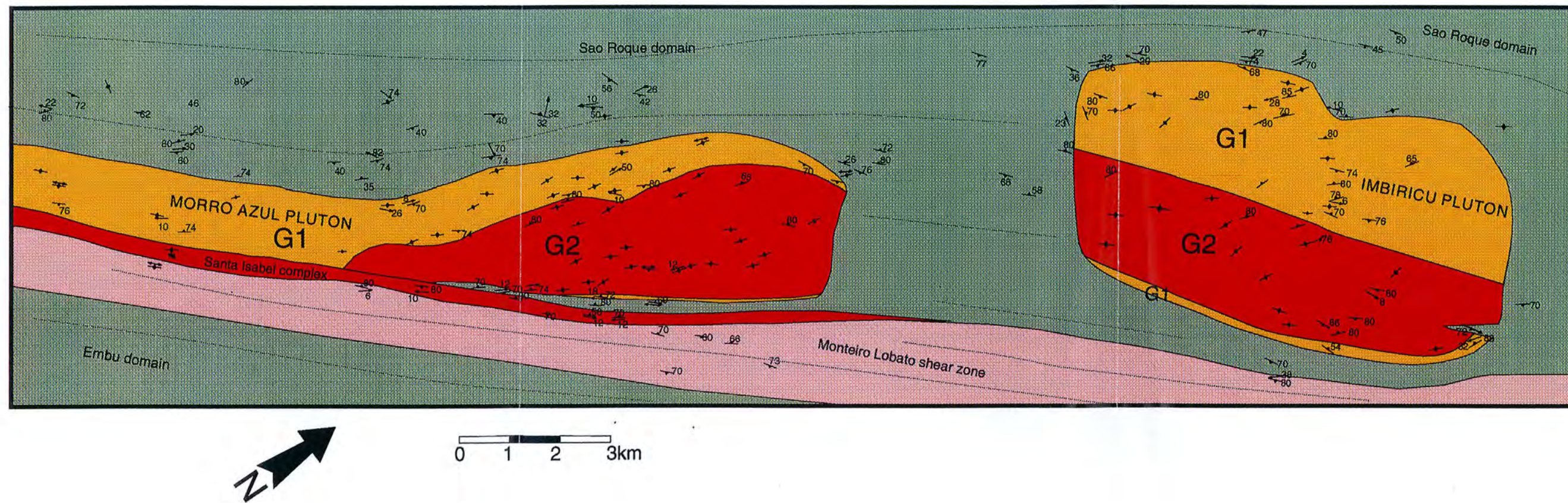


Figure 5.1 Geological map of the Morro Azul and Imbiricu plutons

5.2 Mapping: the Imbiricu pluton

During this work both the country rock and intrusive rocks around the pluton have been structurally and petrographically mapped at a 1:25,000 scale. The results of this work are shown in Map 3 and Figure 5.2. Reference was also made to the regional map of Campos Neto *et al* (1983) which has been redrawn in modified form as Map 8.

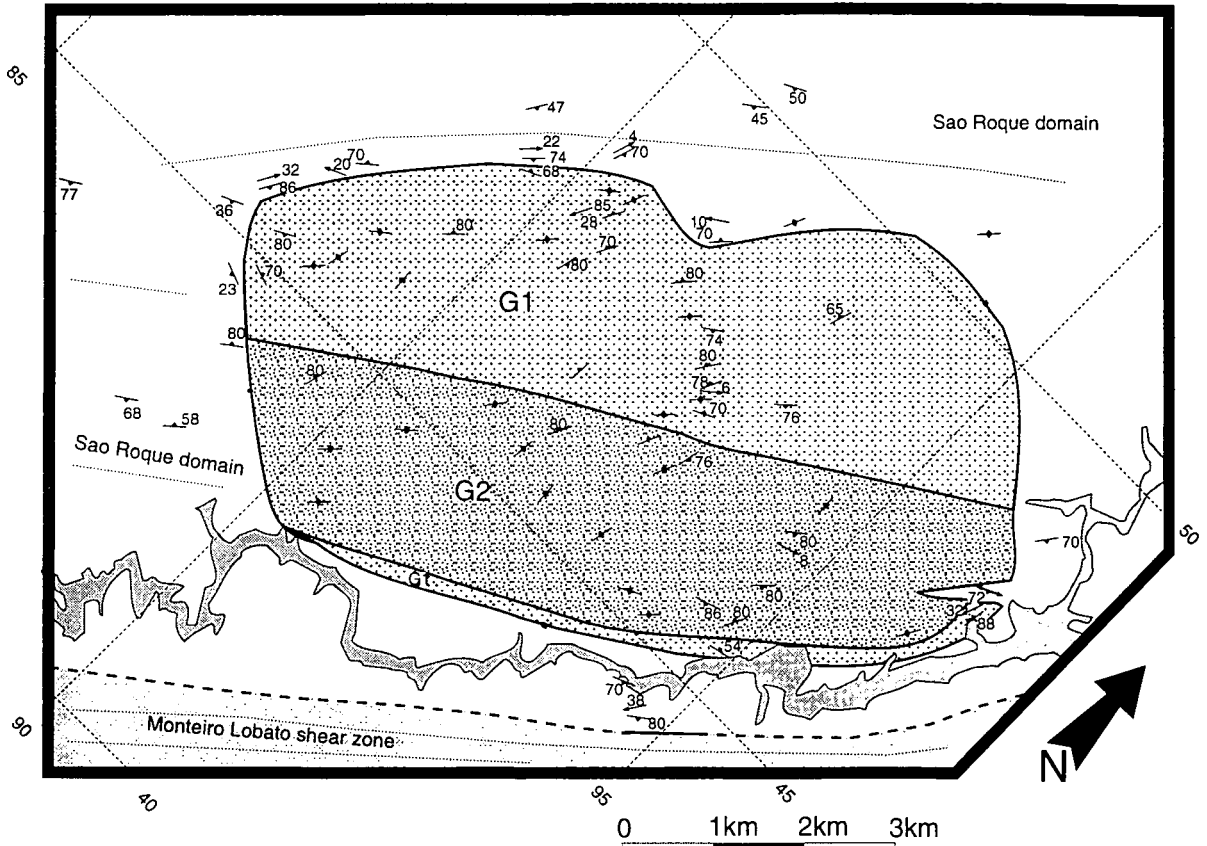


Figure 5.2 Geological map of the Imbiricu pluton

5.2.1 Country rock

The country rock on both sides of the pluton forms part of the Sao Roque domain, although southeastward of the pluton the rocks of the Embu domain are observed both within and beyond the Monteiro Lobato shear zone. The Sao Roque preserves metamorphic ages of 550-600Ma (using various methods, Tassinari 1988). It consists of a relatively homogeneous stack of foliated, schistose, greenschist facies meta-volcano-sedimentary rocks; which shows the development of metamorphic biotite, staurolite and rare sillimanite, but the absence of migmatites (commonly seen in other areas) (Campos Neto *et al* 1983). Very different structural styles occur on each side of the pluton as described below:

Southeast of the pluton

The rocks to the southeast of the pluton trend sub-parallel to the northernmost part of the Jaguari reservoir. They consist of intensely deformed and strongly foliated schistose rocks, which are sub-vertically dipping, trend north-northeastwards and display a sub-

horizontal mineral stretching lineation (Figure 5.3, Plate 5.1). Mineralogically this fabric is formed from strongly commuted grains of quartz, feldspar and mica. No additional metamorphic minerals could be identified within this mylonitic fabric. In general these rocks appear to show little deformation which can be directly associated with intrusion of the granite, although on the southeastern shoreline of the Jaguari reservoir (GR 94204475) m-scale sheets of deformed G2 granite are seen intruding sub-parallel to the regional foliation. Southeastwards of these immediate contact rocks the intensity of deformation increases further as the Monteiro Lobato shear zone exerts a greater tectonic control. This shear zone is 3-4km wide here.



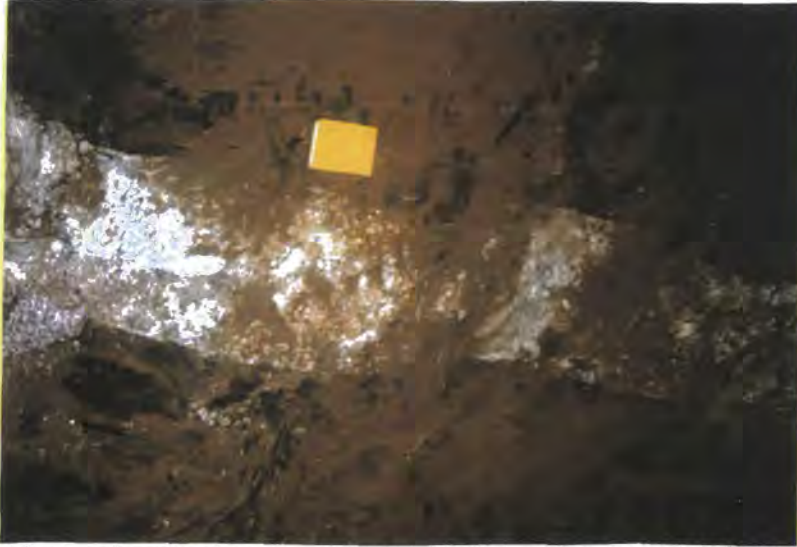
Plate 5.1 *Contact rocks from the southeastern side of the Imbiricu pluton (GR 45009500)*

Northwest of the pluton

On travelling northwestwards from the country rocks southeast of the pluton contact the intensity of the deformation, preserved within the wallrocks, becomes much lower. In these areas the country rock is poorly exposed but shows a strong schistose to gneissic foliation striking in a northeastwards direction (Figure 5.3). At a distance from the pluton contact the foliation generally dips moderately southeastwards, whereas close to the pluton this fabric becomes steepened and deflected until it becomes sub-parallel to the contact and sporadically develops a sub-horizontal mineral stretching lineation (Figure 5.3b). The country rocks immediately adjacent to this northwestern contact show the development of sillimanite which might suggest a thermal intensification of the regional metamorphic grade close to the pluton. Within 50m of the pluton contact itself this fabric shows the injection of cm- to m-scale sheets of relatively undeformed granitoid material compositionally similar to the pluton itself, with evidence for a degree of thermal baking around the dyke contacts (Plate 5.2).

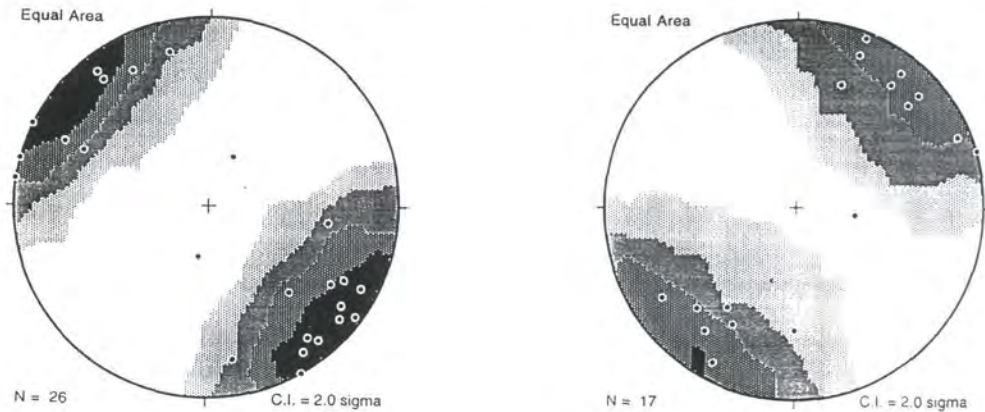
Conclusions

The country rock around the Imbiricu pluton preserves a high intensity shear zone along its southeastern side. Around the remaining sides of the pluton the country rock preserves a low-angle, regional fabric, which has been locally steepened close to the contact during emplacement.



Sheeting of granite along the country rock foliation, northwestern side Imbiricu pluton (GR 92734765)

Plate 5.2



a) Contoured stereonet of poles to country rock foliation, Imbiricu pluton

b) Contoured stereonet of stretching lineations, Imbiricu pluton

Figure 5.3

5.2.2 Nature of the contact

Southeast of the pluton

To the southeast of the pluton the contact between the country rocks and the granite itself can only be observed in a single area around GR 94804561. This area shows a highly deformed outcrop of G1 granite, which displays a finely divided solid state foliation and a sub-horizontal lineation. A few metres southeast of here the country rock can be

observed and displays a similar, vertically orientated fabric. As stated above there are no granite sheets or other such intrusions observed along this contact, which suggests a sharp, initially magmatic, but later tectonised, contact between the country rock and granite in this area.

In other areas the contact is less well exposed but is broadly characterised by a weak break in slope and an increase in the degree of solid state deformation preserved within granite outcrops. Those closest to the contact show a very strong gneissic solid state fabric (Plate 5.3), associated with a low angle stretching lineation.

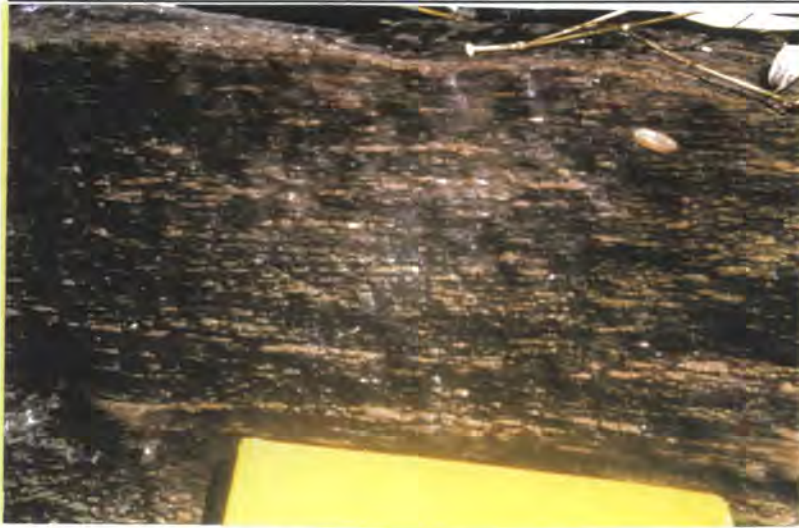


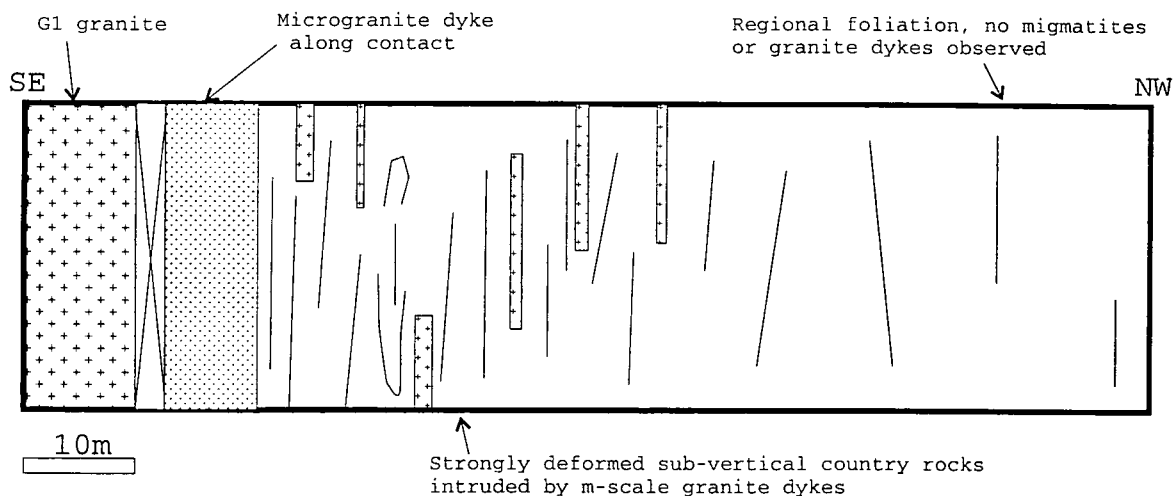
Plate 5.3 *Gneissic solid state fabric adjacent to the southeastern contact, Imbiricu pluton (GR 96554775)*

Northwest of the pluton

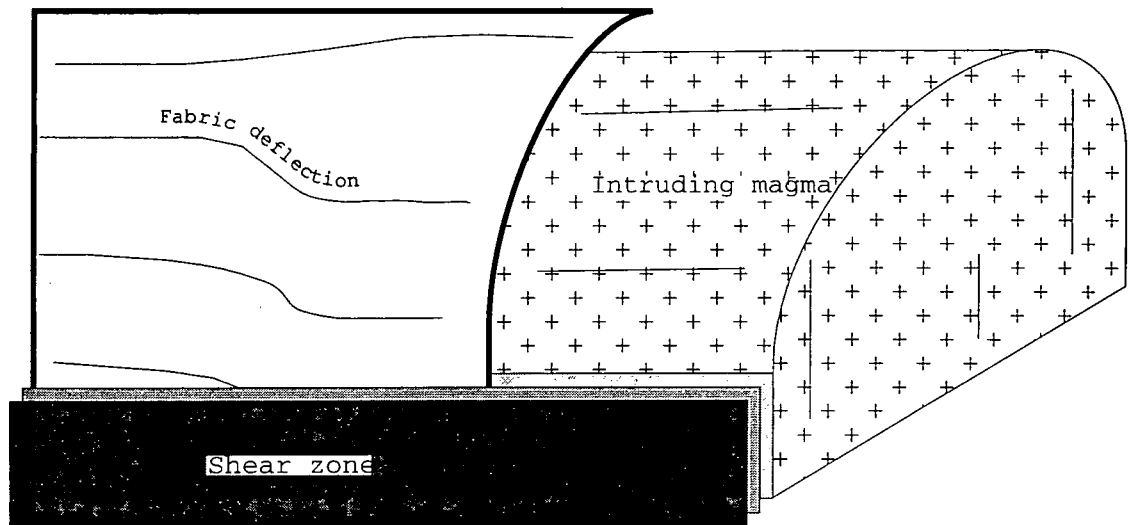
As stated in part 5.1.1 the north-western contact of this pluton commonly preserves granitoid sheets which appear to have been emplaced sub-parallel to the country rock foliation. These are first observed 50-100m from the contact and represent a maximum of ~10% of the contact rock (Plate 5.2). The contact with the pluton itself is generally marked by sub-vertically orientated foliation which may be strongly folded, before a 5-10m wide microgranitoid sheet is observed: This feature can be picked out along 70% of this contact and after it is crossed the G1 granite can be picked out. This granite shows a heterogeneous solid state fabric which does not appear to increase in intensity with increasing proximity to the outer contact. A summary log across this contact is shown in Figure 5.4.

Southwest contact

Country rocks to the southwest of the pluton contain moderately dipping fabrics roughly concordant with the pluton. Further southwest similar fabrics are steeply dipping and trend sub-parallel to the shear zone present to the southeast. This suggests the local deflection of the fabrics around the pluton (Figure 5.5).



A summary log through the northwestern contact of the Imbiricu pluton (GR 89584781 to GR 89754798)
Figure 5.4



A possible interpretation of structural fabrics along the southwest contact of the Imbiricu pluton
Figure 5.5

Northeast contact

The northeastern part of the pluton is the most poorly exposed area of this pluton and no fabrics less than a kilometre from the supposed external contact of the pluton could be found. The outer contact of the pluton has been determined from remote sensing and geomorphological analysis of this region. Regionally, the fabrics are continuous between the pluton and country rock but it is suggested that a ‘roof contact’ similar to the one observed in the southwest might be observed in this area given sufficient exposure.

Conclusions

The Imbiricu pluton preserves a southeastern contact which was strongly tectonised before, during and after the emplacement of the pluton. The northwestern contact preserves only a weak, post-emplacement deformation but it incorporates sheets of granite material which were intruded along the regional foliation during the intrusion of the granite. The lateral contacts are interpreted as representing roof contacts of the pluton with the surrounding wallrock. In summary, it appears from these data that the magma was emplaced by sheeting into the existing country rock, close to a major tectonic discontinuity.

5.2.3 Granite

In outcrop the Imbiricu pluton has been recognised as consisting of two plutonic phases whose interior and exterior contacts are orientated sub-parallel to the regional foliation and the Monteiro Lobato shear zone: G1 is present in a thin band along the southeastern contact and in a much wider band on the northwestern side of the pluton; and G2, intruded into the southeastern portion of the pluton (Figure 5.2, Map 4). In general these intrusive phases preserve a sub-vertical, northeast-southwest trending foliation, formed predominantly in the solid state with a rarely developed sub-horizontal mineral stretching lineation. Where the solid state fabric is not developed the magma becomes almost isotropic preserving only a very weak magmatic fabric.

The outer phase, G1

The distribution of this phase was described above, it forms the lateral boundaries to G2 and is the phase most commonly sheeted into the country rock. Examining G1 in outcrop (Plate 5.4) shows it to consist of a light-coloured, coarsely crystalline texture, containing abundant potassium feldspar crystals 1-2cm in size, within a matrix of smaller potassium feldspars, plagioclase feldspar, quartz and biotite. Point counting 20 thin sections to 500 points (Figure 5.9a) shows, an alkali granite to granite composition. In general it is compositionally homogenous but retains a number of interesting structural features which are outlined in more detail below:

Northwest G1

The majority of the preserved G1 is exposed in this area: In general it is relatively well-exposed and shows a planar fabric sub-parallel to the pluton axis, or rotated anti-clockwise relative to it. The foliation is vertically dipping and occasionally develops an along strike, sub-horizontal mineral stretching lineation (Figure 5.2, 5.6). In outcrop the foliation plane is defined by weak alignment of the potassium feldspar phenocrysts and deformation of the crystalline matrix. It appears to be a dominantly solid state fabric (Plate 5.5, 5.6). Outcrops which do not show a strong solid state overprint preserve only a very weak magmatic fabric.

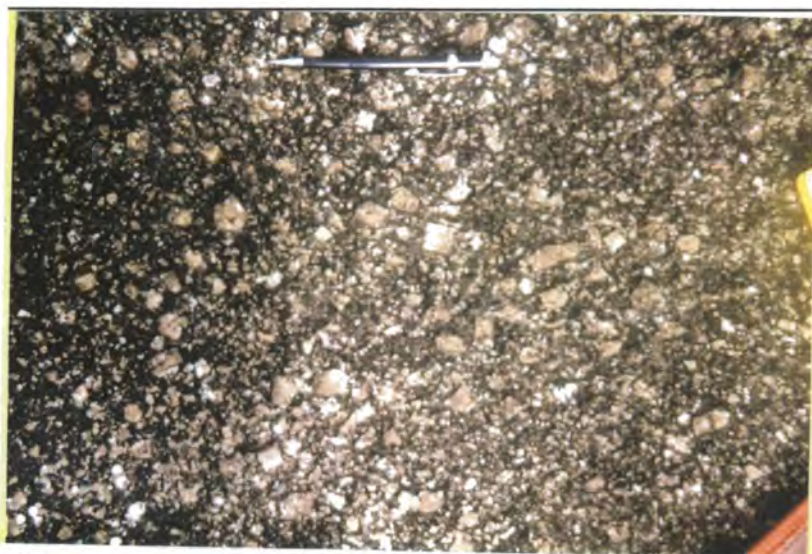


Plate 5.4 Imbiricu G1 in outcrop (GR 92754733)

Within this broadly homogenous pluton there are a number of well exposed granitoid sheets or dykes which have intruded the existing foliation (most commonly in the vicinity of GR 92334783). These are distinct from the microgranitoid dykes described below, which commonly emplace into plutons in this region, because they are discontinuous along strike, have a similar grain size and a qualitatively similar composition when compared to the surrounding granite, except for the absence of phenocrystic potassium feldspar (Plate 5.7). As a consequence of this mineralogy (which is similar to G2) it is suggested that they represent sheets of G2 material emplaced into G1. In outcrop they are generally dm- to m-scale in width and show sharp (mm-scale) contacts between individual phases, although one sheet shows the preferential growth of potassium feldspar close to the contact which may indicate a degree of diffusion occurring in this area in the time after injection. This suggests that injection of these features took place while the magma remained hot and/or melt/volatile phases were present to facilitate such transfer. In general these sheets are orientated sub-parallel to the regional foliation. Across all of these outcrops the fabric is weak (solid or magmatic), which suggests that these sheets are preserved close to the injection orientation.



Plate 5.5 Solid state fabric northwest G1, Imbiricu pluton (GR 92754733)

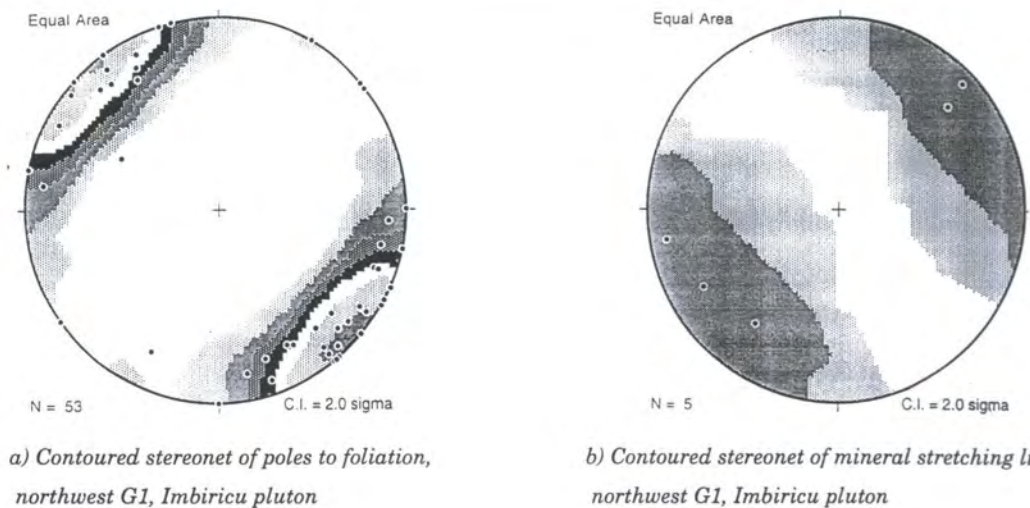


Figure 5.6

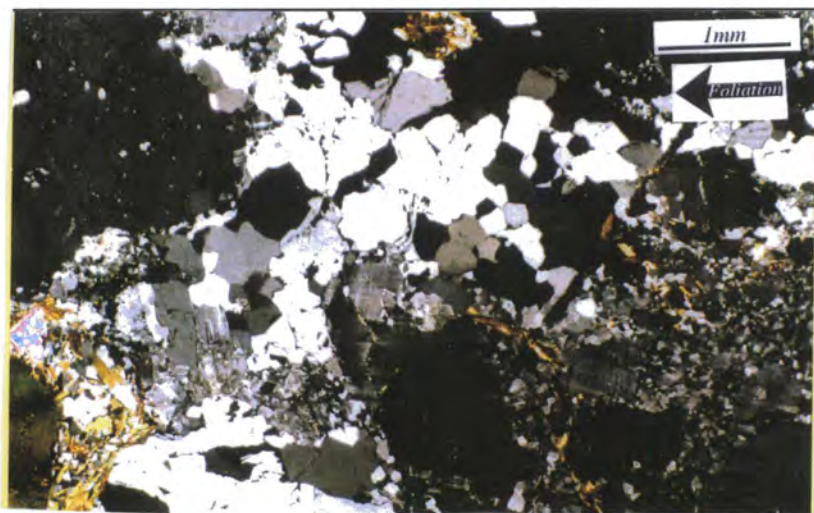


Plate 5.6 Photomicrograph of solid state deformation within G1, Imbiricu pluton (GR 93284780)

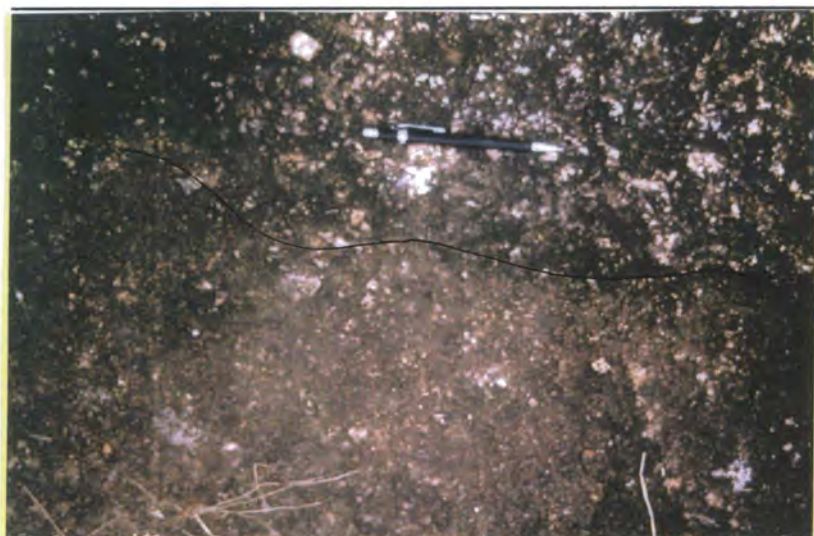


Plate 5.7 Sheeting in the Imbiricu pluton (GR 92234783)

Southeast G1

Along the southeastern contact of the pluton the G1 body can be distinguished in a few places (GR 94804561, GR 96554775, Plate 5.8) and is estimated to be approximately 200m wide. It shows intensely deformed feldspar phenocrysts, which are cracked and re-orientated within the foliation plane along the direction of the low-angle mineral stretching lineation. Stereonets of the fabrics from this area are shown in Figure 5.7.

The inner phase, G2

G2 lies between exposures of G1. It is often poorly exposed and erodes easily but generally it displays a light-coloured, coarsely crystalline outcrop with a matrix of similar crystal size to that of G1, consisting of quartz, biotite, and feldspar (Plate 5.9). In outcrop the principal difference between G2 and G1 is the sporadic occurrence of large potassium feldspar phenocrysts. These phenocrysts are rectangular, up to 3-4cm in length, occur individually or in agglomerates and are generally orientated oblique to the preserved foliation direction. In one outcrop (GR 90384433) the potassium feldspars occur heterogeneously in narrow zones (<1m wide) sub-parallel to the foliation and it is suggested that these zones may preserve the outlines of cryptic (compositionally similar) sheeting during emplacement. In general the fabric is a solid state foliation, which overprints a very weak magmatic fabric, defined by poorly aligned potassium feldspar phenocrysts (Plate 5.10). Point counting of the few samples that could be collected from this area (Figure 5.9b, n= 3, 500 points) show the composition of this pluton to be broadly similar to G1 as an alkali granite.

The fabric within G2 is orientated as elsewhere within the pluton: sub-vertical, and generally sub-parallel to the pluton long axis and the regional dominant trend (Figure 5.8), with a rarely developed sub-horizontal solid state mineral stretching lineation. Anti-clockwise rotation of the fabric within the most central outcrops.

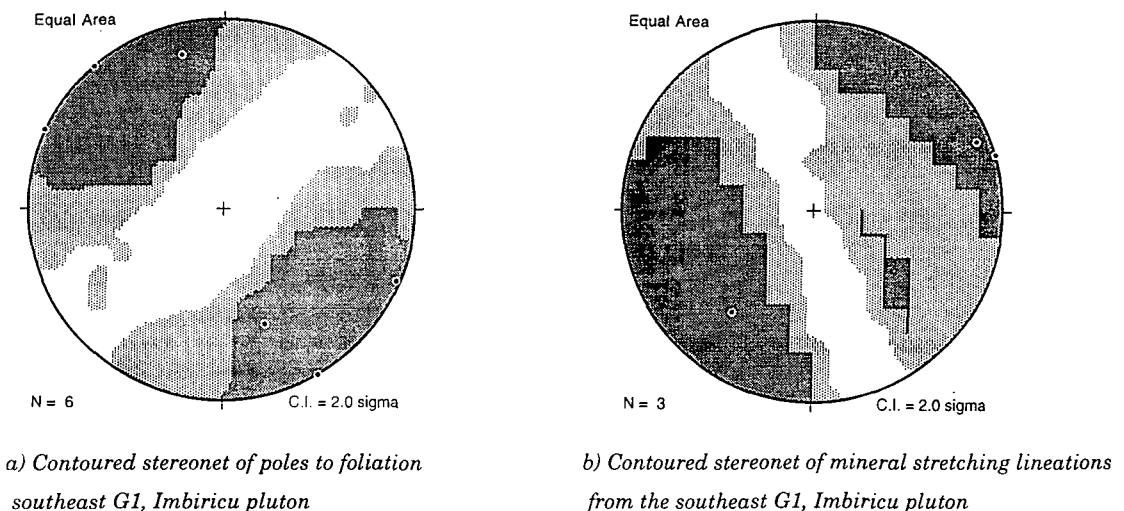


Figure 5.7



Plate 5.8 South-west G1, Imbiricu pluton (GR 94684600)



Plate 5.9 G2 in outcrop, Imbiricu pluton (GR 90384433)

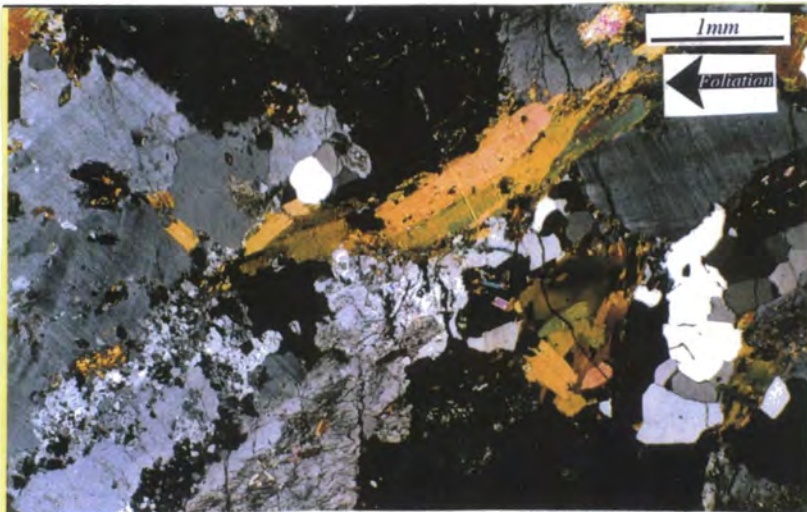


Plate 5.10 Photomicrograph of fabric preserved in G2, Imbiricu pluton (GR 94484750)

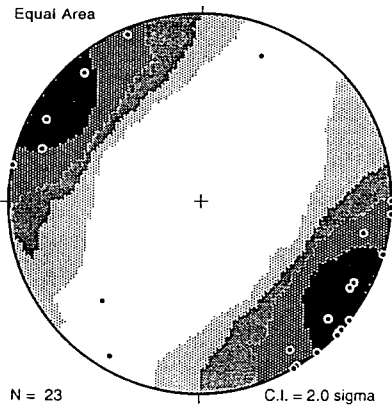
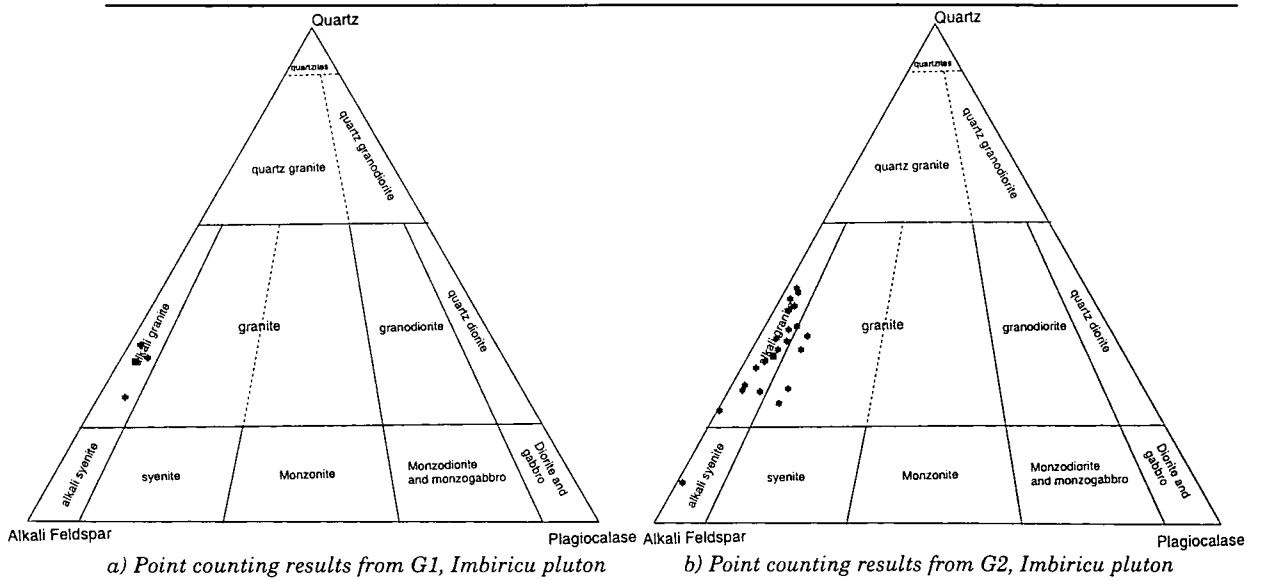


Figure 5.8 Contoured stereonet of poles to foliation from G2, Imbiricu pluton



a) Point counting results from G1, Imbiricu pluton

b) Point counting results from G2, Imbiricu pluton

Figure 5.9

The contact between G1 and G2

The contact between G1 and G2 is not exposed at any point along the southeast side of G2, although along the northwest side of G2 the contact and some of the outcrops closely related to it can easily be examined. This area shows (Figure 5.10): i) an uniformly weak solid state G2 fabric with occasional large potassium feldspar phenocrysts; ii) a distance of approximately 10m of no exposure before; iii) uniformly developed smaller potassium feldspar crystals are observed, consistent with transition from G2 into G1 within a (qualitatively) more intense ductile solid state fabric. This suggests that the contact between these units is relatively well defined, comparatively sharp and subvertical: no intruding sheets have been preserved along this contact.

Conclusions

The data presented above demonstrates that the pluton consists of 2 magmatic phases, compositionally similar but differing in detail. G1 intruded first as sheets into the country rock, before forming a single body which is internally compositionally homogenous. Subsequently, while magmatic fluids remained present, the early pluton was split by a second phase, G2, which emplaced a large magma body, preserving individual sheets, within G1 and may preserve sheets intruded into the major regional structure. Both of these early phases preserve a qualitatively weak magmatic fabric but were overprinted by a ductile solid state fabric. The coincidence of the internal petrographic zonation and the pluton fabric, with the orientation of the regional structure, suggests that the latter exerted a strong control in the focusing of magma during emplacement.

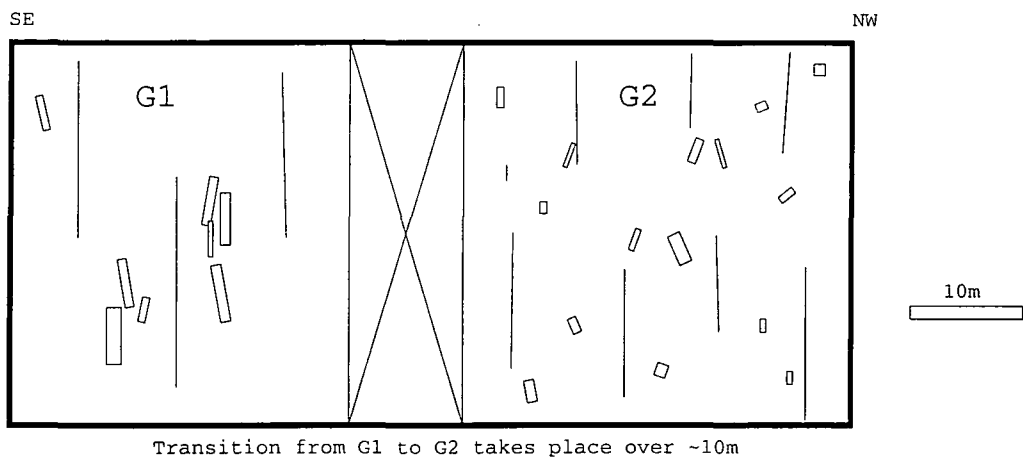


Figure 5.10 Summary log through the G1/G2 contact GR92664710, Imbiricu pluton

5.2.4 Microgranitoid stocks, dykes, enclaves and country rocks xenoliths

Around and within the Imbiricu pluton there are a number of other bodies which indicate that magmatic activity occurred at various times in this area.

Microgranitoid stocks

Along strike to the northeast of the pluton (GR 960540) exposures of fine grained, intensely deformed microgranitoid rocks can be observed (Plate 5.11). These show an intense shear induced solid state fabric of feldspar, broken and cracked during brittle processes, and ribbon quartz, pervasively overprinting any original magmatic fabric. This fabric is broadly consistent with deformation at or less than 300°C (Passchier & Trouw 1996). The exact limits, contact relationships or age of this feature is unknown, but it is tentatively interpreted as being intruded during at an earlier stage than the pluton itself,

since it was cold (relative to the temperature of deformation in the pluton) during solid state overprinting.

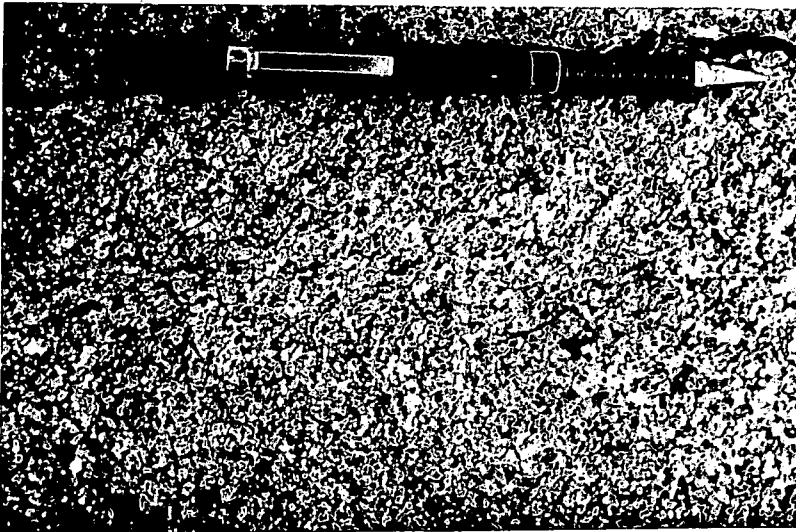


Plate 5.11 *Microgranitoid stock northeast of the Imbiricu pluton (GR 92105235)*

Microgranitoid dykes

A small number of cm-scale microgranitoid dykes are observed within the pluton in both G1 and G2. They show intrusion non-parallel to the regional fabric and a fine grained appearance that is qualitatively similar in composition to the bulk granite (Plate 5.12). In outcrop they appear to be cross-cut, but not significantly deformed by the overprinting solid state deformation: This interpretation is consistent with the observations from the Atibaia pluton, suggesting that the overprinting solid state deformation was of a relatively low intensity and that the microgranitoid dykes predate it. Additionally, there is a regularity in dyke orientation which is kinematically analysed in part 5.6.

Also worthy of remark is the m-scale dyke intruding along the northwesternmost contact of the pluton (see Figure 5.4). This feature shows a finely crystalline matrix and a foliation sub-parallel to that of the pluton. The exact age relationships of the dyke could not be ascertained, but it is suggested that it is contemporaneous or slightly post-dates the intrusion of the pluton since similar features are not observed as sheets within the country rock and it does display a fabric similar to that developed within the pluton.



Plate 5.12 Microgranitoid dyke from within the Imbiricu pluton (GR 91404708)

Microgranitoid enclaves

The microgranitoid enclaves identified within the pluton fall into two categories:

1. **Ellipsoidal enclaves** - These are the most common variety and are generally relatively small, with a smooth outer contact to the surrounding *granite* (Plate 5.13). They display an obvious axial elongation direction sub-parallel to the regional foliation and preserve a fine grained homogenous internal fabric of basic composition. These microgranitoid enclaves conform to the criteria laid down for use as strain markers in part 1.5.1.
2. **Blocky enclaves** - Occasionally within the pluton there are large (>50cm radius) microgranitoid enclaves (Plate 5.14), which can be easily distinguished from the previously described population by: i) their blocky angular shape; ii) a preserved internal magmatic 'stratigraphy'; and iii) an alignment non-parallel with the regional foliation. These could be broken up mafic dykes, smaller intrusions or parts of the magma chamber. In any case the enclaves have such a high competency contrast they fail to conform to any of the criteria laid down for their use as strain markers and have been isolated from the enclave axial ratio strain analysis.

In addition to these features there are, within G2, occasional sub-circular, possibly spheroidal, m-scale features (Plate 5.15), which appear to consist of an annulus 10-20cm wide composed almost entirely of biotite and subsidiary hornblende. The host granitoid both within and around the feature appears to be unaltered. The origin or possible function of these features is unknown, although it is suggested that they could have been 'globules' of more basic material emplaced contemporaneously with the granitoid magma and have been subsequently resorbed during cooling and homogenisation of the magma immediately after emplacement.



Plate 5.13 *Ellipsoidal enclave from within the Imbiricu pluton (GR 92474778)*



Plate 5.14 *Blocky enclave from within the Imbiricu pluton (GR 90384433)*



Plate 5.15 *Annulus of basic material preserved within G2 of the Imbiricu pluton (GR 89654618)*

Country rock xenoliths and screens

Slivers of country rock within the Imbiricu pluton are rare but, where they are preserved they form rectangular fragments with an internal 'stratigraphy' and are generally orientated sub-parallel to the pluton foliation (Plate 5.16). These are easily distinguishable and are isolated from the axial ratio measurements used for strain analysis.

In addition to these minor xenoliths at the northeastern corner of the pluton (GR 96234710) there is a major (>200m wide) country rock apophysis. This screen is orientated sub-parallel to the country rock and the pluton foliation and appears to cross-cut the petrographic zonation of the pluton. These exposures are interpreted to be a country rock screen which was resistant to the intrusion of the magma and was subsequently incorporated into the pluton. There may be additional such screens but lack of exposure prohibits their description.



Plate 5.17 *Country rock xenoliths within the Imbiricu pluton (GR 89654618)*

Conclusions

Within the Imbiricu pluton a number of populations of xenolithic material have been preserved. Of primary importance to the analysis of the pluton are the small ellipsoidal microgranitoid enclaves, which fulfil all of the criteria necessary for their use as strain markers, and the minor country rock screens which demonstrate the sheeted nature of the intrusion. There are, in addition, blocky basic xenoliths, which appear to be formed from incorporated fragments of 'stratified' basic rock, and annular accumulations of basic material, which may have formed in response to absorption/dissolution of basic globules into the surrounding magma. In similarity to other plutons from the RPSSB, the Imbiricu pluton preserves a number of cm-scale microgranitoid dykes/sheets which cross-cut the internal foliation and contain finely crystalline material of a composition qualitatively similar to the bulk magma.

5.2.5 Conclusion and discussion

Mapping of the plutonic phases and country rock around the Imbiricu pluton show that it consists of two magmatic phases, which were emplaced consecutively, by: i) initial sheeting into the regional fabric by G1; ii) assimilation and homogenisation of a large magma body; and iii) intrusion of a second magma phase G2. A number of different types of xenolith were incorporated into these magmas including microgranitoid enclaves, blocky basic enclaves and country rock. Initial intrusion occurred, associated with a weak magmatic fabric which was overprinted by a heterogeneous solid state fabric, most intensively developed within G1. The country rock along the southeast side of the pluton preserves the imprint of intense shearing, whereas on the northwestern side it has been locally deflected to become sub-parallel to the pluton contact over the 100-200m closest to the granite. After the intrusion of both the magma phases, and apparently before the overprinting by the solid state fabric, microgranitoid dykes were emplaced non-parallel to the pluton foliation.

5.3 Deformation: the Imbiricu pluton

In the following section the deformation fabrics preserved within and around the pluton are correlated with the regional deformation sequence outlined in part 3.3.4.

5.3.1 Country rock

The deformation within the country rock consists of near- and far-field components and varies depending upon which side of the pluton is examined. In general the far-field fabric consists of a northeasterly trending fabric, which dips at varying angles, mostly towards the southeast. Field examination of this fabric and interpreting it using Map 8 demonstrates that the fabric is a steepened S_{n+1} low-angle foliation, which has been steepened in response to dextral transpression during D_{n+2} . Closer to the pluton the situation becomes more complex and is described below:

Southeast of the pluton

On the southeastern side of the pluton the fabric is defined by a steeply dipping shear fabric, which preserves intense deformation associated with the Monteiro Lobato shear zone (considered to be a regional D_{n+2} feature). This intense deformation is observed up to 20 km southeastwards of the contact and consists primarily of zones of well developed, sub-vertical fabric (named Monteiro Lobato, Buquira and Paratei shear zones) and occasional portions of more moderately dipping material. Given the scale of this zone it is probable that these shear zones record lateral movements of many kilometres (as suggested by Ebert & Hasui *in press*). Detailed examination of the fabric demonstrates that deformation occurred at a temperature sufficient to cause recrystallisation of quartz, and possibly feldspar, but the absence of additional metamorphic minerals does not permit an accurate estimate of the upper temperature associated with deformation. It is merely possible to suggest that the minimum temperature of deformation is 300°C (lowest greenschist facies). The formation of a mineral stretching lineation occurs in the granite itself and so it is suggested that the lowest temperature fabrics recorded here are associated with the D_{n+4} post-intrusion reactivation of the major structures.

Northwest of the pluton

To the northwest of the pluton the regional fabric ($S_{n+1/2}$) is deflected until it becomes sub-vertical to the pluton margin in the 100-200m closest to the contact. The intrusion of Imbiricu G1 granite sheets sub-parallel to this fabric and the re-orientation of this fabric close to the pluton margin suggests that it was formed in response to granite emplacement and therefore it is a D_{n+3} fabric. Along this contact metamorphic sillimanite has been observed within the country rock which suggests that, during the intrusion of the pluton, temperatures probably in excess of 500°C were present.

Additionally, along this contact there is sporadic development of a sub-horizontal mineral stretching lineation, which, despite the absence of the solid state shear fabrics that

are normally associated with this feature, suggest that the D_{n+4} overprinting deformation only weakly affected this area.

Conclusions

The country rock surrounding the Imbiricu pluton preserves, along its southeastern side, a D_{n+2} regional structure formed in response to regional dextral transpression and reactivated after the granite intrusion during D_{n+4} greenschist facies deformation. Along the northwestern side of the pluton the country rock fabric was deflected until it became sub-parallel to the pluton contact and developed metamorphic sillimanite during D_{n+3} deformation; D_{n+4} only weakly affected this area.

5.3.2 Granite

The granite itself preserves a fabric which is orientated sub-parallel to the pluton long axis. In order to better describe the deformation associated with this fabric it has been sub-divided by pluton:

The outer phase, G1

Northwest G1

The preserved fabric in the northern area is generally northeast-southwest trending, but is rotated northwards in an anti-clockwise fashion in the centre of the pluton. In general the fabric is defined by solid state deformation (Plate 5.17) sub-parallel to an earlier magmatic fabric (Plate 5.18). The solid state fabric in outcrop is generally described by ribbon quartz, the production of S-C fabrics and the weak augening of feldspar. In thin section (Plate 5.19) the solid state fabric can be seen to be locally intense producing the complete recrystallisation of quartz, cracking of feldspar, the development of strong 'core and mantle' feldspar fabrics and the elongation of biotite. These fabrics suggest that deformation took place at temperatures of at least 400-500°C (Passchier & Trouw 1996).

Remnants of the magmatic deformation can be observed in many of the outcrops where the solid state fabric is weakest, although magmatic state fabrics are only seen within a few thin sections from the central part of the pluton, where anticlockwise rotation is strongest. In general, the magmatic state fabric is defined by a weak alignment of the feldspar phenocrysts and matrix, which can be unobservable in places making the pluton appear almost isotropic. In thin section the magmatic fabric can be seen in the tiling relationships of unrecrystallised feldspar phenocrysts and the equant nature of the biotite crystals (Plate 5.20). No thin section was observed where the quartz was not at least partially recrystallised. In this area there are a few mylonites (compared to G2), which cross-cut the internal fabric at a high angle. They are kinematically analysed in part 5.7.



Plate 5.17 Solid state fabric within G1, Imbiricu pluton (GR 90634798)



Plate 5.18 Magmatic fabric within G1, Imbiricu pluton (GR 93584770)

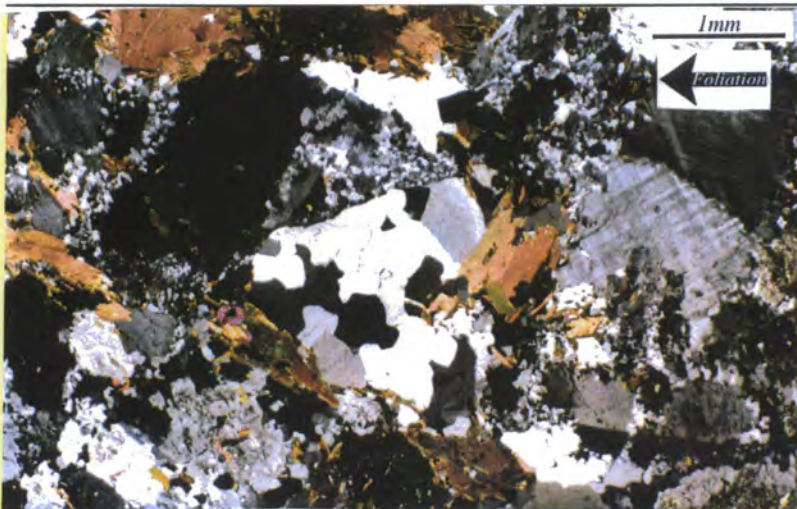
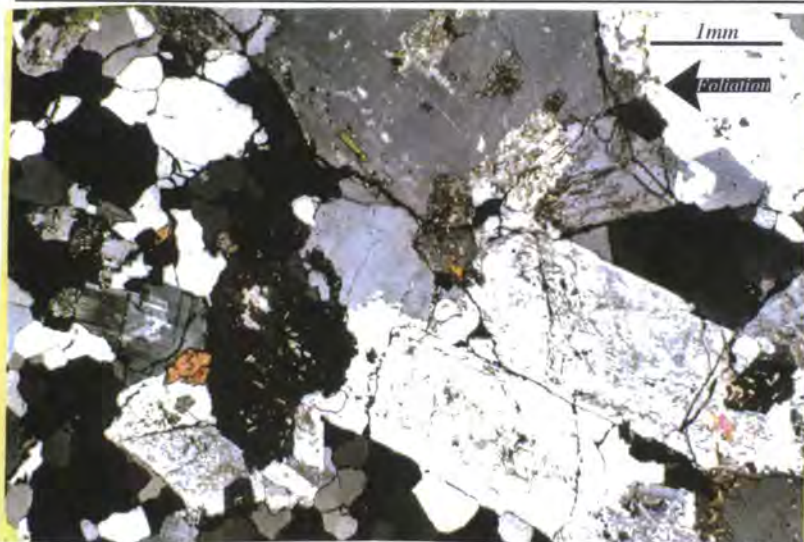


Plate 5.19 Photomicrograph of solid state deformation from the G1, the Imbiricu pluton (GR 92484778)



Photomicrograph of magmatic state deformation from the G1, the Imbiricu pluton (GR 90754513)

Plate 5.20

Southeast G1

The southeastern portion of G1 is narrow and poorly exposed but shows a very strong solid state overprint of the earlier magmatic fabric, displaying a finely divided fabric, augening of feldspar and a well developed sub-horizontal lineation. The magmatic state fabric is not preserved in any part of this area. The fabric was formed entirely within the solid state, representing an intense D_{n+4} overprint of the earlier D_{n+3} fabric. Additionally, a few mylonites cross-cut this area and their occurrence is believed to be associated with the proximity to the Monteiro Lobato shear zone a short distance to the southeast.

The inner phase, G2

As described previously G2 consists of large rectangular phenocrystic potassium feldspars within a matrix of quartz, biotite and feldspar. These outcrops preserve a fabric which, in the field, appears to be relatively weak and orientated approximately sub-parallel to the pluton long axis or rotated anticlockwise relative to it. Solid state deformation increases in intensity as the southeastern contact and the Monteiro Lobato shear zone are approached. In outcrop this solid state fabric is preserved largely in the matrix and does not appear to have altered the orientation of the larger potassium feldspar phenocrysts (Plate 5.22). This solid state deformation of the matrix shows the development of ribbon quartz and occasional S-C fabrics. In thin section weak recrystallisation of quartz and qualitatively weak core and mantle structures around feldspar phenocrysts (Plate 5.23) suggest that, in general, the solid state deformation event (D_{n+4}) had a relatively weak magnitude within this pluton phase. However, the type of structures present are consistent with a deformation taking place at 400°C-500°C (Passchier & Trouw 1996). Additionally, the presence of relatively undeformed magmatic biotite around the smaller feldspars suggest that these are preserved in the magmatic orientation i.e. sub-parallel to the overprinting

fabric. At no single locality could the magmatic fabric be unequivocally identified, an observation which is consistent with the thin sections which show recrystallisation and elongation of quartz even in the most weakly deformed sections. Observations of preserved phenocryst distributions suggested that this magmatic fabric was of a very weak intensity.

Within the largest G2 outcrops there are a number of discrete mylonites, which cross-cut the pluton fabric at a high angle with various shear senses. They become much more common as the southeasternmost contact of the pluton is approached. See part 5.7 for a kinematic analysis of these structures.



Solid state fabric within G2, Imbiricu pluton showing randomly orientated potassium feldspar phenocrysts (GR 94734633)

Plate 5.21

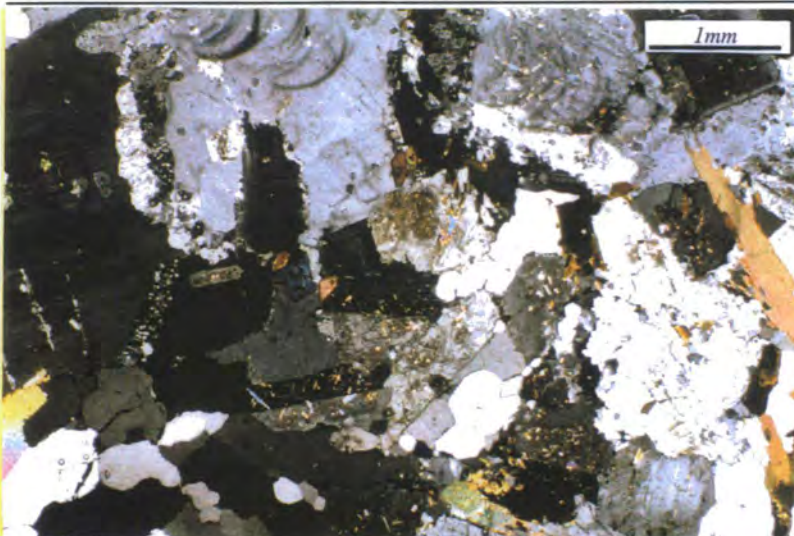


Plate 5.22 Photomicrograph of the fabric within G2, Imbiricu pluton (GR 94484750)

Conclusions

The granite phases within the Imbiricu pluton were emplaced with a low intensity magmatic D_{n+3} fabric, which was subsequently overprinted by a solid state deformation when the pluton had cooled to around 400°C-500°C. The intensity of this solid state deformation was linked to proximity to the outer contacts and, additionally, to proximity to the Monteiro Lobato shear zone along the southeastern contact. As a result G1 generally preserves a more intense fabric than can be found within G2. Also, in the central parts of the pluton, the fabric, whether solid state or magmatic state, is rotated anti-clockwise relative to the long axis of the pluton; This is interpreted to be an emplacement shear induced phenomena and will be discussed in greater detail in part 5.5.

5.3.3 Conclusion and discussion

Examining the deformation data from the Imbiricu pluton suggests that there are fabrics formed within the country rocks and the granite which can be associated with both intrusion and later deformation:

1. **Monteiro Lobato shear zone** - The country rocks along the southeastern side of the pluton are deformed by a major shear zone which can be shown to be an early pre-granite D_{n+2} structure that was reactivated, probably during, and certainly after, the emplacement of the pluton, thus controlling the style of D_{n+4} deformation in the surrounding area.
2. **Syn-intrusion fabrics** - Around the northwestern side of the pluton deflection of the regional foliation into parallelism with the contact and the magmatic fabric within the pluton record deformation associated with the intrusion event. Within the pluton itself these fabrics have a relatively low-intensity, which suggests that the pluton generally has a low emplacement strain, although sufficient force was exerted upon the country rocks to deflect them into parallelism with the contact
3. **Temperature of deformation** - The solid state fabric within the pluton records deformation occurring around 400°C-500°C; This is below the maximum metamorphic temperature recorded in this area but greater than the temperature recorded in the Atibaia pluton and the minimum temperature (~300°C) recorded in the country rocks from this region (Ebert *et al* 1996).
4. **Solid state deformation** - The intensity of solid state deformation which affects the pluton is controlled by proximity to the outer contacts and proximity to the Monteiro Lobato shear zone. Hence, it is concluded that the regional tectonics imposed external deformation on the pluton (which acted as a semi-rigid body), partitioning deformation into the outer margins of the pluton.
5. **Discrete deformation** - Discrete cm-scale mylonites were nucleated within the pluton. These features have regular orientations which are analysed in part 5.7.

5.4 Strain measurement: the Imbiricu pluton

5.4.1 Introduction

As with the other plutons studied within the RPSSB, an attempt has been made to quantify the strain preserved within the Imbiricu pluton using strain estimates from the country rocks, measurements of mafic enclave axial ratio and the Fry fabric strain.

5.4.2 Microgranitoid enclaves

Methodology

As described in part 5.2.4, there are a number of distinct populations of xenolithic material preserved within the Imbiricu pluton. In this analysis only microgranitoid enclaves that preserve an ellipsoidal shape in outcrop, are orientated along the foliation direction and preserve no internal 'magmatic stratigraphy' have been measured and analysed using the techniques detailed in part 1.5.1. This is a relatively small number of enclaves and hence, in order to produce a statistical sample of enclaves, individual outcrop populations have been combined. This results in two principal populations of measurements from the horizontal outcrop plane which are detailed in Table 5.1, Figure 5.11 and Appendix 9.

Results

These data, although small in number, suggest that the finite strain recorded through the deformation within the pluton was less than that preserved in the Atibaia pluton ($R_s \sim 2.46-2.90$) and homogenous across both intrusive phases. It could be suggested that G1 preserves a higher strain but additional data would be required to fully test this hypothesis. As a consequence of the lack of quantitative data from the vertical plane no statements can be made about the type of strain preserved. The lack of a consistently orientated magmatic lineation suggests that, during emplacement, the induced strain had a strong flattening component. However, it should be noted that the overprinting solid state deformation commonly preserves a sub-horizontal lineation. It is known from observations of this fabric overprinting, but not obviously rotated, post-emplacement features (microgranitoid dykes), that this deformation did not induce a significant strain within the main body of the pluton. If the microgranitoid enclaves are assumed to preserve pure flattening emplacement induced strain then this suggests that the pluton was subject to a northwest-southeast directed shortening of 45-50%, equivalent to a 34% northeast-southwest directed extension, during emplacement.

Conclusions

The mafic enclave axial ratio finite strain measurements record an homogenous horizontal strain in both of the analysed populations. This has been interpreted to be a consequence of shortening during the emplacement process. It is suggested that the later solid state strain was not of sufficient intensity and homogeneity to produce such strains.

The values measured are similar to those recorded within other plutons studied from the RPSSB.

Table 5.1 Results of mafic enclave axial ratio finite strain analyses from the Imbiricu pluton.

Localities	Orientations	Grid References	Mean axial ratio	Number of analysed enclaves	St. Dev.	Smallest axial ratio	Largest axial ratio	ω Log	% Variation in size
CH1	Horizontal	GR 90384433	2.46	40	1.52	1.04	7.62	0.86	62
CB6, CC7, CE8, CE10 & CG1	Horizontal	GR 92984759, GR 93584770, GR 90684798, GR 90634798 & GR 89654618	2.90	17	1.35	1.17	3.21	0.78	47

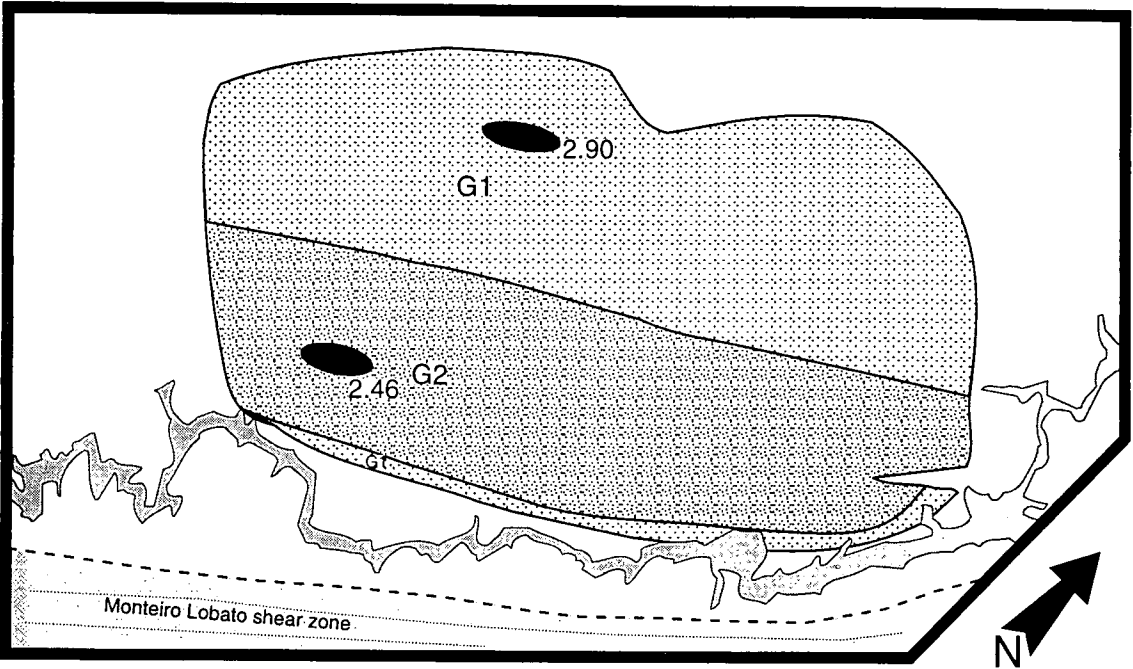


Figure 5.11 Horizontal plane mafic enclave axial ratios from the Imbiricu pluton

5.4.3 Fry strain

Methodology

In this study 21 Fry strain determination have been made at localities across the pluton. Each of these determinations were processed using the method set out in part 1.5.2 and collated with other results from adjacent localities to produce a consistent and reliable value for the Fry strain. The small number of measurements is a consequence of the sparsity of outcrop, the large size and small number of phenocrysts in outcrop and solid state deformation; but the consistency of the results is believed to reflect the robustness of this relatively small dataset. The results are plotted in Figure 5.10, a summary given in table 5.2 and a full list of results shown in Appendix 10.

Results

These data produce four principal populations in the horizontal outcrop plane and only two measurements from the vertical plane. There are a number of interesting points from these data: i) that there is a remarkable consistency across the pluton in the ellipticity of the Fry strain ellipse produced ($R_s = 1.69-1.78$); ii) that it would appear that the values produced from the horizontal plane are mimicked in the vertical plane, suggesting a strong flattening component to the emplacement strain; iii) that the ellipticity values are lower than those produced by measuring the axial ratios of mafic enclaves (as observed in other studied plutons Ardara, Atibaia, Morro Azul, Itapeti); and iv) that these values are lower than those produced from similar measurements in the Atibaia pluton.

Conclusions

These data suggest that the Imbiricu pluton was subject to an approximately flattening strain $R_{xz}=R_{yz}\sim 1.7$, equivalent to a northwest-southeast directed pure shear shortening of ~30% and along axis extension of 20%. The values recorded by this method are lower than those recorded within the Atibaia pluton, which may reflect the qualitative observation that the magmatic fabric (which is probably dominant in producing the distribution of phenocrysts) is very weak throughout this pluton.

Table 5.2 Summary table of Fry strain measurements from the Imbiricu pluton.

Localities	Grid Ref.	Orientation	Fry strain	Number of analyses	Smallest Fry strain	Largest Fry strain	St. Dev.	Log K-value
CA2, CB2, CH3, CH5	GR 94684600, GR 92734633, GR 93704535, GR 92354553	HORIZ.	1.78	4	1.50	2.13	0.26	
CH1, CG10	GR 93084433, GR 9068 4850	HORIZ.	1.80	2	1.59	2.00	0.29	
CE2, CE3, CF3, CG3	GR 89584781, GR 90784860, GR 89534781, GR 88484555	HORIZ.	1.69	5	1.29	1.97	0.31	
CA11, CF4, CB3-4, CC7-8, CD1	GR 92804758, GR 91904619, GR 92664716, GR 92084788, GR 93284780	HORIZ.	1.69	8	1.21	2.18	0.38	0.16
CD1,CB1	GR 93284780, GR 92484778	VERT.	1.84	2	1.61	2.06	0.32	

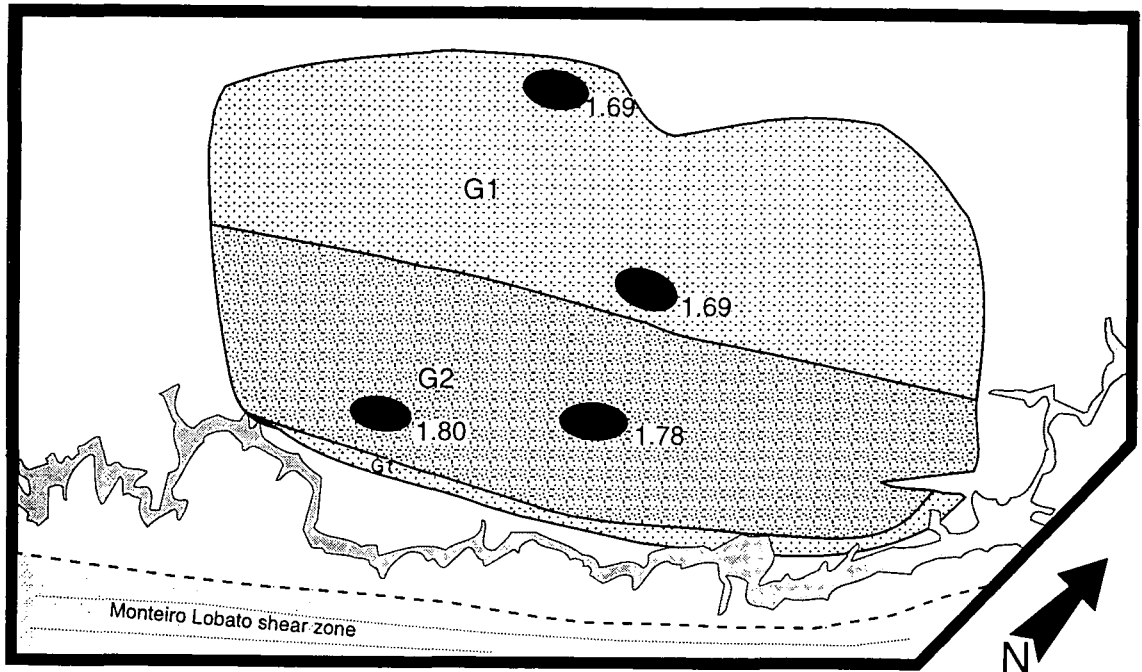
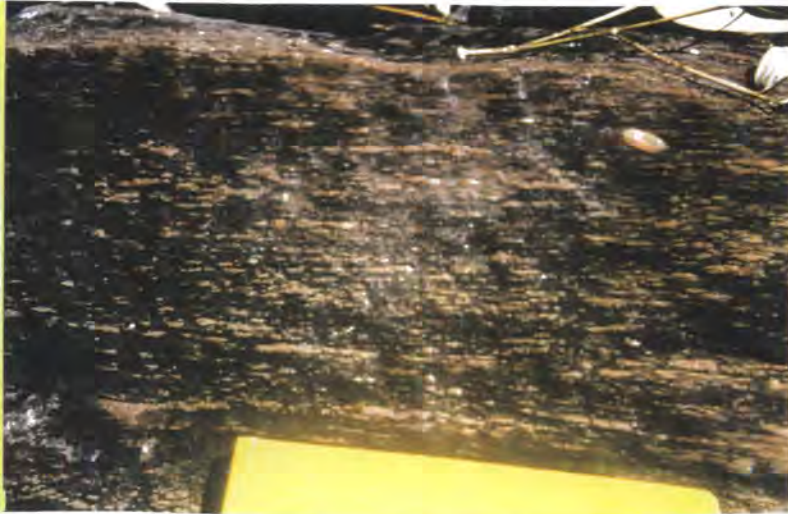


Figure 5.12 Horizontal plane Fry fabric strains from the Imbiricu pluton

5.4.4 Other strain indicators

As stated previously a heterogeneous solid state fabric overprints the Imbiricu pluton; This fabric becomes particularly intense along the southeast contact of the pluton. At one outcrop in particular (GR 96284783) there is a well preserved, intense, sub-vertically orientated LS-type fabric within the G1 granite, whose lineation is sub-horizontal. In the XZ/horizontal plane of this outcrop there are feldspar phenocrysts which have experienced deformation sufficient to induce an axial ratio of 10:1 (Plate 5.23), and similarly within the YZ/vertical plane phenocrysts are relatively undeformed. Interpretation of these observations, assuming that the feldspars were initially equant and $R_{YZ} \sim 1$, suggests a local X axis stretching of greater than 400% along the southwest contact of the pluton. Elsewhere within the pluton this deformation was weak, inducing recrystallisation of quartz and feldspar, while often preserving their original crystal shape. In conclusion, D_{n+4} was partitioned predominantly along the southeastern pluton contact.



Elongate feldspar phenocrysts along the southeastern contact of the Imbiricu pluton (GR 96554775)

Plate 5.23

5.4.5 Country rock strain

A further observation of country rocks around the pluton shows strongly deformed rocks preserving an LS-type fabric along the southeast side of the pluton, within which no adequate strain markers are preserved. It can merely be stated that the ultramylonitic fabric within the country rocks suggests that a high magnitude of strain has been accommodated within these rocks, probably during multiple events.

Along the northwest side of the pluton the country rocks preserve a regional fabric which generally dips moderately to the southeast ($\sim 45^\circ$), although close to the pluton this dip becomes steep to sub-vertical ($\sim 80^\circ$). Taking these data, using the equation of Ramsay (1967) set out in Equation 2.4 and assuming a pure flattening strain, suggests that a finite strain of $R_{XZ}=R_{YZ} \sim 5.6$ was induced during the intrusion of the pluton. This is equivalent to a northwest-southeast directed pure shear shortening of $\sim 65\%$. Field observations suggest that this re-orientation of regional foliation took place over only the 250m closest to the pluton and hence may represent the creation of around 450m of space for the pluton.

5.4.6 Conclusion and discussion

A number of points arise from these analyses:

1. **Pluton strain** - Microgranitoid enclave axial ratios from the horizontal outcrop plane record an homogenous along pluton axial extension. Fry fabric strain measurements produce similar data, albeit with smaller values. These data, taken with field observations of syn-emplacement sheeting, suggest that individual batches of magma were subject to a weak northeast-southwest directed stretching during their emplacement and homogenisation into the major magma body.

2. **Country rock strains** - Estimates of strain can only be made by assuming that the regional foliation was deflected into parallelism with the pluton contact during emplacement. This technique suggests that around 500m of space could be created for the pluton in this way and therefore it is proposed that approximately 4.5km of space for the pluton must have been created using other mechanisms.
3. **Fry strains** - The Fry strain values recorded within this pluton are lower than those recorded within the other plutons studied in the RPSSB. This result is entirely consistent with the very low intensity magmatic fabric observed within this pluton and therefore it can be unequivocally concluded that the emplacement related strain was comparatively low in this area.
4. **Overprinting strain** - The southeastern contact of the pluton was overprinted by an intense solid state shear strain. This strain was predominantly partitioned into the rocks of this area and only weakly overprinted the remaining parts of the pluton.

5.5 Shear senses: the Imbiricu pluton

5.5.1 Introduction

Shear senses (where preserved) were analysed by making comparisons to the ideal situations detailed in part 1.4, the majority of determinations are made from outcrop observations of magmatic and solid state fabrics, although a small number have been made from thin sections.

5.5.2 Country rock

As a consequence of the very different intensities of deformation on either side of the pluton they are described separately.

Southeast of the pluton

This is the area of the pluton most strongly affected by the influence of the Monteiro Lobato shear zone. The fabric is intense everywhere and any small porphyroclast or foliation plane capable of preserving a fabric has often been too heavily deformed to easily facilitate the recognition of shear sense indicators. There are however a number of places in the outer margins of the pluton (GR 96554775), where the solid state fabric is most intense, and dextral asymmetric porphyroclasts, or dextral S-C fabrics can be easily identified (Plate 5.24). Examining the vertical plane of outcrop shows that this fabric is dominantly an LS-fabric, with no demonstrable shear sense in this orientation. The foliation plane shows the development of a sub-horizontal mineral stretching lineation, which leads to the interpretation that this solid state fabric is the result of a dextral shear.

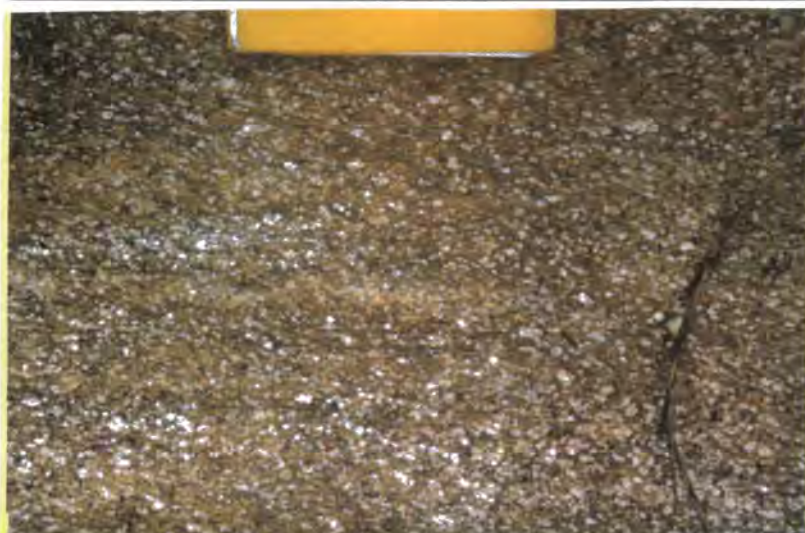


Plate 5.24 Dextral fabrics within the southeasternmost part of the Imbiricu pluton (GR 96554775)

Northwest of the pluton

To the northwest of the Imbiricu pluton the country fabric away from the immediate vicinity of the pluton preserves only the $D_{n+1/2}$ composite fabric which displays no evidence for shearing during emplacement. In the immediate vicinity of the pluton,

where the fabric has been re-orientated sub-parallel to the pluton contact no identifiable shear fabric from any stage during or post emplacement of the pluton can be seen. Although there are a few scattered localities where a sub-horizontal stretching lineation can be found (Figure 5.2), a feature which is regionally associated with D_{n+4} dextral horizontal planar shear. In conclusion there are no intrusion related shear fabrics preserved within the country rocks.

Conclusions

The country rock around the Imbiricu pluton rarely exposes shear sense fabrics, either ones which can be related to the intrusion of the pluton or other events. When they can be identified, the fabrics are consistent with dextral movement, which increases in intensity as the Monteiro Lobato shear zone is approached.

5.5.3 Granite

As described previously the Imbiricu pluton preserves a relatively weak fabric formed in the magmatic state and a stronger solid state fabric which overprints this earlier fabric heterogeneously. Shear senses determined from each of their deformation environments are outlined below:

Magmatic state fabrics

The outcrops where the magmatic fabric is preserved have a very weak fabric, and in outcrop no preferential orientation of phenocrysts or bi-modality of fabric which might aid the identification of the magmatic state shear sense was seen. Thin section analysis showed a very low intensity fabric within which no preferential shear sense could be identified.

Solid state fabrics

As described previously solid state fabrics are present in most outcrops across the pluton. In general they display a deformed and recrystallised matrix around the larger more competent phenocrysts within the matrix. Examination of the horizontal plane shows in general, asymmetric porphyroblasts, S-C fabrics σ - and δ -fabrics consistent with a dextral sense of shear (Plate 5.25, Figure 5.13a). The spatial occurrence of these fabrics is shown in Figure 5.13b). The foliation plane can preserve a solid state sub-horizontal mineral stretching lineation (Figures 5.6b, 5.7b, 5.8b), whereas the vertical outcrop plane shows porphyroclasts with no preferred asymmetry or other fabric. These deformation fabrics are interpreted to indicate that the Imbiricu pluton underwent a dextral simple shear deformation after the pluton had cooled to 400°C-500°C.

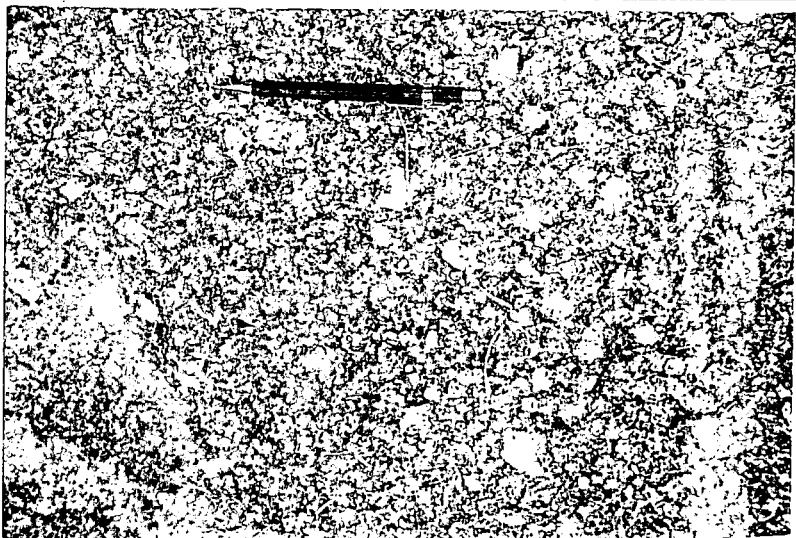
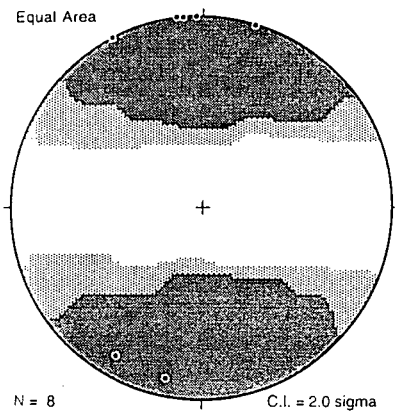


Plate 5.25 Solid state fabrics from the Imbiricu pluton (GR 90684850)



a) Contoured stereonet of poles to C-planes from across the Imbiricu pluton

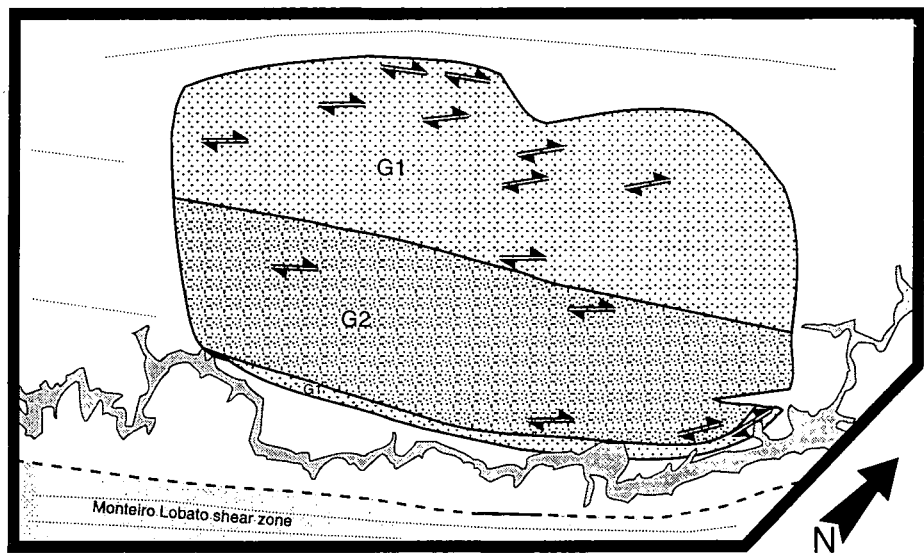


Figure 5.13 b) Plot of observed solid state shear senses from across the Imbiricu pluton

Deflection of the internal pluton fabric

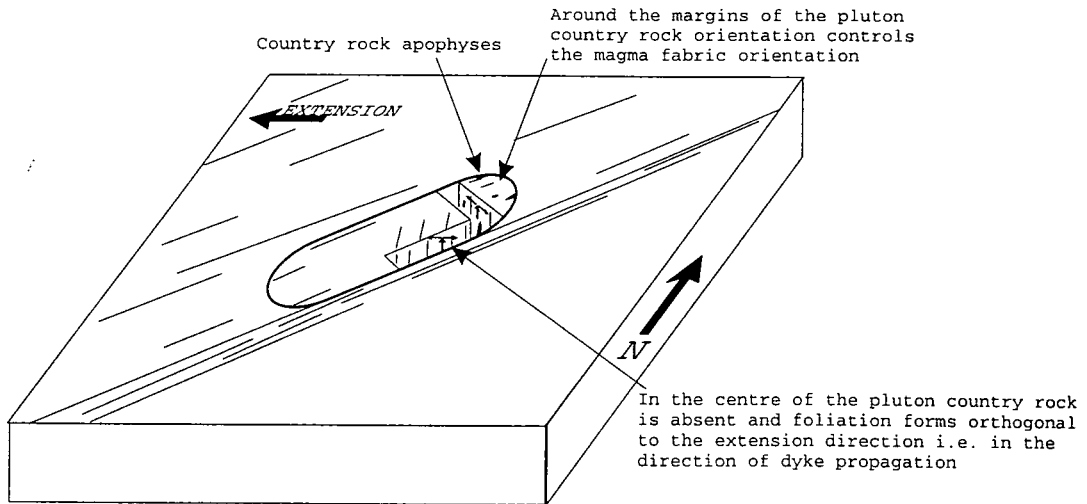
Examining Figure 5.2 shows that while in general the pluton fabric is sub-vertical and sub-parallel to the long axis of the pluton, in the central parts of the pluton the fabric is rotated anti-clockwise relative to the pluton axis. Additionally this rotated fabric is apparently independent of whether the rocks preserve a predominantly magmatic or a solid state fabric. Additionally these outcrops display no preferential or intensified shear sense fabric.

This fabric has been interpreted to have formed in response to regional deformation acting on the body at large during the emplacement of the magma and subsequently during deformation (Figure 5.14). Explaining this idea in more detail; regionally it has been observed that emplacement of the pluton was coincident with east-west directed extension (Chapters 3, 4, 6). If this is the case in the Imbiricu area then extension would have occurred slightly oblique to the present-day pluton long axis. Magma upwelling into such a 'cavity' through dykes would be orientated perpendicular to the local extension direction. Therefore around the margins of the pluton the country rock foliation, into which the magma was sheeting, would exert a strong control on this elongation direction, inducing a sinistral shear as observed in other plutons from the RPSSB. On the other hand in the centre of the pluton it can be hypothesised that magma would be less controlled by the local foliation and rather more by than regional tectonics (sheeting might occur more through a magma conduit and less through the country rocks). As a consequence magma would upwell into the sites of lowest pressure, and extend sub-parallel to the pluton long axis orthogonal to the extension direction, and preserve the observed fabric (Figure 5.14a).

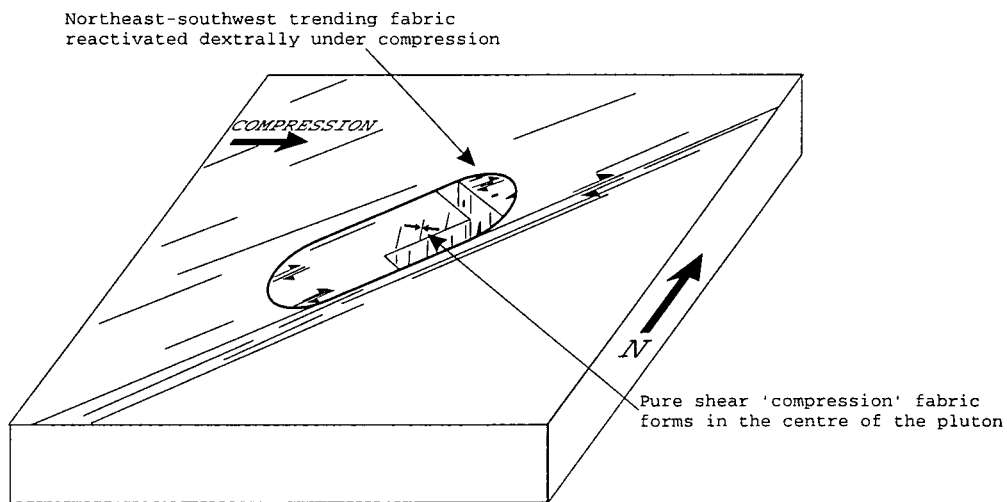
Similarly in the solid state the pluton fabric was formed in response to dextral shear along northeast-southwest trending shear zones i.e. an east west directed compression. Therefore close to the pluton margins a shear induced reactivation of the magmatic fabric occurred, whereas in the centre of this undeformed body, reactivation of the earlier magmatic state fabric as a pure shear fabric orthogonal to the principal stress would be preferential over the formation of a new overprinting fabric. In summary the rotation of this foliation is consistent with emplacement during extension and overprinting during dextral solid state deformation.

Conclusions

The Imbiricu pluton preserves few shear sense fabrics which can be associated with the emplacement of the pluton, although the internal rotation of the fabric can be interpreted as representing the orientation of a fabric formed during regional east-west directed extension. After the emplacement and cooling of the pluton the dextral solid state deformation overprinted the earlier fabric in a similar orientation and resulted in an heterogeneous solid state fabric being found predominantly around the margins of the pluton.



a) Block diagram to explain the formation of the magmatic state rotated fabric within the Imbiricu pluton



b) Block diagram to explain the formation of the solid state rotated fabric within the Imbiricu pluton

Figure 5.14

5.5.4 Conclusion and discussion

The shear sense fabrics present within and around the Imbiricu pluton suggest that emplacement of the pluton was accompanied by the formation of a number of different types of fabrics:

1. **Pre-granite deformation** - While it is difficult to identify unequivocal evidence of pre-granite shearing the major Monteiro Lobato shear zone and steepened and re-orientated country rocks to the north of the pluton suggests deformation associated with D_{n+2} regional dextral transpression.

2. **Emplacement of magma** - In this Imbiricu area the country rocks were deformed by a flattening fabric during intrusion to the northwest of the pluton. Whereas within the pluton only a weak fabric was preserved which appears to show no preferred shear sense in any of the principal planes. Although interpreting the orientation and rotation of this magmatic fabric suggests that it could have formed in response to east-west orientated extension.
3. **Overprinting fabric** - After emplacement of the pluton and significant cooling the pluton and the country rocks to the southeast of the pluton were extensively overprinted by a dextral planar deformation associated with reactivation of the Monteiro Lobato shear zone during D_{n+4} .

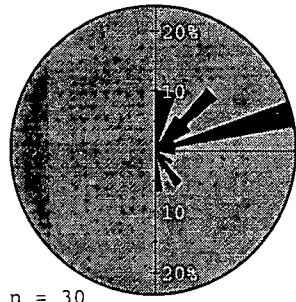
5.6 Emplacement kinematics of microgranitoid dykes/sheets: the Imbiricu pluton

5.6.1 Introduction and methodology

Within the Imbiricu pluton a small number of sub-vertically orientated cm-scale microgranitoid dykes have been emplaced. They are not as prevalent as those recorded within the Atibaia pluton, but have been analysed using identical methods. In order to produce a statistically sized sample these data have been integrated to produce a single rose diagram for the whole pluton (Figure 5.15).

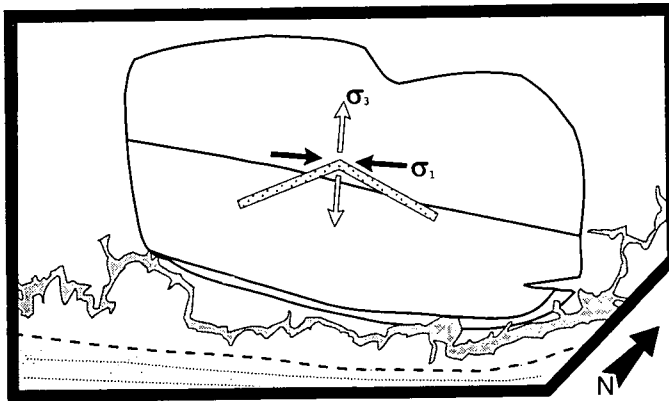
5.6.2 Results and conclusions

A total of 30 individual dyke orientation which came predominantly from localities in the northwestern part of the pluton. They show a prominent peak between 070° and 080°, and subsidiary peaks at 000°-020° and 040°-050°. None of these dykes have recognisable shear senses associated with them. The two subsidiary peaks are taken to represent a broad population whose mean would be at approximately 025°. Therefore one dominant orientation is taken as being at approximately 025° and the second as being at 075°. These results imply a Type 3 origin, where σ_3 is orientated at approximately 140° and σ_1 orientated at approximately 050°. These directions are consistent with injection of the microgranitoid dykes during northeast-southwest directed extension perpendicular to the long axis of the pluton.



n = 30
 Vector mean = 045°
 Circular St. Dev. = 43°
 Max. = 23.3%

a) A rose diagram of microgranitoid dykes orientations from across the whole of the Imbiricu pluton



b) a sketch map of microgranitoid dyke average orientations within the Imbiricu pluton

Figure 5.15

5.7 Overprinting discrete mylonitic shear zones: the Imbiricu pluton

5.7.1 Introduction

As with other plutons studied from the RPSSB a number of sub-vertically orientated, discrete, cm-scale mylonites were found within the pluton which; preserve an identifiable shear sense; occur in conjugate sets; and have inconclusive cross-cutting relationships. In general they have a glassy recrystallised appearance, within which individual grains cannot be identified, except as occasional strongly abraded and rotated δ - and σ -clasts (Plate 5.26). In this pluton mylonites are not as commonly developed as in other plutons examined from this area, although they are more usually observed close to the southeastern contact, where solid state deformation is strongest and there is greatest proximity to the Monteiro Lobato shear zone. Examining them in thin section (Plate 5.27) shows: a matrix of quartz which is commuted in size and shows evidence of dynamic recrystallisation; surrounded by highly deformed fragments of biotite and feldspar. Observations which suggest a formation temperature of up to 400°C, although the caveats to this temperature detailed in part 4.7.1 should be remembered. The age of these fabrics is controversial and was discussed in part 4.7.1.

5.7.2 Methodology

In each analysis the methods described in part 4.7 were used, with rose diagrams being plotted for the mylonites present within each phase of the pluton. Subsequent interpretation assumed that the mylonites formed in a single event. The rose diagrams are shown in Figure 5.16a, b and the interpreted principle stress orientations in Figure 5.16c, d.

5.7.3 Results

G1

The 29 mylonites observed from G1 show a single broad distribution of orientations from 040° to 100° with a prominent mean occurring between 060° and 070°, the vector mean of the data is 067° Figure 5.16a. The dominant shear sense associated with these data is dextral, although many show inconclusive shear sense criteria. These data suggest an environment, where σ_1 can be inferred as being orientated at approximately 112° and σ_3 at approximately 022°, σ_2 being sub-vertical. Results that are consistent with an approximately east southeast-west northwest orientated direction of compression (Figure 5.16c, d)

G2

Far more mylonites are observed within G2 (n=113) and these show a broader and more complex distribution consisting of: i) a prominent peak, coincident with the vector

mean of 079° , between 070° and 090° ; ii) a subsidiary peak at 150° to 170° ; and iii) a minor peak between 030° and 050° (Figure 5.16b). The shear senses associated with these data demonstrate that the mylonites associated with the dominant peak always show a dextral shear sense, whereas those from the subsidiary peaks have a sinistral, or unidentifiable shear sense. Interpreting these results suggest that the data form a conjugate set whose principal stresses and the local anisotropy were orientated in such a way as to produce a dominantly dextral shear sense. By bisecting the angle between individual conjugate sets of mylonites it is possible to suggest that σ_1 must have been orientated between 120° and 150° , and σ_3 must have been orientated between 030° and 060° , σ_2 being sub-vertical in orientation (Figure 5.16c, d). These data are consistent with an approximately southeast-northwest directed direction of compression.

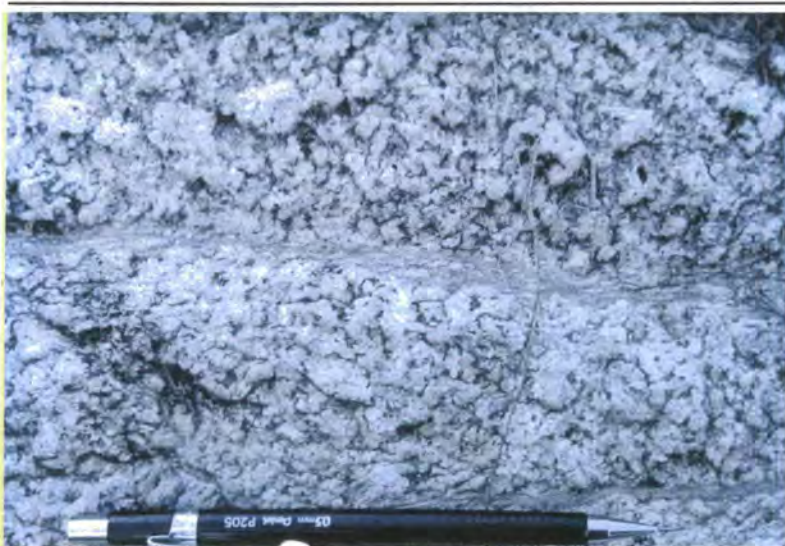
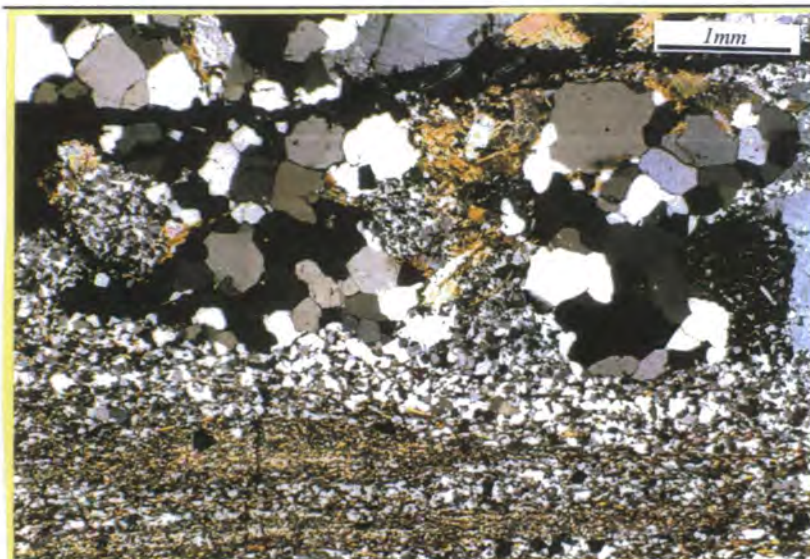


Plate 5.26 *Discrete mylonite from the Imbiricu pluton (GR 90684388)*



Photomicrograph of the sharp boundary zone of a mylonite to the surrounding deformed granite (GR 93134680)

Plate 5.27

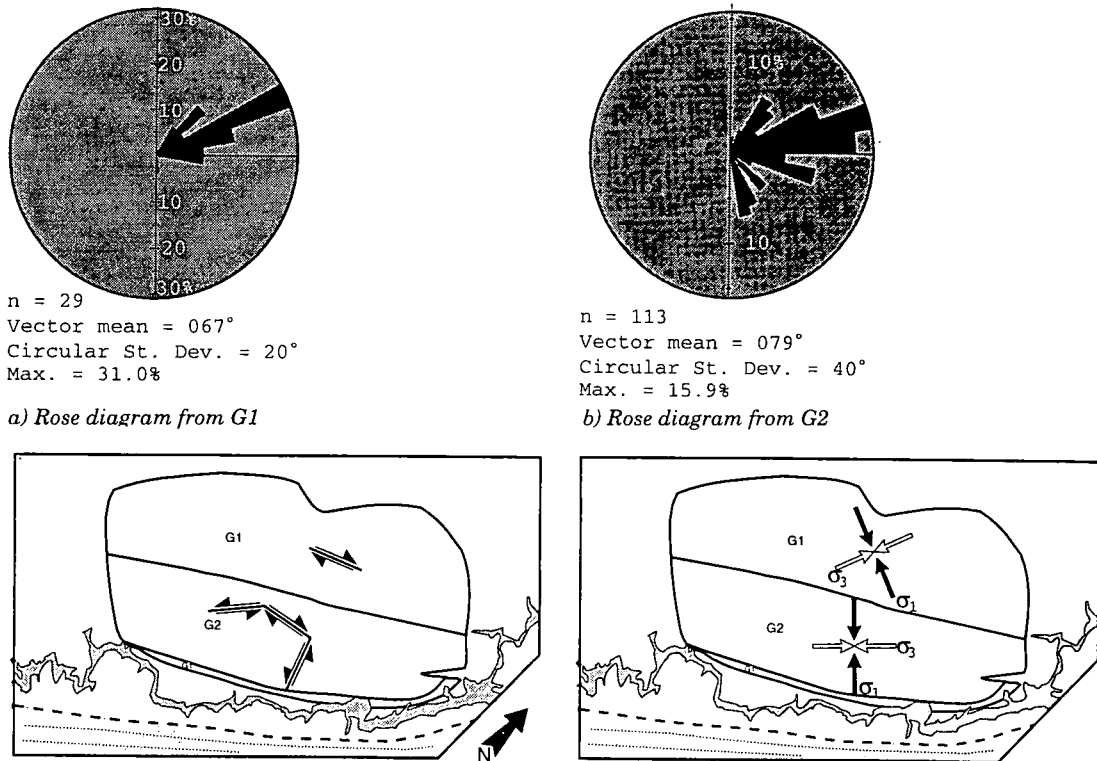


Figure 5.16 Analysis of discrete mylonites from the Imbiricu pluton

5.7.4 Conclusion and discussion

The Imbiricu pluton suffered a number of deformation events after the emplacement of the magma, the last of these was the discrete overprinting of this earlier fabric by the formation of cm-scale mylonitic shear. The results detailed above suggest:

1. That they were formed predominantly close to the Monteiro Lobato shear zone, in response to an east-southeast to southeast directed compression orthogonal to the shear zone itself.
2. In this pluton a single dominant orientation is observed within each of the analysed populations, whereas other orientations are strongly sub-ordinate to this. Twiss & Moores (1992, p.179) demonstrate that fractures will form most easily close to the orientation of the foliation, where the principal compressive stress has an angle of 20° to 50° to that foliation. Hence in such a situation a dominant set of fractures forms (as above), but fractures at high angles to the foliations (the sub-ordinate sets above) are less favourable.
3. The presence of mylonite populations orientated at a high angle and a low angle to the inferred principal stresses (Figure 5.16b, d) may suggest a variability in the magnitude of the sub-ordinate confining stresses during formation.

5.8 Mapping: the Morro Azul pluton

During this work the Morro Azul pluton and its surrounding country rock up to a distance of 4-5km from the pluton was re-mapped at a 1:25,000 scale. The results of this work can be seen in Figures 5.1 & 5.17, Map 4. Reference was also made to the regional map of Campos Neto *et al* (1983) which is redrawn in modified form and included as Map 8.

5.8.1 Country rock

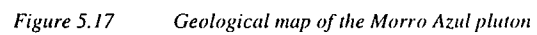
The country rock adjoining each side of the pluton belongs to a different regional domain. To the northwest, and along the northern contact of the pluton are the meta-volcano-sedimentary rocks of the Sao Roque group which were described in part 5.2.1. On the eastern side closest to the pluton there are exposures of strongly foliated schistose rocks, whose stratigraphical heritage is unclear. Further away from the granite are the strongly folded, sheared and sheeted rocks of the Santa Isabel gneisses considered regionally to be part of the Embu domain (Tassinari 1988).

Southeast of the pluton

The country rocks southeast of the Morro Azul pluton are relatively well exposed between the northwestern shoreline of the Jaguari reservoir and the contact of the pluton itself.

Santa Isabel gneisses

The Santa Isabel gneisses are an approximately 1.5km wide group of heterogeneous highly strained gneisses. They are steeply to vertically dipping and strike northeastwards, sub-parallel to the regional trend along the southeastern contact of the pluton and are composed of up to seven compositionally distinct phases (Plate 5.28). Two principal phases are dominant within the outcrops together making up more than 75% of the exposure. These are medium to finely crystalline, containing mm-scale plagioclase feldspar phenocrysts within a matrix of quartz and mica and a composition of granodiorite to tonalite. Each constituent phase within the outcrops is continuous orthogonal to strike for a maximum of only a few metres before it is replaced by different material. Sheets of particular composition types may occur at a number of points across the outcrop. The contacts between individual types are sharp and appear to be have been initially intrusive in nature but have later become reoriented during deformation. The age of these gneisses was measured by Tassinari (1988) who recorded an Rb-Sr whole rock age of 710 ± 30 Ma and a poorly defined Pb-Pb whole rock age of approximately 1300 Ma, which were interpreted to represent the metamorphic age and a possible age of re-working respectively.



The rocks preserve a well developed sub-vertical foliation and weak sub-horizontal lineation, which is sub-parallel to the internal sheet contacts. The latest phase within the complex are a set of complexly folded and deformed pegmatitic dykes, consisting of coarsely crystalline potassium feldspar, muscovite, biotite and quartz, which appear to be compositionally distinct from, and probably pre-date, the intrusion of the Morro Azul granitoids. A strain analysis of these features is detailed in part 5.10.3.



Plate 5.28 The vertical plane from the principal outcrop of the Santa Isabel gneisses (GR 80733359)

Outcrops closest to the pluton

Between the rocks of the Santa Isabel complex and the pluton itself a thin sliver of rock whose outcrops are consistent with them being part of the Sao Roque domain is preserved. These outcrops appear to be meta-volcano sedimentary schists and gneisses which strike sub-parallel to the pluton contact and have a dip which is partitioned into narrow zones showing moderate southeasterly dips, and more common zones displaying sub-vertical dips and, preserving a sub-horizontal mineral stretching lineation (Figure 5.18).

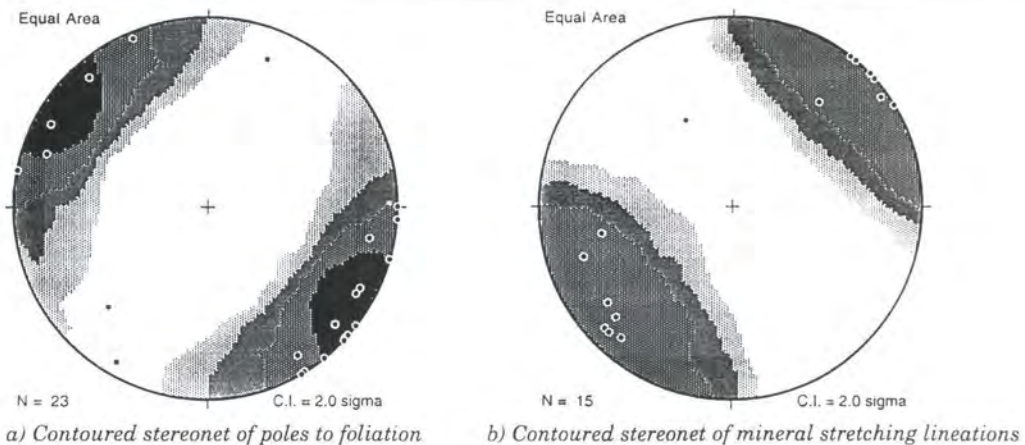


Figure 5.18 Country rock southeast of the Morro Azul pluton

Northwest of the pluton

To the northwest of the pluton the meta-volcano-sedimentary gneisses of the Sao Roque domain are easily identified. These rock generally show a moderate to low angle southeasterly dip and a down dip stretching lineation (Plate 5.29, Figure 5.19a, b). On approaching the pluton the country rocks show a different style of deformation depending upon their position along the contact:



Plate 5.29 Country rock northwest of the Morro Azul pluton (GR 74232980)

Northern end of the pluton

The northern end of the pluton corresponds to the area where G2 is present within G1. The country rock from this area has a southeasterly dip, which switches to a steep northwestwards dipping to upright foliation within 250m of the pluton. This suggests the existence of an upright antiform in this area (Figure 5.19), the attitude of which suggests its formation in response to the intrusion of the Morro Azul pluton.

Southern end of the pluton

Along the southern part of the pluton regionally developed moderate angle southeastwards dips are preserved throughout. Except within approximately 50m of the pluton, where the rocks dip sub-vertically.

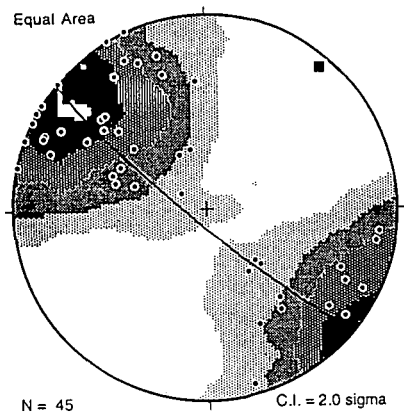
North of the pluton

There are almost no exposures of country rocks in the vicinity of the northern contact of the pluton. Those that are present appear to suggest the country rocks continue to dip sub-vertically, although the existence of a roof contact such as that present at the southern end of the Imbiricu pluton cannot be ruled out (Figure 5.5.).

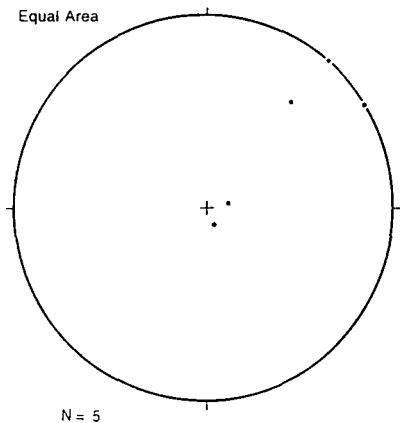
Conclusions

The rocks around the Morro Azul pluton display different characteristics depending upon their spatial relationship with the pluton. On the southwestern side of the pluton they display sub-vertical orientations and evidence of extensive ductile deformation before the intrusion of the pluton took place. On the northeastern side of the pluton however, the

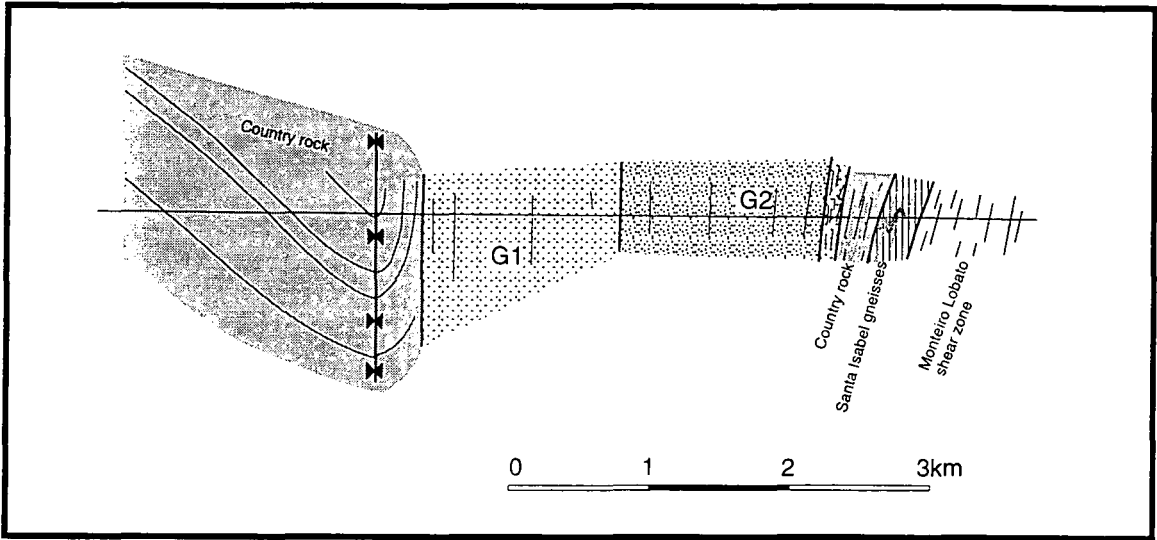
rocks show a moderate angle southeasterly dip, which is steepened such that it becomes sub-parallel with the pluton contact, producing an identifiable fold around the northern portion. The northernmost contact is very poorly exposed and does not show whether a roof contact similar to that preserved around the southwest contact of Imbiricu pluton is present or not.



a) Contoured stereonet of poles to foliation country rock northwest of the Morro Azul pluton, with a great circle which shows a fold axial plane trending sub-vertically at 040°



b) Stereonet of mineral stretching lineations country rock northwest of the Morro Azul pluton



c) A cross section through the Morro Azul pluton (GR 87003425 to GR 80803940)

Figure 5.19

5.8.2 Nature of the contact

The characteristics of the contact itself vary depending upon which side of the pluton is examined. In both areas the geomorphological position of the contact can be found by observing a change from undulating countryside to an area of steep hills and incised valleys. The outcrop features of the contact are described below:

Southeast of the pluton

As described above, the country rocks adjacent to the southeastern contact of the pluton are defined by packets of moderately dipping rocks delimited by zones with a much more intense sub-vertical foliation. In general the contact appears sharp and can be delimited to a distance of less than 20m. Where it can be examined in greatest detail (GR 82883405 to GR 83233500) it shows m-scale packages of sub-vertically foliated G1 surrounded by similarly foliated country rocks. These sheets of granite do not appear to show a greatly intensified foliation relative to nearby outcrops and thus it is suggested that they represent intrusive material fractured off from the granite during post-emplacement deformation (Plate 5.30).



Fractured portion of G1 granite incorporated into the country rocks southeast of the Morro Azul pluton (GR 82883405)

Plate 5.30

Nearby outcrops of granite show an intensification of their solid state foliation on approaching the contact itself: an observation which is consistent with extensive solid state deformation taking place along this contact post-emplacement.

Northwest of the pluton

The outer granite contact is relatively poorly exposed along this northwestern side of the pluton. Where it can be observed in detail (in particular around GR 77703185 and GR 82003810) the pluton shows a very sharp contact with the sub-vertically dipping surrounding rocks (country rock and granite outcrops less than 2m apart). There appears to be no associated granitoid intrusive sheeting and no thermal metamorphism. Within the

pluton itself the solid state fabric is intensified within 10m of the pluton. This is most noticeable around the northern end of the pluton because of the comparatively weak nature of the foliation in this area. In the southern part of the pluton the very intense solid state foliation appears to show no change intensity on approaching the outer contact.

Northeast of the pluton

The contact to the northeast of the pluton is not observed at any point. Its position has been inferred from a prominent break of slope and the geomorphological change that occurs in this area.

Southwestern end of the pluton

The southwestern end of the pluton shows a gradual thinning in the width of granite exposure. The continuation of slightly elevated topography suggests that it may be present, but not exposed further southwest of the last observed around GR 75002900. The country rock in this area maintains a northeast-southwest, sub-vertical orientation.

Conclusions

The Morro Azul pluton preserves a differing contact style depending upon position relative to the pluton. Along the northwestern and northern contacts of the pluton a very sharp intrusive contact can be observed with no extensive sheeting into the country rock, but with a deflection of the contact rocks into parallelism with the granite and a weak intensification of the solid state foliation. Along the southeastern contact the granite becomes heavily overprinted by a solid state foliation and the country rock shows intense, but partitioned, deformation. Within the country rock broken-off fragments of the granite are preserved demonstrating the post-emplacement nature of this event. It could be suggested that before the tectonism this southeastern contact would have preserved a sharp tectonic contact.

5.8.3 Granite

The Morro Azul pluton is a two-phase pluton consisting of: i) an outer G1, present as a thin sliver along the southeastern side of the pluton and most commonly in the southern and northwestern parts of the pluton; and ii) an inner G2, which is found between outcrops of G2 in the northeastern part of the pluton. Each of these and their contact relationships are described below:

The outer phase, G1

The outer phase of the pluton is well exposed and consists of a coarsely crystalline groundmass of potassium feldspar, plagioclase feldspar, biotite and quartz within which there are abundant rectangular potassium feldspar phenocrysts (Plate 5.31, 5.32) up to 5cm in length. Point counting of 24 thin sections to 500 points shows it to have a granitic composition (Figure 5.22a).

Examining Figure 5.17 shows that G1 is present both northwest, south and southeast of G2. While each of these areas shows a very similar petrographic composition and style of outcrop their deformation characteristics are very different (see part 5.9.2). In general terms, the foliation is everywhere sub-vertically dipping and strikes sub-parallel to the long axis of the pluton (Figure 5.20a, c). In all outcrops the phenocrysts and matrix show a strong alignment into this foliation, independent of whether the outcrops shows a magmatic or solid state fabric. Where the solid state deformation is well developed a sub-horizontal mineral stretching lineation is commonly preserved in the foliation plane (Figure 5.20b, d).



Plate 5.31 Morro Azul, G1 in outcrop (GR 79943384)

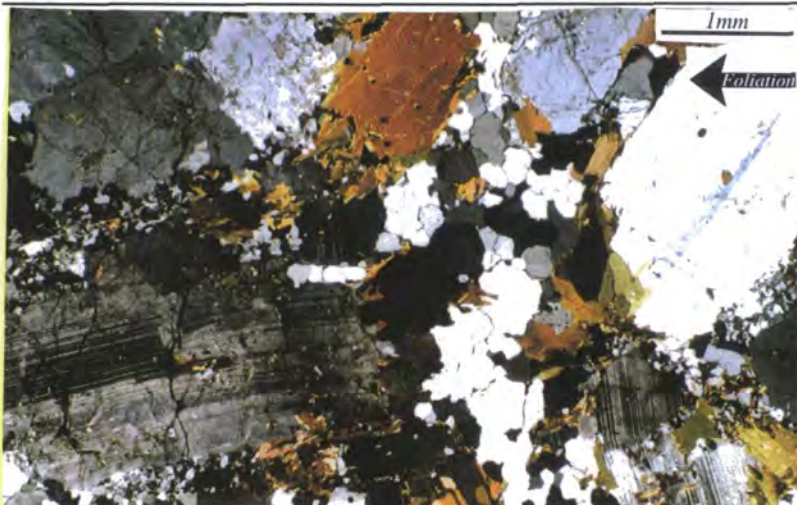


Plate 5.32 Photomicrograph of fabric preserved in G1, Morro Azul pluton (GR 82103675)

Northwestern G1

This area represents G1 outcrops north and west of outcrops of G2, in this area the foliation has its lowest intensity. The pluton is characterised by homogenous phenocryst

rich exposures, containing relatively abundant microgranitoid enclaves and very rare small country rocks screens. The foliation in this area is a weak solid state fabric, overprinting an earlier magmatic fabric.

Southeastern G1

This area consists of the thin sliver of G1 which outcrops southeast of G2. Outcrops in this area are distinguished by a very strong solid state fabric deforming the matrix and phenocrysts. Additionally this area preserves a number of heavily deformed country rock screens, which appear to have been incorporated into the outcrop during magmatic sheeting sub-parallel to the foliation.

Southern G1

This area comprises outcrops in the southern part of the pluton where no G2 can be distinguished. Exposures in this area preserve a strong solid state fabric, within which phenocrysts and the matrix have been extensively deformed and recrystallised. The intensity of this fabric is reduced as the distance from the southeastern pluton contact is increased. A number of microgranitoid enclaves can be distinguished in this area, but xenolithic fragments of country rock are rare.

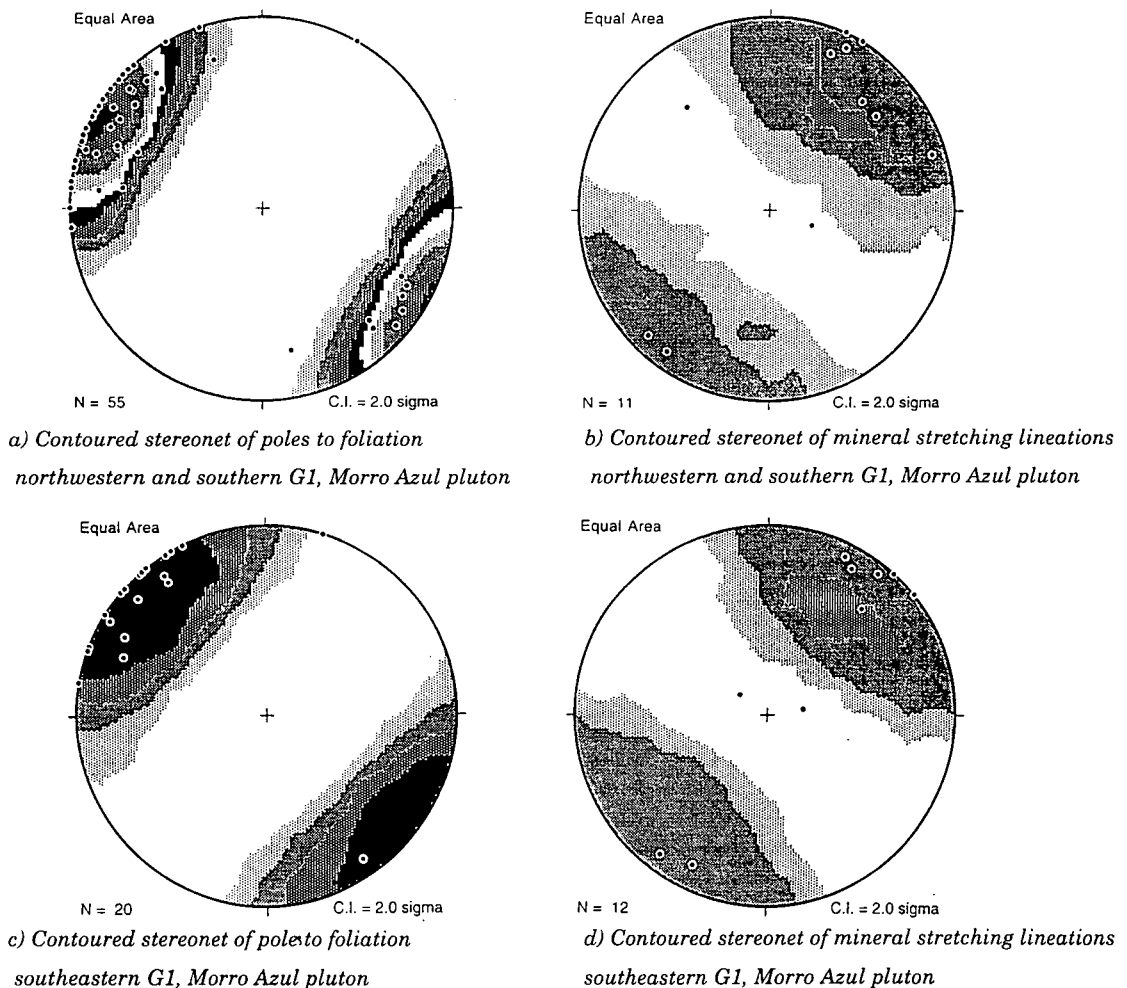


Figure 5.20

The inner phase, G2

In a remarkable similarity to G2 of the Imbiricu pluton outcropping to the northeast, G2 of the Morro Azul pluton shows a coarsely crystalline matrix of potassium feldspar, plagioclase feldspar, biotite and quartz, within which is preserved rare large potassium feldspar phenocrysts up to 5-6cm in size (Plate 5.33, 5.34). Point counting of 12 thin sections to 500 points, shows that this phase has an average granitic composition (Figure 5.22b).

The foliation preserved within G2 shows a sub-vertically dipping planar fabric which strikes sub-parallel to the long axis of the pluton itself and, where a strong solid state fabric is preserved, a sub-horizontal mineral stretching lineation can be seen (Figure 5.21a, b). All outcrops show the presence of a fabric independent of whether it was formed in the magmatic or solid state.

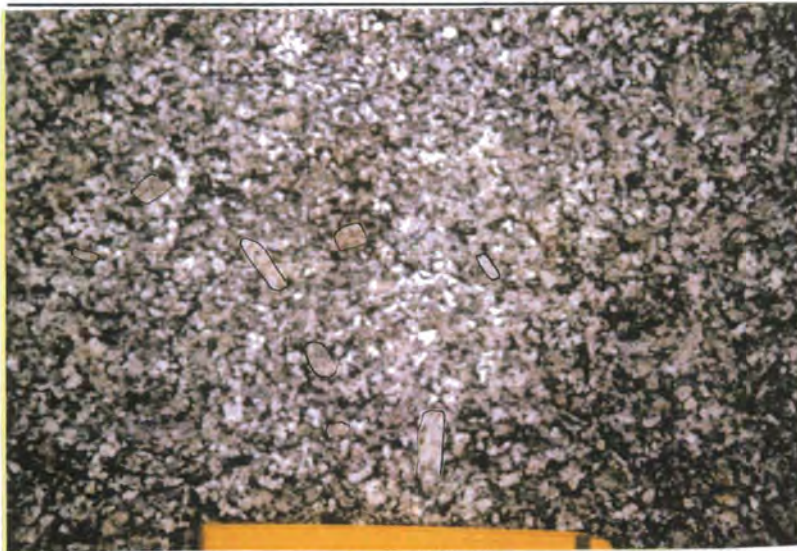


Plate 5.33 Outcrop photograph of G2, Morro Azul pluton (GR 83103583)

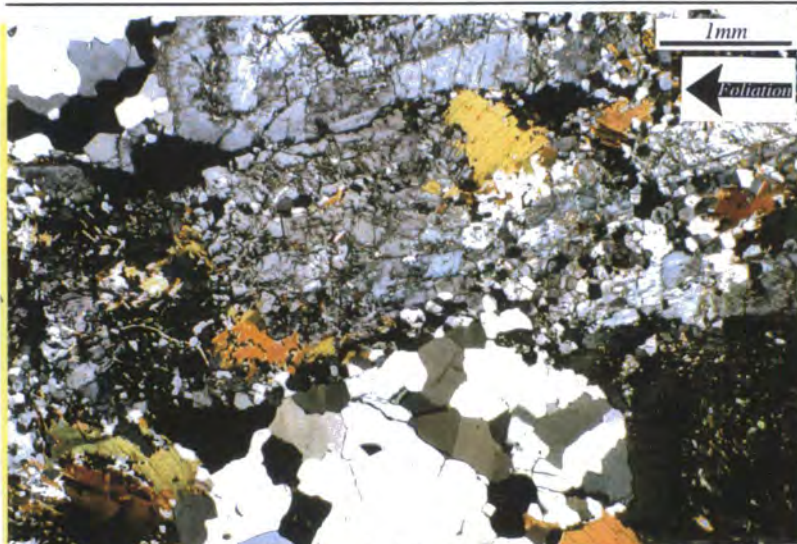
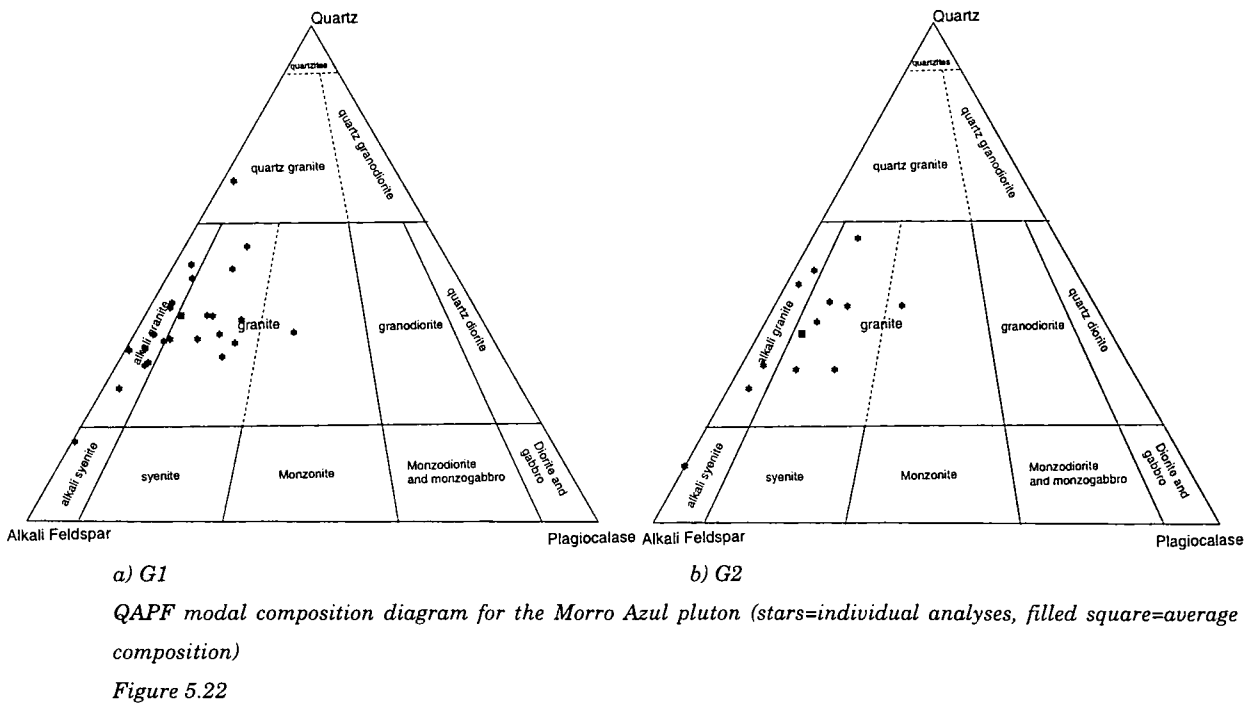
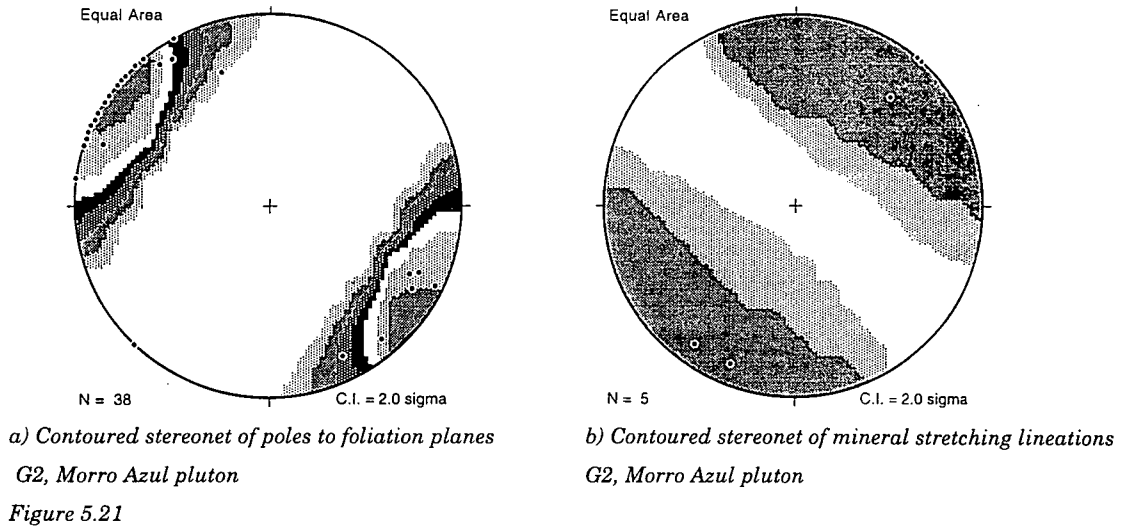


Plate 5.34 Photomicrograph of the fabric preserved within G2, Morro Azul pluton (GR 83603628)



The contact between G1 and G2

The contact between G1 and G2 in the Morro Azul pluton is well exposed on two hillside localities: One at the northwestern side of G2 (GR 83053790); and the second on the southeastern side of G2 (GR 84758780). Each of these is described below:

Northwestern G1-G2 contact

The northwestern contact between G1 and G2 coincides with a prominent valley which trends at approximately 035° from the quarry at GR 81033565 as far as GR 83453915. Outcrops on the western side of this valley show conspicuous development of large potassium feldspar phenocrysts, whereas on the eastern side the outcrops show an

absence of such phenocrysts, which are preserved only rarely. The outcrops around GR 83053790 show a section through the contact (reproduced in schematic form in Figure 5.23). On travelling eastwards from G1 to G2 the outcrops show:

1. The presence of pervasive 5-6cm long rectangular feldspar phenocrysts orientated along the foliation direction, overprinted by a relatively intense solid state shear fabric (Plate 5.35).
2. Traversing 50m eastwards from these outcrops bands of phenocryst-rich material (G1) are observed, divided by cm-scale bands of phenocryst-poor material (G2) (Plate 5.36). Each of these bands, while showing sharp linear boundaries between each other, show slight asperities and possible material transfer along and across the contacts. This feature suggests that neither phase was entirely solid during their formation and is interpreted to represent the contacts between screens of pre-existing G1 sheeted into by G2 before either was entirely cohesive enough to prevent material transfer across the contacts.
3. A continuing traverse westwards shows that over the next hundred metres sheets of G1 become less common, and G2 becomes the dominant phase, G1 remains present as small deformed ellipsoidal rafts of phenocryst rich material (Plate 5.37). This feature conclusively demonstrates that G2 intruded G1. The boundaries of individual sheets of G2 material can no longer be distinguished in outcrop and the material is apparently homogenous in appearance.
4. At GR 83253800 G2 is now homogenous (Plate 5.39) and no rafts of xenocrystic remnants of G1 can be found. Also note that the contact drawn on maps is of the first appearance of G2, although selvages of G1 may be present up to 300m perpendicular to strike from this point.
5. Additionally the G1/G2 contact in this area preserves a more intense solid state fabric than elsewhere within the pluton. It is suggested that the petrographic contacts or unseen structural discontinuities at depth may have been responsible for focusing this deformation into this area.

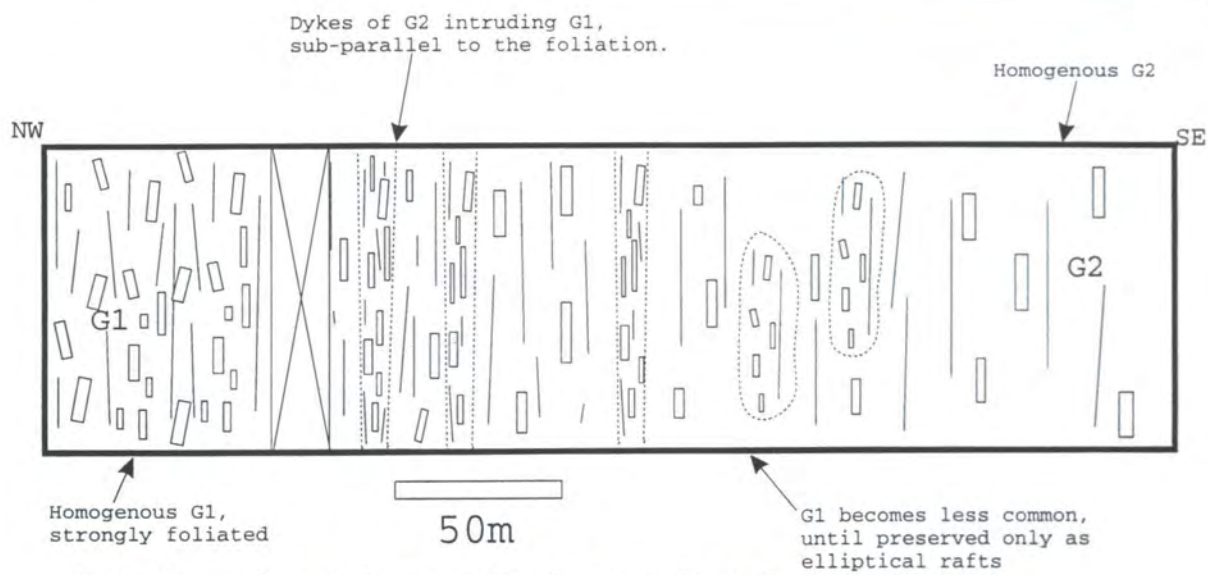


Figure 5.23 Summary log through the contact between G1 and G2 around GR 83053790



Plate 5.35 Homogenous G1 granite (GR 82633530)



Plate 5.36 Outcrop of G1 preserving sheets of intruded G2 (GR 82763674)



Plate 5.37 Rafts of G1 present within homogenous G2 (GR 82853700)



Plate 5.38 Homogenous G2 granite (GR 82633616)

Southeastern G1-G2 contact

This G1-G2 contact is rarely exposed, apparently sharp, and is best examined in a short section around GR 84758780. A schematic log through the contact is shown in Figure 5.24 and it is described in more detail below:

1. The contact section begins with outcrops of G1 material which preserve a strong solid state foliation. Intercalated between these outcrops are screens of strongly foliated, sub-vertically orientated country rocks, striking sub-parallel to the pluton foliation (Plate 5.39).
2. These country rock screens are present on various scales along strike approximately 20m before an homogenous outcrop of G1 is observed. This more homogenous outcrop shows an intense gneissose solid state fabric (Plate 5.40). Up to this point G2 is observed.

3. This intensely deformed outcrop continues for approximately 15m perpendicular to strike before a prominent band of basic biotite rich material about 2-10cm in width is encountered. To the southeast of this band the prominent feldspar phenocrysts _{1A} of G1 are common, whereas to the northwest of this band these phenocrysts are almost absent (Plate 5.41). This band of basic material defines the contact.
4. Traversing further northwestwards shows no additional outcrops or xenolithic fragments of G1 preserved within outcrops of G2. The solid state fabric maintains a similar intensity within these outcrops of G2 to that found within adjacent outcrops of G1.

These contact localities are interpreted to represent an area of country rock that was originally sheeted into by G1, before being split by the intrusion of G2 along a very sharp magmatic contact. In this area G2 did not sheet across the contact zone and G1 is not preserved as xenolithic fragments within G2

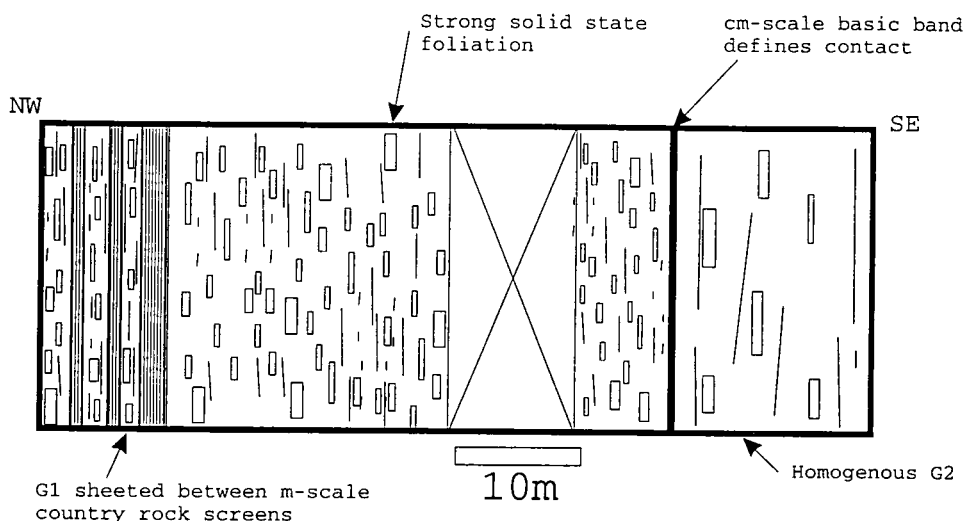


Figure 5.24 A summary log through the southeastern contact between G1 and G2 around GR 84758780



Plate 5.39 Country rock screens preserved within southeastern G1 (GR 84803675)



Intense gneissose fabric preserved within G1 close to its southeastern contact with G2 (GR 8403675)

Plate 5.40



Plate 5.41 *Band of basic material defining the southeastern G1-G2 contact (GR 84033675)*

Conclusions

The Morro Azul pluton consists of two intrusive phases which occur in a spatially and petrographically similar manner to those observed in the Imbiricu pluton a few kilometres to the northeast. G1 preserves megacrystic potassium feldspars within a coarsely crystalline matrix, whereas G2 preserves fewer, smaller potassium feldspars within a matrix petrographically similar to G1. In all localities a planar fabric, dipping sub-vertically and striking sub-parallel to the pluton long axis is preserved. This fabric had a similar orientation whether it was formed in the magmatic or solid state.

The contact localities show that G2 intruded G1 preserving a sharp southeastern contact, but sheeting into its northwestern contact and subsequently deflecting that part of G1 northwestwards. The northwestern contact is diffuse with the transition from G1 into G2 taking place over approximately 300m. Preserved magmatic crystal orientations show that the sheeting occurred sub-parallel to the pluton long axis and that neither phase was

entirely solid during the intrusion process. This type of intrusion is very similar to that seen within the internal contacts of the Main Donegal Granite (Price 1997). Both contacts preserve a strong solid state overprint of the earlier magmatic fabric, which when comparing the qualitative strength of this fabric to elsewhere within the pluton, appears to have been intensified in the contact areas.

5.8.4 Microgranitoid stocks, dykes, enclaves and country rocks xenoliths

Microgranitoid stocks

Unlike other plutons studied within the RPSSB neither the Morro Azul pluton, nor the country rock surrounding the pluton shows the preservation of microgranitoid stocks. Although the preservation of the older Santa Isabel gneisses, the Buquira and Santa Luzia low-angle sheeted complexes to the southeast of the pluton demonstrate that this area has been a focus for intruding magma of a long period of time.

Microgranitoid dykes

The Morro Azul pluton preserves a number of microgranitoid dykes which preserve similar characteristics to those seen in other plutons in this area (Chapters 4, 6), although within the quarry at GR 81003428 some coarser pegmatitic dykes have been recorded. These dykes have been kinematically analysed in part 5.12.

Microgranitoid enclaves

Microgranitoid enclaves are relatively common throughout the Morro Azul pluton, although in similarity with the Imbiricu pluton there are few enclaves preserved within outcrops of G2. The majority of enclaves appear to consist of ellipsoidal inclusions of microgranitoid rather than basic composition, which are elongated and orientated within the principal outcrop planes. These enclaves conform to the criteria laid down in part 1.5.1 for their use as finite strain markers within the intruding granite magma.

Although there are additional enclaves of a more basic composition which can be best observed in the quarry at GR 81003428. These enclaves occur in swarms, show poor alignment within the foliation plane and are often blocky, appearing to spall from larger dykes, and are only weakly ellipsoidal in shape (Plate 5.42). These enclaves are not used in strain analyses.

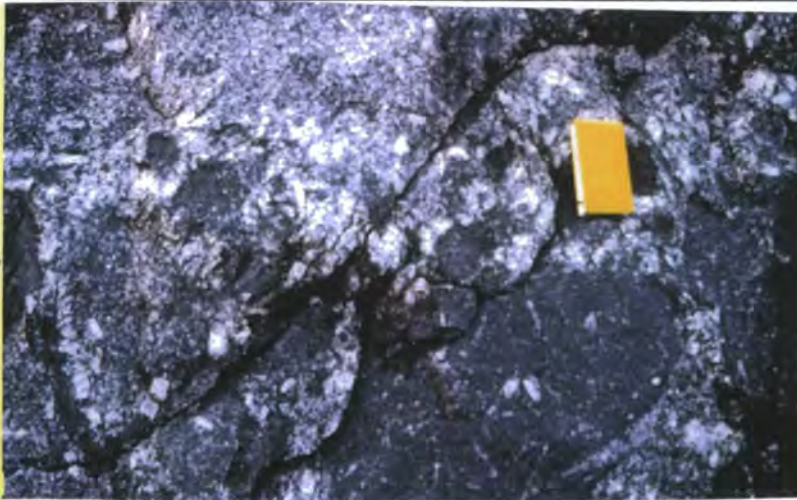


Plate 5.42 Microgranitoid enclaves present in the quarry at GR 81003428

Country rock xenoliths

Country rock xenoliths present within the Morro Azul occur as two separate populations within G1. G2 preserves almost no xenolithic material of any sort. The two populations are:

- 1. Xenolithic country rock screens** - These features are best exposed in the southeastern part of G1 (Plate 5.39), although large incorporated blocks can be seen within the quarry at GR 81003428. In general they are a few metres wide by up to 10 metres long, orientated sub-parallel to the pluton foliation and strongly deformed both internally and along their external margins. They have been used in part 5.11.4 to infer shear senses prevailing during and post-emplacement.
- 2. Deformed xenoliths** - In addition to these large blocks are cm-scale fragments of country rock, which may or may not be parallel to the pluton foliation, preserving an internal stratification which has been folded and deformed during and after emplacement of the pluton (Plate 5.43). The orientations of these internal fabrics have been used to infer shear senses during emplacement.



Country rock xenolith orientated and deformed perpendicular to the pluton foliation (GR 82103549)

Plate 5.43

Conclusions

Within the Morro Azul pluton various populations of xenolithic material are present within the pluton. In particular there is a large population of ellipsoidal microgranitoid enclaves which can be used for finite strain analysis. There are also a number of incorporated country rock xenoliths and screens which show internal deformation and simple shear fabrics sub-parallel to the pluton foliation. Many of the characteristics of enclaves from this area are similar to those observed in enclaves from the Imbiricu pluton.

5.8.5 Conclusion and discussion

The Morro Azul pluton contains two separate intrusive phases. The first a potassium feldspar phenocryst rich granite and the second which was sheeted into the northern part of the pluton an almost aphyric granite. The contact shown on either side of the pluton with the country rock is sharp, although the preservation of country rock screens within the granite on the southeastern side reflects the importance of sheeting as a method of intrusion. Everywhere within the pluton there is a sub-vertically dipping foliation which strikes sub-parallel to the pluton long axis, independent of whether the fabric was formed in the solid or magmatic state.

The country rock around the pluton was deformed by the intrusion of the pluton, preserving slivers of granite along the southeastern side, associated with deformation along the contact post-emplacement. Along the northwestern contact it has been deflected and folded becoming sub-parallel to the contact. Within the pluton small xenoliths of country rock are preserved, as are microgranitoid enclaves and small microgranitoid dykes.

While the intrusion of the Morro Azul pluton shows a number of tectonic similarities to the Imbiricu pluton there are some important differences, in particular: i) the Morro Azul pluton is more basic than the Imbiricu pluton; ii) a fabric is present everywhere within the pluton and phenocrysts are always aligned along the foliation direction; iii) the body obviously folds and deforms its northwestern contact rather than sheeting into it; and iv) the principal (northwestern) contact between the intrusive phases is very obviously sheeted rather than sharp. This suggests that the two plutons were emplaced in a similar tectonic environment, had only very slightly different magma sources, but induced deformation within the magma and in the surrounding rocks in different ways.

5.9 Deformation: the Morro Azul pluton

In the following section the deformation fabrics preserved within and around the pluton are correlated with the regional deformation sequence set up in part 3.3.4.

5.9.1 Country rock

As with other plutons examined from the RPSSB the deformation preserved on either side of the pluton varies dramatically.

Southeast of the pluton

Adjacent to the contact

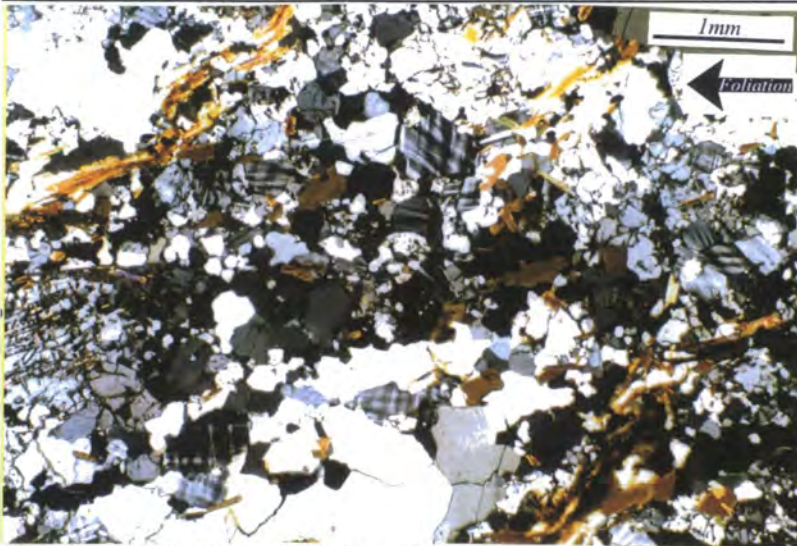
Examination of the fabric from this area (Plate 5.44) shows a schistose fabric within which quartz and mica have been recrystallised to produce a finely divided LS-type fabric. Occasionally this fabric develops pervasive crenulating S-C shear fabrics (see part 5.11.2). In thin section (Plate 5.45) this fabric shows a pervasively recrystallised fabric of quartz, microcline and biotite, which suggests deformation temperatures in excess of 400°C (Passchier & Trouw 1996).

These fabrics are interpreted as representing an narrow D_{n+2} shear zone, which formed before the intrusion of the granite. After the intrusion of the granite this shear zone was reactivated breaking off and incorporating sheets of the outer granite as a D_{n+4} structures, developing an L_{n+4} lineation.



Plate 5.44

Close-up of $D_{n+2/4}$ fabric at the southeastern contact of the Morro Azul pluton (GR 82883548)



Photomicrograph of $D_{n+2/4}$ fabric from the southeastern contact of the Morro Azul pluton (GR 77952943)

Plate 5.45

The Santa Isabel gneisses

The Santa Isabel gneisses preserve a sub-vertical, metamorphic compositional (ductile) fabric (Plate 5.46). The fabric itself preserves no shear sense indicators and only rarely preserves a lower grade solid state mineral stretching lineation. This suggests that these outcrops were subject to a ductile flattening event of greater intensity, and at higher metamorphic grade, than any other outcrop studied in this area. As a consequence these fabrics are interpreted to represent a S_{n+2} , which pre-dates the intrusion of the granite plutons, since the plutons preserve no evidence of such a strong flattening, which as fluid bodies they might be expected to localise. This fabric was only weakly overprinted during later regionally lower grade, D_{n+4} deformation. Thus they demonstrate unequivocally the development of local high strains in the RPSSB (pre-dating the granites).



Plate 5.46

Close-up of the ductile fabric preserved within the Santa Isabel gneisses (GR 81563308)

Northwest of the pluton

The country rock to the northwest of the Morro Azul pluton is defined by southeasterly dipping country rocks which are deflected to become sub-parallel to the pluton contact (Plate 5.47). These rocks do not develop a L_{n+4} sub-horizontal lineation, but often develop an L_{n+1} down-dip lineation (Figure 5.19b). Thus these country rocks are interpreted as preserving a D_{n+1} fabric, which has been deflected during intrusion into a sub-vertical D_{n+3} fabric close to the pluton. Neither D_{n+2} nor D_{n+4} extensively affected the deformation of this region.



Plate 5.47 *Sub-vertical country rock fabric northwest of the Morro Azul pluton (GR 80983224)*

Conclusions

In conclusion the deformation of the country rocks from this area describe a southeastern contact which has been extensively deformed during D_{n+2} deformation and later reactivated during D_{n+4} . The rocks to the northwest of the pluton on the other hand, preserve few fabrics related to $D_{n+2/4}$ and appear to preserve only local D_{n+3} deflection, associated with the intrusion of the pluton itself.

5.9.2 Granite

The outer phase, G1

In general G1 preserves a strong, sub-vertical fabric which is orientated sub-parallel to the pluton long axis. Within this simple scheme there are three separate areas:

Northwestern area

The northwestern part of G1 preserves the qualitatively weakest fabric of anywhere within the pluton. In general the matrix preserves a magmatic (D_{n+3}) to weak solid state (D_{n+4}) fabric within which the potassium feldspar phenocrysts show varying degrees of alignment (Plate 5.48, 5.49). The sub-horizontal mineral stretching lineation is not common in this area. Although when the outcrop foliation plane can be examined a number of

variably plunging magmatic lineations can be made out, suggesting some degree of bulk magma deformation during emplacement (Plate 5.50, Figure 5.25).

In thin section the strength of the deformation preserved varies enormously. Some outcrops develop an intense D_{n+4} solid state deformation showing extensive recrystallisation of quartz and feldspar (Plate 5.51). Whereas other sections show a much lower intensity of solid state deformation and appear to preserve some original magmatic crystal orientations in addition to weak solid state D_{n+4} fabrics (Plate 5.52).

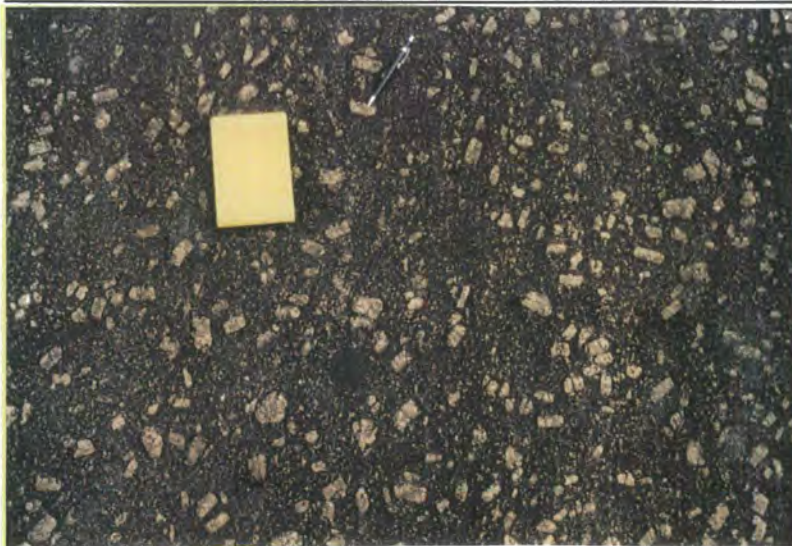


Plate 5.48 *Northwestern area G1, poorly aligned feldspar phenocrysts (GR 84734059)*

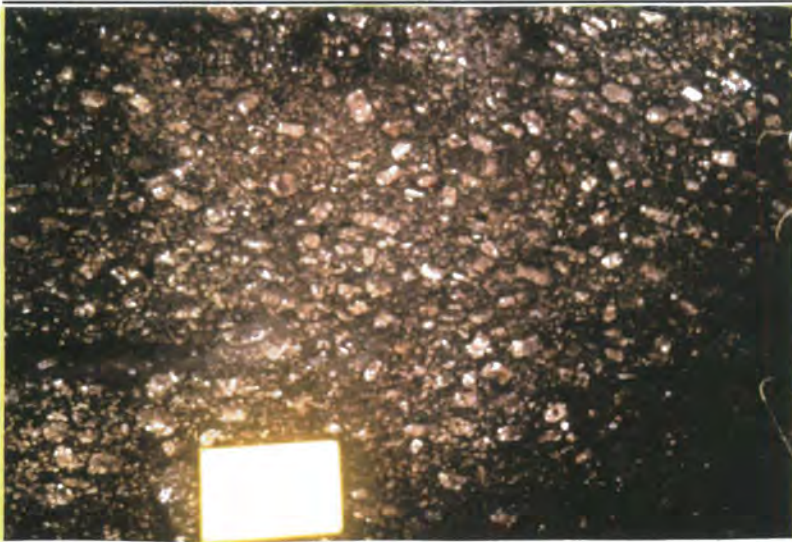
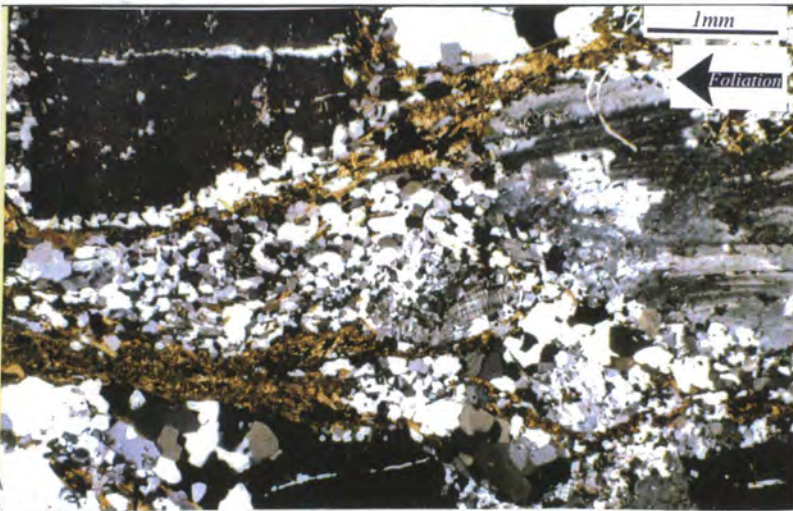


Plate 5.49 *Northwestern area G1, aligned feldspar phenocrysts (GR 82103675)*

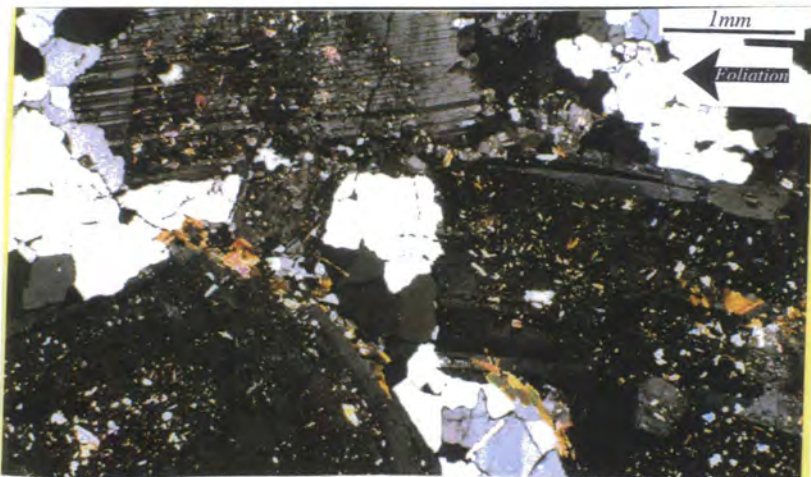


Plate 5.50 Northwestern area G1, magmatic state feldspar lineation (GR 82333661)



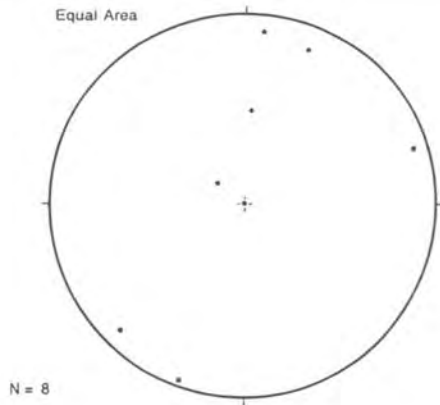
Photomicrograph of strong solid state deformation fabrics from the northwestern area, G1, Morro Azul pluton (GR 80683353)

Plate 5.51



Photomicrograph of weakest solid state deformation fabrics from the northwestern area, G1, Morro Azul pluton (GR 84734059)

Plate 5.52



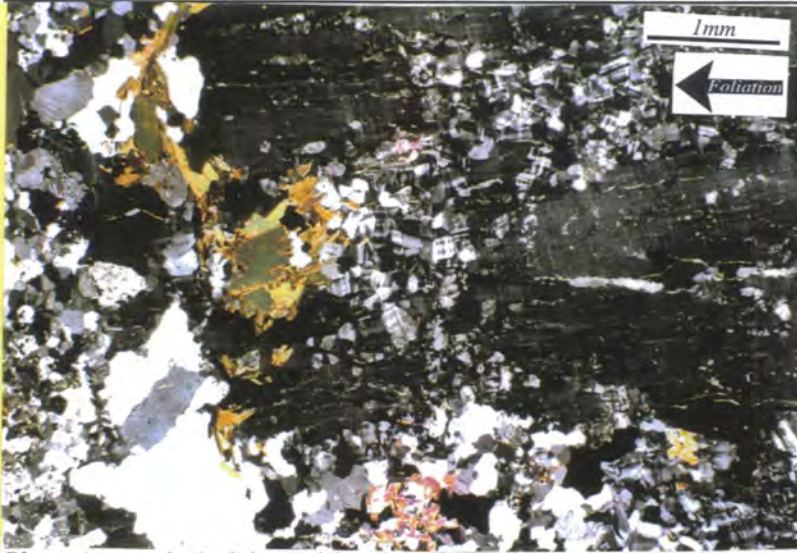
Stereonet showing recorded magmatic state lineations from the Northwestern area, G1, Morro Azul pluton
Figure 5.25

Southeastern area

This area is the part of the granite closest to the southeastern contact, the intensely sheared country rock and the Monteiro Lobato shear zone. In outcrop the granite has a strong gneissic texture (Plate 5.53) with rotated, abraded porphyroclasts around which quartz has been deformed into recrystallised ribbons forming S-C and σ - or δ -type shear sense fabrics, resulting in an LS-type fabric with a sub-horizontally orientated lineation (D_{n+4}). In thin section (Plate 5.54), the fabric can be seen to consist of resistant fractured feldspar phenocrysts, whose fractures have filled with recrystallised quartz. Around these phenocrysts are zones of more intense deformation where grain size has been greatly reduced. Biotite is extensively elongated, but not obviously recrystallised.



Plate 5.53 Southeastern area G1, showing intense solid state fabric (GR 82983453)



Photomicrograph of solid state fabric from the Southeastern area, G1, Morro Azul pluton (GR 84803685)

Plate 5.54

Southern area

The southern area preserves many fabrics similar to those described for the southeastern area. For example close to the southeastern contact it displays an intense (D_{n+4}) gneissic fabric preserving ribbon quartz and deformed phenocrysts, within an LS-type fabric (Plate 5.55, 5.56). Further away from the southeastern pluton contact the deformation reduces in its intensity. Outcrops in this area preserve a solid state fabric (D_{n+4}) (Plate 5.57), but individual phenocrysts have close to their original shape and quartz has not been deformed and recrystallised into ribbons.



Horizontal plane solid state fabric from the southern area, G1, Morro Azul pluton (GR 74582904)

Plate 5.55



Plate 5.56 Vertical plane solid state fabric from the southern area, G1, Morro Azul pluton (GR 74582904)



Plate 5.57 Weak solid state fabric from the southern area, G1, Morro Azul pluton (GR 77233015)

The inner phase, G2

Examination of the G2 fabric in detail shows a wide variation in the intensity of this fabric. In most localities some selvage of the magmatic fabric is preserved (Plate 5.58), where occasionally magmatic fabric can be distinguished within a fabric defined by weak alignment of quartz and biotite crystals. Examination of these localities in thin section, shows feldspar crystals which are generally in magmatic orientation preserving an original internal fabric, and no recrystallisation around their margins (Plate 5.61). Biotite is similarly undeformed, but within the matrix it can be seen that quartz has been recrystallised, but does not display any particular elongated and recrystallised fabrics.

In other localities a pervasive solid state fabric can be found. This is particularly true of areas close to the G1-G2 contact, where an elongation and ribboning of quartz defines a matrix within which the large feldspar phenocrysts are partially aligned (Plate

5.60). Additionally there are rare localities where the solid state fabric becomes locally intensified producing strong solid state fabrics defined by ribbon quartz and deformed and abraded feldspar phenocrysts. Examining thin sections of this fabric shows variable grades of quartz recrystallisation, crystal fracturing, and core and mantle fabrics around feldspar phenocrysts.



Plate 5.58 Magmatic fabric from G2, Morro Azul pluton (GR 85033863)

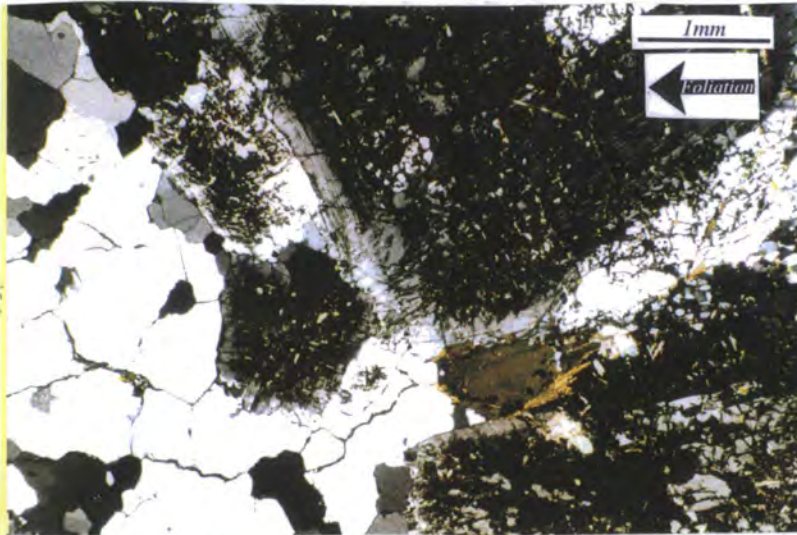


Plate 5.59 Photomicrograph of preserved magmatic fabric from G2, Morro Azul pluton (GR 84133948)



Plate 5.60 Pervasive solid state fabric from G2, Morro Azul pluton (GR 83953650)

Each of these areas of the pluton shows cm-scale discrete mylonites which cross-cut the fabric and post-date the solid state foliation. These mylonites are preserved relatively homogeneously across the pluton.

Conclusions

Deformation within the granite has taken place in two stages the first produced a magmatic fabric which was orientated sub-vertically, sub-parallel to the long axis of the pluton with associated lineations and shear sense fabrics representing flow material transport during intrusion. This D_{n+3} fabric has been overprinted by a heterogeneous solid state (D_{n+4}) fabric which produced variable intensity deformation during the formation of an LS-type fabric at an inferred temperature of 400-500°C. This solid state deformation becomes most intense on approaching the southeastern contact of the pluton and at the contacts the plutonic phases.

5.9.3 Conclusion and discussion

A few general conclusions are worthy of additional discussion:

1. **Contact shear zone** - The intensification of the country rock fabric and the gradational increase in the strength of the solid state deformation along the plutons southeastern contact suggests that there is a shear zone in this area, 300-400m wide delimiting the boundary between the pluton and the Santa Isabel gneisses. This shear zone was present before the intrusion of the plutons, deforming the Santa Isabel gneisses and it is suggested that it was intimately associated with their intrusion dynamics. Although it cannot be distinguished as a separate entity further north around the Imbiricu pluton, which might suggest that it becomes incorporated into the larger Monteiro Lobato shear zone in this area.

2. **Emplacement deformation** - The pluton was emplaced forming a magmatic fabric sub-parallel to the plutons long axis. This wallrocks preserve an intrusion related fabric which extends for up to 300m from the pluton.
3. **Comparison to Imbiricu pluton** - The nature of the overprinting deformation seen in the Morro Azul pluton is very similar to that seen in the Imbiricu pluton exposed a few kilometres further north. Although the magmatic state fabric, within the Morro Azul pluton, is qualitatively much more intense.

5.10 Strain measurement: the Morro Azul pluton

5.10.1 Introduction

In the following sections strain markers from the country rock and the intrusive phases have been used in an attempt to quantify the strain induced within the country rocks before, during and after the emplacement of the Morro Azul pluton. The first two sections use the measurements of mafic enclave axial ratios and the distribution of crystal phases to quantify the finite strain preserved within the pluton itself. The remaining sections use various techniques to quantify finite strain within the country rock.

5.10.2 Microgranitoid enclaves

Methodology

The types of mafic enclaves present within this pluton were described in part 5.8.4, in the following analysis the ellipsoidal enclaves are used to determine the finite strain preserved within the pluton using the methods outlined in part 1.5.1. Small but spatially related outcrops are combined together to produce a statistically robust sample. The results of these analyses are given in Table 5.3, Figure 5.26a, b, c and Appendix 9.

Results

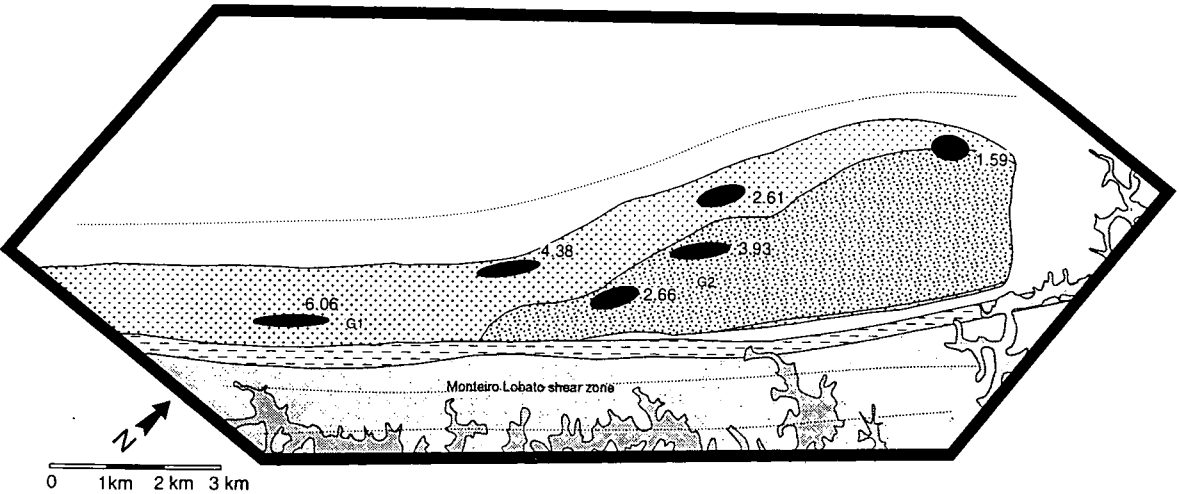
The principal results are:

1. **Data distribution** - As a consequence of the preserved distribution of mafic enclaves, far more determinations could be made of the finite strain preserved within G1 than preserved within G2. Although, there is much less exposure of the vertical or foliation plane of outcrop which makes statistically robust determinations in this orientation rare.
2. **Flattening strain** - Where obtained, K-values are generally from the flattening field ($K < 0$), but appear to show a small plane strain component i.e. $K \rightarrow 1$ with the principal finite strain axis orientated sub-vertically. This is interpreted to represent a component of vertical stretching/extrusion associated with emplacement.
3. **Strain gradients** - Enclave axial ratios in the horizontal outcrop plane axial ratios show a variation. At the northernmost corner of the pluton the lowest horizontal plane axial ratios are recorded ($R_s \sim 1.56$), but on travelling southwestwards along the body of the pluton this value is seen to increase reaching value of $R_s \sim 6$, at the southernmost extremity of the pluton. These values demonstrate that the pluton becomes increasingly deformed as its width diminishes, which can be corroborated by the increasing fabric strength in these southernmost outcrops. Whereas small populations from the vertical plane appear show that in this orientation there was a degree of strain homogeneity.
4. **G2 strain** - The distribution of the data shows that G2 preserves lower enclave axial ratios, and hence a lower finite strain ($R_s < 3$ cf. $R_s > 3.5$), than similarly positioned G1 localities. This may be a consequence of the increased deformation and strain induced into G1 during the intrusion of G2.

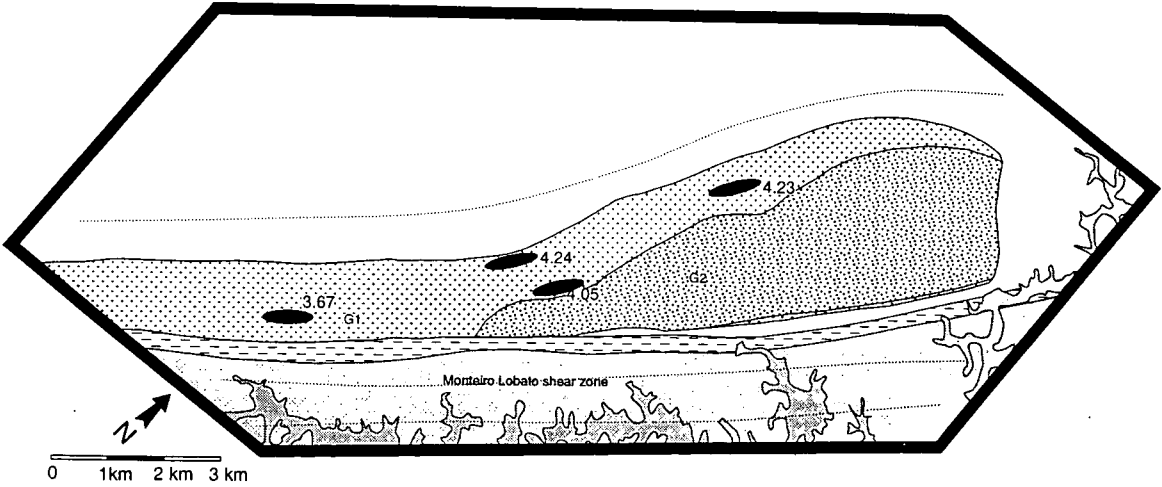
5. Shortening and extension - During emplacement the Morro Azul pluton was subject to a possible along axis extension of between -15% and +215% and axis perpendicular shortening of between 45% and 65%, during vertical extension of between 124% and 30%.

Conclusions

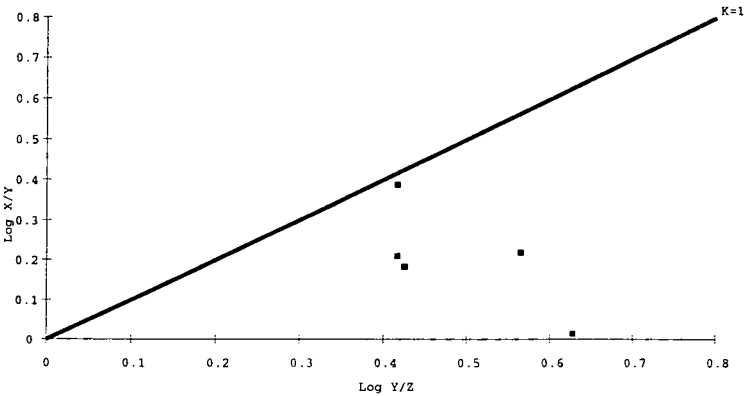
The Morro Azul pluton preserves a more comprehensive dataset of microgranitoid enclaves than any other studied pluton from the RPSSB. Interpreting these data as representing finite strain values demonstrates that the pluton was subject to a flattening strain, whose X-axis was generally vertically orientated, the Y-axis was horizontally orientated parallel to the foliation plane and the Z-axis was orthogonal to each of these and the foliation plane. The finite strain in the vertical plane was relatively homogenous ($R_s \sim 4$), whereas in the horizontal plane it becomes increasingly intensified on travelling southwestwards along the pluton axis. This is interpreted to be a consequence of low magmatic state strain at the northeastern end, and an increasing magmatic state and solid state strain on moving along the pluton axis. The increasing axial ratio in the southern area demonstrates the very intense and homogenous nature of the solid state fabric in this area. In the remainder of the pluton however the magmatic state emplacement related strain is the most dominant.



a) Average mafic enclave axial ratios from the horizontal outcrop plane of the Morro Azul pluton



b) Average mafic enclave axial ratios from the vertical outcrop plane of the Morro Azul pluton



c) A Flinn-type plot for the mafic enclave data from the Morro Azul pluton

Figure 5.26

Table 5.3 Results of mafic enclave axial ratio finite strain analyses from the Morro Azul pluton.

Localities	Orientations	Grid References	Mean axial ratio	Number of analysed enclaves	St. Dev.	Smallest axial ratio	Largest axial ratio	ω Log	Log K-value	% Variation in size
CR10, CR11	Horizontal	GR 81953525, GR 80703773	3.214	25	1.23	1.29	6.19	0.68		38
CK1, CK4	Horizontal	GR 80093393, GR 79943384	4.38	32	2.49	1.07	15	1.15		57
CK1, CK4	Vertical	GR 80093393, GR 79943384	4.24	28	2.22	1.14	12.86	1.05	0.023	52
CN	Horizontal	GR 81003428	2.66	32	3.29	1.1	17.14	1.18		123
CN	Vertical	GR 81003428	4.05	21	2.36	2.10	12.57	0.77	0.43	58
CO5, CO6	Horizontal	GR 82083523, GR 82163543	3.93	38	1.58	1.86	8.21	0.64		40
CP9	Horizontal	GR 84734059	1.59	29	0.52	1.05	2.85	0.44		33
CQ1, CQ2, CQ8, CR1	Horizontal	GR 75482904, GR 75732985, GR 77903170, GR 77233015	6.06	11	1.86	1.14	6.63	0.77		31
CQ1, CQ2, CQ8, CR1	Vertical	GR 75482904, GR 75732985, GR 77903170, GR 77233015	3.67	6	0.80	2.79	5.00	0.25	0.38	22
CS7, CS8, CS10	Horizontal	GR 8210675, GR 82383661, GR 81953703	2.61	33	0.76	1.51	4.82	0.50		29
CS7, CS8, CS10	Foliation, enclave long axes sub-vertical	GR 82103675, GR 82383661, GR 81953703	2.44	4	1.04	1.79	4.08	0.36	0.93	29
CS7, CS8, CS10	Vertical	GR 82103675, GR 82383661, GR 81953703	4.23	12	3.23	1.96	11.87	0.39	0.50	76

5.10.3 Fry strain

Methodology

During this study 28 determinations of the Fry fabric strain were made from various localities across the pluton. These have been processed using the methods outlined in part 1.5.2 and collated with data from neighbouring localities to produce a consistent and robust value for the Fry strain. The results of these analyses are given in Table 5.4, Figure 5.27a, b, c and Appendix 10.

Results

Despite their small number these data produce very consistent values for the Fry fabric strain preserved in localities across the Morro Azul pluton. A number of general points are worthy of remark, in particular:

- 1. Flattening strain** - As observed during measurement of preserved finite strain using microgranitoid enclaves the Fry fabric strain data show a broadly flattening strain ($K < 1$) whose principle preserved X-strain axis was sub-vertical, with the Y-axis sub-horizontal and similarly contained in the plane of foliation.
- 2. Lower values** - As with all other measurements of Fry strain from plutons examined in this study the Fry strain shows a lower ellipticity than that recorded by microgranitoid enclaves. Although in this case the Morro Azul pluton records higher Fry Strains than

the Imbiricu pluton and Itapeti pluton, but lower values than those preserved and recorded within the Atibaia pluton.

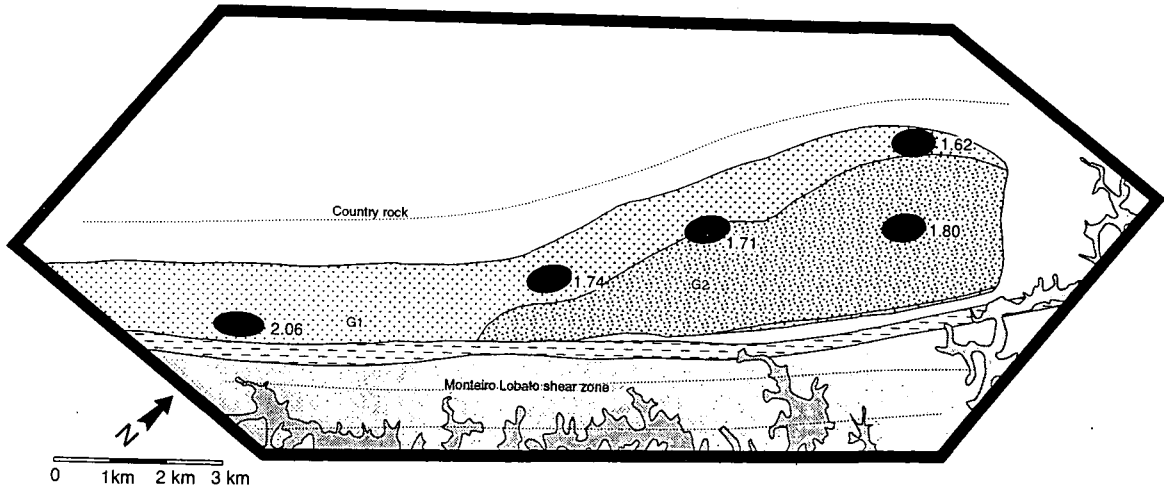
3. **Spatial variation** - There appears to be little variation in the magnitude of Fry strains recorded across the pluton, although at the southwestern end an increase in the magnitude of the horizontal plane reading can be identified. This result reflects the homogeneity of preserved finite strain within this pluton. Identical results have been recorded in other plutons from the RPSSB.
4. **Shortening and extension** - If these Fry strains accurately reflect the preserved finite strain within the Morro Azul pluton then the pluton was subject to an average along axis extension of approximately 13%, a vertical extension of approximately 28% and axis perpendicular shortening of approximately 30%.

Conclusions

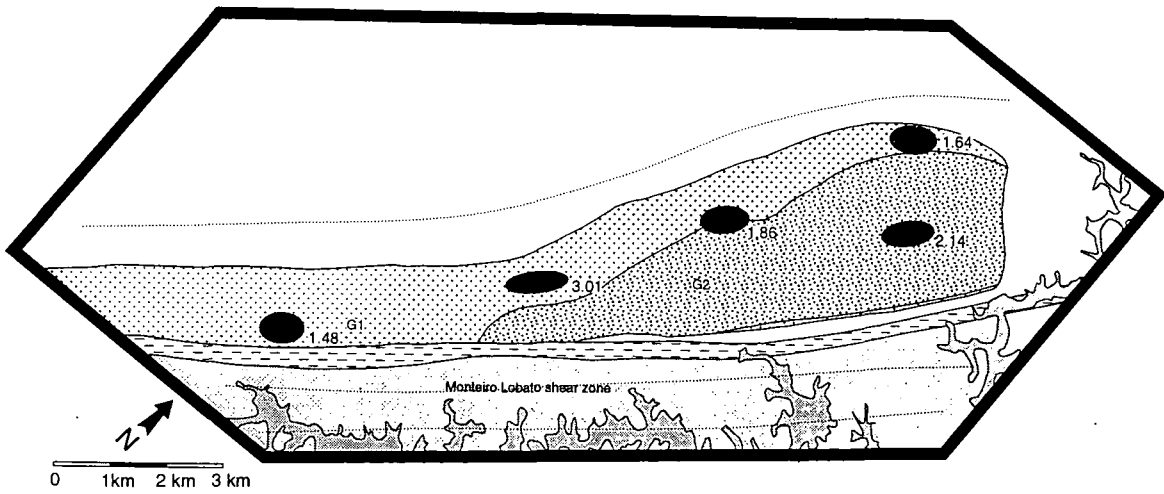
The Morro Azul pluton fabric preserves a finite strain which was predominantly homogenous, of a lower magnitude than that suggested by measurements of microgranitoid enclave ellipticities and flattening in nature. Similarly to the enclave data the Fry strains suggested that the principal finite strain axis (X-axis) was sub-vertically orientated, with a marginally greater magnitude than the sub-horizontally orientated Y-axis. The Z-axis was also sub-horizontal and orthogonal to the foliation plane and the X- and Y-axes.

Table 5.4 Summary table of Fry strain measurements from the Morro Azul pluton, a full table of data is given in Appendix 10.

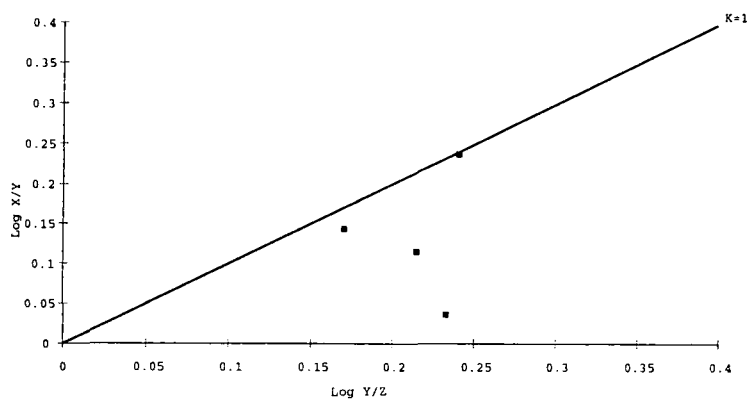
Localities	Grid References	Orientation	Fry strain	Number of analyses	Smallest Fry strain	Largest Fry strain	St. Dev.	Log K-value
CQ5	GR 77683040	Horiz.	2.06	1				
CQ1	GR 75482904	Vert.	1.48	1				0.84
CK1, CN, CO2	GR 80093393, GR 81003428, GR 8103 3399	Horiz.	1.74	4	1.55	1.89	0.17	
CN	GR 81003428	Vert.	3.01	1				0.99
CM1, CM5, CM6, CO7, CO8, CS8	GR 82633530, GR 82853700, GR 83053790, GR 81603638, GR 82383661	Horiz.	1.71	6	1.48	2	0.21	
CM5, CO6	GR 82853700, GR 82103549	Vert.	1.86	2	1.43	1.64	0.60	0.09
CO9, CP6, CU1, CU6	GR 83453915, GR 84633630, GR 85633973, GR 85033863	Horiz.	1.64	5	1.40	2.07	0.29	
CP6, CU6	GR 85033863, GR 84633630	Vert.	2.14	2	2.07	2.16	0.10	0.54
CT2, CT6	GR 84103573, GR 83953650	Horiz.	1.80	2	1.77	1.83	0.03	



a) Average Fry strains from the horizontal outcrop plane of the Morro Azul pluton



b) Average Fry strains from the vertical outcrop plane of the Morro Azul pluton



c) A Flinn-type plot for the Fry strain data from the Morro Azul pluton

Figure 5.27

5.10.4 Country rock strain

When compared to other plutons from this region the country rock around the Morro Azul pluton is relatively well exposed. This has facilitated the partial quantification of the finite strain preserved within country rocks on both sides of the pluton:

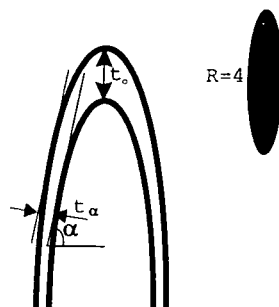
Southeast of the pluton, The Santa Isabel gneisses

Introduction

As described in part 5.8.1 and 5.9.1 the Santa Isabel gneisses (Plate 5.28) are exposed immediately southeast of the Morro Azul pluton and consist of a set of sheeted granodioritic gneisses, cut through by a set of intensely folded pegmatitic dykes which made up the last intrusive event preserved in the pluton. These pegmatites show parallel sided folds which qualitatively appear to represent a strong flattening strain, in an attempt to quantify this finite strain the folded layers were analysed using the t - α method described by Ramsay (1967, p411-412)

Methodology

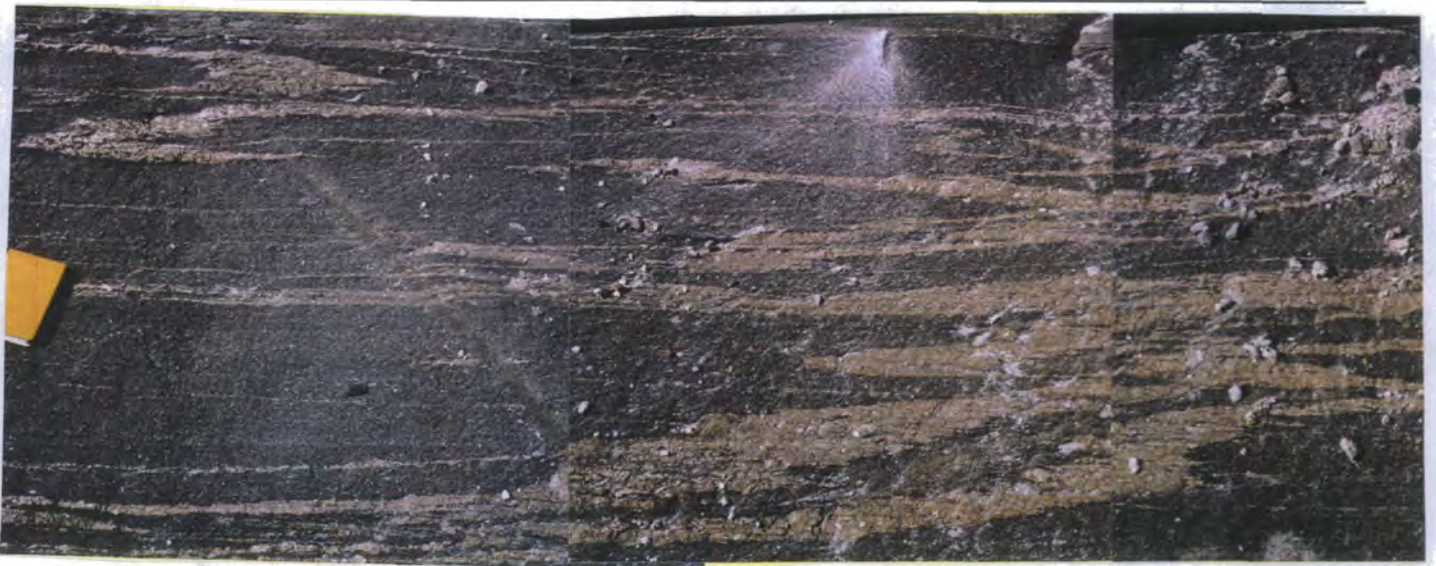
In this technique it is assumed that the structure to be analysed formed initially parallel sided layers which were buckled during the formation of *flattened parallel folds*. Given that magma often intrudes along parallel sided fractures this assumption would appear to be valid in this case. In order to produce a value for the flattening strain induced it is necessary to measure, on a number of folds, from each of the principal planes of the outcrop: i) the thickness of the layer at the fold axis, t_0 ; ii) the perpendicular layer thickness on the fold limb, t_α ; and iii) the angle α , the dip of the fold layer (Figure 5.28). Then using equation 5.1, a value for the ellipticity of the 2-D strain ellipse, R can be calculated. Since individual pegmatites may have not been particularly parallel sided and there may have been enhanced material flow into the apices of the folds a large number of individual strain determinations were made from across the largest outcrops using the photo montages of the horizontal outcrop plane shown in Plate 5.62, and the vertical outcrop plane shown in Plate 5.63. The results are detailed below, and list of the raw data given in Appendix 11.



Sketch of the measurements required for strain determinations from a flattened layer parallel fold (after Ramsay 1967)

Figure 5.28

Equation 5.1	$R^2 = \sin^2 \alpha / ((t_\alpha / t_0)^2 - \cos^2 \alpha)$
--------------	--



Horizontal plane exposure of deformed pegmatites within the Santa Isabel gneisses (GR 81563308)
Plate 5.62

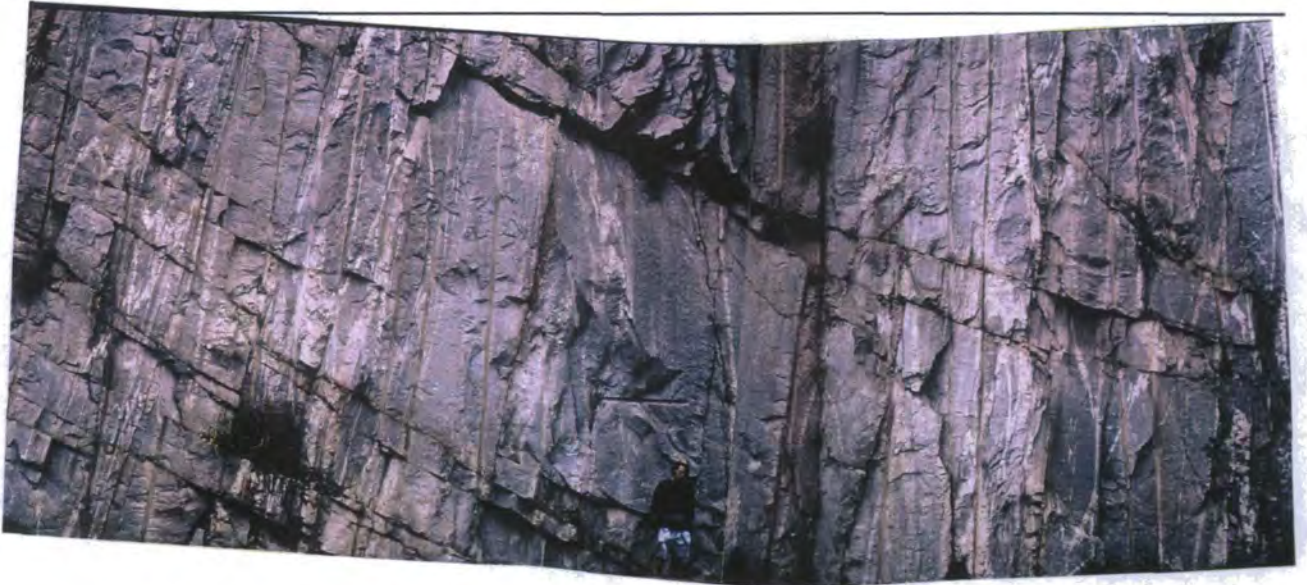


Plate 5.63 *Vertical plane exposure of deformed pegmatite within the Santa Isabel gneisses (GR 81563308)*

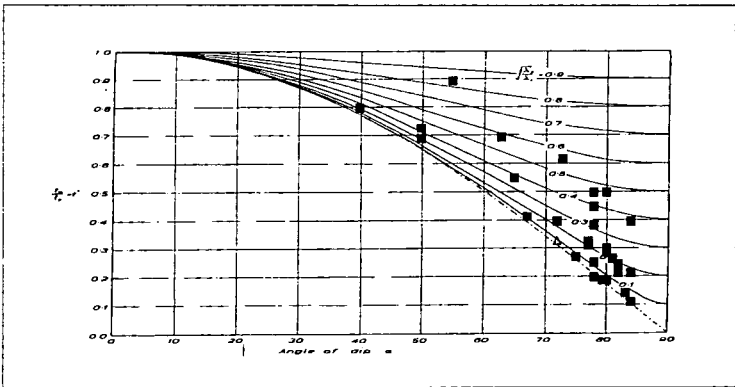
Results

The results obtained from outcrops in the horizontal and the vertical plane show (Table 5.5, Figure 5.29): i) that the gneisses was subject to a predominantly flattening strain after the injection of the pegmatites; ii) there is a large variation within each of the measured populations, but that the data is clustered around the mean value. The variation is probably induced by measurement inaccuracies and incompetent deformation of the pegmatites during deformation, i.e. squeezing of magma into the axial zone; iii) these gneisses have undergone a minimum layer perpendicular shortening of 70%; iv) this shortening was primarily accommodated by extension in the horizontal plane of at least

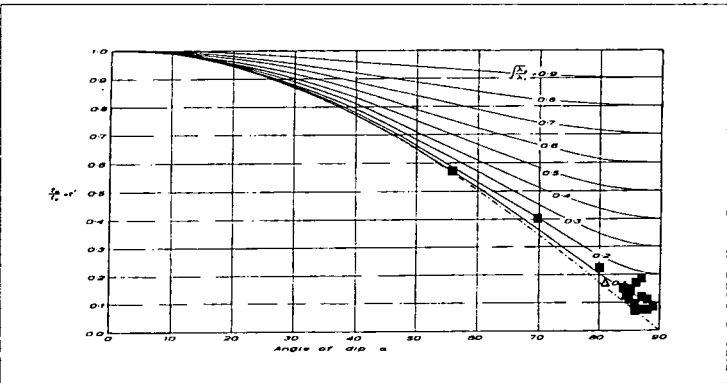
150%; and v) a dominant horizontal principal strain axis is consistent with qualitative observations of the outcrops which suggest that more strain is preserved within horizontal plane exposures.

Table 5.4 Mean strain ellipsoid axial ratios from the Santa Isabel gneisses.

	Mean axial ratio/ R	Standard deviation	Log K-value
Horizontal plane, X/Y	8.27	28.5	0.40
Vertical plane, X/Y	4.52	8.82	



a) Horizontal plane



b) Vertical plane

Ramsay (1967) t - α diagrams for folded pegmatites from the Santa Isabel gneisses (rectangles = data points, triangle=geometric mean value)

Figure 5.29

Conclusions

The Santa Isabel gneisses were subject to an homogenous minimum layer orthogonal shortening of 70%, which was accommodated primarily by stretching in the horizontal plane. This deformation which was the last major event to affect these rocks, whose metamorphic age is estimated at 710Ma (Tassinari 1988); was of greater magnitude than any subsequent deformation identified within the pluton or its immediate contact rocks. Therefore it is suggested that this deformation represents an approximately pure shear shortening which occurred during dextral transpression associated with D_{n+2} (Ebert

& Hasui 1992). It is the authors opinion that these gneisses represent a pure shear domain sandwiched between two shear zones, the dominant Monteiro Lobato shear zone to the south and a narrow shear zone rooted beneath the southeastern contact of the Morro Azul pluton which is responsible for the heterogeneous nature of solid state deformation within that pluton.

Additionally this high strain deformation within this zone demonstrates that the major shear zone controlled deformation in this area long before the intrusion of the granite plutons. Therefore during and post-intrusion of the plutons the shear zones were reactivated.

Northwest of the pluton

As shown in part 5.8.1 the country rocks to the northwest of the pluton have been folded and deformed in response to the intrusion of the pluton. In this section two estimates of the strain preserved within the country rocks will be made. The first from the folded rocks at the northern part of the pluton, and the second from the deflected rocks in the westernmost area.

Restoration of cross sections

In Figure 5.19c a scaled cross-section has been drawn through the country rocks along the northwestern contact of the pluton. This shows the existence of an upright synformal structure at the pluton contact, whose axial plane is situated approximately 300m from the pluton contact and which first begins to steepen the regional southeastward dipping foliation at 2.2km from the pluton contact.

Using this data an attempt was made to restore this cross-section to its pre-intrusion orientation assuming a regional southeastward dip of 25° . This showed that the fold may represent approximately 1.2km of northeastward directed shortening (35%) associated with intrusion. Although the lack of good marker beds and the possibility of pre-intrusion folding associated with transpression in this area and their possible effect on the accuracy of this result should be borne in mind. This amount of space creation would be sufficient to accommodate 30% of the lateral space required for intrusion of the Morro Azul pluton.

Deflection of country rocks

In this section Equation 2.4 is used to estimate the magnitude of strain required to deflect the southeastwards dipping country rock into a sub-vertical orientation and the associated space creation that might take place, assuming an applied principal stress orthogonal to the pluton contact and an acute angle of deflection. The results are detailed in Table 5.6 and show a wide variation depending upon the dip of the country rocks at the contact. The specific values quoted for space creation in the aureole may be slightly misleading, but interpreting these data in a general way shows a reduction in the strain accommodated within the country rocks on travelling southeastwards along the pluton

contact. A result which is consistent with qualitative observation from along this contact which suggest the greatest emplacement related deformation occurred around the northernmost contact area. Additionally it should be noted that even the largest values of space creation quoted would be insufficient to accommodate the entire lateral extent of the pluton.

Table 5.6 Estimates of contact strain associated with country rock deflection around the northwestern contact of the Morro Azul pluton.

Grid Reference	Country rock regional dip	Contact zone dip	Deflection strain, R	Width of contact zone/m	Approx. % shortening	Estimated pluton space created/m
Fold area, GR 380818	25°	85°	24	300	88	2100
Road section, GR 804358	40°	74°	4.45	250	64	450
Southern contact, GR 777318	60°	74°	2.01	50	38	80

5.10.5 Qualitative estimates of strain

In this section some inferences on the finite strain preserved within and around the pluton are made using the observations detailed in parts 5.8 and 5.9.

1. That the solid state deformation in the southwest of the pluton (south of Grid Line 32) becomes pervasive and relatively homogenous, showing its most intense fabrics along the southeast contact. The fabrics from the southeast contact show the shear induced boudinage of feldspar phenocrysts, which is estimated to represent a extension of at least 50% (Plate 5.64). This increase in fabric strength is corroborated by large enclave axial ratios in the horizontal plane.
2. The G1-G2 contact shows a localised increase in intensity of solid state strain which shows elongation of feldspar phenocrysts of up to 100% (Plate 5.65) which may take place in response to the rheological/compositional contrast in this area
3. The intensity of the solid state fabric in the remainder of outcrops is much weaker and probably represents only a very small component of any recorded finite strain values. Therefore the majority of strain reflected by the fabrics was induced in the magmatic state.



Plate 5.64 *Boudinage of feldspar phenocrysts during dextral solid state deformation (GR 79963224)*

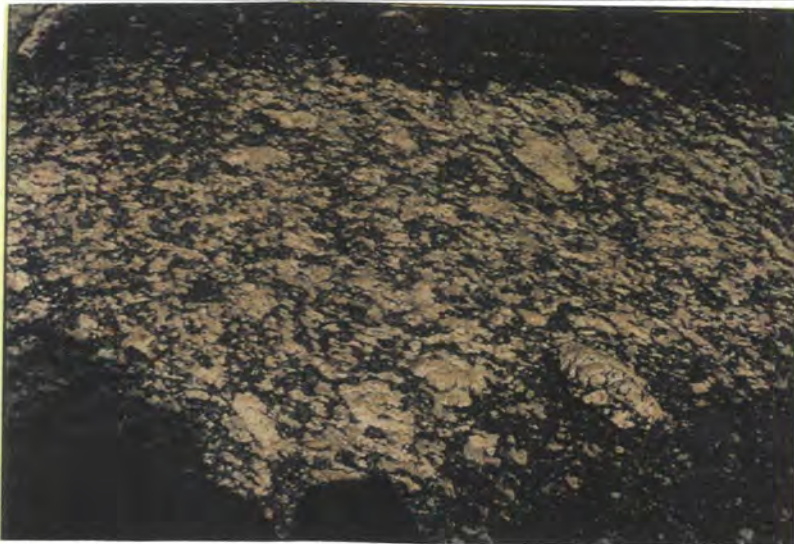


Plate 5.65 *Intense solid state shear induced fabric along the G1-G2 contact (GR 81033399)*

5.10.6 Conclusion and discussion

During this study it has been possible to use a variety of finite strain measurements within the country rock and the pluton phases themselves. This results in the following conclusions:

1. **Flattening strain** - As with other plutons from this region the Morro Azul pluton records a dominantly flattening strain within the intrusive phases themselves (using both Fry strain and enclave ellipticities as measurements). The microgranitoid enclaves in particular record a higher magnitude strain than observed elsewhere which may reflect the more 'forceful' nature of intrusion in this area. The relatively low solid state strains within the majority of the pluton suggests that the preserved finite strains are generally magmatic in origin.

2. **Vertically orientated X-axis** - In both measurements of the preserved granitoid finite strain the principle finite X-strain axis is vertically orientated, indicating that during intrusion there was a predominance of vertical stretching over horizontal lateral extrusion. This feature may demonstrate that during intrusion local space creation mechanisms facilitated vertical extrusion over its horizontal counterparts.
3. **Space creation** - Various estimates can be made for the amount of strain induced through deformation and deflection of the country rock. Converting these values into estimates of created space suggests that no more than 30% of the width of the pluton could have been made through external deformation, and that additional processes are required to account for the majority of the pluton volume.
4. **Fry strains** - Estimates of Fry strains are much lower than the finite strain estimates made from mafic enclave axial ratio measurement, although they display similar characteristics. This may be a consequence of initial axial ratio of the enclaves or the problems associated with the measurement of Fry strains examined in Part 8.5.
5. **Transpressional domains** - It appears that parts of the area adjacent to the Morro Azul pluton were subject to extensive ductile transpressional deformation during the D_{n+2} event. The magnitude of the pure shear strains associated with this deformation were greatly in excess of those induced during any subsequent deformation event. This demonstrates the pre-granite inception of the shear zones. This conclusion can be extended on a regional basis to suggest that all the shear zones associated with the studied granites existed before the intrusion of the plutons, and therefore that: i) emplacement of the plutons is probably genetically related to these shear zones; and ii) that their subsequent deformation is a post-intrusion reactivation of these zones.

5.11 Shear senses: the Morro Azul pluton

5.11.1 Introduction

Within the Morro Azul pluton and the surrounding country rocks there are a number of specific shear sense indicators which can be interpreted by comparison with the ideal situations defined in part 1.4. These are detailed below:

5.11.2 Country rock

As with all other aspects of the pluton the deformation fabrics present in the country rock vary depending upon which side of the pluton is observed.

Northwest of the pluton

To the northwest of the Morro Azul pluton the country rock generally preserves a flattening fabric associated with deformation during intrusion of the pluton and deflection of the regional fabric. Although in a single locality (GR 85434085) at the northernmost extremity of the pluton an outcrop of vertically dipping metabasite is observed (Plate 5.66) which contains quartz filled tension gashes which record a sinistral shear sense. This structure is interpreted as representing a country rock expression of the D_{n+3} pluton intrusion event.

Southeast of the pluton

The country rocks to the southeast of the pluton preserve LS-type dextral shear sense fabrics (Plate 5.67) almost identical to those observed around the Imbiricu pluton further north, and are not discussed further.



Sinistral quartz filled tension gashes at the northernmost extremity of the Morro Azul pluton (GR 85434085)
Plate 5.66



Crenulating fabric forming dextral S-C fabrics southeast of the Morro Azul pluton (GR 83303481)

Plate 5.67

Conclusions

Exterior to the pluton the majority of preserved shear sense fabrics record planar dextral deformation associated with post-emplacement deformation of the country rocks. Although around the northern contact of the pluton it is possible to recognise tension gashes which demonstrate sinistral deformation interpreted to be contemporaneous to pluton intrusion.

5.11.3 Granite

Shear sense from both the magmatic and solid state are described below:

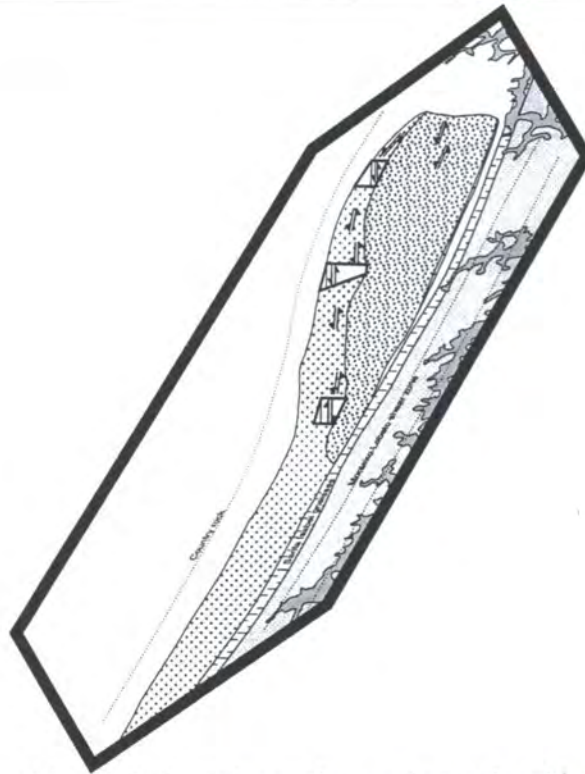
Magmatic state fabrics

As described in part 5.9.2 above there are only a very few small vestiges of the magmatic fabric preserved and within these the magmatic state shear sense is often difficult to identify. Those that can be observed consist of two types: i) sinistral bimodal fabrics (Plate 5.68); or ii) tiling relationships within phenocryst rich outcrops. However only a single unequivocally sinistral bimodal fabric could be identified in thin section. As a consequence of the lack of vertical exposure the shear sense in the vertical plane is difficult to observe, in outcrop, and no equivocal shear sense fabrics could be identified. In thin section however tiling fabrics which suggest a pluton centre up sense of shear have been observed in two close to pristine sections from the northernmost corner of the pluton. Examining the stereonet of magmatic state lineations (Figure 5.25) shows a variable plunge, suggesting that magmatic simple shear may take place during material transport in a number of directions during emplacement. Whilst this would vary depending upon position within the pluton, it does demonstrate a component of vertical plane strain during the pluton intrusion process. A sketch block diagram of the location and inferred magmatic

state shear senses is shown in Figure 5.30. Interpreting this small number of data suggests uplift of the centre of the pluton in response to magma injection during a sinistral shear.



Plate 5.68 Sinistral bimodal magmatic state fabric from the Morro Azul pluton (GR 85033902)



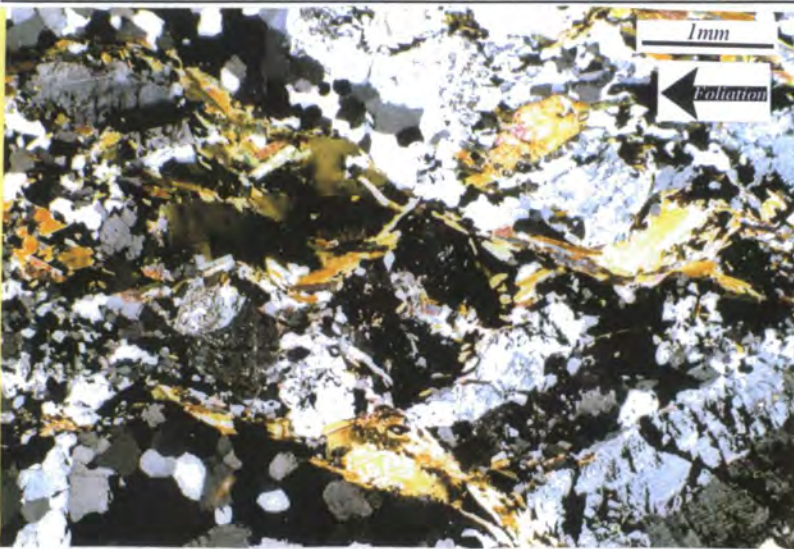
*Sketch block diagram of the distribution and sense of magmatic state shear fabrics from the Morro Azul pluton
Figure 5.30*

Solid state fabrics

Solid state shear sense fabrics within this pluton are very similar to those preserved further north in the Imbiricu pluton. These are entirely dextral, associated with the LS-type fabric produced during this deformation (Plate 5.69, 5.70 and Figure 5.31).



Plate 5.69 Dextral solid state shear sense fabric from the Morro Azul pluton (GR 84103573)



Photomicrograph of dextral solid state shear sense fabrics from the Morro Azul pluton (GR 75482904)

Plate 5.70

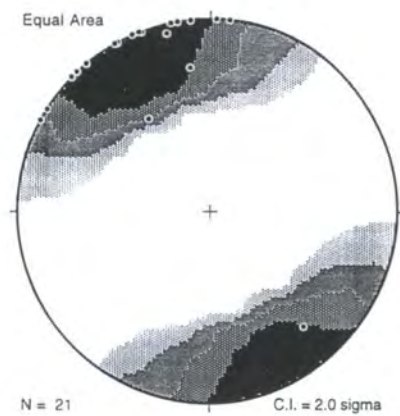


Figure 5.31 Contoured stereonet of poles to C-planes from the Morro Azul pluton (compare with poles to foliation planes in Figure 5.20a, c)

Conclusions

The granite itself preserves two generations of shear sense fabrics the first from magmatic state deformation of the pluton which shows horizontal sinistral shear associated with pluton centre-up. Subsequently the pluton was overprinted by a dextral planar shear as seen in all the other plutons from this region.

5.11.4 Other shear sense indicators

Occasionally incorporated within the Morro Azul pluton are foliated screens of country rock which are sub-vertically dipping, oblique or sub-parallel to the pluton foliation. These screens incorporate minor folds (Plate 5.43) which have a characteristic southwestward sense of vergence (Figure 5.32), demonstrating formation during a sinistral shearing event. Although it is possible that the genesis of these folds could be the result of country rock deformation before incorporation, the presence of crenulating southwesterly verging folds sub-parallel to the pluton fabric at GR 82163543, suggests that shear induced compression caused buckling of the country rock while the xenolith was hot and weak before the pluton had completely cooled. In every case the deformation of these xenolith appears to have been in the high temperature ductile state and there are no later cross-cutting lower temperature fabrics.

Additionally in the large quarry at GR 81003428 an incorporated country rock xenolith can be observed which shows a ductile down to the east sense of shear along slip surfaces within the xenolith itself. Whether this represents a bulk magma deformation or local stoping of the country rock block itself is unknown, but it demonstrates a hot ductile magmatic state process since the pluton is only very weakly overprinted by the solid state fabric in this area. If it represents a magmatic flow it suggests a pluton centre down sense of shear in this area: in contrast to the shear fabrics observed within the magmatic state fabric itself.

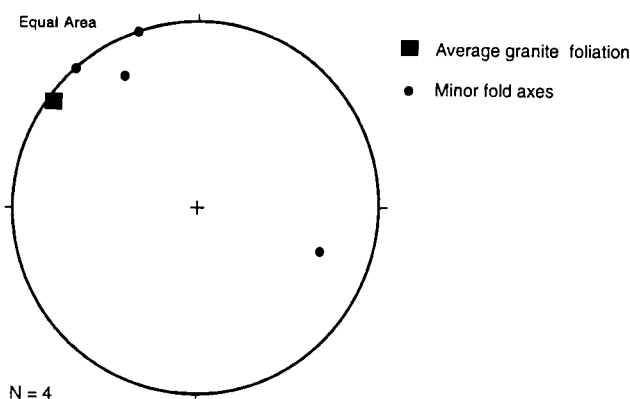


Figure 5.32 Stereonet of minor fold axes compared to average foliation direction, the Morro Azul pluton

5.11.5 Conclusion and discussion

The intrusion of the Morro Azul pluton was associated with a number of shearing events of various styles which are summarised below:

1. **Pre-granite deformation** - As with all other plutons studied in this area shear senses associated with deformation before the intrusion of the pluton cannot be unequivocally proved in this area, although the presence of the Santa Isabel gneisses and quantifying their deformation demonstrates that transpressional deformation occurred in this area before the intrusion of the plutons.
2. **Emplacement of magma** - Magmatic state shear sense can be identified in a number of places across the Morro Azul pluton, most commonly in the northernmost parts where the overprinting solid state fabric is at its weakest. These magmatic fabrics and other shear sense indicators in the country rocks and xenoliths (which are interpreted to represent contemporaneous deformation) demonstrate that sinistral shear was taking place in the horizontal outcrop plane. The vertical plane deformation is more complex to determine and shows evidence of pluton centre-up and pluton centre-down magmatic shear fabrics.
3. **Overprinting fabric** - After the emplacement of the pluton and significant cooling of the intrusion the pluton underwent a dextral solid state overprinting. The fabric associated with this deformation is concentrated along rheological or compositional discontinuities along and around the pluton and appears to have been controlled by a spur of the Monteiro Lobato shear zone which runs sub-parallel to the southeastern contact of this pluton.

5.12 Emplacement kinematics of microgranitoid dykes/sheets: the Morro Azul pluton

5.12.1 Introduction and methodology

As with the other studied plutons from this region the Morro Azul preserves a number of sub-vertically orientated, cm-scale microgranitoid dykes or sheets, which show consistent preferred orientations and a composition which is qualitatively similar to that of the pluton itself. The following section outlines the preferred orientations of these features, in an identical manner to that described in part 4.6, with a division being made depending upon which part of the pluton they came from.

5.12.2 Results

In order to examine any variation with orientation around the pluton the pluton was divided into three areas as follows: *Southern area* - area of the pluton southwest of a northwest trending line from grid reference GR 830340; *Central area* - area of the pluton northeast of the Southern area, but southwest of a northwest trending line from grid reference GR 850370; *Northern area* - the remaining northeasternmost parts of the pluton. The orientations and interpretation of the microgranitoid dykes from these various areas are detailed below (Figure 5.33):

Southern area

The southern areas preserves the largest number of microgranitoid dykes observed anywhere within the pluton ($n=22$). These structures when plotted on a rose diagram (Figure 5.33a) show a single broad peak between 010° and 050° , coincident with the vector mean of the data at 033° . Examination of individual dykes showed no preserved shear senses associated with intrusion or later deformation. Therefore these data are interpreted as Type 1 (see part 4.6.2), where the dykes were intruded perpendicular to σ_3 . Therefore σ_3 is interpreted to have been orientated sub-horizontally trending at 123° , and σ_1 and σ_2 orientated orthogonally within the plane of the dykes.

Central area

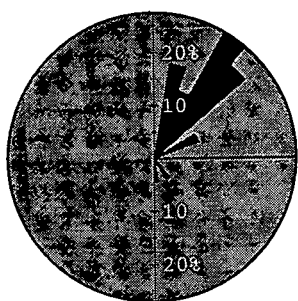
Only a small number of microgranitoid sheets were observed in this area ($n=7$) these show a relatively broad distribution, although the majority of the data is between 010° and 070° , with a vector mean at 043° (Figure 5.33b). Examining individual dykes suggests that there is no predominant shear sense associated with emplacement. As a consequence these data are interpreted to represent Type 1 dykes. In such case σ_3 would be sub-horizontal trending approximately 133° , with σ_1 and σ_2 contained in the plane of the dyke itself.

Northern area

No microgranitoid sheets are preserved anywhere in the northern part of the Morro Azul pluton, this portion of the pluton remained passive with respect to this intrusion phase.

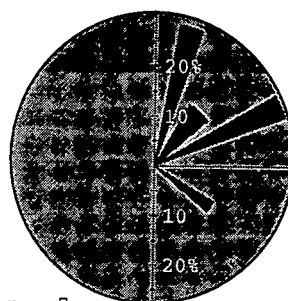
5.12.3 Conclusion and discussion

In this pluton these dykes are intruded approximately sub-parallel to the long axis of the pluton (Figure 5.33c) and preserve no internal shear fabrics. Therefore the dykes have been interpreted as forming during an extensional stress approximately orthogonal to the regional structures in this area. The observation that these dykes predominate in the southern half of the pluton suggests that the extension was most prevalent in this area, and was not accommodated in the northern portion of the pluton.



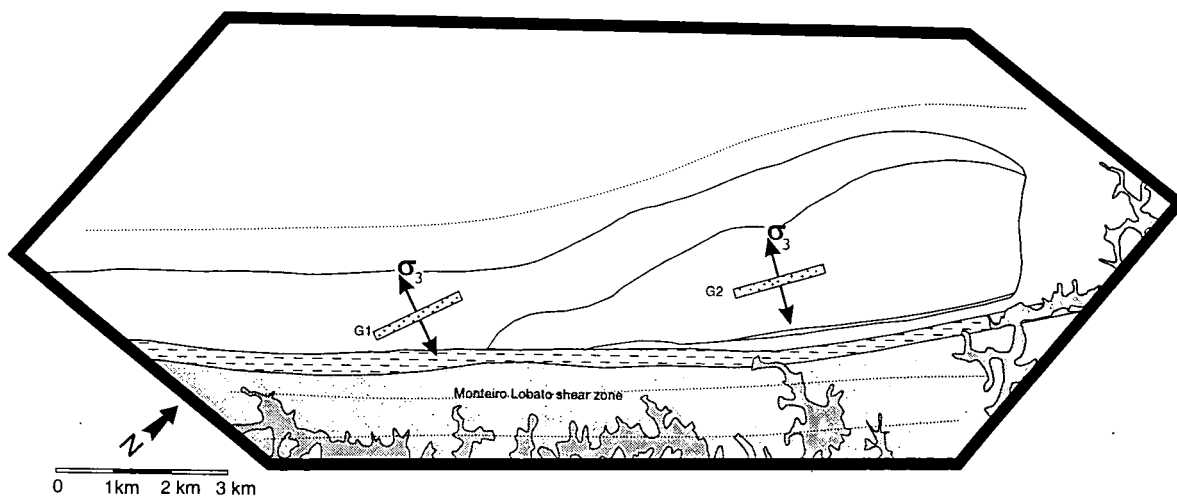
n = 22
Vector mean = 033°
Circular St. Dev. = 21°
Max. = 27.3%

a) Rose diagram of microgranitoid dykes
Central area, Morro Azul pluton



n = 7
Vector mean = 043°
Circular St. Dev. = 33°
Max. = 28.6%

b) Rose diagram of microgranitoid dykes
Southern area Morro Azul pluton



c) Sketch map of principal microgranitoid dyke orientations and inferred extensional stresses during their emplacement, Morro Azul pluton

Figure 5.33

5.13 Overprinting discrete mylonitic shear zones: the Morro Azul pluton

5.13.1 Introduction and methodology

Similarly to the other studied plutons from the RPSSB there are a large number of discrete, cm-scale mylonitic shear zones preserved in various localities across the Morro Azul pluton (Plate 4.71). In the following section they are analysed in a manner identical to that detailed in part 4.7.



Plate 5.71 Discrete mylonite from the Morro Azul pluton (GR 82983453)

5.13.2 Results

Southern area

The Southern area of the pluton preserves mylonites ($n=25$) with a very well developed mean value orientated at 170° - 190° (Figure 5.34a). Although there is a subsidiary, but significant population orientated between 070° - 090° . The shear senses associated with the either of these data groups appear to show no consistent orientation, with dextral and sinistral shear sense fabrics being found in all orientations. As a consequence of this lack of consistency within the data it is impossible to make any valid interpretation as to the dominant principal stresses prevalent in this area during their formation.

Central area

The Central area of the pluton preserves a large number of discrete mylonites ($n=76$) which describe a bimodal distribution (Figure 5.34b). The largest peak of this distribution is found in the region of 020° - 030° and the second peak in the interval between 140° - 170° . Examining the shear senses associated with these data shows that dextral shear senses occur associated with mylonites with an orientation of approximately 025° , whereas mylonites with an average orientation of 155° preserve sinistral shear senses. Interpreting

these data as a conjugate set would make σ_1 orientated at 090° and σ_3 at approximately 180° in the horizontal plane, σ_2 would be sub-vertical.

Northern area

The outcrops from the northern area also preserve a large number of discrete mylonites ($n=67$). They show (Figure 5.34c) two adjacent peaks within the dataset; the first between 010° - 020° , and the second between 030° - 050° . The vector mean of the data is 034° . Examining the shear senses associated with these data suggests that they describe two separate populations, the first with a sinistral shear sense along $\sim 015^\circ$, and the second with a dextral shear sense at $\sim 040^\circ$. Interpreting these data as a conjugate set suggests that σ_1 would be orientated at 118° and σ_3 at 028° in the horizontal plane during formation of these features, σ_2 being sub-vertical.

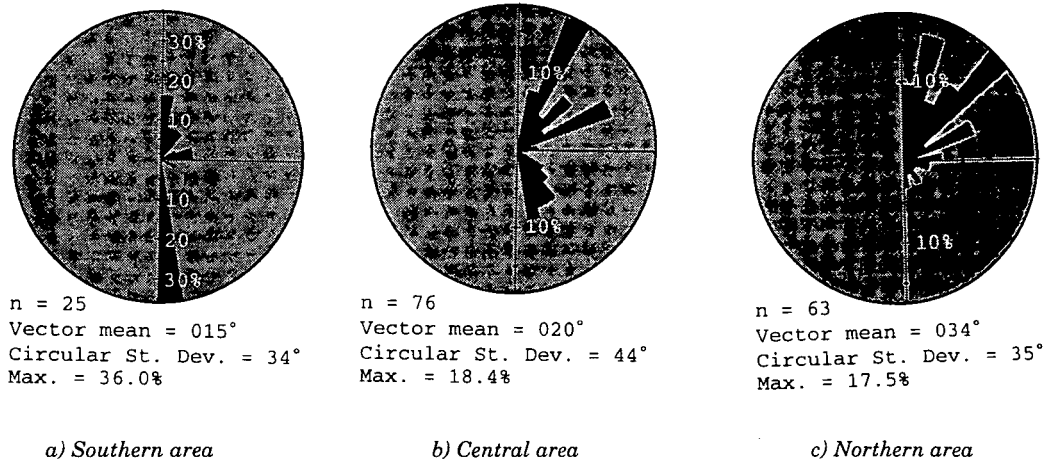


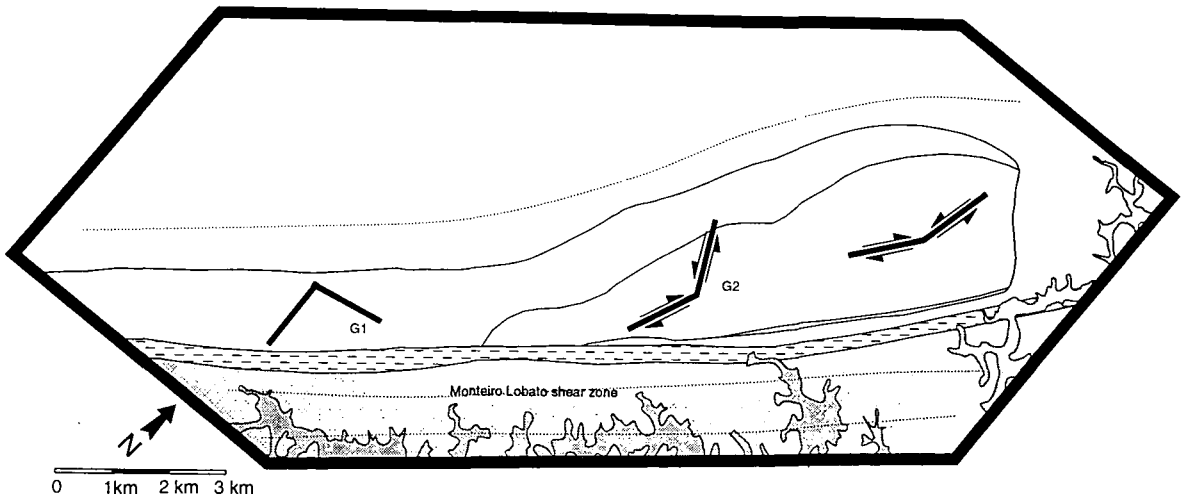
Figure 5.34 Rose diagrams of discrete mylonite orientations from the Morro Azul pluton

5.13.3 Conclusion and discussion

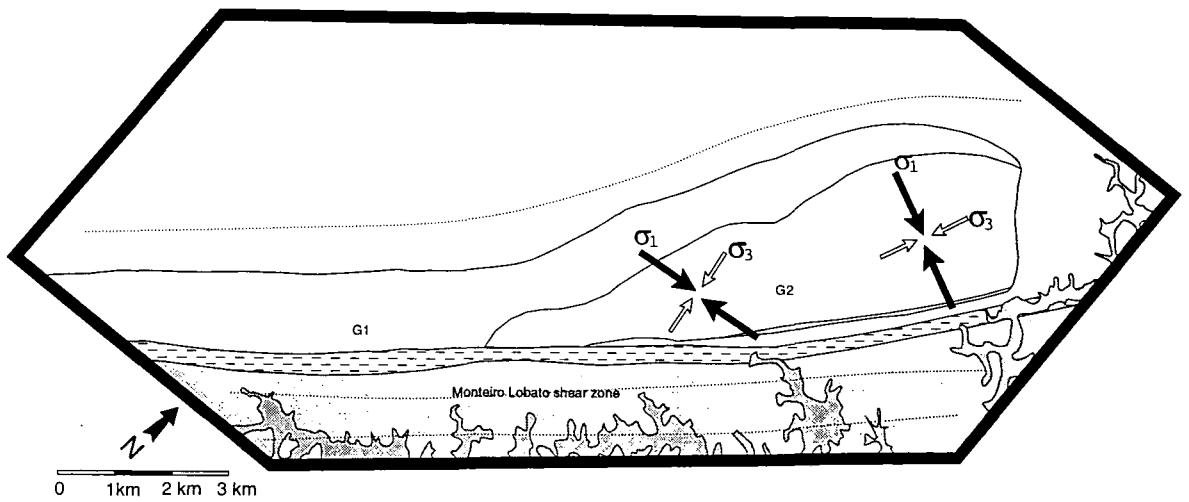
These mylonites which can be seen to cross-cut and post-date the solid state fabric within the Morro Azul pluton are present in many areas throughout the pluton. Examining their orientations suggests that (Figure 5.35):

1. They were formed in response to an east-west directed local compressional deformation.
2. These data produce a less defined and more complex dataset than has been observed in other plutons from the RPSSB. The reasons for this are unknown.
3. There are high angles ($>45^\circ$) between the principal compressive stresses and the fracture orientations. A number of possible reasons for this were explained in part 4.7, in this case these mylonite fabrics could have formed in response to any of these scenarios, but in the authors opinion the preservation of east-west orientated compression direction from the majority of the studied plutons in this area suggests that these mylonites formed in response to a strongly confined compression which was primarily

accommodated along the existing (therefore weaker) shear zones and their adjacent rocks without nucleating additional structures.



a) Average discrete mylonite orientations from the Morro Azul pluton



b) Inferred principal compressive stress orientations for discrete mylonites from the Morro Azul pluton

Figure 5.35

5.14 Dykes or diapir ?

5.14.1 The Imbiricu pluton

Although the Imbiricu pluton could be approximated to a sub-circular shape consistent with intrusion as a diapir it preserves none of the other features normally understood to be consistent with intrusion as a diapir. For example there are no pluton up kinematics, no prolate strains, there is no centre margin zonation, there is no sub-circular foliation and there are no vertically orientated stretching lineations. In fact the field evidence is highly consistent with intrusion along dykes. Since there are granite dykes intruded sub-parallel to the foliation in the wallrocks, a petrographic zonation sub-parallel to the supposed conduit (the Monteiro Lobato shear zone), ^{and} some cryptic magma sheets within G2 and G2 magma sheets present within G1. All of which suggest sheeting/dyking during emplacement. As a consequence the Imbiricu pluton is interpreted to have emplaced by sheeting of magma along the existing regional structural discontinuity (Monteiro Lobato shear zone) before homogenisation after emplacement

5.14.2 The Morro Azul pluton

Whereas the Imbiricu pluton preserved at least some of the shape criteria required to explain intrusion through diapiric processes, the Morro Azul pluton is a wedge-shaped pluton that is strongly elongate along regional strike. Similarly, there are no vertically orientated lineations, no prolate strains, no centre-margin petrographic zonation and no pluton-up kinematic indicators within the wallrocks. Although inside the pluton itself there magmatic state shear senses that can be observed display a pluton centre-up sense of shear, but on balance it seems as though diapiric ascent during emplacement of this pluton is unfavourable. Indeed there is a much larger body of evidence to suggest that emplacement of the pluton was facilitated, by sheeting into the country rock, preserving wallrock xenoliths within the pluton itself, followed by subsequent intrusion of a second phase by sheeting along the internal contact. In such a situation the pluton-up kinematics recognised are merely a function of the supply of magma preferentially towards the centre of the pluton.

5.14.3 General conclusions

The statements in the previous two parts demonstrate that these two plutons, both intruded close to a similar regional structure show a similar emplacement history. Showing: i) sheeting into the country rock; ii) emplacement of a feldspar phenocryst rich G1; iii) the splitting of this early phase by sheeting of a feldspar phenocryst poor G2; and iv) during development of a magmatic fabric and later overprinting by a solid state fabric which had a similar shear sense in both plutons. As a consequence it is suggested that both these plutons were emplaced approximately coevally, by dyking from a similar but not identical

source ascending along different points of a similar conduit. Field evidence suggest that the Monteiro Lobato shear zone or associated shear zone splays of that major structure probably controlled the siting and ascent of the magma and its later deformation.

5.15 Emplacement and deformation

5.15.1 A sequence of events

In the following section a possible series of tectonic events responsible for the intrusion of these plutons is made on the basis of the data described in the preceding sections:

- 1. Initial scenario** - As described in Chapter 3 this area was subject to an east-west directed transpressional crustal thickening during the Brasiliano orogeny, which was responsible for the generation of the regional low-angle fabric and its cross-cutting by high angle shear zones ($D_{n+1/2}$). It was into this environment that the Morro Azul and Imbiricu plutons were emplaced.
- 2. Initiation of ascent and emplacement** - As described in the previous section this area was subject to a dextral transpression before the intrusion of the granitoid plutons. In such an environment the areas around these plutons would have been subjected to intense contraction related deformation. Despite this the plutons themselves demonstrate that during emplacement there was only a very weak induced fabric which is consistent with sinistral shearing in the horizontal outcrop plane (Figure 5.36). Thereby suggesting principal stress orientations consistent with a component of east-west extension, such an extension associated with a major structural discontinuity (shear zones) would be a low-pressure, pull-apart site that could penetrate a magma source at depth and promote ascent, with the shear zone acting as the magma conduit. Such ascent would continue providing that, either the magma retained sufficient internal pressure to deform the pre-existing magma and the surrounding country rock, or sufficient space was being created for the magma itself. The preservation of magma sheeting within the country rocks and the pluton itself proves unequivocally that magma emplacement occurred as a result of the supply of magma through dykes.
- 3. Continued magma ascent and emplacement** - The compositional homogeneity, comparatively low intensity of the magmatic fabric and intrusion related deformation of the country rock suggests that space was being created for the magma almost as fast as it was being supplied and that it took place in two stages. The Morro Azul pluton however displays a stronger magmatic fabric and more 'forceful' deformation of the country rock indicating that tectonic space creation in this area (possibly because of the thinning of the pluton cavity) was probably slower than in the almost isotropic Imbiricu pluton further north.
- 4. Granitic magma source** - While the pluton is believed to be source from melting of an lower crustal protolith the field evidence allows some general comments about the distribution of magma at depth to be made. In particular: i) that the presence of these two plutons of qualitatively similar composition spaced along strike indicates the presence of a laterally continuous homogenous source; ii) each of these plutons probably

tapped this source at different points, before ascent along separate conduits associated with the major shear zone in this area; iii) evolution of this source through time is reflected in the compositional variation seen between the two intrusive phases.

- 5. Post-emplacement magmatic activity** - After the intrusion of the majority of the pluton magma a number of cm-scale microgranitoid dykes were emplaced within each of the plutons, the orientations and fabrics associated with these features demonstrate their intrusion during continued axis orthogonal extension.
- 6. Post-emplacement tectonic activity** - Following the intrusion of the microgranitoid dykes the pluton cooled and was overprinted by an horizontal dextral shear, induced by reactivation of the shear zones along the southeastern contact of the pluton.
- 7. Formation of discrete mylonites** - Overprinting and cross-cutting the solid state and earlier magmatic state fabric the Morro Azul and Imbiricu plutons contain discrete mylonites. The particular orientation and conjugate nature of these fabric demonstrate their formation during confined compression locally orientated perpendicular to the major structures in this area.

5.15.2 Pluton shape

The Imbiricu pluton

The Imbiricu pluton displays a lozenge shape with an axial ratio of $R_s \sim 1.7$ and sharp sub-vertical contacts at the northwestern and southeastern edges. Although at the southwestern edge a supposed roof contact is preserved (Figure 5.5), whereas at the northeastern edge an elongate country rock apophysis intrudes the contact. As a consequence the pluton shape is interpreted to be formed from a horizontal planar section through an arcuate pluton roof (Figure 5.5), which contained subvertical country rock screens and deflected country rock. It is suggested that the magma body is semi-continuous underneath the southwestern contact, and related to the Morro Azul pluton observed to the southwest.

The Morro Azul pluton

The Morro Azul pluton preserves a wedge shape which tapers southwestwards along strike. Its contacts are steep with the surrounding country rock and appear to have formed in response to a flattening deformation. At its northern edge the contact is unexposed, but is of similar width and sub-parallel to the Imbiricu contact exposed to the northeast. As a consequence of these features the pluton shape is interpreted to have formed as magma intruded into an wedge-like extensional zone within the crust. Extension took place preferentially in the northern part associated with making space for the Imbiricu pluton. In the southern section extension was smaller and the magma intrusion was confined. The intense solid state shear (enclave axial ratio =6) strains affecting the

southern may have also been responsible for additional elongation of the pluton 'tail' in this area.

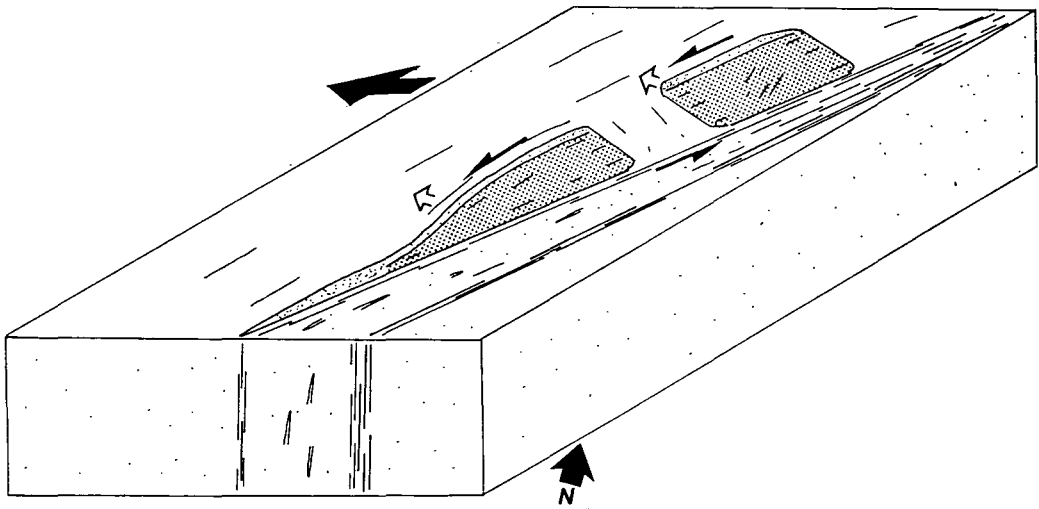


Figure 5.36 East-west directed extension inducing sinistral shear during the intrusion of the Morro Azul and Imbiricu plutons

5.16 Conclusions

5.16.1 The Imbiricu pluton

The Imbiricu pluton is a two-phase pluton, spatially associated with the continental scale Monteiro Lobato shear zone. It shows a sub-vertical fabric, and an homogenous emplacement related strain. This was a qualitatively weak magmatic fabric with no recorded associated shear sense that was overprinted by a ductile horizontal planar dextral solid state deformation which was partitioned into the country rock and outer margins of the pluton itself. Examination of the magma and country rock fabrics and the quantification of the finite strain preserved suggests that the country rocks accommodated approximately 500m of the space required for the pluton, whereas the ^{state fabric} magmatic ^{magmatic} suggests northwest-southeast directed internal shortening of up to 50% during emplacement. This suggests that while the pluton preserves an emplacement strain the country rocks do not preserve sufficient emplacement related deformation to accommodate the pluton.

These results have been interpreted to show that emplacement of the pluton took place during a regional extensional deformation episode (D_{n+3}). During this event magma was intruded, sub-parallel to the country rock foliation under its own pressure into a magma filled 'cavity', exerting deformation onto the surrounding country rocks. As a consequence of the confining effect of the country rocks, a magmatic fabric and emplacement induced finite strain were recorded by the magma itself. The intensity of this intra-pluton deformation was probably controlled by how much the rate of magma injection exceeded the rate of space creation. The presence of two individual homogenous pluton phases suggests that injection took place rapidly in two distinct events.

5.16.2 The Morro Azul pluton

The Morro Azul pluton shows many features which are similar to the Imbiricu pluton such as the bi-modal outcrop (which is compositionally similar to the Imbiricu pluton and similarly homogeneous) and the sub-vertically dipping fabric sub-parallel to the pluton long axis. The pluton was emplaced by sheeting into the country rock surrounding the pluton before coalescing into an homogenous magma body, occasionally incorporating some of this country rock material. Into this early phase G2 was intruded by sheeting along the contact before G1 was entirely solidified and hence there is evidence for fluid exchange along some of these dyke contacts.

The strain associated with intrusion is remarkable for showing a predominance of vertical stretching, which suggests that ^{the} intrusion may have had a greater component of lateral confinement than elsewhere within the RPSSB. The strain induced into the wallrocks may, at least in some areas, have been significantly higher than elsewhere in the RPSSB. The shear senses associated with this intrusion are sinistral in the horizontal plane and variable in the vertical plane. After intrusion the pluton was overprinted by a planar

dextral shear which was most intense along rheological or compositional discontinuities and becomes highly pervasive and intense towards the southeastern end of the pluton.

These data demonstrate that the pluton was sourced from a similar magma to the Imbiricu pluton, but was intruded more forcefully recording a greater intrusion strain within the pluton i.e. space creation in the wallrock remained minimal, during a regional east-west directed extension although the rate of magma supply was much greater than the rate of tectonic space creation. Later deformation overprinted this fabric during dextral reactivation of the major shear zone along the southeastern border of the pluton.

5.16.3 General conclusions

The features of the Morro Azul and Imbiricu plutons also demonstrate some more general considerations:

- 1. Structural architecture** - The preservation of an older transpression domain close to the southeast contact of the Morro Azul pluton demonstrates that there was extensive transpression before the intrusion of the plutons, and most importantly that the shear zones existed before the emplacement of the plutons. This demonstrates the genetic association of these plutons with the regional shear zones.
- 2. Dyking ascent** - The presence of sheets of both compositionally variable and compositionally similar cryptic dykes within both of these plutons demonstrates the general applicability of the sheeting method of magma emplacement through dykes, associated with shear zones, as envisaged by Petford *et al* (1993).
- 3. Space creation** - Neither of these plutons preserves adequate contractional deformation within the country rocks to account for the amount of space required for the magma. As a result it is necessary to invoke far-field mechanisms such as regional extension forming a pull-apart to account for the pluton space.

Chapter 6

The Itapeti pluton

6.1 Introduction

6.1.1 Preamble

In this chapter the Itapeti pluton is described. This pluton was not comprehensively mapped during this work, instead existing maps (Morais 1996) were used in an attempt to elucidate the tectonic framework within which deformation and granite emplacement took place. The pluton (Figure 3.4b, 6.1, Maps 5, 9) is situated north and east of the city of Moji das Cruzes, and southwest of the cities of Guararema and Jacarei, about 50km east of Sao Paulo city. It outcrops over approximately 75km² and comprises parts of the 1:50,000 map sheets named Moji das Cruzes, Santa Isabel, Jacarei and Itaquacetuba.

6.1.2 Previous work

Despite its proximity to the city of Sao Paulo this pluton has received very little detailed geological investigation. It was first examined by Knecht (1964), who remarked upon the porphyritic nature of the intrusion. However it was not until the regional mapping studies of Hasui *et al* (1978), Theodorovicz *et al* (1990) and Bistrichi *et al* (1991) that the setting of the pluton became clear. It is east-west trending, wedge shaped and very strongly elongated eastwards, with a continental-scale shear zone (the Taxaquara shear zone) defining its northernmost contact (Figure 6.1). Isotopic investigations by Tassinari (1988) suggested an Rb-Sr whole rock age of 625±25Ma, a (⁸⁷Sr/⁸⁶Sr)_i ratio of between 0.704 and 0.725 and a K-Ar biotite age of ~460Ma for the pluton. These data are interpreted to correspond to the age of intrusion and the time at which the intrusion had cooled respectively. Whereas, the country rocks have an age which has been estimated at 750±25Ma (Rb-Sr whole rock, Tassinari 1988).

The most recent work is by Morais (1996) who carried out a 1:50,000 mapping, petrographic and geochemical study on the pluton, concluding that:

1. The pluton has three distinct phases (G1, G2, G3) (Figure 6.1, Map 5) which were broadly potassium feldspar rich granites in composition (G1 = Grey coloured phenocrystic (3b) granite, G2 = Pink coloured phenocrystic (3b) granite, G3 = phenocrystic (3a) melanogranite). These conclusions are broadly in agreement with point counting to 500 points of 10 thin sections (shown in Figure 6.2) which demonstrates a granitic to alkali granite composition for the pluton.
 2. The intrusion has a strong, sub-vertical foliation which was classified as solid state and protomylonitic to ultramylonitic in nature.
-

3. The pluton is meta-aluminous, rich in potassium and became progressively more alkaline on travelling eastwards along the pluton axis.
4. Zircon topology suggested that the conditions of formation were essentially anhydrous, with little differentiation between magmas, and a crystallisation temperature of 800-850°C.

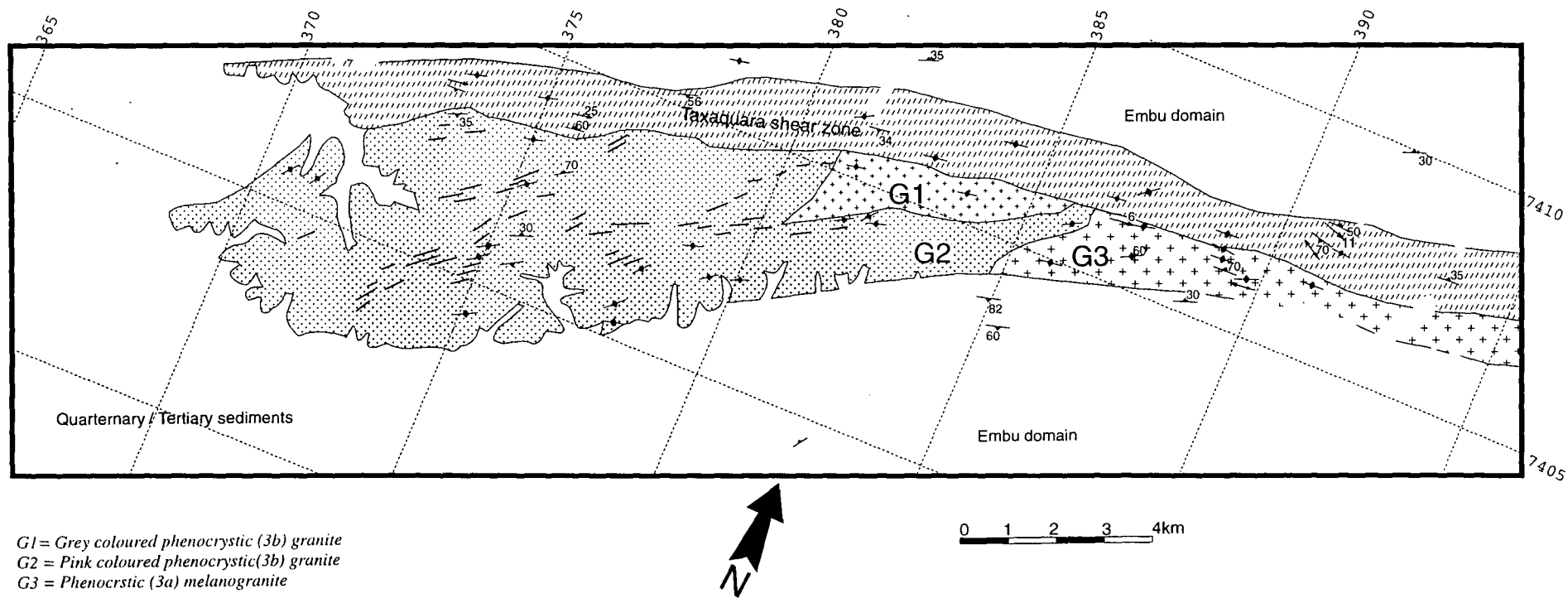


Figure 6.1 Map of the Itapeti pluton (modified after Morais 1996)

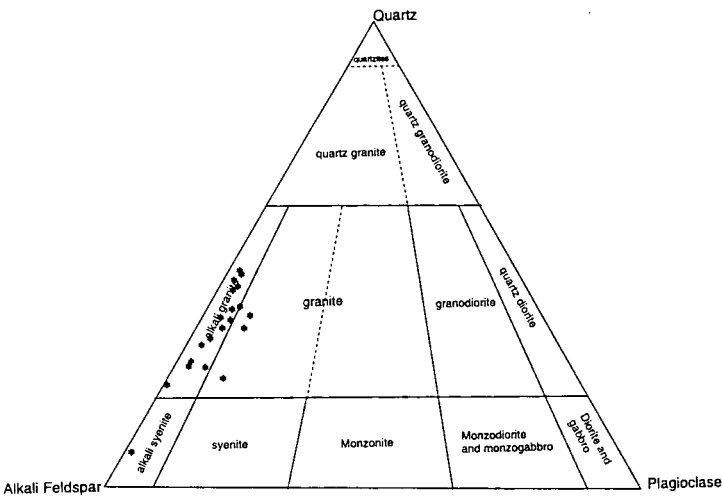


Figure 6.2 Tertiary QAPF-type plot for rocks of a granitic composition for the Itapeti pluton

6.2 Mapping and deformation

6.2.1 Introduction

In the following section the structure and nature of the magmatic and ductile solid state deformation affecting the pluton and the country rock in the immediate vicinity of the pluton contact are examined. The pluton has been split into zones which broadly encompass the areas of principal exposure within and around the pluton (Figure 6.3).

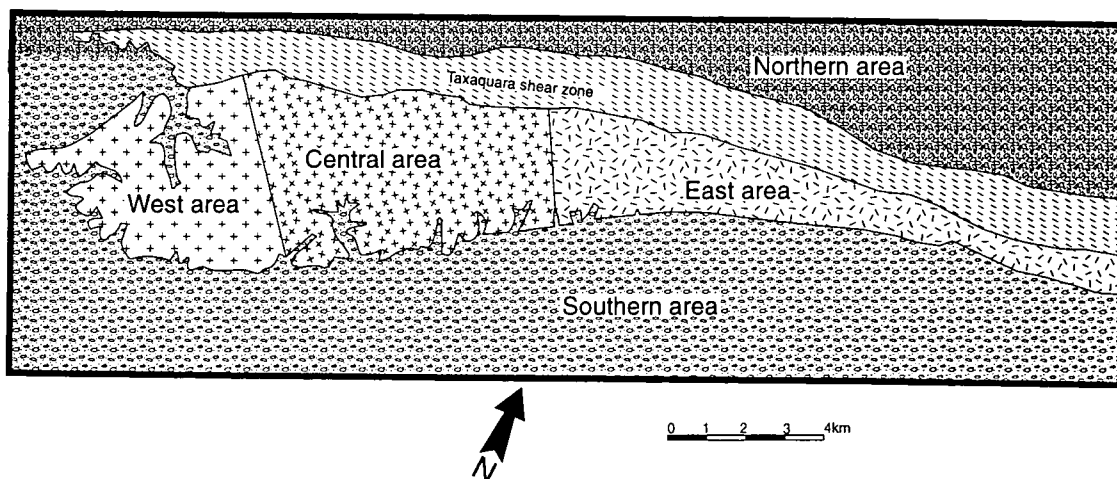


Figure 6.3 Subdivision of the pluton and country rocks used in this study

6.2.2 Country rock

The basement country rock around the pluton is part of the Precambrian Embu domain and consists of strongly foliated, variably migmatized gneisses which are regionally metamorphosed to amphibolite grade, but retrogressed to greenschist facies in the vicinity of the Taxaquara shear zone. This basement is overlain in places by Tertiary age alluvial sediments.

Northern area

The country rocks to the north of the pluton correspond either to sediments associated with the western termination of the Taubate basin or to migmatitic gneisses strongly deformed by the Taxaquara shear zone. These gneisses are generally east-west trending, sub-vertically foliated and, in places, preserve sub-vertical but southward verging isoclinal folds (which are interpreted to be regional F_{n+2} folds) (Figure 6.4a). On approaching the shear zone the metamorphic grade is reduced (from regional amphibolite facies), the fabric becomes finely spaced and displays a sub-horizontal stretching lineation (Plate 6.4) with fabrics indicating a dextral shear sense. The granite contact cannot be examined in detail, but the best exposures show a transition from a country rock gneiss to a granite gneiss occurring over 200-300m of unexposed ground. As in other shear zones across the study area, the Taxaquara shear zone and its associated fabrics are interpreted

to have formed in response to the D_{n+2} deformation event and reactivated during D_{n+4} , since additional deformation overprints both the granite and the country rocks.

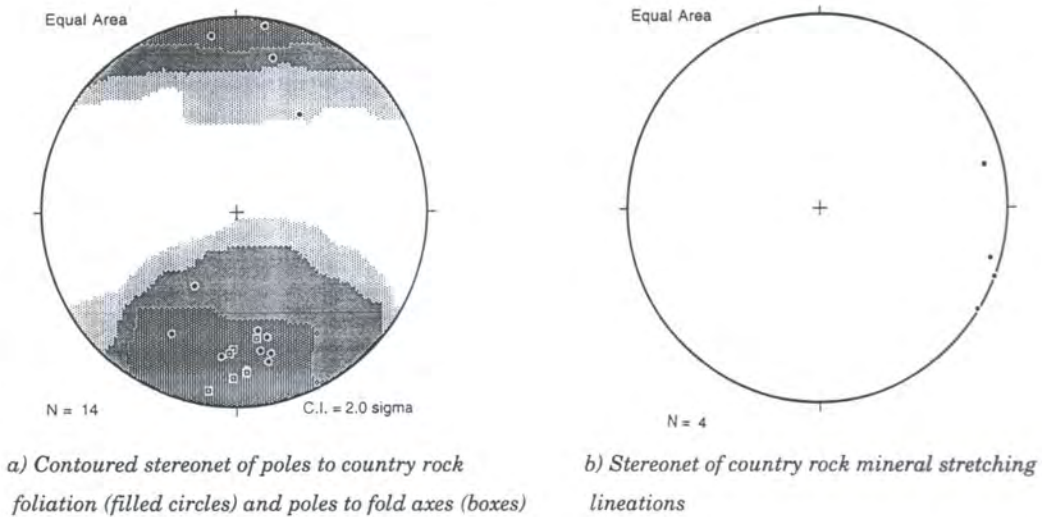


Figure 6.4 Country rock to the north of the Itapeti pluton

Southern area

The country rocks south of the Itapeti pluton consist of migmatitic gneisses, identical to those observed on the northern contact, but with a much lower intensity of deformation. As with the northern contact much of these rocks are overlain by Tertiary sediments. In general these gneisses are very poorly exposed, but where they can be observed show a $D_{n+1/2}$ fabric, which is locally deflected to become concordant with the granite contact. This fabric is interpreted to have formed in response to the intrusion of the magma body itself, and hence is a D_{n+3} fabric.



Stretching lineation in finely divided country rock gneiss close to the northern contact of the Itapeti pluton (GR 375774039)

Plate 6.1

6.2.3 Granite

The pluton has a poorly exposed contact with the surrounding country rocks, which corresponds to a sharp break in slope. In outcrop the intrusion is composed of three similar phases (Figure 6.2), which generally consist of: phenocrysts of potassium feldspar up to 3-4cm in length; set in a coarsely crystalline matrix of potassium feldspar, plagioclase feldspar, biotite (up to 20%) and quartz; which has been deformed during solid state deformation (Plate 6.2). Within each individual phase the granitic material is essentially homogeneous, although individual magma sheets of similar composition have been observed along the northern contact (GR 389374063) (Plate 6.3). The pluton preserves occasional microgranitoid enclaves which have been used as strain markers (Plate 6.3). Almost no microgranitoid dykes occur, unlike other plutons examined during this study.

The pluton fabric is east-west trending, sub-vertical and sub-parallel to the pluton long axis (Plate 6.4, Figure 6.1, Figure 6.5a). The fabric occasionally develops a sub-horizontal stretching lineation (Plate 6.5, Figure 6.5b) most commonly along the northern contact in the vicinity of the shear zone. In general magmatic deformation is confined to the southwestern corner, whereas solid state deformation occurs most intensely along the northern contact and becomes more pervasive on travelling eastwards along the pluton length.

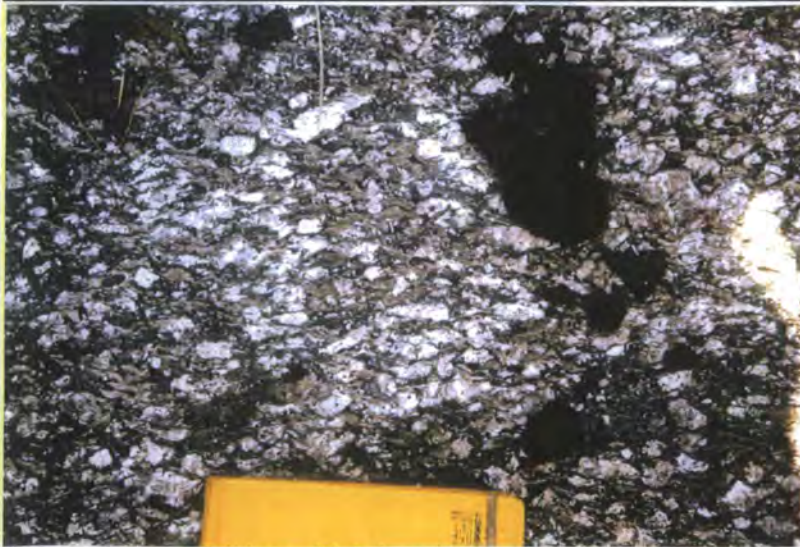


Plate 6.2

Solid state fabric from the Itapeti granite (GR 3760740929)

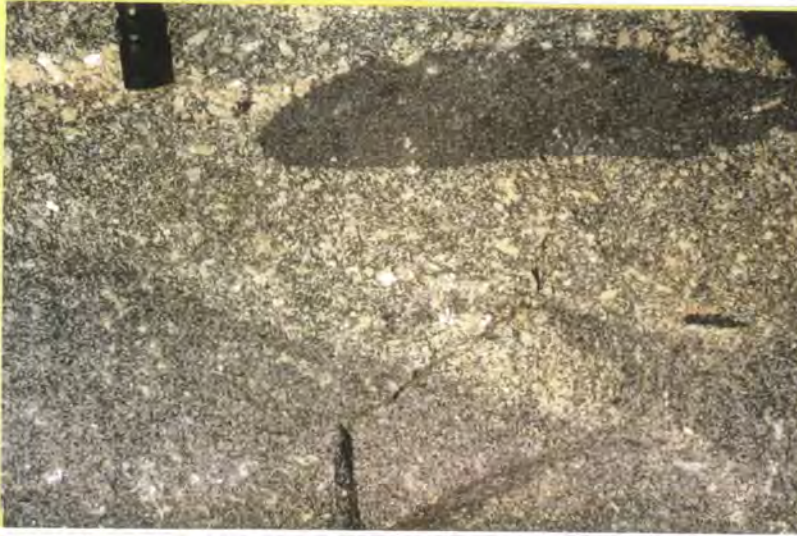
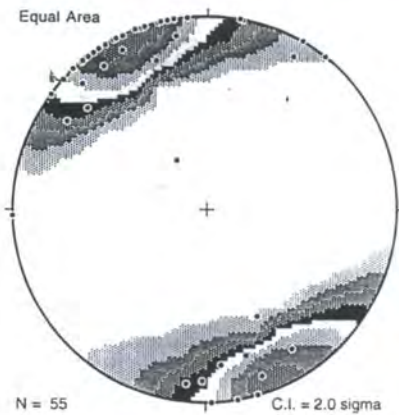
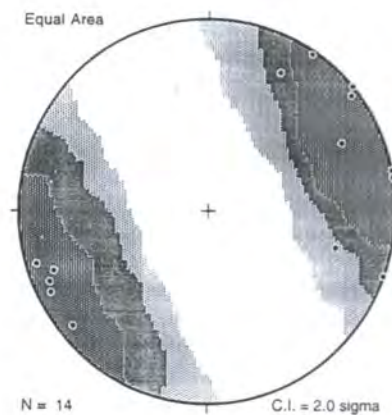


Plate 6.3

Sheeting of similar granite types along the northern contact (GR 389374063)



a) Contoured stereonet of poles to foliation from the Itapeti pluton



b) Contoured stereonet of stretching lineations from the Itapeti pluton

Figure 6.5

Solid state deformation

This deformation creates a strongly foliated, lineated, granitoid gneiss texture defined by ribbon quartz and augened feldspar phenocrysts (Plate 6.4). In thin section the fabric shows the development of recrystallised quartz, diffuse core and mantle feldspar fabrics, rarely formed feldspar internal subgrains and strongly deformed biotite crystals. Such fabrics can be ascribed to deformation occurring probably in excess of 500°C (Plate 6.6) (Passchier & Trouw 1996). The intensity of this fabric is strongly related to position within the pluton; it is very strong within 1km of the contact producing a granitoid gneiss texture; whereas in the pluton body as a whole it is much weaker and original crystal shapes are maintained. Traversing eastward across the pluton the solid state fabric becomes much more pervasive and increases in intensity.

Morais (1996) qualitatively details the deformation of the eastern extremities of the pluton and shows that the solid state deformation becomes much more intense in this area. Interpretation of these observations suggests that the shear zone was responsible for this solid state deformation and may be in part responsible for the extreme elongation of the pluton eastwards along strike. These are D_{n+4} fabrics overprinting an earlier magmatic fabric described below.



Plate 6.4 Solid state fabric from close to the northern contact of the Itapeti pluton (GR 385974059)

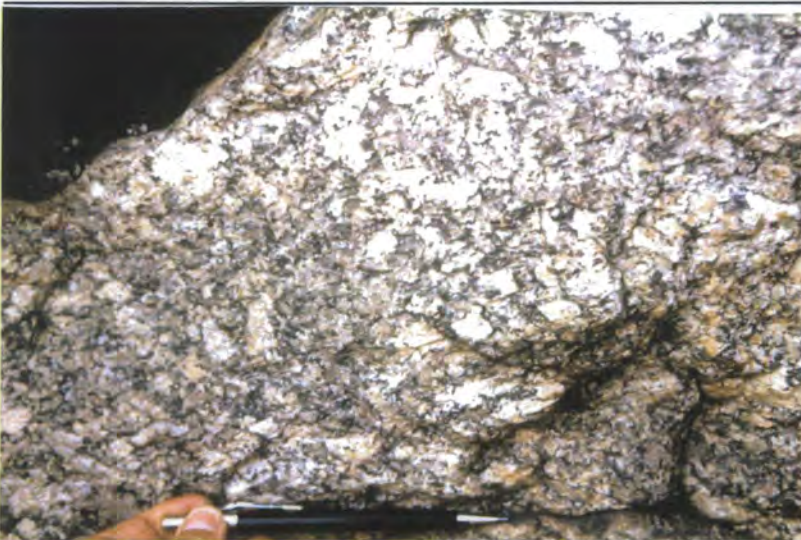


Plate 6.5 Sub-horizontal mineral stretching lineation from close to the northern contact of the Itapeti pluton (GR 375674032)

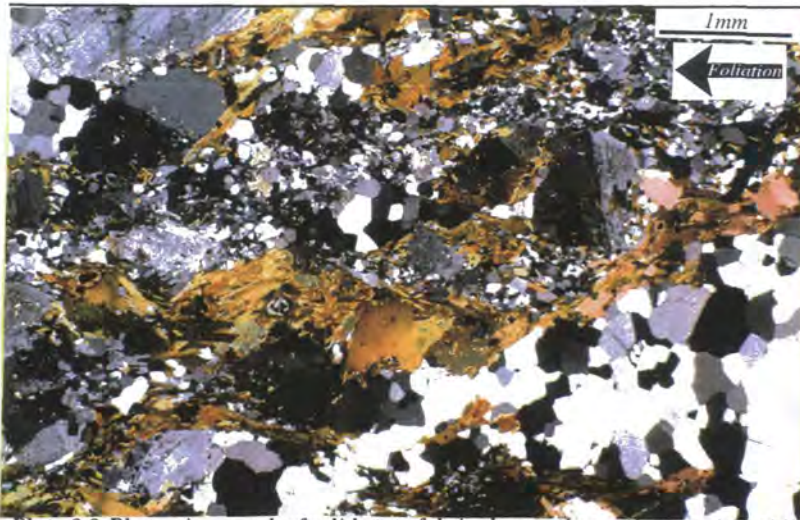


Plate 6.6 Photomicrograph of solid state fabric close to the northern contact of the Itapeti pluton (GR 376074029)

Magmatic state deformation

At the southwestern end of the pluton the outcrop displays a well-formed sub-vertical fabric, which is unlineated and sub-parallel to the previously described solid state fabric and defined by rectangular potassium feldspar phenocrysts within an apparently undeformed matrix of feldspar, quartz and biotite (Plate 6.7). The qualitative intensity of this fabric is much greater than is observed in any other pluton studied in this area. Examination of this fabric in thin section (Plate 6.8) shows individual feldspar crystals with almost pristine tilting fabrics, within a matrix of recrystallised quartz and undeformed rectangular biotites. This suggests that the fabric represents a strong, almost original, magmatic fabric only very weakly overprinted in the solid state and, consequently, are interpreted as magmatic D_{n+3} fabrics, whose orientation was controlled by the strike of and tectonic movements on, the existing D_{n+2} shear zone. After formation the magmatic fabric was generally overprinted by solid state D_{n+4} deformation associated with reactivation of the shear zone, but preserved in the parts of the pluton at greatest distance from this structure.



Plate 6.7 Magmatic fabric from close to the southern contact of the Itapeti pluton (GR 378074006)

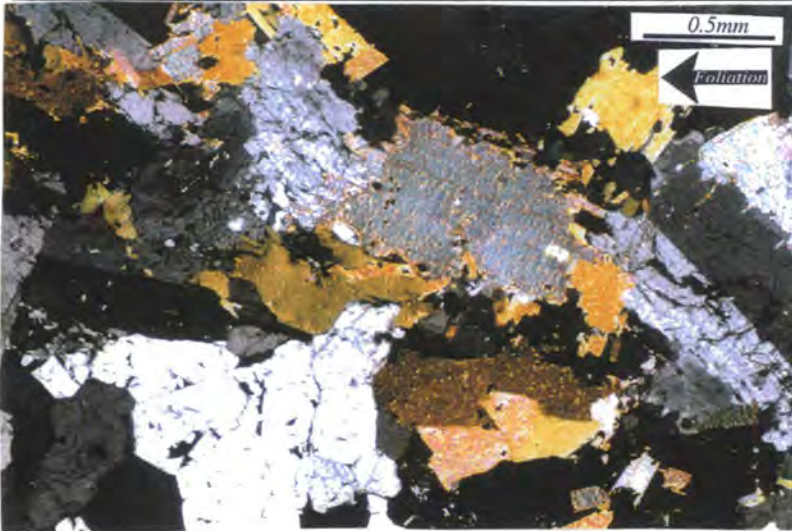


Plate 6.8 Photomicrograph of magmatic fabric from close to the southern contact of the Itapeti pluton (GR 378074006)

Other magmatic/deformation events

The Itapeti pluton does not appear to preserve any microgranitoid dykes, nor are there any identifiable contemporaneous granitoid stocks in the surrounding country rock. However, outcrops within the pluton occasionally preserve discrete mylonites which were formed within the pluton after the emplacement of the magma. These features are kinematically analysed in part 6.5.

6.2.4 Conclusions

The Itapeti pluton was emplaced along the southern boundary of an existing D_{n+2} intercontinental shear zone. As a consequence of its emplacement it formed a strong S-type magmatic foliation, which is preserved in the southwestern portion of the pluton. After cooling of the pluton (to $\sim 500^\circ\text{C}$), this early fabric was overprinted by similarly orientated solid state (LS-type) D_{n+3} fabric. This overprinting fabric is most intense in the vicinity of the Taxaquara shear zone. The country rock preserves the early D_{n+1} fabric in places but is generally overprinted by a D_{n+2} transpressional fabric (planar shear and partitioned pure shear folding), D_{n+3} emplacement related fabric and a D_{n+4} fabric sub-parallel to and reactivating earlier D_{n+2} structures. It is suggested that the high intensity of the solid state fabrics in the far east of the pluton indicates that there may have been intense D_{n+4} solid state elongation of the pluton eastwards along strike. The shear senses associated with each of these deformations will be detailed in part 6.4. After the development of these fabrics the pluton was overprinted by discrete mylonite shear zones.

6.3 Strain measurement

6.3.1 Introduction

In order to attempt to quantify the emplacement and overprinting strain which has affected the Itapeti pluton qualitative examination of the country rock and measurements of mafic enclaves and the Fry fabric strain from the granite itself have been made using the methods outlined in part 1.5. As a consequence of the absence of good exposures and mafic enclaves it has been necessary to collate statistically robust populations from diverse outcrops and therefore internal variations in strain may have been masked.

6.3.2 Granite

The results of quantitative strain measurements made within the pluton are outlined below. Individual populations have been collated within the internal boundaries set out in Figure 6.3.

Microgranitoid enclaves

Applying the methods detailed in part 1.5.1 to the Itapeti pluton produces the results shown in Figure 6.6, summarised in Table 6.1, and the raw data is given in Appendix 12. As with other plutons from the area vertically orientated and the foliation plane data is insufficient to make-up statistically robust populations, but the available data has been detailed in Table 6.1 for illustrative purposes.

Table 6.1 Summary table of microgranitoid enclave axial ratios from across the Itapeti pluton.

Localities	Orientations	Grid References	Mean axial ratio	Number of analysed enclaves	St. Dev	Smallest axial Ratio	Largest axial ratio	σ Log	% Variation in size
CY3, CZ4,	Horizontal	GR 38875740630, GR 38870740660	3.15	21	21.68	2.11	10.37	0.69	
CZ4	Foliation, long axes are sub-horizontal	GR 38870740660	2.83	3	0.30	2.60	3.18	0.09	10
CX7, DC2, DC3	Horizontal	GR 37630740256, GR 37800740050, GR 37780740060	4.20	65	1.82	1.25	10.00	0.90	43

These data indicate that the Itapeti pluton preserves similar microgranitoid enclave axial ratio strains to those that have been observed within the other studied plutons from this area (R_s 2.35-4.2): If this horizontal plane data represents a flattening strain it implies a shortening, perpendicular to the pluton long axis, of 45-60% and, a extension sub-parallel to the long axis of the pluton of 32-60%. Of particular interest is that the highest measured axial ratios occur in the centre of the pluton, away from the eastern portion where the highest solid state strains are recorded. However it should be

noted that the enclaves measured in this study are not from the most intensely deformed areas. This suggests, in accordance with observations made in other plutons (Chapters 4, 5), that the overprinting solid state strain was of a generally relatively low magnitude, despite altering the appearance of the granites themselves, and that therefore that the plutons preserve a predominance of magmatic state strain. Similarly, the emplacement of the granite in the Itapeti area induced a higher magnitude strain compared to the Atibaia, Imbiricu and Morro Azul plutons.

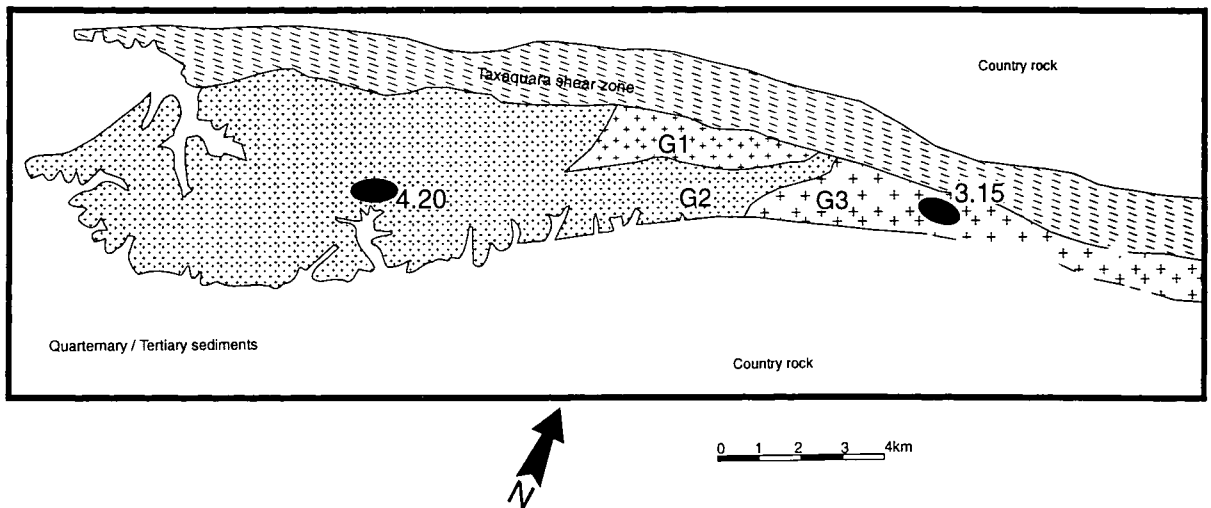


Figure 6.6 Horizontal plane microgranitoid enclaves axial ratios from the Itapeti pluton

Fry strain

The Itapeti pluton preserves few small crystals, either in thin section or hand specimen, and therefore outcrop photographs of phenocryst distributions provide the only way of measuring sufficient crystals to provide accurate determinations of Fry strain. In this study 12 determinations of Fry strain have been made, using digitised tracings of horizontal and vertical outcrop photographs, which have been processed using the method outlined in part 1.5.2. Table 6.2 is a summary table of the data and Figure 6.7 shows a spatial plot of the results for the horizontal plane.

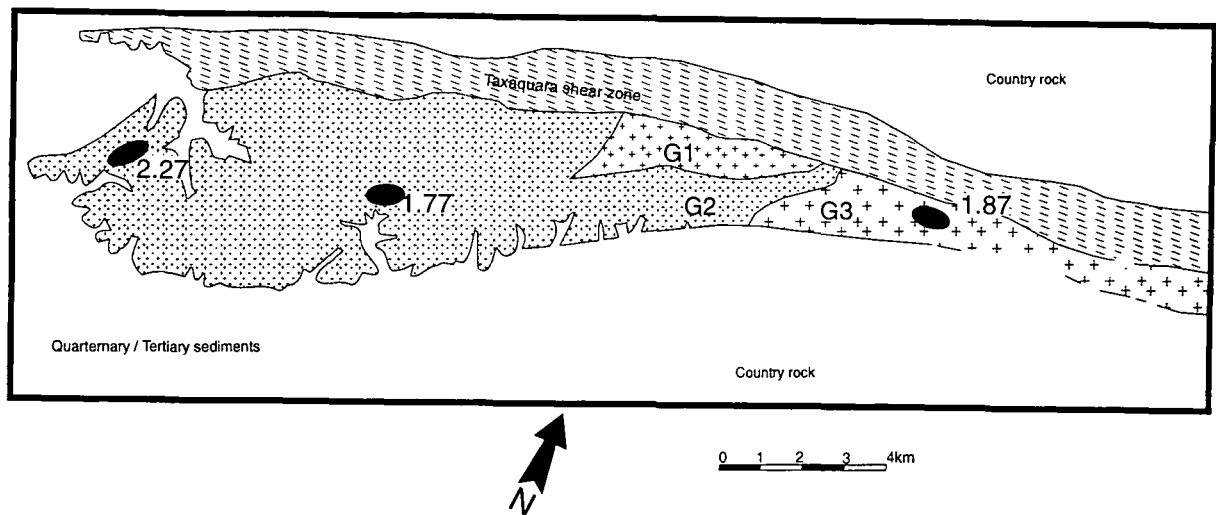


Figure 6.7 Average Fry strains from the Itapeti pluton

Table 6.2 Summary table of Fry strain measurements from the Itapeti pluton
(Division of pluton as detailed in Figure 9.3)

Locality	Grid References	Orientation	Fry strain	Number of points	St. Dev.	Log K-value
Western area						
DC5	GR 370374006	Horiz.	2.27	117		
DC5	GR 370374006	Vert.	1.67	88		0.60
Central area						
CX7	GR 376074029	Horiz.	1.83	73		
DC3	GR 378074006	Horiz.	1.87	108		
DC3	GR 378074006	Horiz.	1.99	72		
DC3	GR 378074006	Horiz.	1.4	70		
Average		Horiz	1.77		0.22	
CX5	GR 375674015	Vert.	2.41	89		0.54
Eastern area						
CY2	GR 389674062	Horiz.	1.70	59		
CY3	GR 389374063	Horiz.	2.07	70		
CY3	GR 389374063	Horiz.	2.07	77		
CZ3	GR 385974059	Horiz.	1.65	70		
Average			1.87		0.20	
CY3	GR 389374063	Vert.	1.96	68		0.08

These data show much lower values for the ellipticity of the Fry strain ellipse than the microgranitoid enclave axial ratio strain described in the previous section. Most remarkably these data show an homogeneity of finite strain across the pluton which, similarly to the microgranitoid enclave strain, has not been increased in magnitude by proximity to the increased solid state strain at the eastern end of the pluton. Calculating K-values from these data it is possible to suggest that these data demonstrate a flattening type strain, but lack of additional data in this orientation makes further corroboration of this statement difficult.

6.3.3 Country rock

As with most of the other studied plutons there is inadequate exposure of the country rock around the Itapeti pluton to enable a quantitative study of the strain preserved in the vicinity of the granite itself. It is merely possible to make the statements that:

1. In the *Northern area* the country rocks were intensely strained during a strong ductile deformation which produced the finely foliated fabric and the associated sub-horizontal lineation, the deformation was most intense in the rocks closest to the pluton contact.
2. In the *Southern area* the country rocks were not intensely deformed, but underwent deflection/deformation close to the contact, which was of sufficient intensity to produce a recognisable fabric sub-parallel to the pluton contact for approximately 300m.
3. If this fabric is assumed to have been deflected by rotation from a regional dip of 65° southwards (Theodorovicz *et al* 1990) to become sub-parallel to the pluton contact then using Equation 2.4 an estimate can be made of the finite strain preserved within the country rock. This calculation suggests a strain ellipsoid axial ratio of $R_s \sim 5.3$, which equivalent to a local shortening (assuming flattening strain) of 65% that could have accommodated up to 600m of the space required for the intrusion of the granite in this area.

6.3.4 Conclusions

The data examined above demonstrates that:

1. The Itapeti pluton preserves an homogenous strain that is preserved as a consequence of emplacement rather than overprinting solid state deformation.
2. This deformation was induced as a consequence of an axis parallel extension/axis perpendicular shortening during emplacement of the magma, similar to that observed in each of the previously described plutons from the RPSSB. The observation of individual magma sheets along the northern contact suggests that single undeformed sheets may have experienced this along axis extension during their homogenisation, after injection, with the surrounding granitic material.
3. The finite strain within the pluton could possibly have a strong horizontal plane strain component ($K > 0$). This may be a consequence of the tectonics responsible for emplacement.
4. The magnitude of the Fry strain is relatively low ($R_s < 2$) compared with values determined from the axial ratio of microgranitoid enclaves ($R_s \sim 2.5-4.0$). This may be a consequence of a number of factors which are discussed in part 8.5.
5. Estimates of country rock strain suggest that 600m of space could have been created by the pluton itself.

6.4 Shear senses

6.4.1 Introduction

Using the criteria laid down in part 1.4, shear senses have been determined from a number of localities within the country rock and the granite during magmatic state and overprinting solid state deformation. The modes of occurrence of these fabrics are detailed below:

6.4.2 Country rock

The country rock north of the pluton, despite being intensely deformed, has few recognisable shear sense fabrics. Those that have been observed show a dextral sense of shear associated with a low angle lineation, which demonstrates the plane strain nature of the imposed deformation. This interpretation is consistent with the regional interpretation of Theodorovicz *et al* (1990). To the south of the pluton the country rock appears to show no evidence for simple shear of any sort along the granite contact. In this area the country rock has been deformed 'passively' in response to the emplacement of the magma.

6.4.3 Granite

In contrast to the country rock surrounding the pluton the granite preserves well developed shear sense fabrics formed in the solid and magmatic state.

Solid state fabrics

Associated with the overprinting solid state deformation there are abundant solid state shear sense indicators such as: S-C fabrics, asymmetric phenocrysts, crystal rotation etc. (Plate 6.9, Figure 6.8). All of these indicators are associated with a dextral solid state shear sense.



Asymmetric phenocrysts and S-C fabrics associated with the solid state deformation of the Itapeti pluton (GR 387274062)

Plate 6.9

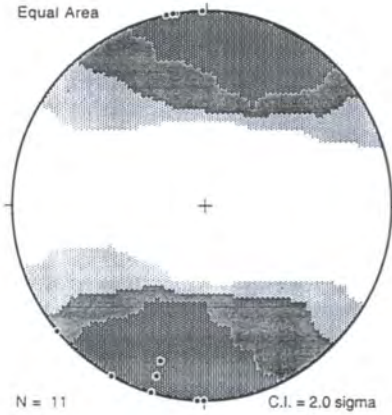


Figure 6.8 Contoured stereonet of poles to the C-planes of S-C fabrics (compare with Figure 6.5)

Magmatic state fabrics

As described in part 6.2, the southwestern end of the pluton preserves an almost pristine magmatic fabric. In outcrop it is possible to observe bi-modal fabrics and tiled porphyroclast relationships, which indicate the preservation of a sinistral magmatic state shear sense (Plate 6.10, Figure 6.9). The vertical plane magmatic shear sense is more difficult to determine (due to lack of outcrop) but examination of thin sections suggests a 'pluton centre up' sense of shear predominates in the areas it can be identified. This is consistent with the movement of material upwards and outwards from a magma supply zone to the north of these outcrops.

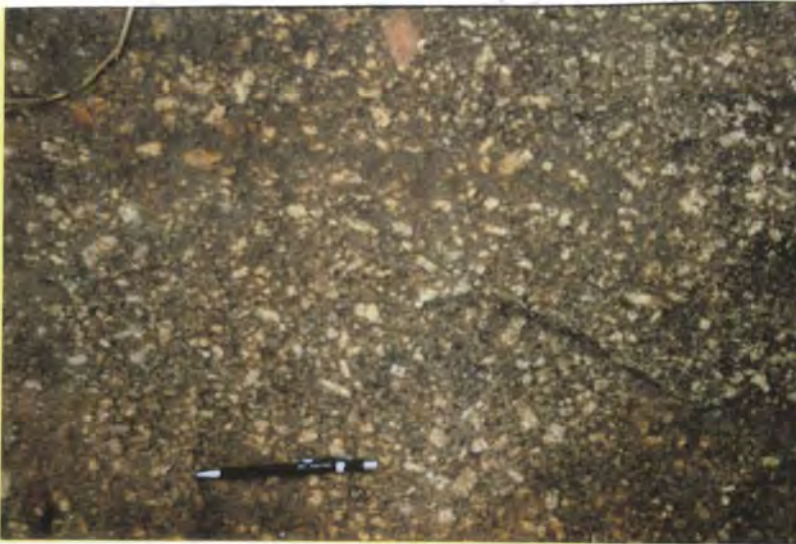


Plate 6.10 Magmatic state fabric from the Itapeti pluton (GR 378074006)

6.4.4 Conclusions

An examination of shear sense data from across the Itapeti pluton shows that in the magmatic state there was the development of a strong sinistral and centre up shear sense fabric, D_{n+3} (Figure 6.9). This sense of shear is consistent with 'central' magma supply into a dilatational zone. Later this fabric was strongly overprinted by a D_{n+4} lower temperature, ductile, heterogeneous, solid state, horizontal dextral shear (Figure 6.9).

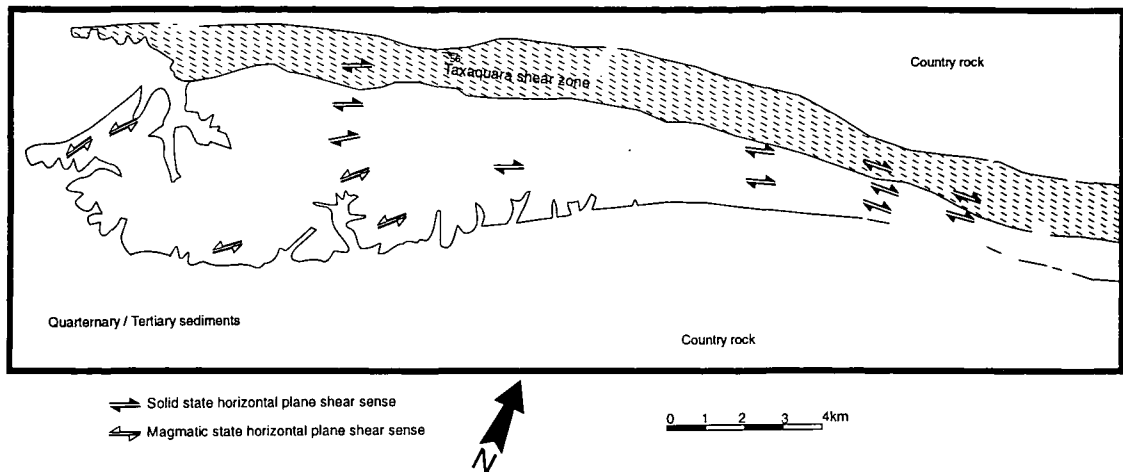


Figure 6.9 Composite map of solid state and magmatic state shear senses of the Itapeti pluton

6.5 Overprinting discrete mylonitic shear zones

6.5.1 Introduction

Overprinting both the solid state fabric and the earlier magmatic state fabric are discrete cm-scale mylonitic shear zones, which were detailed from various localities across the pluton. These fabrics are identical in outcrop form and style to those observed in other plutons in this area and are similarly interpreted (see part 4.7.2). Representative populations have been formed using the delimited areas defined by Figure 6.3. Their orientations and associated dominant shear sense fabrics are shown in Figures 6.10, 6.11 and are described below.

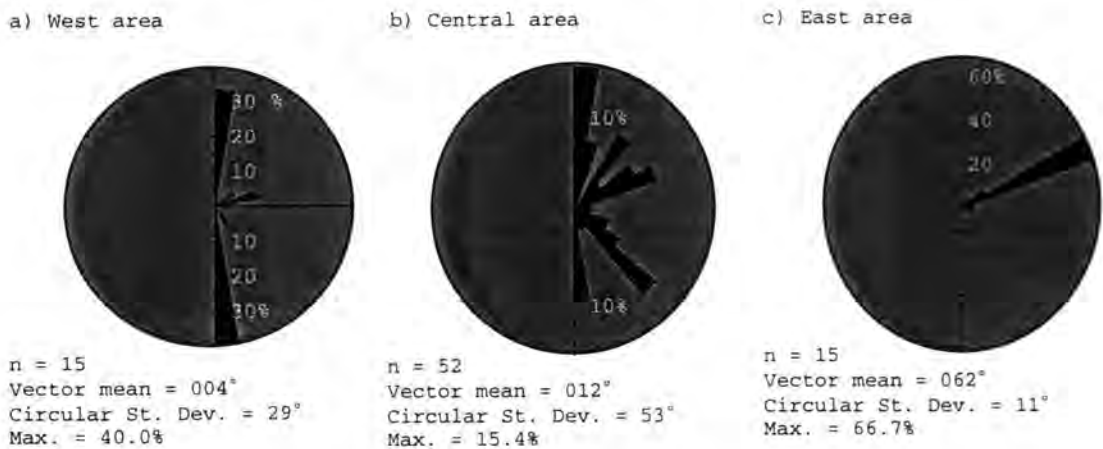


Figure 6.10 Rose diagrams showing mylonite orientations from the Itapeti pluton

6.5.2 Results

Western area

Mylonites from this area show a single dominant population orientated between 350° and 010° (n=15) (Figure 6.10a), of which the majority display sinistral shear sense fabrics. These data suggest an orientation of ~315° for σ_1 of and of 045° for σ_3 (Figure 6.11a, b)

Central area

The large number of outcrops in the central area preserve a large population of associated mylonites (n=52). These demonstrate a complex pattern of peaks on the Rose diagram (Figure 6.10b) with the dominant peak at 350°-010°, a second peak at 130°-140° and a broad spread of data between 010° and 070°. Associated with these data are shear senses which are dominantly sinistral between 000° and 060° and dextral between 120° and 150°.

These data are interpreted to represent a conjugate set which was dominantly sinistral at $\sim 020^\circ$ and dextral at 135° . In such a scenario σ_1 would be orientated at approximately 347° and σ_3 at approximately 077° (Figure 6.11a, b)

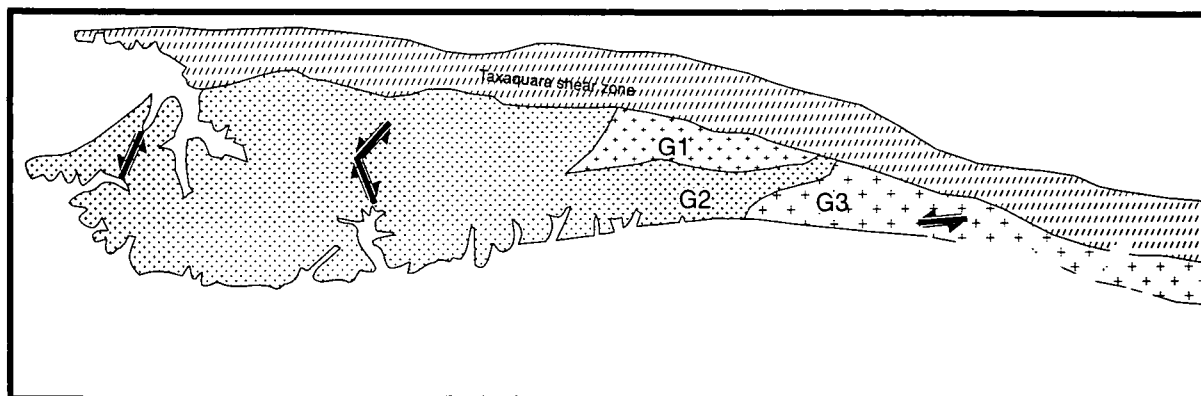
Eastern area

The mylonites from the eastern area define a single, well-constrained population peak ($n=15$) at 060° - 070° and a vector mean at 062° (Figure 6.10b). The shear senses associated with this population are entirely sinistral. These data can be interpreted as being formed while the principle compressive stress (σ_1) was orientated at 017° and minimum compressive stress (σ_3) at 107° (Figure 6.11a, b).

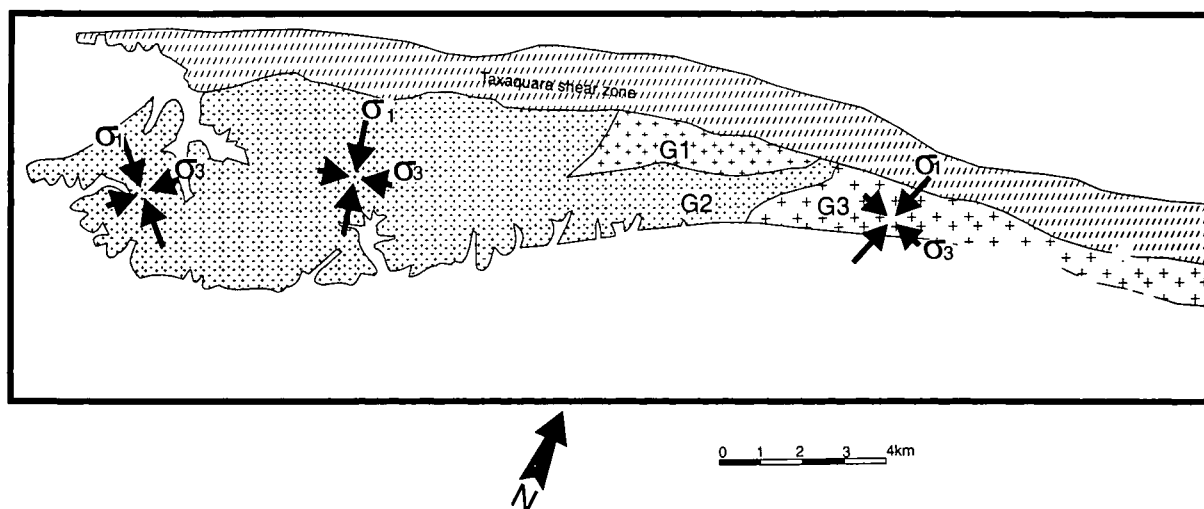
6.4.3 Conclusion and discussion

Interpretation of these data leads to a number of conclusions that are illustrated below:

1. The mylonites suggest an orientation of between north-west and north-northeast for the principal compressive stress σ_1 (Figure 6.11). An orientation which is approximately perpendicular to the Taxaquara shear zone.
2. In contrast to the data collected from the Atibaia pluton, there is generally only a single dominant population of mylonites. The reason for this is unclear.
3. In the only area where a conjugate array is observed (Central area) the principal stress is seen to bisect the minor angle (in contrast to Atibaia and Morro Azul/Imbiricu plutons where it bisects the major angle). After examining a number of possible hypotheses for such a situation, discussed by Twiss & Moores (1993), it was concluded that an environment where the intermediate principle stress is reduced ($\sigma_2 \rightarrow \sigma_3$) would be most appropriate in this case.



a) Average principal mylonite orientations within the Itapeti pluton



b) Inferred principal compressive stress orientations within the Itapeti pluton

Figure 6.11

6.6 Emplacement and deformation

The Itapeti pluton is not as well exposed as other granites that have been examined in the RPSSB but, nevertheless, it has been possible to identify fabrics within the pluton and surrounding rocks which elucidate its emplacement history. This is broadly similar to the other plutons detailed in Chapters 4 and 5.

6.6.1 A sequence of events

1. **Initial scenario** - The Itapeti area was deformed during the formation of the regional southeast dipping, low-angle D_{n+1} fabric, in the early stages of the Brasiliano orogeny. This fabric was later overprinted by the Taxaquara continental scale D_{n+2} ductile shear zone which has an east-west trend in this area.
2. **Initiation of emplacement** - Preserved regional deformation indicators suggest that these early phases formed in response to an east-west directed, regional, dextral transpression, which produced the dextral shear zones and flattening fabrics (upright isoclinal folds) in the Itapeti area. However, the preserved fabrics within the pluton show none of the fabrics consistent with emplacement into a compressional setting (part 1.6.3). The pluton fabrics (homogenous strain, sinistral centre-up shear senses) suggest that at least some component of tectonic reversal was associated with the intrusion and therefore, it is concluded that the injection of magma was initiated by sheeting of granitoid magma from depth along an existing tectonic feature (the Taxaquara shear zone). Once magma ascent had begun the inferred regional tectonic framework producing sinistral (i.e. extensional) fabrics facilitated the intrusion of additional magma into this zone (Figure 6.12).
3. **Continued magma ascent and emplacement** - Magma ascent would have continued for as long as the magma had sufficient internal fluid pressure to overcome the imposed regional stresses (Hutton 1997a, b). The emplacement related deformation within and without the pluton suggests that: i) the pluton created a component of its own space, but the comparative narrowness of the deformation zone suggests that this may not have been significant; ii) during homogenisation of the magma into the main pluton body it underwent a degree of along axis extension/axis perpendicular shortening, forming the magmatic pluton fabric and associated shear senses; iii) this fabric formation may have had a weak plane strain ($K \rightarrow 1$); and iv) the southern contact of the pluton was relatively passive with relation to the regional deformation.
4. **Granitic magma source** - This study gives no clues as to the source of the magma for the pluton. However the work of Morais (1995) suggested that the granite was may have formed through the fusion of an evolved lower crustal protolith with a small additional mantle melt contribution.

5. **Post emplacement tectonic activity** - After the emplacement and cooling of the magma the pluton was overprinted by a D_{n+4} horizontal planar dextral reactivation of the Taxaquara shear zone which resulted in solid state deformation of the earlier fabric: This is concentrated towards the northern contact with the shear zone itself. Deformation occurred at a higher temperature ($>500^{\circ}\text{C}$) than that observed in other plutons from this region, which suggests either a later time of intrusion (i.e. magma was still hot during deformation) or that metamorphic temperatures were locally higher in this area.
6. **Formation of discrete mylonites** - Overprinting both the magmatic and solid state fabrics are discrete mylonites, which formed at a lower temperature than the main fabric. Their orientations suggest that they formed in response to a local approximately north-south orientated, compression/east-west extension.

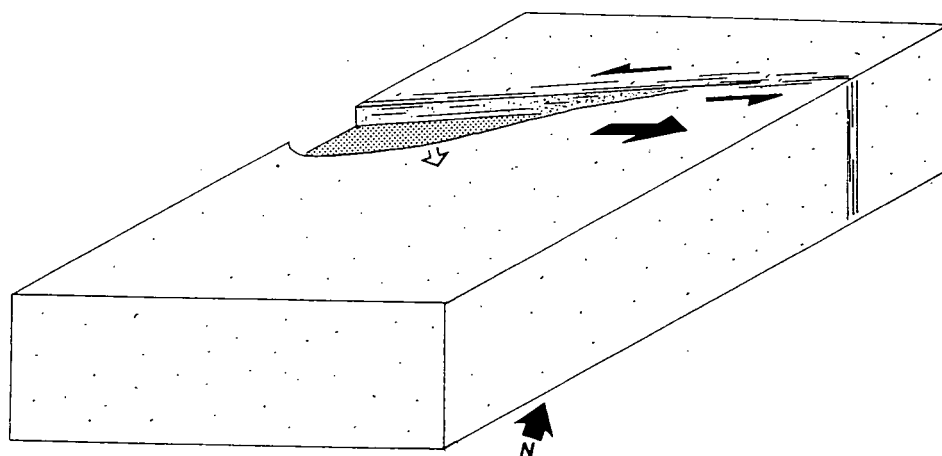


Figure 6.12 A model for the emplacement of the Itapeti pluton

6.6.2 The shape of the pluton

The pluton is strongly elongate along strike. Broadly its shape is consistent with an east-west orientated extension, resulting in the opening of a transtensional pull-apart 'fracture' which propagated eastwards, forming sinistral shear fabrics and allowing the injection and homogenisation of individual granite sheets. The emplacement strains preserved within the pluton demonstrate along axis extension of 32-60% (assuming approximately flattening strain) which, if the pluton is estimated to have a pre-solid state deformation length of 20km, suggests an injection conduit length of 12-15km.

It must be pointed out that such a pluton shape could be formed as a consequence of north-south directed extension, and it is difficult to distinguish between these two

scenarios. However during north-south directed extension (i.e. axis perpendicular), magmatic shear fabrics should be weak, and possibly dextral, and the foliation should be orientated along the pluton axis. The key piece of evidence for east-west extension lies in the strong intensity (compared to other studied plutons in this area) of the magmatic shear fabrics: an east-west extension would require a principal extension direction orientated only slightly southwards of the pluton long axis, which would be more inclined to produce simple shear than pure shear fabrics (Figure 6.13). However, the internal fabrics (foliation, orientations of strain marker etc.) were not entirely under tectonic control and formed in orientations sub-parallel to the pluton axis, indicating that internal magma forces were dominant during emplacement. Therefore, in concordance with the studied plutons from the remainder of the RPSSB, the Itapeti pluton is interpreted as forming during east-west directed extension.

Additionally, the pluton is remarkably elongated along strike: Hasui *et al* (1978) describe magmatic material occurring up to 40km along the strike of the main pluton. This could occur in response to eastward migration of intruding dykes during emplacement or, alternatively, as the result of intense stretching of the granite in the vicinity of the Taxaquara shear zone. From observations in this eastern area it is suggested that this 'tail' formed in response to dextral elongation of pluton during overprinting solid state deformation.

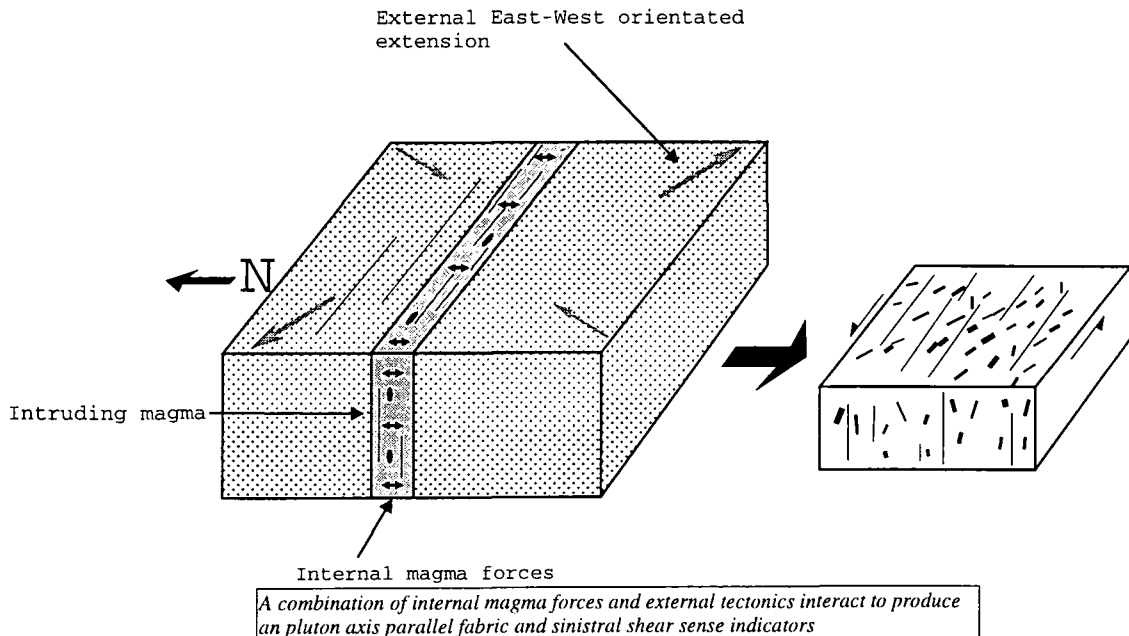


Figure 6.13 Production of sinistral shear fabrics during intrusion of the Itapeti pluton

6.7 Conclusions and discussion

The Itapeti pluton preserves very similar deformation and intrusion characteristics to those observed in other plutons from the RPSSB. As a consequence it is concluded that it was intruded during a similar east-west orientated, extension event which occurred during the dextrally transpressive Brasiliano orogeny. Of particular interest are:

1. **Sinistral shear fabrics** - These are strong bi-modal fabrics in outcrops which preserve the early magmatic sinistral shear sense fabric in the horizontal plane and pluton centre-up fabrics in the vertical plane. This data is entirely consistent with the model of east-west orientated extension developed from observations in other plutons.
2. **Internal strain fabric** - The strain within the pluton does not show any variation with intensity of solid state fabric and therefore it is suggested that the strain preserved in the majority of the pluton is primarily an emplacement related strain, associated with along axis extension/axis perpendicular shortening. Fry strains and enclave axial ratios suggest that the strain may, in addition, have a weak linear component ($K > 0$) which is ascribed to intrusion into a narrow sub-east-west trending pull-apart during east-west extension.
3. **Overprinting fabric** - The pluton has had its early magmatic fabric heterogeneously overprinted by an horizontal planar dextral shear, which is most prominent along the northern contact of the pluton and occurred at higher temperatures than the solid state deformation observed in other plutons.
4. **Mylonite orientations** - The orientation of the mylonites in this area appear to suggest that during their formation they were subject to a north-south orientated compression, in contrast to the east-west orientated compression observed in other areas.

Chapter 7

The tectonic evolution of the RPSSB

7.1 Introduction

7.1.1 Preamble

The purpose of this chapter is to bring together each of the strands of evidence elucidated above, to explain the pre-, syn- and post-emplacement deformation of each of the studied plutons. Then using this evidence, a general model for the Brasiliano and later tectonic evolution of the RPSSB is developed to attempt to explain the intrusion dynamics of a number of other coeval and possibly consanguineous granitoid plutons.

7.1.2 Background

Each of the plutons and their settings (described in the Chapters 4-6) have a very similar structural and intrusive heritage consisting of:

1. **Pre-existing country rock fabric** - A generally low to moderate southeasterly dipping fabric produced as a consequence of D_{n+1} thrusting which has been locally steepened to high or moderate dips during D_{n+2} transpression. S_{n+1} was the predominant regional fabric until at least 609Ma, when migmatites were injected sub-parallel to the foliation plane.
2. **Strike-slip shear zones** - The country rock fabric has been cross-cut by numerous continental scale, sub-vertical, strike-slip shear zones which overprint and deflect the regional fabric. Their formation was associated with regional scale dextral transpression and re-orientation of the regional fabric (Ebert & Hasui 1992). This fabric may have been formed as early as 710Ma (metamorphic age of the transpressional Santa Isabel complex), but was certainly in existence after 650 Ma (age of granitoids sub-parallel to the low-angle fabric, but extensively overprinted by strike-slip deformation Ebert *et al* 1996).
3. **Intrusion of the granites** - Each of the studied granitoid plutons have low internal strain, but have been emplaced in locations which would have been in local compression during the dextral transpression which affected this region. Each of the granites was emplacement into an extensional pull-apart, spatially related to one of the major shear zones, during a phase of east-west directed extension. The age of the studied plutons is between 623-525Ma, although data from other plutons in this area suggests an average regional age of approximately 610-570Ma for plutons of this type (Brito Neves & Cordani 1991, Tassinari 1988).

4. **Emplacement of microgranitoid dykes** - After the plutons were emplaced and had cooled such that they were cohesive enough to undergo 'brittle' fracture, cm-scale microgranitoid dykes were injected into the pluton. Their orientation demonstrates continued extension orthogonal to the local pluton contact. No absolute age determinations on these features have been made.
5. **Overprinting fabric** - After the intrusion of the granites, they and their surrounding rocks were overprinted by a dextral, plane strain reactivation of the existing shear zones. This occurred when the plutons had cooled to ~300°C in the Atibaia area, and to 500°C in the Itapeti area. The absolute age of this deformation is unknown.
6. **Discrete mylonites** - Overprinting each of the earlier fabrics are discrete, conjugate cm-scale mylonites. Kinematic analysis of each of these populations generally shows a maximum principle stress orientated orthogonal to the local shear zone. These features may either demonstrate a discrete continuation of the regional overprinting dextral deformation, or may be related to a reactivation of major structures associated with the opening of the Atlantic Ocean during the Mesozoic.

7.2 Intrusion of the studied granites

7.2.1 Genesis of the magma

While the fieldwork does not directly describe the genesis of the magma some general inferences can be made from the available geochemical data, the outcrop features and the petrographic composition.

Composition of the melt zone

Each of the plutons studied in this area was emplaced in the midcrust (15-18km) (Ebert *et al* 1996) and shows an isotopic signature consistent with derivation from melting of material, which had been highly fractionated by previous melting and crystallisation events ($^{87}\text{Sr}/^{86}\text{Sr}_i \approx 0.71$ (Tassinari 1988, Melhem 1995, *unpublished data*). This has been interpreted to suggest derivation from the anatexis and fractional crystallisation of an upper crustal protolith, although ϵ_{Nd} values from the Morro Azul pluton (*unpublished data*) suggest that there may have been a component of more primitive material. Such data is consistent with the petrographic composition of the plutons, but the presence of mafic dykes and mafic stratified xenoliths demonstrates that there was at least some, possibly mantle derived material, associated with magma genesis. Additionally Melhem (1995) and Morais (1995), using zircon topology techniques, showed that the magma was anhydrous, forming in a zone of complete magma homogeneity at a temperature of approximately 850°C. Such features are exactly consistent with the anhydrous granulite facies melt zone envisaged by Petford (1995) for the production of granite melt.

Size of the melt zone

Each of the plutons is relatively homogeneous within itself, suggesting that a large quantity of similar melt was present in the melt zone. The production of two petrographically similar plutons (Imbiricu and Morro Azul plutons) whose conduits were separated by a minimum of 5km demonstrates that the melt zone was laterally continuous. Similarly the presence of a suite of similar and comparatively coeval plutons across the region may suggest the presence of a cognate melt horizon within the lower crust.

Evolution of magma production

Examining the regional magmatic evolution of this area shows that there was the injection of subduction I-type magmas at ~650Ma (Brito Neves & Cordani 1991) intimately associated with the low-angle fabric, before the emplacement of migmatites at ~610Ma similarly associated with the low-angle fabric, and followed by the emplacement of the studied plutons. It is possible to suggest that: i) the low-angle sheeted complexes represented the last expression of westward directed subduction; and ii) the migmatites represented a component of wet-melting; which slightly pre-dates, or is synchronous with dry melting in the lower crust forming magma for the studied plutons. Additionally the bulk petrographic similarity of the multi-intrusive phase plutons and the later

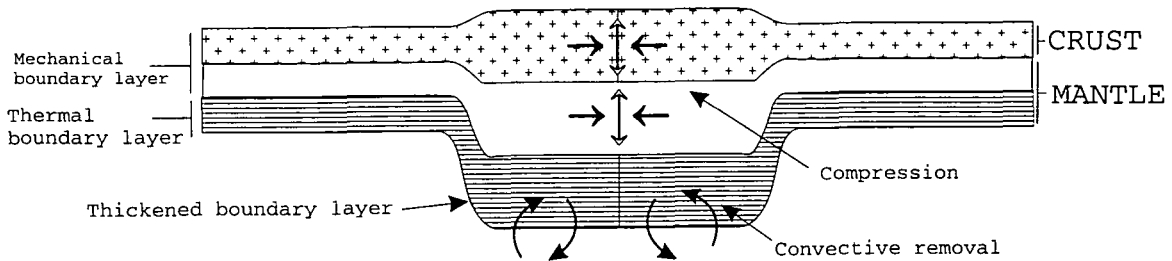
microgranitoid dykes, demonstrates that there may have been a widespread melt horizon and continued magma production after the main emplacement event.

Reasons for crustal anatexis

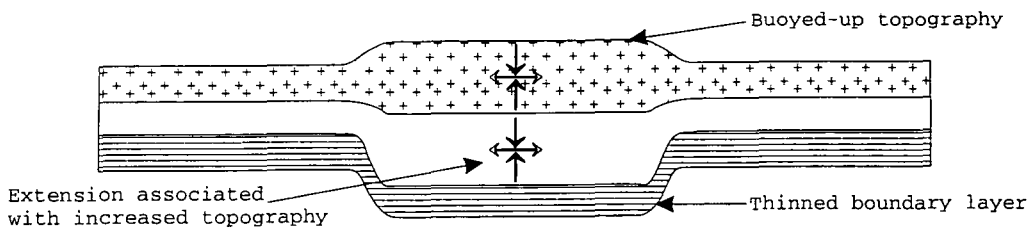
Melting to form granitic melt can be envisaged as occurring in four principal tectonic environments (modified after Pitcher 1993):

1. **Extension and decompression** - During extension there is a thinning of the crust, and the associated adiabatic decompression of the mantle and crust, introducing an increased crustal heat flow. This high temperature, comparatively low pressure melting, results in bimodal volcanism, consisting of mafic intrusions and volatile rich alkalic granites. The regional tectonics and features of the studied plutons suggest that this process is not occurring within the study area.
2. **Subduction related** - The release of water from subducting oceanic crust triggers melting within both the mantle and the lower crust. The resulting granitoids are Cordilleran I-types, commonly tonalites to granodiorites, emplaced into extensional or contractional tectonic environments. The low-angle plutons, in the study area, display these characteristics (Brito Neves & Cordani 1991), whereas the studied plutons are more evolved.
3. **Crustal thickening** - Continental collision and associated crustal thickening increases the volume of radiogenic crust. As such, the release of energy associated with radiogenic decay may be sufficient to induce melting within the crustal pile. This melting will be characterised by the re-melting and fractional crystallisation of already evolved material and the lack of a primitive component, and could produce granitoids of a granitic to alkali granite composition, emplaced into any tectonic setting. It is possible that the studied plutons were sourced in this way.
4. **Orogenic delamination** - When two continental blocks collide there is extensive crustal thickening during the development of a thickened lithospheric root, which will produce a mountain belt limited to approximately 3km in vertical height above sea level (Houseman *et al* 1981, Dewey 1988)(Figure 7.1a). Such a thickened lithospheric root is dynamically unstable and mantle convection will act to remove this 'boundary layer' supplying hot, convecting, 'fertile' asthenospheric mantle to the base of the crust (Houseman *et al* 1981, Dewey 1988) (Figure 7.1b). This hot material buoys up the orogenic belt, increasing vertical elevation, but also increases the heat flow at depth. This increase in heat flow, in combination with the decompression melting of 'fertile' mantle, would introduce quantities of basic melt into the lower crust. As such this would induce crustal anatexis (through higher heat flow) and the production of abundant granitoid melt of a granitic to alkali granite composition. The production of crustal melt, associated with a minor more primitive component, and emplacement during regional extension is highly consistent with the features observed in the study area.

Therefore, although a specific study of the source of the granitoids has not been carried out, it is most likely that the granitoid melt formed in a Type 3 of 4 environment. Type 1 or 2 appear unlikely on compositional and tectonic grounds. It is the authors personal opinion that a Type 4 origin is most probable for the studied plutons.



a) Double thickness continental lithosphere produced during continental collision (after England & Houseman 1988)



b) Convective removal of the lithospheric root producing extension and uplift (after England & Houseman 1988)
Figure 7.1

Expulsion of melt

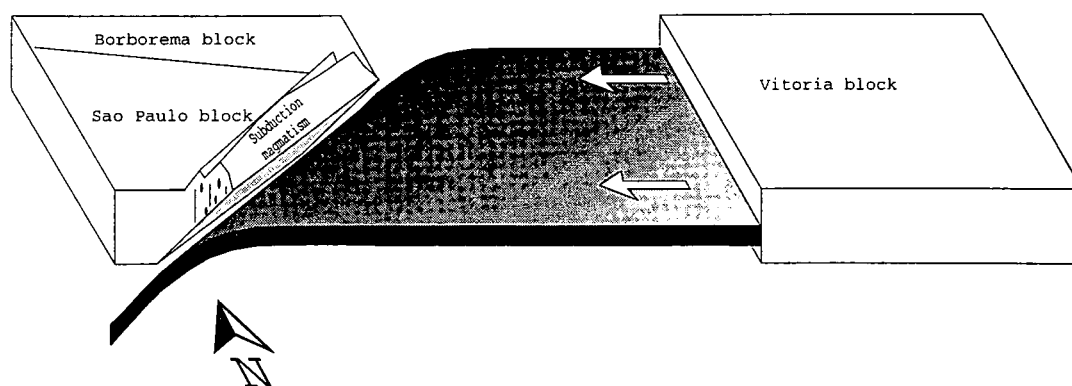
The creation of small quantities of melt within the lower crust and the lithospheric mantle is envisaged as a semi-continuous process (McKenzie & Bickle 1988) and the volume increase induced by such melting (Clemens & Mawer 1992) could be contained within the lower crust. Large scale melt production, as required for batholith formation, would result in a very large volume increase in the lower crust (up to 18%, under the dry melting envisaged by Clemens & Mawer 1992). Such a volume increase could induce local dynamic (overpressuring) and buoyancy instabilities within the crust. Additionally tectonic stresses could pressurise the magma. For example during extensional collapse orogenic convergence could occur at lower crustal levels, but with extension occurring contemporaneously in the mid to upper crust. Any crustal discontinuity that penetrates this zone (e.g. shear zone, crustal fracture) will act as a conduit for magma from depth (overpressured) towards the surface (unpressured) (Clemens & Mawer 1992, Petford *et al* 1993, Hutton 1997a,b). This process will continue until the mechanical instability is removed.

7.2.2 Tectonics associated with emplacement

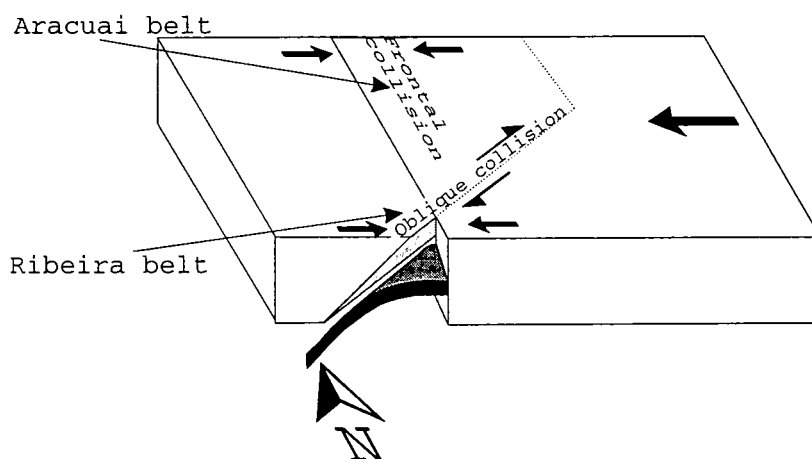
Each of the plutons that has been studied has an association with the tectonic structures in the surrounding rocks. In the following section this association is examined and the possible dynamics required for the formation of each type of fabric discussed.

Brasiliano - low angle fabric

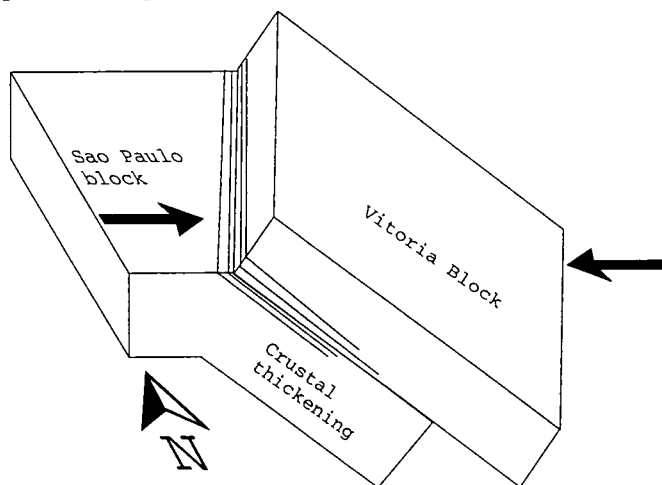
As described by a number of other authors (Cunningham *et al* 1996, Ebert *et al* 1996, Ebert & Hasui *in press*, Vauchez *et al* 1994) the D_{n+1} fabric was induced by east-west directed collision along a northeast-southwest trending continental margin (Figure 7.2a,b,c), which resulted in oblique collision in the Aracuai belt, and dextrally transpressive collision in the Ribeira belt and more specifically the RPSSB. This collision can be envisaged using a quasi-Andersonian model where the forces due to convergence (F_{conv}), lateral confinement (F_{lat}) and topography (F_{top}) apply stresses upon the orogenic belt (σ_{conv} , σ_{lat} , σ_{top}) that interact to form three orthogonal principal stresses (σ_1 , σ_2 , σ_3). Therefore applying this simplistic model to the initial collision, (Figure 7.3a) σ_1 is orientated sub-horizontally east-west (equal to the stress due to convergence σ_{conv}), σ_3 sub-vertical (equal to the stress due to topography σ_{top}) and σ_2 sub-horizontal and sub-parallel to the elongation axis of the orogen (equal to the lateral stress σ_{lat}). In such a convergent environment deformation is envisaged as having been concentrated in the vicinity of the mechanically favourable, northeast-southwest trending continental suture zone (Figure 7.2c), forming the preserved D_{n+1} fabric. Such a deformation would be most favourable while $\sigma_{conv} \gg \sigma_{lat} \gg \sigma_{top}$.



a) Initial scenario, westwards directed subduction into a northeast-southwest trending subduction zone



b) Continental collision with orthogonal collision to the north and oblique transpressional collision further south



c) Oblique collision and crustal thickening during continued convergence

Figure 7.2

Early evolution of the RPSSB

Brasiliano - strike-slip fabric

As convergence continued, topography would increase until it reached what is viewed as the limiting topographic height (~3km, England & Houseman 1988, Dewey 1988). In reaching the point when topography can no longer increase and the forces of lateral spreading exceed the forces of convergence (σ_1 is vertical), a number of intermediate states of stress will take place within the orogen. These intermediate states can be envisaged (Figure 7.3b) and have three possible interpretations:

1. ($\sigma_1 = \sigma_{\text{conv.}}$) > ($\sigma_2 = \sigma_{\text{lat.}}$) \geq ($\sigma_3 = \sigma_{\text{top.}}$) - In this environment the low angle fabric would continue to accommodate crustal thickening, by oblique thrusting along the northeast-southwest trending thrusts, but with increasing crustal height, $\sigma_{\text{top.}}$ will increase such that it exceeds $\sigma_{\text{lat.}}$.
2. ($\sigma_1 = \sigma_{\text{conv.}}$) > ($\sigma_2 = \sigma_{\text{lat.}}$) = ($\sigma_3 = \sigma_{\text{top.}}$) - This would produce pure flattening strain-plane strain, on an orogen scale. Such a deformation could be accommodated by continued thrusting or bulk pure shear in the deformable zones orientated orthogonally to the local principal stress axis: In this situation the pure shear domains would be sub-vertically orientated and would occur most often where previously deformed sub-vertical fabrics already existed e.g. on lateral ramps.
3. ($\sigma_1 = \sigma_{\text{conv.}}$) > ($\sigma_2 = \sigma_{\text{top.}}$) \geq ($\sigma_3 = \sigma_{\text{lat.}}$) - If bulk pure shear took place, sufficient to induce a limiting topographic height, it would feedback such that σ_2 and σ_3 would interchange, and given a continued westwards orientation for σ_1 , northeast-southwest directed, dextral strike-slip along the pre-existing structural fabric accommodated by any suitably orientated sub-vertical fabric would take place. Such deformation would continue until lateral stresses $\sigma_{\text{lat.}}$ were again sufficient to exceed topographic stresses $\sigma_{\text{top.}}$ (since constant volume elongation along the orogenic belt would reduce stresses due to topography) and a similar feedback into a pure shear environment would take place.

During continued oblique convergence, without outside disturbance, there should be a smooth transgression from low-angle thrusting into pure shear and then strike-slip deformation. These latter two categories will then dynamically feedback between each other resulting in an overall dextral transpression (Sanderson & Marchini 1984), which on the geological timescale will appear to be a single continuous deformation, cross-cutting the earlier fabric: The extent to which pure ($K=0$) flattening deformation will take place over horizontally or vertically orientated plane strain ($K=1$) will depend upon the strength of the boundary conditions to the deforming zone, this assumes that lateral extrusion can take place i.e. $\sigma_{\text{lat.}}$ is variable. Such an evolution can explain the apparent temporal partitioning of transpressional fabrics during oblique collision. It is a development of the ideas of Hasui *et al* (1978), Ebert & Hasui 1992, Ebert & Hasui *in press*, who have discussed the field

evidence for a continuous tectonic evolution during the production of thrust related (D_{n+1}) and transpressional (D_{n+2}) fabrics.

Emplacement of the granites

The syn-emplacement structures that have been identified within the country rocks and the granites demonstrate that there must have been a significant component of extension during emplacement (see Lagarde *et al* 1990, Klemens & Schwertner 1997 and Kusky 1993 for other examples of this style of emplacement) and that the principal extension direction was directed approximately east-west (see part 7.3.3 for further analysis). Therefore, considering the orogen as a single body, the principal convergent stress $\sigma_{\text{conv.}}$, becomes the minimum principal stress σ_3 (Figure 7.3c). Such a reorientation requires that $\sigma_{\text{lat.}}$ and $\sigma_{\text{top.}}$ both exceed the convergent stress $\sigma_{\text{conv.}}$; an environment which in an orogen with a dynamically limited topographic height, requires that convergence, at that level (see below), be rapidly slowed or stopped entirely. Although if the topography of the pluton is buoyed up by boundary layer delamination, as envisaged by England & Houseman (1988), and the orogen is strongly confined along its axis i.e. $\sigma_{\text{lat.}} \geq \sigma_{\text{conv.}}$, then east-west directed extension of the orogen will take place (Dewey 1988)(Figure 7.3c). In such an environment σ_1 must be orientated either sub-parallel to the orogen $\sigma_{\text{lat.}}$ or sub-vertically $\sigma_{\text{top.}}$, and orthogonal to σ_2 .

Additionally it may be possible to have orogenic extension taking place at the emplacement level (Figure 7.3c) while convergence was dominant at greater depth (Figure 7.3b). This requires that the lower crust and the middle/upper crust are mechanically decoupled, with a free surface acting as the dominant boundary condition at the emplacement level. To distinguish this process from that outlined in the previous paragraph would require the study of coeval lower crustal plutons which should show contractional magmatic state fabrics. The studied exposures represent a single crustal level and thus it is difficult to test this hypothesis.

Previous sections have demonstrated that there could be appropriate magma 'reservoirs' and conduits to facilitate the emplacement of magma into the RPSSB (Figure 7.4). Providing there are sufficient dynamic forces to drive magma ascent plutons will emplace into the extending middle crust in the mechanically most favourable areas (extensional pull-aparts). Orogenic extension will continue until the orogen achieves a stress balance, but magma emplacement will only continue while magma ascent is mechanically favourable. Indeed the emplacement of microgranite dykes demonstrates that extension took place after the emplacement of the plutons.

Post emplacement deformation

All the plutons and the country rocks record D_{n+4} solid state overprinting which appears to consist of a dextral LS-type fabric, there is no evidence for any post-intrusion related transpression. As such, a dextral deformation suggests that the convergent stress

has again become dominant, although $\sigma_{top.}$ must exceed $\sigma_{lat.}$ (Figure 7.3d). Comparison of geochronological data from K-Ar dating, which has an isotope blocking temperature of approximately 400°C, with similar inferred temperatures from deformation fabrics within the plutons, suggests that this deformation must have occurred before 450Ma (Tassinari 1988).

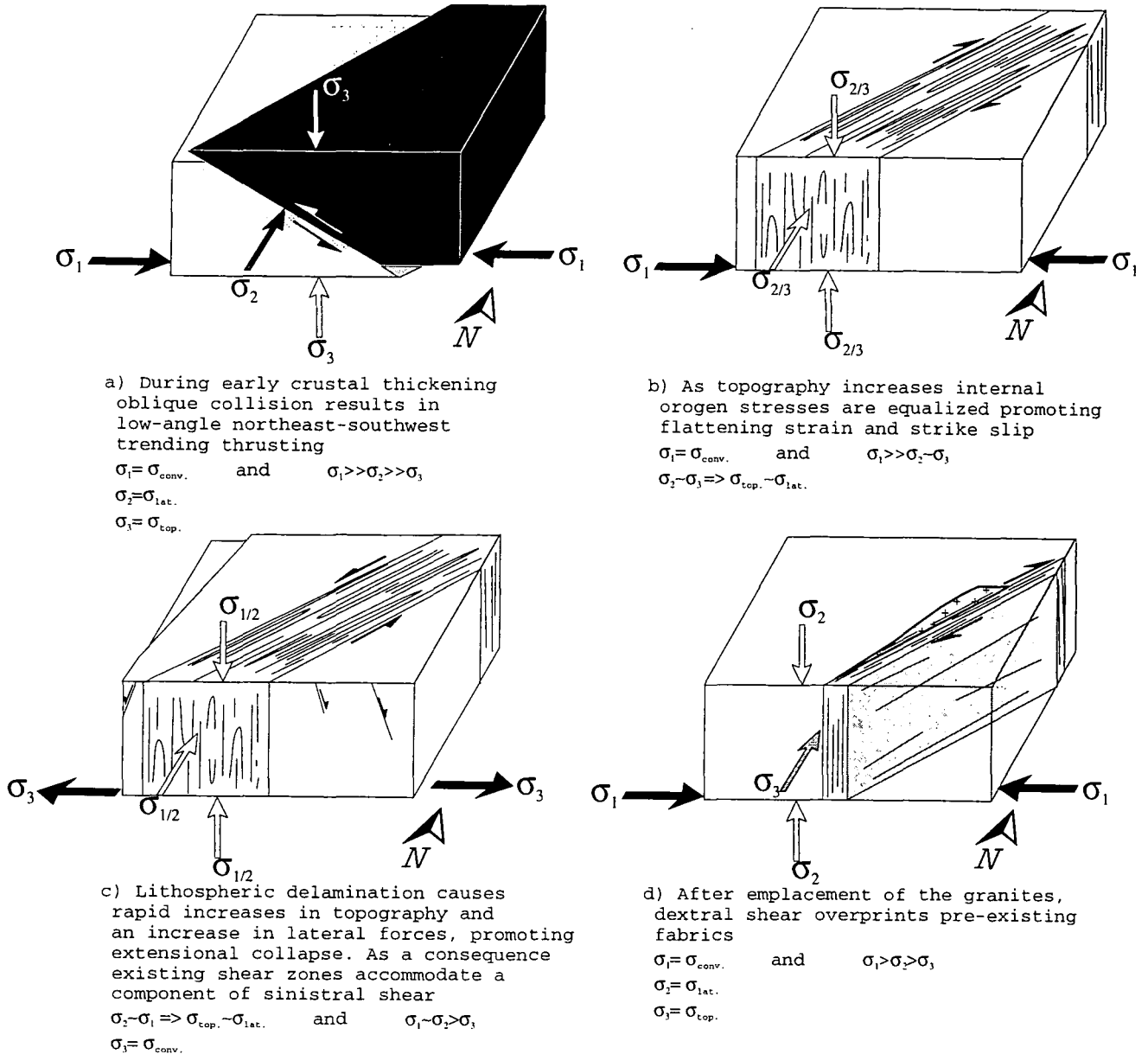
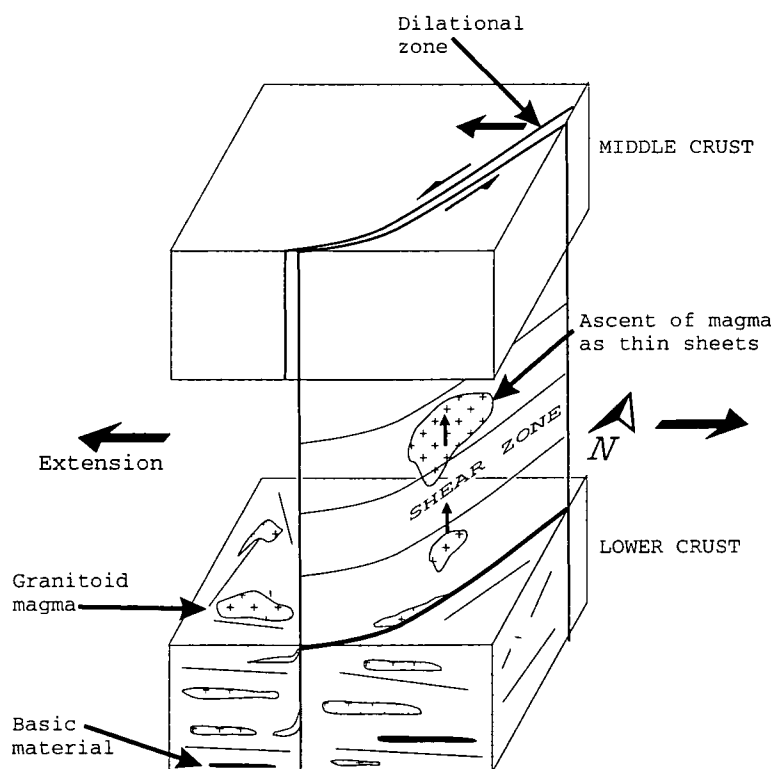


Figure 7.3 Dynamics associated with evolution of the RPSSB



Mid crustal deformation accommodated along shear zones, penetrating the lower crust. Magma formed at depth ascends as thin sheets along the shear zone discontinuity, into the dilation zone

Figure 7.4 Ascent of magma sheets along a conduit penetrating a melt zone at depth

Mylonites

Overprinting the earlier fabrics are discrete mylonites, which show an inferred principle stress perpendicular to the regional structure, associated with each pluton, that was strongly confined i.e. $\sigma_1 \approx \sigma_2 \approx \sigma_3$. As a consequence it is suggested that this represents a partitioning of some degree of strike orthogonal compression into the granites. As a consequence of the poor exposure of the country rocks it is difficult to recognise the degree, or the style of deformation accommodated by the shear zones in response to this event.

It is considered by a number of local authors that these features appear to represent a Cretaceous to Eocene event (see part 4.7.1 for references); and indeed it is possible that these structures represent at least part of the dextral deformation of the South American continent as visualised by Unternehr *et al* (1988) and Nurnberg & Miller (1991). These authors demonstrated that the simple restoration of the African and South American continents provides an inadequate 'tectonic fit', and that a degree of dextral strike slip and regional extension must have taken place during the post-Atlantic rifting phase in order to restore the continents to their pre-rift positions (Figure 7.5). In addition Rabinowitz & LaBreque (1979) and Chang *et al* (1992) demonstrate that the RPSSB lies onshore of the Sao Paulo plateau basalts, one of the first offshore expressions of the Trindade hotspot, and

due south of the Sao Paulo-Walvis Ridges. The Sao Paulo Ridge is a fracture zone which controlled ocean rifting in this area such that south of this structure rifting was occurring at 127Ma; whereas rifting did not occur north of this structure until 113Ma. Such a hiatus during the early stages of ocean basin rifting would have induced a northwest-southeast directed compression into the surrounding continents; a direction which is sub-orthogonal to the major regional structures in this area. It is this deformation that could be considered to be responsible for the nucleation of the mylonitic structures observed in this area.

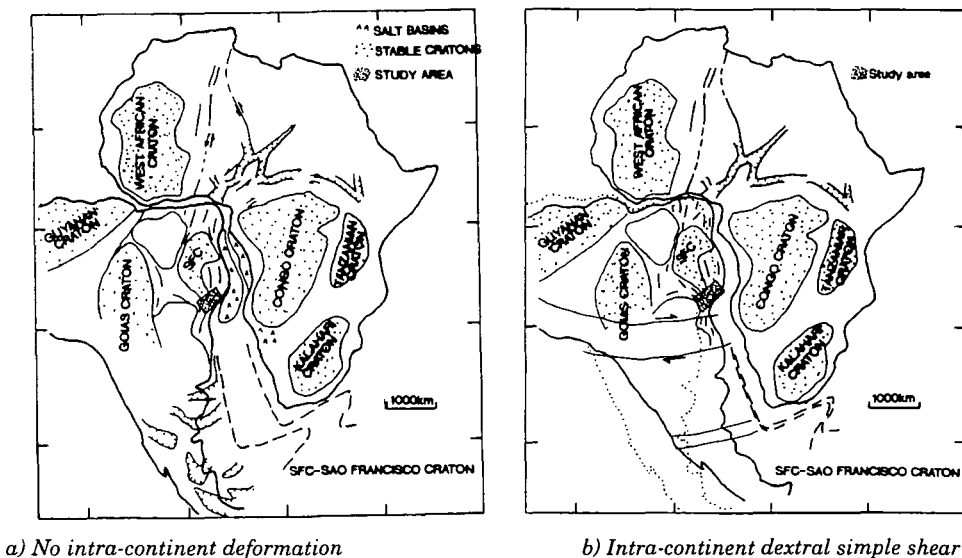


Figure 7.5 Restoring continents to their pre-rift positions after Unternehr et al (1988)

7.2.3 Reason for ascent

As stated above, the ascent and emplacement of magma will occur only if it mechanically favourable. Hutton (1997a,b) used the principle of effective stress (Equation 1.12) to describe how magma can alter the local stress conditions. Applying this principle to pluton emplacement shows that in a 'collapsing' orogen environment, σ the total principal stress will be controlling primarily by the regional confining stresses ($\sigma_{lat.}$ and $\sigma_{top.}$ above), but space can be created in the Andersonian model if, the fluid pressure exceeds the local minimum principal stress ($\sigma_{conv.}$ at the time of pluton emplacement). During extension σ should be small, zero or even negative, depending upon the rate of local dilation. Therefore considering a single pluton there are two possible scenarios:

1. **Positive minimum stress** - In this environment the magma must have sufficient fluid pressure to ascend through a conduit and overcome the local minimum stress at the emplacement level, and therefore rate of magma supply \geq rate of tectonic space creation. If this fluid pressure significantly exceeds the minimum stress then it controls the effective stress and will deform the minimum stress boundary, expanding in-situ (Figure 7.6a) e.g. Main Donegal Granite (Hutton 1982b). In the study area the strong magmatic

fabric and deformation of the outer contacts of the Morro Azul and the Itapeti pluton suggest that there was at least a component of this type of deformation.

- 2. Negative minimum stress** - In this environment there is dilation within the deforming zones, though as cavities cannot exist within the crust these zones will be filled by other crustal material or intruding magma. Given a mechanical connection between the dilatational zone and the magma 'reservoir', magma ascent must take place providing that the resultant effective stress at the emplacement level is positive or zero. Therefore even an underpressured magma reservoir can be exploited and 'sucked dry' by the extending orogen. In the limiting case of principal stress = fluid pressure, the rate of space creation can regulate the rate of magma supply, and there would be no emplacement related deformation of the wallrocks and little internal fabric within the pluton (Figure 7.6b). However if the local resultant effective stress is positive then even an underpressured magma can exert emplacement related strain on the pluton walls and form a fabric within the pluton. All the studied plutons show, to a varying degree, this sort of deformation.

These scenarios demonstrate that the emplacement of plutons into dilatational zones within the crust is a mechanically favourable process, and that even a magma which is under-pressured at the emplacement level can be intruded, and preserve structures which demonstrate a degree of forceful emplacement. The Morro Azul pluton has a strong magmatic fabric and strong deformation of the wallrocks suggesting that its fluid pressures exceeded the minimum regional stress, though the fluid pressure need not have been positive. Conversely the Imbiricu and Atibaia plutons, preserve weaker magmatic fabrics and almost no deformation of their wallrocks which suggest that the effective stress was close to zero and therefore that the minimum principle tectonic stress may have regulated magma supply from a comparatively under-pressured reservoir.

7.2.4 Siting of the pluton

The siting of intrusive bodies is widely debated in the literature (Pitcher 1979, Hutton & Reavy 1992, Jaques & Reavy 1994, Hutton & Alsop 1996, Schmidt *et al* 1995). The consensus of discussion suggests that major shear zones which penetrate the lower crust, intersect the magma 'reservoir' and act as a mechanical linkage and magma conduit to the level of emplacement higher in the crust. Jacques & Reavy (1994) extend this argument a stage further and suggest that the lower crust is segmented into rhomboids defined by shear zones and lineaments. While from this study it is impossible to comment on the validity of such arguments it is necessary to remark upon the fact that the principal northeast-southwest trending shear zones in the field area are spaced at 10-15km intervals and plutons can be observed at approximately similar intervals along strike of these shear

zones. Observations which might suggest a rhomboidal segmentation of the lower crust in the RPSSB, although no across strike lineaments could be identified.

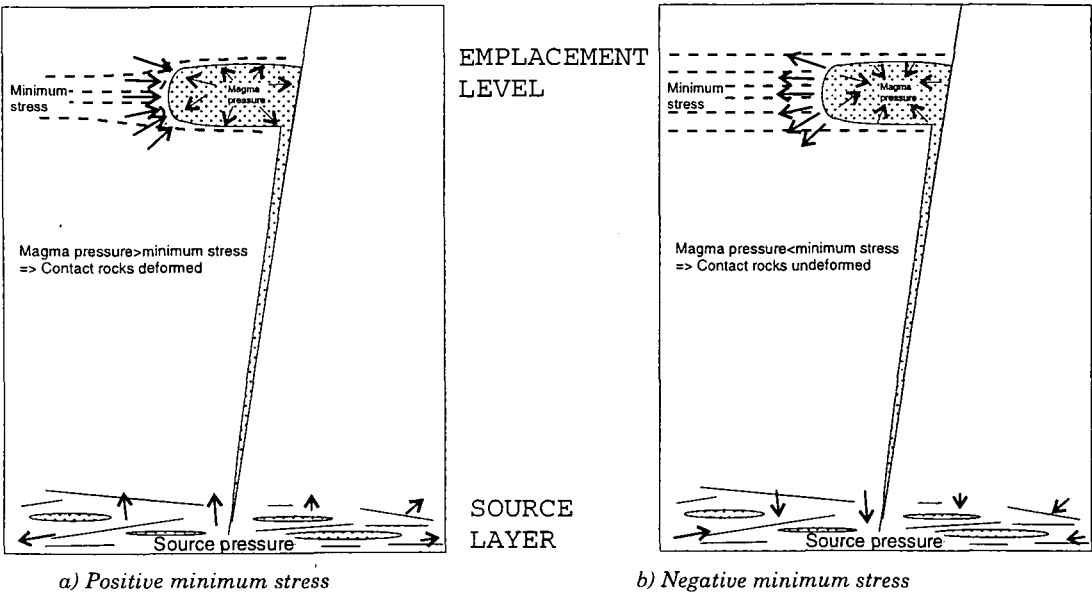


Figure 7.6 Applying the principle of effective stress to pluton emplacement

7.3 The creation of space for the pluton

7.3.1 Strain preserved within the plutons

Each of the studied plutons shows an internal and approximate regional homogeneity of emplacement related finite strains, with average mafic enclave axial ratios recording average flattening strains of the order of $R_s \sim 2.5-3.5$, and Fry fabric crystallographic strains recording similarly flattening strains with average $R_s \sim 1.8-2.1$. As such this suggests that individual magma sheets ascending and homogenising, experienced a flattening strain orthogonal to the short axis of the pluton; equivalent to a shortening of approximately 30-60%. Such a stretching is consistent with the magma ascent and emplacement scenario described above (part 7.2.3), whereby pressurised magma is emplaced into a dilational zone. In general this magma will preserve sufficient fluid pressure to flatten against the wallrock and existing magma, but in addition there will be a tendency for magma to preferentially stretch along the direction of the propagating dyke tip (Clemens & Mawer 1992) i.e. the long axis of the pluton. This injection and deformation would occur independent of where, within the pluton, the dyke is emplaced, and explains the finite strain homogeneity observed.

There are two additional points that are worthy of remark:

- 1. A vertical stretch within the Morro Azul pluton** - The calculation of a sub-vertically orientated X-axis, is consistent with the more forceful, greater fluid pressure intrusion, envisaged for this pluton.
- 2. A horizontal stretch in the Itapeti pluton** - The Itapeti pluton is emplaced at a high angle to the inferred extension direction, and preserves strong magmatic sinistral shear fabrics and as such it is possible that there would be a stronger plane strain component to deformation during emplacement.

7.3.2 Strain in the country rocks

In Chapters 4-6 the emplacement related finite strain within the contact rocks was estimated. These exercises demonstrated that the country rock did not appear to preserve strain sufficient to account for the creation of more than 20% of the width of the pluton: However it was impossible to quantify the possible space creation through the influence of volume loss or material incorporation. Even if these processes accounted for significant additional space creation, external tectonic and regional space creation mechanisms would still be required to create space for the pluton.

7.3.3 External space creation mechanisms

In parts 7.2.2 and 7.2.3 the feasibility of injecting the pluton within an orogen which was undergoing east-west directed extension was demonstrated and indeed the field evidence suggests that this type of deformation is probably taking place. In this section an

attempt is made to quantify this extension by approximating each of the unsheared pluton contacts to a rotated line. Thus regional finite stretch induced during the intrusion of the pluton can be calculated using an assumed principal stress direction and Equation 2.4. Extending this approach and obtaining a best-fit solution for the extension direction by simultaneously solving Equation 2.4 for each of the studied plutons demonstrates:

1. A best fit minimum required extension orientation of 080°. A value that is probably within error of the east-west directed extension inferred from field data.
2. North-South orientated extension requires very high regional strains to open granite cavities the shape of those observed in the field.
3. A minimum of 40% regional, sub east-west orientated extension is required to facilitate pluton cavities the shape of those observed in the field.

As such emplacement of the studied plutons required a regional emplacement related extension of ~40km to extend the RPSSB to the 200km now exposed.

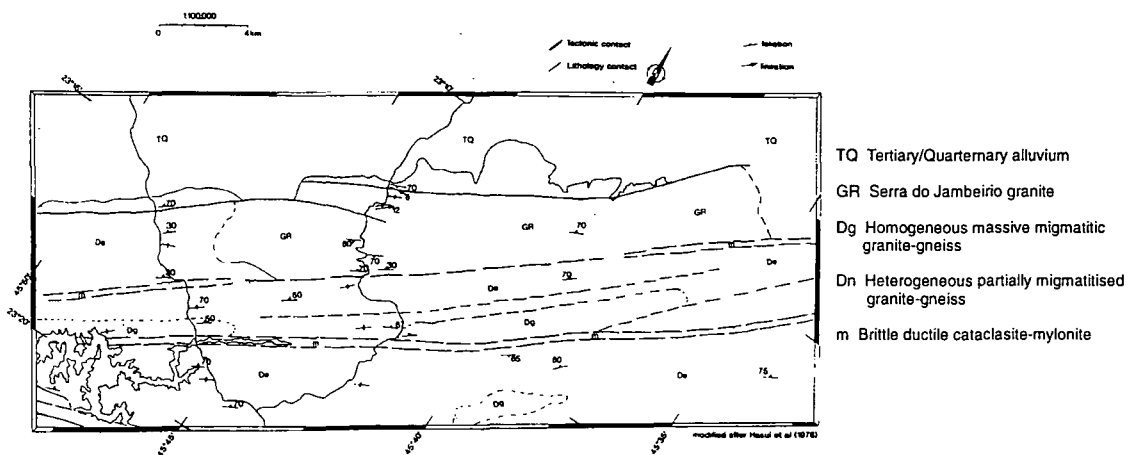
7.4 Emplacement of other granitoids from the RPSSB

7.4.1 Introduction

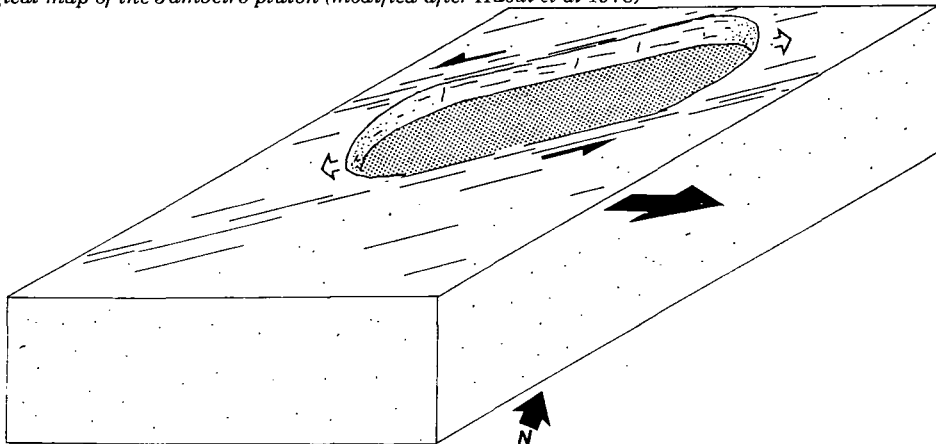
In the literature there are a number of other granitoids which were emplaced pene-contemporaneous to the studied plutons and preserve many similar outcrops features i.e. compositional homogeneity, a single sheared contact and at least one undeformed contact and a wedge-like shape. It is suggested that similar emplacement mechanisms to those described for the plutons in Chapters 4-6, can be applied to these plutons.

7.4.2 The Jambeiro pluton

The Jambeiro pluton is exposed on the southeastern side of the Taubate basin (Figure 7.9a) and was the subject of a brief field study. It showed: i) a granite matrix which has been extensively deformed in the solid state; ii) shear zones defining its outer contact on both sides of the pluton; and iii) no internal petrographic variation. Hasui *et al* (1978) suggests that this pluton is contemporaneous with the others detailed above and as such its emplacement can be envisaged as occurring during regional east-west directed extension (Figure 7.7b).



a) Geological map of the Jambeiro pluton (modified after Hasui *et al* 1978)



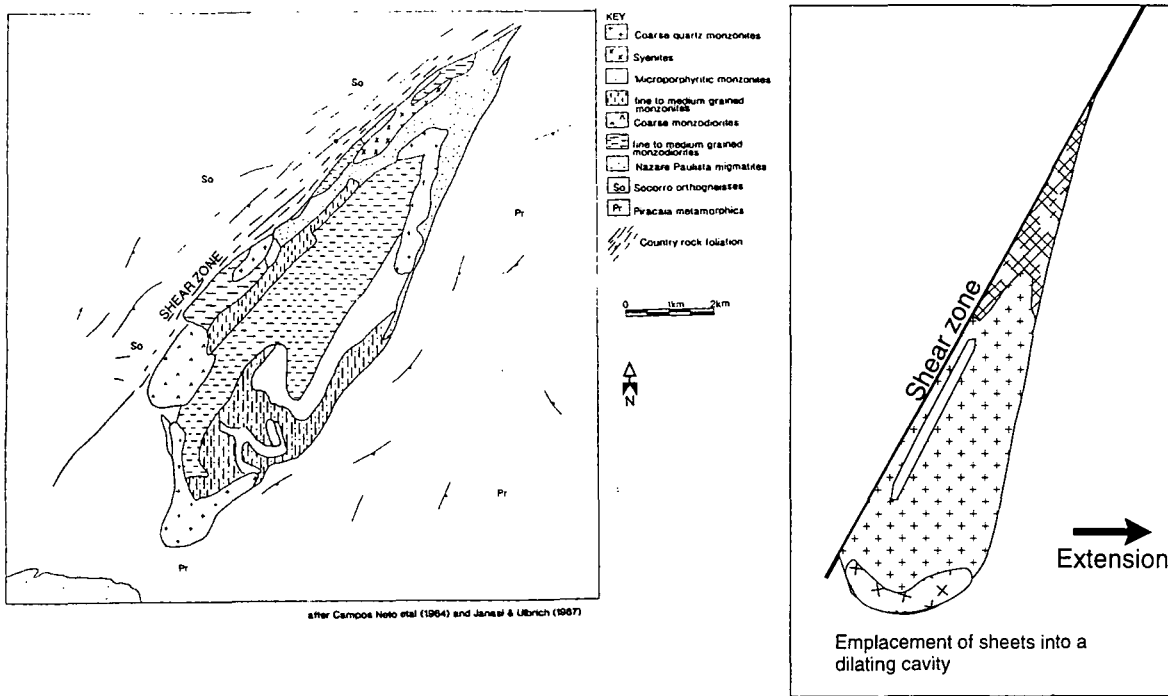
b) Possible tectonics associated with emplacement

Figure 7.7

7.4.3 The Piracaia pluton

The Piracaia pluton is exposed 20km northeast of the Atibaia pluton. It is wedge-shaped, thinning northwards and is associated with a north-northeast trending shear zone along its westernmost contact (Figure 7.8a). It is petrographically heterogeneous consisting of north-northeast striking km-scale sheets of granitic to syenitic composition. It has previously been mapped by Campos Neto *et al* (1983) and Janasi & Ulbrich (1987) and has been dated using Rb-Sr whole rock methods to 573 ± 12 Ma by Tassinari (1988).

There have been no structural studies of the emplacement mechanism but applying the model of east-west directed extension and sheeted emplacement of granitoid sheets would explain the observed distribution of petrographic phases. It might be expected that almost no magmatic shear senses would be preserved, since cavity opening would be sub-orthogonal to the extension direction (cf. Imbiricu pluton).



a) Summary map of the Piracaia pluton
(after Janasi & Ulbrich 1987)

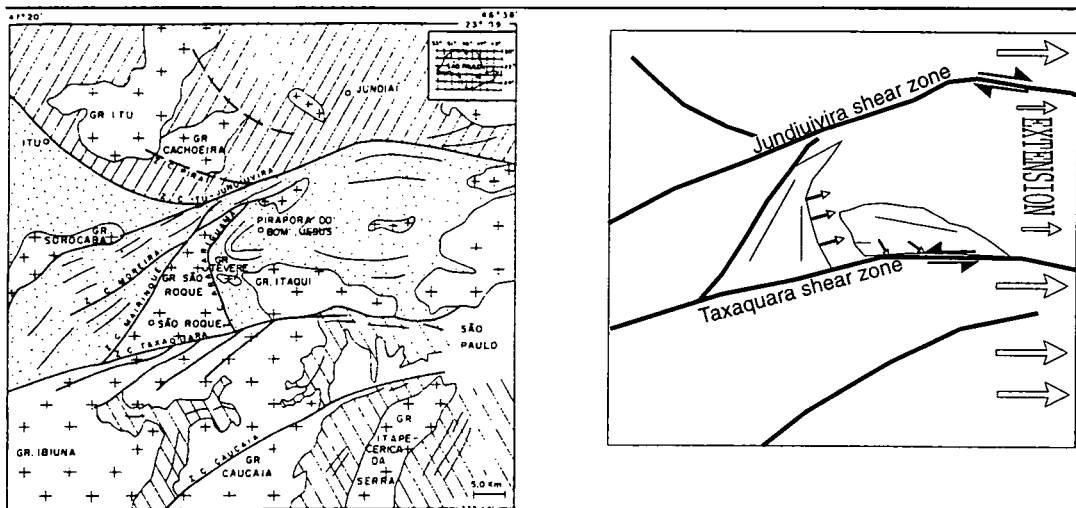
b) Possible tectonics associated with intrusion

Figure 7.8

7.4.4 The Itaquí and São Roque plutons

These are two plutons exposed due west of the city of São Paulo, south of the Jundiivira and north of the Taxaquara shear zones (Figure 7.9a). Both of these plutons preserve a sub-vertical fabric, sub-parallel to the long axis of the pluton, a dominantly granitic composition, low mafic enclave axial ratios ($R_s=1.8-3.5$), sheeting along internal contacts and overprinting by a solid state dextral transcurrent shear; although there is no detailed information available upon the preserved shear senses (Ferreira & Wernick 1995, 1997, Wernick *et al* 1993, Hackspacher *et al* 1993). The Itaquí pluton has been U-Pb dated by Toepfner (1997) at 624 ± 11 Ma, and the São Roque pluton is considered to be of a similar age.

Hackspacher *et al* (1993) suggests that the intrusion of the São Roque pluton during transtension associated with dextral deformation on the Jundiivira and Taxaquara shear zones. Although in the light of the field evidence presented in Chapters 4-6, suggesting east-west D_{n+3} regional extension and additional in relation to the Jundiivira shear zone (inducing dextral magmatic shear sense during pluton emplacement in the Atibaia area), and Taxaquara shear zone (inducing sinistral magmatic shear sense during pluton emplacement in the Itapeti area) it is suggested that the tectonic scenario for intrusion presented in Figure 7.9b might also be possible. In such a situation east-west extension which occurs preferentially in the blocks north and south of the confining shear zones, induces a pull-apart structure against the Marínique shear zone facilitating granite emplacement along its eastern side. Similarly, extensional space can be created against the Taxaquara shear zone enabling intrusion of the Itaquí plutons. It is hypothesised that examination of the magmatic shear sense fabric within each of these plutons should show weakly sinistral fabrics in the São Roque pluton, but much more intense sinistral fabrics within the Itaquí pluton *vis a vis* the Itapeti pluton.



a) Summary map of the São Roque and Itaquí plutons (after Wernick *et al* 1993)

b) Possible tectonics associated with emplacement

Figure 7.9

7.4.5 The Sindacta pluton

The Sindacta pluton is situated due south of the Sao Roque and Itaquí plutons that have been described in the previous section and has been structurally mapped by Spanner & Kruhl (*in press*) (Figure 7.10). In summary, their work demonstrates that this Granitic pluton was emplaced by sheeting during east-west extension associated with east-northeast trending D_{n+2} shear zones. Where the magma preserves syn-emplacement fabrics these show well developed sinistral magmatic shear senses, very similar to those described from the Itapeti pluton (which had a similar orientation relative to the extension direction).

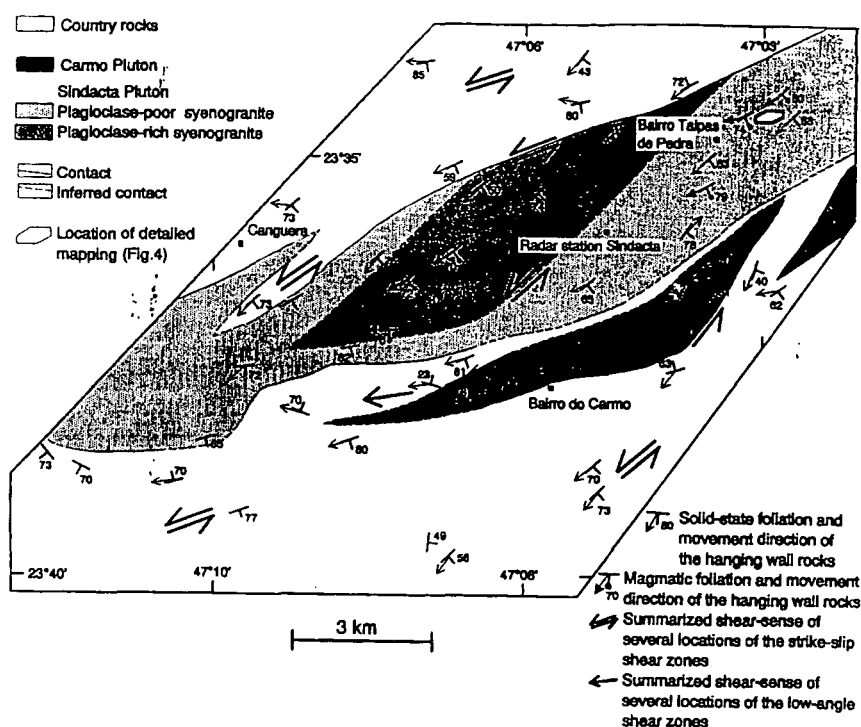


Figure 7.10 Summary map and tectonic interpretation of the Sindacta pluton (Spanner & Kruhl *in press*)

7.4.6 Conclusions

While there are few studies which have comprehensively interpreted the emplacement related structures preserved within granitoid plutons pene-contemporaneous within the studied plutons, a number of mapped plutons show internal and external field relationships comparable to those from the studied plutons. This suggests that a structural analysis of these plutons might elucidate similar magmatic fabrics to those observed within the studied granites. Henceforth it is suggested that regional east-west extensional collapse facilitated granitoid intrusion in most parts of the RPSSB between 630 and 520Ma.

7.5 Conclusion and discussion

The purpose of this Chapter was to bring together the data analysed in the previous Chapters 4-6 to produce a regional tectonic model, for the ascent and emplacement of granitoid magma. The principal features of this model are:

- Regional orogenic dextral transpression took place before the intrusion of the plutons. This process is interpreted to have caused extensive crustal thickening, before inferred lithospheric delamination took place.
- Such delamination increases the topographic height of the orogen, causing dynamic instability and extensional collapse. While the increased heat flow in the root of the orogen causes crustal anatexis and granitoid magma genesis.
- The orogen is laterally confined and thus extension leading perhaps to collapse must take place in the convergence direction: This results in greater than 40% eastwards extension. Granite emplacement accommodates that extension.
- Granite emplacement took place by ascent along shear zones and sheeting into dilatational cavities or local transtensional pull-aparts. Such magma generally exerted a relatively low effective stress on the surrounding rocks during emplacement with less than 20% of the width of the pluton being created by in-situ expansion.
- Extension continued after pluton emplacement and was recorded by the orientations of microgranitoid dykes.
- After a significant amount of cooling the pluton was overprinted by a dextral planar shear associated with a reassertion of convergence.
- All these earlier fabrics were cross-cut by discrete mylonites recording compressive deformation.
- Similar field relationships, internal structure and magmatic shear sense fabrics can be found within pene-contemporaneous plutons elsewhere within the RPSSB.

SECTION 4

Analytical considerations and final conclusions

*“Granite is not a rock which is simple in origin but might be
produced in more ways than one” - a quote of J.B. Jukes,
taken from Pitcher (1993)*

Chapter 8

Analytical considerations

8.1 Preamble

The granite plutons can be described from field evidence, but fieldwork only illustrates the final solution. At best it provides indications as to the methods or processes at work during ascent and emplacement. By modelling emplacement and related features in a dimensionally consistent manner, hypotheses about magma intrusion can be tested.

In this chapter a number of mathematically simplistic but appropriately scaled models have been used to illustrate particular features associated with the studied plutons.

8.2 Modelling mafic enclave shape during deformation

8.2.1 Introduction

Throughout the preceding section the axial ratio of incorporated mafic enclaves has been used to describe the strain state of magma during emplacement. This method is known to provide consistent and applicable results (Hutton 1977, 1988, Ingram 1992, Ingram & Hutton 1994, Molyneux & Hutton *in press* and this work), though some workers argue that at best it provides a significant underestimate of the imposed finite strain (Fowler & Paterson 1997). The methods and statistical analysis used during field analysis were described in Chapter 1. There are two assumptions inherent within that method: i) that the enclaves have strong mechanical coupling with the magma around them; and ii) that the enclaves were initially spherical before deformation. Both these assumptions were extensively discussed in Chapters 1 and 2. In this section a model is illustrated which analyses the three dimensional shape characteristics of an ellipsoid, analogous to an enclave, both before and after an imposed deformation.

8.2.2 Methodology

Examination of outcrops which contain abundant mafic enclaves show that they describe an elliptical shape with variable axial ratio (longest axis/shortest axis). Their three dimensional shape is difficult to describe from a single outcrop but serial sectioning of an enclave demonstrates that they are ellipsoidal, with minor lobate apophyses (Vernon 1983, Flinders & Clemens 1996). This study uses an ellipsoid as an approximation to an enclave. A section through the ellipsoid, parallel to one of the principle deformation planes, will give an ellipse, with a corresponding axial ratio.

For a population of ellipsoids sectioned parallel and perpendicular to the principal strain planes of the strain/fabric ellipsoid will yield a series of apparent strain planes for the enclaves. In order to model the deformation characteristics of an ellipsoid population each enclave was defined mathematically, in terms of three orthogonal principle vectors, the magnitude of which are the principal axial lengths (Figure 8.1a, Equation 8.1 a-c) and axial ratios. In each of the principal strain planes (X-Y, X-Z, Y-Z), each enclave has apparent initial axial ratios (R_{ixy} , R_{ixz} , R_{iyz}) (Figure 8.1a). These can be determined using projection (Equation 8.3, 8.4). In this way each ellipsoid can be defined with specific parameters (size, orientation, axial ratio), so defining the population characteristics.

Equation of a sphere, of unit radius centred on the origin:

$$x^2 + y^2 + z^2 = 1$$

Equation of an ellipsoid, centred on the origin, with axes parallel to the datum:

$$(ax)^2 + (by)^2 + (cz)^2 = 1 \quad \text{where } a, b, c \text{ are the orthogonal radial lengths}$$

Equation 8.1a Equation of an ellipsoid, centred on the origin, with any set of three orthogonal principal vectors:

$$(ax+by+cz)^2 + (dx+ey+fz)^2 + (gx+hy+iz)^2 = 1$$

where $ax+by+cz$, $dx+ey+fz$ and $gx+hy+iz$ are the cartesian form of any set of three orthogonal vectors which describe axial lengths:

Equation 8.1b

$$|L_1| = \sqrt{a^2 + b^2 + c^2}$$

$$|L_2| = \sqrt{d^2 + e^2 + f^2}$$

$$|L_3| = \sqrt{g^2 + h^2 + i^2}$$

Equation 8.1c Expansion of Equation 8.1a produces:

$$Ax^2 + By^2 + Cz^2 + Dxy + Exz + Fyz = 1$$

where, $A = a^2 + b^2 + c^2$, etc.

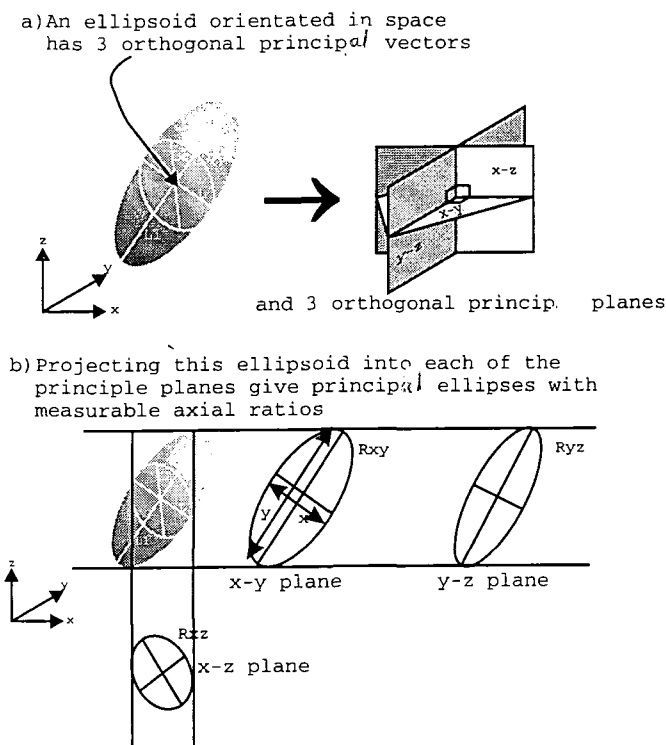


Figure 8.1 Characteristics of an ellipsoid / mafic enclave population

Pre-deformation the principal vectors define the enclave ellipsoid uniquely in space. However if the ellipsoid is deformed, by pure or simple shear, these vectors continue to define the ellipsoid but are generally no longer orthogonal (Figure 8.2). The post-deformation orientation of these vectors can be determined using a deformation matrix (Equation 8.2)(Tikoff & Teyssier 1993). In order to determine the new enclave ellipsoid principal vectors (Figure 8.2) the general ellipsoid equation (Equation 8.1) must be iterated, such that the deformed vectors are solutions.

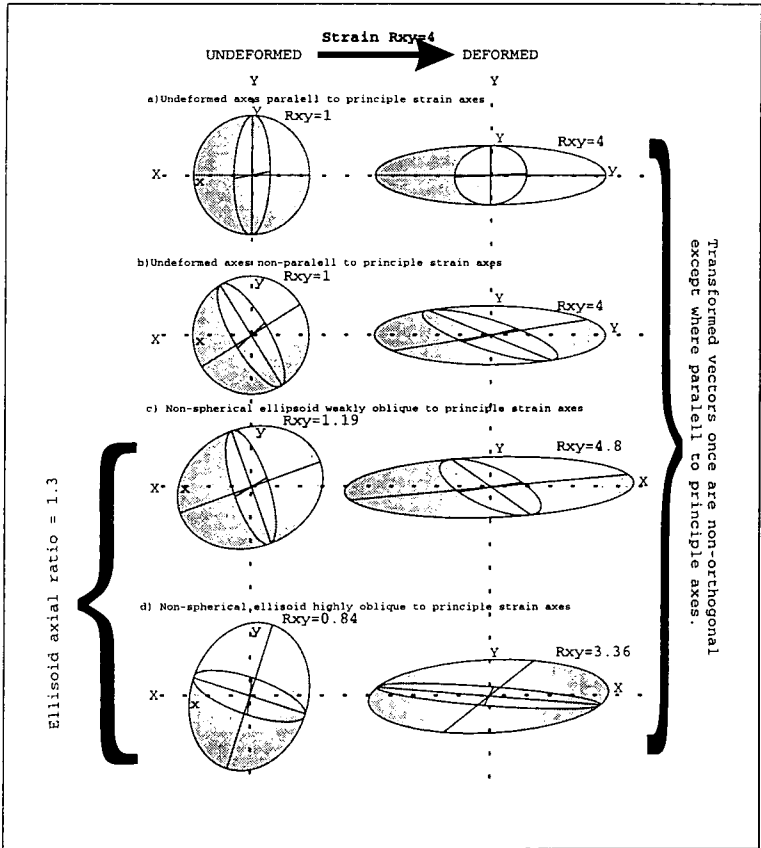


Figure 8.2 Orientations of the principal vectors before and after deformation

Equation 8.2 The deformation matrix is defined by nine components and is symmetrical about its centre line, enabling the mapping of points before and after a pure and/or simple shear deformation (as used by Tikoff & Teyssier 1993).

$$\text{The deformation matrix, } D = \begin{bmatrix} A & b & c \\ b & B & d \\ c & d & C \end{bmatrix}$$

components A, B, C describe pure shear deformation along the principal axes, and components b, c, d describe simple shear deformation. This work describes deformation only during constant volume pure shear conditions and in these cases:

$$A \cdot B \cdot C = 1 \text{ and,} \\ b = c = d = 0$$

Hence to describe mapping of a vector $\mathbf{a} = a\mathbf{i} + b\mathbf{j} + c\mathbf{k}$, to \mathbf{a}' during pure shear is simply:

$$\begin{bmatrix} A & 0 & 0 \\ 0 & B & 0 \\ 0 & 0 & C \end{bmatrix} * \begin{bmatrix} a \\ b \\ c \end{bmatrix} = \begin{bmatrix} A.a \\ B.b \\ C.c \end{bmatrix}$$

$$\text{i.e. } \mathbf{a}' = (A.a)\mathbf{i} + (B.b)\mathbf{j} + (C.c)\mathbf{k}$$

where A/B, B/C and A/C are the principle axial ratios of the strain ellipsoid X/Y, Y/Z and X/Z respectively.

This iteration is most simply carried out by considering the two dimensional planar projected ellipses formed by this deformation i.e. set one of the axial components to zero (since the vectors are defined around the origin) and optimise the solution for these components, subject to the constraints outlined in Equation 8.3. The non-linear optimisation code of Lasdon & Warren (1983) is used, as implemented in Microsoft Excel v4.0.

Equation 8.3, An ellipsoid is defined by the equations:

$$(ax+by+cz)^2 + (dx+ey+fz)^2 + (gx+hy+iz)^2 = 1 \quad [8.1a]$$

$$Ax^2 + By^2 + Cz^2 + Dxy + Exz + Fyz = 1 \quad [8.2b]$$

If projected onto the X-Y plane i.e. $z=0$ this becomes:

$$Ax^2 + By^2 + Dxy = 1 \quad \text{the equation of an ellipse.}$$

Therefore given three non-orthogonal transformed vectors:

$$\mathbf{a}' = a'\mathbf{i} + b'\mathbf{j} + c'\mathbf{k}$$

$$\mathbf{b}' = d'\mathbf{i} + e'\mathbf{j} + f'\mathbf{k}$$

$$\mathbf{c}' = g'\mathbf{i} + h'\mathbf{j} + i'\mathbf{k}$$

which are solutions to the equation 8.2b, where A-F are unknowns. A complete solution can be obtained by deriving three mutually consistent solutions, for the appropriate unknowns A-F, to each of the projected ellipses.

For example, the projected transformed vectors:

$$\mathbf{a}' = a'\mathbf{i} + b'\mathbf{j}$$

$$\mathbf{b}' = d'\mathbf{i} + e'\mathbf{j}$$

$$\mathbf{c}' = g'\mathbf{i} + h'\mathbf{j}$$

$$\text{are solutions to } Ax^2 + By^2 + Dxy = 1$$

$$\text{i.e. } A.a'^2 + B.b'^2 + D.a'.b' = 1$$

but A, B and D are unknown, and hence during optimisation A, B, D are varied such that \mathbf{a}' , \mathbf{b}' , \mathbf{c}' are solutions and the mathematical definition of an ellipse;

$D^2 - 4.A.B \leq 0$ is satisfied

since if, $D^2 - 4.A.B = 0$, the solution is a circle, or if, $D^2 - 4.A.B < 0$, the solution is an ellipse.

This process is carried out concurrently for projected ellipses in each of the principal planes X-Y, X-Z and Y-Z. Iterating a solution for the equation of the ellipsoid.

Note: This optimisation may represent a non-unique solution i.e. three vectors may be the solution of more than one ellipsoid.

When iteration is complete and the final shapes and orientations of the entire ellipsoid population is known, each of the ellipsoids can be projected to the principal planes to determine their apparent axial ratios and orientations. These projected axial ratios (R_{fXZ} , R_{fYZ} and R_{fXY}) are a realistic representation of what would be measured in outcrop (Figure 8.3) (Equation 8.4).

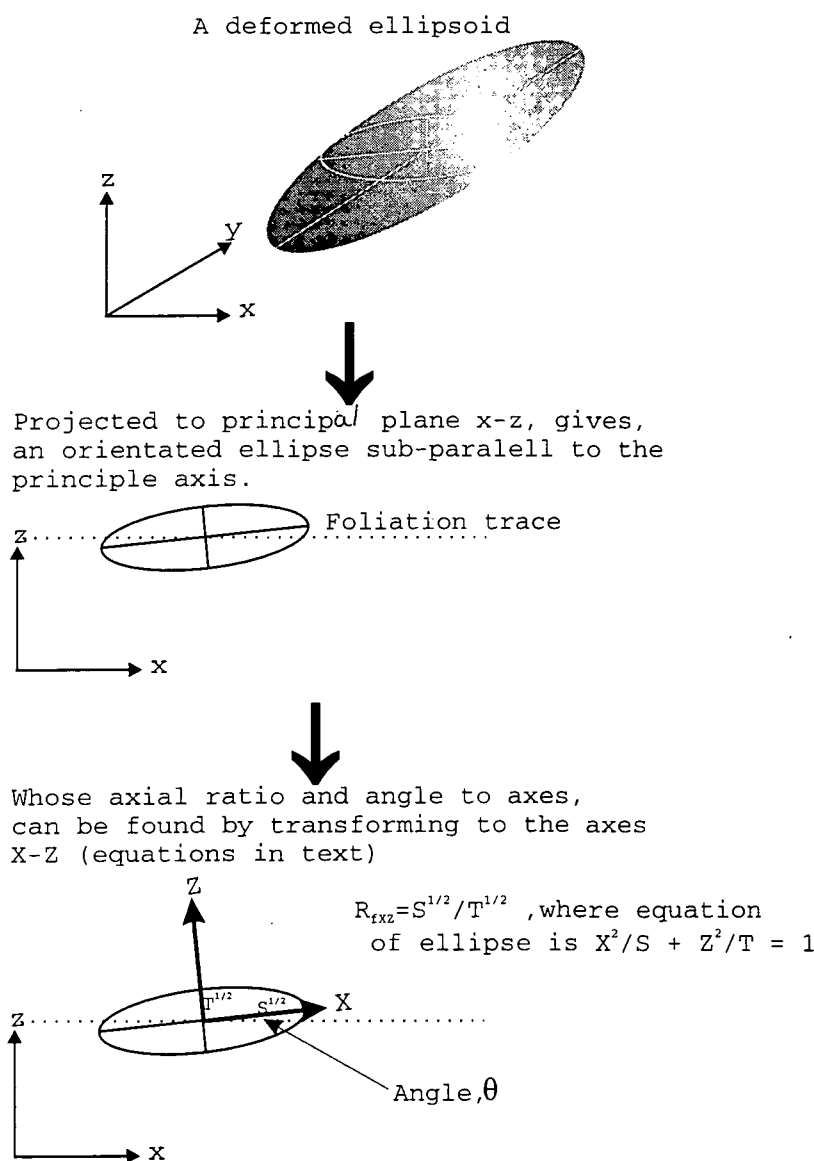


Figure 8.3

Projection, apparent axial ratio, axis transformation and orientation

Equation 8.4, The angle of orientation of the apparent axial ratio is defined by;
 $\tan 2\theta = B/(A - C)$ where $Ax^2 + Bxy + Cy^2$ is the equation of the projected ellipse
 Then defining θ , the ellipse can be transformed to a set of co-ordinate axes which correspond to the long and short axes of the ellipse using the equations;
 $x = X\cos\theta - Y\sin\theta$ and $y = X\sin\theta + Y\cos\theta$
 This produces a new simplified ellipse equation;
 $SX^2 + TY^2 = 1$ where;
 major axis length $X' = 1/\sqrt{S}$ and, minor axis length $Y' = 1/\sqrt{T}$
 Hence, the apparent axial ratio is X'/Y'

Completion of the analysis results in a set of orientated axial ratio data which can be analysed statistically in a similar way to field mafic enclave data, as detailed in Chapter 1, the results of these analyses are detailed below for each of the studied populations.

8.2.3 Results

The iteration and deformation described above has been applied to five different initial ellipsoid populations of 35 ellipsoids, which had no prominent initial preferred orientation, deformed in 13 different, constant volume, finite strain environments (5 pure flattening strain, 3 plane strain and 5 prolate strain). Each of these populations and the results of the deformations are described below:

These first three populations were defined such that the ellipsoids were initially sub-spherical, any shape distributions being controlled by the initial conditions.

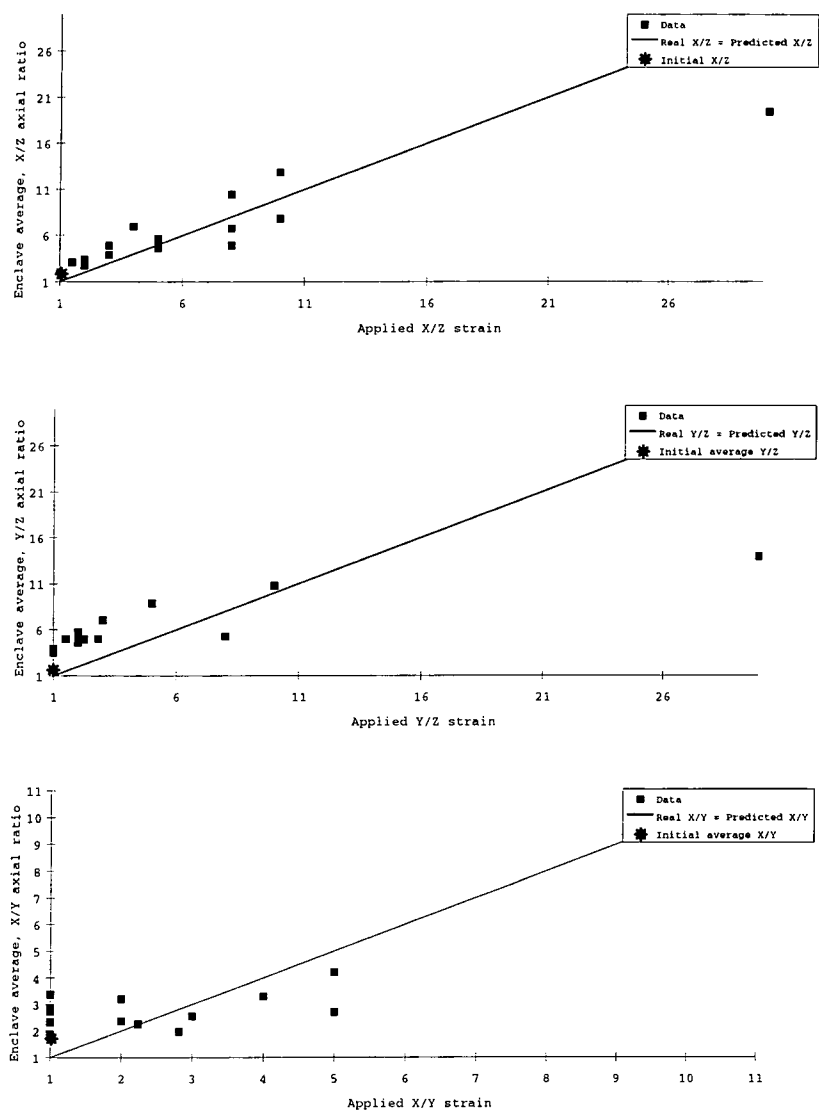
Uniform distribution

The uniform population consists of ellipsoids whose initial axial lengths were uniformly distributed over a range of 0 to 10 units in each of the three principal directions. The undeformed ellipsoid population has the characteristics listed in Table 8.1, note in particular the high degree of initial shape variability indicated by the standard deviation and ω log values.

Table 8.1 Initial characteristics of the Uniformly distributed ellipsoid population

Number	35		
Average axial ratio X/Y	1.74	Standard deviation X/Y	1.41
Average axial ratio X/Z	2.09	Standard deviation X/Z	2.18
Average axial ratio Y/Z	1.77	Standard deviation Y/Z	0.95
Largest X	20.6	Smallest X	3.16
Largest Y	14.5	Smallest Y	6.80
Largest Z	14.8	Smallest Z	3.04
ω log X	0.814		
ω log Y	0.329		
ω log Z	0.687		

The post-deformation finite strain data recorded for this population is shown in Table 8.2. Of particular remark is the strong deviation within any recorded sample (up to 200%) of the mean value, probably reflecting a magnification of the strong initial variation. Correlation between the imposed finite strain and the recorded axial ratio (Fig 8.4, Table 8.11) is relatively poor. This is possibly a function of the poor definition of the mean value. This poor mean definition is further reflected comparing the outcrop and modelled histograms of axial ratios in Figure 8.10a, b, where the calculated mean is 5.62, standard deviation 17, but the graphical mean is 3.



Correlation between imposed finite strain and recorded mafic ellipsoid axial ratio for the uniform population
Figure 8.4

Table 8.2 *Imposed finite strains and recorded ellipsoid axial ratios for uniform population*

Imposed finite strains				Modelled ellipsoid axial ratios						
X/Z	Y/Z	X/Y	log K-value	X/Z	Standard deviation	Y/Z	Standard deviation	X/Y	Standard deviation	log K-value
1.5	1.5	1	0	3.07	15.97	4.99	22.11	3.37	12.76	0.76
2	2	1	0	2.76	39.7	5.32	4.21	1.8	13.9	0.35
3	3	1	0	3.9	25.12	7.06	14.3	2.73	12.8	0.51
5	5	1	0	5.62	17.3	8.89	21.9	2.81	14.1	0.47
8	8	1	0	4.90	15.0	5.30	11.78	1.88	7.32	0.38
10	10	1	0	7.84	14.31	10.78	40.7	2.33	4.68	0.36
30	30	1	0	11.72	11.58	13.89	10.5	2.72	13.22	0.38
4	2	2	1	6.95	32.6	5.77	9.35	3.29	11.2	0.76
8	2.82	2.82	1	6.74	11.99	5	8.84	1.98	5.36	0.42
5	2.24	2.24	1	5.24	7.86	4.96	8.80	2.26	7.86	0.51
8	2	4	2	11.91	40.76	2.72	16.22	4.77	16.57	0.68
10	2	5	2.32	12.85	16.26	4.59	18.5	4.21	19.6	2.32
2	1	1	∞	3.4	22.46	3.9	13.92	2.37	15.65	0.63
3	1	1	∞	4.91	19.41	3.57	35.54	2.55	9.62	0.73
5	1	1	∞	4.65	8.37	3.52	9.45	2.7	15.05	0.79

Normal population 1

This ellipsoid distribution consists of ellipsoids whose initial axial ratios were defined as being normally distributed with a mean value of 10, and a standard distribution of 1. Examination of the populations initial characteristics (Table 8.3) shows that the population has initial projected axial ratios close to unity and a well defined mean value (small standard deviation).

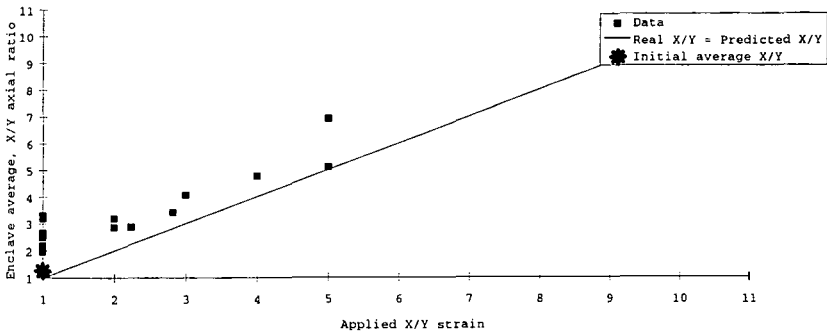
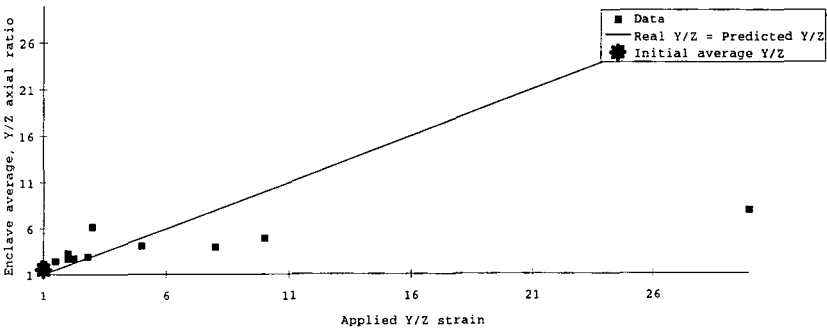
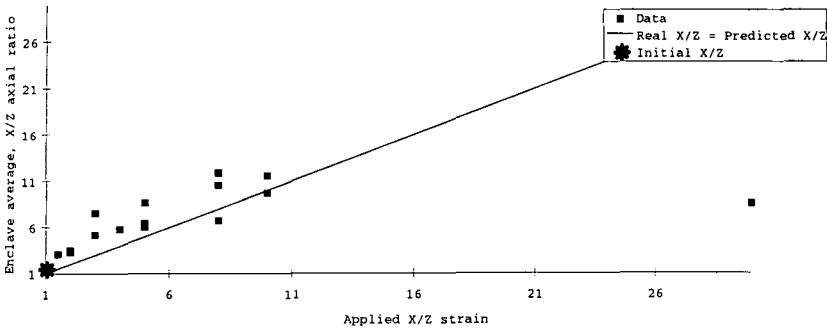
Table 8.3 *Initial characteristics of Normal population 1, axial length mean 10, standard deviation, 1*

Number	35		
Average axial ratio X/Y	1.24	Standard deviation X/Y	0.2
Average axial ratio X/Z	1.30	Standard deviation X/Z	0.48
Average axial ratio Y/Z	1.32	Standard deviation Y/Z	0.44
Largest X	18.34	Smallest X	8.03
Largest Y	33.11	Smallest Y	8.11
Largest Z	10.00	Smallest Z	6.18
ω log X	0.36		
ω log Y	0.61		
ω log Z	0.21		

Post deformation (Table 8.4) the ellipsoids mimic imposed finite strain well (correlation co-efficient ~0.8) (Figure 8.5, Table 8.11), except at very high finite strains where the ellipsoid axial ratio significantly underestimates the imposed finite strain. Around the mean there is often a strong deviation, as shown in Figure 8.10c, which illustrates that for an imposed flattening Y/Z finite strain of 5, (the population mean is 4.1, standard deviation 16) that the mean is identifiable. However there are additional spurious peaks, probably due to iterative error.

Table 8.4 *Imposed finite strains and recorded ellipsoid axial ratios for Normal population 1*

Imposed finite strains				Modelled ellipsoid axial ratios						
X/Z	Y/Z	X/Y	log K-value	X/Z	Standard deviation	Y/Z	Standard deviation	X/Y	Standard deviation	log K-value
1.5	1.5	1	0	3.05	6.83	2.39	4.03	2.18	2.36	0.89
2	2	1	0	3.51	9.77	3.31	9.23	2.49	5.42	0.76
3	3	1	0	7.57	18.0	6.21	15.58	1.98	2.76	0.37
5	5	1	0	8.67	25.6	4.1	16.38	3.2	19.05	0.82
8	8	1	0	6.74	15.0	4.01	11.8	2.63	18.0	0.69
10	10	1	0	9.75	16.7	4.94	17.9	2.66	8.06	0.61
30	30	1	0	8.53	12.0	7.92	25.7	3.31	9.43	0.58
4	2	2	1	5.83	15.3	2.7	3.56	3.21	13.4	1.17
8	2.82	2.82	1	10.56	18.2	2.95	3.53	3.42	9.56	1.13
5	2.24	2.24	1	6.02	7.18	2.75	3.41	2.88	4.45	1.05
8	2	4	2	11.91	18.2	2.72	18.05	4.77	9.56	1.56
10	2	5	2.32	11.56	26.0	3.08	4.03	6.91	11.4	1.72
2	1	1	∞	3.29	4.27	2.1	1.87	2.88	4.16	1.43
3	1	1	∞	5.2	11.52	2.16	1.85	4.07	10.27	1.82
5	1	1	∞	6.43	9.17	2.09	1.61	5.1	9.03	2.21



Correlation between imposed finite strain and recorded mafic ellipsoid axial ratio for Normal population 1

Figure 8.6

Normal population 2

This ellipsoid distribution consists of ellipsoids whose initial axial ratios were defined as being normally distributed with a mean value of 10 and a standard distribution of 2. The populations initial characteristics are listed in Table 8.5, demonstrating slightly increased projected initial axial ratios and standard deviations compared with Normal population 1, consistent with the increased deviation.

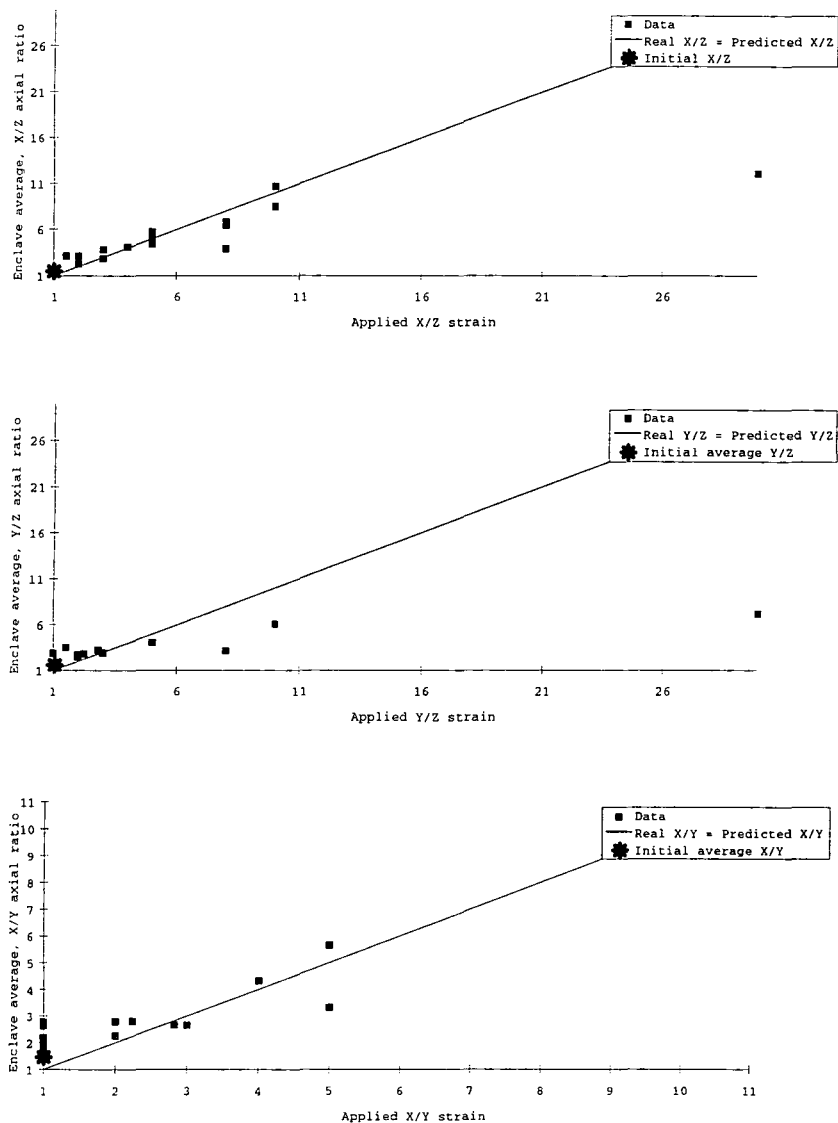
Table 8.5 Initial characteristics of Normal population 2, axial mean length 10, standard distribution 2

Number	35		
Average axial ratio X/Y	1.42	Standard deviation X/Y	0.32
Average axial ratio X/Z	1.40	Standard deviation X/Z	0.47
Average axial ratio Y/Z	1.42	Standard deviation Y/Z	0.56
Largest X	39.4	Smallest X	15.75
Largest Y	65.1	Smallest Y	15.53
Largest Z	24.9	Smallest Z	11.81
$\omega \log X$	0.40		
$\omega \log Y$	0.62		
$\omega \log Z$	0.32		

The post deformation population characteristics are detailed in Table 8.6. Figure 8.6 and Table 8.11 show that there is good correlation between imposed finite strain and recorded average axial ratios (correlation co-efficient ~0.85), with the relationship breaking down at high finite strains similarly to Normal population 1. Furthermore, as seen in all other populations deformed ellipsoids show a strong deviation around the mean values, as illustrated by Figure 8.10d, where imposed finite strain $X/Z=5$ and recorded mean finite strain is 4.44, standard deviation 7.65.

Table 8.6 Imposed finite strains and recorded ellipsoid axial ratios for Normal population 2

Imposed finite strains				Modelled ellipsoid axial ratios						
X/Z	Y/Z	X/Y	log K-value	X/Z	Standard deviation	Y/Z	Standard deviation	X/Y	Standard deviation	log K-value
1.5	1.5	1	0	3.16	5.14	3.52	4.53	2.78	4.15	0.81
2	2	1	0	2.3	3.03	2.48	2.13	1.85	1.59	0.68
3	3	1	0	2.88	3.63	2.93	3.77	2.1	2.71	0.69
5	5	1	0	4.44	7.65	4.05	6.99	2.16	2.93	0.55
8	8	1	0	3.95	7.43	3.18	6.46	1.78	1.45	0.50
10	10	1	0	8.49	14.8	6.09	9.22	2.19	4.03	0.43
30	30	1	0	12.11	17.5	7.18	12.9	2.64	4.86	0.49
4	2	2	1	4.13	7.03	2.74	7.31	2.8	4.13	1.02
8	2.82	2.82	1	6.8	10.23	3.28	8.48	2.68	3.55	0.83
5	2.24	2.24	1	5.72	10.73	2.82	4.34	2.82	6.66	1
8	2	4	2	6.47	10.78	2.59	2.21	4.33	8.48	1.54
10	2	5	2.32	10.67	19.0	2.54	2.40	5.65	8.94	1.86
2	1	1	∞	3.15	4.86	2.89	5.36	2.26	4.79	0.77
3	1	1	∞	3.83	6.28	2.84	6.03	2.66	4.00	0.94
5	1	1	∞	5.23	8.90	2.84	5.84	3.31	4.27	1.15



Correlation between imposed finite strain and recorded mafic ellipsoid axial ratio for Normal population 2
Figure 8.6

In order to explore the effects of having a significant initial axial ratio associated with deformation two elongate populations were defined where one axial length was greater than the others. The characteristics and results are as follows:

Elongate population 1

The undeformed ellipsoids were defined as having one direction with a mean length of 10 and two directions with a mean length of 5, each of these directions having a standard deviation of 2. This sample produces initial ellipsoids with larger projected initial axial ratios than in either of the sub-spherical distributions (Table 8.7) and a larger deviation, but no specific elongation in any particular direction.

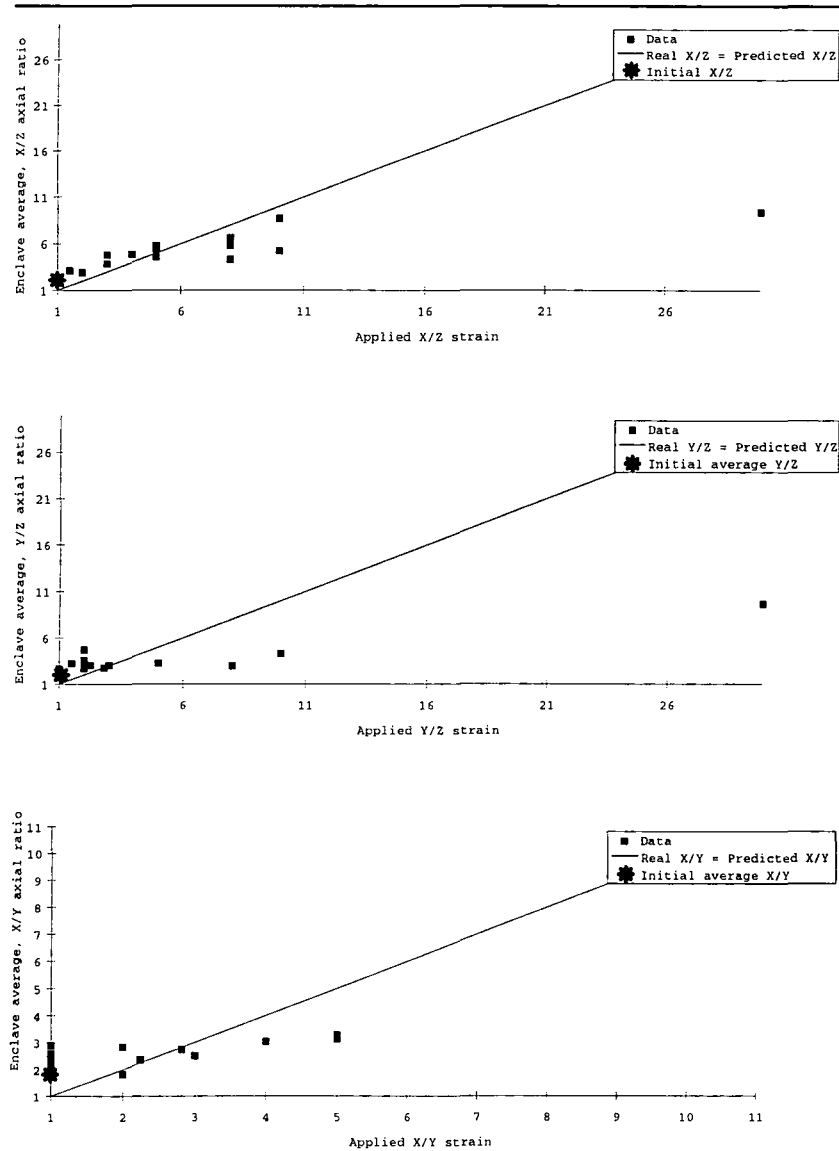
Table 8.7 Initial characteristics of the Elongate population 1, one direction mean 10, standard deviation 2, two directions mean 5, standard deviation 2

Number	35		
Average axial ratio X/Y	1.89	Standard deviation X/Y	0.76
Average axial ratio X/Z	1.78	Standard deviation X/Z	0.69
Average axial ratio Y/Z	1.74	Standard deviation Y/Z	0.65
Largest X	27.27	Smallest X	10.75
Largest Y	40.57	Smallest Y	11.53
Largest Z	16.42	Smallest Z	5.31
$\omega \log X$	0.40		
$\omega \log Y$	0.55		
$\omega \log Z$	0.49		

After deformation the mean recorded axial ratio (Table 8.8) mimics the imposed finite strains well for lower values up to the imposed finite strain of 10, but for the higher imposed finite strain of axial ratio 30 a significant underestimate is recorded in the modelled axial ratio population (Figure 8.7, Table 8.11). This behaviour is consistent with that recorded for each of the sub-spherical populations. In contrast to these sub-spherical populations R^2 values are significantly lower in the Y/Z and X/Y planes. This indicates that there is strong variation associated with this linear trend, which is due to the more elongate initial shapes. Similarly, the modelled populations show a strong deviation around the mean value, which is reflected in an example histogram Fig 8.10d, imposed deformation $X/Z=5$ (modelled mean 4.44, standard deviation 7.65), where the mean is identifiable, but with spurious peaks at the upper and lower ends of the distribution. These upper and lower ends peaks are understood to be due to iterative error in the calculation process.

Table 8.8 Imposed finite strains and recorded ellipsoid axial ratios for elongate population 1

Imposed finite strains				Modelled ellipsoid axial ratios						
X/Z	Y/Z	X/Y	log K-value	X/Z	Standard deviation	Y/Z	Standard deviation	X/Y	Standard deviation	log K-value
1.5	1.5	1	0	3.1	7.23	3.21	6.09	2.19	2.89	0.67
2	2	1	0	2.89	3.48	3.58	3.77	1.92	1.97	0.51
3	3	1	0	3.84	4.70	2.98	9.17	2.47	4.06	0.83
5	5	1	0	4.6	5.34	3.24	3.07	2.89	8.23	0.90
8	8	1	0	4.3	1.5	2.96	6.54	2.12	6.45	0.69
10	10	1	0	5.2	9.17	4.24	12.64	2.59	6.62	0.67
30	30	1	0	9.42	34.1	9.66	34.77	2.52	8.34	0.41
4	2	2	1	4.85	7.71	4.72	9.46	2.84	4.72	0.67
8	2.82	2.82	1	5.78	9.92	2.73	4.12	2.71	3.44	1.00
5	2.24	2.24	1	5.75	n/a	3.06	n/a	2.36	n/a	0.77
8	2	4	2	6.62	19.88	2.72	4.39	3.04	7.99	1.11
10	2	5	2.32	8.70	19.8	2.85	3.34	3.26	5.54	1.12
2	1	1	∞	2.96	2.13	1.86	1.56	1.82	1.27	0.96
3	1	1	∞	4.76	6.75	2.61	2.87	2.51	3.07	0.96
5	1	1	∞	5.46	5.88	2	2.21	3.14	5.46	1.65



Correlation between imposed finite strain and recorded mafic ellipsoid axial ratio for Elongate population 1
Figure 8.7

Elongate population 2

This population was defined with a very significant initial axial ratio to each of the ellipsoids, one length was defined as having mean length 30, and the other two lengths as having mean length 5, with both lengths having standard deviation of 2. This produces a set of ellipsoids with the initial projected characteristics listed in Table 8.9, most notable here are the very high initial axial ratios and significant deviations, relative to any of the previously studied populations.

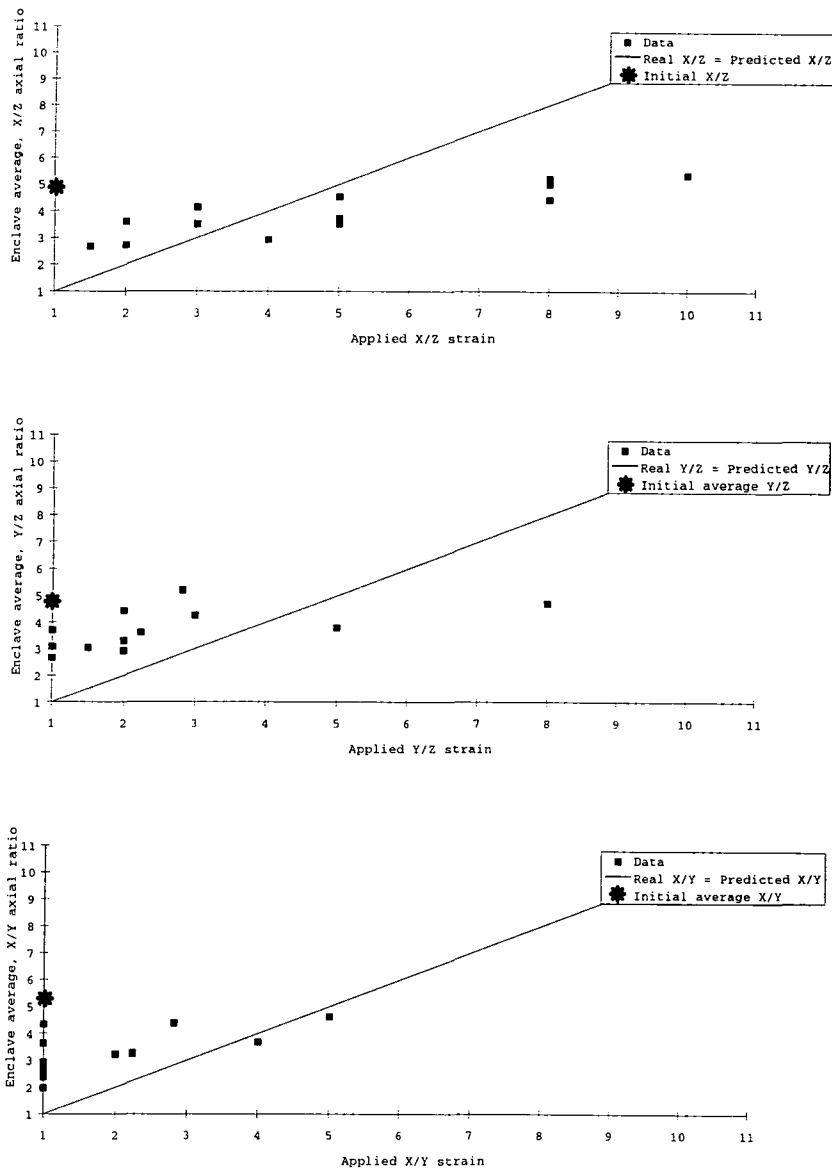
Table 8.9 Initial characteristics of Elongate population 2, one direction mean 30 standard deviation 2, two direction mean 5, standard deviation 2

Number	35		
Average axial ratio X/Y	5.25	Standard deviation X/Y	2.76
Average axial ratio X/Z	4.89	Standard deviation X/Z	2.13
Average axial ratio Y/Z	4.71	Standard deviation Y/Z	1.79
Largest X	29.73	Smallest X	19.70
Largest Y	26.93	Smallest Y	20.76
Largest Z	10.06	Smallest Z	3.11
$\omega \log X$	0.18		
$\omega \log Y$	0.11		
$\omega \log Z$	0.51		

After deformation the ellipsoid axial ratios (Table 8.10) record a strong, and well defined linear increase with applied finite strain (Table 8.11, Figure 8.8). In detail this shows that, at low imposed finite strains ($X/Z=Y/Z=X/Y < 4$), the recorded axial ratio is in excess of the unity line but, at higher imposed finite strains recorded axial ratio data plots below the unity line (Figure 8.8). Within each sample the variation is very high, an example histogram (Figure 8.10f, applied flattening $X/Z=3$, mean 4.15, standard deviation, 7.87) shows an almost flat distribution across a wide range of possible axial ratios. These characteristics are a result of the elongate initial characteristics of the ellipsoid population.

Table 8.10 Imposed finite strains and recorded ellipsoid axial ratios for elongate population 2

Imposed finite strains				Modelled ellipsoid axial ratios						
X/Z	Y/Z	X/Y	log K-value	X/Z	Standard deviation	Y/Z	Standard deviation	X/Y	Standard deviation	log K-value
1.5	1.5	1	0	2.67	5.38	3.05	7.93	2.39	6.37	0.78
2	2	1	0	3.61	7.07	3.31	10.0	2.82	4.59	0.87
3	3	1	0	4.15	7.87	4.26	16.9	1.98	2.41	0.47
5	5	1	0	3.73	n/a	3.8	n/a	2.52	n/a	0.69
8	8	1	0	4.45	10.2	4.72	9.03	2.69	3.93	0.64
4	2	2	1	2.93	9.33	3.31	12.4	3.23	5.38	0.98
8	2.82	2.82	1	5.03	9.74	5.2	20.6	4.38	5.29	0.89
5	2.24	2.24	1	4.54	6.36	3.61	7.26	3.27	5.64	0.92
8	2	4	2	5.23	8.38	2.93	5.21	3.69	2.47	1.21
10	2	5	2.32	5.39	13.57	4.45	21.94	4.63	9.68	1.03
2	1	1	∞	2.73	3.90	2.67	5.10	2.93	3.10	1.09
3	1	1	∞	3.52	5.79	3.71	16.05	3.63	3.48	0.98
5	1	1	∞	3.53	5.75	3.08	10.66	4.34	9.38	1.3



Correlation between imposed finite strain and recorded mafic ellipsoid axial ratio for Elongate population 2
Figure 8.8

log K-values

For each of the studied populations, at each of the imposed finite strains the log K-value (Flinn 1962) was calculated as is recorded in each of the Tables 8.2, 8.4, 8.6, 8.8 , 8.10. Figure 8.9 shows a graph of these values, imposed against calculated, showing that the modelled K-value shows very high variation relative to the predicted value. This is largely a result of the strong deviation in all of the post-deformation datasets.

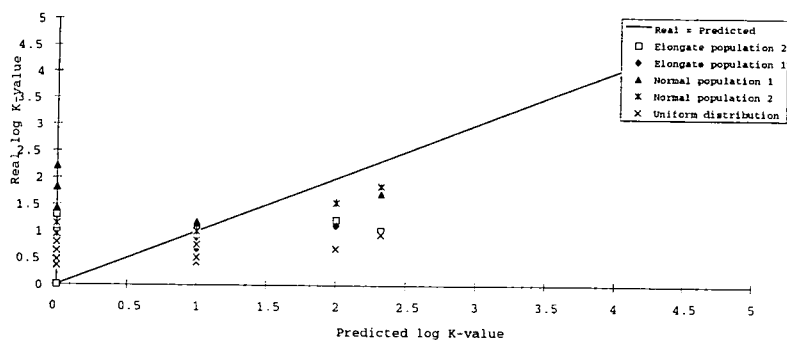


Figure 8.9 log K-values for predicted and modelled datasets

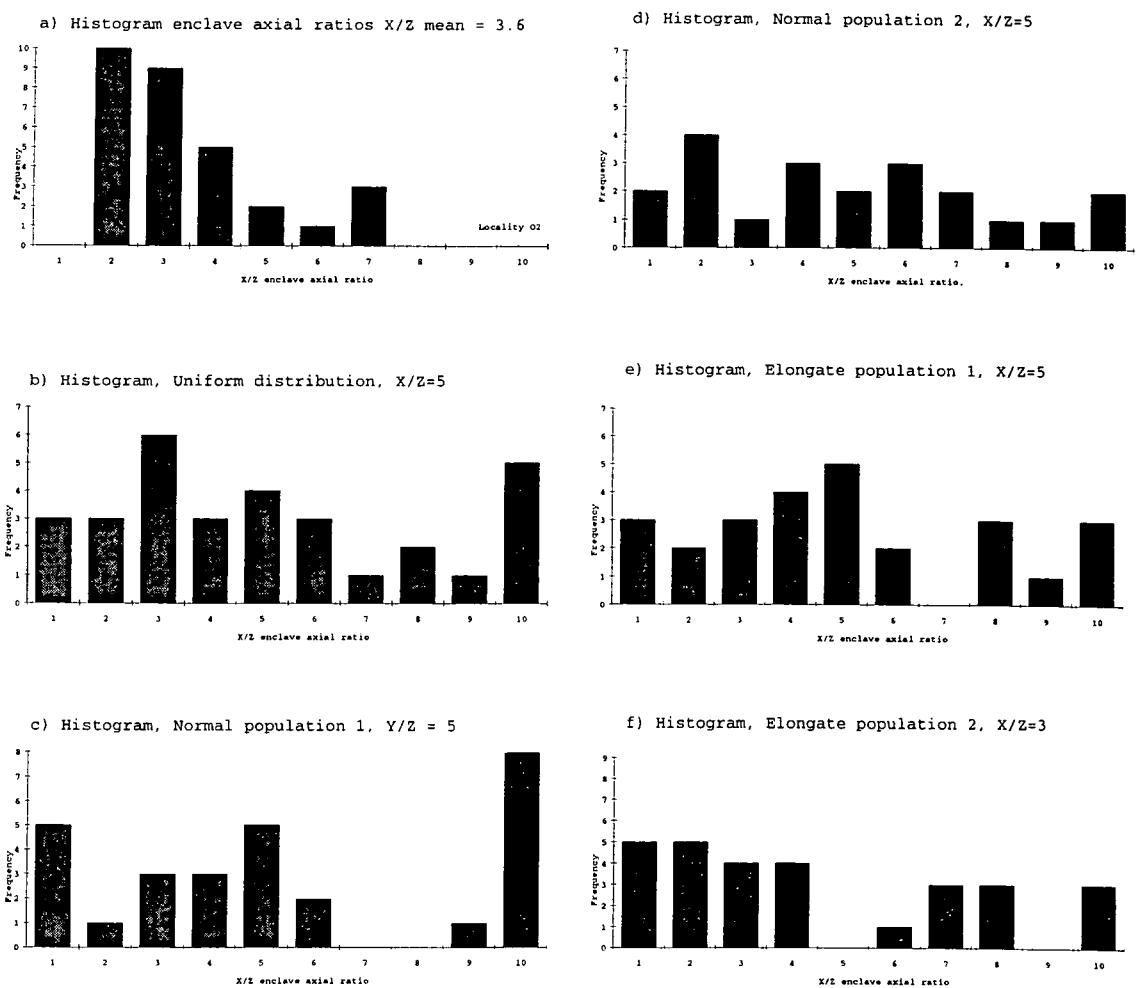


Figure 8.10 Histograms of outcrops and modelled ellipsoid / enclave axial ratio populations

Table 8.11 Correlation co-efficients for each individual dataset

Correlation co-efficient = A , where for a straight line through the origin $y = Ax$; A being the gradient. R^2 is the degree of variability in the data set which describes the straight line $y = Ax$

Pearson correlation co-efficient and R^2 , of imposed vs. modelled finite strains for each individual data set					
X/Z	R^2	Y/Z	R^2	X/Y	R^2
Correlation co-effs all data					
0.672988	0.452912	0.727595	0.529394	0.640873	0.410718
Correlation co-effs uniform population					
0.723605	0.523604	0.875227	0.766022	0.46761	0.218659
Correlation co-effs normal population 1					
0.464176	0.21546	0.833402	0.694559	0.905617	0.820141
Correlation co-effs normal population 2					
0.848768	0.720407	0.888474	0.789387	0.819819	0.672103
Correlation co-effs elongate population 1					
0.865991	0.749941	0.570463	0.325428	0.655698	0.42994
Correlation co-effs elongate population 2					
0.95276	0.907752	0.912682	0.828909	0.497388	0.247394

8.2.4 Conclusions and discussion

The data above demonstrates that a deformation matrix can be used to model the finite strain applied to a population of ellipsoids randomly orientated in space. As a mathematical exercise it demonstrates that: i) imposed deformation will be mimicked by the ellipsoids irrespective of the initial shape characteristics of the population; ii) that the iteration/optimisation method used produces ellipsoids which may not be a unique solution to the supplied data, inducing a wide variation into the results; iii) the linear relationship between imposed finite strain and recorded axial ratio breaks down at high imposed finite strains, axial ratio >10 .

If the assumptions made at the beginning of this analysis, that an enclave can be modelled as a deforming ellipsoid and that there is strong coupling between granitic magma and enclave are valid, then the results of this model imply that: i) irrespective of even major initial shape obliquity, enclaves preserve a valid record of the imposed finite strains; ii) the strain record is easily interpretable for $X/Z = Y/Z/X/Y < 10$, but more complex at higher values; iii) measurement of mafic enclave axial ratios provides an accurate method of quantifying magmatic strain.

The validity of the assumptions is questioned by Fowler & Paterson (1997) but the enclave axial ratio data measured as part of this study (see Chapters 2-8) and their field characteristics e.g. rings of concentrically increasing enclave axial ratio, used in conjunction with the models, demonstrates the general validity of using enclave axial ratio population measurements as strain markers. In particular this analysis invalidates the comments of

Vernon & Paterson (1993) who disregard enclave axial ratio measurements on the basis of axial ratio variation across an outcrop. Population variation is inherent and due to the initial characteristics of a population, enhancing through its variability, rather than inhibiting the analysis process.

8.2.5 Further work

The model described above illustrates the usefulness of this sort of modelling in correlating field data but there are some problems with it, in particular the variability within a sample. Any future, more robust analysis should include more ellipsoids and more ellipsoid defining vectors. Three vectors allows a variation to exist in the iterative solution.

8.3 Modelling aureole deformation

8.3.1 Introduction

In Chapter 2 the deformation both within and around the Ardara pluton, NW Ireland were described and discussed. This pluton displays the remarkable co-existence of: i) concentrically increasing finite strain values within the pluton from the 'injection point' to the contact; ii) surrounding country rocks which display very high finite strain at the contact, and a rapid reduction in finite strain, approximately 500m from the contact (Figure 2.8, 2.17a).

The following analysis takes a line-section through the wallrock and aureole surrounding a pluton of identical size to the Ardara pluton. This modelled pluton is assumed to have been emplaced into homogenous country rock by in-situ expansion processes. The magma supply is taken as constant, maintaining steady-state temperature conditions in the aureole. The line-section is used to model the deformation in the aureole, given the conditions above, for a rheology which can be generally modelled using the power-law equation (Equation 8.5).

It is known from experimental work that under medium-low experimental strain conditions deformation can be modelled using a power-law equation e.g. Kirby 1983, Paterson 1987, Twiss & Moores 1992, Wilks & Carter 1990 (Equation 8.5, rheological theory was described in Chapter 1). In a power-law environment there is no linear relationship between stress and strain. The induced strain rate is dependent upon the applied differential stress σ_d to the power n ; when $n=1$ the material behaves truly viscously, as a Newtonian fluid, but with increasing values of n greater plasticity is observed, until $n>3$ where the material becomes truly plastic. There is also a temperature exponent, which controls an energy barrier to deformation. The larger the value of the activation energy, Q , the greater temperature or differential stress is required to produce a given strain rate.

Equation 8.5 A power-law rheology,

$$\dot{\epsilon} = A \sigma_d^n \exp(-Q/RT)$$

where σ_d is the differential stress ($\sigma_1 - \sigma_3$), T is in Kelvin, Q is the activation energy, R is the gas constant, A is constant and n is the power law exponential. For crustal rocks $n=2-3$, $Q=150-260$ kJ/mol and $A=10^{-3}-10^{-6}$ Pa^{- n /s} (Twiss & Moores 1992)

Using this 1-dimensional power-law equation and applying it to deformation under a variety of possible conditions across the line-section (through the model aureole) while changing the value of n and Q , and varying the speed of expansion, it was hoped to provide an insight into the processes at work during the emplacement of the Ardara pluton.

8.3.2 Methodology

The line-section is divided into elements, each 50m in width, each subject to a temperature and a differential stress, which can be shortened during pure shear deformation (Figure 8.11). the section will preserve a cumulative finite strain through time integration of the strain rate.

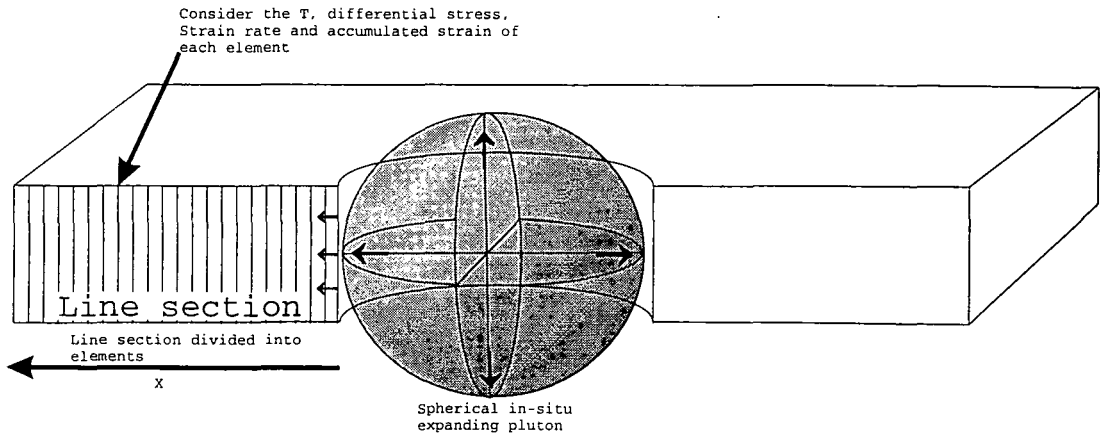


Figure 8.11 Elemental approach to aureole deformation

Temperature regime

The temperature within the aureole of any pluton, which might be expanding during emplacement, is unknown unless recourse is made to theoretical models of hot cooling bodies. In this analysis the temperature profile is assumed to be steady state at all times across the aureole, and equivalent to that derived for the aureole of the Ardara pluton by Kerrick (1987). Figure 8.12 shows a parameterisation of that data which predicts a temperature of $\sim 650^\circ\text{C}$ at the contact dropping to around 350°C at 1km distant.

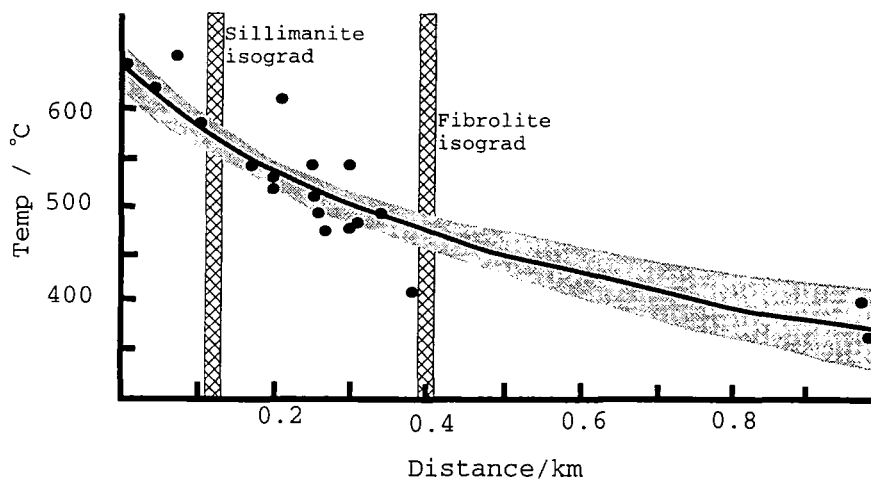
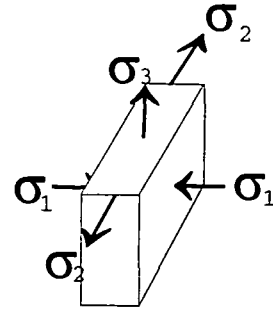
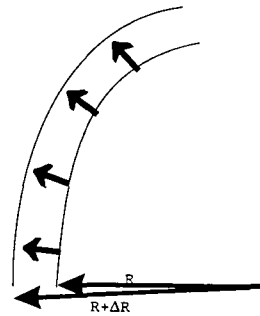


Figure 8.12 Temperature variation estimate across the aureole of the Ardara pluton, from Kerrick (1987)

Differential stress

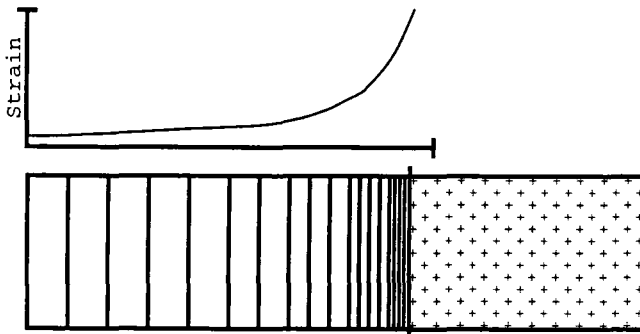
The differential stress affecting the wallrock is taken as the result of stress induced by the forceful expansion of the spherical pluton (Figure 8.13a) and is defined by Equation 8.6, where, σ_1 is orientated perpendicular to the pluton contact. for the purpose of this calculation on the line section $\sigma_3 = \sigma_2$ are orientated parallel to the pluton contact have an effective value of zero. This stress is recalculated for each element, for each increment of pluton volume, ΔV , occurring with every increment of time, Δt .

A pluton expanding from radius R to a radius $R+\Delta R$ exerts a differential stress on any wallrock element

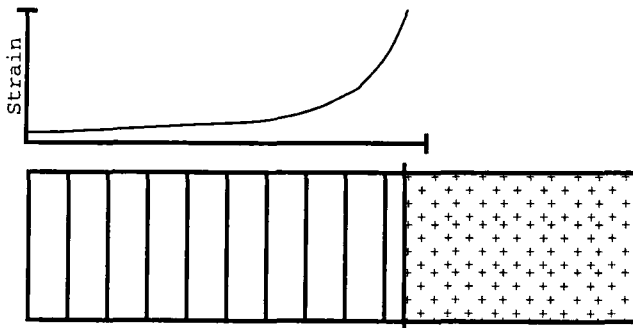


where σ_1 = expansion stress + regional stress and σ_2, σ_3 = regional stress

a) Differential stress due to pluton emplacement



For each expansion increment, stress, induces a strain which shortens wallrock elements, which are re-sized, elemental strain is re-calculated before the next expansion increment.



b) Strain accumulation through shortening

Figure 8.13

If a pluton emplaces a volume of magma ΔV which increases the pluton radius from R_0 to $R_0 + \Delta R$ this requires the movement of country rock away from the pluton a distance ΔR , which is achieved through applying a differential stress, σ_d , to induce a strain.

Stress = Force/Area hence,

Equation 8.6 Differential stress at the contact is simply,

$$\sigma_d = \Delta V \cdot (\rho_g - \rho_{cr}) / 4\pi R_0^2$$

where ρ_g and ρ_{cr} are granite and country rock densities respectively.

Differential stress can be found throughout the aureole by substituting distance from pluton centre for $R_0 + \Delta R$.

In the case of Ardara $\rho_g - \rho_{cr} = 70 \text{ kg/m}^3$ (Akaad 1956a, Young 1966)

Strain accumulation

For each element during each time increment Equation 8.5 describes an induced strain rate. Time integrating this strain rate over Δt , describes the finite strain (extension/length) recorded in the plane of the model by this element. In order to calculate the accumulated finite strain it is necessary to take account of the shortening (wallrock shortening) of each element due to the incremental strain. When this shortening has been calculated, the average strain for initial element size is calculated (Figure 8.13b). This averaged incremental value can then be added to the accumulated finite strain value for each element.

The model was devised and run using Fortran 77 code (listing in Appendix 14), implemented on a HP-UX workstation. The results obtained are detailed below.

8.3.3 Results

A number of different emplacement environments were modelled, firstly varying the power-law exponential, secondly varying the activation energy and thirdly examining the effect of variable speed of intrusion. In all cases element size is 50m. The accumulated strains (referred to as finite strains) are plotted to a distance of 4000m from the contact. Each set of results is accompanied by a set of graphs detailing the results: the first shows the accumulated strain (extension/length) on a log scale, the second has this finite strain re-calculated as strain ellipse axial ratio on a log scale, the third shows the same data on a uniform scale and the final plot has finite strain re-calculated as accumulated country rock shortening. Where not stated the time allowed for emplacement is 10,000yrs and the time increment is 1 yr. The other calculation co-efficients used are $n=2.5$, $A=10^{-4} \text{ Pa}^{-n}/\text{s}$ and $Q=10^5 \text{ kJ/mol}$, values which are consistent with experimentally derived power-law deformation co-efficients.

Variation in power-law exponential

From Equation 8.5 increasing the value of n increases the rate at which increasing differential stresses can overcome the retarding effect of the temperature exponential. Published studies suggest a large variation in the value of the power-law exponential ($n=1$ through to $n=83$ Shea & Kronenburg 1993) though most experiments suggest n is between 1 and 4 (Twiss & Moores 1992). A number of scenarios were run for an expanding pluton, using large variation in n .

The results showed that with increasing n there is a zone which increases in width, into which finite strains are partitioned (Figure 8.14). When n is greater than 6, this zone of high strain extends throughout the measured section. Any, even a small differential stress, results in very high strains, i.e. plastic behaviour. For $n=1$ there is no deformation partitioning and deformation is entirely viscous. At intermediate values of n (2-3) there is an inner zone of high strain plastic deformation, before a rapid drop in finite strain (Figure 8.14c) to a viscous zone where little to no finite strain is recorded.

Using the accumulated finite strain at the contact and at ~500m from the model pluton contact suggests a time averaged strain rate of 10^{-5}s^{-1} and 10^{-10}s^{-1} respectively for $n=2.5$, values which are consistent with laboratory experiments and possibly similar to those experienced in the fastest geological processes.

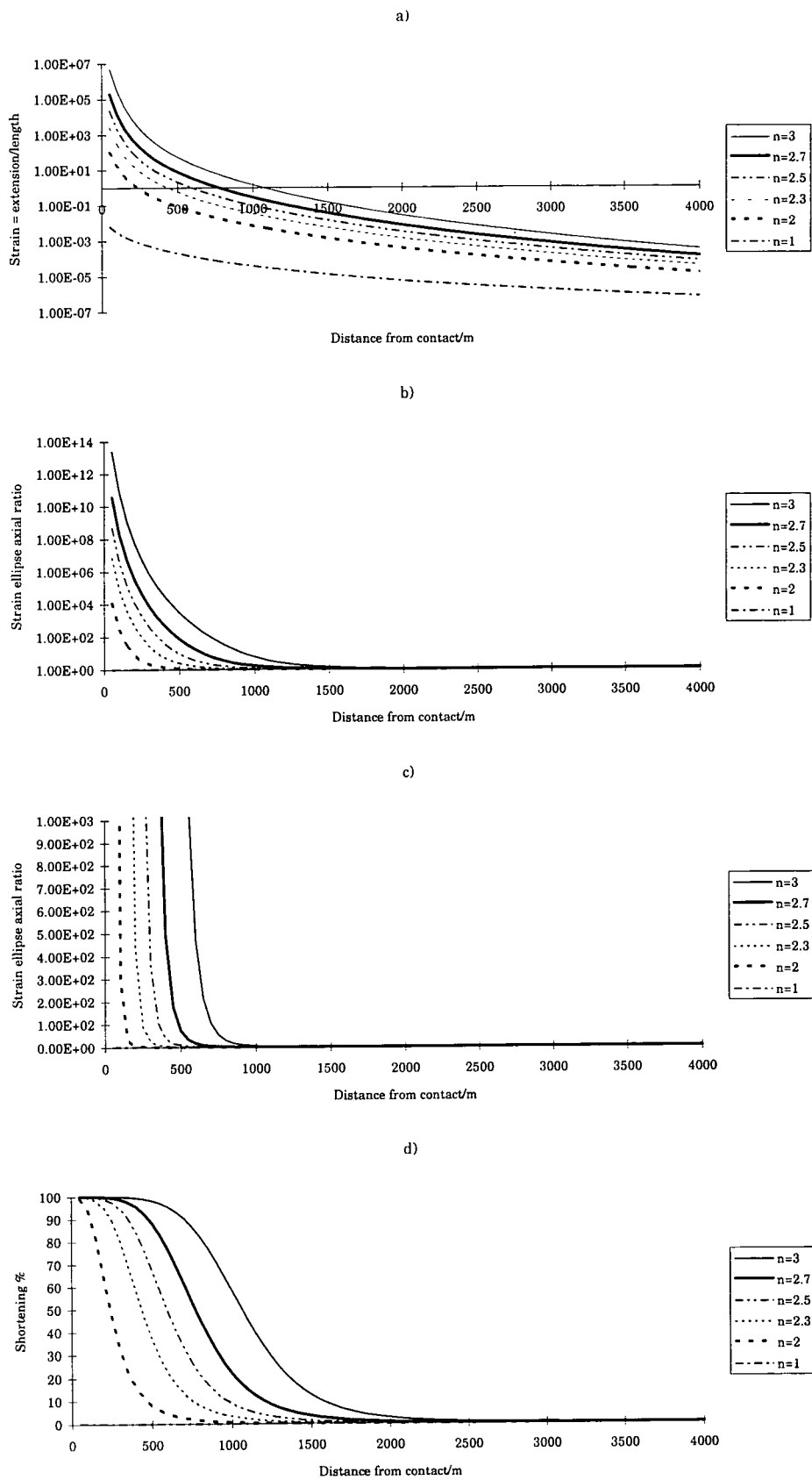


Figure 8.14 Variation in the power law exponential during deformation

Variation in activation energy

Variation of the activation energy affects the influence of temperature in the exponential term of Equation 8.6. Increasing activation energy results in increased retardation for a given applied stress at a given temperature i.e. a higher temperature is required to induce a given finite strain at a given applied differential stress. For the standard criteria defined above the model was run varying activation energy, Q between 10^3 and 10^6 kJ/mol.

This variation in Q produces changes in the width and character of the partitioned high strain zone closest to the pluton contact (Figure 8.15). At low Q , 10^3 kJ/mol, any energy barrier to deformation is quickly overcome and high finite strains are recorded across the model but at high Q , greater than 2×10^5 kJ/mol, the energy barrier is too great and almost no finite strain is recorded for the differential stresses induced in this model. When Q is intermediate between these values there is a variation in the width of the deformed zone and also in the rate of change from a viscous to a plastic regime. Increasing Q results in a more distributed variation with a consequent sharp change in deformation intensity implying a lower Q value.

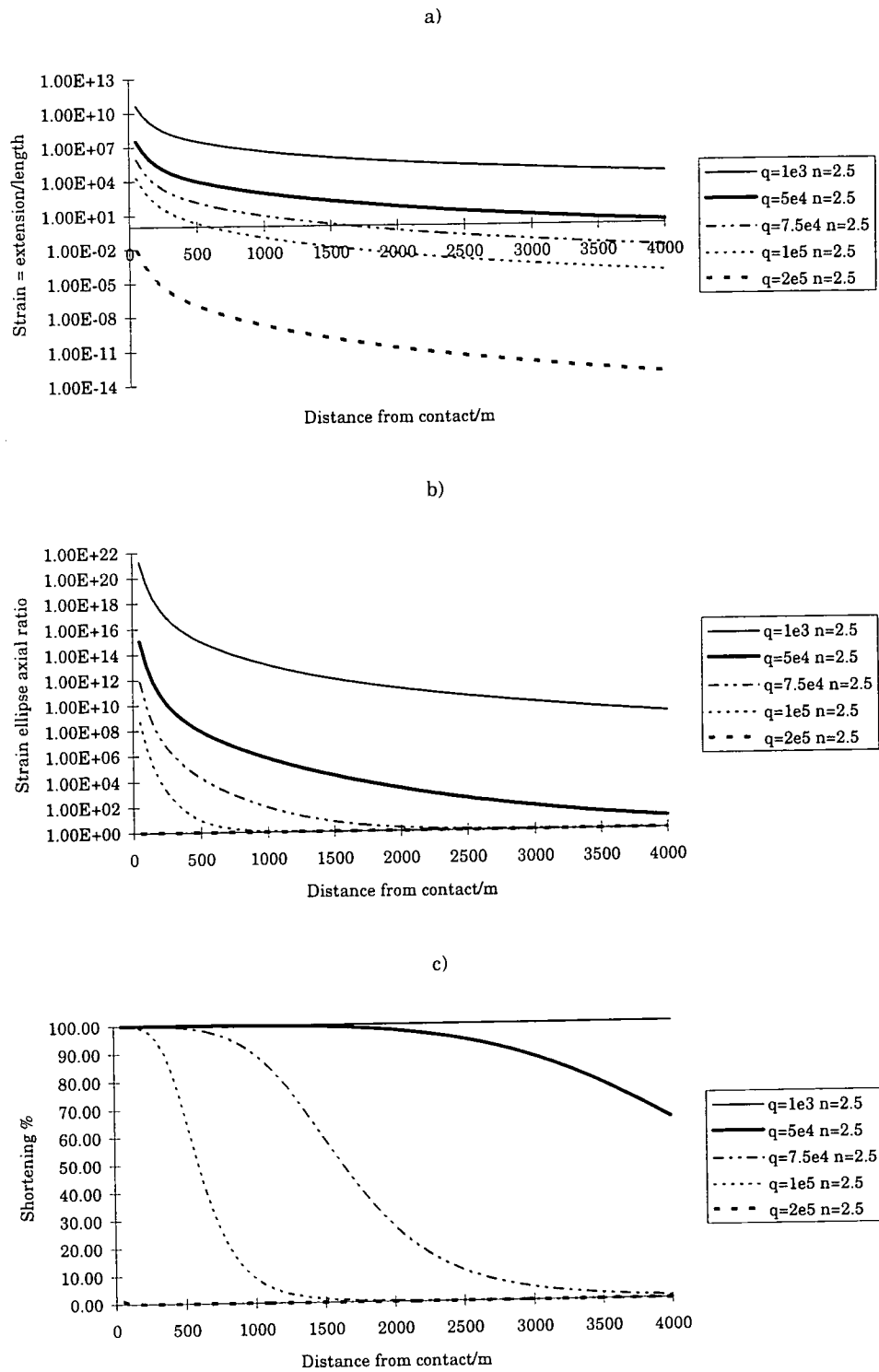


Figure 8.15 Variation in activation energy and its effect on deformation

Variation in emplacement timescales

Petford *et al* (1993) demonstrate that magma ascent through dykes could result in the emplacement of very large volumes of granitic magma in a very short timescale (10^2 - 10^3 yrs), whereas ascent as diapirs results in magma emplacement over a period of $\sim 10^6$ yrs. By varying the volume of magma emplaced during each increment the emplacement period was varied between 10^3 and 2×10^4 yrs.

Examining Figure 8.16, shows that reducing the timescale increases the width of the inner zone of partitioned high finite strain. This is a result of the increased differential stresses induced by increased volumes of magma being emplaced in a given time, hence sufficient stress exists to overcome the 'energy barrier'. A thinner zone of high finite strain implies a shorter period of emplacement.

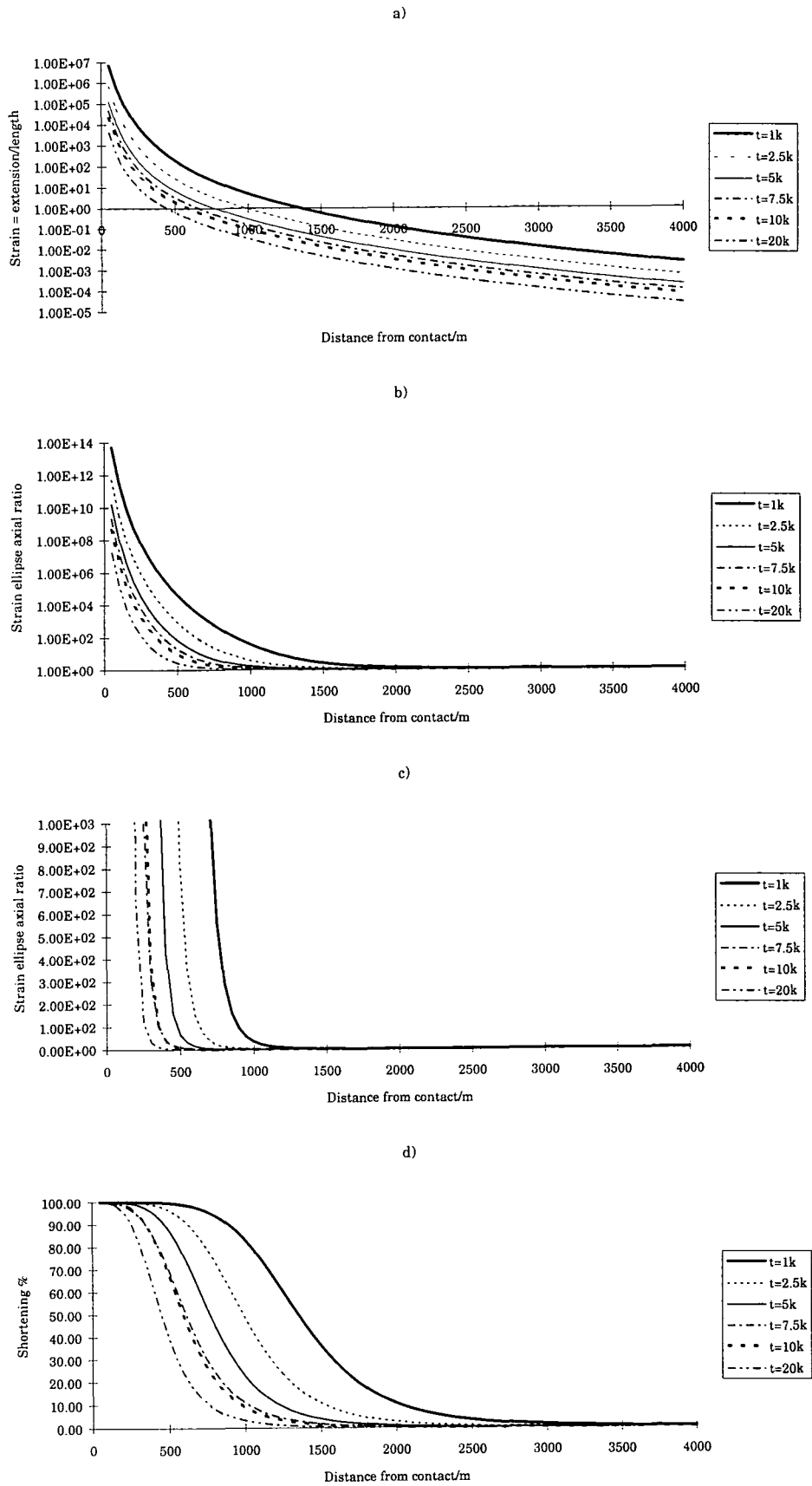


Figure 8.16 Variation in magma supply rate and its influence upon deformation preserved

8.3.4 Conclusions and discussion

In the analysis above data has been collected on the deformation characteristics of power-law wallrock around an in-situ expanding ideal pluton, assuming steady-state thermal conditions. There are three primary conclusions that can be made: i) that a power-law rheology is trivariate, depending upon the exponential co-efficient, applied differential stress, and activation energy. All three affect the width of the inner high finite strain zone, but activation energy also affects the nature of the transition between high and low finite strain; ii) in-situ expansion, given these boundary conditions, results in an inner zone of very high finite strain, before rapid transition to a lower finite strain zone as the distance from the contact increases; and iii) any real pluton is unlikely to display the homogenous wallrock rheology and steady-state conditions set-up here.

Given these data and applying it to observations made around the Ardara pluton, detailed in Chapter 2, is particularly interesting. The wallrock surrounding the pluton shows relatively low, but quantifiable finite strains in the far-field wallrock recognisable up to 7km from the pluton. At a distance of approximately 1.5km from the pluton a pervasive intrusion related cleavage forms (Meneilly 1982). At 500m from the contact bedding, early cleavages are deflected such that they are sub-parallel to the intrusion related cleavage implying that a very high finite strain is present in the wallrock (Fig 2.18). Strain measurement within the pluton also suggest that there is a strong component of in-situ expansion (part 2.3). This transition is similar to that identified in the power-law model. Therefore it is reasonable to consider the Ardara pluton as being analogous to the model and that during in-situ expansion, the wallrock was acting as a power-law fluid. Hence, given an assumed timescale for emplacement of 10,000yrs (consistent with estimates of pluton filling through dykes Petford *et al* 1993, Part 8.4), the Ardara pluton wallrock rheology had co-efficients of $A=10^{-4}$ Pa $^{-n}$ /s, $n=2.5$, and $Q=10^5$ kJ/mol. Given that there is no precise knowledge of the rheology co-efficients in the wallrock there is necessarily a quadrivariate field of possible solutions (time, A, n and Q dependent).

It is interesting to contrast this work with that of Weinberg & Podlanchikov (1994, 1995) on diapiric rise through a power-law crust. These authors demonstrate for the rise of a body through a power-law fluid the width of cumulative strain aureole actually gets smaller for increasing n (power-law exponential). This is a consequence of the cumulative strain field formed by material travelling past the rising diapir. Therefore if the width of the strain 'aureole' and the rheological coefficients of the wallrock are known, it could be possible to distinguish between the relative importance of diapiric and in-situ expansion processes during ascent and emplacement.

Similarly if this model were applied more generally, to a pluton aureole whose country rock and magma, finite strain and deformation characteristics are well known, it could be possible to establish a field of possible wallrock and emplacement criteria. If, in addition,

appropriate experimental data was available on the deformation characteristics of the wallrocks a narrowing of the field would take place, and estimates of the length of time of emplacement could be made, assuming that in-situ expansion was entirely responsible for emplacement.

8.4 Speed of emplacement

8.4.1 Introduction

Magma ascent through the crust has physical constraints which, through proper examination of the conditions prevailing in the lithosphere during formation ascent and emplacement, can be modelled to demonstrate how fast plutons can be emplaced at high crustal levels. Chapter 1 reviewed this area. In summary, if it is accepted that magma forms through a combination of mantle melt and crustal anatexis and travels through the crust to its point of emplacement, then there are two end-member solutions to magma transport, that of diapirism and that of dyking/magma sheeting.

Diapirism

This process assumes that magma travelled from a source region through the crust to its level of emplacement as a single magma body or multiple large bodies. This method has been described extensively in the literature, in early work by Ramberg (1967, 1970) and more recently by Marsh (1982), Schmeling *et al* (1988) Cruden (1988, 1990) and Weinberg & Podlanchikov (1994, 1995). In the following analysis the easily applicable equations describing a 'Hot Stokes' diapir, Marsh (1982), and their modifications by England (1988) are used to calculate 'ballpark' ascent rates for each studied pluton. Each pluton is considered as an *equivalent diapir*, this being a sub-spherical body, whose volume is estimated to be similar to the emplaced pluton, irrespective of the final outcrop shape.

Dyking/sheeting

In this process magma travels from its source, along discrete conduits as dykes or sheets and is assembled piecemeal at the level of emplacement. Leake (1978) and Pitcher (1979) first suggested sheeting as an emplacement method from field evidence, but only with the calculations of Clemens & Mawer (1992) and Petford *et al* (1993) have the implications of this process become apparent. In the following analysis the calculations set out by Petford *et al* (1993) are used to assemble plutons of similar volume to the studied plutons, through dyke-like conduits of varying sizes.

8.4.2 Methodology

Hot Stokes diapirs

The Stokes (1851) equation (Equation 8.7) describes the buoyant ascent of a solid spherical body through a medium of uniform viscosity e.g. air bubbles in water. This equation has limited applicability to a magma emplacement setting given that the Earth's crust is not isoviscous, a magmatic diapir may not be entirely solid and magma is generally hot relative to the surrounding crust, resulting in additional heat transfer related criteria. Marsh (1982) integrated these criteria into the 'Hot Stokes' model for ascent of hot (relative to the surroundings) spherical bodies through a material whose viscosity is dependent on

temperature (Equation 8.8) (Figure 8.17a). The material (wallrock) viscosity is defined as varying exponentially with a value μ_1 at the contact increasing to μ_∞ at ∞ (Equation 8.9).

Equation 8.7 Ascent velocity of a spherical body in an isoviscous system, Stokes' Law.

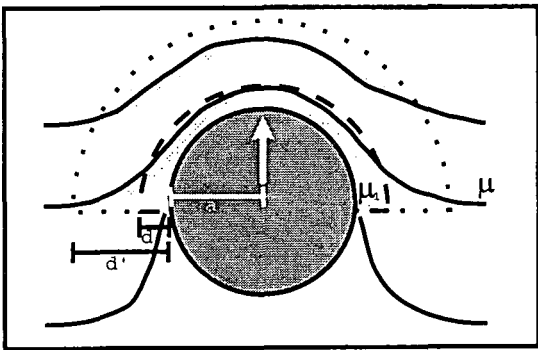
$$v = 2a^2(\rho_H - \rho_L)g/9\mu$$

Equation 8.8 Hot Stokes' equation for ascent of a sphere through a variable viscosity medium.

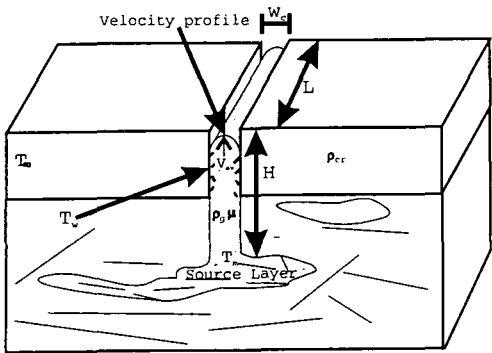
$$v = 2\Delta\rho ga^2 f^2 / 3A(1 + 0.5Pe^{0.5})^2 \mu_1$$

where Pe = Peclet number = va/κ where κ is the thermal diffusivity, v velocity of ascent and a the radius of the ascending body. μ_1 is the contact viscosity, and $\Delta\rho$ the density difference between the medium and the ascending sphere. f is a co-efficient which refers to the difference between the width of the thermal aureole (taken as $f=0.33$ through out), d' , and the width of a softened boundary layer d , such that:

$$d = f \cdot d', \text{ where } d' \text{ can be defined as } d' = a/(1 + 0.5Pe^{0.5})$$



a) Parameters affecting diapiric ascent



b) Parameters affecting dyking ascent

Figure 8.17

Equation 8.9 Assumed viscosity variation in the wallrock,

$\mu(y) = \mu_1 \exp(Ay/d)$ where y is distance from ascending sphere, μ_1 is viscosity at contact, d is the width of the softened boundary zone pluton and A is a co-efficient. A can be estimated by taking estimates of μ at the contact (10^{18} Pa.s) and in the far field (10^{22} Pa.s).

As it stands this equation has no unique solution given that the calculated ascent velocity v , appears on both sides of the equation. It can be solved iteratively for particular deformation zone thicknesses or contact viscosities. To eliminate this variation England (1988) defines a minimum Peclet number (Equation 8.10) based on the minimum strain rate recorded in the far-field, which allows a minimum ascent velocity to be uniquely defined after substitution into Equation 8.8. Marsh (1982) also recognised the possible importance of multiple pluton ascent along a single conduit and used the equation for a spheres ascent through a fluid filled cylinder to define it (Equation 8.11).

In the following analysis the equations 8.8-8.11 are used to determine possible ascent rates and times of emplacement for each of the studied plutons. For simplicity the diapirs are considered as isothermal, ascending through a homogenous medium.

Equation 8.10 Minimum Peclet number after England (1988),

$Pe = 4a^2\epsilon' / \kappa$, where ϵ' is the minimum strain which might be recorded in the aureole taken as 10^{-14} s^{-1} .

Equation 8.11 Repeated ascent along a single conduit.

$V \approx a^2 \Delta\rho g / 52\mu_1^* \cdot (f/(1 + f + 0.5Pe^{0.5}))$

where $\mu_1^* = A \mu$

Dyking/sheeting

Petford *et al* (1993) take a mechanistically simplistic approach, to modelling the ascent of magma as dykes or sheets which exploit existing faults, fractures, shear zones or lineaments, forming feeder dykes. This is a development of the theoretical and experimental models of Lister & Kerr (1991) and Clemens & Mawer (1992). Neglecting the forces required to nucleate a dyke, and using appropriate thermal and rheological constraints to laminar fluid flow between two parallel plates leads to Equation 8.12, which describes the critical minimum dyke width required for fluid flow (Figure 8.17b). Extending this allows calculation of the average velocity in Equation 8.13, and the time required for emplacement of an entire pluton (Equation 8.14) assuming uniform and constant magma supply.

Equation 8.12 Equation for critical dyke width,

$w_c = 1.5(S_m/S_\infty^2)^{3/4}(\mu\kappa H/g\Delta\rho)^{1/4}$, where w_c is the critical dyke width, H is the length of the dyke (zone of anatexis to the surface), κ thermal diffusivity, μ the magma viscosity and S_∞ and S_m Stefan numbers defined by

$$S_\infty = L/c(T_w - T_\infty)$$

$S_m = L/c(T_m - T_w)$, where L is the latent heat of solidification, c the specific heat, T_w the temperature at the dyke wall where the magma is effectively frozen, T_∞ the far-field temperature of the crust and T_m the initial magmatic temperature

Equation 8.13 Horizontally averaged ascent velocity V_{av} ,

$$V_{av} = g\Delta\rho w_c^2/12\mu$$

Equation 8.14 Time taken to emplace an entire pluton of volume, Q

$$\Delta t = Q/V_{av}w_c l, \text{ where } l \text{ is the lateral extent of the conduit.}$$

In applying these equations to the studied plutons a number of variable conduit lateral lengths were used (detailed in the results) and each dyke was assumed to travel up through 30km (dyke length) of crust, from source to emplacement. Using these boundary conditions a population of possible results was defined by varying the possible magma conditions by changing magma viscosity from 10^4 to 10^8 Pas, magma initial temperature (T_m) between 900 and 700°C, and the magma freezing temperature (T_w) between 750 and 550°C. Only magma far-field temperature was kept constant at 350°C, consistent with field evidence from both field areas. These populations defined a range of possible conditions the characteristics of which are described below.

8.4.3 Results

Each of the emplacement analyses carried out has used a similar set of defined physical parameters which are known to be consistent across the majority of the country rocks and granites. These are detailed in Table 8.12 below:

Table 8.12 *Physical properties of granite and metamorphosed country rock, where no specific reference is made the general parameters set out by Petford et al (1993) have been used*

Properties	Granite Ardara	Atibaia / Morro Azul / Imbiricu / Itapeti	Country rock Donegal	Brazil
Density, ρ / Kgm^{-3}	2.68 Akaad (1956a)	2.65 Telford et al (1990)	2.75 Young (1966)	2.96 Telford et al (1990)
Specific heat, C_p / $\text{J}^{-1}\text{°C}^{-1}$	1.2	1.2	1.2	1.2
Latent Heat magma L/ J/Kg	3×10^5	3×10^5		
Thermal diffusivity, κ / m^2/s	8×10^{-7}	8×10^{-7}	8×10^{-7}	8×10^{-7}
Far field country rock viscosity/ Pas			1×10^{22}	1×10^{22}
Granite viscosity range/ Pas	$10^4 - 10^8$	$10^4 - 10^8$		

The Ardara pluton

As described extensively in Chapter 2, the Ardara pluton is a sub-spherical pluton which has been cited as a type example of both a diapirically emplaced and a ballooning pluton, expanding in-situ from a central magma source. In this analysis pluton volume is taken as a sphere, or spheres (where each sphere is the volume of one magmatic phase), whose radius is equivalent to the pluton radius, or the equivalent pluton radius for that magmatic phase respectively. These pluton volumes are then analysed as a single Hot Stokes diapir, multiple diapirs following a similar path and as an in-situ expanding spherical pluton fed from a linear source, the results are:

- 1. A Hot Stokes diapir** - The ascent of the Ardara pluton as a single Hot Stokes diapir has been modelled in two ways. The first uses an iterative solution to Equation 8.8 for a fixed contact viscosity, the second uses the far field Peclet number defined by England (1988), Equation 8.10. The results of this first analysis, using a contact viscosity of 1×10^{18} Pas (an experimentally determined value for high temperature wallrock creep, quoted by England 1988) are shown in Table 8.13. Of particular remark is that the calculations predict an inner deformed zone of width 800m and a thermal aureole of 2.5km, in conjunction with a time for ascent along a 30km conduit of 2.9Ma.

Table 8.13 Optimised diapiric ascent characteristics for the Ardara pluton

ascent velocity/m/s	3.21×10^{-10}
$\Delta\rho/\text{kg/m}^3$	70
radius pluton/m	4000
d / deformed zone	808
μ_1 , contact viscosity	1×10^{18}
f	0.33
Peclet number/Pe	1.61
Conductivity/ m^2/s	8×10^{-7}
d', thermal aureole/m	2448
g	9.81
viscosity co-efficient	0.93
Emplacement time/ Ma	2.9

Applying the minimum Peclet number using a number of different contact viscosities (10^{14} - 10^{18} Pas) produces the data in Table 8.14 which shows that the minimum far-field Peclet number is a factor of 2 lower than that calculated by iteration, and in this case predicts a deformed zone 900m in width and a thermal aureole 2.7km wide. In particular these data demonstrate that strong variation in ascent rate is caused by variation in contact viscosity. If contact viscosity was reduced to 10^{14} Pas then ascent of a diapir through 30km of crust would occur in less than 500yrs, alternatively setting viscosity at 10^{18} Pas and the emplacement time is 131Myrs.

Table 8.14 Ascent data for far-field Peclet number and variable contact wallrock viscosity, Ardara pluton

ascent velocity/m/s	7.25×10^{-12}	4.83×10^{-11}	3.63×10^{-10}	2.9×10^{-9}	2.42×10^{-8}	2.07×10^{-7}	1.81×10^{-6}
$\Delta\rho/\text{kg/m}^3$	70	70	70	70	70	70	70
radius pluton/m	4000	4000	4000	4000	4000	4000	4000
d, deformed zone/m	912	912	912	912	912	912	912
μ_1 , contact viscosity	1×10^{20}	1×10^{19}	1×10^{18}	1×10^{17}	1×10^{16}	1×10^{15}	1×10^{14}
f	0.33	0.33	0.33	0.33	0.33	0.33	0.33
Minimum Peclet number	0.8	0.8	0.8	0.8	0.8	0.8	0.8
Conductivity/ m^2/s	8×10^{-7}	8×10^{-7}	8×10^{-7}	8×10^{-7}	8×10^{-7}	8×10^{-7}	8×10^{-7}
d', thermal aureole/m	2763	2763	2763	2763	2763	2763	2763
g	9.81	9.81	9.81	9.81	9.81	9.81	9.81
Viscosity co-efficient, A	0.52	0.78	1.05	1.31	1.58	1.84	2.10
Emplacement time/yrs	1.31×10^8	1.96×10^7	2.62×10^6	3.27×10^5	3.9×10^4	4590	524

2. Multiple diapirs - In this case each of the plutonic phases present within the pluton (3 in Ardara) are considered to have ascended as individual diapirs (Equation 8.8), with unique ascent paths, and also as single diapirs, following the same ascent path (Equation 8.11), using pluton volume estimates to calculate the *effective diapiric radius* of each phase. The results are shown in Table 8.15 and demonstrate that: i) if the plutons are considered as having unique ascent paths their ascent velocity is low, ($\sim 10^{-10}$

m/s) resulting in individual ascent times of 3-4Ma (total time ~11Ma) and deformed zones around the contact of each plutonic phase of ~650m; ii) if the plutons use a similar ascent path (one is encased in an annular shell of the previous phase) then G2 and G3 ascend an order of magnitude faster than when a unique path is considered, giving a total time for ascent of ~4Ma.

Table 8.15 Ascent rates of multiple diapirs along a single conduit

Phase	G1	G2	G3
Ascent velocity if individual single plutons /m/s	2.7x10 ⁻¹⁰	2.68x10 ⁻¹⁰	2.54x10 ⁻¹⁰
Δρ/kg/m ³	70	70	70
radius pluton/m	3110	3085	2855
d, deformed zone/m	678	674	638
μ ₁ , contact viscosity	1.0x10 ¹⁸	1.0x10 ¹⁸	1.0x10 ¹⁸
f	0.33	0.33	0.33
Minimum Peclet number	1.04	1.03	0.906
Conductivity/m ² /s	8.0x10 ⁻⁷	8.0x10 ⁻⁷	8.0x10 ⁻⁷
d', thermal aureole/m	2056	2045	1934
g	9.81	9.81	9.81
Viscosity co-efficient, A	0.78	0.77	0.73
Emplacement time/yrs	3.52x10 ⁶	3.54x10 ⁶	3.74x10 ⁶
Volume of each phase/m ³	1.26x10 ¹¹	1.23x10 ¹¹	9.75x10 ¹⁰
Then recalculating for multiple diapirs using the same conduit			
Ascent velocity / m/s		G2 after G1 2.83x10 ⁻⁹	G3 after G1 & G2 2.8x10 ⁻⁹
Emplacement time using identical conduit / yrs		3.36x10 ⁵	3.3x10 ⁵

3. Sheeting / dyking - Equations 8.12-8.14 were used with variable initial magma conditions, to calculate a population of critical fracture sizes and ascent rates. Pluton filling periods were then calculated using the lateral dyke extent. Two estimates were made; the first of 750m, the estimated minimum radius of the injection zone (see Chapter 2); the second of 7000m, the approximate length of the southern shear zone and the maximum possible conduit length. The conditions were set with the aim of defining a population of values within which all possible magma and conduit conditions for this pluton would lie. The results are plotted in Figure 8.18 and raw data collated in Appendix 15. Figure 8.18 shows that the majority of data clusters around an emplacement time of 10³ to 10⁴ yrs and corresponding conduit widths of 0-20m, the mean emplacement time being 4140 yrs and mean fracture width 10m. These values are for continuous magma supply and hence probably a significant under-estimate. However the emplacement time, if magma supply is sufficient to achieve critical dyke width only 10% of the time, is 10⁵ yrs.

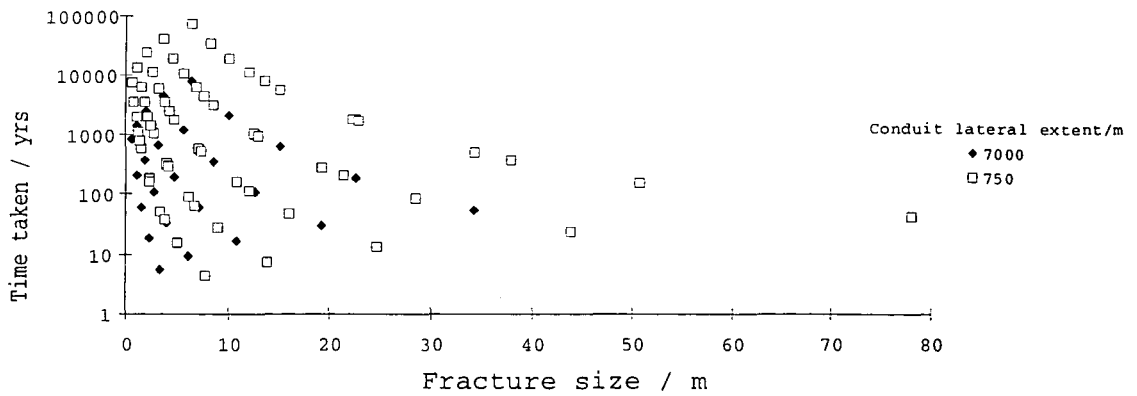


Figure 8.18 Ardara pluton, emplacement time against critical fracture size

Plutons from the Rio Paraíba do Sul shear belt

Each of the plutons from the Rio Paraíba do Sul shear belt has been modelled using similar calculations to those set out for the Ardara pluton. The plutons of the belt all have a linear shape, or a determinable three dimensional shape. Their volume has been determined using best estimates of average pluton depth, determined from geophysical data (5km from Vignerresse 1988). From this volume estimate *effective diapir sizes* have been calculated, before modelling them as Hot Stokes diapirs. Furthermore this volume estimate has been used to determine critical dyke widths and pluton filling times using a dyking sheeting model. For each pluton three conduit lengths were modelled: i) the undeformed length of the pluton; ii) half the undeformed length of the pluton; and iii) 1000m.

1. **A Hot Stokes diapir** - Each of the plutons has been modelled using the iterative approach of Equation 8.8 and, for a contact viscosity of 10^{18} Pas, the results of these calculations are shown in Table 8.16. Generally each pluton would have been an *equivalent diapir*, which rose at a speed of $5-7 \times 10^{-10}$ m/s, and produced a deformed zone of 500-700m width within a thermal aureole 1.5-2.0km wide. These values would have resulted in diapiric ascent through 30km of crust in 1.2-1.6 Ma.

Table 8.16 Optimised diapiric ascent data for the plutons of the Rio Paraiba do Sul shear belt

Pluton	Atibaia	Imbiricu	Itapeti	Morro Azul
ascent velocity/m/s	7.81×10^{-10}	7.08×10^{-10}	5.60×10^{-10}	6.68×10^{-10}
$\Delta\rho/\text{kg/m}^3$	201	201	201	201
radius pluton/m	4160	3541	2462	3228
d, deformed zone/m	683	620	490	585
μ_1 , contact viscosity	1×10^{18}	1×10^{18}	1×10^{18}	1×10^{18}
f	0.33	0.33	0.33	0.33
Peclet number	4.0	3.12	1.72	2.69
Conductivity/ m^2/s	8×10^{-7}	8×10^{-7}	8×10^{-7}	8×10^{-7}
d', thermal aureole/m	2070	1880	1486	1773
g	9.81	9.81	9.81	9.81
Viscosity co-efficient, A	0.787	0.714	0.564	0.673
Emplacement time/Ma	1.2×10^6	1.3×10^6	1.6×10^6	1.4×10^6

Using the alternative method for calculating the Peclet number described by England (1988) (Equation 8.10), and a far field strain rate of 10^{-14} s^{-1} , results in minimum ascent speeds controlled by the contact viscosity (Table 8.17), enlarged deformed zones and thermal aureoles, relative to the iterative approach (Table 8.16). Using two possible limiting cases for the wallrock viscosity shows, the very wide variation in the ascent speed (10^{-6} - 10^{-11} m/s) and emplacement time (10^7 - 10^2 yrs) depending upon the viscosity of the wallrock (10^{20} - 10^{14} Pas).

Table 8.17 Ascent data for far-field Peclet number for plutons from the Rio Paraiba do Sul shear belt

Pluton	Atibaia		Imbiricu		Itapeti		Morro Azul	
ascent velocity/m/s	2.14×10^{-11}	5.35×10^{-6}	1.91×10^{-11}	4.78×10^{-6}	1.45×10^{-11}	3.64×10^{-6}	1.79×10^{-11}	4.47×10^{-6}
$\Delta\rho/\text{kg/m}^3$	201	201	201	201	201	201	201	201
radius pluton/m	4162	4162	3541	3541	2462	2462	3228	3228
d, deformed zone/m	937	937	837	837	637	637	782	782
μ_1 , contact viscosity	1×10^{20}	1×10^{14}	1×10^{20}	1×10^{14}	1×10^{20}	1×10^{14}	1×10^{20}	1×10^{14}
f	0.33	0.33	0.33	0.33	0.33	0.33	0.33	0.33
Peclet number	0.86	0.86	0.62	0.62	0.30	0.30	0.52	0.52
Conductivity/ m^2/s	8×10^{-7}	8×10^{-7}	8×10^{-7}	8×10^{-7}	8×10^{-7}	8×10^{-7}	8×10^{-7}	8×10^{-7}
d', thermal aureole/m	2840	2840	2536	2536	1930	1930	2371	2371
g	9.81	9.81	9.81	9.81	9.81	9.81	9.81	9.81
Viscosity co-efficient, A	0.540	2.16	0.482	1.93	0.367	1.47	0.451	1.80
Emplacement time/yrs	4.44×10^7	177	4.97×10^7	199	6.53×10^7	261	5.32×10^7	212

2. Sheeting / dyking - Applying calculations of Petford *et al* (1993) to the plutons of the Rio Paraiba do Sul shear belt, and using similar criteria to those used for the Ardara pluton for each of three conduit lengths (see above) is shown in Figure 8.19 and Appendix 16. Similarly to the Ardara pluton data these show that the data population favours conduit critical widths of 0-10m (average 8.5m) with average pluton emplacement periods of between 300 and 1500yrs, (average 1495yrs for Atibaia, 973yrs

for Imbiricu, 726yrs Morro Azul and 322yrs for Itapeti). Allowing for intermittent magma supply to achieve critical dyke width, with magma flowing perhaps only 10% of the time, these calculations predict very short periods for pluton emplacement.

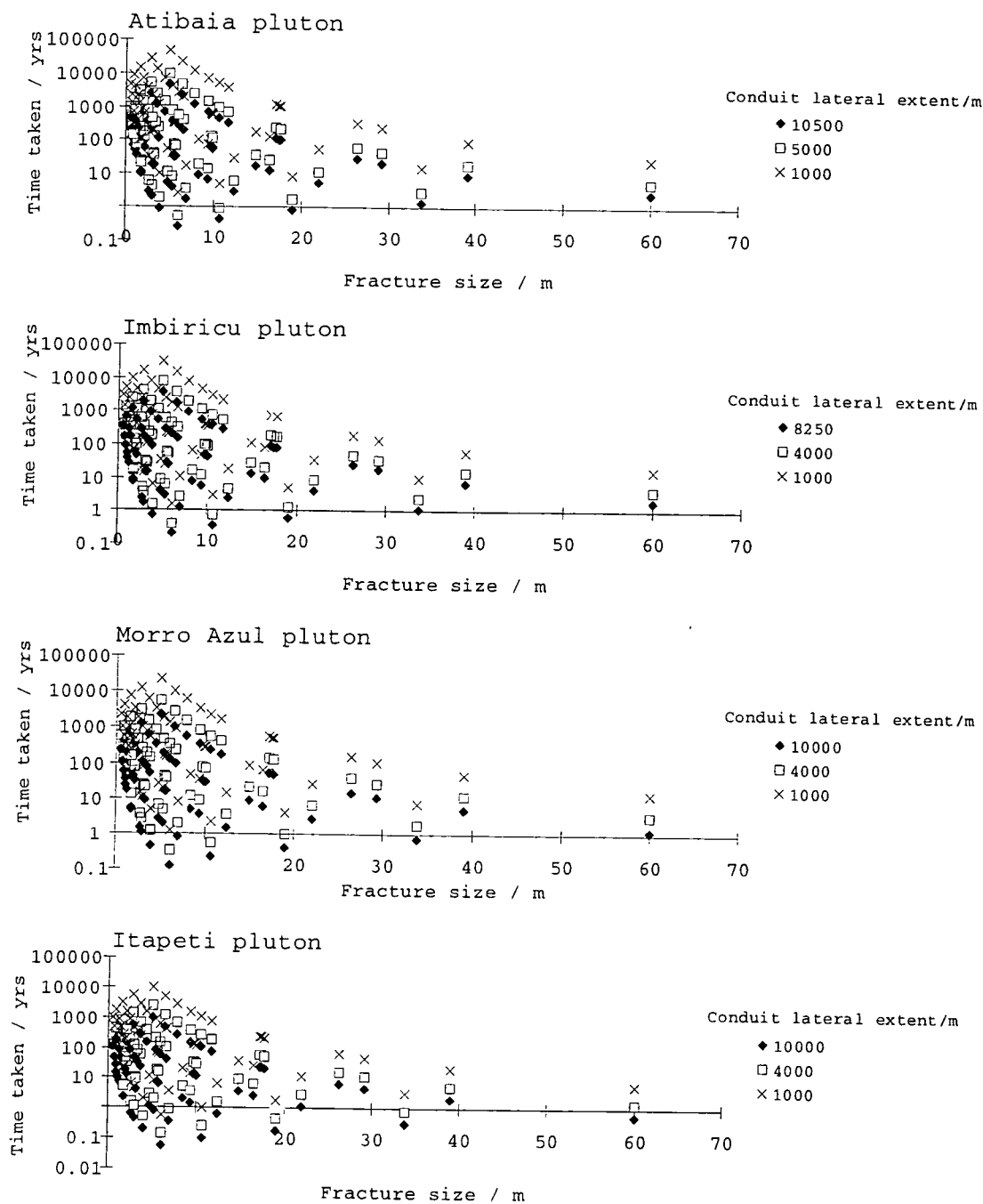


Figure 8.19 Plutons from Rio Paraíba do Sul shear belt, emplacement time against critical fracture size

8.4.4 Conclusion and discussion

The calculations described above provide a simple comparison of the ease of emplacement of granitoid plutons by diapiric or sheeting processes. In particular they illustrate the following points:

1. **Speed** - The time required for the emplacement of diapirs of the sizes studied in this work, is of the order of millions of years. Whereas using magmatic sheets to assemble the pluton emplacement can occur in hundreds to thousands of years, even with an intermittent supply.
2. **Heat transfer** - These results do not take into account the problems associated with heat loss during ascent through a heterothermal crust. Since dyke ascent is so rapid, and thermal conductivity of wallrock is very low Petford *et al* (1993) suggest that this is not a significant effect during sheeting, but during the long ascent times of Hot Stokes diapirs such an effect is significant (Marsh 1982). The production of realistic, accurate models of heat transfer is complex and beyond the scope of this study.
3. **Conduit width** - In order to understand the possible variation in critical dyke width during emplacement of a single or multiple plutons a wide range of magma properties were used. These show a strong clustering of data around critical widths of 0-10m. A result which is largely controlled by S_w , and hence, T_w , the far-field metamorphic temperature of 350°C (assumed to be identical in both areas). Hence, for greenschist conditions the critical dyke width is 0-10m and, more generally, given variable magma conditions, metamorphic temperature controls dyke width.
4. **Contact viscosity** - In the study of diapirs, whether 'Hot Stokes' or any other sort, the contact viscosity and the viscosity variation around the ascending body is the primary controlling factor on the speed of ascent, as recognised by Weinberg & Podlanchikov (1994, 1995). This leads to the conclusion, which echoes Weinberg & Podlanchikov (1994, 1995), that if co-efficients affecting wallrock viscosity and its rheology were better quantified then estimated rates of diapiric ascent would be more realistic.
5. **Aureole width** - Each of the Hot Stokes diapir analyses predicts a wide deformed zone around the pluton and a significant thermal aureole. Only in the case of the Ardara pluton is a thermal aureole developed (to 1km from the contact), in conjunction with an inner deformed zone of 500m, significantly below the values predicted by the model. These values would change if the wallrock viscosity were varied (see point 4). None of the plutons from the Rio Paraiba do Sul shear belt develop an observable thermal aureole, and none have an emplacement related intense deformation zone of more than 200-300m in width. These observations suggest that the Hot Stokes diapir model is not modelling the features associated with emplacement of any of the studied plutons.
6. **Model inadequacy** - Each of the methods described requires significant assumptions to be made about initial and final conditions of magma and wallrock. The validity of these

assumptions is not known and the calculated results should be viewed in the light of such observations.

8.5 Using the Fry (1979) method to measure fabric strain in granitoid rocks

8.5.1 Introduction

During this work more than 300 Fry strain determinations have been made, the basic methodology was outlined in Chapter 1. In this section the validity of this technique as a method for measuring fabric strain will be discussed.

In summary, using an image of particle (phenocryst) distributions, on an outcrop from either a tracing, photograph, polished slab or thin section, the Fry (1979) method provides a way of quantifying the finite strain preserved in that image, by auto-correlating the inter crystal spacings i.e. plotting the position of each crystal relative to one other crystal on a trace, then repeating for each other measured crystal. The original Fry (1979) method assumed each particles could be represented by a point in space, which deformed homogeneously, and required very large numbers of points to produce a reliable result. Erslev (1988) presented a non-circular particle modification to the method, which normalised the inter-granular distance, thereby compensating for shape preferred orientation in the fabric, and producing a better defined Fry ellipse for fewer measured particles.

8.5.2 Results

In Chapter 2, a spatial plot was shown which showed an weak increase in 'Fry strain' with increasing distance from the injection point of the Ardara pluton (Figure 2.15) and of the correlation between the Fry strain and the mafic enclave axial ratio (Figure 2.15d). Approximately 300 analyses were used in the collation of those plots, and another 100 analyses in the fabric strain data collected for the plutons of the Rio Paraiba do Sul shear belt (listed on Appendices 3,7 and 10). Analysing these data has shown:

1. The Fry strain ellipse generally underestimates the, mafic enclave axial ratio.
2. Despite increasing qualitative intensity of finite strain in the magmatic fabric, little increase in Fry strain ellipse is observed.
3. Fry strain determinations, using different crystal phases are of similar magnitudes independent of their position in the crystallisation sequence.
4. Some crystal phases produce consistently poorly defined Fry strain ellipses.

8.5.3 Conclusions

Concluding from results 1 and 2 shows, that while the 'Fry strain' of a fabric is a quantification of the finite strain recorded in that fabric, it is an under-estimate. Which suggests that the Fry method should be used with caution, as a measure of the finite strain recorded in magmatic rocks.

Intuitively, it might be expected that the later crystallised mineral phases might produce lower values of Fry strain, than their earlier produced neighbours. Result 3 shows that this is not the case, demonstrating that either small crystallising nuclei, or simply the cavities required for crystallisation are preserved within the matrix during the entire deformation process. The later formed crystals may only be present during the final increments of deformation i.e. during deformation early crystals form a coherent matrix within which there are cavities, that are deformed and translated similarly to full crystals.

Importantly all crystals do not record a well-developed Fry strain ellipse. Biotite and quartz in particular, can produce poorly orientated and ill-defined ellipses. These are also the mostly easily deformed rocks post-crystallisation (Passchier & Trouw 1996), suffering crystallographic re-orientation, and boundary migration, hence their position and shape could change heterogeneously. Any attempt to measure the distribution of such deformed phases, is not recording a true representation of the 'Fry strain'.

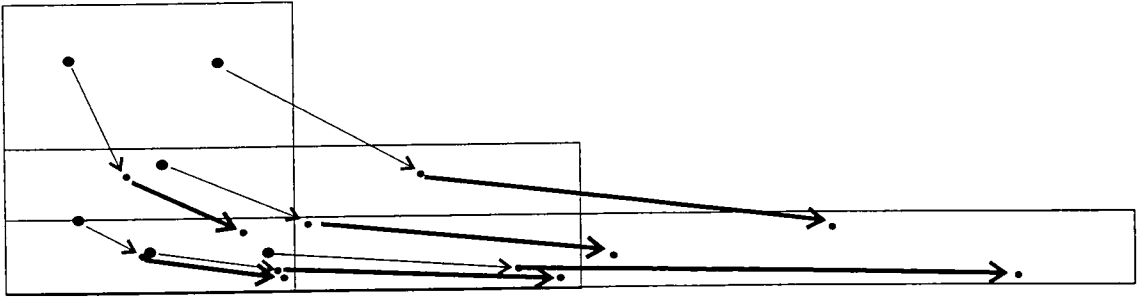
8.5.4 Discussion

The general assumption made when measuring the 'Fry strain' of a sample, is that the deformation is homogenous and the particle number remains constant on the scale, and within the plane of observation. Essentially the Fry (1979) technique requires a two dimensional deformation to take place, but does this type of deformation take place in magmatic rocks? Erslev (1988) recognised this two dimensionality, showing that despite having a fabric that was isotropic and uniform in three dimensions. Such a fabric is not wholly isotropic in two dimensions, and produced a modified Fry algorithm to compensate for this.

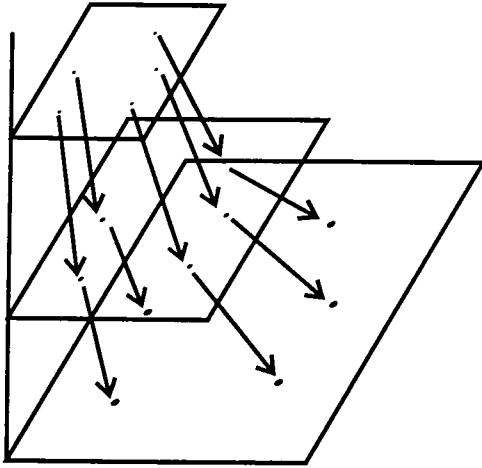
Even so, such modifications do not account for the flow that occurs during deformation. Ramsay & Huber (1983) show the flow lines of particles during a pure shear deformation (Figure 8.20a). Extending this concept to three dimensions (Figure 8.20b) shows that material always flows towards the principal strain axes. Measuring particle distributions in any plane within such a deforming medium, will show increasing anisotropy along the principal axes, but importantly there will be a constant supply of additional isotropic particles to the measurement plane. Therefore the measurement of Fry strain in this plane of deformation, will be constantly reduced by the incorporation of these isotropic particles. Explaining, why despite increasing qualitative fabric strain, there is little increase in the 'Fry strain' value.

This reduction of the 'Fry strain' is likely to be affected by the viscosity. In magmas, viscosities are generally low (cf. metamorphic rocks), hence for a particular applied stress there is an increased strain rate i.e. any particle velocity is higher. Therefore, the trajectory of any particle is potentially variable, generally increasing the isotropy. In

metamorphic rocks, particle velocity is lower, incorporation into the strain plane is irreversible, and consequently Fry strain is more reliable.



a) Two dimensional particles flow lines during pure shear (after Ramsay & Huber 1983)



b) Three dimensional particles flow lines during pure shear

Figure 8.20

8.6 Conclusions

Each of the three parts of this Chapter lead to wide-ranging conclusions which can be summarised as:

- Providing there is significant mechanical coupling between magma and wallrock, ellipsoidal mafic enclaves incorporated within granitic magma will record accurately the imposed finite strain through their axial elongation. This relationship is valid even if there is significant initial shape obliquity.
- Using a power-law rheology to model deformation surrounding an ideal in-situ expanding spherical pluton, demonstrates features which are identical to those observed around the Ardara pluton. Suggesting that if the wallrock had a power-law rheology, then there was a strong component of in-situ expansion associated with its emplacement. A conclusion which is entirely consistent the internal finite strain history of the pluton. Additional knowledge of the strain state and rheology of the country rock could enable the calculation of constraints on the timescale and proportion of in-situ expansion 'ballooning' of this pluton.
- Modelling the ascent of each of the studied plutons as 'Hot Stokes' diapirs suggest ascent and emplacement times of the order of 1-4Ma, wide deformed zones and extensive thermal aureoles. Features for which there is little/no field evidence, hence these plutons did not ascend using a 'Hot Stokes' method.
- Using the alternative ascent scenario of dyking and sheeting shows that each of the studied plutons could be emplaced completely in around 1000yrs through a single conduit less than 10m in width, which had a lateral extent only a fraction of the final conduit dimensions. Given the supposed timescale of geological processes these emplacement speeds are very fast, and possibly occur only rarely interspersed by prolonged periods of quiescence.
- Examining the validity of the Fry method for measuring finite strain in magmatic rocks shows; that while it records a measurement of finite strain, similar in each mineral phase, through crystallisation of the matrix; this finite strain value is consistently reduced as a result of, three-dimensional particle flow, introducing isotropic particles into the fabric, reducing the average inter-particle distance. The relative low viscosity (compared to metamorphic rocks) of magmas, enhances large particle flow, and inhibits the finite strain value recorded by the Fry(1979) technique.

Chapter 9

Conclusions

9.1 Conclusions from Section 2:

The emplacement of an in-situ expanding pluton

In Section 2 the preserved field relationships from the Ardara pluton were discussed, the principal conclusions were:

- Within the pluton there are emplacement induced finite strains which increase smoothly from the 'injection point' in the Moolagh Townlands towards the outer pluton contacts. Modelling of the pluton, using a spherical geometry, demonstrates that these strains could have been produced by the radially directed ballooning of an early magma body of less than 2km radius.
- The country rocks around the pluton show emplacement related structures developed up to 7km from the outer pluton contact. This deformation increases in intensity as the pluton is approached, and becomes pervasive within 500m of the pluton. Estimates of the finite strain preserved within the wallrocks suggests that there has been an average of at least 40% shortening over the 4km closest to the pluton, a measure of shortening which is consistent with a pluton of less than 1.3km initial radius.
- Emplacement-related shear sense fabrics, within the magma and wallrocks, demonstrate that magma was supplied at the 'injection point' before moving outwards and upwards, relative to the existing magma and wallrocks. Expansion took place in all directions, but had a stronger northwards directed component, resulting into the country rocks preserving fabrics which indicate that they were shouldered aside westwards and eastwards during emplacement.
- The southern contact is defined by a sinistrally transpressive shear zone which was active before, during and post-emplacement. This shear zone swings from northeast-southwest trending to sub-east-west trending along the pluton contact and, as such, would have defined a local 'pull-apart'. Such a structure may have created 'space' sufficient to initiate the emplacement process.
- None of the field relationships / structures are entirely consistent with emplacement of magma as a consequence diapir-like processes. Indeed the pluton appears to represent a spheroidal magmatic body which expanded in-situ, as a 'balloon', deforming the surrounding wallrocks.

These conclusions demonstrate that granitoid magma can be emplaced and expand in-situ, akin to the inflation of a balloon, preserving appropriate strains within the magma

and the wallrock. Quantitative methods have demonstrated that the majority of space within the pluton can be accounted for, but that random, unavoidable errors during the measurement process prohibit a comprehensive, and final, solution to the 'space problem' for this pluton.

9.2 Conclusions from Section 3:

Granitoid pluton emplacement in the Rio Paraíba do Sul shear belt, SE Brazil

In Chapters 3-7 the regional framework, field relationships, emplacement mechanisms and possible models for regional evolution of the RPSSB area were examined. The principal conclusions can be summarised as follows:

- These granites correspond to a regional suite of granitic to alkali granite composition which was emplaced towards the end of the Brasiliano orogeny (570 ± 50 Ma) and are intimately associated with major continent-scale, sub-vertical shear zones, formed during dextral transpression (east-west directed convergence) prior to the emplacement of the plutons.
- Each of the plutons has an internal homogeneity, weak emplacement related deformation and wallrocks which were almost passive during the emplacement process. A number of them preserve evidence for having emplaced as a consequence of the large-scale sheeting of magma, into the country rocks and within the pluton itself, sub-parallel to the regional foliation. The majority of these sheets have been homogenised into the main pluton.
- Every studied body shows an internal finite strain which is roughly homogeneous, orientated sub-parallel to the pluton long axis, and flattening. This demonstrates an approximately equal elongation of magma pulses sub-parallel to the regional foliation during emplacement.
- The plutons commonly preserve two distinct contacts the first associated with the shear zone, which preserves intense post-emplacement deformation, and the second which is comparatively undeformed. Estimates of the finite strain preserved within these less deformed contact rocks suggest that they accommodated only a small fraction of the deformation that would be required for emplacement as a consequence of in-situ expansion alone.
- Preserved magmatic state shear sense indicators demonstrate a variable intensity, but dominantly, sinistral shear sense which, in conjunction with the weak intensity nature of the emplacement fabrics, demonstrates east-west directed extension during the intrusion process.
- After this extensional event the region experienced a dextral plane strain which was partitioned into the major shear zones and their surrounded rocks.
- Examination of the tectonic evolution of the RPSSB region suggests that these plutons were emplaced during a period of east-west directed extension at the end of the Brasiliano orogenic event. By comparing the features seen here with models derived from younger orogenic belts it is suggested that the coeval production of large volumes

of magma and regional extension, during a broadly convergent orogeny, is consistent with extension of the orogen, induced by a cessation of continental convergence, or lithospheric delamination and a consequent extensional collapse.

As such this area has been interpreted as having experienced dyke driven ascent of magma along fractures sub-parallel to the dominant regional trend. This magma deformed the wallrocks only weakly and the majority of the space for the pluton was made in local dilatational pull-aparts associated with regional east-west directed extension. Subsequent tectonic reactivations of the regional fabric altered the appearance of these plutons.

9.3 Conclusions from Section 4:

Analytical considerations

In addition to the field study of plutons a number of simple models were constructed in an attempt to quantify some of the specific processes at work during the emplacement of the studied plutons. This work produced the following conclusions:

- A set of randomly orientated ellipsoids subject to a particular pure shear strain will accurately mimic that deformation. An accurate representation of the finite strain is preserved even if the such ellipsoids have a prominent initial elongation. Therefore if ellipsoidal mafic enclaves have a mechanical coupling to the deforming magma they are an accurate and reliable strain marker.
- Modelling the aureole of a hot, in-situ expanding pluton as a Power-Law fluid demonstrates that very high finite strains can be partitioned into the inner aureole. The characteristics of this high strain zone are controlled by the equation parameters and the timescale of emplacement. If these characteristics are compared to those seen in the aureole around the Ardara pluton a very strong similarity is observed. This suggests that during the emplacement of the Ardara pluton the aureole wallrocks behaved as a Power-Law fluid and, given appropriate data on the rheological characteristics of the wallrock, an estimation of the time taken for emplacement could be made.
- The Petford *et al* (1993) model for dyke driven ascent of granitoid magma has been applied, with a wide variation in possible magma properties, to estimate the minimum emplacement time of the studied plutons. These calculations showed that emplacement of the Ardara pluton could occur through a 10m wide fracture in a minimum time of 4140yrs. Similarly the plutons from the RPSSB could be emplaced in between 322 and 1500yrs along conduits with an average width of 8.5m. Even allowing for a highly intermittent magma supply these results demonstrate that emplacement of any of the studied plutons could occur in much less than one million years.
- Applying the Marsh (1982) model for Hot Stokes diapiric ascent to the studied plutons demonstrates a strong variability in the ascent rates/emplacement times depending upon the wallrock rheology used. Generally the envisaged emplacement times are of the order of a million years a timescale, which when viewed in terms of the possible heat loss from the pluton, is excessively large if it is hoped to preserve magmatic emplacement fabrics.
- The Fry (1979) strain when applied to magmatic rocks preserves a component of the finite strain, which has been affected by the three-dimensional nature of the magma deformation and flow. As such it preserves an indication of the finite strain preserved within the magma, but may not accurately mimic it.

REFERENCES

References

- AKAAD, M.K. 1956a. The Ardara granitic diapir of County Donegal, Ireland. *Quarterly Journal of the Geological Society of London*, **112**, 263-288.
- AKAAD, M.K. 1956b. The northern aureole of the Ardara pluton of County Donegal. *Geological Magazine*, **93**, 337-392.
- ALMEIDA, F.F.M. 1977. O Craton do Sao Francisco. *Revista Brasileiro de Geociencias*, **7**, 349-364.
- ALMEIDA, F.F.M., AMARAL, G., CORDANI, U.G. & KAWASHITA, K. 1973. The Precambrian evolution of the South American Cratonic Margin South of the Amazon River. In: NAIRN, C. & STELLI, J. (eds). *The Ocean Basin Margins*, Plenum, New York p1,441-1,446.
- ALMEIDA, F.F.M. & HASUI, Y. 1984. *O Pre-Cambriano do Brasil*. Edgard Blucher, Sao Paulo. 378pp.
- ARZI, A.A. 1978. Critical phenomena in the rheology of partially melted rocks. *Tectonophysics*, **44**, 173-184.
- BALK, R. 1937. Structural behaviour of igneous rocks. *Memoir of the Geological Society of America*, **5**, 177p.
- BASEI M.A.S., CAMPOS NETO, M.S., BERGMANN, M. & FIGUEIREDO, M.C. 1986. Geologia da Folha Amparo 1:50,000, Pro-Minerio-SICCT, Sao Paulo. *Relatorio Final*, 109pp.
- BATEMAN, B. 1985. Aureole deformation by flattening around a diapir during in-situ ballooning: The Cannibal Creek Pluton. *Journal of Geology*, **93**, 293-310.
- BERGANTZ, G.W. 1989. Underplating and partial melting: implications for melt generation and extraction. *Science*, **254**, 1093-1095.
- BERGER, A.R. & PITCHER, W.S. 1970. Structures in granitic rocks. A commentary and a critique on granite tectonics. *Proceedings of the Geological Society of London*, **81**, 441-461.
- BERTHE, D., CHOUKROUNE, P. & JEGOUZO, P. 1979. Orthogneiss, mylonite and non-coaxial deformation of granites: the example of the South American shear zone. *Journal of Structural Geology*, **1**, 31-42.
- BISTRICHI, C. *et al* 1991. Geologia das folhas Jacarei, Tremembe, Taubate e Pindamonhangaba escala do 1:50,000, Estado de Sao Paulo: Pro-Minerio/IPT Relatorio Final 345pp.
- BLUMENFELD, P. & BOUCHEZ, J-L. 1988. Shear criteria in granite and migmatite deformed in the magmatic and solid states. *Journal of Structural Geology*, **10**, 361-372.
- BOUCHEZ, J-L., DELAS, C., GLEIZES, G., NODELEC, A. & CUNEY, M. 1992. Submagmatic microfractures in granites. *Geology*, **20**, 35-38.
- BRAUN, O.P.G. 1972. Faixas ruteis do Escudo Brasileiro. Mimeographado.
- BRAUN, O.P.G. 1974. Principais tracos estruturais do Escudo Brasileiro. *Boletim Especial do XXVII Congresso Brasileiro de Geologia*, 1551-1553.
- BRAUN, O.P.G. & BAPTISTA, M. M. 1977. Consideracoes sobre a geologia Pre-Cambriana da Regiao Sudeste e parte da Regiao Centro-este do Brasil. *Publicacao Especial do Societe Brasileira Geologia*, **3**, 225-368.
- BRITO NEVES, B.B. & CORDANI, U.G. 1991. Tectonic evolution of South America during the Late Proterozoic. *Precambrian Research*, **53**, 23-40.
- BROWN, M., YURI, A. A. & McLELLON, E. L. 1995. Melt segregation in migmatites. *Journal of Geophysical Research*, **100**, 15655-15879.
- BRUN, J.P., GAPAIS, D., COGNE, J.P., LEDRU, P. & VIGNERESSE, J.L. 1990. The Flamanville Granite (NW France): an unequivocal example of a syntectonically expanding pluton. *Geological Journal*, **25**, 271-286.
- BUDDINGTON, A.F. 1959. Granite emplacement with special reference to North America. *Bulletin of the Geological Society of America*, **70**, 671-747.
- BURG, J.P. & WILSON, C.J.L. 1988. A kinematic analysis of the southernmost part of the Bega Batholith. *Australian Journal of Earth Sciences*, **35**, 1-73.
- CAMPANHA, G.A.C., FERNANDES, L.A. & GIMENEZ FILHO, A. 1983. Quadriculas Moji-Guacue Aquas de Lindoia. *1ª Jornada sobre a Carta Geologia do Estado de Sao Paulo em 1:50,000 SICCT-Pro Minerio*. 137-153.
- CAMPANHA, G.A.C., ENS, H.H. & PONCANO, W.L. 1994. Analise morphotectonica do planalto do Juqueriquere, Sao Sebastiao. *Revista Brasileira de Geociencias*, **24**, 32-42.
- CAMPOS NETO, M.C., BASEI, M.A.S. & ARTUR, A.C. 1983. Geologia das folhas de Piracaia e Igarata. *Relatorio Final*, 75pp.
- CAMPOS NETO, M.C., FIGUEREIDO, M.C.H., BASEI, M.A.S. & ALVES, F.R. 1984. Os granitoides da regioao de Braganca Paulista, SP. *Anais do XXXIII Congresso Brasileiro de Geologia*, 2854-2867.
- CAMPOS NETO, M.C. & FIGUEREIDO, M.C.H. 1994. The Rio Doce Orogeny, Southeastern Brazil. *Journal of South American Earth Sciences*, **8**, 143-162.
-

- CAMPOS NETO, M.C. & VASCOCELOS, A.C.B.C. 1986. Geologia da Faixa Alto Rio Grande (Sao Paulo e Sudoeste de Minas Gerais). *Relatorio Final* 127pp.
- CAVALCANTE, J.C. 1979. Projeto Sapucaí. *Ministerio das Minas e Energia*, 2,299pp
- CHANG, H.K., KOWSMANN, R.O., FIGUEIREDO, A.M.F. & BENDER, A.A. 1992. Tectonics and stratigraphy of the East Brazil Rift system: an overview. *Tectonophysics*, **213**, 97-138.
- CHAPPELL, B.W. & STEPHENS, W.E. 1988. Origin of infracrustal (I-type) granite magmas. *Transactions of the Royal Society of Edinburgh (Earth Sciences)*, **79**, 71-86.
- CHAPPELL, B.W. & WHITE, A. J.R. 1984. I- and S- type granites in the Lachlan Fold Belt, south-eastern Australia. In: XU KEGIN & TU GUANGCHI (eds). *Geology of granites and their metallogenic relations*. Beijing, Science Press, 87-101.
- CHAPPELL, B.W., WHITE, A.J.R. 1974. Two contrasting granite types. *Pacific Geology*, **8**, 173-174.
- CHEESMAN, R.L. 1952. The geology of the granitic and metamorphic rocks of the Loughros Peninsula, County Donegal. *MSc thesis, Imperial College, London*.
- CLEMENS, J.D. & MAWER, C.K. 1992. Granite magma transport by fracture propagation. *Tectonophysics*, **204**, 339-360.
- COLE, G.A.J. 1902. On composite gneisses in Boylagh, west Donegal. *Proceedings of the Royal Irish Academy*, **24B**, 203-228.
- COLE, G.A.J. 1905. On the marginal phenomena of granite domes. *Geological Magazine*, **3**, 80.
- COLE, G.A.J. 1906. On a hillside in Donegal: a glimpse into the great Earth cauldron. *Scientific Progress, London*, **1**, 343-360
- CORDANI, U.G. 1973. Evolucao geologica pre-cambriano da faixa costeira do Brasil entre Salvador e Vitoria. *PhD thesis, University of Sao Paulo*.
- CORREA-GOMES, L.C. & OLIVEIRA, E.P. 1997. O exame radial gigante de diques maficos da provincia Bahia-Congo. Implicacoes reologico e tectonica da resenca de uma pluma mantelica na interfície America do Sul-Afric, 1.0 Ga Atras. *Anais do VI Simposio Nacional de Estudo Tectonicos*, 52-55.
- COURRIOUX, G. 1987. Oblique diapirism: the Criffel granodiorite/granite zoned pluton, SW Scotland. *Journal of Structural Geology*, **9**, 313-330.
- COWARD, M.P. 1981. Diapirism and gravity tectonics. *Journal of Structural Geology*, **3**, 89-95.
- CRUDEN, A.R. 1988. Deformation around a rising diapir modelled by creeping flow past a sphere. *Tectonics*, **7**, 1091-1101.
- CRUDEN, A.R. 1990. Flow and fabric development during diapiric rise of magma. *Journal of Geology*, **98**, 681-698.
- CUNNINGHAM, W.D., MARSHAK, S. & ALKIMM, F.F. 1996 Structural style of basin inversion at mid-crustal levels: 2 transects of the Brasiliano Aracuaí belt, MG, Brazil. *Precambrian Research*, **77**, 1-15.
- DEMPSEY, C.S., HALLIDAY, A.N. & MEIGHAN, I.G. 1990. Combined Sm-Nd and Rb-Sr isotope systematics in the Donegal granitoids and their petrogenetic implications. *Geological Magazine*, **127**, 75-80.
- DERBY, O.A. 1878. A regio diamantífera do Parana. *Archive do Museu Nacional*, **3**.
- DERBY, O.A. 1906. The Serra do Espinhaco, Brazil. *Journal of Geology*, **14**, 398.
- DEWEY, J.F. 1969. Evolution of the Appalachian/Caledonian orogen. *Nature*, **222**, 124-129.
- DEWEY, J.F. 1988. Extensional collapse of orogens. *Tectonics*, **7**, 1123-1139.
- EBERT, H. 1968. Occurencias da facies granulitica no sul de Minas e em areas adjacentes, em dependencias da estrutura orogenica: hypotheses sobre sua origem. *Anais Academie Brasileiro das Ciencias*, **40**, 215-229.
- EBERT, H.D. & HASUI, Y. 1992. Transpressive evolution of a collisional suture zone in SE Brazil. *29th IGC, Kyoto, Japan*, II-6-2, P-49, 486.
- EBERT, H.D. & HASUI, Y. *in press* Transpressional tectonics and strain partitioning during oblique collision between three plates in the Precambrian of South-East Brazil. *Special Publication of the Geological Society on Transpressional and Transtensional Tectonics*.
- EBERT, H.D., HASUI, Y., COSTA, J.B.S. 1991. O carater Transpressivo do Cinturao de Cisalhamento Rio Paraíba do Sul. *Anais do III Simposio Nacional dos Estudos Tectonicos*, 139-141
- EBERT, H.D., HASUI, Y., SARTORATO, G., ALMEIDA, S.H. & COSTA, J.B.S. 1993a. Arcabouco estrutural e tectonica transpressiva das faixas moveis da bordas sul e sudeste do craton do Sao Francisco e da sintaxe de Guaxupe. *Anais do IV Simposio Nacional dos Estudos Tectonicos*. 166-171.
- EBERT, H.D., NEVES, M.A., HASUI, Y., SZATMARI, P & AIRES, J.R. 1993b. Evolucao dos cinturoes de cisalhamento entre os blocos Sao Paulo, Vitoria e Brasilia atraves da tectonica colisional obliqua: uma modelagem fisica. *Anais do IV Simposio Nacional dos Estudos Tectonicos*, 254-258
- EBERT, H.D., CHEMALE, F., BABINSKY, M., ARTUR, A.C. & VAN SCHMUS, W.V. 1996. Tectonic setting & U/Pb zircon dating of the plutonic Socorro complex in the Transpressive Rio Paraíba do Sul Shear Belt, SE Brazil. *Tectonics*, **15**, 688-699.

- EBERT, H.D., FILHO, W.M., HASUI, Y., HARLYI, N.E., HACKSPACHER, P.C., MORALES, N. & DE SOUZA, C.A. 1997. Compartimentacao crustal do sul de Minas Gerais a partir de dados gravimetricos e litotecturais. *Anais do VI Simposio Nacional dos Estudos Tectonicos*, 31-35.
- ENGLAND, P.C. & HOUSEMAN, G.A. 1988. The mechanics of the Tibetan Plateau. *Philosophical Transactions of the Royal Society of London*, **A326**, 301-326.
- ENGLAND, R.W. 1988. The ascent and emplacement of Granite magma: The Northern Arran Granite. *PhD thesis, University of Durham*.
- ENGLAND, R.W. 1990. The identification of granite diapirs. *Journal of the Geological Society of London*, **147**, 931-933.
- ERSLEV, E.A. 1988. Normalised centre-centre strain analysis of packed aggregates. *Journal of Structural Geology*, **10**, 201-209.
- EVANS, D.J., ROWLEY, W.J., CHADWICK, R.A. & MILLWARD, D. 1993. Seismic reflectors from within the Lake District batholith, Cumbria, northern England. *Journal of the Geological Society of London*, **150**, 1043-1046.
- FERNANDES, L.A.D., TOMMASI, A. & PORCHER, C.C. 1992. deformation patterns in the Southern Branch of the Dom Feliciano Belt: A reappraisal. *Journal of South American Earth Sciences*, **5**, 77-96.
- FIGUEREIDO, M.C.H., BERGMANN, M., PENALVA, F. & TASSINARI, C.G.G. 1982. Occurrence de *pillow lavas* no Grupo Sao Roque, Estado de Sao Paulo. *Ciencias da Terra*, **2**, 6-8.
- FLINDERS, J. & CLEMENS, J.C. 1996. Nonlinear dynamics, chaos, complexity and enclaves in granitoid magmas. *Transactions of the Royal Society of Edinburgh-Earth Sciences*, **87**, 217-223.
- FLINN, D. 1962. On folding during 3-D progressive deformation. *Quarterly Journal of the Geological Society*, **118**, 385-428.
- FOWLER, T.K. & PATERSON, S.R. 1997. Timing and nature of magmatic fabrics from structural relations around stope blocks. *Journal of Structural Geology*, **19**, 209-224.
- FRY, N. 1979. Random point distributions and strain measurement in rocks. *Tectonophysics*, **60**, 89-105.
- FYFE, W.S. 1988. Granites in a wet convecting ultramafic planet. *Transactions of the Royal Society of Edinburgh (Earth Sciences)*, **79**, 339-346.
- GEIKE, A. 1888, Report on the recent work of the Geological Survey in the north-west Highlands of Scotland. *Quarterly Journal of the Geological Society of London*, **44**, 378-441.
- GIBSON, S.A., THOMPSON, R.N., LEONARDOS, O.H., DICKIN, A.P. & MITCHELL, J.G. 1995. The Late Cretaceous Impact of the Trindade Mantle Plume: Evidence from Large-volume, Mafic, potassic Magmatism in SE Brazil. *Journal of Petrology*, **36**, 189-230.
- GINDY, 1951, The country rocks and associated granites north east of Gweebarra Bay, County Donegal. *PhD thesis, Imperial College, London*.
- GINDY, A.R. 1953, The plutonic history of the district around Trawenagh Bay, County Donegal. *Quarterly Journal of the Geological Society of London*, **44**, 378-441.
- GRESSE, P.G., CHEMALE, F., DA SILVA, L.C., WALRAVEN, F. & HARTMANN, L.A. 1996. Late- to post-orogenic basins of the pan-African-Brasiliano collision orogen in southern Africa and southern Brazil. *Basin Research*, **8**, 157-171.
- HACKSPACHER, P.C. 1994. Tectonica Transtensiva/Transpressiva e Alojamento de Rochas plutonicas, a Exemplo da Folha Cabreuva (SP) 1:50,000. *Livre Docente, UNESP, Rio Claro*, 210pp.
- HACKSPACHER, P.C. & GODOY, A.M. 1996. Trantensional/Transpressional tectonic and plutonic rock emplacement: The calc- to alkaline granites of the Ribeira belt: Sao Paulo, Brazil. *Abstract from symposium on Rapakivi granites and related rocks, Belem, Brazil*, 40-41.
- HACKSPACHER, P.C., DANTAS, E.L., VAN SCHMUS, W.R. & FETTER, A. 1997. Terrenos exoticos na faixa Ribeira, sim ou nao ? *Anais do VI Simposio Nacional de Estudos Tectonicos*, 70-71.
- HACKSPACHER, P.C., GODOY, A.M. & OLIVEIRA, M.A.F. 1993. Evolucao crustal do Bloco Sao Roque, na regioa sudeste do Estado de Sao Paulo. *Revista Brasileira de Geociencias*, **23**, 260-264.
- HALL, A. 1966. The Ardara pluton: A study of the chemistry and crystallisation of a contaminated granitic intrusion. *Proceedings of the Royal Irish Academy*, **65B**, 203-235.
- HALLIDAY, A.N. 1980. A revised age for the Donegal granite. *Nature*, **284**, 542-543.
- HANMER, S. & PASSCHIER, C. 1991. Shear sense indicators: A review. *Geological Survey of Canada Paper*, **90-17**, 67pp.
- HARLAND, W.B. 1971. Tectonic transpression in Caledonian Spitzbergen. *Geological Magazine*, **108**, 27-42.
- HARALYI, N.L.E. & HASUI, Y. 1982. Compartimentacao geotectonica do Brasil oriental com base na informacao geofisica. *Anais do XXXII Congresso Brasileira do Geologia*, **1**, 374-385.
- HASUI, Y. 1982. The Mantiquera Province ; Archaean structure and Proterozoic evolution. *Abstract for an International Symposium on Archaean and Early Proterozoic Geological Evolution and Metallogenesis, Salvador, Brazil*.

- HASUI, Y. 1983. Aspectos geológicos essenciais da secção Caconde-Caraguatatuba e suas implicações na reconstituição da organização e evolução do Pré-Cambriano do leste Paulista. *1ª Jornada sobre a Carta Geológica do Estado de São Paulo em 1:50,000 SICCT-Pro Minerio*
- HASUI, Y., CARNEIRO, C.D.R. & COIMBRA, A.M. 1975. The Ribeira folded belt. *Revista Brasileira de Geociências*, **5**, 257-266.
- HASUI, Y., CARNEIRO, C.D.R. & BISTRICHI, C.A. 1978. Os granitos e granitóides da região de dobramentos sudeste nos Estados de São Paulo e Paraná. *Anais do XXX Congresso Brasileiro de Geologia*, **6**, 2,579-2,593.
- HASUI, Y., BISTRICHI, C.A., STEIN, D.P., NETO, A.G.P., DE MELO, M.S. & CARNEIRO, C.D.R. 1978. Geologia da região administrativa 3 (Vale do Paraíba) e parte da região administrativa 2 (litoral) do estado de São Paulo, escala 1:100,000. São Paulo, IPT Relatório Final 65pp
- HASUI, Y., AGAMENON, S.L.D., CARNEIRO, C.D.R. & BISTRICHI, C.A. 1981. O embasamento Pré-Cambriano e Eo-Paleozoico em São Paulo. In: *Mapa Geológico de Estado de São Paulo 1:500,000 monograph*. **1**, 12-45.
- HASUI, Y. & OLIVEIRA, M.A.F. 1984. Província Mantiqueira. Setor Central. In: Almeida, F.F.M. & Hasui, Y. (eds) *O Precambriano do Brasil*, 308-344.
- HOLDER, M.T. 1979. An emplacement mechanism for post-tectonic granites and its implications for the geochemical features. In: ATHERTON, M.P. & TARNEY, J. (eds). *Origin of granite batholiths: geochemical evidence*, Shiva, Nantwich. p 116-128.
- HOUSEMAN, G.A., MCKENZIE, D.P. & MOLNAR, P. 1981. Convective instability of a thickened boundary layer and its relevance for the thermal evolution of Continental convergent belts. *Journal of Geophysical Research*, **86**, 6115-6132.
- HULL, E., KINAGHAN, G.H., NOLAN, J., CRUISE, R.J., EGAN, F.W., KILROE, J.R., MITCHELL, W.F. & M'HENRY, A. 1891. Explanatory memoir to accompany sheets 3, 4, 5(in part), 9, 10, 11(in part), 15 and 16 of the maps of the Geological Survey of Ireland comprising north-west and Central Donegal. *Memoir of the Geological Survey of Ireland*, 174p.
- HUTTON, D.H.W. 1977. A structural cross-section from the aureole of the Main Donegal Granite. *Geological Journal*, **12**, 99-112.
- HUTTON, D.H.W. 1982a. A method for the determination of the initial shapes of deformed xenoliths in granitoids. *Tectonophysics*, **85**, T45-T50.
- HUTTON, D.H.W. 1982b. A tectonic model for the emplacement of the Main Donegal granite, NW Donegal. *Journal of the Geological Society of London*, **139**, 615-631.
- HUTTON, D.H.W. 1987. Strike-slip terranes and a model for the evolution of the British and Irish Caledonides. *Geological Magazine*, **124**, 405-425.
- HUTTON, D.H.W. 1988. Granite emplacement mechanisms and tectonic controls: inferences from deformation studies. *Transactions of the Royal Society of Edinburgh*, **79**, 245-255.
- HUTTON, D.H.W. 1992. Granite sheeted complexes: evidence for dyking ascent mechanism. *Transactions of the Royal Society of Edinburgh*, **83**, 377-382.
- HUTTON, D.H.W. 1997a. Syntectonic granites and the principle of effective stress: a general solution to the space problem? In: BOUCHEZ, J.-L. et al (eds). *Granite: from segregation of melt to emplacement fabrics*. Elsevier, Amsterdam. p187-197.
- HUTTON, D.H.W. 1997b. The 'space problem' in the emplacement of granite. *Episodes*, **19**, 114-119.
- HUTTON, D.H.W. & ALSOP, G.I. 1995. Extensional geometries as a result of regional scale thrusting: tectonic slides of the Dunlewy, NW Donegal area, Ireland. *Journal of Structural Geology*, **17**, 1279-1292.
- HUTTON, D.H.W. & ALSOP, G.I. 1996. The Caledonian strike swing and associated lineaments in NW Ireland and adjacent areas - sedimentation, deformation and igneous intrusion patterns. *Journal of the Geological Society of London*, **153**, 245-360.
- HUTTON, D.H.W., DEMPSTER, T.J., BROWN, P.E. & BECKER, S.D. 1990. A new mechanism of granite emplacement: intrusion in active extensional shear zones. *Nature*, **343**, 452-455.
- HUTTON, D.H.W. & INGRAM, G.W. 1992. The Great Tonalite Sill of SE Alaska and British Columbia: emplacement into and active contractional reverse shear zone. *Transactions of the Royal Society of Edinburgh*, **83**, 383-386.
- HUTTON, D.H.W. & REAVY, R.J. 1992. Strike-slip tectonics and granite petrogenesis. *Tectonics*, **11**, 960-967.
- INGER, S. 1994. Magmagenesis associated with extension in orogenic belts: examples from the Himalaya and Tibet. *Tectonophysics*, **238**, 183-197.
- INGRAM, G.H. & HUTTON, D.H.W. 1994. The Great Tonalite Sill-Emplacement into a contractional shear zone and implications for Late Cretaceous to Early Eocene tectonics in SE Alaska and British Columbia. *Bulletin of the Geological Society of America*, **106**, 715-728.
- INGRAM, G.H. 1992. Deformation, emplacement and tectonic inferences: the Great Tonalite Sill, south-east Alaska, USA. *PhD thesis, University of Durham*.

- IYENGAR, S.V.P., PITCHER, W.S. & READ, H.H. 1954. The plutonic history of the Maas area, County Donegal. *Quarterly Journal of the Geological Society of London*, **439**, 203-230.
- IYER, S.S., CHOUDHURI, A., PATTISON, D.R.M. & DE PAOLI, G.R. 1996. Petrology and geochemistry of the Neoproterozoic Guaxupe granulite facies terrain, southeastern Brazil. *Precambrian Research*, **77**, 23-40.
- JACQUES, J.M. & REAVY, R.J. 1994. Caledonian plutonism and major lineaments in the SW Scottish Highlands. *Journal of the Geological Society of London*, **151**, 955-969.
- JANASI, V.A. & ULBRICH, H.H.G.J. 1987. Petrogenesis of the monzonitic-monzodioritic Piracaia massif, State of Sao Paulo, Southern Brazil, field and petrographic aspects. *Revista Brasileira do Geociencias*, **17**, 524-534.
- JANASI, V.A. & ULBRICH, H.H.G.J. 1991. Late Proterozoic granitoid magmatism in the State of Sao Paulo, SE Brazil. *Precambrian Research*, **51**, 351-374.
- KERRICK, D.M. 1987. Fibrolite in contact aureoles of Donegal, Ireland. *American Mineralogist*, **72**, 240-254.
- KING, R.F. 1966. The magnetic fabric of some Irish granites. *Geological Journal*, **5**, 43-66.
- KIRBY, S.H. 1983. Rheology of the Lithosphere. *Reviews of Geophysics*, **21**, 1458-1487.
- KLEMENS, W.P. & SCHWERTNER, W.M. 1997. Emplacement and deformation of granite pegmatite dykes in a mid-crustal regime of Late-orogenic extension Grenville province, Ontario. *Geological Magazine*, **134**, 287-295.
- KNECHT, T. 1964. Escala geologica do tempo Pre-Cambriano Inferior. *Boletim Instituto Geographia e Geologia do estado do Sao Paulo*, **41**, 14-36.
- KNIPE, R. 1989. Deformation mechanisms - Recognition from Natural Tectonites. *Journal of Structural Geology*, **11**, 127.
- KRONER, A. 1982. Rb-Sr Geochronology and Tectonic Evolution of the Pan-African Damara belt of Namibia-SW Africa. *American Journal of Science*, **282**, 1,471-1,507.
- KUSKY, T.M. 1983. Collapse of Archaean orogens and the generation of late- to post-kinematic granitoids. *Geology*, **21**, 925-928.
- LASDON, L.S. & WARREN, A.D. 1983. Large-scale non-linear programming. *Computers and Chemical Engineering*, **7**, 595-604.
- LEAKE, B.E. 1978. Granite emplacement; the granites of Ireland and their origin. In: Bowes, D.R., & Leake, B.E. (eds) Crustal evolution of northwest Britain and adjacent regions. *Geological Journal Special Publication*, **10**, 221-248.
- LISLE, R.J. 1977. Estimation of the tectonic strain ratio from the mean shape of deformed elliptical markers. *Geologie en mijnbouw*, **56**, 140-144.
- LISTER, G.S. & SNOKE, W.A. 1984. S-C mylonites. *Journal of Structural Geology*, **6**, 617-638.
- LISTER, J.R. & KERR, R.C. 1991. Fluid mechanical models of crack propagation and their application to magma transport in dykes. *Journal of Geophysical Research*, **96**, 10049-10077.
- MARRE, J. 1986. *The structural analysis of granitic rocks*. North Oxford Academic Press; translated by John Renouf. pp181.
- MARSH, B.D. 1982. On the mechanics of igneous diapirism, stoping and zone melting. *American Journal of Science*, **282**, 808-855.
- McBIRNEY, A.R. & MURASE, T. 1984. Rheological properties of magmas. *Annual Review of Earth and Planetary Sciences*, **12**, 337-357.
- McCAFFREY, K.J.W. 1989. The emplacement and deformation of granitic rocks in a transpressional shear zone: The Ox Mountains Igneous Complex. *PhD thesis, University of Durham*.
- McERLEAN, M.A. 1993. Granitoid emplacement and deformation: a case study of the Thorr pluton, Ireland, with contrasting examples from Scotland. *PhD thesis, University of Durham*.
- McKENZIE, D.P. 1984. The generation and compaction of partially molten rock. *Journal of Petrology*, **25**, 713-765.
- McKENZIE, D.P. & BICKLE, M.J. 1988. The volume and composition of melt generated by extension of the lithosphere. *Journal of Petrology*, **29**, 625-679.
- MELHEM, M.M. 1995. Geologia e Petrografia das Rochas Granitoides do Macico Atibaia e adjacencias, SP. *MSc thesis, University of Sao Paulo*.
- MENEILLY, A.W. 1981. The Structural Geology of the Lower Dalradian rocks around Gweebarra Bay, Co. Donegal, Ireland. *PhD thesis, University of Belfast*.
- MENEILLY, A.W. 1982. Regional structure and syn-tectonic granite intrusion in the Dalradian of the Gweebarra Bay area, County Donegal. *Journal of the Geological Society of London*, **139**, 633-646.
- MITHAL, R.S. 1952. The geology of the Portnoo district, County Donegal. *PhD thesis, Imperial College, London*.
- MOLYNEUX, S.J. & HUTTON, D.H.W. (in press) The emplacement of the Ardara granite, County Donegal, Ireland: evidence for ballooning. *Bulletin of Geological Society of America*.

- MORAIS, S.M. 1996. Granito Itapeti, SP: Petrografia, Litoquímica e Tipologia de Zircão. *MSc thesis, UNESP, Rio Claro*.
- MORGAN, S. 1995. Discussion of: 'The Ardara pluton, Ireland: deflating an expanded intrusion', VERNON, R.H. & PATERSON, S.R. *Lithos*, **35**, 129-133.
- MORGAN, S., LAW, R., SAINT BLANQUAT, M. & BOUCHEZ, J.-L. 1995. Kilometer Scale Vertical Translation Concordancy and Nonrotation of Porphyroblasts Surrounding the Papoose Flat Pluton: Inclusion Trails and AMS Reveal the Kinematics of Emplacement. *United States Geological Survey Circular*, **1129**, 100-101.
- MRAZEC, L. 1927. Les plis diapirs et le diapirisme en general. *Contributions Seances Institute Geologique Roumanie VI (1914-1915)*, 226-70.
- NICOLESCO, C.P. 1929. Anticlimax diapirs sedimentares, volcaniques et plutoniques. *Bulletin Societe Geologique Francais*, **29**, 21-24.
- NURNBERG, D. & MULLER, R.D. 1991. the tectonic evolution of the South Atlantic from late Jurassic to present. *Tectonophysics*, **191**, 27-53.
- O'CONNOR, P.J., LONG, C.B. & EVANS, J.A. 1987. Rb-Sr whole-rock isochron studies of the Barnesmore and Fanad plutons, Donegal, Ireland. *Geological Journal*, **22**, 11-23.
- O'CONNOR, P.J., LONG, C.B., BASHAM, I.R., SWAINBANK, I.G. & BEDDOESTEPHENS, B. 1984. Age and geological setting of uranium mineralization associated with the Main Donegal Granite, Ireland. *Transaction of the Institution of Mining and Metallurgy*, **93**, B190-B194.
- O'CONNOR, P.J., LONG, C.B., KENNAN, R.S., HALLIDAY, A.N., MAX, M.D. & RODDICK, J.C. 1982. Rb-Sr isochron study of the Thorra and Main Donegal granites, Ireland. *Geological Journal*, **17**, 279-295.
- OLIVEIRA, M.A.F., MORALES, N., FULFARO, V.J. & CAMPOS, E.G. 1985. Geologia da folha Atibaia. *Relatorio Final*, 117pp.
- PASSCHIER, C.W. & SIMPSON, C. 1988. Porphyroclast systems as kinematic indicators. *Journal of Structural Geology*, **8**, 831-843.
- PASSCHIER, C.W. & TROUW, R.A.J. 1996. *Microtectonics*. Springer-Verlag, Berlin. 289pp.
- PATERSON, S.R. & FOWLER, T.K. 1993. Re-examining pluton emplacement processes. *Journal of Structural Geology*, **15**, 191-206.
- PATERSON, S.R. & VERNON, R.H. 1995. Bursting the bubble of ballooning plutons: A return to nested diapirs emplaced by multiple processes. *Bulletin of the Geological Society of America*, **107**, 1356-1380.
- PATERSON, S.R., VERNON, R.H. & TOBISCH, O.T. 1989. A review of the criteria for the identification of magmatic and tectonic foliations in granitoids. *Journal of Structural Geology*, **11**, 349-363.
- PEDROSA-SOARES, A.C., NOCE, C.M., VIDAL, P., MONTERO, R.L.B.P. & LEONARDES, O.H. 1992. Toward a new tectonic model for the late proterozoic Aracui (SE Brazil)-West Congolian (SW Africa) belt. *Journal of South American Earth Sciences*, **6**, 33-47.
- PETFORD, N. 1996. Dykes or diapirs. *Transactions of the Royal Society of Edinburgh (Earth Sciences)*, **87**, 105-114.
- PETFORD, N., KERR, R.C. & LISTER, J.R. 1993. Dike transport of granitoid magmas. *Geology*, **21**, 845-848.
- PIMENTAL, M.M., FUCK, R.A. & ALVARENGA, C.J.S. 1996. Post-Brasiliano (Pan-African) high-K granitic magmatism in Central Brazil: the role of Late Precambrian-Early Palaeozoic extension. *Precambrian Research*, **80**, 217-238.
- PINHEIRO, R.V.L. 1997. Reactivation history of the Carajas and Cinzento strike-slip systems, Amazon, Brazil. *PhD thesis, University of Durham*.
- PITCHER, W.S. 1978. The anatomy of a batholith. *Journal of the Geological Society of London*, **135**, 157-182.
- PITCHER, W.S. 1979. The nature, ascent and emplacement of granitic magmas. *Journal of the Geological Society*, **136**, 627-662.
- PITCHER, W.S. 1987. Granites and yet more granites forty years on. *Geologische Rundschau*, **76**, 51-79.
- PITCHER, W.S. 1993. *The nature and origin of granite*. Chapman and Hall, London, 321pp.
- PITCHER, W.S. & BERGER, A.R. 1972. *The geology of Donegal: a study of granite emplacement and unroofing*. London: Wiley Interscience. 270pp.
- PITCHER, W.S. & READ, H.H. 1960. The aureole of the Main Donegal Granite. *Quarterly Journal of the Geological Society*, **116**, 1-36.
- PORADA, H. 1989. Pan-African Rifting and Orogenesis in Southern to Equatorial Africa and Eastern Brazil. *Precambrian Research*, **44**, 103-136.
- PORCHER, C.C. & FERNANDES, L.A.D. 1997. Metamorphic evolution of a Lower crustal transcurrent shear zone: The Tres Rios-Alem-Paraiba lineament. *Anais do VI Simposio Nacional dos Estudos Tectonicos*. 85-87.
- PRESS, F. & SIEVER, R. 1986. *Earth*. W.H. Freeman & Co., New York. 656pp.

- PRICE, 1997. Multiple sheeting as a mechanism of pluton construction: the Main Donegal Granite, NW Ireland. *PhD thesis, University of Durham*.
- RABINOWITZ, P.D. & LABREQUE, J. 1979. The Mesozoic South Atlantic Ocean and the evolution of its continental margins. *Journal of Geophysical Research*, **84**, 5973-6002.
- RAGATKY, D., TUPINAMBA, M. & TASSINARI, C. 1988. Sm/Nd and Rb/Sr isotopic studies from a garnet bearing peraluminous granite (Nazare Paulista) from the Ribeira belt, southeastern Brazil. *Bulletin South-American Symposium on Isotope Geology-Brazil, June 1997*, 247- 249.
- RAMBERG, H. 1967. *Gravity, deformation and the Earth's crust as studied by centrifuged models*. Academic Press, New York, 214pp.
- RAMBERG, H. 1970. Model studies in relation to intrusion of plutonic bodies. In, Mechanisms of Igneous Intrusion, Newall, G. & Rast, N. (eds) *Geological Journal Special Publication*, **2**, 261-286.
- RAMSAY, J.G. 1967. *The folding and fracturing of rocks*. International series in the Earth and Planetary Sciences, McGraw-Hill, New York. 563pp.
- RAMSAY, J.G. 1975. The structure of the Chindamora Batholith. *19th Annual Report, Institute African Geology, University of Leeds*, **81**.
- RAMSAY, J.G. 1989. Emplacement kinematics of a granite diapir: The Chindamora Batholith, Zimbabwe. *Journal of Structural Geology*, **11**, 191-209.
- RAMSAY, J.G. & HUBER, M.I. 1983. *The techniques of modern Structural Geology Volume 1 & 2: Strain analysis & Folds and Fractures*. Academic Press, London, 307pp.
- READ, H.H. 1957. *The Granite controversy*. Thomas Murby & Co, London, 430pp.
- RIBEIRO, L.F.B., HACKSPACHER, P.C., HASUI, Y., HADLER, N., IUNES, P.J. & TELLO, S. 1996. Datacao pelo metodo Tracos de fissao de Apatites presentes em falhas da Regiao de Branganca Paulista (SP). *Anais do V Simposio Nacional dos Estudos Tectonicos*, 391-394.
- RICCOMINI, C. 1995. Padrao de Fracturamentos do macico alcalino de Cananea estado de Sao Paulo: Relacoes com a tectonica Mesozoico-Cenozoico de sudeste do Brasil. *Revista Brasileira de Geociencias*, **25**, 79-84.
- RIDDIHOUGH, R.P. & YOUNG, D.G.G., 1969. Gravity and magnetic surveys of Inishowen and adjoining areas off the north coast of Ireland. *Proceedings of the Geological Society of London*, **1644**, 215-220.
- ROMAN-BERDIEL, T., GAPAIS, D. & BRUN, J.P. (in press) Analogue models of laccolith formation. *Journal of Structural Geology*
- ROSIER, G.F. 1957. A geologia da Serra do mar entre os picos Maria Comprida e do Desengano, Estado do Rio de Janeiro. *Boletim do Divisao Geologia e Minerologie, DNPM, Rio de Janeiro*, **166**.
- ROSIER, G.F. 1965. Pesquisas geograficas na parte oriental do estado do Rio de Janeiro e na vizinha do Estado de Minas Gerais. *Boletim do Divisao Geologia e Minerologie, DNPM, Rio de Janeiro*, **222**.
- RUBIN, A.M. 1993. Dikes vs. diapirs in viscoelastic rock. *Earth and Planetary Science letters*, **119**, 641-659.
- RUTTER, E.H. & NEUMANN, D.H.K. 1995. Experimental deformation of partially molten Westerly granite under fluid absent conditions, with implications for the extraction of granitic magmas. *Journal of Geophysical Research*, **100**, 15697-15715.
- SAADI, A., HASUI, Y. & MARGALHAES, F.S. 1991. Informacoes sobre a neotectonica e morphogenese de Minas Gerais. *Boletim do III Simposio Nacional de Estudo Tectonicos*. 105-106.
- SALVADOR, E.D. & RICCOMINI, C. 1995. Neotectonica da regio do alto estrutural de Queluz (SP-RJ, Brasil). *Revista Brasileira de Geociencias*, **25**, 151-164.
- SANDERSON, D.J. & MARCHINI, W.R.D. 1984. Transpression. *Journal of Structural Geology*, **6**, 449-458.
- SANDERSON, D.J. & MENEILLY, A.W. 1981. Analysis of 3-D strain modified uniform distributions: andalusite fabrics from a granite aureole. *Journal of Structural Geology*, **3**, 109-116.
- SAWYER, E.W. 1996. Melt segregation and magma flow in migamtites: implications for the generation of granite magmas. *Transactions of the Royal Society of Edinburgh (Earth Sciences)*, **87**, 85-94.
- SCHMELING, H., CRUDEN, A.R. & MARQUART, G. 1988. Finite deformation in and around a fluid sphere moving through a viscous medium: implication for diapiric ascent. *Tectonophysics*, **149**, 17-34.
- SCMIDT, K.L., PATERSON, S.R. & LUND, S.P. 1995. Quantifying Spatial Relationships Between Faults and Plutons. *United States geological Survey Circular*, **1129**, 138-139.
- SETZER, J. 1953. Zona de Atibaia (Folha de Junidiai). *IGG, Sao Paulo*, **11**, 27-34.
- SHAW, H.R. 1972. Viscosities of magmatic silicate liquids an empirical method of prediction. *American Journal of Science*, **272**, 870-893.
- SHEA, W.T. & KRONENBURG, A.K. 1992. Rheology and deformation mechanisms of an isotropic mica schist. *Journal of Geophysical Research*, **97**, 15201-15237.
- SOARES, P.C. 1988. Tectonica colisional em torno do Bloco Parana, Brasil. *Abstract, VII Congress on LatinAmerican geology, Belem*. **1**, 63-79.
- SOARES, P.C. & ROSTIROLLA, S.P. 1997. Tectonica de escape tardicollisional nos cinturaoes Ribeira e Dom Feliciano. *Anais do VI Simposio Nacional dos Estudos Tectonicos*, 65-68.

- SOPER, N.J. & ENGLAND, R.W. 1995. Vendian and Riphean rifting in NW Scotland. *Journal of the Geological Society of London*, **152**, 11-14.
- SOPER, N.J., STRACHAN, R.A., HOLDSWORTH, R.E., GAYER, R.A. & GREILING, R.O. 1992. Sinistral transpression and the Silurian closure of Iapetus. *Journal of the Geological Society of London*, **149**, 871-880.
- SPANNER, B.G. & KRUHL, J.H. *in review* Varying mechanisms of magma emplacement due to a change of tectonic setting during the Brasiliano Orogeny: The Carmo and the Sindacta plutons (SE Brazil). *Tectonics*.
- SPARKS, R.S.J., PINKERTON, H. & McDONALD, R. 1977. The transport of xenoliths in magmas. *Earth and Planetary Science Letters*, **35**, 234-238.
- STOKES, G.G. 1851. On the effect of the internal friction of fluids on the motion of pendulums. *Cambridge Philosophical Society Transactions*, **9**, 8.
- SWAN, A.R.H. & SANDILANDS, M. 1994. *Introduction to Geological Data Analysis*. Blackwell Scientific Press, Oxford, 446pp.
- SYLVESTER, A.G. 1988. Strike-slip faults. *Geological Society of America Bulletin*, **100**, 1666-1703.
- SYLVESTER, A.G., OERTEL, G., NELSON, C.A. & CHRISTIE, J.M. 1978. papoose Flat: A granitic blister in the Inyo mountains, California. *Geological Society of America Bulletin*, **89**, 1205-1219.
- TASSINARI, C.C.G. 1988 As idades das rochas e dos eventos metamorficos da porcao Sudeste do Estado de Sao Paulo e sua Evolucao crustal. *PhD thesis, University of Sao Paulo*. 236pp.
- TELFORD, W.M., GELDARD, L.P., SHERIFF, R.E. 1990. *Applied Geophysics*. Cambridge University Press, 770pp.
- THEODOROVICZ, A., YAMATO, A.A., TAKAHASHI, A.T., VASCONCELOS, C.S., SANTAREM, P.C. & DA SILVA, V.A. 1990. Geologia das folhas Santa Isabel e Moji das Cruzes. *Relatorio Final*. 193pp.
- TIKOFF, B. & TEYSSIER, C. 1990. Strain modelling of displacement-field partitioning in transpressional orogens. *Journal of Structural Geology*, **16**, 1575-1588.
- TOEPFNER, C. 1997. Age and origin of Brasiliano-granitoids in the southern Ribeira mobile belt, Brazil, by mena of UPb-zircon and Rb/Sr-whole rock dating. *South-American symposium on Isotope Geology-Brazil*, 314-316.
- TOMMASI, A., VAUCHEZ, A. & FERNANDES, L.A.D. 1994. Magma assisted strain localization in an orogen-parallel transcurrent shear zone of Southern Brazil. *Tectonics*, **13**, 421-437.
- TORQUATO, J.R. & CORDANI, U.G. 1981. Brazil-Africa geological links. *Earth Science Reviews*, **17**, 155-176.
- TRIBE, I.R. & D'LEMONS, R.S. 1996. Significance of a hiatus in down temperature fabric development within syn-tectonic quartz diorite complexes, Channel Islands, UK. *Journal of the Geological Society of London*, **153**, 127-138.
- TWISS, R.J. & MOORES, E.M. 1992. *Structural Geology*. W.H. Freeman & Co., New York. 532pp.
- UNTERNEHR, P., CURIE, D., OLIVET, J.L., GOSLIN, J. & BEUZART, P. 1988. South Atlantic fits and intraplate boundaries in Africa and South America. *Tectonophysics*, **155**, 169-179.
- VAN DER MOLEN, I. & PATERSON, M.S. 1979. Experimental deformation of partially melted granite. *Contributions to Mineralogy and Petrology*, **70**, 299-318.
- VASCOCELOS, A.C.B.C. 1988. O grupo Andrelandia na regioa a norte de Ouro Fino, MG. *MSc thesis, University of Sao Paulo*.
- VAUCHEZ, A., TOMMASI, A. & MARCES, E-S. 1994. Self indentation of a heterogeneous continental Lithosphere. *Geology*, **22**, 967-970.
- VERNON, R.H. 1983. Restite, Xenolith and Microgranitoid Enclaves in granites. *Journal and proceedings, Royal Society of New South Wales*, **116**, 77-103.
- VERNON, R.H. 1984. Microgranitoid enclaves in granite, globule of hybrid magma quenched in a plutonic environment. *Nature*, **309**, 438-439.
- VERNON, R.H. 1990. Crystallisation and hybridism in microgranitoid magmas: microstructural evidence. *Journal of Geophysical Research*, **95**, 17849-17859.
- VERNON, R.H. & PATERSON, S.R. 1993. The Ardara pluton: deflating an expanded intrusion. *Lithos*, **31**, 17-32.
- VERNON, R.H. & PATERSON, S.R. 1995. Reply: to comment on: The Ardara pluton: deflating an expanded intrusion. *Lithos*, **35**, 135-138.
- VERNON, R.H., ETHERIDGE, M.A. & WALL, V.J. 1988. Shapes and microstructures of microgranitoid enclaves: indicators of magma mixing and flow. *Lithos*, **22**, 1-11
- VIGNERESSE, J.L. 1995. Crustal regime of deformation and ascent of granitic magma. *Tectonophysics*, **249**, 187-202
- WEGMANN, C.E. 1930. Uber diapirismus (Besonders im Grundebirge) *Bulletin of Commercial Geology of Finland*, **92**, 58-76.

- WEINBERG, R.F. 1993. Re-examining pluton emplacement processes: discussion. *Journal of Structural Geology*, **15**, 743-748.
- WEINBERG, R.F. & PODLANCHIKOV, Y.Y. 1994. Diapiric ascent of magmas through Power Law crust and mantle. *Journal of Geophysical Research*, **99**, 9543-9559.
- WEINBERG, R.F. & PODLANCHIKOV, Y.Y. 1995. The rise of solid state diapirs. *Journal of Structural Geology*, **17**, 1183- 1195.
- WERNICK, E. 1978. Contribucao a geologia do macico Guaxupe, SP e MG. *Anais Academie Brasileira do Ciencias*, **50**, 338-352.
- WERNICK, E., OLIVEIRA, M.A.F., KAWASHITA, K., CORDANI, U.G. & DELHAL, J. 1976. Estudo geocronologico pelo metodo Rb/Sr em rochas do Bloco Jundiá e regioes adjacentes. *Revista Brasileira de Geociencias*, **6**, 125-135.
- WERNICK, E., FERREIRA, C.J. & HORMANN, P.K. 1993. Evolucao das unidades magmaticas do Complexo Granitoide Itaquí (Precambriano Superior), Estado de São Paulo, Brasil: Aspectos Geologicos, Petrograficos e Geoquimicos (elementos maiores). *Revista Brasileira de Geociencias*, **23**, 274-281.
- WHITE, A.J.R. & CHAPPELL, B.W. 1988. Some supracrustal (S-type) granites of the Lachlan Fold belt. *Transactions of the Royal Society of Edinburgh (Earth Sciences)*, **79**, 169-191.
- WHITTON, D.G.A. & BROOKS, J.R.V. 1972. *Dictionary of Geology*. Penguin Books, London. 495pp.
- WILKS, K.R. & CARTER, N.L. 1990. Rheology of some Continental Lower Crustal Rocks. *Tectonophysics*, **182**, 57-77.
- WOHLERS, A. 1964. Explicacao do mapa Geologico. *Boletim do IGG, São Paulo*, **41**, 9-165.
- YARDLEY, B.W.D. 1989. *An introduction to Metamorphic Petrology*. Longman Scientific and technical, Harlow. 248pp.
- YOUNG, D.G.G. 1966. The Donegal Granite: A gravity analysis. *Proceedings of the Royal Irish Academy*, **74**, 63-73.

APPENDICES

Appendix 1

Locality grid references for the Ardara pluton

Locality	Northings	Eastings	Locality	Northings	Eastings
A0	7278	9221	I3	7169	9525
A1	7267	9237	I4	7154	9484
A2	7275	9279	I5	7188	9419
A3	7308	9159	J1	7578	9817
A4	7326	9169	J2	7593	9784
A5	7313	9148	J3	7632	9753
A6	7315	9211	J4	7708	9693
A6*	7323	9204	J5	7814	9665
A7	7327	9178	J5*	7840	9659
A8	7327	9159	K1	7872	9563
B1	7168	9248	K2	7829	9578
B2	7167	9286	K3	7795	9609
B3	7141	9293	K4	7761	9632
B4	7106	9297	L1	7597	9704
B5	7126	9336	L2	7597	9649
B6	7078	9380	L3	7578	9557
C1	7194	9842	L4	7546	9499
C10	7388	9704	L5	7485	9476
C11	7363	9636	L6	7419	9380
C2	7234	9840	L7	7376	9186
C3	7262	9846	M1	7440	9155
C3*	7271	9844	M2	7561	9132
C3**	7293	9847	M3	7617	9139
C4	7308	9861	M4	7623	9193
C5	7355	9829	M5	7874	9311
C6	7359	9823	M5*	7882	9340
C7	7359	9793	M6	7953	9323
C8	7363	9777	M7	8017	9369
C9	7369	9757	N1	7504	9674
D1	7032	9569	N2	7474	9623
D2	7061	9592	N3	7413	9629
D2*	7102	9597	N4	7437	9553
D3	7164	9563	N5	7376	9492
D4	7211	9527	O1	7259	9342
D4*	7251	9534	O2	7158	9319
D4**	7267	9532	O3	7282	9274
D4***	7276	9532	O3	7284	9274
D5	7288	9525	O4	7346	9227
E1	8078	9608	O5	7356	9113
E2	8095	9593	O6	7353	9316
E3	8091	9557	P1	7138	9753
E4	8121	9514	P2	7306	9761
E5	8063	9486	P3	7321	9713
E6	7995	9457	P4	7300	9623
E7	7963	9407	P5	7334	9560
F1	7678	9151	P6	7311	9486
F2	7646	9325	P7	7242	9555
F3	7642	9342	Q1	8104	9444
F4	7623	9416	Q2	8186	9642
F5	7591	9448	Q3	8123	9615
G1	7159	9800	Q4	8129	9554
G2	7100	9749	Q5	8184	9580
G3	7038	9678	Q6	7982	9553
G4	7042	9637	R2	7691	9560
G4*	7067	9638	R3	7652	9549
G5	7169	9720	R4	7691	9529
H1	7311	9865	R6	7525	9421
H2	7378	9866	R7	7546	9671
H3	7463	9874	S1	7472	9444
H4	7438	9821	S2	7542	9378
H5	7465	9825	S3	7513	9359
H5*	7438	9753	S4	7478	9308
H6	7402	9813	U1	7274	9415
I1	7222	9674	U2	7307	9378
I2	7151	9657	U3	7284	9452

Appendix 2

LOCALITY I4								LOCALITY A0							
PLUTON G2								PLUTON G2/G3							
HORIZONTAL				VERTICAL				HORIZONTAL				VERTICAL			
NUMBER	X	Z	X/Z	Y	Z	Y/Z		NUMBER	X	Z	X/Z	Y	Z	Y/Z	
1	13.500	12.500	1.080	8.000	8.000	1.000		1	1.200	0.800	1.500	3.300	2.000	1.650	
2	13.000	10.000	1.300	100.000	100.000	1.000		2	7.000	4.500	1.556	6.000	3.500	1.714	
3	2.600	1.800	1.444	15.000	13.000	1.154		3	6.000	2.600	2.308	5.000	2.600	1.923	
4	4.200	2.900	1.448	3.500	3.000	1.167		4	1.500	0.600	2.500	1.900	0.700	2.714	
5	3.200	2.200	1.455	17.000	14.000	1.214		5	23.000	8.700	2.644	5.500	2.000	2.750	
6	1.200	0.800	1.500	5.400	4.000	1.350		6	3.400	1.100	3.091	1.700	0.600	2.833	
7	3.100	2.000	1.550	19.000	14.000	1.357		7	1.600	0.500	3.200	2.300	0.700	3.286	
8	2.200	1.400	1.571	26.000	18.000	1.444		8	3.000	0.900	3.333	2.000	0.600	3.333	
9	3.200	2.000	1.600	9.000	6.000	1.500		9	8.000	2.400	3.333	8.500	2.500	3.400	
10	7.000	4.100	1.707	31.000	20.000	1.550		10	4.000	1.200	3.333	10.000	2.900	3.448	
11	10.700	6.000	1.783	1.400	0.900	1.556		11	3.200	0.900	3.556	2.200	0.600	3.667	
12	1.100	0.600	1.833	2.800	1.800	1.556		12	4.200	1.100	3.818	1.900	0.500	3.800	
13	9.000	4.900	1.837	11.000	7.000	1.571		13	2.000	0.500	4.000	4.600	1.200	3.833	
14	2.600	1.400	1.857	3.200	2.000	1.600		14	1.600	0.400	4.000	3.900	1.000	3.900	
15	2.800	1.500	1.867	15.000	9.000	1.667		15	1.600	0.400	4.000	7.900	2.000	3.950	
16	6.200	3.200	1.938	27.000	16.000	1.688		16	4.900	1.100	4.455	9.800	2.100	4.667	
17	9.800	5.000	1.960	110.000	65.000	1.692		17	13.000	2.900	4.483	20.000	4.200	4.762	
18	4.000	2.000	2.000	3.600	2.100	1.714		18	2.300	0.500	4.600	5.400	1.100	4.909	
19	3.200	1.600	2.000	20.000	11.500	1.739		19	1.900	0.400	4.750	6.000	1.200	5.000	
20	9.500	4.400	2.159	2.500	1.400	1.786		20	19.000	4.000	4.750	4.000	0.800	5.000	
21	4.400	2.000	2.200	7.000	3.800	1.842		21	12.000	2.500	4.800	6.000	1.000	6.000	
22	5.000	2.100	2.381	1.900	1.000	1.900		22	6.600	1.200	5.500	5.500	0.900	6.111	
23	5.000	1.900	2.632	25.000	12.000	2.083		23	3.000	0.500	6.000	10.500	1.700	6.176	
24	2.500	0.900	2.778	1.500	0.700	2.143		24	28.000	4.400	6.364	16.000	2.400	6.667	
25	6.000	2.100	2.857	31.000	14.000	2.214		25	4.500	0.700	6.429	4.700	0.600	7.833	
26	4.000	1.400	2.857	2.000	0.900	2.222		26	7.800	1.000	7.800	8.000	1.000	8.000	
27	9.000	3.000	3.000	6.600	2.400	2.750		27	5.000	0.600	8.333	1.600	0.200	8.000	
28	5.400	1.800	3.000	72.000	25.000	2.880		28	6.000	0.700	8.571	4.200	0.400	10.500	
29	3.200	1.000	3.200	4.000	1.200	3.333		29	7.000	0.600	11.667	7.900	0.700	11.286	
30	20.000	4.400	4.545	87.000	4.600	18.913		30	2.700	0.200	13.500	2.900	0.200	14.500	
Length av.	3.591	1.810		5.294	2.847			Length av.	3.179	0.713		3.847	0.772		
AREAS OF XENOLITHS			5.106			11.838	AREAS OF XENOLITHS				1.780			2.333	
VOLUME OF XENOLITHS						28.341	VOLUME OF XENOLITHS							4.944	
NUMBER			30			30	NUMBER				30			30	
Axial ratio							Axial ratio								
MEAN ARITHMETIC			2.111			2.320	MEAN ARITHMETIC				4.939			5.187	
HARMONIC MEAN			1.874			1.619	HARMONIC MEAN				3.756			3.876	
GEOMETRIC MEAN			2.007			1.816	GEOMETRIC MEAN				4.340			4.513	
STANDARD DEVIATION			0.731			3.179	STANDARD DEVIATION				2.749			2.969	
SMALLEST			1.08			1	SMALLEST				1.5			1.65	
LARGEST			4.54545455			18.913	LARGEST				13.5			14.500	
K VALUE						0.30247762	K VALUE							0.02325882	
w log			0.62415356			1.27676142	w log				0.95424251			0.94388406	

LOCALITY A2								LOCALITY A4							
PLUTON G1								PLUTON G1							
HORIZONTAL				VERTICAL				HORIZONTAL				VERTICAL			
NUMBER	X	Z	X/Z	Y	Z	Y/Z		NUMBER	X	Z	X/Z	Y	Z	Y/Z	
1	4.500	3.000	1.500	7.000	5.500	1.273		1	15.000	6.000	2.500	5.000	2.000	2.500	
2	7.500	5.000	1.500	4.000	3.000	1.333		2	9.000	3.000	3.000	2.500	1.000	2.500	
3	16.000	9.000	1.778	3.500	2.000	1.750		3	9	3	3.000	7.000	2.500	2.800	
4	16.000	9.000	1.778	14.000	8.000	1.750		4	4	1.3	3.077	7.000	2.500	2.800	
5	25.000	14.000	1.786	9.000	5.000	1.800		5	13.000	4.000	3.250	15.000	5.000	3.000	
6	15.000	8.000	1.875	8.000	4.000	2.000		6	5.000	1.500	3.333	8.500	2.500	3.400	
7	5.000	2.500	2.000	14.000	7.000	2.000		7	18.000	5.000	3.600	6.000	1.500	4.000	
8	5.000	2.500	2.000	20.000	8.000	2.500		8	11.000	3.000	3.667	6.000	1.500	4.000	
9	6.500	3.000	2.167	17.000	6.000	2.833		9	10.000	2.500	4.000	6.000	1.500	4.000	
10	5.500	2.500	2.200	3.000	1.000	3.000		10	4.000	1.000	4.000	8.000	2.000	4.000	
11	10.000	4.500	2.222	15.000	5.000	3.000		11	4.000	1.000	4.000	15.000	3.500	4.286	
12	4.500	2.000	2.250	9.000	3.000	3.000		12	6.000	1.500	4.000	3.500	0.800	4.375	
13	3.500	1.500	2.333	3.000	1.000	3.000		13	4.000	1.000	4.000	3.000	0.600	5.000	
14	17.500	7.500	2.333	9.000	3.000	3.000		14	4	1	4.000	13.000	2.500	5.200	
15	6.000	2.500	2.400	8.000	2.500	3.200		15	4	1	4.000	5.500	1.000	5.500	
16	5.000	2.000	2.500	5.000	1.500	3.333		16	2.5	0.6	4.167	6.000	1.000	6.000	
17	5.000	2.000	2.500	10.000	3.000	3.333		17	7.000	1.500	4.667	4.000	0.600	6.667	
18	6.500	2.500	2.600	10.000	3.000	3.333		18	15.000	3.000	5.000			#DIV/0!	
19	5.500	2.000	2.750	10.000	3.000	3.333		19	10.000	2.000	5.000			#DIV/0!	
20	2.000	0.700	2.857	3.500	1.000	3.500		20	4.000	0.800	5.000			#DIV/0!	
21	6.000	2.000	3.000	18.000	5.000	3.600		21	3.500	0.700	5.000			#DIV/0!	
22	4.500	1.500	3.000	30.000	7.000	4.286		22	2.500	0.500	5.000			#DIV/0!	
23	9.000	3.000	3.000	3.500	0.700	5.000		23	1.5	0.3	5.000			#DIV/0!	
24	15.000	5.000	3.000			#DIV/0!		24	3.500	0.600	5.833			#DIV/0!	
25	12.500	4.000	3.125			#DIV/0!		25	6.000	1.000	6.000			#DIV/0!	
26	6.500	2.000	3.250			#DIV/0!		26	4.000	0.600	6.667			#DIV/0!	
27	7.000	2.000	3.500			#DIV/0!		27	1.5	0.2	7.500			#DIV/0!	
28	2.500	0.700	3.571			#DIV/0!		28	4.000	0.500	8.000			#DIV/0!	
29	50.000	12.000	4.167			#DIV/0!		29	4.000	0.500	8.000			#DIV/0!	
30	25.000	4.000	6.250			#DIV/0!		30	2.500	0.300	8.333			#DIV/0!	
Length av.	6.030	2.317		6.558	2.286			Length av.	4.190	0.801		5.563	1.342		
AREAS OF XENOLITHS			10.972			11.772	AREAS OF XENOLITHS				2.635			5.862	
VOLUME OF XENOLITHS						47.321	VOLUME OF XENOLITHS							16.375	
NUMBER			30			23	NUMBER				30			17	
Axial ratio							Axial ratio								
MEAN ARITHMETIC			2.640			2.833	MEAN ARITHMETIC				4.753			4.119	
HARMONIC MEAN			2.345			2.510	HARMONIC MEAN				4.215			3.782	
GEOMETRIC MEAN			2.513			2.677	GEOMETRIC MEAN				4.523			3.947	
STANDARD DEVIATION			0.936			0.922	STANDARD DEVIATION				1.590			1.238	
SMALLEST			1.5			1.27272727	SMALLEST				2.5			2.5	
LARGEST			6.25			5.000	LARGEST				8.33333333			6.670	
K VALUE						0.0740168	K VALUE							0.08143316	
w log			0.61978876			0.59423465	w log				0.52287875			0.42618583	

LOCALITY B1				LOCALITY B5			
PLUTON G1		VERTICAL		PLUTON G2/G3		VERTICAL	
HORIZONTAL				HORIZONTAL			
NUMBER	X	Z	X/Z	Y	Z	Y/Z	
1	5.2	2.8	1.857	19.000	14.000	1.357	
2	9	4.3	2.093	0.600	0.300	2.000	
3	4.500	2.000	2.250	5.2	2.3	2.261	
4	10.500	4.500	2.333	7.000	2.900	2.414	
5	11.5	4.6	2.500	20.000	8.000	2.500	
6	4.2	1.6	2.625	7	2.5	2.800	
7	12	4	3.000	3.200	1.100	2.909	
8	9	2.9	3.103	11	3.5	3.143	
9	3.800	1.200	3.167	9	2.6	3.462	
10	3	0.9	3.333	4.300	1.200	3.583	
11	6.700	2.000	3.350	9.000	2.500	3.600	
12	6.7	2	3.350	5.500	1.500	3.667	
13	12	3.5	3.429	5.500	1.500	3.667	
14	6.300	1.800	3.500	2.6	0.7	3.714	
15	7.000	1.900	3.684	2.3	0.6	3.833	
16	13.000	3.500	3.714	4	1	4.000	
17	12	3.2	3.750	6.500	1.600	4.063	
18	19	4	4.750	4.500	1.100	4.091	
19	5.300	1.100	4.818	4.700	1.100	4.273	
20	6.300	1.300	4.846	11.000	2.500	4.400	
21	12.000	2.400	5.000	5.5	1.2	4.583	
22	4	0.8	5.000	4.200	0.900	4.667	
23	18	3.6	5.000	7.5	1.3	5.769	
24	5.700	1.100	5.182	12	2	6.000	
25	11.000	2.000	5.500	4.2	0.7	6.000	
26	10.500	1.900	5.526	6.200	1.000	6.200	
27	6.300	1.100	5.727	6.3	0.9	7.000	
28	8.000	1.300	6.154	9.300	1.200	7.750	
29	1.900	0.300	6.333	3.000	0.300	10.000	
30	4.500	0.700	6.429	8	1.5	5.333	
Length av.	6.058	1.441		4.172	1.060		
AREAS OF XENOLITHS			6.857			3.474	AREAS OF XENOLITHS
VOLUME OF XENOLITHS						14.032	VOLUME OF XENOLITHS
NUMBER			30			30	NUMBER
Axial ratio							Axial ratio
MEAN ARITHMETIC			4.043			4.301	MEAN ARITHMETIC
HARMONIC MEAN			3.510			3.545	HARMONIC MEAN
GEOMETRIC MEAN			3.818			3.953	GEOMETRIC MEAN
STANDARD DEVIATION			1.347			1.840	STANDARD DEVIATION
SMALLEST		1.85714286			1.35714286	SMALLEST	
LARGEST		6.42857143			10.000	LARGEST	
K VALUE					-0.00787779	K VALUE	
w log		0.53926916			0.86737443	w log	

LOCALITY A6				LOCALITY A6			
PLUTON G2		VERTICAL		PLUTON G2		VERTICAL	
HORIZONTAL				HORIZONTAL			
NUMBER	X	Z	X/Z	Y	Z	Y/Z	
1	2	1.5	1.333	3.000	1.500	2.000	
2	4.5	2	2.250	3.500	1.700	2.059	
3	4.5	2	2.250	11	4.5	2.444	
4	26.000	10.000	2.600	10.000	4.000	2.500	
5	8.000	3.000	2.667	1.100	0.400	2.750	
6	13.000	4.500	2.889	2.000	0.700	2.857	
7	9.000	3.000	3.000	2.000	0.700	2.857	
8	6.000	2.000	3.000	10.000	3.500	2.857	
9	3.2	1	3.200	5.600	1.700	3.294	
10	5.000	1.500	3.333	17	5	3.400	
11	13.500	4.000	3.375	2.500	0.700	3.571	
12	6.7	1.8	3.722	12.000	3.000	4.000	
13	7.500	2.000	3.750	10.000	2.500	4.000	
14	12	3.2	3.750	45	10	4.500	
15	6.3	1.6	3.938	3.500	0.700	5.000	
16	4.000	1.000	4.000	3.5	0.7	5.000	
17	1.6	0.4	4.000	5	1	5.000	
18	3	0.7	4.286	6.500	1.200	5.417	
19	6.500	1.500	4.333	4.000	0.700	5.714	
20	3.500	0.800	4.375	4.500	0.700	6.429	
21	7.000	1.500	4.667	4.5	0.7	6.429	
22	7	1.5	4.667	5.000	0.700	7.143	
23	1.900	0.400	4.750	5.000	0.700	7.143	
24	3.000	0.600	5.000			#DIV/0!	
25	5.500	1.100	5.000			#DIV/0!	
26	6	1.2	5.000			#DIV/0!	
27	17	3	5.667			#DIV/0!	
28	6.000	1.000	6.000			#DIV/0!	
29	13.000	2.000	6.500			#DIV/0!	
30			#DIV/0!			#DIV/0!	
Length av.	4.699	1.226		3.877	0.971		
AREAS OF XENOLITHS			4.525			2.958	
VOLUME OF XENOLITHS						9.265	
NUMBER			29			23	
Axial ratio							
MEAN ARITHMETIC			3.907			4.190	
HARMONIC MEAN			3.410			3.617	
GEOMETRIC MEAN			3.714			3.894	
STANDARD DEVIATION			1.187			1.622	
SMALLEST		1.33333333				2	
LARGEST		6.5				7.140	
K VALUE						0.04585334	
w log		0.68797462				0.55266822	

LOCALITY				LOCALITY			
PLUTON		B6		PLUTON		B6	
		G1				G1	
		HORIZONTAL				HORIZONTAL	
		VERTICAL				VERTICAL	
NUMBER	X	Z	X/Z	Y	Z	Y/Z	
1	16.000	9.000	1.778				
2	4.300	2.000	2.150				
3	5.000	2.300	2.174				
4	7.700	3.400	2.265				
5	3.200	1.400	2.286				
6	5.000	2.100	2.381				
7	4.000	1.600	2.500				
8	12.000	4.500	2.667				
9	3.500	1.300	2.692				
10	7.500	2.600	2.885				
11	12.000	4.000	3.000				
12	27.000	9.000	3.000				
13	6.000	2.000	3.000				
14	13.000	4.000	3.250				
15	19.000	5.500	3.455				
16	9.000	2.600	3.462				
17	5.000	1.400	3.571				
18	20.000	5.500	3.636				
19	3.000	0.800	3.750				
20	5.300	1.400	3.786				
21	14.000	3.500	4.000				
22	4.000	1.000	4.000				
23	12.300	3.000	4.100				
24	4.500	1.000	4.500				
25	7.000	1.500	4.667				
26	7.500	1.600	4.688				
27	17.000	3.500	4.857				
28	10.000	2.000	5.000				
29	5.300	0.900	5.889				
30	2.900	0.400	7.250				
Length av.	5.864	1.611		#DIV/0!	#DIV/0!		
AREAS OF XENOLITHS		7.417		#DIV/0!			#DIV/0!
VOLUME OF XENOLITHS				#DIV/0!		17.555	#DIV/0!
NUMBER		30		30		30	30
Axial ratio							
MEAN ARITHMETIC		3.555		0.000		4.275	0.000
HARMONIC MEAN		3.131		#DIV/0!		2.941	#DIV/0!
GEOMETRIC MEAN		3.372		0.000		3.449	0.000
STANDARD DEVIATION		1.216		#DIV/0!		4.040	#DIV/0!
SMALLEST		1.77777778		#DIV/0!		1.28571429	#DIV/0!
LARGEST		7.25		#DIV/0!		23.3333333	#DIV/0!
K VALUE				#DIV/0!			#DIV/0!
w log		0.61046053		#DIV/0!		1.25883232	#DIV/0!

LOCALITY				LOCALITY			
PLUTON		C1		PLUTON		C1	
		G1				G1	
		HORIZONTAL				HORIZONTAL	
		VERTICAL				VERTICAL	
NUMBER	X	Z	X/Z	Y	Z	Y/Z	
1	6.500	2.900	2.241	5.500	3.100	1.774	
2	6.500	2.500	2.600	3.200	0.900	3.556	
3	8.500	3.000	2.833	3.800	0.600	6.333	
4	6.500	2.200	2.955	16.500	2.200	7.500	
5	2.8	0.9	3.111	13.500	1.800	7.500	
6	5.000	1.600	3.125	15.000	1.600	9.375	
7	21.000	6.500	3.231				
8	6.800	2.100	3.238				
9	5.200	1.600	3.250				
10	9	2.5	3.600				
11	4.4	1.2	3.667				
12	3.500	0.900	3.889				
13	7.500	1.900	3.947				
14	1.600	0.400	4.000				
15	3.4	0.8	4.250				
16	5.8	1.3	4.462				
17	9.3	1.9	4.895				
18	8.4	1.7	4.941				
19	11.000	2.200	5.000				
20	4	0.8	5.000				
21	3.6	0.7	5.143				
22	2.100	0.400	5.250				
23	19.000	3.400	5.588				
24	16	2.4	6.667				
25	6.4	0.9	7.111				
26	8.000	1.100	7.273				
27	4.7	0.6	7.833				
28	21.000	2.500	8.400				
29	12.000	1.400	8.571				
30	7.8	0.9	8.667				
Length av.	5.307	1.166		6.258	1.267		
AREAS OF XENOLITHS		4.858				6.227	
VOLUME OF XENOLITHS						22.032	
NUMBER		30				6	
Axial ratio							
MEAN ARITHMETIC		4.825				6.006	
HARMONIC MEAN		4.117				4.360	
GEOMETRIC MEAN		4.495				5.255	
STANDARD DEVIATION		1.896				2.823	
SMALLEST		2.24137931				1.77419355	
LARGEST		8.66666667				9.380	
K VALUE						-0.03902012	
w log		0.58733673				0.72320184	

LOCALITY				C4				LOCALITY							
PLUTON				G2				PLUTON							
HORIZONTAL				VERTICAL				HORIZONTAL				VERTICAL			
NUMBER	X	Z	X/Z	Y	Z	Y/Z		NUMBER	X	Z	X/Z	Y	Z	Y/Z	
1	39.000	28.500	1.368	3.100	1.400	2.214		1	2.500	1.700	1.471	1.400	0.900	1.556	
2	1.7	1.1	1.545	7.500	3.300	2.273		2	8.500	5.600	1.518	15.000	9.000	1.667	
3	11.000	7.000	1.571	10.000	4.000	2.500		3	4.200	2.000	2.100	2.000	1.100	1.818	
4	5.000	2.800	1.786	8.000	3.200	2.500		4	4.500	2.000	2.250	9.500	4.800	1.979	
5	4.500	2.200	2.045	10.500	4.000	2.625		5	2.700	1.200	2.250	1.800	0.900	2.000	
6	4.800	2.300	2.087	3.000	1.100	2.727		6	6.000	2.600	2.308	1.800	0.900	2.000	
7	4.5	2.1	2.143	6.500	2.200	2.955		7	7.000	3.000	2.333	11.000	5.000	2.200	
8	11.000	5.000	2.200	5.500	1.800	3.056		8	3.500	1.400	2.500	4.500	2.000	2.250	
9	0.900	0.400	2.250	9.500	3.000	3.167		9	1.800	0.700	2.571	1.400	0.600	2.333	
10	3.500	1.400	2.500	13.000	4.000	3.250		10	2.400	0.900	2.667	7.500	3.200	2.344	
11	11.000	4.000	2.750	3.100	0.900	3.444		11	1.900	0.700	2.714	5.400	2.100	2.571	
12	9	3.2	2.813	7.000	2.000	3.500		12	6.000	2.100	2.857	9.000	3.300	2.727	
13	2.100	0.700	3.000	9.500	2.700	3.519		13	7.000	2.400	2.917	1.100	0.400	2.750	
14	4.2	1.4	3.000	8.500	2.400	3.542		14	5.400	1.800	3.000	1.400	0.500	2.800	
15	3.7	1.2	3.083	3.200	0.900	3.556		15	1.800	0.600	3.000	16.000	5.500	2.909	
16	3.5	1.1	3.182	9.000	2.300	3.913		16	2.700	0.900	3.000	1.200	0.400	3.000	
17	2.400	0.700	3.429	5.500	1.400	3.929		17	1.900	0.600	3.167	4.700	1.500	3.133	
18	7	2	3.500	12.500	3.000	4.167		18	5.100	1.600	3.188	3.500	1.100	3.182	
19	7.4	2	3.700	4.200	1.000	4.200		19	5.500	1.600	3.438	8.500	2.500	3.400	
20	4.500	1.200	3.750	8.500	2.000	4.250		20	2.200	0.600	3.667	2.100	0.600	3.500	
21	1.200	0.300	4.000	9.000	2.100	4.286		21	3.400	0.900	3.778	1.200	0.300	4.000	
22	16	4	4.000	0.900	0.200	4.500		22	4.200	1.100	3.818	4.100	1.000	4.100	
23	2.5	0.6	4.167	2.900	0.500	5.800		23	1.600	0.400	4.000	3.500	0.800	4.375	
24	9.000	2.000	4.500					24	2.400	0.600	4.000	3.100	0.700	4.429	
25	4.5	1	4.500					25	18.000	4.500	4.000	1.800	0.400	4.500	
26	3.7	0.8	4.625					26	1.300	0.300	4.333	1.400	0.300	4.667	
27	6.5	1.4	4.643					27	22.000	4.500	4.889	1.900	0.400	4.750	
28	1.900	0.400	4.750					28	2.000	0.400	5.000	31.500	6.500	4.846	
29	7.000	1.400	5.000					29	3.600	0.700	5.143	5.500	1.100	5.000	
30	9.000	1.800	5.000					30	2.200	0.300	7.333	4.600	1.100	4.182	
Length av.	3.570	1.115		4.456	1.192			Length av.	2.976	0.866		2.587	0.821		
AREAS OF XENOLITHS			3.125			4.170		AREAS OF XENOLITHS			2.023			1.667	
VOLUME OF XENOLITHS						9.926		VOLUME OF XENOLITHS						3.308	
NUMBER			30			23		NUMBER			30			30	
Axial ratio								Axial ratio							
MEAN ARITHMETIC			3.230			3.473		MEAN ARITHMETIC			3.307			3.166	
HARMONIC MEAN			2.753			3.284		HARMONIC MEAN			2.863			2.756	
GEOMETRIC MEAN			3.025			3.377		GEOMETRIC MEAN			3.114			2.987	
STANDARD DEVIATION			1.122			0.851		STANDARD DEVIATION			1.216			1.074	
SMALLEST		1.36842105				2.21428571		SMALLEST		1.47058824				1.55555556	
LARGEST		5				5.800		LARGEST		7.33333333				5.000	
K VALUE						0.14818449		K VALUE						0.03775567	
w log		0.56275026				0.41819434		w log		0.69781034				0.50708448	

LOCALITY				C10				LOCALITY							
PLUTON				G3				PLUTON							
HORIZONTAL				VERTICAL				HORIZONTAL				VERTICAL			
NUMBER	X	Z	X/Z	Y	Z	Y/Z		NUMBER	X	Z	X/Z	Y	Z	Y/Z	
1	0.600	0.600	1.000	0.700	0.700	1.000		1	3.400	1.400	2.429	1.400	1.200	1.167	
2	1.000	0.900	1.111	0.600	0.500	1.200		2	5.000	2.000	2.500	20.000	10.000	2.000	
3	0.700	0.600	1.167	1.400	1.100	1.273		3	3.100	1.200	2.583	2.400	1.200	2.000	
4	1.600	1.200	1.333	0.900	0.700	1.286		4	13.500	5.000	2.700	2.900	1.400	2.071	
5	1.000	0.700	1.429	2.000	1.400	1.429		5	3.900	1.400	2.786	25.000	12.000	2.083	
6	1.500	1.000	1.500	2.000	1.400	1.429		6	3.100	1.100	2.818	3.000	1.200	2.500	
7	0.900	0.600	1.500	1.600	1.100	1.455		7	26.000	9.200	2.826	1.800	0.700	2.571	
8	1.400	0.900	1.556	1.200	0.800	1.500		8	8.500	2.900	2.931	2.000	0.700	2.857	
9	1.100	0.700	1.571	1.200	0.800	1.500		9	2.700	0.900	3.000	10.000	3.500	2.857	
10	1.400	0.800	1.750	0.900	0.600	1.500		10	5.500	1.800	3.056	7.500	2.600	2.885	
11	2.200	1.200	1.833	1.400	0.900	1.556		11	16.500	5.400	3.056	5.500	1.900	2.895	
12	1.100	0.600	1.833	1.400	0.900	1.556		12	2.800	0.900	3.111	3.500	1.200	2.917	
13	2.100	1.100	1.909	1.400	0.900	1.556		13	2.800	0.900	3.111	6.500	2.100	3.095	
14	7.000	3.600	1.944	0.700	0.400	1.750		14	6.400	2.000	3.200	2.800	0.900	3.111	
15	0.800	0.400	2.000	0.700	0.400	1.750		15	4.200	1.300	3.231	7.700	2.200	3.500	
16	1.400	0.700	2.000	0.900	0.500	1.800		16	23.000	6.400	3.594	4.000	1.100	3.636	
17	2.100	1.000	2.100	11.000	6.000	1.833		17	7.000	1.900	3.684	5.100	1.300	3.923	
18	3.600	1.600	2.250	1.700	0.900	1.889		18	2.600	0.700	3.714	3.600	0.900	4.000	
19	8.000	3.500	2.286	1.700	0.900	1.889		19	7.500	2.000	3.750	9.000	2.200	4.091	
20	1.900	0.800	2.375	1.400	0.700	2.000		20	4.500	1.200	3.750	5.600	1.300	4.308	
21	0.800	0.300	2.667	0.900	0.400	2.250		21	14.500	3.700	3.919	3.800	0.800	4.750	
22	1.600	0.600	2.667	2.100	0.800	2.625		22	2.900	0.700	4.143	3.400	0.700	4.857	
23	5.700	2.100	2.714	2.100	0.800	2.625		23	17.000	3.800	4.474	9.200	1.700	5.412	
24	0.600	0.200	3.000	3.500	1.200	2.917		24	7.200	1.600	4.500	10.000	1.800	5.556	
25	0.900	0.300	3.000	1.200	0.400	3.000		25	16.000	3.500	4.571	9.200	1.600	5.750	
26	5.500	1.800	3.056	0.900	0.300	3.000		26	21.500	4.700	4.574				
27	3.400	1.000	3.400	0.900	0.300	3.000		27	3.400	0.700	4.857				
28	1.400	0.400	3.500	1.400	0.400	3.500		28	6.100	1.200	5.083				
29	0.400	0.100	4.000	10.000	2.400	4.167		29	3.100	0.600	5.167				
30	3.200	0.800	4.000	1.100	0.800	1.375		30	16.000	1.900	8.421				
Length av.	1.243	0.562		1.194	0.642			Length av.	5.024	1.418		3.971	1.299		
AREAS OF XENOLITHS			0.549			0.602		AREAS OF XENOLITHS			5.597			4.052	
VOLUME OF XENOLITHS						0.499		VOLUME OF XENOLITHS						13.573	
NUMBER			30			30		NUMBER			30			25	
Axial ratio								Axial ratio							
MEAN ARITHMETIC			2.215			1.987		MEAN ARITHMETIC			3.718			3.392	
HARMONIC MEAN			1.896			1.728		HARMONIC MEAN			3.371			2.885	
GEOMETRIC MEAN			2.071			1.864		GEOMETRIC MEAN			3.574			3.174	
STANDARD DEVIATION			0.828			0.770		STANDARD DEVIATION			1.196			1.218	
SMALLEST		1				1		SMALLEST		2.42857143				1.16666667	
LARGEST		4				4.170		LARGEST		8.42105263				5.750	
K VALUE						0.16933415		K VALUE						0.14690165	
w log		0.60205999				0.62013605		w log		0.5400155				0.69272106	

LOCALITY PLUTON	E3 G1	HORIZONTAL			VERTICAL			LOCALITY PLUTON	E7 G2	HORIZONTAL			VERTICAL		
NUMBER	X	Z	X/Z	Y	Z	Y/Z		NUMBER	X	Z	X/Z	Y	Z	Y/Z	
1	3.600	1.600	2.250	4.500	3.300	1.364		1	6.800	5.400	1.259				
2	4.100	1.600	2.563	2.400	1.400	1.714		2	2.600	1.400	1.857				
3	15.000	5.800	2.586	1.800	0.900	2.000		3	27.000	14.500	1.862				
4	4.700	1.800	2.611	0.600	0.300	2.000		4	21.200	10.500	2.019				
5	5.600	2.100	2.667	4.500	2.200	2.045		5	4.900	2.200	2.227				
6	1.900	0.700	2.714	2.100	0.900	2.333		6	6.000	2.500	2.400				
7	6.500	2.300	2.826	15.000	6.200	2.419		7	5.400	2.200	2.455				
8	2.600	0.900	2.889	8.800	3.600	2.444		8	3.000	1.200	2.500				
9	2.400	0.800	3.000	13.000	5.000	2.600		9	23.000	8.900	2.584				
10	4.200	1.400	3.000	5.500	2.100	2.619		10	20.000	7.600	2.632				
11	3.700	1.200	3.083	2.100	0.700	3.000		11	12.000	4.500	2.667				
12	7.000	2.200	3.182	1.500	0.400	3.750		12	17.000	6.200	2.742				
13	3.600	1.100	3.273	1.600	0.400	4.000		13	3.400	1.200	2.833				
14	9.500	2.800	3.393	1.600	0.400	4.000		14	2.000	0.700	2.857				
15	7.600	2.100	3.619	7.500	1.800	4.167		15	3.800	1.200	3.167				
16	18.700	4.600	4.065	9.500	2.200	4.318		16	1.300	0.400	3.250				
17	12.000	2.900	4.138					17	4.100	1.200	3.417				
18	4.700	0.900	5.222					18	7.200	2.100	3.429				
19	11.000	1.800	6.111					19	3.600	1.000	3.600				
20	10.000	1.600	6.250					20	3.000	0.800	3.750				
21	4.400	0.700	6.286					21	3.800	1.000	3.800				
22	4.500	0.700	6.429					22	8.000	2.100	3.810				
23	16.000	2.100	7.619					23	3.500	0.900	3.889				
24	2.400	0.300	8.000					24	14.000	3.500	4.000				
25	26.500	3.200	8.281					25	13.000	3.200	4.063				
26								26	4.600	1.100	4.182				
27								27	7.500	1.700	4.412				
28								28	2.700	0.600	4.500				
29								29	8.000	1.500	5.333				
30								30	6.400	0.900	7.111				
Length av.		4.785	1.201		2.413	0.885		Length av.		4.502	1.357		#DIV/0!	#DIV/0!	
AREAS OF XENOLITHS			4.514					AREAS OF XENOLITHS			4.797		#DIV/0!	#DIV/0!	
VOLUME OF XENOLITHS								VOLUME OF XENOLITHS					#DIV/0!	#DIV/0!	
NUMBER			25					NUMBER			30				30
Axial ratio								Axial ratio							
MEAN ARITHMETIC			4.242					MEAN ARITHMETIC			3.287				0.000
HARMONIC MEAN			3.547					HARMONIC MEAN			2.845				#DIV/0!
GEOMETRIC MEAN			3.889					GEOMETRIC MEAN			3.099				0.000
STANDARD DEVIATION			1.912					STANDARD DEVIATION			1.171				#DIV/0!
SMALLEST			2.25			1.36363636		SMALLEST			1.25925926			#DIV/0!	SMALLEST
LARGEST			8.28			4.320		LARGEST			7.11111111			#DIV/0!	LARGEST
K VALUE						0.38035531		K VALUE						#DIV/0!	
w log			0.56584782			0.50078517		w log			0.75182231			#DIV/0!	

LOCALITY PLUTON	F1 G1	Horizontal			Vertical			LOCALITY PLUTON	F2 G3	Horizontal			Vertical		
NUMBER	Y	Z	Y/Z	X	Z	X/Z		NUMBER	Y	Z	Y/Z	X	Z	X/Z	
1	2.700	1.400	1.929	2.800	2.100	1.333		1	1.100	1.000	1.100				3.154
2	10.000	5.000	2.000	3.500	1.900	1.842		2	3.400	2.900	1.172				
3	3.400	1.600	2.125	1.600	0.800	2.000		3	6.800	5.700	1.193				
4	4.100	1.900	2.158	15.000	5.500	2.727		4	16.000	13.000	1.231				
5	4.800	2.100	2.286	9.000	3.200	2.813		5	2.100	1.600	1.313				
6	3.800	1.600	2.375	2.400	0.800	3.000		6	2.100	1.600	1.313				
7	16.500	6.700	2.463	9.900	3.300	3.000		7	1.200	0.900	1.333				
8	14.000	5.500	2.545	14.000	4.600	3.043		8	2.400	1.700	1.412				
9	6.600	2.400	2.750	7.500	2.400	3.125		9	1.600	1.100	1.455				
10	5.900	2.100	2.810	14.000	4.400	3.182		10	8.600	5.500	1.564				
11	14.500	5.100	2.843	2.600	0.800	3.250		11	3.700	2.300	1.609				
12	8.000	2.700	2.963	3.600	1.100	3.273		12	2.100	1.200	1.750				
13	12.100	4.000	3.025	9.500	2.800	3.393		13	6.500	3.700	1.757				
14	9.700	3.100	3.129	5.000	1.400	3.571		14	4.600	2.600	1.769				
15	11.000	3.500	3.143	1.800	0.500	3.600		15	2.400	1.300	1.846				
16	14.500	4.600	3.152	4.800	1.300	3.692		16	3.900	2.100	1.857				
17	15.000	4.500	3.333	6.400	1.700	3.765		17	1.400	0.700	2.000				
18	74.000	22.000	3.364	7.600	2.000	3.800		18	4.200	2.000	2.100				
19	9.000	2.600	3.462	8.000	2.100	3.810		19	3.900	1.800	2.167				
20	13.500	3.600	3.750	4.300	1.100	3.909		20	7.200	3.100	2.323				
21	7.600	1.600	4.750	2.400	0.600	4.000		21	3.500	1.500	2.333				
22	2.900	0.600	4.833	6.400	1.600	4.000		22	2.700	1.100	2.455				
23	15.400	3.100	4.968	5.000	1.200	4.167		23	3.600	1.400	2.571				
24	7.100	1.400	5.071	3.400	0.800	4.250		24	1.300	0.500	2.600				
25	11.000	2.100	5.238	14.000	3.200	4.375		25	3.200	1.200	2.667				
26	8.600	1.600	5.375	14.000	3.200	4.375		26	3.100	1.100	2.818				
27	11.500	2.100	5.476	6.100	1.300	4.692		27	4.600	1.600	2.875				
28	7.800	1.400	5.571	20.000	4.100	4.878		28	4.700	1.600	2.938				
29	18.000	3.110	5.788	19.000	3.200	5.938		29	3.400	1.100	3.091				
30	38.000	4.100	9.268	4.100	0.600	6.833		30	6.700	2.000	3.350				
Length av.		7.434	2.217		4.643	1.357		Length av.		2.736	1.438		#DIV/0!	#DIV/0!	
AREAS OF XENOLITHS			12.943					AREAS OF XENOLITHS			3.091				#DIV/0!
VOLUME OF XENOLITHS								VOLUME OF XENOLITHS							#DIV/0!
NUMBER			30					NUMBER			30				30
Axial Ratio								Axial Ratio							
MEAN ARITHMETIC			3.731					MEAN ARITHMETIC			1.999				0.105
HARMONIC MEAN			3.161					HARMONIC MEAN			1.761				#DIV/0!
GEOMETRIC MEAN			3.455					GEOMETRIC MEAN			1.898				0.000
STANDARD DEVIATION			1.610					STANDARD DEVIATION			0.650				#DIV/0!
SMALLEST			1.92857143			1.33333333		SMALLEST			1.1				3.15384615
LARGEST			9.26829268			6.833		LARGEST			3.35				#DIV/0!
K VALUE						0.01487904		K VALUE							#DIV/0!
w log			0.68176401			0.70969387		w log			0.48365212				#DIV/0!

LOCALITY	F3						LOCALITY	G1					
PLUTON	Horizontal			Vertical			PLUTON	Horizontal			Vertical		
NUMBER	Y	Z	Y/Z	X	Z	X/Z	NUMBER	Y	Z	Y/Z	X	Z	X/Z
1	7.500	4.200	1.786	1.400	1.400	1.000	1	4.300	2.100	2.048	2.500	2.100	1.190
2	4.500	2.300	1.957	4.300	4.000	1.075	2	4.600	2.200	2.091	16.000	7.000	2.286
3	2.400	1.200	2.000	11.500	9.700	1.186	3	20.000	9.500	2.105	21.000	8.500	2.471
4	2.800	1.400	2.000	3.000	2.100	1.429	4	5.700	2.500	2.280	2.200	0.800	2.750
5	3.800	1.800	2.111	4.900	3.400	1.441	5	12.000	4.800	2.500	5.600	1.600	3.500
6	4.600	2.100	2.190	2.400	1.600	1.500	6	5.700	2.200	2.591	5.600	1.600	3.500
7	4.500	2.000	2.250	2.500	1.600	1.563	7	6.000	2.300	2.609	7.000	2.000	3.500
8	4.300	1.900	2.263	2.100	1.300	1.615	8	4.700	1.800	2.611	5.600	1.400	4.000
9	5.600	2.400	2.333	4.000	2.400	1.667	9	6.800	2.600	2.615	5.600	1.300	4.308
10	2.600	1.100	2.364	14.000	8.000	1.750	10	10.000	3.600	2.778	3.800	0.800	4.750
11	6.000	2.500	2.400	1.600	0.900	1.778	11	20.000	7.000	2.857			
12	5.600	2.300	2.435	2.500	1.400	1.786	12	5.200	1.800	2.889			
13	13.500	5.500	2.455	13.000	7.000	1.857	13	9.000	3.000	3.000			
14	7.500	3.000	2.500	6.400	3.400	1.882	14	8.500	2.800	3.036			
15	4.900	1.900	2.579	8.700	4.600	1.891	15	52.000	16.500	3.152			
16	2.600	1.000	2.600	2.000	1.000	2.000	16	38.000	12.000	3.167			
17	5.000	1.900	2.632	6.500	3.000	2.167	17	38.000	11.500	3.304			
18	7.000	2.600	2.692	8.000	3.600	2.222	18	5.300	1.600	3.313			
19	3.000	1.100	2.727	16.000	7.000	2.286	19	5.300	1.600	3.313			
20	1.700	0.600	2.833	11.500	5.000	2.300	20	7.000	2.000	3.500			
21	4.600	1.600	2.875	6.500	2.800	2.321	21	5.100	1.400	3.643			
22	10.000	3.400	2.941	2.600	1.100	2.364	22	9.000	2.200	4.091			
23	6.500	2.200	2.955	4.100	1.700	2.412	23	62.500	15.000	4.167			
24	3.100	1.000	3.100	2.200	0.900	2.444	24	17.000	4.000	4.250			
25	10.000	3.200	3.125	28.000	11.000	2.545	25	3.000	0.700	4.286			
26	23.000	7.000	3.286	6.000	2.200	2.727	26	18.000	4.100	4.390			
27	11.000	3.000	3.667	7.000	2.500	2.800	27	7.000	1.400	5.000			
28	7.000	1.800	3.889	1.400	0.500	2.800	28	28.000	5.000	5.600			
29	9.000	2.300	3.913	4.000	1.300	3.077	29	7.000	1.000	7.000			
30	4.500	1.000	4.500	4.100	1.300	3.154	30	30.500	4.300	7.093			
Length av.	4.366	1.664		3.597	1.827		Length av.	7.619	2.299		4.796	1.546	
AREAS OF XENOLITHS			5.706			5.160	AREAS OF XENOLITHS			13.755			5.822
VOLUME OF XENOLITHS						15.020	VOLUME OF XENOLITHS						29.571
NUMBER			30				NUMBER			30			10
Axial Ratio							Axial Ratio						
MEAN ARITHMETIC			2.712			2.035	MEAN ARITHMETIC			3.509			3.225
HARMONIC MEAN			2.517			1.821	HARMONIC MEAN			3.089			2.781
GEOMETRIC MEAN			2.646			1.953	GEOMETRIC MEAN			3.321			3.028
STANDARD DEVIATION			0.638			0.572	STANDARD DEVIATION			1.292			1.062
SMALLEST		1.78571429				1	SMALLEST		2.04761905				1.19047619
LARGEST		4.5				3.154	LARGEST		7.09302326				4.750
K VALUE						-0.35038407	K VALUE						-0.0930879
w log		0.40140054				0.4988405	w log		0.53958222				0.6009729

LOCALITY	G2						LOCALITY	G4					
PLUTON	Horizontal			Vertical			PLUTON	Horizontal			Vertical		
NUMBER	Y	Z	Y/Z	X	Z	X/Z	NUMBER	Y	Z	Y/Z	X	Z	X/Z
1	3.100	1.400	2.214				1	34.000	24.000	1.417	2.200	1.300	1.692
2	3.100	1.200	2.583				2	14.000	9.000	1.556	6.600	3.600	1.833
3	6.200	2.400	2.583				3	5.500	3.200	1.719	1.900	0.900	2.111
4	4.200	1.600	2.625				4	6.600	3.500	1.886	2.600	1.200	2.167
5	8.600	3.200	2.688				5	2.100	1.000	2.100	2.000	0.900	2.222
6	3.000	1.100	2.727				6	3.800	1.800	2.111	4.000	1.500	2.667
7	17.000	6.000	2.833				7	2.600	1.200	2.167	3.600	1.300	2.769
8	3.400	1.100	3.091				8	29.000	12.500	2.320	4.000	1.400	2.857
9	17.000	5.500	3.091				9	10.000	4.000	2.500	3.200	1.100	2.909
10	9.000	2.900	3.103				10	2.000	0.800	2.500	16.000	5.200	3.077
11	9.500	2.900	3.276				11	11.500	4.500	2.556	8.000	2.600	3.077
12	8.000	2.300	3.478				12	1.800	0.700	2.571	4.100	1.200	3.417
13	7.500	2.100	3.571				13	3.600	1.300	2.769	3.100	0.900	3.444
14	16.500	4.500	3.667				14	10.000	3.500	2.857	4.500	0.900	5.000
15	13.500	3.600	3.750				15	3.500	1.200	2.917	10.000	1.900	5.263
16	8.300	2.200	3.773				16	4.500	1.400	3.214			
17	7.600	2.000	3.800				17	3.800	1.100	3.455			
18	18.000	4.400	4.091				18	4.600	1.300	3.538			
19	18.400	4.000	4.600				19	5.200	1.400	3.714			
20	3.300	0.700	4.714				20	12.500	3.000	4.167			
21							21	4.200	1.000	4.200			
22							22	2.600	0.600	4.333			
23							23	3.100	0.600	5.167			
24							24						
25							25						
26							26						
27							27						
28							28						
29							29						
30							30						
Length av.	6.183	1.946		#DIV/0!	#DIV/0!		Length av.	4.099	1.373		3.586	1.325	
AREAS OF XENOLITHS			9.448			#DIV/0!	AREAS OF XENOLITHS			4.421			3.731
VOLUME OF XENOLITHS						#DIV/0!	VOLUME OF XENOLITHS						10.196
NUMBER			20				NUMBER			23			15
Axial Ratio							Axial Ratio						
MEAN ARITHMETIC			3.313			0.000	MEAN ARITHMETIC			2.858			2.967
HARMONIC MEAN			3.184			#DIV/0!	HARMONIC MEAN			2.558			2.691
GEOMETRIC MEAN			3.247			0.000	GEOMETRIC MEAN			2.704			2.820
STANDARD DEVIATION			0.686			#DIV/0!	STANDARD DEVIATION			0.978			1.030
SMALLEST		2.21428571				#DIV/0!	SMALLEST		1.41666667				1.69230769
LARGEST		4.71				#DIV/0!	LARGEST		5.16				5.230
K VALUE						#DIV/0!	K VALUE						0.05401969
w log		0.32778725				#DIV/0!	w log		0.56138203				0.49002236

LOCALITY	G5						LOCALITY	H1					
PLUTON	G2						PLUTON	G1					
	Horizontal			Vertical				Horizontal			Vertical		
NUMBER	Y	Z	Y/Z	X	Z	X/Z	NUMBER	Y	Z	Y/Z	X	Z	X/Z
1	7.500	4.200	1.786	3.000	2.600	1.154	1	4.100	2.900	1.414	5.000	2.600	1.923
2	9.000	5.000	1.800	6.000	4.500	1.333	2	4.500	2.500	1.800	90.000	41.000	2.195
3	3.600	2.000	1.800	4.000	2.200	1.818	3	4.500	2.200	2.045	7.000	3.000	2.333
4	3.100	1.600	1.938	1.500	0.800	1.875	4	4.600	2.200	2.091	9.000	3.700	2.432
5	4.400	2.000	2.200	9.000	4.200	2.143	5	11.000	5.000	2.200	11.000	4.500	2.444
6	6.900	2.700	2.556	7.000	3.100	2.258	6	15.000	6.500	2.308	9.000	3.500	2.571
7	4.200	1.600	2.625	10.000	4.400	2.273	7	13.000	5.300	2.453	1.800	0.700	2.571
8	7.400	2.800	2.643	4.800	2.100	2.286	8	4.800	1.900	2.526	1.600	0.600	2.667
9	3.900	1.400	2.786	1.200	0.500	2.400	9	13.000	5.000	2.600	2.800	1.000	2.800
10	3.200	1.100	2.909	5.200	2.000	2.600	10	10.000	3.800	2.632	1.700	0.600	2.833
11	3.600	1.200	3.000	0.400	0.150	2.667	11	16.000	6.000	2.667	3.500	1.200	2.917
12	2.100	0.700	3.000	6.000	2.200	2.727	12	13.500	5.000	2.700	9.500	3.200	2.969
13	2.800	0.900	3.111	33.000	11.500	2.870	13	3.000	1.100	2.727	9.600	3.100	3.097
14	5.800	1.800	3.222	3.800	1.200	3.167	14	5.000	1.800	2.778	2.800	0.900	3.111
15	10.000	2.900	3.448	4.500	1.400	3.214	15	10.000	3.100	3.226	3.500	1.100	3.182
16	2.100	0.600	3.500	30.000	9.200	3.261	16	33.000	10.000	3.300	3.500	1.100	3.182
17	6.500	1.800	3.611	15.000	4.600	3.261	17	10.000	3.000	3.333	8.600	2.400	3.583
18	4.400	1.200	3.667	8.500	2.600	3.269	18	25.000	7.000	3.571	4.000	1.100	3.636
19	15.000	3.800	3.947	4.000	1.200	3.333	19	4.500	1.200	3.750	7.100	1.800	3.944
20	6.700	1.600	4.188	6.400	1.900	3.368	20	20.000	5.200	3.846	12.000	3.000	4.000
21	4.200	1.000	4.200	8.500	2.400	3.542	21	8.000	2.000	4.000	7.000	1.700	4.118
22	11.000	2.600	4.231	14.000	3.900	3.590	22	6.400	1.600	4.000	23.000	5.400	4.259
23	7.800	1.800	4.333	4.000	1.000	4.000	23	13.500	3.200	4.219	7.600	1.700	4.471
24	10.000	2.300	4.348	3.800	0.900	4.222	24	5.600	1.200	4.667	6.300	1.400	4.500
25	4.500	1.000	4.500	32.000	7.300	4.384	25	29.000	6.000	4.833	2.800	0.600	4.667
26	8.500	1.800	4.722	10.300	2.200	4.682	26	23.000	4.500	5.111	7.500	1.400	5.357
27	19.000	3.800	5.000	7.000	1.400	5.000	27	21.000	4.000	5.250	8.500	1.500	5.667
28	82.000	12.500	6.560	1.000	0.200	5.000	28	18.500	3.300	5.606	7.500	1.200	6.250
29	16.000	2.300	6.957	11.000	2.000	5.500	29	12.000	1.800	6.667	4.600	0.700	6.571
30	8.600	1.100	7.818	2.500	0.300	8.333	30	3.400	0.500	6.800	14.000	2.000	7.000
Length av.	5.152	1.568		3.150	0.979		Length av.	7.405	2.215		4.648	1.343	
AREAS OF XENOLITHS			6.343			2.421	AREAS OF XENOLITHS			12.883			4.903
VOLUME OF XENOLITHS						8.313	VOLUME OF XENOLITHS						24.204
NUMBER			30			30	NUMBER			30			30
Axial Ratio							Axial Ratio						
MEAN ARITHMETIC			3.680			3.318	MEAN ARITHMETIC			3.504			3.708
HARMONIC MEAN			3.114			2.740	HARMONIC MEAN			2.967			3.234
GEOMETRIC MEAN			3.422			3.052	GEOMETRIC MEAN			3.257			3.497
STANDARD DEVIATION			1.482			1.438	STANDARD DEVIATION			1.390			1.353
SMALLEST		1.78571429				1.15384615	SMALLEST		1.4137931				1.92307692
LARGEST		7.81818182				8.333	LARGEST		6.8				7.000
K VALUE						-0.11265694	K VALUE						0.07937383
w log		0.64129379				0.85867085	w log		0.68212305				0.56110138

LOCALITY	H4						LOCALITY	H3					
PLUTON	G2						PLUTON	G1					
	Horizontal			Vertical				Horizontal			Vertical		
NUMBER	Y	Z	Y/Z	X	Z	X/Z	NUMBER	Y	Z	Y/Z	X	Z	X/Z
1	2.200	1.500	1.467	20.000	12.000	1.667	1	5.200	3.500	1.486	0.900	0.800	1.125
2	3.000	1.700	1.765	30.000	18.000	1.667	2	5.000	2.800	1.786	3.700	1.500	2.467
3	7.300	4.100	1.780	7.000	3.100	2.258	3	7.100	3.900	1.821	7.500	2.600	2.885
4	3.100	1.400	2.214	2.800	1.200	2.333	4	2.600	1.400	1.857	8.800	3.000	2.933
5	40.000	18.000	2.222	3.000	1.100	2.727	5	8.500	3.000	2.833	13.000	4.100	3.171
6	3.600	1.600	2.250	10.500	3.300	3.182	6	0.900	0.300	3.000	2.300	0.700	3.286
7	6.600	2.700	2.444	2.100	0.600	3.500	7	3.000	1.000	3.000	9.500	2.800	3.393
8	16.000	6.500	2.462	7.000	1.300	5.385	8	6.400	2.100	3.048	3.100	0.900	3.444
9	1.000	0.400	2.500	6.000	1.100	5.455	9	2.800	0.900	3.111	23.000	6.300	3.651
10	16.500	6.000	2.750	14.000	2.000	7.000	10	13.000	4.000	3.250	4.400	1.200	3.667
11	1.700	0.600	2.833				11	3.000	0.900	3.333	4.500	1.200	3.750
12	4.000	1.400	2.857				12	3.200	0.900	3.556	2.300	0.600	3.833
13	4.100	1.300	3.154				13	4.800	1.300	3.692	3.600	0.900	4.000
14	2.000	0.600	3.333				14	24.000	6.000	4.000	6.400	1.500	4.267
15	8.100	2.400	3.375				15	3.800	0.900	4.222	1.300	0.300	4.333
16	1.500	0.400	3.750				16	3.400	0.800	4.250	8.500	1.900	4.474
17	9.700	2.400	4.042				17	4.800	1.100	4.364	6.300	1.400	4.500
18	5.500	1.300	4.231				18	11.000	2.500	4.400	10.000	2.200	4.545
19	2.700	0.600	4.500				19	3.200	0.700	4.571	4.200	0.900	4.667
20	6.500	1.400	4.643				20	6.000	1.300	4.615	10.000	2.100	4.762
21	10.700	2.100	5.095				21	12.000	2.400	5.000	4.500	0.900	5.000
22	1.600	0.300	5.333				22	2.000	0.400	5.000	15.000	2.800	5.357
23	13.000	2.100	6.190				23	1.600	0.300	5.333	3.600	0.600	6.000
24	2.100	0.300	7.000				24	3.000	0.500	6.000	2.500	0.400	6.250
25	2.200	0.300	7.333				25	4.300	0.700	6.143	4.600	0.700	6.571
26							26	5.600	0.800	7.000	17.000	2.500	6.800
27							27	14.000	1.900	7.368	1.500	0.200	7.500
28							28	27.000	3.600	7.500	7.000	0.900	7.778
29							29	20.000	2.600	7.692	1.600	0.200	8.000
30							30	42.000	4.800	8.750	10.500	1.200	8.750
Length av.	3.085	0.833		5.350	1.574		Length av.	3.871	0.971		3.561	0.786	
AREAS OF XENOLITHS			2.019			6.616	AREAS OF XENOLITHS			2.952			2.198
VOLUME OF XENOLITHS						13.608	VOLUME OF XENOLITHS						5.672
NUMBER			25			10	NUMBER			30			30
Axial Ratio							Axial Ratio						
MEAN ARITHMETIC			3.008			3.517	MEAN ARITHMETIC			4.399			4.705
HARMONIC MEAN			2.939			2.817	HARMONIC MEAN			3.528			3.876
GEOMETRIC MEAN			3.265			3.134	GEOMETRIC MEAN			3.999			4.359
STANDARD DEVIATION			1.618			1.824	STANDARD DEVIATION			1.897			1.797
SMALLEST		1.46666667				1.66666667	SMALLEST		1.48571429				1.125
LARGEST		7.33				7.000	LARGEST		8.75				8.750
K VALUE						-0.0392945	K VALUE						0.07465173
w log		0.69877255				0.62324929	w log		0.77007275				0.89085553

LOCALITY	J3			LOCALITY	J1		
PLUTON	G1			PLUTON	G1		
	horizontal				horizontal		
NUMBER	Y	Z	Y/Z	NUMBER	Y	Z	Y/Z
1	1.5	0.7	2.143	1	2.2	1.4	1.571
2	10.5	4.8	2.188	2	6.5	4	1.625
3	7.1	3.1	2.290	3	6.4	3.8	1.684
4	2.6	1.1	2.364	4	4	2.3	1.739
5	5.8	2.4	2.417	5	13	7.4	1.757
6	9.7	3.9	2.487	6	2.6	1.4	1.857
7	7.5	2.9	2.586	7	5.6	3	1.867
8	10	3.2	3.125	8	1.5	0.8	1.875
9	5.9	1.8	3.278	9	5	2.6	1.923
10	12	3.6	3.333	10	7.7	3.9	1.974
11	16.5	4.9	3.367	11	3.4	1.7	2.000
12	3.8	1.1	3.455	12	3.2	1.6	2.000
13	17	4.9	3.469	13	3.6	1.7	2.118
14	5	1.4	3.571	14	3	1.4	2.143
15	16.9	4.6	3.674	15	1.5	0.7	2.143
16	2.4	0.6	4.000	16	3	1.4	2.143
17	3.4	0.8	4.250	17	2.6	1.2	2.167
18	7.7	1.8	4.278	18	2.5	1.1	2.273
19	3.6	0.8	4.500	19	2.1	0.9	2.333
20	6	1.3	4.615	20	2.6	1.1	2.364
21	15	3.2	4.688	21	26	10.5	2.476
22	18	3.8	4.737	22	4	1.6	2.500
23	24	4.6	5.217	23	3.8	1.5	2.533
24	10	1.9	5.263	24	3	1.1	2.727
25	6	1.1	5.455	25	12.5	4.4	2.841
26	6	1	6.000	26	32	11	2.909
27	7	1.1	6.364	27	12	3.9	3.077
28	13	2	6.500	28	9	2.2	4.091
29	5.6	0.8	7.000	29	2.5	0.6	4.167
30	14.5	1.1	13.182	30	10	1.6	6.250
Length av.	5.641	1.441		Length av.	3.456	1.509	
AREAS OF XENOLITHS			6.384	AREAS OF XENOLITHS			4.095
VOLUME OF XENOLITHS				VOLUME OF XENOLITHS			2.672
NUMBER			30	NUMBER			30
Axial Ratio				Axial Ratio			
MEAN ARITHMETIC			4.327	MEAN ARITHMETIC			2.438
HARMONIC MEAN			3.583	HARMONIC MEAN			2.167
GEOMETRIC MEAN			3.955	GEOMETRIC MEAN			2.314
STANDARD DEVIATION			2.158	STANDARD DEVIATION			0.954
SMALLEST		2.14285714		SMALLEST		1.57142857	
LARGEST		13.1818182		LARGEST		6.25	
K VALUE				K VALUE			
w log	w log	0.7889821		w log		0.59958537	

LOCALITY	J5			LOCALITY	J4		
PLUTON	G1			PLUTON	G2		
	horizontal				horizontal		
NUMBER	Y	Z	Y/Z	NUMBER	Y	Z	Y/Z
1	2	1.6	1.250	1	1.6	1	1.600
2	1.5	0.9	1.667	2	6.1	3.1	1.968
3	3	1.7	1.765	3	2.8	1.4	2.000
4	1.6	0.9	1.778	4	9	4.5	2.000
5	18	9	2.000	5	2.7	1.3	2.077
6	4.3	2.1	2.048	6	3	1.4	2.143
7	3.8	1.8	2.111	7	2.5	1.1	2.273
8	1.5	0.7	2.143	8	24	9.5	2.526
9	5.6	2.6	2.154	9	3.2	1.1	2.909
10	2.2	1	2.200	10	11	3.5	3.143
11	2.2	1	2.200	11	6.3	2	3.150
12	3.1	1.4	2.214	12	3.2	1	3.200
13	9.5	4	2.375	13	3	0.9	3.333
14	3.4	1.4	2.429	14	3.9	1.1	3.545
15	1.7	0.7	2.429	15	3.2	0.9	3.556
16	1	0.4	2.500	16	21.5	6	3.583
17	4	1.6	2.500	17	2.9	0.8	3.625
18	5.5	2	2.750	18	3	0.8	3.750
19	4	1.4	2.857	19	7	1.8	3.889
20	2.6	0.9	2.889	20	4	1	4.000
21	22	7	3.143	21	2	0.5	4.000
22	2	0.6	3.333	22	1.8	0.45	4.000
23	5.5	1.6	3.438	23	2.1	0.5	4.200
24	31	9	3.444	24	3	0.7	4.286
25	2.4	0.6	4.000	25	3	0.6	5.000
26	1.9	0.4	4.750	26	3.2	0.6	5.333
27	5.4	0.7	7.714	27	2.8	0.5	5.600
28				28	4	0.7	5.714
29				29	2.9	0.4	7.250
30				30	4.2	0.4	10.500
Length av.	2.715	1.046		Length av.	3.282	0.863	
AREAS OF XENOLITHS			2.231	AREAS OF XENOLITHS			2.224
VOLUME OF XENOLITHS				VOLUME OF XENOLITHS			2.592
NUMBER			27	NUMBER			30
Axial Ratio				Axial Ratio			
MEAN ARITHMETIC			2.744	MEAN ARITHMETIC			3.805
HARMONIC MEAN			2.355	HARMONIC MEAN			3.131
GEOMETRIC MEAN			2.556	GEOMETRIC MEAN			3.480
STANDARD DEVIATION			1.249	STANDARD DEVIATION			1.808
SMALLEST		1.25		SMALLEST		1.6	
LARGEST		7.71		LARGEST		10.5	
K VALUE				K VALUE			
w log	w log	0.79014437		w log		0.81706932	

LOCALITY J5*				LOCALITY K2			
PLUTON G1				PLUTON G1			
horizontal				horizontal			
NUMBER	Y	Z	Y/Z	X	Z	X/Z	
1	2.4	1.6	1.500		2	1.5	1.333
2	3.1	1.7	1.824		3	1.700	4.6
3	6.1	2.4	2.542		4	1.727	13
4	4.9	1.9	2.579		5	2.083	7.5
5	0.8	0.3	2.667		6	2.111	15
6	14.5	5.4	2.685		7	2.350	2.1
7	7	2.6	2.692		8	2.421	2.1
8	3	1.1	2.727		9	2.667	2.1
9	4.5	1.6	2.813		10	2.731	3
10	4.6	1.6	2.875		11	2.769	0.5
11	2.6	0.8	3.250		12	2.857	12
12	2.6	0.8	3.250		13	2.857	2
13	3	0.9	3.333		14	2.952	4.5
14	7.5	2.2	3.409		15	3.000	1.2
15	3.6	1	3.600		16	3.091	4.7
16	4	1.1	3.636		17	3.111	3.4
17	6	1.6	3.750		18	3.182	11.2
18	5	1.3	3.846		19	3.333	3.8
19	3.5	0.9	3.889		20	3.500	12
20	7	1.8	3.889		21	3.538	6.5
21	6	1.5	4.000		22	3.571	2.2
22	6.4	1.5	4.267		23	3.643	1.1
23	4	0.9	4.444		24	3.857	6
24	6.2	1.2	5.167		25	4.000	10
25	6	1.1	5.455		26	4.750	3.6
26	5.1	0.9	5.667		27	4.800	2.8
27	26	4.4	5.909		28	5.333	4.2
28	12	2	6.000		29	5.333	2.7
29	5.6	0.9	6.222		30	5.667	6.7
30	39	5.1	7.647				3
Length av.	3.942	1.167		#DIV/0!	3.132	0.925	2.824
AREAS OF XENOLITHS		3.615	#DIV/0!	AREAS OF XENOLITHS		2.276	2.234
VOLUME OF XENOLITHS			#DIV/0!	VOLUME OF XENOLITHS			4.663
NUMBER		30	30	NUMBER		29	30
Axial Ratio				Axial Ratio			
MEAN ARITHMETIC		3.851	0.000	MEAN ARITHMETIC		3.251	2.873
HARMONIC MEAN		3.307	#DIV/0!	HARMONIC MEAN		2.817	2.396
GEOMETRIC MEAN		3.611	0.000	GEOMETRIC MEAN		3.069	2.648
STANDARD DEVIATION		1.423	#DIV/0!	STANDARD DEVIATION		1.109	1.213
SMALLEST		1.5	#DIV/0!	SMALLEST		1.33333333	1.26829268
LARGEST		7.64705882	#DIV/0!	LARGEST		5.67	6.000
K VALUE			#DIV/0!	K VALUE			-0.15606501
w log		0.70740317	#DIV/0!	w log		0.62864432	0.67493176

LOCALITY L2				LOCALITY L1			
PLUTON G3				PLUTON G2			
horizontal				horizontal			
NUMBER	Y	Z	Y/Z	X	Z	X/Z	
1	4.1	3.4	1.206	2.2	2.1	1.048	1.545
2	2.6	1.9	1.368	1.5	1.1	1.364	1.750
3	5.5	3.4	1.618	9	6.5	1.385	1.846
4	3.4	2.1	1.619	1.6	1.1	1.455	1.923
5	0.9	0.5	1.800	2.4	1.6	1.500	1.938
6	7.8	4.2	1.857	3	2	1.500	2.077
7	3.4	1.8	1.889	2.4	1.4	1.714	2.105
8	4	2.1	1.905	2.4	1.4	1.714	2.111
9	2.5	1.3	1.923	1.9	1.1	1.727	2.118
10	1.2	0.6	2.000	3	1.6	1.875	2.333
11	2.8	1.4	2.000	4	2.1	1.905	2.368
12	1.2	0.6	2.000	1.8	0.9	2.000	2.444
13	2.8	1.3	2.154	0.4	0.2	2.000	2.500
14	5.2	2.4	2.167	5.7	2.8	2.036	2.500
15	11.5	5	2.300	2.1	1	2.100	2.636
16	11.1	4.8	2.313	3	1.4	2.143	2.667
17	1.9	0.8	2.375	1.5	0.7	2.143	2.813
18	2.3	0.9	2.556	7.4	3.4	2.176	2.857
19	4.2	1.6	2.625	4	1.8	2.222	2.857
20	3.7	1.4	2.643	13	5.8	2.241	3.500
21	2.3	0.8	2.875	10.6	4.6	2.304	3.600
22	1.5	0.5	3.000	1.4	0.6	2.333	3.600
23	1.3	0.4	3.250	7.5	3.2	2.344	3.750
24	4.1	1.2	3.417	4.6	1.9	2.421	4.000
25	2.4	0.7	3.429	11	4.5	2.444	4.000
26	1.4	0.4	3.500	3	1.2	2.500	4.250
27	8.5	2.4	3.542	3.8	1.4	2.714	4.762
28	4	1.1	3.636	3	1.1	2.727	5.357
29	1.7	0.2	8.500	10.5	3.8	2.763	5.429
30	10	0.7	14.286	2.6	0.8	3.250	5.727
Length av.	2.490	0.886		2.375	1.194		2.951
AREAS OF XENOLITHS		1.733	2.228	AREAS OF XENOLITHS		4.514	2.326
VOLUME OF XENOLITHS			3.700	VOLUME OF XENOLITHS			5.957
NUMBER		30	30	NUMBER		30	30
Axial Ratio				Axial Ratio			
MEAN ARITHMETIC		2.992	2.068	MEAN ARITHMETIC		2.746	3.045
HARMONIC MEAN		2.268	1.896	HARMONIC MEAN		2.373	2.628
GEOMETRIC MEAN		2.546	2.010	GEOMETRIC MEAN		2.559	2.853
STANDARD DEVIATION		2.500	0.489	STANDARD DEVIATION		1.361	1.167
SMALLEST		1.20588235	1.04761905	SMALLEST		1.46153846	1.54545455
LARGEST		14.2857143	3.250	LARGEST		9.0625	5.727
K VALUE			-0.21871742	K VALUE			0.11768523
w log		1.07359702	0.49167997	w log		0.79243777	0.56889163

LOCALITY	L7							LOCALITY	L3						
PLUTON	G2	horizontal			vertical			PLUTON	G3	horizontal			vertical		
NUMBER		Y	Z	Y/Z	X	Z	X/Z	NUMBER		Y	Z	Y/Z	X	Z	X/Z
1		3	1.9	1.579	5.5	4	1.375	1		0.9	0.8	1.125	3.7	2.8	1.321
2		6	2.9	2.069	8	4.8	1.667	2		7	5.7	1.228	3.6	2.6	1.385
3		7	3.2	2.188	14	6.5	2.154	3		4.6	3.3	1.394	1.7	1.2	1.417
4		2.5	1	2.500	2.6	1.2	2.167	4		1.7	1.1	1.545	2.6	1.8	1.444
5		2.4	0.9	2.667	9	4	2.250	5		2.2	1.4	1.571	4.2	2.8	1.500
6		2.7	1	2.700	1.6	0.7	2.286	6		1.8	1.1	1.636	2.5	1.6	1.563
7		3	1.1	2.727	17	7.4	2.297	7		4.6	2.6	1.769	3.8	2.4	1.583
8		4.1	1.5	2.733	12	5.2	2.308	8		4	2.2	1.818	1.8	1.1	1.636
9		4.4	1.6	2.750	8.6	3.5	2.457	9		7.5	3.9	1.923	4.1	2.4	1.708
10		14	5	2.800	3.6	1.4	2.571	10		7.2	3.7	1.946	1.6	0.9	1.778
11		6.3	2.2	2.864	16	6	2.667	11		6.5	3.1	2.097	2.5	1.4	1.786
12		3.8	1.2	3.167	4	1.4	2.857	12		8.2	3.8	2.158	1.5	0.8	1.875
13		7	2.2	3.182	3	1	3.000	13		5.2	2.4	2.167	6	3.1	1.935
14		3.5	1.1	3.182	9	3	3.000	14		6.8	3.1	2.194	0.8	0.4	2.000
15		2.5	0.7	3.571	5.6	1.8	3.111	15		5.6	2.5	2.240	0.6	0.3	2.000
16		7.6	2.1	3.619	3	1.5	3.250	16		4.8	2.1	2.286	1.8	0.9	2.000
17		2.5	0.6	4.167	9	2.4	3.750	17		2.1	0.9	2.333	5.1	2.5	2.040
18		2.1	0.5	4.200	4	1	4.000	18		2.2	0.9	2.444	3.6	1.7	2.118
19		4.2	1	4.200	6	1.5	4.000	19		1.4	0.55	2.545	2.9	1.3	2.231
20		4	0.9	4.444	4.1	1	4.100	20		2.4	0.9	2.667	0.9	0.4	2.250
21		4	0.9	4.444	7	1.6	4.375	21		3.5	1.3	2.692	0.7	0.3	2.333
22		8	1.8	4.444	16	3.6	4.444	22		4	1.4	2.857	4.6	1.9	2.421
23		18	4	4.500	8.5	1.9	4.474	23		4.2	1.4	3.000	4.6	1.7	2.706
24		4.6	1	4.600	4.5	1	4.500	24		4	1.3	3.077	0.6	0.2	3.000
25		2.7	0.5	5.400	9.5	2	4.750	25		2.2	0.7	3.143	5	1.6	3.125
26		10.5	1.7	6.176	2.6	0.5	5.200	26		6	1.8	3.333	8.5	0.2	3.250
27		3.8	0.6	6.333	8.6	1.5	5.733	27		4	1.2	3.333	0.9	0.25	3.600
28		7	1.1	6.364	6	1	6.000	28		4.6	1.3	3.538	3	0.8	3.750
29		4.5	0.7	6.429	4.5	0.6	7.500	29		1.6	0.4	4.000	1.6	0.4	4.000
30		2.6	0.4	6.500	38	5	7.600	30		4.5	1	4.500	1.7	0.3	5.667
Length av.		3.838	0.999		5.164	1.493		Length av.		2.844	1.207		1.731	0.647	
AREAS OF XENOLITHS				3.010			6.054	AREAS OF XENOLITHS				2.697			0.879
VOLUME OF XENOLITHS							15.489	VOLUME OF XENOLITHS							1.667
NUMBER				30			30	NUMBER				30			30
Axial Ratio								Axial Ratio							
MEAN ARITHMETIC				3.883			3.661	MEAN ARITHMETIC				2.419			2.314
HARMONIC MEAN				3.318			3.012	HARMONIC MEAN				2.114			1.998
GEOMETRIC MEAN				3.636			3.356	GEOMETRIC MEAN				2.290			2.162
STANDARD DEVIATION				1.429			1.591	STANDARD DEVIATION				0.814			0.970
SMALLEST				1.57894737			1.375	SMALLEST				1.125			1.32142857
LARGEST				6.5			7.600	LARGEST				4.5			5.667
K VALUE							-0.08072522	K VALUE							-0.0756428
w log				0.6145457			0.74251089	w log				0.60205999			0.63228397

LOCALITY	M2							LOCALITY	M1						
PLUTON	G2	horizontal			vertical			PLUTON	G1	horizontal			vertical		
NUMBER		Y	Z	Y/Z	X	Z	X/Z	NUMBER		Y	Z	Y/Z	X	Z	X/Z
1		7	3.8	1.842	4	1.9	2.105	1		4.7	2.4	1.958	7	3.5	2.000
2		3.7	2	1.850	2.6	1.2	2.167	2		6.8	3	2.267	3.2	1.5	2.133
3		5.7	3	1.900	2.5	1.1	2.273	3		3.2	1.4	2.286	5.5	2.5	2.200
4		4.6	2.4	1.917	1.7	0.7	2.429	4		15	6.1	2.459	2.8	1.1	2.545
5		6	2.8	2.143	4	1.6	2.500	5		1	0.4	2.500	0.8	0.3	2.667
6		7	2.9	2.414	5.4	2	2.700	6		2.6	1	2.600	6.5	2.4	2.708
7		3.9	1.6	2.438	6.5	2.4	2.708	7		13	5	2.600	2.5	0.9	2.778
8		2.2	0.9	2.444	2	0.7	2.857	8		2.4	0.9	2.667	7	2.4	2.917
9		2.7	1.1	2.455	7.4	2.4	3.083	9		6	2.2	2.727	2.4	0.8	3.000
10		5.5	2.2	2.500	3.4	1.1	3.091	10		10	3.5	2.857	9	3	3.000
11		8.5	3.2	2.656	4.6	1.4	3.286	11		9.8	3.4	2.882	2.8	0.9	3.111
12		3	1.1	2.727	10.5	3.1	3.387	12		8	2.6	3.077	1.9	0.6	3.167
13		8.8	3.2	2.750	14	3.9	3.590	13		7.4	2.3	3.217	0.8	0.25	3.200
14		3.4	1.2	2.833	9.5	2.5	3.800	14		7	2.1	3.333	5.5	0.9	6.111
15		2.6	0.9	2.889	2.4	0.6	4.000	15		2.7	0.8	3.375	3	0.9	3.333
16		7	2.1	3.333	2.5	0.6	4.167	16		3.9	1.1	3.545	2.6	0.7	3.714
17		9.5	2.7	3.519	4.7	1	4.700	17		7	1.9	3.684	8.1	2.1	3.857
18		4	1.1	3.636	6.9	1.4	4.929	18		4.5	1.2	3.750	6.4	1.6	4.000
19		5.8	1.5	3.867	5.5	1.1	5.000	19		9	2.4	3.750	7.4	1.8	4.111
20		3.1	0.8	3.875	2	0.4	5.000	20		3.4	0.9	3.778	25	6	4.167
21		2	0.5	4.000	3.5	0.7	5.000	21		1.9	0.5	3.800	5	1.2	4.167
22		10	2.4	4.167	4.6	0.9	5.111	22		7.7	1.9	4.053	1.7	0.4	4.250
23		6	1.4	4.286	2.2	0.4	5.500	23		4.6	1.1	4.182	8.2	1.9	4.316
24		19.6	4.5	4.356	3.6	0.6	6.000	24		16	3.4	4.706	3.4	0.7	4.857
25		2.8	0.6	4.667	5	0.8	6.250	25		6.3	1.3	4.846	4.4	0.9	4.889
26		11	2.3	4.783	6.8	1	6.800	26		5.4	1.1	4.909	16	2.9	5.517
27		2.5	0.5	5.000	7	1	7.000	27		6	1.2	5.000	3.4	0.6	5.667
28		9.5	1.9	5.000	4.5	0.6	7.600	28		3.2	0.6	5.333	8	1.4	5.714
29		7	1.2	5.833	4.7	0.6	7.833	29		5.8	0.9	6.444	0.9	0.4	7.600
30		3.5	0.6	5.833	4	1.6	2.500	30				#DIV/0!	9	1	9.000
Length av.		4.294	1.270		3.713	0.910		Length av.		4.247	1.247		2.933	0.868	
AREAS OF XENOLITHS				4.284			2.654	AREAS OF XENOLITHS				4.160			2.000
VOLUME OF XENOLITHS							7.597	VOLUME OF XENOLITHS							5.663
NUMBER				30			30	NUMBER				29			30
Axial Ratio								Axial Ratio							
MEAN ARITHMETIC				3.397			4.246	MEAN ARITHMETIC				3.537			4.023
HARMONIC MEAN				2.950			3.575	HARMONIC MEAN				3.182			3.447
GEOMETRIC MEAN				3.201			3.931	GEOMETRIC MEAN				3.392			3.757
STANDARD DEVIATION				1.189			1.701	STANDARD DEVIATION				1.070			1.617
SMALLEST				1.84210526			2.10526316	SMALLEST				1.95833333			2
LARGEST				5.83333333			7.800	LARGEST				6.44			9.000
K VALUE							0.17752886	K VALUE							0.06910486
w log				0.50060235			0.56878821	w log				0.51699925			0.65321251

LOCALITY	N5						LOCALITY	M5					
PLUTON	G3						PLUTON	G2					
NUMBER	horizontal			vertical			NUMBER	horizontal			vertical		
	Y	Z	Y/Z	X	Z	X/Z		Y	Z	Y/Z	X	Z	X/Z
1	1.6	1.6	1.000	1.2	1.2	1.000	1	8.5	5.1	1.667			
2	1.6	1.4	1.143	1.6	1.5	1.067	2	3.9	2.1	1.857			
3	1.8	1.5	1.200	0.7	0.5	1.400	3	6.5	2.6	2.500			
4	0.9	0.7	1.286	2.5	1.7	1.471	4	10.6	4.2	2.524			
5	0.9	0.7	1.286	2.5	1.7	1.471	5	6.7	2.4	2.792			
6	0.8	0.6	1.333	0.9	0.6	1.500	6	5.4	1.9	2.842			
7	2.8	1.9	1.474	6.5	4.2	1.548	7	3.9	1.1	3.545			
8	0.6	0.4	1.500	1.1	0.7	1.571	8	4.4	1.2	3.667			
9	1.4	0.9	1.556	3.8	2.4	1.583	9	4.1	1.1	3.727			
10	1.6	1	1.600	2.8	1.7	1.647	10	5.4	1.3	4.154			
11	1	0.6	1.667	1	0.6	1.667	11	6	1.3	4.615			
12	1	0.6	1.667	1.2	0.7	1.714	12	9	1.9	4.737			
13	0.7	0.4	1.750	2	1.1	1.818	13	6.1	1.2	5.083			
14	0.7	0.4	1.750	1.1	0.6	1.833	14	7.8	1.1	7.091			
15	0.7	0.4	1.750	1.5	0.8	1.875	15	4.5	0.6	7.500			
16	0.9	0.5	1.800	4.4	2.3	1.913	16						
17	1.1	0.6	1.833	1.2	0.6	2.000	17						
18	1.6	0.8	2.000	1.2	0.6	2.000	18						
19	0.6	0.3	2.000	1.7	0.8	2.125	19						
20	0.9	0.4	2.250	2.6	1.2	2.167	20						
21	1.9	0.8	2.375	2.4	1.1	2.182	21						
22	1	0.4	2.500	2	0.9	2.222	22						
23	1.3	0.5	2.600	7.6	3.2	2.375	23						
24	2.4	0.9	2.667	4.1	1.7	2.412	24						
25	2.4	0.9	2.667	1.5	0.6	2.500	25						
26	1.6	0.6	2.667	2	0.8	2.500	26						
27	2.5	0.9	2.778	2.2	0.8	2.750	27						
28	4	1.3	3.077	2	0.7	2.857	28						
29	2.9	0.7	4.143	3.6	1.2	3.000	29						
30	7	1.5	4.667	3.2	1	3.200	30						
Length av.	1.115	0.598		1.681	0.899		Length av.	5.636	1.447		#DIV/0!	#DIV/0!	
AREAS OF XENOLITHS			0.523			1.186	AREAS OF XENOLITHS			6.407			#DIV/0!
VOLUME OF XENOLITHS						0.882	VOLUME OF XENOLITHS						#DIV/0!
NUMBER			30			30	NUMBER			15			30
Axial Ratio							Axial Ratio						
MEAN ARITHMETIC			2.066			1.979	MEAN ARITHMETIC			3.887			0.000
HARMONIC MEAN			1.772			1.787	HARMONIC MEAN			3.256			#DIV/0!
GEOMETRIC MEAN			1.928			1.906	GEOMETRIC MEAN			3.557			0.000
STANDARD DEVIATION			0.845			0.547	STANDARD DEVIATION			1.719			#DIV/0!
SMALLEST			1			1	SMALLEST			1.6666667			
LARGEST			4.6666667			3.200	LARGEST			7.5			#DIV/0!
K VALUE						0.01537708	K VALUE						#DIV/0!
w log			0.66900678			0.50514998	w log			0.65321251			#DIV/0!

LOCALITY	O3						LOCALITY	O2					
PLUTON	G3						PLUTON	G27					
NUMBER	horizontal			vertical			NUMBER	horizontal			vertical		
	Y	Z	Y/Z	X	Z	X/Z		Y	Z	Y/Z	X	Z	X/Z
1	7.8	6.7	1.164	3.1	2.2	1.409	1	1	0.8	1.250	2.6	1.1	2.364
2	6	4.7	1.277	7.2	5	1.440	2	5.7	4	1.425	3.4	1.3	2.615
3	3.4	2	1.700	3.4	2.1	1.619	3	4.3	2.9	1.483	7	1.1	6.364
4	3.8	2.2	1.727	2.5	1.5	1.667	4	5.6	3	1.867			
5	4.3	2	2.150	3.6	2.1	1.714	5	2.8	1.5	1.867			
6	2.6	1.2	2.167	4	2.3	1.739	6	3.1	1.5	2.067			
7	2.6	1.2	2.167	2.4	1.2	2.000	7	5.8	2.8	2.071			
8	1.1	0.5	2.200	8	3.8	2.105	8	1.5	0.7	2.143			
9	8.3	3.7	2.243	4.2	1.9	2.211	9	5.6	2.6	2.154			
10	8.7	3.7	2.351	3.3	1.4	2.357	10	2.7	1.2	2.250			
11	1.9	0.8	2.375	3	1.2	2.500	11	3.4	1.5	2.267			
12	3.4	1.4	2.429	3.3	1.3	2.538	12	6.2	2.7	2.296			
13	4	1.6	2.500	8	3	2.667	13	5.2	2	2.600			
14	6	2.4	2.500	4.3	1.6	2.688	14	0.8	0.3	2.667			
15	8.7	3.4	2.559	3	1.1	2.727	15	3.8	1.4	2.714			
16	5.4	2.1	2.571	3.6	1.3	2.769	16	2.8	1	2.800			
17	1.8	0.7	2.571	4	1.4	2.857	17	2.8	1	2.800			
18	3.9	1.4	2.786	2.9	1	2.900	18	5.4	1.9	2.842			
19	3.4	1.2	2.833	3	1	3.000	19	3.9	1.3	3.000			
20	8.2	2.8	2.929	2.2	0.7	3.143	20	9.7	3.2	3.031			
21	22	7.5	2.933	5.5	1.7	3.235	21	2.8	0.9	3.111			
22	6	2	3.000	3.5	1	3.500	22	3.5	1.1	3.182			
23	4.2	1.4	3.000	6.7	1.9	3.526	23	1.6	0.5	3.200			
24	4.4	1.4	3.143	12	3.4	3.529	24	12	3.6	3.333			
25	1.9	0.6	3.167	5.2	1.4	3.714	25	6	1.6	3.750			
26	3.5	1.1	3.182	9	2.4	3.750	26	4	1	4.000			
27	7.6	2.3	3.304	4	1	4.000	27	5.8	1.4	4.143			
28	2.2	0.5	4.400	0.8	0.2	4.000	28	6.8	1.6	4.250			
29	2.2	0.5	4.400	3	0.7	4.286	29	7.1	1.6	4.438			
30	3.1	0.7	4.429	3.4	0.6	5.667	30	5.5	1.1	5.000			
Length av.	3.367	1.226		3.254	1.109		Length av.	3.080	1.187		#DIV/0!	#DIV/0!	
AREAS OF XENOLITHS			3.242			2.833	AREAS OF XENOLITHS			2.871			#DIV/0!
VOLUME OF XENOLITHS						6.360	VOLUME OF XENOLITHS						#DIV/0!
NUMBER			30			30	NUMBER			30			3
Axial Ratio							Axial Ratio						
MEAN ARITHMETIC			2.672			2.842	MEAN ARITHMETIC			2.800			3.781
HARMONIC MEAN			2.374			2.472	HARMONIC MEAN			2.441			3.117
GEOMETRIC MEAN			2.557			2.684	GEOMETRIC MEAN			2.651			3.401
STANDARD DEVIATION			0.791			0.974	STANDARD DEVIATION			0.931			2.240
SMALLEST			1.1641791			1.40909091	SMALLEST			1.25			2.36363636
LARGEST			4.42857143			5.667	LARGEST			5			6.360
K VALUE						0.04644958	K VALUE						0.27387432
w log			0.58024385			0.60438865	w log			0.60205999			0.42987645

LOCALITY O4							LOCALITY O3						
PLUTON G2/G3							PLUTON G3						
horizontal				vertical			horizontal				vertical		
NUMBER	Y	Z	Y/Z	X	Z	X/Z	NUMBER	Y	Z	Y/Z	X	Z	X/Z
1	4	2.9	1.379	2.9	1.4	2.071	1	7.8	6.7	1.164	3.1	2.2	1.409
2	9.5	5.8	1.638	3	1.4	2.143	2	6	4.7	1.277	7.2	5	1.440
3	7	3.9	1.795	3.5	1.6	2.188	3	3.4	2	1.700	3.4	2.1	1.619
4	14.5	7	2.071	6.2	2.7	2.296	4	3.8	2.2	1.727	2.5	1.5	1.667
5	10	4.8	2.083	2.5	1	2.500	5	4.3	2	2.150	3.6	2.1	1.714
6	7.5	3.4	2.206	11	4.3	2.558	6	2.6	1.2	2.167	4	2.3	1.739
7	6.4	2.9	2.207	4.3	1.6	2.688	7	2.6	1.2	2.167	2.4	1.2	2.000
8	9	3.9	2.308	3	1.1	2.727	8	1.1	0.5	2.200	8	3.8	2.105
9	5.4	2.3	2.348	2.6	0.9	2.889	9	8.3	3.7	2.243	4.2	1.9	2.211
10	5.4	2.2	2.455	7	2.4	2.917	10	8.7	3.7	2.351	3.3	1.4	2.357
11	4	1.6	2.500	5.4	1.8	3.000	11	1.9	0.8	2.375	3	1.2	2.500
12	6.4	2.5	2.560	2.8	0.9	3.111	12	3.4	1.4	2.429	3.3	1.3	2.538
13	3.7	1.4	2.643	5.1	1.6	3.188	13	4	1.6	2.500	8	3	2.667
14	8.5	3.2	2.656	4.3	1.3	3.308	14	6	2.4	2.500	4.3	1.6	2.688
15	13.6	4.8	2.833	8	2.4	3.333	15	8.7	3.4	2.559	3	1.1	2.727
16	2	0.7	2.857	10	2.7	3.704	16	5.4	2.1	2.571	3.6	1.3	2.769
17	5.5	1.9	2.895	1.9	0.5	3.800	17	1.8	0.7	2.571	4	1.4	2.857
18	8	2.7	2.963	5.5	1.4	3.929	18	3.9	1.4	2.786	2.9	1	2.900
19	4.3	1.3	3.308	1.6	0.4	4.000	19	3.4	1.2	2.833	3	1	3.000
20	2.8	0.8	3.500	16	4	4.000	20	8.2	2.8	2.929	2.2	0.7	3.143
21	5	1.4	3.571	8.5	2.1	4.048	21	22	7.5	2.933	5.5	1.7	3.235
22	13	3.5	3.714	4.7	1.1	4.273	22	6	2	3.000	3.5	1	3.500
23	7	1.8	3.889	3.1	0.7	4.429	23	4.2	1.4	3.000	6.7	1.9	3.526
24	5	1.2	4.167	3.5	0.7	5.000	24	4.4	1.4	3.143	12	3.4	3.529
25	9.5	2.2	4.318	3.5	1	3.500	25	1.9	0.6	3.167	5.2	1.4	3.714
26	4.8	1.1	4.364	16	2.8	5.714	26	3.5	1.1	3.182	9	2.4	3.750
27	3.6	0.8	4.500	4.5	0.7	6.429	27	7.6	2.3	3.304	4	1	4.000
28	15	3.3	4.545	4.2	0.6	7.000	28	2.2	0.5	4.400	0.8	0.2	4.000
29	5.5	1.2	4.583	22	3.1	7.097	29	2.2	0.5	4.400	3	0.7	4.286
30	2.8	0.6	4.667	5	0.7	7.143	30	3.1	0.7	4.429	3.4	0.6	5.667
Length av.		5.216	1.658		3.788	1.035	Length av.		3.367	1.226		3.254	1.109
AREAS OF XENOLITHS				6.794	3.081 AREAS OF XENOLITHS			3.242				2.833	
VOLUME OF XENOLITHS					10.712 VOLUME OF XENOLITHS			6.360				6.360	
NUMBER				30	30 NUMBER			30				30	
Axial Ratio					Axial Ratio								
MEAN ARITHMETIC				3.051	3.833 MEAN ARITHMETIC			2.672				2.842	
HARMONIC MEAN				2.686	3.309 HARMONIC MEAN			2.374				2.472	
GEOMETRIC MEAN				2.897	3.589 GEOMETRIC MEAN			2.557				2.684	
STANDARD DEVIATION				0.976	1.496 STANDARD DEVIATION			0.791				0.974	
SMALLEST				1.37931034	2.07142857 SMALLEST			1.1641791				1.40909091	
LARGEST				4.66666667	7.143 LARGEST			4.42857143				5.667	
K VALUE					0.21119607 K VALUE			0.04644958				0.04644958	
w log				0.52934479	0.537602 w log			0.58024385				0.60438865	

LOCALITY P2							LOCALITY O5							
PLUTON G2							PLUTON G3							
horizontal				vertical			horizontal				vertical			
NUMBER	Y	Z	Y/Z	X	Z	X/Z	NUMBER	Y	Z	Y/Z	X	Z	X/Z	
1	3.2	2	1.600	3	2	1.500	1	4	2.6	1.538	7.8	4	1.950	
2	4.4	2.6	1.692	3.4	2.2	1.545	2	3.6	1.9	1.895	10	4.8	2.083	
3	4.6	2.5	1.840	6.2	3.1	2.000	3	5.4	2.6	2.077	8.5	3.4	2.500	
4	2.7	1.4	1.929	6.8	3.3	2.061	4	1.7	0.8	2.125	3.5	1.4	2.500	
5	5.4	2.7	2.000	4.5	2	2.250	5	5.4	2.3	2.348	5.5	1.9	2.895	
6	2.6	1.3	2.000	3.8	1.6	2.375	6	8	3.4	2.353	7	2.4	2.917	
7	7.6	3.6	2.111	6.2	2.6	2.385	7	4.5	1.9	2.368	6	1.9	3.158	
8	9.8	4.6	2.130	5.2	2.1	2.476	8	3.8	1.6	2.375	3.5	1.1	3.182	
9	3	1.4	2.143	2.3	0.9	2.556	9	6	2.5	2.400	7.3	2.2	3.318	
10	3.5	1.6	2.188	13	5	2.600	10	6.2	2.4	2.583	13	3.6	3.611	
11	3.5	1.5	2.333	9.5	3.6	2.639	11	15	5.7	2.632	4.2	1.1	3.818	
12	6.2	2.6	2.385	9	3.4	2.647	12	16	6	2.667	4.6	1.2	3.833	
13	3.6	1.5	2.400	1.6	0.6	2.667	13	7.6	2.8	2.714	5	1.3	3.846	
14	19.5	7.7	2.532	1.9	0.7	2.714	14	6	2.2	2.727	9	2.2	4.091	
15	5.5	2.1	2.619	3.1	1.1	2.818	15	5.5	1.9	2.895	4.3	0.8	5.375	
16	6.1	2.3	2.652	5.5	1.9	2.895	16	12.5	4.2	2.976	28	5	5.600	
17	6	2.2	2.727	2.4	0.8	3.000	17	6	2	3.000				
18	2.2	0.8	2.750	2.7	0.9	3.000	18	7.4	2.4	3.083				
19	6.2	2.1	2.952	13.6	3.9	3.487	19	6.2	1.9	3.263				
20	2.4	0.8	3.000	2.1	0.6	3.500	20	12	3.6	3.333				
21	1.5	0.5	3.000	6	1.7	3.529	21	9.5	2.7	3.519				
22	5.5	1.8	3.056	3.6	1	3.600	22	4.6	1.3	3.538				
23	4.3	1.4	3.071	2.4	0.6	4.000	23	4.7	1.3	3.615				
24	2.8	0.8	3.500	1.7	0.4	4.250	24	3.5	0.9	3.889				
25	9.5	2.7	3.519	4.8	1.1	4.364	25	15.6	4	3.900				
26	3.1	0.8	3.875	10.5	2.3	4.565	26	7.5	1.9	3.947				
27	6.8	1.6	4.250	2.8	0.6	4.667	27	3.4	0.8	4.250				
28	6	1.4	4.286	6.6	1.2	5.500	28	6.6	1.4	4.714				
29	3.1	0.7	4.429	7.7	1.4	5.500	29	14.5	3	4.833				
30	5.8	1.1	5.273	2.7	0.45	6.000	30	4	0.6	6.667				
Length av.		3.893	1.398		3.601	1.109	Length av.		5.353	1.747		6.021	1.779	
AREAS OF XENOLITHS				4.275	3.136 AREAS OF XENOLITHS				7.346				8.413	
VOLUME OF XENOLITHS					8.138 VOLUME OF XENOLITHS								30.020	
NUMBER				30	30 NUMBER				30				16	
Axial Ratio					Axial Ratio									
MEAN ARITHMETIC				2.808	3.236 MEAN ARITHMETIC				3.141				3.417	
HARMONIC MEAN				2.511	2.810 HARMONIC MEAN				2.795				3.148	
GEOMETRIC MEAN				2.683	3.048 GEOMETRIC MEAN				2.994				3.279	
STANDARD DEVIATION				0.901	1.164 STANDARD DEVIATION				1.049				1.029	
SMALLEST				1.6	1.5 SMALLEST				1.53846154				1.95	
LARGEST				5.27272727	6.000 LARGEST				6.66666667				5.600	
K VALUE					0.1222418 K VALUE								0.11596569	
w log				0.51791533	0.60205999 w log				0.6368221				0.45815342	

LOCALITY	P5							LOCALITY	P3						
PLUTON	G3	horizontal			vertical			PLUTON	G3	horizontal			vertical		
NUMBER	Y	Z	Y/Z	X	Z	X/Z		NUMBER	Y	Z	Y/Z	X	Z	X/Z	
1	20	11	1.818	3.1	2.1	1.476		1	5.9	4.1	1.439	2.6	1	2.600	
2	2.4	1.2	2.000	9.1	6	1.517		2	14.5	10	1.450	1.7	0.6	2.833	
3	2.4	1.1	2.182	3.1	1.8	1.722		3	2.1	1.3	1.615	1.9	0.6	3.167	
4	1.8	0.6	3.000	4.8	2.7	1.778		4	3.4	2	1.700				
5				6.5	3.6	1.806		5	2.7	1.4	1.929				
6				2.4	1.2	2.000		6	3.2	1.6	2.000				
7				2.2	1	2.200		7	2.2	1.1	2.000				
8				1.9	0.7	2.714		8	2.3	1.1	2.091				
9								9	17	8	2.125				
10								10	5.3	2.4	2.208				
11								11	3.7	1.6	2.313				
12								12	1.9	0.8	2.375				
13								13	10	4.2	2.381				
14								14	4	1.6	2.500				
15								15	2.5	0.9	2.778				
16								16	1.8	0.6	3.000				
17								17	3.1	1	3.100				
18								18	3.5	1.1	3.182				
19								19	7.8	2.1	3.714				
20								20	10	2.6	3.846				
21								21	1.6	0.4	4.000				
22								22	4.7	1.1	4.273				
23								23							
24								24							
25								25							
26								26							
27								27							
28								28							
29								29							
30								30							
Length av.	2.780	1.143		3.181	1.566			Length av.	3.267	1.258		#DIV/0!	#DIV/0!		
AREAS OF XENOLITHS			2.495			3.913		AREAS OF XENOLITHS			3.229			#DIV/0!	
VOLUME OF XENOLITHS						7.251		VOLUME OF XENOLITHS						#DIV/0!	
NUMBER			4			8		NUMBER			22			3	
Axial Ratio								Axial Ratio							
MEAN ARITHMETIC			2.250			1.902		MEAN ARITHMETIC			2.546			2.867	
HARMONIC MEAN			2.172			1.836		HARMONIC MEAN			2.309			2.848	
GEOMETRIC MEAN			2.209			1.867		GEOMETRIC MEAN			2.423			2.857	
STANDARD DEVIATION			0.522			0.404		STANDARD DEVIATION			0.837			0.285	
SMALLEST			1.81818182			1.47619048		SMALLEST			1.43902439			2.6	
LARGEST			3			2.710		LARGEST			4.27			3.170	
K VALUE						-0.21647212		K VALUE						0.25091235	
w log			0.21748394			0.26382689		w log			0.47235972			0.08608591	

LOCALITY	Q1							LOCALITY	P7						
PLUTON	META-SEDIMENTS	horizontal			vertical			PLUTON	G3	horizontal			vertical		
NUMBER	Y	Z	Y/Z	X	Z	X/Z		NUMBER	Y	Z	Y/Z	X	Z	X/Z	
1	3	1.5	2.000					1	1.1	1.1	1.000	1.3	1.1	1.182	
2	3	1.2	2.500					2	1.9	1.6	1.188	1.1	0.9	1.222	
3	10.5	3.4	3.088					3	2.4	2	1.200	0.9	0.7	1.286	
4	5	1.4	3.571					4	0.6	0.5	1.200	3.6	2.5	1.440	
5	5.8	1.6	3.625					5	1.1	0.9	1.222	1.3	0.9	1.444	
6	7	1.6	4.375					6	3.1	2.5	1.240	1.9	1.2	1.583	
7	95	20	4.750					7	0.9	0.7	1.286	0.8	0.5	1.600	
8	1.5	0.3	5.000					8	1.5	1.1	1.364	2.3	1.4	1.643	
9	7	1.3	5.385					9	0.6	0.4	1.500	1	0.6	1.667	
10	11	2	5.500					10	0.9	0.6	1.500	2	1.2	1.667	
11	11	1.8	6.111					11	1.5	1	1.500	0.9	0.5	1.800	
12	6.8	1.1	6.182					12	1.4	0.9	1.556	1	0.5	2.000	
13	9	1.4	6.429					13	3.8	2.4	1.583	5	2	2.500	
14	2	0.3	6.667					14	1.5	0.9	1.667	1.1	0.4	2.750	
15	4	0.6	6.667					15	2	1.2	1.667	12	4.2	2.857	
16	4.4	0.6	7.333					16	3.1	1.7	1.824	1.6	0.3	5.333	
17	10.5	1.4	7.500					17	2.6	1.4	1.857				
18	4.7	0.6	7.833					18	1.5	0.8	1.875				
19	4.7	0.6	7.833					19	5	2.6	1.923				
20	21	2	10.500					20	3.7	1.9	1.947				
21	11	1	11.000					21	1.6	0.8	2.000				
22	8.5	0.7	12.143					22	4.1	2	2.050				
23	13	0.8	16.250					23	2.1	1	2.100				
24	5	0.3	16.667					24	3.4	1.6	2.125				
25								25	1.7	0.7	2.429				
26								26	5	2	2.500				
27								27	2.5	1	2.500				
28								28	1.4	0.5	2.800				
29								29	2.2	0.6	3.667				
30								30	1.5	0.4	3.750				
Length av.	5.229	0.820		#DIV/0!	#DIV/0!			Length av.	1.594	0.914		1.394	0.741		
AREAS OF XENOLITHS			3.368			#DIV/0!		AREAS OF XENOLITHS			1.143			0.812	
VOLUME OF XENOLITHS						#DIV/0!		VOLUME OF XENOLITHS						0.863	
NUMBER			25			30		NUMBER			30			16	
Axial Ratio								Axial Ratio							
MEAN ARITHMETIC			6.756			0.000		MEAN ARITHMETIC			1.867			1.998	
HARMONIC MEAN			5.577			#DIV/0!		HARMONIC MEAN			1.641			1.730	
GEOMETRIC MEAN			5.717			0.000		GEOMETRIC MEAN			1.768			1.837	
STANDARD DEVIATION			3.856			#DIV/0!		STANDARD DEVIATION			0.673			1.026	
SMALLEST			2			#DIV/0!		SMALLEST			1			1.18181818	
LARGEST			16.7			#DIV/0!		LARGEST			3.75			5.330	
K VALUE						#DIV/0!		K VALUE						0.10669565	
w log			0.92168648			#DIV/0!		w log			0.57403127			0.65417654	

LOCALITY	Q6								LOCALITY	Q2							
PLUTON	G2								PLUTON	G1							
	horizontal					vertical				horizontal					vertical		
NUMBER	Y	Z	Y/Z			X	Z	X/Z	NUMBER	Y	Z	Y/Z			X	Z	X/Z
1	3.8	3.4	1.118				2.3	0.6	3.833	1	1.6	0.5	3.200				
2	1.4	1.1	1.273				2.9	0.4	7.250	2	2.4	0.6	4.000				
3	2.6	1.9	1.368							3	2.8	0.7	4.000				
4	2.2	1.6	1.375							4	3.5	0.8	4.375				
5	2	1.4	1.429							5	5.7	1.3	4.385				
6	6.8	4.6	1.478							6	5.5	1.2	4.583				
7	0.9	0.6	1.500							7	1.9	0.4	4.750				
8	2.7	1.8	1.500							8	3	0.6	5.000				
9	2.6	1.7	1.529							9	3	0.6	5.000				
10	3.7	2.4	1.542							10	4.7	0.9	5.222				
11	3.3	2.1	1.571							11	4.8	0.9	5.333				
12	8.6	5.3	1.623							12	11	2	5.500				
13	2.6	1.5	1.733							13	4.2	0.7	6.000				
14	4.5	2.4	1.875							14	12	1.9	6.316				
15	5	2.6	1.923							15	2.6	0.4	6.500				
16	2.7	1.4	1.929							16	7.3	1.1	6.636				
17	2.4	1.2	2.000							17	2	0.3	6.667				
18	2	1	2.000							18	4	0.6	6.667				
19	2	1	2.000							19	3	0.4	7.500				
20	2	1	2.000							20	8	0.9	8.889				
21	2.5	1.2	2.083							21	3	0.3	10.000				
22	2.1	1	2.100							22	4	0.4	10.000				
23	2	0.9	2.222							23	2.2	0.2	11.000				
24	3.5	1.4	2.500							24	8.4	0.7	12.000				
25	4.6	1.8	2.556							25	5.4	0.4	13.500				
26	10	3.8	2.632							26	4.4	0.3	14.667				
27	1.1	0.4	2.750							27	6	0.4	15.000				
28	1.7	0.6	2.833							28	2.4	0.15	16.000				
29	10.7	3.4	3.147							29	6	0.3	20.000				
30	3	0.9	3.333							30	4.5	0.2	22.500				
Length av.	2.397	1.237				#DIV/0!	#DIV/0!			Length av.	3.459	0.437			#DIV/0!	#DIV/0!	
AREAS OF XENOLITHS				2.329				#DIV/0!		AREAS OF XENOLITHS				1.189			#DIV/0!
VOLUME OF XENOLITHS								#DIV/0!		VOLUME OF XENOLITHS							#DIV/0!
NUMBER				30						NUMBER				30			30
Axial Ratio										Axial Ratio							
MEAN ARITHMETIC				1.964				5.542		MEAN ARITHMETIC				8.506			0.000
HARMONIC MEAN				1.779				5.015		HARMONIC MEAN				6.441			#DIV/0!
GEOMETRIC MEAN				1.890				5.272		GEOMETRIC MEAN				7.384			0.000
STANDARD DEVIATION				0.569				2.416		STANDARD DEVIATION				5.001			#DIV/0!
SMALLEST				1.11764706				3.83333333		SMALLEST				3.2			#DIV/0!
LARGEST				3.33333333				7.250		LARGEST				22.5			#DIV/0!
K VALUE								1.799309		K VALUE							#DIV/0!
w log				0.47457407				0.27676142		w log				0.84703254			#DIV/0!

LOCALITY	R2								LOCALITY	R1							
PLUTON	G3								PLUTON	G2							
	horizontal					vertical				horizontal					vertical		
NUMBER	Y	Z	Y/Z			X	Z	X/Z	NUMBER	Y	Z	Y/Z			X	Z	X/Z
1	2.6	1.9	1.368						1	2.8	2.1	1.333			3	1.8	1.667
2	3	1.8	1.667						2	2.4	1.5	1.600			4	2.1	1.905
3	8	4.8	1.667						3	2.2	1.3	1.692			3.6	1.8	2.000
4	2	1	2.000						4	5	2.6	1.923			3.7	1.5	2.467
5	1.5	0.7	2.143						5	1.2	0.6	2.000			6	2.3	2.609
6	5.7	2.6	2.192						6	28	12.5	2.240			5.5	2.1	2.619
7	2.5	1.1	2.273						7	3.6	1.5	2.400			2.1	0.8	2.625
8	2.1	0.9	2.333						8	5.7	2.2	2.591			8	3	2.667
9	1.4	0.6	2.333						9	1.4	0.5	2.800			4.1	1.3	3.154
10	10	3.8	2.632						10	4.2	1.4	3.000			6.7	2.1	3.190
11	8.5	3.1	2.742						11	4	1.3	3.077			4	1.2	3.333
12	2.2	0.8	2.750						12	2.8	0.9	3.111			4.2	1.2	3.500
13	1.2	0.4	3.000						13	2	0.6	3.333			1.5	0.4	3.750
14	3	0.8	3.750						14	1.4	0.4	3.500			4	1	4.000
15	2	0.5	4.000						15	1.4	0.4	3.500			1.2	0.3	4.000
16	7.2	1.7	4.235						16	2.1	0.6	3.500			3.2	0.8	4.000
17									17	2.6	0.7	3.714			1.6	0.4	4.000
18									18	1.5	0.4	3.750			3	0.7	4.286
19									19	1.6	0.4	4.000			2.7	0.6	4.500
20									20	1.6	0.4	4.000			5.3	1.1	4.818
21									21	1.6	0.4	4.000			2	0.4	5.000
22									22	3	0.7	4.286			3	0.6	5.000
23									23	1.8	0.4	4.500			1.6	0.3	5.333
24									24	1.5	0.3	5.000			1.2	0.2	6.000
25									25	2.6	0.5	5.200					
26									26	7.5	1.4	5.357					
27									27	1.9	0.3	6.333					
28									28	2.7	0.4	6.750					
29									29	5	0.6	8.333					
30									30	2.7	0.3	9.000					
Length av.	2.559	1.002				#DIV/0!	#DIV/0!			Length av.	2.173	0.568			2.607	0.659	
AREAS OF XENOLITHS				2.014				#DIV/0!		AREAS OF XENOLITHS				0.969			1.350
VOLUME OF XENOLITHS								#DIV/0!		VOLUME OF XENOLITHS							1.955
NUMBER				16						NUMBER				30			24
Axial Ratio										Axial Ratio							
MEAN ARITHMETIC				2.568				0.000		MEAN ARITHMETIC				3.861			3.601
HARMONIC MEAN				2.337				#DIV/0!		HARMONIC MEAN				3.065			3.150
GEOMETRIC MEAN				2.449				0.000		GEOMETRIC MEAN				3.476			3.414
STANDARD DEVIATION				0.832				#DIV/0!		STANDARD DEVIATION				1.861			1.157
SMALLEST				1.36842105				#DIV/0!		SMALLEST				1.33333333			1.66666667
LARGEST				4.24				#DIV/0!		LARGEST				9			6.000
K VALUE								#DIV/0!		K VALUE							0.0243825
w log				0.49114611				#DIV/0!		w log				0.82930377			0.5563025

LOCALITY		S2				LOCALITY		R7					
PLUTON		G3				PLUTON		G3					
		horizontal				vertical				horizontal		vertical	
NUMBER	Y	Z	Y/Z	X	Z	X/Z	NUMBER	Y	Z	Y/Z	X	Z	X/Z
1	1.1	0.6	1.833	1.2	0.6	2.000	1	3.5	2.5	1.400	3	1.7	1.765
2	2.3	1.2	1.917	1.4	0.7	2.000	2	1.8	1	1.800	4.5	2.4	1.875
3	1.6	0.8	2.000	1.2	0.6	2.000	3	2.2	1.1	2.000	2.7	1.3	2.077
4	1.4	0.7	2.000	2.4	1.1	2.182	4	2.7	1.3	2.077	1.7	0.8	2.125
5	1.5	0.7	2.143	1.9	0.8	2.375	5	4	1.9	2.105	2.4	1.1	2.182
6	2.1	0.9	2.333	1.8	0.7	2.571	6	6.8	3.2	2.125	12	5.4	2.222
7	2.1	0.9	2.333	1.1	0.4	2.750	7	1.1	0.5	2.200	3.2	1.4	2.286
8	5.4	2.3	2.348	1.4	0.5	2.800	8	2	0.9	2.222	3	1.3	2.308
9	1.2	0.5	2.400	2.2	0.7	3.143	9	0.9	0.4	2.250	2	0.8	2.500
10	2.6	1	2.600	1.3	0.4	3.250	10	2.5	1.1	2.273	2.3	0.9	2.556
11	1.6	0.6	2.667	1.3	0.4	3.250	11	7	3	2.333	6.4	2.5	2.560
12	1.1	0.4	2.750	1	0.3	3.333	12	4	1.7	2.353	5.6	2.1	2.667
13	1.7	0.6	2.833	1.7	0.4	4.250	13	2.9	1.2	2.417	6.5	2.4	2.708
14	2.9	1	2.900	1.8	0.4	4.500	14	4.4	1.7	2.588	14	5	2.800
15	1.3	0.4	3.250				15	14	5.3	2.642	2.3	0.8	2.875
16	3.1	0.9	3.444				16	5.7	2.1	2.714	5.5	1.8	3.056
17	1.4	0.4	3.500				17	2.2	0.8	2.750	5	1.6	3.125
18	4	1.1	3.636				18	4.4	1.6	2.750	1.6	0.5	3.200
19	2.6	0.7	3.714				19	1.4	0.5	2.800	6	1.8	3.333
20	1.5	0.4	3.750				20	2	0.7	2.857	1	0.3	3.333
21	1.5	0.4	3.750				21	11.4	3.6	3.167	1.7	0.5	3.400
22	1.6	0.4	4.000				22	1.5	0.4	3.750	2.9	0.8	3.625
23	2	0.5	4.000				23	29	7.5	3.867	1.1	0.3	3.667
24	2.8	0.7	4.000				24	2.8	0.7	4.000	1.1	0.3	3.667
25	1.2	0.3	4.000				25	1.6	0.4	4.000	2.6	0.7	3.714
26	2.5	0.6	4.167				26	3	0.7	4.286	1.9	0.5	3.800
27	2.1	0.5	4.200				27	2.8	0.6	4.667	5.6	1.4	4.000
28	2.6	0.6	4.333				28	2.8	0.6	4.667	1.3	0.3	4.333
29	4	0.9	4.444				29	7.6	1.6	4.750	1.8	0.4	4.500
30	4	0.4	10.000				30	15.5	3	5.167	2.2	0.4	5.500
Length av.	1.828	0.575		1.452	0.507		Length av.	2.538	0.901		2.390	0.737	
AREAS OF XENOLITHS			0.826	0.578 AREAS OF XENOLITHS						1.795	1.383		
VOLUME OF XENOLITHS				0.705 VOLUME OF XENOLITHS							2.340		
NUMBER			30	14 NUMBER						30	30		
Axial Ratio				Axial Ratio									
MEAN ARITHMETIC			3.375	2.886 MEAN ARITHMETIC						2.966	3.059		
HARMONIC MEAN			2.913	2.703 HARMONIC MEAN						2.614	2.771		
GEOMETRIC MEAN			3.155	2.791 GEOMETRIC MEAN						2.811	2.947		
STANDARD DEVIATION			1.501	0.796 STANDARD DEVIATION						1.014	0.863		
SMALLEST			1.83333333	2 SMALLEST						1.4	1.76470588		
LARGEST			10	4.500 LARGEST						5.16666667	5.500		
K VALUE				-0.07001337 K VALUE							0.06073469		
w log			0.73675857	0.35218252 w log						0.56708241	0.49369036		

U2				LOCALITY				S6							
PLUTON	G3							PLUTON	G3						
	horizontal								horizontal						
NUMBER	Y	Z	Y/Z	X	Z	X/Z		NUMBER	Y	Z	Y/Z	X	Z	X/Z	
1	1.2	0.8	1.500		0.7	0.6	1.167	1	2.4	1.4	1.714		2.7	2	1.350
2	1.5	1	1.500		1.1	0.8	1.375	2	1.1	0.6	1.833		0.7	0.5	1.400
3	0.9	0.6	1.500		2.2	1.2	1.833	3	2.1	1.1	1.909		0.7	0.4	1.750
4	3.1	2	1.550		1.2	0.6	2.000	4	1.5	0.7	2.143		1.6	0.8	2.000
5	2.5	1.5	1.667		1.5	0.7	2.143	5	3	1.4	2.143		1.4	0.7	2.000
6	1.6	0.9	1.778		0.9	0.4	2.250	6	3	1.4	2.143		0.7	0.3	2.333
7	0.9	0.5	1.800		2.1	0.9	2.333	7	2.6	1.2	2.167		4	1.6	2.500
8	1.1	0.6	1.833		1.2	0.5	2.400	8	3.1	1.4	2.214		2.6	1	2.600
9	7.6	4.1	1.854		1.2	0.5	2.400	9	2.1	0.9	2.333		1.6	0.6	2.667
10	1.6	0.8	2.000					10	1.7	0.7	2.429		6	2	3.000
11	0.8	0.4	2.000					11	1	0.4	2.500		3.1	1	3.100
12	1.2	0.6	2.000					12	2.1	0.8	2.625		5.6	1.6	3.500
13	1.8	0.9	2.000					13	1.6	0.6	2.667		2.2	0.6	3.667
14	2.1	1	2.100					14	1.6	0.6	2.667		2.2	0.5	4.400
15	1.9	0.9	2.111					15	1.6	0.6	2.667		9.7	2.2	4.409
16	1.7	0.8	2.125					16	2.2	0.8	2.750		3	0.6	5.000
17	1.5	0.7	2.143					17	2.5	0.9	2.778		2.6	0.4	6.500
18	1.1	0.5	2.200					18	2.5	0.9	2.778				
19	2.5	1.1	2.273					19	1.7	0.6	2.833				
20	5.6	2.4	2.333					20	8.5	3	2.833				
21	1.2	0.5	2.400					21	1.5	0.5	3.000				
22	1	0.4	2.500					22	1.5	0.5	3.000				
23	1.2	0.4	3.000					23	4	1.2	3.333				
24	1.2	0.4	3.000					24	2	0.6	3.333				
25	0.9	0.3	3.000					25	1.7	0.5	3.400				
26	1.5	0.5	3.000					26	1.4	0.4	3.500				
27	2.1	0.6	3.500					27	2.5	0.7	3.571				
28	1.2	0.3	4.000					28							
29	1.7	0.4	4.250					29							
30	11	2.5	4.400					30							
Length av.	1.443	0.620		1.193	0.623			Length av.	1.850	0.700		1.761	0.688		
AREAS OF XENOLITHS			0.703			0.583	AREAS OF XENOLITHS				1.018				0.951
VOLUME OF XENOLITHS						0.561	VOLUME OF XENOLITHS								1.173
NUMBER			30			9	NUMBER				27				17
Axial Ratio							Axial Ratio								
MEAN ARITHMETIC			2.377			1.989	MEAN ARITHMETIC				2.639				3.069
HARMONIC MEAN			2.122			1.874	HARMONIC MEAN				2.471				2.561
GEOMETRIC MEAN			2.266			1.935	GEOMETRIC MEAN				2.590				2.801
STANDARD DEVIATION			0.803			0.451	STANDARD DEVIATION				0.514				1.384
SMALLEST			1.5			1.1666667	SMALLEST				1.71428571				1.35
LARGEST			4.4			2.400	LARGEST				3.57				6.500
K VALUE						-0.16509369	K VALUE								0.03986907
w log			0.46736142			0.31326445	w log				0.31858501				0.68257959

Appendix 3

Fry (1979) raw data for each phenocryst type, number of points, a qualitative estimate of 'fit', average and standard error.
THIN = tracing from thin section BIOT = biotite MAFS = identifiable mafic phases (dominantly biotite)
SLAB = tracing from polished slab FELD = plagioclase feldspar QTZ = quartz
FELD2 = K-feldspar

Locality	Phenocryst	Type	Number of points	Fry strain	Comment	AVERAGE	ERROR
A0H	BIOT	THIN	54	4.48	POOR	3.20	0.80
A0H	FELD	SLAB	55	2.49	OK		
A0H	FELD	THIN	107	3.43	OK		
A0H	FELD2	THIN	47	3.56			
A0H	MAFS	SLAB	71	2.33	OK		
A0H	QTZ	THIN	63	2.92	OK		
A0V	BIOT	THIN	66	2.57	GOOD	2.74	0.43
A0V	FELD	SLAB	55	2.27	OK		
A0V	FELD	THIN	114	2.75	GOOD		
A0V	MAFS	SLAB	62	2.66	POOR		
A0V	QTZ	THIN	51	3.43	OK		
A2H	BIOT	THIN	53	2.01	POOR	2.99	0.58
A2H	FELD	THIN	37	2.84	GOOD		
A2H	FELD2	THIN	69				
A2H	QTZ	THIN	70	3.13	GOOD		
A2V	BIOT	THIN	72	3.65	OK	3.36	0.31
A2V	FELD	THIN	40	3.04	V.POOR		
A2V	FELD2	THIN	93	1.15	OK?		
A2V	QTZ	THIN	79	3.38	OK		
B1H	BIOT	THIN	66	2.26	GOOD	2.26	0.22
B1H	FELD	THIN	65	2.46	GOOD		
B1H	FELD2	THIN	51	2.07	OK		
B1H	QTZ	THIN	51	1.96	POOR		
B1V	BIOT	THIN	80	2.31	POOR	2.44	0.13
B1V	FELD	THIN	72	2.44	GOOD		
B1V	FELD2	THIN	55	V. POOR			
B1V	QTZ	THIN	61	2.57	OK		
B5H	BIOT	THIN	73	2.14	POOR	2.37	0.17
B5H	FELD	THIN	118	2.39	GOOD		
B5H	FELD2	THIN	54	2.03	POOR		
B5H	QTZ	THIN	54	2.34	OK		
B5V	BIOT	THIN	76	1.95	OK	2.04	0.16
B5V	FELD	THIN	103	2.02	GOOD		
B5V	FELD2	THIN	51	1.92	OK		
B5V	QTZ	THIN	63	2.27	OK		
B6H	BIOT	THIN	74	2.35	OK	2.58	0.37
B6H	FELD	THIN	86	2.38	OK		
B6H	QTZ	THIN	63	3.00	OK		
B6V	BIOT	THIN	67	2.68	POOR	2.53	0.61
B6V	FELD	THIN	77	2.53	GOOD		
B6V	FELD2	THIN	21				
B6V	QTZ	THIN	47	1.56	POOR		
C1H	BIOT	THIN	66	2.18	OK	2.35	0.36
C1H	FELD	THIN	48	2.38	OK		
C1H	FELD2	THIN	73	1.67	POOR		
C1H	QTZ	THIN	86	2.49	OK		
C1V	BIOT	THIN	47	1.73	POOR	2.03	0.38
C1V	FELD	THIN	50	2.19	POOR		
C1V	FELD2	THIN	74	2.50			
C1V	QTZ	THIN	67	1.71	OK		
C3H	BIOT	THIN	42	2.03	OK	2.49	0.37
C3H	FELD	THIN	89	2.93	OK		
C3H	FELD2	THIN	28	2.50	POOR		
C3H	QTZ	THIN	58	2.50	POOR		
C3V	BIOT	THIN	70	2.49	GOOD	2.44	0.35
C3V	FELD	THIN	75	2.37	OK		
C3V	FELD2	THIN	23	2.03	V.V. POOR		
C3V	QTZ	THIN	84	2.87	OK		
C4H	BIOT	THIN	73	1.89	OK	2.45	0.48
C4H	FELD	THIN	70	2.85	GOOD		
C4H	FELD2	THIN	42	2.20	OK		
C4H	QTZ	THIN	74	2.84	GOOD		
C4V	BIOT	THIN	85	1.99	V.POOR	2.75	0.69
C4V	FELD2	THIN	65				
C4V	QTZ	THIN	91	2.94			
C4V	FELD	THIN	42	3.32	GOOD		
C6H	FELD	SLAB	43	2.43	OK	2.43	0.43
C6H	MAFS	SLAB	45	1.82	POOR		
C6V	FELD	SLAB	39	3.00	POOR	2.66	0.24
C6V	MAFS	SLAB	37	2.66	OK		
C7H	BIOT	THIN	82	1.92	OK	2.43	0.49
C7H	FELD	THIN	59	2.11	GOOD		
C7H	FELD	SLAB	52	1.62	POOR		
C7H	FELD2	THIN	75	2.70	OK		
C7H	MAFS	SLAB	56	2.55	OK		
C7H	QTZ	THIN	97	2.86	OK		
C7V	BIOT	THIN	45	2.67	POOR	2.41	0.42
C7V	FELD	THIN	62	2.49	OK		

Locality	Phenocryst	Type	Number of points	Fry strain	Comment	AVERAGE	ERROR
C7V	FELD	SLAB	32		2.18 POOR		
C7V	FELD2	THIN	81		2.07 OK		
C7V	MAFS	SLAB	44		2.17 GOOD		
C7V	QTZ	THIN	87		3.19 OK		
D1H	BIOT	THIN	55		1.68 OK	2.06	0.32
D1H	FELD	SLAB	62		2.64 POOR		
D1H	FELD	THIN	106		1.87 GOOD		
D1H	FELD2	THIN	85		2.00 OK		
D1H	MAFS	SLAB	62		2.10 V.POOR		
D1H	QTZ	THIN	63		2.07 OK		
D1V	BIOT	THIN	79		1.84 OK	1.91	0.43
D1V	FELD	SLAB	47		2.31 POOR		
D1V	FELD	THIN	89		1.16 POOR		
D1V	FELD2	THIN	64		2.06 POOR		
D1V	MAFS	SLAB	50		1.61 OK		
D1V	QTZ	THIN	62		1.49 V.POOR		
D1V	QTZ	THIN	68		2.27 OK		
D4H	BIOT	THIN	43		1.41 V.POOR	1.60	0.82
D4H	FELD	THIN	96		1.60 OK		
D4H	FELD2	THIN	18		2.91 POOR		
D4V	BIOT	THIN	51		1.37 POOR	1.43	0.12
D4V	FELD	THIN	68		1.57 OK		
D4V	FELD2	THIN	21		1.35 POOR		
D4V	QTZ	THIN	39	3?	POOR		
E1V	FELD	SLAB	58		2.04 OK	2.23	0.26
E1V	MAFS	SLAB	55		2.41 OK		
E5H	BIOT	THIN	75		2.54 OK	2.30	0.25
E5H	FELD	THIN	93		2.05 OK		
E5H	FELD2	THIN					
E5H	QTZ	THIN	53		2.31 POOR		
E5V	BIOT	THIN	92		1.81 OK	1.83	0.34
E5V	FELD	THIN	50		1.50 POOR		
E5V	QTZ	THIN	73		2.18 POOR		
E7H	BIOT	THIN	87		2.57 OK	2.43	0.66
E7H	FELD	THIN	32		1.49 POOR		
E7H	FELD2	THIN	65		2.58 POOR		
E7H	QTZ	THIN	88		3.06 OK		
E7V	BIOT	THIN	51		2.21 OK	2.31	0.51
E7V	FELD	THIN	34		1.85 OK		
E7V	FELD2	THIN	38		2.86 OK		
E7V	QTZ	THIN	73		1.00 OK		
F1H	BIOT	THIN	60		1.81 POOR	1.86	0.07
F1H	FELD	THIN	51		1.91 OK		
F1H	QTZ	THIN	64	3.65?	POOR		
F1V	BIOT	THIN	65		2.04 OK	2.00	0.04
F1V	FELD	THIN	37		1.96 OK		
F1V	FELD2	THIN	30		V.V.POOR		
F1V	QTZ	THIN	59		2.00 OK		
G2H	BIOT	THIN	56		1.65 POOR	1.55	
G2H	FELD	THIN	37		1.45 POOR		
G2V	BIOT	THIN	54		1.90 OK	2.19	
G2V	FELD	THIN	26		2.48 OK		
G4H	BIOT	THIN	64		2.14 POOR	2.01	
G4H	FELD	THIN	68		1.87 OK		
G4V	BIOT	THIN	61		1.84 POOR	2.09	
G4V	FELD	THIN	74		2.33 OK		
G5H	BIOT	THIN	79		1.62 POOR	2.16	
G5H	FELD	THIN	60		2.69 GOOD		
G5V	BIOT	THIN	59		3.21 GOOD	2.98	
G5V	FELD	THIN	61		2.74 GOOD		
H3H	BIOT	THIN	20		2.51 POOR	2.56	0.38
H3H	BIOT	THIN	59		1.73 POOR		
H3H	FELD	THIN	31		2.38 POOR		
H3H	FELD	THIN	38		2.58 OK		
H3H	FELD2	THIN	42		2.50 OK		
H3H	QTZ	THIN	78		1.79		
H3H	QTZ	THIN	77		2.60 GOOD		
H3V	BIOT	THIN	50		2.41 OK	2.82	0.72
H3V	BIOT	THIN	59		3.64 OK		
H3V	FELD	THIN	47		3.84 OK		
H3V	FELD	THIN	60		1.95 POOR		
H3V	FELD2	THIN	25		2.10 POOR		
H3V	FELD2	THIN	54		2.42 GOOD		
H3V	QTZ	THIN	73		2.10 OK		
H3V	QTZ	THIN	66		2.50 OK		
H5H	BIOT	THIN	58		1.64 OK	2.09	0.26
H5H	FELD	THIN	77		2.27 GOOD		
H5H	FELD2	THIN	50		1.96 OK		
H5H	QTZ	THIN	42		2.00 POOR		
H5V	BIOT	THIN	58		2.59 V.POOR	2.04	0.51
H5V	FELD	THIN	92		1.79 GOOD		
H5V	FELD2	THIN	29		3.00 POOR		
H5V	QTZ	THIN	44		2.29 OK		
H6H	BIOT	THIN	73		1.81 GOOD	2.32	0.34
H6H	FELD	SLAB	60		2.22 POOR		

Locality	Phenocryst	Type	Number of points	Fry strain	Comment	AVERAGE	ERROR
H6H	FELD	THIN	79		2.63 OK		
H6H	FELD2	THIN	52		2.60 OK		
H6H	MAFS	SLAB	66		2.25 OK		
H6H	QTZ	THIN	72		1.93 POOR		
H6V	BIOT	THIN	77		2.61 POOR	2.80	0.63
H6V	FELD	SLAB	38				
H6V	FELD	THIN	64		3.32 OK		
H6V	FELD2	THIN	43		3.46 OK		
H6V	MAFS	SLAB	50		2.47 OK		
H6V	QTZ	THIN	66		1.94 OK		
I5H	BIOT	THIN	73		1.30	1.94	0.57
I5H	FELD	THIN	65		2.15		
I5H	FELD2	THIN	15		POOR		
I5H	QTZ	THIN	65		2.38		
I5V	BIOT	THIN	58		1.00	2.22	0.31
I5V	FELD	THIN	38		2.44		
I5V	FELD2	THIN					
I5V	QTZ	THIN	52		2.00		
J3H	BIOT	THIN	56		2.08 OK	2.27	0.29
J3H	FELD	THIN	60		2.60 GOOD		
J3H	QTZ	THIN	50		2.12 POOR		
J3V	BIOT	THIN	40		1.44 V.POOR	1.67	0.29
J3V	FELD	THIN	62		1.78 OK		
J3V	FELD2	THIN	47		1.43 POOR		
J3V	QTZ	THIN	64		2.02 POOR		
J4H	BIOT	THIN	58			1.78	0.36
J4H	FELD	THIN	26		2.18 OK		
J4H	FELD2	THIN	42		1.47 POOR		
J4H	QTZ	THIN	92		1.68		
J4V	BIOT	THIN	59		2.51 OK	2.53	0.49
J4V	FELD	THIN	11				
J4V	FELD2	THIN	27		3.37 POOR		
J4V	QTZ	THIN	122		2.54 OK		
J5H	BIOT	THIN	58		2.44 GOOD	2.65	0.54
J5H	BIOT	THIN	69		2.36 OK		
J5H	FELD	THIN	43		2.67 GOOD		
J5H	FELD	THIN	58		2.34 V.GOOD		
J5H	FELD2	THIN					
J5H	FELD2	THIN	29		2.37 OK		
J5H	QTZ	THIN	29		3.72 OK		
J5H	QTZ	THIN	30				
J5V	BIOT	THIN	43		3.58 OK	2.90	0.67
J5V	BIOT	THIN	44		2.65 OK		
J5V	FELD	THIN	30		1.79 POOR		
J5V	FELD	THIN	73		2.19 GOOD		
J5V	FELD2	THIN	13				
J5V	QTZ	THIN	65		3.19 GOOD		
J5V	QTZ	THIN	24		2.26 POOR		
K4H	BIOT	THIN	73		1.76	1.82	0.18
K4H	FELD	THIN	34		1.63		
K4H	FELD	SLAB	49				
K4H	FELD2	THIN	18				
K4H	MAFS	SLAB	45		2.06		
K4H	QTZ	THIN	63		1.82		
K4V	BIOT	THIN	89		1.67	1.99	0.39
K4V	FELD	THIN	50		2.30		
K4V	FELD	SLAB	37		1.64		
K4V	FELD2	THIN	36	7.5?			
K4V	MAFS	SLAB	39				
K4V	QTZ	THIN	123		2.35		
L1H	BIOT	THIN	48			2.75	0.34
L1H	FELD	SLAB	37		2.52 OK		
L1H	FELD	THIN	56		2.98 OK		
L1H	FELD2	THIN	19		2.23 POOR		
L1H	QTZ	THIN	39		2.28 POOR		
L1V	BIOT	THIN	78		2.48 POOR	2.79	0.67
L1V	FELD	THIN	79		2.30 V.GOOD		
L1V	FELD2	THIN	38		3.25 POOR		
L1V	MAFS	SLAB	63		1.70 POOR		
L1V	QTZ	THIN	95		3.28 OK		
L4H	BIOT	THIN	55		3.02 GOOD	2.74	0.53
L4H	FELD	THIN	33		2.45 OK		
L4H	FELD2	THIN	27		3.50 POOR		
L4H	QTZ	THIN	65				
L4V	BIOT	THIN	50		3.30 POOR	2.59	0.72
L4V	FELD	THIN	55		2.00 POOR		
L4V	FELD2	THIN	24		3.12 POOR		
L4V	QTZ	THIN	90		1.93		
L7H	BIOT	THIN	73		3.00 POOR	2.61	0.30
L7H	FELD	THIN	65		2.32 OK		
L7H	FELD2	THIN	30		2.64 V.V.POOR		
L7H	QTZ	THIN	63		2.90 OK		
L7V	BIOT	THIN	81		1.81 GOOD	1.79	0.10
L7V	FELD	THIN	106		1.76 GOOD		
L7V	FELD2	THIN	57		1.80 OK		

Locality	Phenocryst	Type	Number of points	Fry strain	Comment	AVERAGE	ERROR
L7V	QTZ	THIN	71	1.60	POOR		
M6V	BIOT	THIN	67	2.68	POOR	3.04	0.47
M6V	FELD	THIN	41	2.88	OK		
M6V	FELD2	THIN					
M6V	QTZ	THIN	64	3.57	OK		
N3H	BIOT	THIN	60	2.50		2.38	0.28
N3H	FELD	THIN	75	1.97			
N3H	FELD2	THIN	44	2.41			
N3H	QTZ	THIN	41	2.62			
N3V	BIOT	THIN	41	1.48		1.71	0.45
N3V	FELD	THIN	56	2.30			
N3V	FELD2	THIN	28	1.25			
N3V	QTZ	THIN	45	1.79			
O2H	BIOT	THIN	43	3.09	POOR	2.29	0.48
O2H	BIOT	THIN	74	1.68	POOR		
O2H	FELD	THIN	77	2.30	OK		
O2H	FELD	SLAB	47	2.35	POOR		
O2H	FELD	THIN	73	2.27	OK		
O2H	FELD2	THIN	13				
O2H	FELD2	THIN	62	2.09	POOR		
O2H	QTZ	THIN	61	1.88	OK		
O2H	QTZ	SLAB	36	2.71	POOR		
O2H	QTZ	THIN	91	1.60	OK		
O2V	BIOT	THIN	56	2.76	OK	2.39	0.46
O2V	BIOT	THIN	112	2.35	OK		
O2V	FELD	THIN	23	2.45	OK		
O2V	FELD	SLAB	47	2.00	OK		
O2V	FELD	THIN	81	2.63	OK		
O2V	FELD2	THIN	41	2.70	POOR		
O2V	FELD2	THIN	57	2.15	GOOD		
O2V	QTZ	THIN	94	1.19	GOOD		
O2V	QTZ	SLAB	44	2.26	POOR		
O2V	QTZ	THIN	59	2.59	POOR		
O4H	BIOT	THIN	49	1.70		2.05	0.49
O4H	FELD	THIN	77	2.60			
O4H	FELD	SLAB	118	2.04	POOR		
O4H	FELD2	THIN	22	1.31			
O4H	MAFS	SLAB	68	2.53	V.POOR		
O4H	QTZ	THIN	36	2.11			
O4V	BIOT	THIN	69	1.80		1.56	0.27
O4V	FELD	THIN	82	1.24			
O4V	FELD	SLAB	75	1.33	POOR		
O4V	FELD2	THIN	44	1.60			
O4V	MAFS	SLAB	51				
O4V	QTZ	THIN	83	1.82			
P5H	BIOT	THIN	59	3.47		2.11	0.81
P5H	FELD	THIN	71	2.24			
P5H	FELD2	THIN	23	2.57			
P5H	QTZ	THIN	116	1.51			
P5V	BIOT	THIN	42	2.02		1.91	0.14
P5V	FELD	THIN	107	1.89			
P5V	FELD2	THIN	26	1.72			
P5V	QTZ	THIN	45	2.02			
Q1H	BIOT	THIN	123	2.29		1.92	0.32
Q1H	FELD	THIN	49	1.69			
Q1H	FELD2	THIN					
Q1H	QTZ	THIN	113	1.79			
Q1V	BIOT	THIN	83	1.67		1.50	0.16
Q1V	FELD	THIN	59	1.46			
Q1V	FELD2	THIN					
Q1V	QTZ	THIN	118	1.36			
Q5H	BIOT	THIN	37	2.06	V.POOR	2.05	0.10
Q5H	FELD	THIN	26	2.14	OK		
Q5H	QTZ	THIN	105	1.95	OK		
Q5V	BIOT	THIN	52	1.74	POOR	2.15	0.36
Q5V	FELD	THIN	47	2.44	OK		
Q5V	QTZ	THIN	103	2.26	OK		
S3H	BIOT	THIN	64	2.12	POOR	1.56	
S3H	FELD	THIN	86	1.00	GOOD		
S3V	BIOT	THIN	54	3.33	POOR	1.72	
S3V	FELD	THIN	69	1.72	OK		
S6H	BIOT	THIN	52	3.27	POOR	2.36	
S6H	FELD	THIN	53	2.36	OK		
S6V	BIOT	THIN	53	2.32	OK	2.07	
S6V	FELD	THIN	76	1.81	OK		

Appendix 4

Country rock shortening data of D. Hutton (unpublished)

Line deflection

Distance from

contact / kr	Strain	% Shortening
0.22	13.38	82.26
0.22	15.58	83.97
0.22	14.03	82.81
0.22	100.00	95.36
0.22	15.58	83.97
0.25	4.40	62.76
0.25	2.91	50.94
0.25	1.44	21.58
0.38	15.31	83.78
0.38	3.55	57.03
0.38	3.27	54.61
0.43	3.26	54.52
0.43	12.93	81.85
0.43	4.29	62.12
0.43	100.00	95.36
0.43	3.06	52.56
0.43	7.24	73.28
0.44	100.00	95.36
0.44	9.43	77.60
0.44	8.46	75.91
0.50	5.03	65.94
0.63	4.83	65.00
0.63	4.01	60.38
0.63	2.37	43.74
0.65	9.67	77.97
0.65	1.59	26.59
0.65	2.04	37.83
0.65	2.67	48.04
0.65	6.28	70.62
0.66	7.26	73.33
0.66	9.44	77.61
0.66	7.55	74.01
0.75	2.44	44.83
0.75	3.89	59.57
0.75	4.07	60.77
0.83	8.50	75.99
0.83	4.76	64.66
0.83	4.67	64.21
0.83	4.07	60.77
0.85	10.42	79.04
0.86	1.37	18.77
0.86	2.93	51.16
0.86	2.20	40.88
0.86	3.28	54.70
0.87	15.87	84.17
0.87	18.60	85.76
0.87	7.00	72.67
0.87	3.78	58.79
1.06	2.06	38.23
1.08	1.22	12.46
1.08	3.21	54.05
1.08	1.97	36.37
1.08	1.89	34.58
1.09	9.30	77.39
1.09	4.04	60.58
1.09	2.22	41.24
1.09	2.22	41.24
1.09	13.36	82.24
1.29	1.39	19.71
1.29	1.58	26.28
1.30	6.61	71.61
1.30	5.91	69.41
1.30	4.59	63.79
1.30	2.30	42.61
1.72	2.30	42.61
1.72	2.74	48.93
1.72	1.67	28.96
1.72	1.31	16.47
1.72	1.38	19.32
1.72	1.79	32.17
1.72	5.49	67.87
1.72	8.93	76.77
1.72	2.40	44.21
2.15	1.07	4.41
2.15	1.77	31.66
2.15	2.74	48.93
2.15	4.03	60.51
2.15	2.36	43.59
2.15	2.29	42.44
2.15	2.52	46.00
2.15	13.35	82.23
2.15	2.15	39.97
2.58	1.61	27.20
2.58	1.68	29.24

Fold related

Distance from contact/km

% shortening	Strain
Dawros head to Rosbeg Harbour	
3.91	6.00
3.81	5.00
3.61	5.00
3.59	9.00
3.58	5.00
3.56	7.00
3.55	7.00
3.53	2.00
3.51	7.00
3.50	7.00
3.49	8.00
3.49	10.00
3.48	10.00
3.46	12.00
3.46	12.00
3.45	14.00
3.45	5.00
3.41	5.00
3.40	5.00
3.40	10.00
3.39	10.00
3.28	9.00
3.26	5.00
3.24	10.00
3.23	16.00
3.21	10.00
3.18	15.00
3.14	10.00
3.14	27.00
3.12	16.00
3.11	17.00
3.10	9.00
2.92	13.00
2.87	7.00
2.85	2.00
2.85	20.00
2.83	10.00
2.83	20.00
2.82	17.00
2.81	35.00
2.75	3.00
2.74	17.00
2.74	18.00
2.74	14.00
2.71	9.00
Dunmore Head to Portnoo Harbour	
3.55	13.00
3.27	11.00
3.04	8.00
2.91	15.00
2.70	13.00
2.48	5.00
2.46	19.00
2.46	23.00
2.44	17.00
2.33	3.00
2.32	18.00
2.31	3.00
2.25	9.00
2.24	10.00
2.21	4.00
2.18	5.00
2.18	5.00
2.17	22.00
2.16	29.00
2.15	8.00
2.12	13.00
2.09	6.00
2.04	15.00
2.02	10.00
1.90	18.00
1.88	24.00
1.88	33.00
1.88	20.00

Andalusite data of Sanderson & Meneilly (1981)

Distance from contact/km

Strain	% shortening
500	1.5
500	1.7
150	3.5
150	11.5

Crenulation cleavage

750m - 2.5km from contact

% shortening

20%

Appendix 5

Locality Grid References from the Atibaia pluton

Locality	X	Y	Locality	X	Y
BA1	4275	4145	BN1	4783	4283
BA10	4358	3970	BN2	4824	3030
BA11	4358	3983	BN3	4885	3175
BA12	4333	3963	BN4	4793	3270
BA2	4284	4134	BN5	4693	3188
BA3	4215	4090	BN6	4670	3108
BA4	4293	4048	BN7	4625	3133
BA5	4364	4008	BN8	4575	3134
BA6	4383	3988	BO1	4383	3215
BA7	4400	4015	BO2	4445	3161
BA8	4423	3998	BO3	4470	3193
BA9	4370	3968	BO4	4465	3236
BB1	4276	3494	BO5	4448	3133
BB10	4233	3515	BP1	4678	3525
BB2	4341	3548	BP2	4613	3453
BB3	4316	3530	BP2X	4618	3470
BB4	4270	3560	BP2XX	4609	3483
BB5	4273	3593	BQ1	4406	3970
BB6	4249	3643	BQ2	4405	3973
BB7	4225	3635	BQ3	4481	3983
BB8	4196	3640	BQ4	4433	3904
BB9	4193	3529	BQ5	4420	3873
BC1	4250	3866	BQ6	4385	3825
BC2	4276	3855	BQ7	4363	3841
BC3	4300	3826	BQ7	4430	3948
BC4	4310	3818	BR1	4443	3648
BC5	4340	3819	BR2	4404	3673
BC6	4380	3798	BR3	4403	3718
BD1	4143	4253	BR4	4530	3838
BD2	4411	4145	BR5	4540	3795
BD3	4423	4133	BR6	4500	3663
BD4	4445	4105	BR7	4436	3693
BD5	4448	4078	BS1	4563	3945
BE1	4811	3498	BS2	4560	3909
BE2	4784	3445	BS3	4563	3888
BE3	4690	3503	BS4	4590	3868
BE4	4725	3590	BS5	4640	3875
BE5	4765	3583	BS6	4670	3880
BE6	4785	3600	BT1	4553	3753
BF1	4891	3121	BT2	4579	3760
BF2	4809	3108	BT3	4600	3784
BF3	4725	3086	BT4	4629	3851
BF4	4803	3170	BT5	4448	3743
BG1	4735	2963	BU1	4355	3780

Locality	X	Y	Locality	X	Y
BG2	4638	2985	BU3	4415	3568
BG3	4600	3010	BU4	4430	3591
BG4	4537	2986	BU5	4410	3630
BG5	4410	2941	BV1	4578	3975
BG6	4374	2903	BV2	4354	3740
BG7	4387	3035	BV2	4534	3900
BH1	4180	2820	BV3	4540	4030
BI1/1	4323	2810	BV4	4518	4055
BI1/10	4253	2923	BV5	4545	4048
BI1/2	4329	2925	BV6	4605	4075
BI1/3	4314	2928	BV7	4618	4088
BI1/4	4300	2914	BV8	4643	4133
BI1/5	4300	2938	BV9	4575	4023
BI1/6	4289	2929	BW1	4500	3600
BI1/7	4273	2949	BW2	4539	3613
BJ1/1	4145	3028	BW3	4570	3623
BJ1/2	4145	3058	BW4	4496	3555
BJ1/3	4125	3025	BW5	4475	3506
BJ1/4	4128	3051	BW6	4500	3506
BJ2	4110	3058	BW7	4413	3439
BJ3	4053	3134	BW8	4430	3355
BJ4	4050	3100	BX1	4248	3851
BJ5	4028	3046	BX2	4314	3843
BJ6	3983	3033	BX3	4318	3830
BK1	4378	3665	BX4	4320	3805
BK2	4361	3690	BX5	4333	3795
BK3	4358	3723	BY1	4435	3331
BK4	4353	3670	BY2	4461	3293
BK5	4340	3714	BY3	4520	3241
BK6	4361	3698	BY4	4410	3235
BL1	4160	3383	BY5	4356	3200
BL10	4136	3275	BY6	4281	3293
BL11	4095	3200	BY8	4435	3331
BL2	4174	3383	BZ1	4653	4163
BL3	4189	3393	BZ2	4663	4213
BL4	4200	3406	BZ3	4625	4238
BL5	4279	3366	BZ4	4729	4208
BL6	4244	3405	BZ5	4770	4119
BL7	4210	3353	BZ6	4773	3906
BL8	4160	3355	BZ7	4755	3933
BL9	4148	3300	BZ8	4728	3934
BM1	4579	4240	BZ9	4781	3876
BM2	4566	1228	CA1	4400	3728
BM3	4558	4209	CB1	4705	3878
BM4	4523	4185	CB2	4706	3916
BM5	4578	4170	CB3	4688	3890
BM6	4550	4131	CB4	4678	3928
BM7	4533	4113	CB5	4668	3895

Appendix 6

Xenolith data from Atibaia pluton, SE Brazil
Data consists of xenolith long and short axes, this is averaged using standard mean geometric mean and harmonic mean using Macros.

LOCALITY CB				LOCALITY BU3				LOCALITY BS1,BS2,BS3&BS4			
PLUTON				PLUTON				PLUTON			
		horizontal				horizontal				horizontal	
NUMBER	Y	Z	Y/Z	NUMBER	Y	Z	Y/Z	NUMBER	Y	Z	Y/Z
1	34	25	1.360	1	88	53	1.660	1	64	44	1.455
2	130	56	2.321	2	181	68	2.662	2	35	24	1.458
3	60	25	2.400	3	29.6	9.9	2.990	3	65	42	1.548
4	154	29	5.310	4	37	12	3.083	4	59	34	1.735
Length av.	86.374	30.225		5	198	61	3.246	5	37	21	1.762
AREAS OF XENOLITHS			1575.648	6	31	6.9	4.493	6	13.5	7.5	1.800
VOLUME OF XENOLITHS				7	33	5.8	5.690	7	75.7	42	1.802
NUMBER			4	Length av.	48.173	12.689		8	57	31	1.839
MEAN ARITHMETIC			2.848	AREAS OF XENOLITHS			480.090	9	76	41	1.854
HARMONIC MEAN			2.259	VOLUME OF XENOLITHS				10	18.2	9.6	1.896
GEOMETRIC MEAN			2.519	NUMBER			7	11	80	42	1.905
STANDARD DEVIATION			1.708	MEAN ARITHMETIC			3.403	12	48	25	1.920
SMALLEST		1.36		HARMONIC MEAN			2.987	13	139	72	1.931
LARGEST		5.310		GEOMETRIC MEAN			3.193	14	33	17	1.941
K VALUE				STANDARD DEVIATION			1.310	15	126	64	1.969
w log	0.59155561			SMALLEST		1.66		16	44	22	2.000
				LARGEST		5.690		17	30	14.9	2.013
				K VALUE				18	82	40.5	2.025
				w log	0.53500418			19	100	49	2.041
								20	31	15	2.067
								21	29	13.8	2.101
								22	61	29	2.103
								23	22	10.4	2.115
								24	32	15	2.133
								25	88	41	2.146
								26	106	49	2.163
								27	40	17	2.353
								28	113	47	2.404
								29	34	14	2.429
								30	76	31	2.452
								31	82	33	2.485
								32	180	72	2.500
								33	35	14	2.500
								34	117	46	2.543
								35	13	5.1	2.549
								36	14	5.2	2.692
								37	38	14	2.714
								38	15	5.4	2.778
								39	81	29	2.793
								40	90	32	2.813
								41	30	10.4	2.885
								42	12.7	4.4	2.886
								43	98	33	2.970
								44	84	28	3.000
								45	76	24	3.167
								46	49	15	3.267
								47	27	7.6	3.553
								48	160	44	3.636
								49	198	46	4.304
								50	28	6.5	4.308
								51	58	13.4	4.328
								52	166	38	4.368
								53	35	7.6	4.605
								54	70	15	4.667
								55	65	11.1	5.856
								56	50	7.6	6.579
								57	103	10.9	9.450
								58	73	7.6	9.605
								Length av.	41.819	15.352	
								AREAS OF XENOLITHS			504.231
								VOLUME OF XENOLITHS			
								NUMBER			58
								MEAN ARITHMETIC			2.917
								HARMONIC MEAN			2.453
								GEOMETRIC MEAN			2.635
								STANDARD DEVIATION			1.642
								SMALLEST	1.455		
								LARGEST	9.605		
								K VALUE			
								w log	0.81963438		

LOCALITY BQ3, BQ4 & BQ7				LOCALITY BP				LOCALITY BK1, BK2, BK3 & BK4			
PLUTON				PLUTON				PLUTON			
NUMBER	Y	horizontal Z	Y/Z	NUMBER	Y	horizontal Z	Y/Z	NUMBER	Y	horizontal Z	Y/Z
1	38	38	1.000	1	38	23	1.652	1	54	42	1.286
2	10	9.1	1.099	2	40	22	1.818	2	16.6	12.5	1.328
3	19	16	1.188	3	111	42	2.643	3	14	9.5	1.474
4	16	13	1.231	4	61.5	21.5	2.860	4	63.5	43	1.477
5	15	12	1.250	5	17	5.8	2.931	5	19.7	12.5	1.576
6	27	19	1.421	6	66	19	3.474	6	50	31	1.613
7	23	15	1.438	Length av.	39.851	15.613		7	10	6.2	1.613
8	30	20.8	1.442	AREAS OF XENOLITHS			488.667	8	22	13.6	1.618
9	27	18	1.500	VOLUME OF XENOLITHS				9	22	13	1.692
10	59	37	1.595	NUMBER			6	10	84	47	1.787
11	53	33	1.606	MEAN ARITHMETIC			2.563	11	18.5	10	1.850
12	19	11.8	1.610	HARMONIC MEAN			2.388	12	63	34	1.853
13	9.9	5.9	1.678	GEOMETRIC MEAN			2.477	13	104	56	1.857
14	63	37	1.703	STANDARD DEVIATION			0.699	14	62	32	1.938
15	35	20.5	1.707	SMALLEST		1.652		15	109	55	1.982
16	57	31	1.839	LARGEST		3.474		16	44.5	21.5	2.070
17	38	20	1.900	K VALUE				17	21.5	10.3	2.087
18	55	28	1.964	w log		0.32281977		18	65	31	2.097
19	138	70	1.971					19	32.5	15.5	2.097
20	45	22.8	1.974					20	30.8	14.5	2.124
21	46	23	2.000					21	15	6.9	2.174
22	64	31	2.065					22	25	11.5	2.174
23	57	27	2.111					23	24.5	11	2.227
24	21	9.8	2.143					24	17	7.4	2.297
25	21	9.6	2.188					25	129	56	2.304
26	22.8	10.2	2.235					26	9.8	4.2	2.333
27	43	19	2.263					27	58	24.5	2.367
28	40	16	2.500					28	12.4	5.2	2.385
29	49	19.6	2.500					29	8.2	3.4	2.412
30	80	31	2.581					30	49	19.8	2.475
31	16	5.9	2.712					31	129	52	2.481
32	30	10.8	2.778					32	9.3	3.6	2.583
33	70	25	2.800					33	20.2	7.5	2.693
34	10.8	3.4	3.176					34	60	21.5	2.791
35	39	12.2	3.197					35	211	73	2.890
36	45	14	3.214					36	10.2	3.5	2.914
37	12.6	3.8	3.316					37	22	7.5	2.933
38	76	19	4.000					38	84	28	3.000
Length av.	27.091	13.465						39	41	13.5	3.037
AREAS OF XENOLITHS			286.507					40	45.5	14.8	3.074
VOLUME OF XENOLITHS								41	13	4.2	3.095
NUMBER		38						42	129	40	3.225
MEAN ARITHMETIC		2.076						43	50.5	15.6	3.237
HARMONIC MEAN		1.863						44	183	56	3.268
GEOMETRIC MEAN		1.967						45	29.5	9	3.278
STANDARD DEVIATION		0.702						46	19.4	5.9	3.288
SMALLEST		1						47	131	39	3.359
LARGEST		4.000						48	11.5	3.3	3.485
K VALUE								49	51.5	14.5	3.552
w log		0.60205999						50	35.6	9	3.956
								51	74	17.8	4.157
								52	262	54.5	4.807
								53	112	21.5	5.209
								54	34	6.5	5.231
								55	21.2	3.9	5.436
								56	39.5	5.8	6.810
								57	225	25.5	8.824
								Length av.	27.061	10.479	
								AREAS OF XENOLITHS			222.713
								VOLUME OF XENOLITHS			
								NUMBER		57	
								MEAN ARITHMETIC		2.828	
								HARMONIC MEAN		2.408	
								GEOMETRIC MEAN		2.589	
								STANDARD DEVIATION		1.376	
								SMALLEST		1.286	
								LARGEST		8.824	
								K VALUE			
								w log		0.83642453	

LOCALITY BB1			
PLUTON			
NUMBER	Y	horizontal	
		Z	Y/Z
1	7	7	1.000
2	13.5	12	1.125
3	23	18	1.278
4	52	37	1.405
5	15	10	1.500
6	27	18	1.500
7	10	6.5	1.538
8	85	55	1.545
9	48	30	1.600
10	49	30	1.633
11	45	27	1.667
12	17	9.5	1.789
13	21.5	11.6	1.853
14	70	37.6	1.862
15	15	8	1.875
16	15.5	7.8	1.987
17	14	7	2.000
18	38	19	2.000
19	43	21	2.048
20	64	31	2.065
21	24	11.5	2.087
22	32	15	2.133
23	78.6	36	2.183
24	9.5	4.3	2.209
25	8	3.5	2.286
26	15	6.4	2.344
27	49	20	2.450
28	35	14	2.500
29	19.5	7.6	2.566
30	36	14	2.571
31	30	11.5	2.609
32	48	18	2.667
33	48	16	3.000
34	53	17	3.118
35	11.5	3.6	3.194
36	80	25	3.200
37	64	17	3.765
38	23	5.4	4.259
Length av. 22.235 10.880			
AREAS OF XENOLITHS 189.997			
VOLUME OF XENOLITHS 0.000			
NUMBER 38			
MEAN ARITHMETIC 2.169			
HARMONIC MEAN 1.964			
GEOMETRIC MEAN 2.064			
STANDARD DEVIATION 0.708			
SMALLEST 1			
LARGEST 4.260			
K VALUE #DIV/0!			
w log 0.6294096			

LOCALITY BJ					LOCALITY BI					LOCALITY BG3				
PLUTON					PLUTON					PLUTON				
NUMBER	Y	horizontal		Y/Z	NUMBER	Y	horizontal		Y/Z	NUMBER	Y	horizontal		Y/Z
		Z					Z					Z		
1	12		9	1.333	1	10		10	1.000	1	45		29	1.552
2	14		9.5	1.474	2	21		19.5	1.077	2	80		48	1.667
3	9.5		6	1.583	3	42		39	1.077	3	37		15	2.467
4	11		6	1.833	4	76		68	1.118	4	55		22	2.500
5	23		12	1.917	5	81		72	1.125	5	10.5		3.6	2.917
6	86		44	1.955	6	10		8.5	1.176	6	25		6.6	3.788
7	24		12	2.000	7	18		14	1.286	7	32		8.2	3.902
8	69		34	2.029	8	49		38	1.289	8	56		13	4.308
9	28		13.5	2.074	9	39		30	1.300	9	27		6	4.500
10	16		7.5	2.133	10	66		49	1.347	10	50		11	4.545
11	13		6	2.167	11	15		11	1.364	11	28		4.5	6.222
12	24		11	2.182	12	59		43	1.372	Length av.	30.810		8.625	
13	22		10	2.200	13	80		58	1.379	AREAS OF XENOLITHS			208.702	
14	19		8.5	2.235	14	29		21	1.381	VOLUME OF XENOLITHS			#VALUE!	
15	23		10	2.300	15	6		4.3	1.395	NUMBER			11	
16	9		3.8	2.368	16	17		12	1.417	MEAN ARITHMETIC			3.488	
17	19		8	2.375	17	26		18	1.444	HARMONIC MEAN			2.935	
18	60		25	2.400	18	14		9.5	1.474	GEOMETRIC MEAN			3.213	
19	11		4.5	2.444	19	23		15	1.533	STANDARD DEVIATION			1.413	
20	23		8	2.875	20	46		30	1.533	SMALLEST			1.552	
21	45		15	3.000	21	10		6.5	1.538	LARGEST			6.220	
22	14		4.5	3.111	22	20		13	1.538	K VALUE			#DIV/0!	
23	25		8	3.125	23	40		26	1.538	w log			0.60289867	
24	27		6.5	4.154	24	73		47	1.553					
25	33		6	5.500	25	37.5		24	1.563					
Length av.	18.708		8.167		26	30		19	1.579					
AREAS OF XENOLITHS				120.004	27	49		31	1.581					
VOLUME OF XENOLITHS					28	80		50	1.600					
NUMBER				25	29	36		22	1.636					
MEAN ARITHMETIC				2.431	30	28		17	1.647					
HARMONIC MEAN				2.222	31	28		17	1.647					
GEOMETRIC MEAN				2.315	32	10		6	1.667					
STANDARD DEVIATION				0.874	33	32		19	1.684					
SMALLEST				1.33	34	93		55	1.691					
LARGEST				5.500	35	11.7		6.8	1.721					
K VALUE					36	19		11	1.727					
w log				0.61651105	37	26		15	1.733					
					38	40		23	1.739					
					39	87		50	1.740					
					40	82		47	1.745					
					41	44		25	1.760					
					42	23		13	1.769					
					43	28		15.8	1.772					
					44	64		36	1.778					
					45	16		9	1.778					
					46	34		19	1.789					
					47	34		19	1.789					
					48	14.5		8	1.813					
					49	31		17	1.824					
					50	35		19	1.842					
					51	35		19	1.842					
					52	24		13	1.846					
					53	103		55	1.873					
					54	15		8	1.875					
					55	94		50	1.880					
					56	16		8.5	1.882					
					57	34		18	1.889					
					58	34		18	1.889					
					59	18		9.5	1.895					
					60	19		10	1.900					
					61	40		21	1.905					
					62	40		21	1.905					
					63	28		14.6	1.918					
					64	27		14	1.929					
					65	56		29	1.931					
					66	31		16	1.938					
					67	39		20	1.950					
					68	39		20	1.950					
					69	42		21.5	1.953					
					70	19		9.6	1.979					
					71	15.5		7.8	1.987					
					72	36		18	2.000					
					73	40		20	2.000					
					74	11		5.5	2.000					
					75	46		23	2.000					
					76	10		5	2.000					
					77	46		23	2.000					
					78	73		36	2.028					
					79	35		17	2.059					
					80	172		83	2.072					
					81	54		26	2.077					
					82	50		24	2.083					
					83	50		24	2.083					
					84	44		21	2.095					
					85	40		19	2.105					
					86	140		66	2.121					
					87	13		6.1	2.131					
					88	64		30	2.133					
					89	77		36	2.139					
					90	15		7	2.143					
					91	15		7	2.143					
					92	12		5.6	2.143					
					93	43		20	2.150					
					94	28		13	2.154					
					95	28		13	2.154					
					96	39		18	2.167					
					97	20		9.2	2.174					
					98	37		17	2.176					
					99	24		11	2.182					
					100	11		5	2.200					
					101	11		5	2.200					
					102	11		5	2.200					

103	42	19	2.211
104	10	4.5	2.222
105	100	45	2.222
106	41	18	2.278
107	24	10.5	2.286
108	16	7	2.286
109	71	31	2.290
110	58	25	2.320
111	35	15	2.333
112	42	18	2.333
113	108	46	2.348
114	26	11	2.364
115	71	30	2.367
116	9	3.8	2.368
117	19	8	2.375
118	31	13	2.385
119	18	7.5	2.400
120	72	30	2.400
121	29	12	2.417
122	17	7	2.429
123	32	13	2.462
124	32	13	2.462
125	16	6.5	2.462
126	170	69	2.464
127	72	29	2.483
128	120	48	2.500
129	24	9.6	2.500
130	10	4	2.500
131	161	64	2.516
132	81	32	2.531
133	127	50	2.540
134	51	20	2.550
135	54	21	2.571
136	62	24	2.583
137	15	5.8	2.586
138	22	8.5	2.588
139	71	27	2.630
140	25	9.5	2.632
141	16	6	2.667
142	80	30	2.667
143	16	6	2.667
144	63	23.5	2.681
145	43	16	2.688
146	97	36	2.694
147	62	23	2.696
148	23	8.5	2.706
149	49	18	2.722
150	85	31	2.742
151	66	24	2.750
152	55	20	2.750
153	47	17	2.765
154	47	17	2.765
155	90	32	2.813
156	130	46	2.826
157	27	9.5	2.842
158	16	5.6	2.857
159	26	9	2.889
160	52	18	2.889
161	50	17	2.941
162	18	6	3.000
163	19.5	6.5	3.000
164	27	9	3.000
165	106	35	3.029
166	79	26	3.038
167	73	24	3.042
168	55	18	3.056
169	62	20	3.100
170	30	9.5	3.158
171	24	7.5	3.200
172	29	9	3.222
173	49	15	3.267
174	72	21	3.429
175	86	25	3.440
176	76	22	3.455
177	23	6.6	3.485
178	109	31	3.516
179	18	5	3.600
180	69	19	3.632
181	22	6	3.667
182	91	24	3.792
183	23	6	3.833
184	53	13.5	3.926
185	32	8	4.000
186	56	14	4.000
187	52	13	4.000
188	72	18	4.000
189	30	7.5	4.000
190	53	13	4.077
191	24	5.6	4.286
192	39	9	4.333
193	53	12	4.417
194	42	9	4.667
195	39	8	4.875
196	38	7.5	5.067
197	113	22	5.136
198	84	16	5.250
199	29	4.8	6.042
200	54.5	9	6.056
201	177	28	6.321
202	82	11.9	6.891
Length av.	28.995	12.735	
AREAS OF XENOLITHS			289.995
VOLUME OF XENOLITHS			
NUMBER			23
MEAN ARITHMETIC			2.459
HARMONIC MEAN			2.169
GEOMETRIC MEAN			2.302
STANDARD DEVIATION			0.987
SMALLEST		1	
LARGEST		6.891	
K VALUE			
w log		0.83828225	

Appendix 7

Fry data collected from the Atibaia pluton SE Brazil, during field season 1995.

Locality	Phenocryst	Type	Number of	Orientation	Fry strain	Average	Error
BC5HORIZ	FELDSPAR	TRACING	67	Only recorded when non-parallel to Foliation	2.33	1.93	0.35
BC5VERT	FELDSPAR	TRACING	71		1.80	2.13	0.42
BE1HORIZ	FELDSPAR	TRACING	36		1.89	2.04	0.13
BE1VERT	FELDSPAR	TRACING	57		1.81		
BE3HORIZ	FELDSPAR	TRACING	79		1.77		
BE3HORIZ2	FELDSPAR	TRACING	50		2.74		
BE3VERT	FELDSPAR	TRACING	48		2.27		
BF2HORIZ	FELDSPAR	TRACING	57		1.62		
BF3HORIZ	FELDSPAR	TRACING	62		1.87		
BF3VERT	FELDSPAR	TRACING	57		1.43		
BF3VERT2	FELDSPAR	TRACING	66		1.70		
BG3HORIZ	FELDSPAR	TRACING	48		1.57		
BG3VERT	FELDSPAR	TRACING	51		1.72		
BG4HORIZ	FELDSPAR	TRACING	88		1.95		
BG4VERT	FELDSPAR	TRACING	64		2.33		
BG6HORIZ	FELDSPAR	TRACING	72		2.32		
BG6VERT	FELDSPAR	TRACING	49		1.81		
BG7HORIZ	FELDSPAR	TRACING	57		1.92		
BG7VERT	FELDSPAR	TRACING	60		2.00		
BH1HORIZ	FELDSPAR	TRACING	64		3.32		
BH1VERT	FELDSPAR	TRACING	44		2.17		
BI1HORIZ1	FELDSPAR	TRACING	73		2.04	1.94	0.41
BI1HORIZ10	FELDSPAR	TRACING	72		1.39		
BI1HORIZ2	FELDSPAR	TRACING	61	30 TO FOLIATION	2.48		
BI1HORIZ3	FELDSPAR	TRACING	74		2.42		
BI1HORIZ4	FELDSPAR	TRACING	72	20 TO FOLIATION	2.19		
BI1HORIZ5	FELDSPAR	TRACING	75		1.83		
BI1HORIZ6	FELDSPAR	TRACING	68		1.62		
BI1HORIZ7	FELDSPAR	TRACING	76		1.56		
BJ1HORIZ	FELDSPAR	TRACING	67		2.31	2.40	0.57
BJ1HORIZ2	FELDSPAR	TRACING	75		1.81		
BJ1HORIZ2	FELDSPAR	TRACING	59		3.50		
BJ1HORIZ3	FELDSPAR	TRACING	0		2.39		
BJ1HORIZ3	FELDSPAR	TRACING	87		2.27		
BJ1VERT4	FELDSPAR	TRACING	73		1.86	2.35	0.69
BJ2HORIZ	FELDSPAR	TRACING	71		2.66		
BJ2VERT	FELDSPAR	TRACING	78		2.83		
BK1HORIZ	FELDSPAR	TRACING	60		2.41	2.24	0.43
BK1VERT	FELDSPAR	TRACING	65		2.00		
BK3HORIZ	FELDSPAR	TRACING	77		1.66	2.13	0.12
BK3VERT	FELDSPAR	TRACING	61		2.14		
BK4HORIZ	FELDSPAR	TRACING	82		2.69		
BK5HORIZ	FELDSPAR	TRACING	69		2.33		
BK6HORIZ	FELDSPAR	TRACING	61		2.41		
BK6HORIZN	FELDSPAR	TRACING	67		2.67		
BK6VERT	FELDSPAR	TRACING	58		2.24		
BL2HORIZ	FELDSPAR	TRACING	57		2.02	2.26	0.29
BL4HORIZ	FELDSPAR	TRACING	62		2.64		
BL5HORIZ	FELDSPAR	TRACING	62		2.50		
BL5VERT	FELDSPAR	TRACING	62		2.24		
BL6HORIZ	FELDSPAR	TRACING	75		2.05	2.12	0.16

Locality	Phenocryst	Type	Number of	Orientation	Fry strain	Average	Error
BL6VERT	FELDSPAR	TRACING	60		1.94		
BL7HORIZ	FELDSPAR	TRACING	92		2.08		
BL7VERT	FELDSPAR	TRACING	44		2.18		
BM5HORIZ	FELDSPAR	TRACING	71		3.07		
BM5VERT	FELDSPAR	TRACING	72		1.97		
BM6HORIZ	FELDSPAR	TRACING	71		1.91		
BM6VERT	FELDSPAR	TRACING	57		1.55		
BM7VERT	FELDSPAR	TRACING	56		1.83		
BM7VERT	FELDSPAR	TRACING	83		1.44		
BN4HORIZ	FELDSPAR	TRACING	76		2.10		
BN4VERT	FELDSPAR	TRACING	59		3.89		
BN5HORIZ	FELDSPAR	TRACING	62		1.57		
BN5HORIZ2	FELDSPAR	TRACING	72		1.88		
BN7HORIZ	FELDSPAR	TRACING	72		2.29		
BN7VERT	FELDSPAR	TRACING	61		2.24		
BN8HORIZ	FELDSPAR	TRACING	73		1.80		
BN8VERT	FELDSPAR	TRACING	57		2.63		
BO1HORIZ	FELDSPAR	TRACING	73		1.59	1.92	0.48
BO1VERT	FELDSPAR	TRACING	72		2.10	2.10	0.24
BO2HORIZ	FELDSPAR	TRACING	60		2.39		
BO2VERT	FELDSPAR	TRACING	73		2.41		
BO3HORIZ	FELDSPAR	TRACING	65		2.30		
BO3VERT	FELDSPAR	TRACING	58		2.12		
BO4HORIZ	FELDSPAR	TRACING	70		2.49		
BO4VERT	FELDSPAR	TRACING	59		2.14		
BP1HORIZ	FELDSPAR	TRACING	75	30 TO FOLIATION	2.52	2.27	0.34
BP2*HORIZ	FELDSPAR	TRACING	78		2.40		
BP2HORIZ	FELDSPAR	TRACING	74		2.26		
BP2HORIZ**	FELDSPAR	TRACING	62		2.30		
BQ1HORIZ	FELDSPAR	TRACING	66		2.05		
BQ1VERT	FELDSPAR	TRACING	71		2.44		
BQ2HORIZ	FELDSPAR	TRACING	70		2.23		
BQ3HORIZ	FELDSPAR	TRACING	68		1.78		
BQ4HORIZ	FELDSPAR	TRACING	59		2.14		
BQ4HORIZ	FELDSPAR	TRACING	76		2.03		
BQ6HORIZ	FELDSPAR	TRACING	68		1.90		
BQ7HORIZ	FELDSPAR	TRACING	68		1.77		
BQ7HORIZ2	FELDSPAR	TRACING	78		1.78		
BQHORIZ	FELDSPAR	TRACING	61		2.23		
BQHORIZ2	FELDSPAR	TRACING	61		2.20		
BR1HORIZ	FELDSPAR	TRACING	58		2.00		
BR1VERT	FELDSPAR	TRACING	49		1.76		
BR2HORIZ	FELDSPAR	TRACING	57		1.54		
BR3HORIZ	FELDSPAR	TRACING	58		2.20		
BR4HORIZ	FELDSPAR	TRACING	61		1.13		
BR4MAF	BIOTITE	TRACING	66	HORIZONTAL MAFIC ENCLA	1.30		
BR4VERT	FELDSPAR	TRACING	67		1.18		
BR5HORIZ	FELDSPAR	TRACING	46		3.41		
BR5HORIZ	FELDSPAR	TRACING	61		1.75		
BR5VERT	FELDSPAR	TRACING	52		2.32		
BR6HORIZ	FELDSPAR	TRACING	47		2.38		
BR7HORIZ	FELDSPAR	TRACING	72		2.01		
BR7HORIZ2	FELDSPAR	TRACING	68		2.87		
BS1HORIZ	FELDSPAR	TRACING	73		2.52		
BS1VERT	FELDSPAR	TRACING	43	30 TO FOLIATION	2.00		

Locality	Phenocryst	Type	Number of	Orientation	Fry strain	Average	Error
BS2HORIZ	FELDSPAR	TRACING	61	60 TO FOLIATION.	2.58	2.12	0.58
BS3HORIZ	FELDSPAR	TRACING	65		1.20		
BS3VERT	FELDSPAR	TRACING	60		2.80	2.40	0.57
BS4HORIZ	FELDSPAR	TRACING	59		2.04		
BS5HORIZ	FELDSPAR	TRACING	74		1.72		
BS6HORIZ	FELDSPAR	TRACING	73		2.68		
BT1HORIZ	FELDSPAR	TRACING	66		2.30		
BT1VERT	FELDSPAR	TRACING	69		2.20		
BT2HORIZ	FELDSPAR	TRACING	71		2.20		
BT2VERT	FELDSPAR	TRACING	50		2.51		
BT3HORIZ	FELDSPAR	TRACING	57		1.47		
BT3VERT	FELDSPAR	TRACING	59		3.20		
BT4HORIZ	FELDSPAR	TRACING	54		1.73		
BU1HORIZ	FELDSPAR	TRACING	61		2.08		
BU1VERT	FELDSPAR	TRACING	62		2.73		
BU2HORIZ	FELDSPAR	TRACING	41		2.26		
BU2VERT	FELDSPAR	TRACING	49		2.18		
BV1HORIZ	FELDSPAR	TRACING	66		2.12	2.33	0.60
BV1VERT	FELDSPAR	TRACING	42		1.71	1.81	0.13
BV2HORIZ	FELDSPAR	TRACING	58	V.V. POOR	1.70		
BV3HORIZ	FELDSPAR	TRACING	52		2.38		
BV3VERT	FELDSPAR	TRACING					
BV8HORIZ	FELDSPAR	TRACING	74		3.13		
BV8VERT	FELDSPAR	TRACING	58	TOO POOR	1.90		
BW1HORIZ	FELDSPAR	TRACING	68		1.86	2.16	0.24
BW1VERT	FELDSPAR	TRACING	66		2.59	2.14	0.42
BW2HORIZ	FELDSPAR	TRACING	71		2.00		
BW2VERT	FELDSPAR	TRACING	59		1.77		
BW3HORIZ	FELDSPAR	TRACING	74		2.22		
BW5HORIZ	FELDSPAR	TRACING	75		2.07		
BW6HORIZ	FELDSPAR	TRACING	65		2.30		
BW7HORIZ	FELDSPAR	TRACING	50		2.53		
BW7VERT	FELDSPAR	TRACING	58		2.06		
BW8HORIZ	FELDSPAR	TRACING		50 TO FOLIATION			
BX2HORIZ	FELDSPAR	TRACING	51		2.53		
BX2VERT	FELDSPAR	TRACING	57		2.13		
BX2VERT	FELDSPAR	TRACING	62		2.84		
BX3HORIZ	FELDSPAR	TRACING	71		1.47		
BX3VERT	FELDSPAR	TRACING	54		1.96		
BX4HORIZ	FELDSPAR	TRACING	60		1.96		
BX4VERT	FELDSPAR	TRACING	65		1.91		
BX5HORIZ	FELDSPAR	TRACING	63		1.69		
BY1HORIZ	FELDSPAR	TRACING	53		2.41		
BY2HORIZ	FELDSPAR	TRACING	75	PARALELL TO FOLIATION D	1.92		
BY3HORIZ	FELDSPAR	TRACING	49		1.28		
BY4FOL	FELDSPAR	TRACING	51		2.22		
BY4HORIZ	FELDSPAR	TRACING	62		1.20		
BY5HORIZ	FELDSPAR	TRACING	42		1.83		
BY6HORIZ	FELDSPAR	TRACING	50		1.47		
BY6VERT	FELDSPAR	TRACING	36		1.74		
CA1HORIZ	FELDSPAR	TRACING	50		2.58		
CB1HORIZ	FELDSPAR	TRACING	70		2.50		

Appendix 8

Grid references for the Morro Azul and Imbiricu plutons

Locality	EASTINGS	NORTHINGS	Locality	EASTINGS	NORTHINGS	Locality	EASTINGS	NORTHINGS
IMBIRICU			MORRO AZUL					
CA1	9480	4561	CK1	8009	3393	CS4	8125	3825
CA10	9293	4733	CK2	7825	3500	CS5	8153	3891
CA11	9280	4758	CK3	7904	3406	CS7	8210	3675
CA12	9253	4758	CK4	7994	3384	CS8	8238	3661
CA15	9180	4860	CK5	8073	3359	CS9	8245	3680
CA16	9238	4789	CK6	8156	3308	CT1	8398	3531
CA2	9468	4600	CL1	8228	3405	CT10	8495	3778
CA3	9473	4633	CL10	8365	3578	CT11	8443	3655
CA4	9455	4590	CL11	8310	3583	CT2	8410	3573
CA5	9420	4638	CL2	8253	3425	CT3	8383	3589
CA6	9373	4665	CL3	8273	3443	CT4	8360	3628
CA7	9313	4680	CL4	8285	3460	CT5	8363	3668
CA8	9306	4669	CL5	8298	3453	CT6	8395	3650
CA9	9288	4693	CL6	8330	3481	CT8	8458	3713
CB1	9248	4778	CL7	8323	3500	CT9	8470	3743
CB2	9273	4683	CL8	8330	3518	CTII	8400	3550
CB3	9266	4716	CL9	8388	3548	CU2	8563	3973
CB4	9275	4733	CM1	8263	3530	CU3	8505	3970
CB5	9293	4741	CM2	8238	3590	CU4	8495	3950
CB6	9298	4759	CM3	8253	3618	CU5	8473	3855
CB7	9185	4823	CM4	8276	3674	CU7	8503	3863
CB8	9203	4788	CM5	8285	3700	CU7	8533	3960
CC2	9273	4765	CM6	8305	3790	CU8	8558	3843
CC5	9323	4893	CM7	8283	3616	CU9	8555	3870
CC8	9358	4770	CM7	8363	3833	CV1	8233	3395
CD1	9328	4780	CM8	8308	3841	CV1	8423	3676
CD3	9223	4783	CN	8100	3428	CV9	8330	3459
CD4	9140	4708	CO1	8103	3399			
CD4?	9193	4770	CO10	8350	3881			
CD5	9165	4720	CO11	8304	3930			
CD6	9148	4763	CO3	8095	3385			
CE1	8948	4858	CO4	8193	3565			
CE10	9073	4823	CO5	8208	3523			
CE3	8958	4781	CO6/1	8210	3549			
CE4	8975	4798	CO6/2	8216	3543			
CE5	9043	4781	CO7	8191	3624			
CE6	9043	4763	CO8	8160	3638			
CE7	8973	4805	CO9	8345	3915			
CE7	9080	4760	CP1	8415	3529			
CE8	9063	4798	CP2	8448	3566			
CE9	9108	4795	CP3	8470	3569			
CF1	9050	4868	CP4	8523	3610			
CF2	9068	4850	CP5	8478	3613			
CF3	9078	4860	CP6	8463	3630			
CF4	9190	4619	CP6	8413	3948			
CF5	8833	4665	CP7	8553	4140			
CF6	8908	4633	CP8	8543	4085			
CF7	8935	4685	CP9	8473	4059			
CF8	9173	4573	CQ1	7548	2904			
CF9	9173	4689	CQ2	7573	2985			
CG1	8965	4618	CQ3	7795	2943			
CG10	9068	4388	CQ4	7795	2996			
CG12	9075	4513	CQ5	7768	3040			
CG2	8923	4598	CQ6	7996	3224			
CG3	8848	4555	CQ7	8098	3224			
CG4	8793	4598	CQ8	7790	3170			
CG5	8845	4483	CQ9	7770	3185			
CG6	8848	4520	CR1	7723	3015			
CG7	8888	4555	CR10	8195	3525			
CG8	8898	4583	CR11	8070	3573			
CG9	8873	4423	CR12	8048	3585			
CH1	9038	4433	CR2	7648	3168			
CH2	9393	4535	CR3	7415	3165			
CH3	9370	4535	CR4	7438	3025			
CH4	9305	4560	CR5	7423	2980			
CH5	9235	4553	CR6	7500	2900			
CH6	9128	4585	CR7	7660	3148			
CI1	9453	4695	CR7	8003	3378			
CI2	9623	4710	CR8	8068	3353			
CI3	9628	4783	CR9	8100	3488			
CI4	9655	4775	CS0	8205	3703			
CI5	9448	4750	CS1	8048	3735			
CJ1	9443	4438	CS10	8195	3703			
CJ2	9418	4468	CS2	8100	3810			
CJ3	9395	4483	CS3	8088	3875			

Mafic enclave axial ratio data from the Morro Azul and Imbiricu plutons

[illegible]

LOCALITY CQ1, CQ2, CQ8, CR1				LOCALITY CQ1, CQ2, CQ8, CR1				LOCALITY CP9			
ORIENTATION		HORIZ		ORIENTATION		VERT		ORIENTATION		HORIZ	
NUMBER	X	Y	X/Y	NUMBER	X	Y	X/Y	NUMBER	X	Y	X/Y
1	6.4	5.6	1.14285714	1	20.9	7.5	2.78666667	1	13.6	13	1.04615385
2	2	1.4	1.42857143	2	7.8	2.5	3.12	2	11.7	11	1.06363636
3	5.3	1.8	2.94444444	3	11.8	3.4	3.47058824	3	3	2.7	1.11111111
4	16.4	4.6	3.56521739	4	10.7	2.8	3.82142857	4	6	5.2	1.15384615
5	55.2	13	4.24615385	5	25.5	6	4.25	5	7	6	1.16666667
6	29	6.2	4.67741935	6	11.5	2.3	5	6	8.8	7.5	1.17333333
7	13.2	2.6	5.07692308	Length av.	12.489	3.359	3.7176088	7	5	4	1.25
8	9	1.6	5.625	AREAS OF XENOLITHS			32.951	8	9.8	7.7	1.27272727
9	21.4	3.7	5.78378378	NUMBER			6	9	10	7.8	1.28205128
10	21.2	3.4	6.23529412	MEAN ARITHMETIC			3.741	10	12.2	9.5	1.28421053
11	12.6	1.9	6.63157895	HARMONIC MEAN			3.605	11	5.2	4	1.3
Length av.	8.342	2.747	3.03672596	GEOMETRIC MEAN			3.672	12	7.5	5.5	1.36363636
AREAS OF XENOLITHS			17.998	STANDARD DEVIATION			0.803	13	10	7	1.42857143
NUMBER			11	SMALLEST			2.79	14	9.7	6.7	1.44776119
MEAN ARITHMETIC			4.305	LARGEST			5.000	15	4.9	3.3	1.48484848
HARMONIC MEAN			3.140	w log			0.253	16	4.4	2.9	1.51724138
GEOMETRIC MEAN			6.056	K-VALUE			0.385	17	7.3	4.7	1.55319149
STANDARD DEVIATION			1.857					18	17	9.7	1.75257732
SMALLEST			1.14					19	6	3.3	1.81818182
LARGEST			6.630					20	7.3	4	1.825
w log			0.765					21	7.5	4	1.875
								22	8	4	2
								23	7.6	3.6	2.11111111
								24	5.5	2.5	2.2
								25	10	4.5	2.22222222
								26	13.5	5.7	2.36842105
								27	7.7	3.1	2.48387097
								28	6.8	2.5	2.72
								29	11.4	4	2.85
								Length av.	7.306	4.508	1.62049027
								AREAS OF XENOLITHS			25.868
								NUMBER			29
								MEAN ARITHMETIC			1.659
								HARMONIC MEAN			1.526
								GEOMETRIC MEAN			1.588
								STANDARD DEVIATION			0.518
								SMALLEST			1.0462
								LARGEST			2.850
								w log			0.4352

LOCALITY CO5, CO6				LOCALITY CN/ZONE3				LOCALITY CN/ZONE3			
ORIENTATION		HORIZ		ORIENTATION		HORIZ		ORIENTATION		VERT	
NUMBER	X	Y	X/Y	NUMBER	X	Y	X/Y	NUMBER	X	Y	X/Y
1	44	23.6	1.86440678	1	15	13.5	1.11111111	1	19.8	9.4	2.10638298
2	34	15	2.26666667	2	22.5	18	1.25	2	23.7	10.9	2.17431193
3	10.2	4.4	2.31818182	3	17.5	13.4	1.30597015	3	43	18	2.38888889
4	11	4.7	2.34042553	4	15.7	12	1.30833333	4	50	20.5	2.43902439
5	11	4.5	2.44444444	5	7.4	5.4	1.37037037	5	38	15.1	2.51655629
6	16	6.4	2.5	6	16.9	12.3	1.37398374	6	51	15.9	3.20754717
7	11	4	2.75	7	11.7	7.7	1.51948052	7	37	10.6	3.49056604
8	23	8	2.875	8	24.7	16	1.54375	8	20.1	5.6	3.58928571
9	34.8	12	2.9	9	24.1	14.4	1.67361111	9	49	13.6	3.60294118
10	23	7.5	3.06666667	10	9.3	5.4	1.72222222	10	39.6	10.6	3.73584906
11	21	6.5	3.23076923	11	11.5	6.5	1.76923077	11	6.8	1.8	3.77777778
12	32	9.7	3.29896907	12	12.9	7	1.84285714	12	26	6.7	3.88059701
13	8	2.4	3.33333333	13	10	5.4	1.85185185	13	20	4.7	4.25531915
14	13.5	3.8	3.55263158	14	13	7	1.85714286	14	35	7.2	4.86111111
15	32	9	3.55555556	15	15.6	8	1.95	15	12.5	2.4	5.20833333
16	31	8.6	3.60465116	16	10	5	2	16	47	9	5.22222222
17	19.6	5.1	3.84313725	17	25.4	12	2.11666667	17	20	3.8	5.26315789
18	10	2.6	3.84615385	18	24.9	11.5	2.16521739	18	64	10.8	5.92592593
19	28	7.2	3.88888889	19	23	9.7	2.37113402	19	42	6.7	6.26865672
20	14.1	3.6	3.91666667	20	20	8	2.5	20	43	5.6	7.67857143
21	8.5	2.1	4.04761905	21	27.8	10	2.78	21	17.6	1.4	12.5714286
22	22	5.4	4.07407407	22	23.5	8.3	2.8313253	Length av.	25.024	5.448	4.59305197
23	31	7.5	4.13333333	23	36	10	3.6	AREAS OF XENOLITHS			107.078
24	20	4.8	4.16666667	24	42	11.4	3.68421053	NUMBER			21
25	25	5.7	4.38596491	25	10	1.9	5.26315789	MEAN ARITHMETIC			4.484
26	15	3.4	4.41176471	26	14	2.4	5.83333333	HARMONIC MEAN			3.712
27	35	7.8	4.48717949	27	13.6	2.1	6.47619048	GEOMETRIC MEAN			4.048
28	13	2.7	4.81481481	28	13	1.9	6.84210526	STANDARD DEVIATION			2.364
29	19	3.9	4.87179487	29	34	4.8	7.08333333	SMALLEST			2.106
30	18.6	3.7	5.02702703	30	8.1	1.1	7.36363636	LARGEST			12.571
31	14.6	2.6	5.61538462	31	34	3.9	8.71794872	w log			0.776
32	14.7	2.6	5.65384615	32	36	2.1	17.1428571	K-VALUE			0.429
33	26	4.5	5.77777778	Length av.	15.673	4.883	3.20939437				
34	51	7.7	6.62337662	AREAS OF XENOLITHS			60.110				
35	25	3.7	6.75675676	NUMBER			32				
36	35	5.1	6.8627451	MEAN ARITHMETIC			3.507				
37	41	5.1	8.03921569	HARMONIC MEAN			2.207				
38	46	5.6	8.21428571	GEOMETRIC MEAN			2.661				
Length av.	18.327	4.668	3.92633386	STANDARD DEVIATION			3.293				
AREAS OF XENOLITHS			67.189	SMALLEST			1.1111				
NUMBER			38	LARGEST			17.143				
MEAN ARITHMETIC			4.194	w log			1.1883				
HARMONIC MEAN			3.691								
GEOMETRIC MEAN			3.930								
STANDARD DEVIATION			1.575								
SMALLEST			1.8644								
LARGEST			8.214								
w log			0.644								

LOCALITY CK1, CK4				LOCALITY CK1, CK4				LOCALITY CR10, CR11			
ORIENTATION		HORIZ		ORIENTATION		VERT		ORIENTATION		HORIZ	
NUMBER	X	Y	X/Y	NUMBER	X	Y	X/Y	NUMBER	X	Y	X/Y
1	4.7	4.4	1.06818182	1	4.9	4.3	1.13953488	1	70.4	54.4	1.29411765
2	4	1.9	2.10526316	2	3.2	2.8	1.14285714	2	23.3	13.5	1.72592593
3	19	8.1	2.34567901	3	21	9	2.33333333	3	23.5	12.5	1.88
4	4	1.5	2.66666667	4	7.6	2.6	2.92307692	4	15.7	6.5	2.41538462
5	18	6	3	5	12	4	3	5	15.9	6.5	2.44615385
6	19	5.9	3.22033898	6	8.8	2.7	3.25925926	6	13.8	5.6	2.46428571
7	22	6.5	3.38461538	7	6.2	1.8	3.44444444	7	28	11	2.54545455
8	15	4.4	3.40909091	8	11	3	3.66666667	8	20.5	7.9	2.59493671
9	3.2	0.9	3.55555556	9	6	1.6	3.75	9	12	4.5	2.66666667
10	11	3	3.66666667	10	17	4.3	3.95348837	10	14.5	5	2.9
11	7	1.9	3.68421053	11	24	6	4	11	41.3	13.9	2.97122302
12	33	8.7	3.79310345	12	16	3.9	4.1025641	12	20	6.2	3.22580645
13	7.6	2	3.8	13	38	9	4.22222222	13	54.6	16	3.4125
14	12	3.1	3.87096774	14	21	4.9	4.28571429	14	31.6	8.7	3.63218391
15	14	3.5	4	15	10.5	2.2	4.77272727	15	80.3	21.6	3.71759259
16	13.6	3.4	4	16	8	1.6	5	16	33	8.8	3.75
17	21	5	4.2	17	12	2.4	5	17	42.3	11.2	3.77678571
18	7.7	1.7	4.52941176	18	12	2.4	5	18	30.9	8	3.8625
19	17	3.5	4.85714286	19	16	3.2	5	19	22.2	5.7	3.89473684
20	10.2	2.1	4.85714286	20	20	3.9	5.12820513	20	30	7.5	4
21	5	0.9	5.55555556	21	15	2.9	5.17241379	21	16	3.6	4.44444444
22	33	5.8	5.68965517	22	36	6.4	5.625	22	17	3.6	4.72222222
23	27	4.7	5.74468085	23	6.2	1	6.2	23	20.7	4	5.175
24	14	2.4	5.83333333	24	18	2.8	6.42857143	24	24	4	6
25	35	5.9	5.93220339	25	16	2.4	6.66666667	25	49.5	8	6.1875
26	41.5	6.9	6.01449275	26	21	3.1	6.77419355	Length av.	23.401	6.998	3.34413723
27	16	2.4	6.66666667	27	15.5	2.1	7.38095238	AREAS OF XENOLITHS			128.609
28	6.1	0.9	6.77777778	28	36	2.8	12.8571429	NUMBER			25
29	48	6.5	7.38461538	Length av.	10.930	2.771	3.94398559	MEAN ARITHMETIC			3.428
30	20	2.7	7.40740741	AREAS OF XENOLITHS			23.792	HARMONIC MEAN			2.994
31	23.7	2.9	8.17241379	NUMBER			28	GEOMETRIC MEAN			3.214
32	13.5	0.9	15	MEAN ARITHMETIC			4.722	STANDARD DEVIATION			1.232
Length av.	10.452	2.455	4.25761326	HARMONIC MEAN			3.678	SMALLEST		1.29	
AREAS OF XENOLITHS			20.154	GEOMETRIC MEAN			4.240	LARGEST		6.190	
NUMBER			32	STANDARD DEVIATION			2.221	w log		0.6811	
MEAN ARITHMETIC			4.881	SMALLEST			1.14				
HARMONIC MEAN			3.893	LARGEST			12.857				
GEOMETRIC MEAN			4.384	w log			1.052				
STANDARD DEVIATION			2.490	K-VALUE			0.023				
SMALLEST			1.07								
LARGEST			15.000								
w log			1.1467								

IMBIRICU PLUTON

LOCALITY CM2, CM7, CM7, CT8				LOCALITY CH1				LOCALITY CB6, CC7, CE7, CE8, CE10, CG1			
ORIENTATION HORIZ				ORIENTATION HORIZ				ORIENTATION HORIZ			
NUMBER	X	Y	X/Y	NUMBER	X	Y	X/Y	NUMBER	X	Y	X/Y
1	25	13	1.92307692	1	6.7	6.4	1.046875	1	42	36	1.16666667
2	5.8	2.6	2.23076923	2	21.6	20.6	1.04854369	2	13.8	7.9	1.74683544
3	19	8.5	2.23529412	3	5.6	5	1.12	3	12.8	6.3	2.03174603
4	12	4.9	2.44897959	4	9.3	8.1	1.14814815	4	15.7	7	2.24285714
5	37	14.5	2.55172414	5	16	13.8	1.15942029	5	29.5	13.1	2.2519084
6	12.5	4.3	2.90697674	6	4	3.1	1.29032258	6	25	10.4	2.40384615
7	10	3	3.33333333	7	23.5	17.5	1.34285714	7	7.1	2.8	2.53571429
8	21.8	5.8	3.75862069	8	25	18	1.38888889	8	14	4.9	2.85714286
9	28	6.4	4.375	9	22	14	1.57142857	9	19	6.4	2.96875
10	30.5	6.7	4.55223881	10	12	7.5	1.6	10	36.8	10.8	3.40740741
Length av.	14.930	5.274	2.83084896	11	79	49	1.6122449	11	27	7.9	3.41772152
AREAS OF XENOLITHS			61.846	12	137.1	84.4	1.62440758	12	35	10.1	3.46534653
NUMBER			10	13	34	19	1.78947368	13	24	6.8	3.52941176
MEAN ARITHMETIC			3.032	14	8	4	2	14	75	21	3.57142857
HARMONIC MEAN			2.798	15	31.5	15	2.1	15	5.4	1.3	4.15384615
GEOMETRIC MEAN			2.909	16	15.3	7	2.18571429	16	33.5	7.2	4.65277778
STANDARD DEVIATION			0.933	17	34	14.3	2.37762238	17	15.6	2.2	7.09090909
SMALLEST			1.92	18	15.5	6.5	2.38461538	Length av.	16.935	5.277	3.20918998
LARGEST			4.550	19	20	8	2.5	AREAS OF XENOLITHS			70.191
w log			0.375	20	9	3.6	2.5	NUMBER			17
				21	6.9	2.7	2.55555556	MEAN ARITHMETIC			3.147
				22	27	10.5	2.57142857	HARMONIC MEAN			2.680
				23	20	7.3	2.73972603	GEOMETRIC MEAN			2.906
				24	22	8	2.75	STANDARD DEVIATION			1.351
				25	15	5.4	2.77777778	SMALLEST			1.17
				26	22	7.5	2.93333333	LARGEST			7.090
				27	27.5	9	3.05555556	w log			0.782
				28	19	6	3.16666667				
				29	83	23.8	3.48739496				
				30	38.5	11	3.5				
				31	21	5.8	3.62068966				
				32	74.5	20	3.725				
				33	26.5	7	3.78571429				
				34	36	8.5	4.23529412				
				35	250	59	4.23728814				
				36	53.2	12	4.43333333				
				37	18	3.5	5.14285714				
				38	24	4	6				
				39	40	6.5	6.15384615				
				40	160	21	7.61904762				
				Length av.	17.194	7.709	2.23046849				
				AREAS OF XENOLITHS			104.100				
				NUMBER			40				
				MEAN ARITHMETIC			2.807				
				HARMONIC MEAN			2.163				
				GEOMETRIC MEAN			2.458				
				STANDARD DEVIATION			1.522				
				SMALLEST			1.0469				
				LARGEST			7.620				
				w log			0.8621				

Appendix 10

Fry fabric strains from the Morro Azul and Imbiricu plutons
SLAB= tracing from hand specimen polished slab
PHOTO= tracing from outcrop photograph

MORRO AZUL								
LOCALITY	Phenocryst	Type	Number	Orientation	Fry Strain	Average	Error	Comment
CK1H	FELDSPAR	PHOTO	97		1.55	1.7425	0.17	OK
CM1H	FELDSPAR	PHOTO	60	Only recorded when non-parallel to foliation	1.86	1.74	0.17	OK
CM3F	FELDSPAR	PHOTO	66		1.81			OK
CM5H	FELDSPAR	SLAB	64		1.6	1.666	0.2	GOOD
CM5V	FELDSPAR	SLAB	47		1.43			GOOD
CM6H	FELDSPAR	PHOTO	68		2			GOOD
CNH	FELDSPAR	PHOTO	47		1.89			GOOD
CNH	FELDSPAR	SLAB	58		1.89			V.GOOD
CNV	FELDSPAR	SLAB	33		3.01			POOR
CO2H	FELDSPAR	PHOTO	78		1.64			OK
CO6V	FELDSPAR	SLAB	40		2.28			OK
CO7H	FELDSPAR	PHOTO	62		1.62			GOOD
CO8H	FELDSPAR	PHOTO	74		1.63			GOOD
CO9H	FELDSPAR	PHOTO	58		2.07			GOOD
CP6H	FELDSPAR	SLAB	59		1.5	1.5975	0.32	V.GOOD
CP6V	FELDSPAR	SLAB	49		2.21	2.14	0.1	GOOD
CP9H	FELDSPAR	PHOTO	127		1.08	1.615	0.76	GOOD
CP9H	FELDSPAR	SLAB	63		2.15			OK
CP9V	FELDSPAR	SLAB	40		1.68	1.68		OK
CQ1V	FELDSPAR	PHOTO	71		1.48			POOR
CQ5H	FELDSPAR	SLAB	61		2.08			GOOD
CS8H	FELDSPAR	PHOTO	81		1.48			POOR
CU1H	FELDSPAR	PHOTO	70		1.42			POOR
CU6H	FELDSPAR	SLAB	55		1.4			OK
CU6V	FELDSPAR	PHOTO	74		2.07			GOOD

IMBIRICU								
LOCALITY	Phenocryst	Type	Number	Orientation	Fry Strain	Average	Error	Comment
CA11H	FELDSPAR	SLAB	50		1.21	1.68857	0.38	POOR
CA2H	FELDSPAR	PHOTO	54	Only recorded when non-parallel to foliation	2.13	1.87	0.23	GOOD
CB1V	FELDSPAR	SLAB	35		1.61	1.835	0.32	OK
CB2H	FELDSPAR	PHOTO	96		1.69			OK
CB3H	FELDSPAR	SLAB	89		1.74			V.GOOD
CB4H	FELDSPAR	PHOTO	88		1.9			GOOD
CC7H	FELDSPAR	SLAB	53		2.07			GOOD
CC8H	FELDSPAR	PHOTO	85		2.18			OK
CC8H2	FELDSPAR	PHOTO	58		1.37			POOR
CD1H	FELDSPAR	PHOTO	52		1.36			OK
CD1V	FELDSPAR	PHOTO	62		2.06			GOOD
CE2H	FELDSPAR	PHOTO	106		1.8	1.785	0.25	GOOD
CE3H	FELDSPAR	PHOTO	65		1.94			GOOD
CF2H	FELDSPAR	PHOTO	74		1.97			GOOD
CF3H	FELDSPAR	PHOTO	80		1.43			OK
CF4H	FELDSPAR	PHOTO	89		1.35			GOOD
CG10H	FELDSPAR	PHOTO	55					V.POOR
CH3H	FELDSPAR	SLAB	58		1.79			OK

Appendix 11

Vertical plane

Using the t-alpha technique to determine the flattening strain on a folded layer
After Ramsay (1967)

Horizontal plane

To	Talpha	Angle (alpha-90)	To/Talpha	Lambda1		
thickness at axial point	thickness on limb			/Lambda2	R	
29	4.5	84	0.155172	1.466077	0.013298	8.671892
29	5.5	87	0.189655	1.518436	0.033321	5.478214
29	5	86.2	0.172414	1.504474	0.025446	6.268878
29	3.2	88	0.110345	1.53589	0.010971	9.547059
34	3.2	85.8	0.094118	1.497492	0.003513	16.87144
34	2.5	85.8	0.073529	1.497492	4.3E-05	152.5494
34	5	85	0.147059	1.48353	0.014138	8.410323
22	1.7	88	0.077273	1.53589	0.004759	14.49596
22	2.8	84.5	0.127273	1.474803	0.007077	11.88713
19	2.8	85.3	0.147368	1.488766	0.015105	8.136552
19	1.8	86	0.094737	1.500983	0.004129	15.56207
124	9.8	87	0.079032	1.518436	0.003517	16.86296
124	6.3	85	0.050806	1.48353	-0.00505	
56	5.2	84	0.092857	1.466077	-0.00233	
65	30	60	0.461538	1.047198	-0.04931	
26	3	85	0.115385	1.48353	0.005761	13.17473
26	3.5	84.5	0.134615	1.474803	0.009018	10.53056
45	8.5	78	0.188889	1.361357	-0.00789	
43	25	56	0.581395	0.977384	0.036845	5.20966
27	3	85	0.111111	1.48353	0.004786	14.45499
11	4.5	70	0.409091	1.22173	0.057051	4.186654
8	1.8	80	0.225	1.396263	0.021108	6.883014
46	5	82	0.108696	1.43117	-0.0077	
46	1.2	84	0.026087	1.466077	-0.01036	
16	2	87	0.125	1.518436	0.012921	8.797236
35	3	89	0.085714	1.553343	0.007044	11.91448
			81.92991543	0.12875	mean value	11.03321
			8.124005265	0.129421	stdev	32.028

Vertical plane

To	Talpha	Angle (alpha-90)	To/Talpha	Lambda1		
thickness at axial point	thickness on limb			/Lambda2	R	
3	2.5	15	0.833333	0.261799	-3.5614	
3	2.7	55	0.9	0.959931	0.716845	1.181102
3	1.2	72	0.4	1.256637	0.071319	3.744535
7	2	80	0.285714	1.396263	0.05308	4.340468
4.5	2.8	73	0.622222	1.27409	0.329878	1.741099
2.9	1.3	78	0.448276	1.361357	0.16485	2.46295
4	2	78	0.5	1.361357	0.216115	2.151086
8	1.7	84	0.2125	1.466077	0.034608	5.375397
8	2.1	81	0.2625	1.413717	0.045549	4.685541
15	4	75	0.266667	1.308997	0.00442	15.04161
11.5	8	50	0.695652	0.872665	0.120575	2.879866
10.5	4	78	0.380952	1.361357	0.106501	3.06424
16	5.2	77	0.325	1.343904	0.057955	4.153896
27	3	79	0.111111	1.37881	-0.02497	
20	3.7	80	0.185	1.396263	0.004198	15.43421
33	3	78.5	0.090909	1.370083	-0.03279	
21.5	3	74	0.139535	1.291544	-0.06115	
21.5	2.3	84	0.106977	1.466077	0.000524	43.7042
9.5	2	74	0.210526	1.291544	-0.03426	
9.5	2.1	75	0.221053	1.308997	-0.01942	
8.5	3.5	67	0.411765	1.169371	0.019921	7.085135
8.5	1.8	82	0.211765	1.43117	0.025978	6.204324
8.2	6	50	0.731707	0.872665	0.208273	2.191207
13	6	50	0.461538	0.872665	-0.34109	
13	7.2	65	0.553846	1.134464	0.156002	2.531829
13	4	77	0.307692	1.343904	0.046421	4.641353
18	2.5	83	0.138889	1.448623	0.004505	14.89902
18	2	76	0.111111	1.32645	-0.04905	
5	1.2	82	0.24	1.43117	0.038986	5.064608
8	1.5	79.5	0.1875	1.387537	0.002013	22.28656
6	1.5	78	0.25	1.361357	0.020143	7.04584
6	1.8	80	0.3	1.396263	0.061707	4.02562
20.5	4	78	0.195122	1.361357	-0.00539	
7	1.2	78	0.171429	1.361357	-0.01446	
2	0.8	84	0.4	1.466077	0.150721	2.575809
2	1	80	0.5	1.396263	0.226682	2.100351
2	1.6	40	0.8	0.698132	0.1287	2.787469
1	0.7	63	0.7	1.099557	0.357596	1.67226
			69.53027143	0.302898	mean value	4.523697
			14.44024328	0.22474	stdev	8.824393

Appendix 12

Grid references for the Itapeti pluton

Locality	EASTINGS	NORTHINGS
CX1	3757	74039
CX2	3756	74032
CX3	3753	74022
CX4	3758	74005
CX5	3756	74015
CX6	3764	74017
CX7	3760	74029
CY1	3980	74080
CY2	3896	74062
CY3	3893	74063
CY4	3891	74064
CZ1	3872	74056
CZ2	3872	74062
CZ3	3859	74059
CZ4	3858	74056
DA1	3825	74046
DA2	3814	74038
DA3	3800	74020
DA4	3793	74017
DC1	3786	74008
DC2	3781	74004
DC3	3780	74006
DC4	3748	73988
DC5	3703	74006
DC6	3734	74029
DC7	3709	74007

Appendix 13

Mafic enclave data from the Itapeti pluton, SE Brazil
Data consists of enclave long and short axes, this is averaged using standard mean, geomoetric mean and harmonic mean.

LOCALITY ORIENTATION				LOCALITY ORIENTATION			
CY3, CZ4		CZ4		Foliation			
HORIZ		X/Y		X/Y			
NUMBER	X	Y	X/Y	NUMBER	X	Y	X/Y
1	19.00	9.00	2.11	1	26.00	10.00	2.60
2	24.50	11.40	2.15	2	13.20	4.80	2.75
3	9.50	3.80	2.50	3	14.00	4.40	3.18
4	16.00	6.30	2.54	Length av.	16.16	5.60	2.89
5	49.00	19.00	2.58	AREAS OF XENOLITHS			71.09
6	13.00	4.70	2.77	NUMBER			3.00
7	11.00	3.30	3.33	MEAN ARITHMETIC			2.84
8	20.50	5.90	3.47	HARMONIC MEAN			2.82
9	16.00	4.60	3.48	GEOMETRIC MEAN			2.83
10	13.00	3.00	4.33	STANDARD DEVIATION			0.30
11	36.00	7.50	4.80	SMALLEST		2.60	
12	16.40	3.40	4.82	LARGEST		3.18	
13	14.00	2.90	4.83	w log		0.09	
14	58.00	11.00	5.27				
15	32.00	5.90	5.42				
16	12.00	2.20	5.45				
17	9.90	1.60	6.19				
18	47.00	6.80	6.91				
19	25.00	2.90	8.62				
20	140.00	15.80	8.86				
21	113.00	10.90	10.37				
Length av.	16.16	0.55	29.58				
AREAS OF XENOLITHS			6.93				
NUMBER			21.00				
MEAN ARITHMETIC			9.43				
HARMONIC MEAN			1.63				
GEOMETRIC MEAN			3.15				
STANDARD DEVIATION			21.68				
SMALLEST		2.11					
LARGEST		10.37					
w log		0.69					

LOCALITY ORIENTATION CX7, DC2, DC3 (cont.)				LOCALITY ORIENTATION CX7, DC2, DC3 (cont.)			
NUMBER	X	Y	HORIZ X/Y	NUMBER	X	Y	HORIZ X/Y
1	43.70	35.00	1.25	56	86.00	13.50	6.37
2	39.00	25.00	1.56	57	150.00	23.30	6.44
3	8.80	5.60	1.57	58	17.00	2.60	6.54
4	22.00	13.80	1.59	59	22.50	3.40	6.62
5	45.00	28.00	1.61	60	81.00	11.10	7.30
6	144.00	70.00	2.06	61	52.00	6.90	7.54
7	31.00	14.80	2.09	62	75.00	9.80	7.65
8	18.20	8.40	2.17	63	19.50	2.50	7.80
9	41.10	18.60	2.21	64	33.20	3.50	9.49
10	59.00	26.00	2.27	65	34.00	3.40	10.00
11	17.00	7.40	2.30	Length av.	20.86	6.41	3.25
12	55.00	23.80	2.31	AREAS OF XENOLITHS			105.09
13	8.60	3.60	2.39	NUMBER			65.00
14	15.10	6.30	2.40	MEAN ARITHMETIC			4.50
15	28.00	11.50	2.43	HARMONIC MEAN			3.96
16	23.00	9.00	2.56	GEOMETRIC MEAN			4.20
17	11.80	4.60	2.57	STANDARD DEVIATION			1.82
18	49.00	19.00	2.58	SMALLEST		1.25	
19	27.00	9.80	2.76	LARGEST		10.00	
20	10.20	3.60	2.83	w log		0.90	
21	29.00	9.80	2.96				
22	9.60	3.20	3.00				
23	33.00	11.00	3.00				
24	21.40	7.10	3.01				
25	35.70	11.60	3.08				
26	61.00	19.80	3.08				
27	82.50	25.40	3.25				
28	39.00	12.00	3.25				
29	24.00	7.20	3.33				
30	21.10	6.10	3.46				
31	16.00	4.50	3.56				
32	18.50	5.20	3.56				
33	14.80	4.10	3.61				
34	46.00	12.70	3.62				
35	28.40	7.80	3.64				
36	13.00	3.40	3.82				
37	12.50	3.20	3.91				
38	15.00	3.80	3.95				
39	38.00	9.60	3.96				
40	19.00	4.80	3.96				
41	38.70	9.70	3.99				
42	25.00	6.20	4.03				
43	48.00	11.80	4.07				
44	23.60	5.80	4.07				
45	11.00	2.70	4.07				
46	47.60	11.40	4.18				
47	86.50	19.50	4.44				
48	131.00	29.40	4.46				
49	44.00	9.20	4.78				
50	54.00	11.10	4.86				
51	20.00	3.80	5.26				
52	68.00	12.50	5.44				
53	35.00	6.40	5.47				
54	24.00	4.00	6.00				
55	48.00	7.70	6.23				

LOCALITY		DC7	
ORIENTATION		HORIZ	
NUMBER	X	Y	X/Y
1	12.80	7.80	1.64
2	10.50	6.10	1.72
3	30.00	14.50	2.07
4	21.00	9.40	2.23
5	8.40	3.70	2.27
6	12.60	5.50	2.29
7	9.70	3.90	2.49
8	20.00	5.60	3.57
9	23.70	6.50	3.65
Length av.	13.89	5.97	
AREAS OF XENOLITHS			65.08
NUMBER			9.00
MEAN ARITHMETIC			2.44
HARMONIC MEAN			2.28
GEOMETRIC MEAN			2.35
STANDARD DEVIATION			0.72
SMALLEST		1.64	
LARGEST		3.65	
w log		0.35	

Appendix 14

Fortran program modelling a Power Law rheology around an hot expanding body.

```
c2345678909123456789
  Program model
c initialise variables
  character*20 namew
  Integer p,i,t,val,n,q,time,incr
  real x,y,a,supply,pi,volume
  real nrate(900,200),dist(900,200),rate(900,200)
  real margint(200),pa(200)
  Real r(200),sigma(200) ,ratetot(200) ,temp(200) ,margin(200)
  supply=30000000
  pi=3.14159
  volume=0
  do 10,i=1,1000
    r(i)=0
    margin(i)=0
    sigma(i)=0
    ratetot(i)=0
10  continue
  time=100
  incr=160
* Calculate temperature at a function of distance
  temp(1)=650
  margin(1)=0
  do 15,i=2,incr
    margin(i)=margin(i-1)+(8000/incr)
15  continue
  do 20,i=2,incr
    temp(i)=848.2-(64.67*log(margin(i)))
20  continue
* Calc radius as a function of time
  r(1)=0
  do 30,i=1,time
    volume=supply + ((4*pi/3)*(r(i)**3))
    r(i+1)=(volume/(4*pi/3))**0.33333333
* Deviatoric stress per unit area as a function of time at pluton margin
    sigma(i+1)=(supply*200)/(4*pi*(r(i+1)**2))
    margin(1)=0.01
*deviatoric stress as a function of distance from the pluton
    do 40,t=1,incr
      dist(i,t)=(supply*200)/(4*pi*((r(i)+margin(t))**2))
40  continue
30  continue
* Calculating strain rate per unit distance per unit time, approx to wet qtz.
  a=0.00012
  do 50,n=1,time
    do 60,q=1,incr
      rate(n,q)=(a*exp(-259000/(8.31*(temp(q)+273))))*(dist(n,q)**8.2)
60  continue
50  continue
* Attempting to quantify the strain at a particular point better
* work out the shortening related to a single increment of strain rate.
  do 90,i=1,time
    margint(1)=0
    do 100,t=2,incr
      val=(8000/incr)/(1+rate(i,t))
```



```

* readjusting division boundaries, for a given shortening
  margint(t)=margint(t-1)+val
* working out average strain rates for individual cells
  x=0
  if (margint(t) .gt. (t*(8000/incr))) then
    stop
  endif
  a=0
  y=0
  do 150,p=1,incr
    if (t+p .gt. incr) goto 150
    n=margint(t)-margint(t+p)
    if ((n.lt.50).and.(n.gt.0))then
      a=a+1
      pa(a)=p
    endif
150  continue
    if (a .eq. 1)then
      x= (margint(t+pa(1))-margint(t))*rate(i,t+pa(1))
    endif
    if (a .gt. 1) then
      do 160, p=2,a
        n=t+pa(p)
        y=y+(margint(n)-margint(n-1))*rate(i,n)
160  continue
      endif
      n=t+pa(a)
      z=(margint(t+1)-margint(n))*rate(i,n+1)
      nrate(i,t)=(x+y+z)/(8000/incr)
* adding up the strain rates over time
      ratetot(t)=ratetot(t)+nrate(i,t)
100  continue
90  continue
* specifying a file to save to.
  PRINT *, 'SPECIFY A FILE TO SAVE TO:'
  READ *,namew
  OPEN (UNIT=4,FILE=namew)
  DO 300, t=1,incr
    write (4,'(f10.0,2x,e10.3)')(margint(t),ratetot(t))
300  continue
  CLOSE (UNIT=4)
  END

```

Appendix 15

Looking at critical dyke widths for the studied plutons

Looking at critical dyke widths for the studied plutons										latent heat J/kg specific heat J-1Kg-1oC-1		3.00E-01 thermal diffus m2/s 1.20E-03 gravity m/s2		8.00E-07 9.81			
Pluton	Volume /m^3	lateral extent /m	Tm,initial oC	Tw,freezing oC	Tinf,far field oC	Magma superheat oC	Magma undercooling oC	Density Kg/m3	diff: viscosity Pas	Dyke length /m	Sinf	Sm	sm/sinf^2	ukH/gp	dyke width /m	average vel/m	time taken /yrs
Ardara	2.70E+11	7000	900	750	350	150	400	70	1.00E+04	30000	0.625	1.66666667	4.26666667	0.3494976	3.423882434	6.71E-02	5.32496533
Ardara	2.70E+11	7000	900	750	350	150	400	70	1.00E+05	30000	0.625	1.66666667	4.26666667	3.49497597	6.088619634	2.12E-02	9.4692762
Ardara	2.70E+11	7000	900	750	350	150	400	70	1.00E+06	30000	0.625	1.66666667	4.26666667	34.9497597	10.82726693	6.71E-03	16.8390189
Ardara	2.70E+11	7000	900	750	350	150	400	70	1.00E+07	30000	0.625	1.66666667	4.26666667	349.497597	19.25390585	2.12E-03	29.9444806
Ardara	2.70E+11	7000	900	750	350	150	400	70	1.00E+08	30000	0.625	1.66666667	4.26666667	3494.97597	34.23882434	6.71E-04	53.2496533
Ardara	2.70E+11	7000	900	700	350	200	350	70	1.00E+04	30000	0.71428571	1.25	2.45	0.3494976	2.258535238	2.92E-02	18.552084
Ardara	2.70E+11	7000	900	700	350	200	350	70	1.00E+05	30000	0.71428571	1.25	2.45	3.49497597	4.016306711	9.23E-03	32.9907891
Ardara	2.70E+11	7000	900	700	350	200	350	70	1.00E+06	30000	0.71428571	1.25	2.45	34.9497597	7.142115528	2.92E-03	58.6668409
Ardara	2.70E+11	7000	900	700	350	200	350	70	1.00E+07	30000	0.71428571	1.25	2.45	349.497597	12.70067699	9.23E-04	104.326035
Ardara	2.70E+11	7000	900	700	350	200	350	70	1.00E+08	30000	0.71428571	1.25	2.45	3494.97597	22.58535238	2.92E-04	185.52084
Ardara	2.70E+11	7000	900	650	350	250	300	70	1.00E+04	30000	0.83333333	1	1.44	0.3494976	1.516087185	1.32E-02	61.3339289
Ardara	2.70E+11	7000	900	650	350	250	300	70	1.00E+05	30000	0.83333333	1	1.44	3.49497597	2.696026624	4.16E-03	109.068863
Ardara	2.70E+11	7000	900	650	350	250	300	70	1.00E+06	30000	0.83333333	1	1.44	34.9497597	4.794288635	1.32E-03	193.954913
Ardara	2.70E+11	7000	900	650	350	250	300	70	1.00E+07	30000	0.83333333	1	1.44	349.497597	8.525584765	4.16E-04	344.906029
Ardara	2.70E+11	7000	900	650	350	250	300	70	1.00E+08	30000	0.83333333	1	1.44	3494.97597	15.16087185	1.32E-04	613.339289
Ardara	2.70E+11	7000	900	600	350	300	250	70	1.00E+04	30000	1	0.83333333	0.83333333	0.3494976	1.005926787	5.79E-03	209.978194
Ardara	2.70E+11	7000	900	600	350	300	250	70	1.00E+05	30000	1	0.83333333	0.83333333	3.49497597	1.788818893	1.83E-03	373.399899
Ardara	2.70E+11	7000	900	600	350	300	250	70	1.00E+06	30000	1	0.83333333	0.83333333	34.9497597	3.181019806	5.79E-04	664.009353
Ardara	2.70E+11	7000	900	600	350	300	250	70	1.00E+07	30000	1	0.83333333	0.83333333	349.497597	5.656742023	1.83E-04	1180.79416
Ardara	2.70E+11	7000	900	600	350	300	250	70	1.00E+08	30000	1	0.83333333	0.83333333	3494.97597	10.05926787	5.79E-05	2099.78194
Ardara	2.70E+11	7000	900	550	350	350	200	70	1.00E+04	30000	1.25	0.71428571	0.45714286	0.3494976	0.641196675	2.35E-03	810.773475
Ardara	2.70E+11	7000	900	550	350	350	200	70	1.00E+05	30000	1.25	0.71428571	0.45714286	3.49497597	1.140226844	7.44E-04	1441.78178
Ardara	2.70E+11	7000	900	550	350	350	200	70	1.00E+06	30000	1.25	0.71428571	0.45714286	34.9497597	2.02764192	2.35E-04	2563.89085
Ardara	2.70E+11	7000	900	550	350	350	200	70	1.00E+07	30000	1.25	0.71428571	0.45714286	349.497597	3.605713877	7.44E-05	4559.3143
Ardara	2.70E+11	7000	900	550	350	350	200	70	1.00E+08	30000	1.25	0.71428571	0.45714286	3494.97597	6.411966746	2.35E-05	8107.73475
Ardara	2.70E+11	750	900	750	350	150	400	70	1.00E+04	30000	0.625	1.66666667	4.26666667	0.3494976	3.423882434	6.71E-02	49.6996764
Ardara	2.70E+11	750	900	750	350	150	400	70	1.00E+05	30000	0.625	1.66666667	4.26666667	3.49497597	6.088619634	2.12E-02	88.3799112
Ardara	2.70E+11	750	900	750	350	150	400	70	1.00E+06	30000	0.625	1.66666667	4.26666667	34.9497597	10.82726693	6.71E-03	157.164176
Ardara	2.70E+11	750	900	750	350	150	400	70	1.00E+07	30000	0.625	1.66666667	4.26666667	349.497597	19.25390585	2.12E-03	279.481819
Ardara	2.70E+11	750	900	750	350	150	400	70	1.00E+08	30000	0.625	1.66666667	4.26666667	3494.97597	34.23882434	6.71E-04	496.996764
Ardara	2.70E+11	750	900	700	350	200	350	70	1.00E+04	30000	0.71428571	1.25	2.45	0.3494976	2.258535238	2.92E-02	173.152784
Ardara	2.70E+11	750	900	700	350	200	350	70	1.00E+05	30000	0.71428571	1.25	2.45	3.49497597	4.016306711	9.23E-03	307.914031
Ardara	2.70E+11	750	900	700	350	200	350	70	1.00E+06	30000	0.71428571	1.25	2.45	34.9497597	7.142115528	2.92E-03	547.557182
Ardara	2.70E+11	750	900	700	350	200	350	70	1.00E+07	30000	0.71428571	1.25	2.45	349.497597	12.70067699	9.23E-04	973.709663
Ardara	2.70E+11	750	900	700	350	200	350	70	1.00E+08	30000	0.71428571	1.25	2.45	3494.97597	22.58535238	2.92E-04	1731.52784
Ardara	2.70E+11	750	900	650	350	250	300	70	1.00E+04	30000	0.83333333	1	1.44	0.3494976	1.516087185	1.32E-02	572.450004
Ardara	2.70E+11	750	900	650	350	250	300	70	1.00E+05	30000	0.83333333	1	1.44	3.49497597	2.696026624	4.16E-03	1017.97605
Ardara	2.70E+11	750	900	650	350	250	300	70	1.00E+06	30000	0.83333333	1	1.44	34.9497597	4.794288635	1.32E-03	1810.24586
Ardara	2.70E+11	750	900	650	350	250	300	70	1.00E+07	30000	0.83333333	1	1.44	349.497597	8.525584765	4.16E-04	3219.12294
Ardara	2.70E+11	750	900	650	350	250	300	70	1.00E+08	30000	0.83333333	1	1.44	3494.97597	15.16087185	1.32E-04	5724.50004
Ardara	2.70E+11	750	900	600	350	300	250	70	1.00E+04	30000	1	0.83333333	0.83333333	0.3494976	1.005926787	5.79E-03	1959.79648
Ardara	2.70E+11	750	900	600	350	300	250	70	1.00E+05	30000	1	0.83333333	0.83333333	3.49497597	1.788818893	1.83E-03	3485.06573
Ardara	2.70E+11	750	900	600	350	300	250	70	1.00E+06	30000	1	0.83333333	0.83333333	34.9497597	3.181019806	5.79E-04	6197.42063
Ardara	2.70E+11	750	900	600	350	300	250	70	1.00E+07	30000	1	0.83333333	0.83333333	349.497597	5.656742023	1.83E-04	11020.7455
Ardara	2.70E+11	750	900	600	350	300	250	70	1.00E+08	30000	1	0.83333333	0.83333333	3494.97597	10.05926787	5.79E-05	19597.9648
Ardara	2.70E+11	750	900	550	350	350	200	70	1.00E+04	30000	1.25	0.71428571	0.45714286	0.3494976	0.641196675	2.35E-03	7567.2191
Ardara	2.70E+11	750	900	550	350	350	200	70	1.00E+05	30000	1.25	0.71428571	0.45714286	3.49497597	1.140226844	7.44E-04	13456.6299
Ardara	2.70E+11	750	900	550	350	350	200	70	1.00E+06	30000	1.25	0.71428571	0.45714286	34.9497597	2.02764192	2.35E-04	23929.6479

Ardara	2.70E+11	750	900	550	350	350	200	70	1.00E+07	30000	1.25	0.71428571	0.45714286	349.497597	3.605713877	7.44E-05	42553.6001
Ardara	2.70E+11	750	900	550	350	350	200	70	1.00E+08	30000	1.25	0.71428571	0.45714286	349.497597	6.411966746	2.35E-05	75672.191
Ardara	2.70E+11	750	800	750	350	50	400	70	1.00E+04	30000	0.625	5	12.8	0.3494976	7.80476417	3.49E-01	4.19595419
Ardara	2.70E+11	750	800	750	350	50	400	70	1.00E+05	30000	0.625	5	12.8	3.49497597	13.87905142	1.10E-01	7.46157894
Ardara	2.70E+11	750	800	750	350	50	400	70	1.00E+06	30000	0.625	5	12.8	34.9497597	24.68083138	3.49E-02	13.2687722
Ardara	2.70E+11	750	800	750	350	50	400	70	1.00E+07	30000	0.625	5	12.8	349.497597	43.88941426	1.10E-02	23.5955844
Ardara	2.70E+11	750	800	750	350	50	400	70	1.00E+08	30000	0.625	5	12.8	3494.97597	78.0476417	3.49E-03	41.9595419
Ardara	2.70E+11	750	800	700	350	100	350	70	1.00E+04	30000	0.71428571	2.5	4.9	0.3494976	3.798388371	8.26E-02	36.4008889
Ardara	2.70E+11	750	800	700	350	100	350	70	1.00E+05	30000	0.71428571	2.5	4.9	3.49497597	6.754595831	2.61E-02	64.7309513
Ardara	2.70E+11	750	800	700	350	100	350	70	1.00E+06	30000	0.71428571	2.5	4.9	34.9497597	12.01155869	8.26E-03	115.109718
Ardara	2.70E+11	750	800	700	350	100	350	70	1.00E+07	30000	0.71428571	2.5	4.9	349.497597	21.3599075	2.61E-03	204.697241
Ardara	2.70E+11	750	800	700	350	100	350	70	1.00E+08	30000	0.71428571	2.5	4.9	3494.97597	37.98388371	8.26E-04	364.008889
Ardara	2.70E+11	750	800	650	350	150	300	70	1.00E+04	30000	0.83333333	1.66666667	2.4	0.3494976	2.223876875	2.83E-02	181.375188
Ardara	2.70E+11	750	800	650	350	150	300	70	1.00E+05	30000	0.83333333	1.66666667	2.4	3.49497597	3.954674458	8.95E-03	322.535762
Ardara	2.70E+11	750	800	650	350	150	300	70	1.00E+06	30000	0.83333333	1.66666667	2.4	34.9497597	7.032516162	2.83E-03	573.558705
Ardara	2.70E+11	750	800	650	350	150	300	70	1.00E+07	30000	0.83333333	1.66666667	2.4	349.497597	12.50577869	8.95E-04	1019.94764
Ardara	2.70E+11	750	800	650	350	150	300	70	1.00E+08	30000	0.83333333	1.66666667	2.4	3494.97597	22.23876875	2.83E-04	1813.75188
Ardara	2.70E+11	750	800	600	350	200	250	70	1.00E+04	30000	1	1.25	1.25	0.3494976	1.36343619	1.06E-02	787.056011
Ardara	2.70E+11	750	800	600	350	200	250	70	1.00E+05	30000	1	1.25	1.25	3.49497597	2.424570504	3.36E-03	1399.6055
Ardara	2.70E+11	750	800	600	350	200	250	70	1.00E+06	30000	1	1.25	1.25	34.9497597	4.311563805	1.06E-03	2488.88964
Ardara	2.70E+11	750	800	600	350	200	250	70	1.00E+07	30000	1	1.25	1.25	349.497597	7.667165139	3.36E-04	4425.9412
Ardara	2.70E+11	750	800	600	350	200	250	70	1.00E+08	30000	1	1.25	1.25	3494.97597	13.6343619	1.06E-04	7870.56011
Ardara	2.70E+11	750	800	550	350	250	200	70	1.00E+04	30000	1.25	1	0.64	0.3494976	0.825253335	3.90E-03	3549.3451
Ardara	2.70E+11	750	800	550	350	250	200	70	1.00E+05	30000	1.25	1	0.64	3.49497597	1.467531014	1.23E-03	6311.72732
Ardara	2.70E+11	750	800	550	350	250	200	70	1.00E+06	30000	1.25	1	0.64	34.9497597	2.609680186	3.90E-04	11224.0147
Ardara	2.70E+11	750	800	550	350	250	200	70	1.00E+07	30000	1.25	1	0.64	349.497597	4.640740541	1.23E-04	19959.4343
Ardara	2.70E+11	750	800	550	350	250	200	70	1.00E+08	30000	1.25	1	0.64	3494.97597	8.252533351	3.90E-05	35493.451
Ardara	2.70E+11	750	700	650	350	50	300	70	1.00E+04	30000	0.83333333	5	7.2	0.3494976	5.069343031	1.47E-01	15.3128156
Ardara	2.70E+11	750	700	650	350	50	300	70	1.00E+05	30000	0.83333333	5	7.2	3.49497597	9.014708335	4.65E-02	27.2304647
Ardara	2.70E+11	750	700	650	350	50	300	70	1.00E+06	30000	0.83333333	5	7.2	34.9497597	16.03067022	1.47E-02	48.4233747
Ardara	2.70E+11	750	700	650	350	50	300	70	1.00E+07	30000	0.83333333	5	7.2	349.497597	28.50701078	4.65E-03	86.1102902
Ardara	2.70E+11	750	700	650	350	50	300	70	1.00E+08	30000	0.83333333	5	7.2	3494.97597	50.69343031	1.47E-03	153.128156
Ardara	2.70E+11	750	700	600	350	100	250	70	1.00E+04	30000	1	2.5	2.5	0.3494976	2.293017209	3.01E-02	165.458145
Ardara	2.70E+11	750	700	600	350	100	250	70	1.00E+05	30000	1	2.5	2.5	3.49497597	4.07762529	9.51E-03	294.230812
Ardara	2.70E+11	750	700	600	350	100	250	70	1.00E+06	30000	1	2.5	2.5	34.9497597	7.251157095	3.01E-03	523.224594
Ardara	2.70E+11	750	700	600	350	100	250	70	1.00E+07	30000	1	2.5	2.5	349.497597	12.89458336	9.51E-04	930.439523
Ardara	2.70E+11	750	700	600	350	100	250	70	1.00E+08	30000	1	2.5	2.5	3494.97597	22.93017209	3.01E-04	1654.58145
Ardara	2.70E+11	750	700	550	350	150	200	70	1.00E+04	30000	1.25	1.66666667	1.06666667	0.3494976	1.210525243	8.39E-03	1124.5753
Ardara	2.70E+11	750	700	550	350	150	200	70	1.00E+05	30000	1.25	1.66666667	1.06666667	3.49497597	2.152652116	2.65E-03	1999.80911
Ardara	2.70E+11	750	700	550	350	150	200	70	1.00E+06	30000	1.25	1.66666667	1.06666667	34.9497597	3.828016934	8.39E-04	3556.21936
Ardara	2.70E+11	750	700	550	350	150	200	70	1.00E+07	30000	1.25	1.66666667	1.06666667	349.497597	6.807283696	2.65E-04	6323.95166
Ardara	2.70E+11	750	700	550	350	150	200	70	1.00E+08	30000	1.25	1.66666667	1.06666667	3494.97597	12.10525243	8.39E-05	11245.753

Appendix 16

Appendix of critical dykes widths for Brazilian plutons

Appendix of critical dykes widths for Brazilian plutons													latent heat specific heat	J/kg J-1Kg-1oC	3.00E-01 1.20E-03	thermal diffusiv m2/s gravity	8.00E-07 m/s2	9.81		
Pluton	length /m	width /m	depth /m	volume /m^3	lateral extent /m	Tm,initial oC	Tw,freezing oC	Tinf,far field oC	Magma superheat oC	Magma undercooling oC	Density difference Kg/m3	viscosity Pas	Dyke length /m	Sint	Sm	sm/sint^2	ukh/gp	dyke width /m	average vel/m /m/s	time taken /hrs
Atibaia	10500	5750	5000	3.02E+11	10500	900	750	350	150	400	200	1.00E+04	30000	0.625	1.66666667	4.26666667	0.12232416	2.633515355	1.13E-01	3.05285319
Atibaia	10500	5750	5000	3.02E+11	10500	900	750	350	150	400	200	1.00E+05	30000	0.625	1.66666667	4.26666667	1.22324159	4.683126132	3.59E-02	5.42882598
Atibaia	10500	5750	5000	3.02E+11	10500	900	750	350	150	400	200	1.00E+06	30000	0.625	1.66666667	4.26666667	12.2324159	8.327906775	1.13E-02	9.65396945
Atibaia	10500	5750	5000	3.02E+11	10500	900	750	350	150	400	200	1.00E+07	30000	0.625	1.66666667	4.26666667	122.324159	14.80934515	3.59E-03	17.1674551
Atibaia	10500	5750	5000	3.02E+11	10500	900	750	350	150	400	200	1.00E+08	30000	0.625	1.66666667	4.26666667	1223.24159	26.33515355	1.13E-03	30.5265319
Atibaia	10500	5750	5000	3.02E+11	10500	900	700	350	200	350	200	1.00E+04	30000	0.71428571	1.25	2.45	0.12232416	1.737176245	4.93E-02	10.636086
Atibaia	10500	5750	5000	3.02E+11	10500	900	700	350	200	350	200	1.00E+05	30000	0.71428571	1.25	2.45	1.22324159	3.089184748	1.56E-02	18.9139327
Atibaia	10500	5750	5000	3.02E+11	10500	900	700	350	200	350	200	1.00E+06	30000	0.71428571	1.25	2.45	12.2324159	5.493433632	4.93E-03	33.6342571
Atibaia	10500	5750	5000	3.02E+11	10500	900	700	350	200	350	200	1.00E+07	30000	0.71428571	1.25	2.45	122.324159	9.768859917	1.56E-03	59.8111068
Atibaia	10500	5750	5000	3.02E+11	10500	900	700	350	200	350	200	1.00E+08	30000	0.71428571	1.25	2.45	1223.24159	17.37176245	4.93E-04	106.36086
Atibaia	10500	5750	5000	3.02E+11	10500	900	650	350	250	300	200	1.00E+04	30000	0.83333333	1	1.44	0.12232416	1.166114479	2.22E-02	35.1633239
Atibaia	10500	5750	5000	3.02E+11	10500	900	650	350	250	300	200	1.00E+05	30000	0.83333333	1	1.44	1.22324159	2.073677368	7.03E-03	62.530215
Atibaia	10500	5750	5000	3.02E+11	10500	900	650	350	250	300	200	1.00E+06	30000	0.83333333	1	1.44	12.2324159	3.687577766	2.22E-03	111.196194
Atibaia	10500	5750	5000	3.02E+11	10500	900	650	350	250	300	200	1.00E+07	30000	0.83333333	1	1.44	122.324159	6.557543615	7.03E-04	197.737902
Atibaia	10500	5750	5000	3.02E+11	10500	900	650	350	250	300	200	1.00E+08	30000	0.83333333	1	1.44	1223.24159	11.66114479	2.22E-04	351.633239
Atibaia	10500	5750	5000	3.02E+11	10500	900	600	350	300	250	200	1.00E+04	30000	1	0.83333333	0.83333333	0.12232416	0.773719218	9.79E-03	120.382493
Atibaia	10500	5750	5000	3.02E+11	10500	900	600	350	300	250	200	1.00E+05	30000	1	0.83333333	0.83333333	1.22324159	1.375808954	3.10E-03	214.073708
Atibaia	10500	5750	5000	3.02E+11	10500	900	600	350	300	250	200	1.00E+06	30000	1	0.83333333	0.83333333	12.2324159	2.446714998	9.79E-04	380.682868
Atibaia	10500	5750	5000	3.02E+11	10500	900	600	350	300	250	200	1.00E+07	30000	1	0.83333333	0.83333333	122.324159	4.350942904	3.10E-04	676.960506
Atibaia	10500	5750	5000	3.02E+11	10500	900	600	350	300	250	200	1.00E+08	30000	1	0.83333333	0.83333333	1223.24159	7.73719218	9.79E-05	1203.82493
Atibaia	10500	5750	5000	3.02E+11	10500	900	550	350	350	200	200	1.00E+04	30000	1.25	0.71428571	0.45714286	0.12232416	0.493183198	3.98E-03	464.824133
Atibaia	10500	5750	5000	3.02E+11	10500	900	550	350	350	200	200	1.00E+05	30000	1.25	0.71428571	0.45714286	1.22324159	0.877017526	1.26E-03	826.587185
Atibaia	10500	5750	5000	3.02E+11	10500	900	550	350	350	200	200	1.00E+06	30000	1.25	0.71428571	0.45714286	12.2324159	1.55958221	3.98E-04	1469.90297
Atibaia	10500	5750	5000	3.02E+11	10500	900	550	350	350	200	200	1.00E+07	30000	1.25	0.71428571	0.45714286	122.324159	2.773372931	1.26E-04	2613.89819
Atibaia	10500	5750	5000	3.02E+11	10500	900	550	350	350	200	200	1.00E+08	30000	1.25	0.71428571	0.45714286	1223.24159	4.93183198	3.98E-05	4648.24133
Atibaia	10500	5750	5000	3.02E+11	10500	800	750	350	50	400	200	1.00E+04	30000	0.625	5	12.8	0.12232416	6.003116837	5.89E-01	0.25774076
Atibaia	10500	5750	5000	3.02E+11	10500	800	750	350	50	400	200	1.00E+05	30000	0.625	5	12.8	1.22324159	10.67521907	1.86E-01	0.45833508
Atibaia	10500	5750	5000	3.02E+11	10500	800	750	350	50	400	200	1.00E+06	30000	0.625	5	12.8	12.2324159	18.98352226	5.89E-02	0.81504783
Atibaia	10500	5750	5000	3.02E+11	10500	800	750	350	50	400	200	1.00E+07	30000	0.625	5	12.8	122.324159	33.75800677	1.86E-02	1.44938278
Atibaia	10500	5750	5000	3.02E+11	10500	800	750	350	50	400	200	1.00E+08	30000	0.625	5	12.8	1223.24159	60.03116837	5.89E-03	2.57740756
Atibaia	10500	5750	5000	3.02E+11	10500	800	700	350	100	350	200	1.00E+04	30000	0.71428571	2.5	4.9	0.12232416	2.921570554	1.40E-01	2.23596164
Atibaia	10500	5750	5000	3.02E+11	10500	800	700	350	100	350	200	1.00E+05	30000	0.71428571	2.5	4.9	1.22324159	5.195368762	4.41E-02	3.97616455
Atibaia	10500	5750	5000	3.02E+11	10500	800	700	350	100	350	200	1.00E+06	30000	0.71428571	2.5	4.9	12.2324159	9.238817296	1.40E-02	7.07073155
Atibaia	10500	5750	5000	3.02E+11	10500	800	700	350	100	350	200	1.00E+07	30000	0.71428571	2.5	4.9	122.324159	16.42919857	4.41E-03	12.5737363
Atibaia	10500	5750	5000	3.02E+11	10500	800	700	350	100	350	200	1.00E+08	30000	0.71428571	2.5	4.9	1223.24159	29.21570554	1.40E-03	22.3596164
Atibaia	10500	5750	5000	3.02E+11	10500	800	650	350	150	300	200	1.00E+04	30000	0.83333333	1.66666667	2.4	0.12232416	1.710518399	4.78E-02	11.1411555
Atibaia	10500	5750	5000	3.02E+11	10500	800	650	350	150	300	200	1.00E+05	30000	0.83333333	1.66666667	2.4	1.22324159	3.04177965	1.51E-02	19.8120874
Atibaia	10500	5750	5000	3.02E+11	10500	800	650	350	150	300	200	1.00E+06	30000	0.83333333	1.66666667	2.4	12.2324159	5.409134121	4.78E-03	35.2314271
Atibaia	10500	5750	5000	3.02E+11	10500	800	650	350	150	300	200	1.00E+07	30000	0.83333333	1.66666667	2.4	122.324159	9.618951833	1.51E-03	62.6513214
Atibaia	10500	5750	5000	3.02E+11	10500	800	650	350	150	300	200	1.00E+08	30000	0.83333333	1.66666667	2.4	1223.24159	17.10518399	4.78E-04	111.411555
Atibaia	10500	5750	5000	3.02E+11	10500	800	600	350	200	250	200	1.00E+04	30000	1	1.25	1.25	0.12232416	1.048701353	1.80E-02	48.3457163
Atibaia	10500	5750	5000	3.02E+11	10500	800	600	350	200	250	200	1.00E+05	30000	1	1.25	1.25	1.22324159	1.864884024	5.69E-03	85.9721919
Atibaia	10500	5750	5000	3.02E+11	10500	800	600	350	200	250	200	1.00E+06	30000	1	1.25	1.25	12.2324159	3.316284862	1.80E-03	152.882579
Atibaia	10500	5750	5000	3.02E+11	10500	800	600	350	200	250	200	1.00E+07	30000	1	1.25	1.25	122.324159	5.897281088	5.69E-04	271.867942
Atibaia	10500	5750	5000	3.02E+11	10500	800	600	350	200	250	200	1.00E+08	30000	1	1.25	1.25	1223.24159	10.48701353	1.80E-04	483.457163

Atibaia	10500	5750	5000	3.02E+11	10500	700	550	350	150	200	200	1.00E+07	30000	1.25	1.66666667	1.06666667	122.324159	5.235894189	4.48E-04	388.455165
Atibaia	10500	5750	5000	3.02E+11	10500	700	550	350	150	200	200	1.00E+08	30000	1.25	1.66666667	1.06666667	1223.24159	9.31088283	1.42E-04	690.781822
Atibaia	10500	5750	5000	3.02E+11	5000	900	750	350	150	400	200	1.00E+04	30000	0.625	1.66666667	4.26666667	0.12232416	2.633515355	1.13E-01	6.41099171
Atibaia	10500	5750	5000	3.02E+11	5000	900	750	350	150	400	200	1.00E+05	30000	0.625	1.66666667	4.26666667	1.22324159	4.683126132	3.59E-02	11.4005345
Atibaia	10500	5750	5000	3.02E+11	5000	900	750	350	150	400	200	1.00E+06	30000	0.625	1.66666667	4.26666667	12.2324159	8.327906775	1.13E-02	20.2733359
Atibaia	10500	5750	5000	3.02E+11	5000	900	750	350	150	400	200	1.00E+07	30000	0.625	1.66666667	4.26666667	122.324159	14.80934515	3.59E-03	36.0516557
Atibaia	10500	5750	5000	3.02E+11	5000	900	750	350	150	400	200	1.00E+08	30000	0.625	1.66666667	4.26666667	1223.24159	26.33515355	1.13E-03	64.1099171
Atibaia	10500	5750	5000	3.02E+11	5000	900	700	350	200	350	200	0.71428571	30000	1.25	2.45	0.12232416	1.737176245	4.93E-02	22.3357805	
Atibaia	10500	5750	5000	3.02E+11	5000	900	700	350	200	350	200	1.00E+05	30000	0.71428571	1.25	2.45	1.22324159	3.089184748	1.56E-02	39.7192586
Atibaia	10500	5750	5000	3.02E+11	5000	900	700	350	200	350	200	0.71428571	30000	1.25	2.45	12.2324159	5.493433632	4.93E-03	70.6319398	
Atibaia	10500	5750	5000	3.02E+11	5000	900	700	350	200	350	200	1.00E+07	30000	0.71428571	1.25	2.45	122.324159	9.768859917	1.56E-03	125.603324
Atibaia	10500	5750	5000	3.02E+11	5000	900	700	350	200	350	200	1.00E+08	30000	0.71428571	1.25	2.45	1223.24159	17.37176245	4.93E-04	223.357805
Atibaia	10500	5750	5000	3.02E+11	5000	900	650	350	250	300	200	1.00E+04	30000	0.83333333	1	1.44	0.12232416	1.166114479	2.22E-02	73.8429803
Atibaia	10500	5750	5000	3.02E+11	5000	900	650	350	250	300	200	1.00E+05	30000	0.83333333	1	1.44	1.22324159	2.073677368	7.03E-03	131.313451
Atibaia	10500	5750	5000	3.02E+11	5000	900	650	350	250	300	200	1.00E+06	30000	0.83333333	1	1.44	12.2324159	3.687577766	2.22E-03	233.512007
Atibaia	10500	5750	5000	3.02E+11	5000	900	650	350	250	300	200	1.00E+07	30000	0.83333333	1	1.44	122.324159	6.557543615	7.03E-04	415.249594
Atibaia	10500	5750	5000	3.02E+11	5000	900	600	350	300	250	200	1.00E+08	30000	0.83333333	1	1.44	1223.24159	11.66114479	2.22E-04	738.429803
Atibaia	10500	5750	5000	3.02E+11	5000	900	600	350	300	250	200	1.00E+04	30000	1	0.83333333	0.83333333	0.12232416	0.773719218	9.79E-03	252.803235
Atibaia	10500	5750	5000	3.02E+11	5000	900	600	350	300	250	200	1.00E+05	30000	1	0.83333333	0.83333333	1.22324159	1.375888954	3.10E-03	449.554788
Atibaia	10500	5750	5000	3.02E+11	5000	900	600	350	300	250	200	1.00E+06	30000	1	0.83333333	0.83333333	12.2324159	2.446714998	9.79E-04	799.434023
Atibaia	10500	5750	5000	3.02E+11	5000	900	600	350	300	250	200	1.00E+07	30000	1	0.83333333	0.83333333	122.324159	4.350942904	3.10E-04	1421.61706
Atibaia	10500	5750	5000	3.02E+11	5000	900	600	350	300	250	200	1.00E+08	30000	1	0.83333333	0.83333333	1223.24159	7.73719218	9.79E-05	2528.03235
Atibaia	10500	5750	5000	3.02E+11	5000	900	550	350	350	200	200	1.00E+04	30000	1.25	0.71428571	0.45714286	0.12232416	0.493183198	3.98E-03	976.130679
Atibaia	10500	5750	5000	3.02E+11	5000	900	550	350	350	200	200	1.00E+05	30000	1.25	0.71428571	0.45714286	1.22324159	0.877017526	1.26E-03	1735.83309
Atibaia	10500	5750	5000	3.02E+11	5000	900	550	350	350	200	200	1.00E+06	30000	1.25	0.71428571	0.45714286	12.2324159	1.55958221	3.98E-04	3086.79624
Atibaia	10500	5750	5000	3.02E+11	5000	900	550	350	350	200	200	1.00E+07	30000	1.25	0.71428571	0.45714286	122.324159	2.773372931	1.26E-04	5489.1862
Atibaia	10500	5750	5000	3.02E+11	5000	900	550	350	350	200	200	1.00E+08	30000	1.25	0.71428571	0.45714286	1223.24159	4.93183198	3.98E-05	9761.30679
Atibaia	10500	5750	5000	3.02E+11	5000	800	750	350	50	400	200	1.00E+04	30000	0.625	5	12.8	0.12232416	6.003116837	5.89E-01	0.54125559
Atibaia	10500	5750	5000	3.02E+11	5000	800	750	350	50	400	200	1.00E+05	30000	0.625	5	12.8	1.22324159	10.67521907	1.86E-01	0.96250367
Atibaia	10500	5750	5000	3.02E+11	5000	800	750	350	50	400	200	1.00E+06	30000	0.625	5	12.8	12.2324159	18.98352226	5.89E-02	1.71160045
Atibaia	10500	5750	5000	3.02E+11	5000	800	750	350	50	400	200	1.00E+07	30000	0.625	5	12.8	122.324159	33.75800677	1.86E-02	3.04370384
Atibaia	10500	5750	5000	3.02E+11	5000	800	750	350	50	400	200	1.00E+08	30000	0.625	5	12.8	1223.24159	60.03116837	5.89E-03	5.61255587
Atibaia	10500	5750	5000	3.02E+11	5000	800	700	350	100	350	200	1.00E+04	30000	0.71428571	2.5	4.9	0.12232416	2.921570554	1.40E-01	4.69551945
Atibaia	10500	5750	5000	3.02E+11	5000	800	700	350	100	350	200	1.00E+05	30000	0.71428571	2.5	4.9	1.22324159	5.195368762	4.41E-02	8.3499455
Atibaia	10500	5750	5000	3.02E+11	5000	800	700	350	100	350	200	1.00E+06	30000	0.71428571	2.5	4.9	12.2324159	9.238817296	1.40E-02	14.8485363
Atibaia	10500	5750	5000	3.02E+11	5000	800	700	350	100	350	200	1.00E+07	30000	0.71428571	2.5	4.9	122.324159	16.42919857	4.41E-03	26.4048463
Atibaia	10500	5750	5000	3.02E+11	5000	800	700	350	100	350	200	1.00E+08	30000	0.71428571	2.5	4.9	1223.24159	29.21570554	1.40E-03	46.9551945
Atibaia	10500	5750	5000	3.02E+11	5000	800	650	350	150	300	200	1.00E+04	30000	0.83333333	1.66666667	2.4	0.12232416	1.710518399	4.78E-02	23.3964265
Atibaia	10500	5750	5000	3.02E+11	5000	800	650	350	150	300	200	1.00E+05	30000	0.83333333	1.66666667	2.4	1.22324159	3.04177965	1.51E-02	41.6053835
Atibaia	10500	5750	5000	3.02E+11	5000	800	650	350	150	300	200	1.00E+06	30000	0.83333333	1.66666667	2.4	12.2324159	5.409134121	4.78E-03	73.9859969
Atibaia	10500	5750	5000	3.02E+11	5000	800	650	350	150	300	200	1.00E+07	30000	0.83333333	1.66666667	2.4	122.324159	9.618951833	1.51E-03	131.567775
Atibaia	10500	5750	5000	3.02E+11	5000	800	650	350	150	300	200	1.00E+08	30000	0.83333333	1.66666667	2.4	1223.24159	17.10518399	4.78E-04	233.964265
Atibaia	10500	5750	5000	3.02E+11	5000	800	600	350	200	250	200	1.00E+04	30000	1	1.25	1.25	0.12232416	1.048701353	1.80E-02	101.526004
Atibaia	10500	5750	5000	3.02E+11	5000	800	600	350	200	250	200	1.00E+05	30000	1	1.25	1.25	1.22324159	1.864884024	5.69E-03	180.541603
Atibaia	10500	5750	5000	3.02E+11	5000	800	600	350	200	250	200	1.00E+06	30000	1	1.25	1.25	12.2324159	3.316284862	1.80E-03	321.053415
Atibaia	10500	5750	5000	3.02E+11	5000	800	600	350	200	250	200	1.00E+07	30000	1	1.25	1.25	122.324159	5.897281088	5.69E-04	570.922678
Atibaia	10500	5750	5000	3.02E+11	5000	800	600	350	200	250	200	1.00E+08	30000	1	1.25	1.25	1223.24159	10.48701353	1.80E-04	1015.26004
Atibaia	10500	5750	5000	3.02E+11	5000	800	550	350	250	200	200	1.00E+04	30000	1.25	1	0.64	0.12232416	0.634752323	6.59E-03	467.846483
Atibaia	10500	5750	5000	3.02E+11	5000	800	550	350	250	200	200	1.00E+05	30000	1.25	1	0.64	1.22324159	1.128766987	2.08E-03	814.178973
Atibaia	10500	5750	5000	3.02E+11	5000	800	550	350	250	200	200	1.00E+06	30000	1.25	1	0.64	12.2324159	2.007263092	6.59E-04	1447.8377
Atibaia	10500	5750	5000	3.02E+11	5000	800	550	350	250	200	200	1.00E+07	30000	1.25	1	0.64	122.324159	3.569474627	2.08E-04	2574.65998
Atibaia	10500	5750	5000	3.02E+11	5000	700	650	350	50	300	200	1.00E+08	30000	1.25	1	0.64	1223.24159	6.347523234	6.59E-05	4578.46483
Atibaia	10500	5750	5000	3.02E+11	5000	700	650	350	50	300	200	1.00E+04	30000	0.83333333	5	7.2	0.12232416	3.899138762	2.49E-01	1.97527109
Atibaia	10500	5750	5000	3.02E+11	5000	700	650	350	50	300	200	1.00E+05	30000	0.83333333	5	7.2	1.22324159	6.933758177	7.86E-02	3.5125839
Atibaia	10500	5750	5000	3.02E+11	5000	700	650	350	50	300	200	1.00E+06	30000	0.83333333	5	7.2	12.2324159	12.3301594	2.49E-02	6.24635563
Atibaia	10500																			

Atibaia	10500	5750	5000	3.02E+11	1000	900	750	350	150	400	200	1.00E+08	30000	0.625	1.66666667	4.26666667	1223.24159	26.33515355	1.13E-03	320.549585
Atibaia	10500	5750	5000	3.02E+11	1000	900	700	350	200	350	200	1.00E+04	30000	0.71428571	1.25	2.45	0.12232416	1.737176245	4.93E-02	111.678903
Atibaia	10500	5750	5000	3.02E+11	1000	900	700	350	200	350	200	1.00E+05	30000	0.71428571	1.25	2.45	1.22324159	3.089184748	1.56E-02	198.596293
Atibaia	10500	5750	5000	3.02E+11	1000	900	700	350	200	350	200	1.00E+06	30000	0.71428571	1.25	2.45	12.2324159	5.493433632	4.93E-03	353.159699
Atibaia	10500	5750	5000	3.02E+11	1000	900	700	350	200	350	200	1.00E+07	30000	0.71428571	1.25	2.45	122.324159	9.768859917	1.56E-03	628.016621
Atibaia	10500	5750	5000	3.02E+11	1000	900	700	350	200	350	200	1.00E+08	30000	0.71428571	1.25	2.45	1223.24159	17.37176245	4.93E-04	1116.78903
Atibaia	10500	5750	5000	3.02E+11	1000	900	650	350	250	300	200	1.00E+04	30000	0.83333333	1	1.44	0.12232416	1.166114479	2.22E-02	369.214901
Atibaia	10500	5750	5000	3.02E+11	1000	900	650	350	250	300	200	1.00E+05	30000	0.83333333	1	1.44	1.22324159	2.073677368	7.03E-03	656.567257
Atibaia	10500	5750	5000	3.02E+11	1000	900	650	350	250	300	200	1.00E+06	30000	0.83333333	1	1.44	12.2324159	3.687577766	2.22E-03	1167.56003
Atibaia	10500	5750	5000	3.02E+11	1000	900	650	350	250	300	200	1.00E+07	30000	0.83333333	1	1.44	122.324159	6.557543615	7.03E-04	2076.24797
Atibaia	10500	5750	5000	3.02E+11	1000	900	650	350	250	300	200	1.00E+08	30000	0.83333333	1	1.44	1223.24159	11.66114479	2.22E-04	3692.14901
Atibaia	10500	5750	5000	3.02E+11	1000	900	600	350	300	250	200	1.00E+04	30000	1	0.83333333	0.83333333	0.12232416	0.773719218	9.79E-03	1254.01618
Atibaia	10500	5750	5000	3.02E+11	1000	900	600	350	300	250	200	1.00E+05	30000	1	0.83333333	0.83333333	1.22324159	1.375888954	3.10E-03	2247.77394
Atibaia	10500	5750	5000	3.02E+11	1000	900	600	350	300	250	200	1.00E+06	30000	1	0.83333333	0.83333333	12.2324159	2.446714998	9.79E-04	3997.17011
Atibaia	10500	5750	5000	3.02E+11	1000	900	600	350	300	250	200	1.00E+07	30000	1	0.83333333	0.83333333	122.324159	4.350942904	3.10E-04	7108.08531
Atibaia	10500	5750	5000	3.02E+11	1000	900	600	350	300	250	200	1.00E+08	30000	1	0.83333333	0.83333333	1223.24159	7.73719218	9.79E-05	12640.1618
Atibaia	10500	5750	5000	3.02E+11	1000	900	550	350	350	200	200	1.00E+04	30000	1.25	0.71428571	0.45714286	0.12232416	0.493183198	3.98E-03	4880.65339
Atibaia	10500	5750	5000	3.02E+11	1000	900	550	350	350	200	200	1.00E+05	30000	1.25	0.71428571	0.45714286	1.22324159	0.877017526	1.26E-03	8679.16544
Atibaia	10500	5750	5000	3.02E+11	1000	900	550	350	350	200	200	1.00E+06	30000	1.25	0.71428571	0.45714286	12.2324159	1.55958221	3.98E-04	15433.9812
Atibaia	10500	5750	5000	3.02E+11	1000	900	550	350	350	200	200	1.00E+07	30000	1.25	0.71428571	0.45714286	122.324159	2.773372931	1.26E-04	27445.931
Atibaia	10500	5750	5000	3.02E+11	1000	900	550	350	350	200	200	1.00E+08	30000	1.25	0.71428571	0.45714286	1223.24159	4.93183198	3.98E-05	48806.5339
Atibaia	10500	5750	5000	3.02E+11	1000	800	750	350	50	400	200	1.00E+04	30000	0.625	5	12.8	0.12232416	6.003116837	5.89E-01	2.70627793
Atibaia	10500	5750	5000	3.02E+11	1000	800	750	350	50	400	200	1.00E+05	30000	0.625	5	12.8	1.22324159	10.67521907	1.86E-01	4.81251833
Atibaia	10500	5750	5000	3.02E+11	1000	800	750	350	50	400	200	1.00E+06	30000	0.625	5	12.8	12.2324159	18.98352226	5.89E-02	8.55800225
Atibaia	10500	5750	5000	3.02E+11	1000	800	750	350	50	400	200	1.00E+07	30000	0.625	5	12.8	122.324159	33.75800677	1.86E-02	15.2185192
Atibaia	10500	5750	5000	3.02E+11	1000	800	750	350	50	400	200	1.00E+08	30000	0.625	5	12.8	1223.24159	60.03116837	5.89E-03	27.0627793
Atibaia	10500	5750	5000	3.02E+11	1000	800	700	350	100	350	200	1.00E+04	30000	0.71428571	2.5	4.9	0.12232416	2.921570554	4.40E-01	23.4775972
Atibaia	10500	5750	5000	3.02E+11	1000	800	700	350	100	350	200	1.00E+05	30000	0.71428571	2.5	4.9	1.22324159	5.195368762	4.41E-02	41.7497278
Atibaia	10500	5750	5000	3.02E+11	1000	800	700	350	100	350	200	1.00E+06	30000	0.71428571	2.5	4.9	12.2324159	9.238817296	1.40E-02	74.2426813
Atibaia	10500	5750	5000	3.02E+11	1000	800	700	350	100	350	200	1.00E+07	30000	0.71428571	2.5	4.9	122.324159	16.42919857	4.41E-03	132.024231
Atibaia	10500	5750	5000	3.02E+11	1000	800	700	350	100	350	200	1.00E+08	30000	0.71428571	2.5	4.9	1223.24159	29.21570554	1.40E-03	234.775972
Atibaia	10500	5750	5000	3.02E+11	1000	800	650	350	150	300	200	1.00E+04	30000	0.83333333	1.66666667	2.4	0.12232416	1.710518399	4.78E-02	116.982133
Atibaia	10500	5750	5000	3.02E+11	1000	800	650	350	150	300	200	1.00E+05	30000	0.83333333	1.66666667	2.4	1.22324159	3.04177965	1.51E-02	208.026918
Atibaia	10500	5750	5000	3.02E+11	1000	800	650	350	150	300	200	1.00E+06	30000	0.83333333	1.66666667	2.4	12.2324159	5.409134121	4.78E-03	369.929984
Atibaia	10500	5750	5000	3.02E+11	1000	800	650	350	150	300	200	1.00E+07	30000	0.83333333	1.66666667	2.4	122.324159	9.818951833	1.51E-03	657.838874
Atibaia	10500	5750	5000	3.02E+11	1000	800	650	350	150	300	200	1.00E+08	30000	0.83333333	1.66666667	2.4	1223.24159	17.10518399	4.78E-04	1169.82133
Atibaia	10500	5750	5000	3.02E+11	1000	800	600	350	200	250	200	1.00E+04	30000	1	1.25	1.25	0.12232416	1.048701353	1.80E-02	507.630022
Atibaia	10500	5750	5000	3.02E+11	1000	800	600	350	200	250	200	1.00E+05	30000	1	1.25	1.25	1.22324159	1.864884024	5.69E-03	902.708015
Atibaia	10500	5750	5000	3.02E+11	1000	800	600	350	200	250	200	1.00E+06	30000	1	1.25	1.25	12.2324159	3.16284862	1.80E-03	1605.26708
Atibaia	10500	5750	5000	3.02E+11	1000	800	600	350	200	250	200	1.00E+07	30000	1	1.25	1.25	122.324159	5.897281088	5.89E-04	2854.61339
Atibaia	10500	5750	5000	3.02E+11	1000	800	600	350	200	250	200	1.00E+08	30000	1	1.25	1.25	1223.24159	10.48701353	1.80E-04	5076.30022
Atibaia	10500	5750	5000	3.02E+11	1000	800	550	350	250	200	200	1.00E+04	30000	1.25	1	0.64	0.12232416	0.634752323	6.59E-03	2289.23241
Atibaia	10500	5750	5000	3.02E+11	1000	800	550	350	250	200	200	1.00E+05	30000	1.25	1	0.64	1.22324159	1.128766987	2.08E-03	4070.89487
Atibaia	10500	5750	5000	3.02E+11	1000	800	550	350	250	200	200	1.00E+06	30000	1.25	1	0.64	12.2324159	2.007263092	6.59E-04	7239.18852
Atibaia	10500	5750	5000	3.02E+11	1000	800	550	350	250	200	200	1.00E+07	30000	1.25	1	0.64	122.324159	3.569474627	2.08E-04	12873.2999
Atibaia	10500	5750	5000	3.02E+11	1000	800	550	350	250	200	200	1.00E+08	30000	1.25	1	0.64	1223.24159	6.347523234	6.59E-05	22892.3241
Atibaia	10500	5750	5000	3.02E+11	1000	700	650	350	50	300	200	1.00E+04	30000	0.83333333	5	7.2	0.12232416	3.899138762	2.49E-01	8.87635543
Atibaia	10500	5750	5000	3.02E+11	1000	700	650	350	50	300	200	1.00E+05	30000	0.83333333	5	7.2	1.22324159	6.933758177	7.86E-02	17.5629195
Atibaia	10500	5750	5000	3.02E+11	1000	700	650	350	50	300	200	1.00E+06	30000	0.83333333	5	7.2	12.2324159	12.3301594	2.49E-02	31.2317781
Atibaia	10500	5750	5000	3.02E+11	1000	700	650	350	50	300	200	1.00E+07	30000	0.83333333	5	7.2	122.324159	21.92646858	7.86E-03	55.538828
Atibaia	10500	5750	5000	3.02E+11	1000	700	600	350	100	250	200	1.00E+04	30000	0.83333333	5	7.2	1223.24159	38.99138762	2.49E-03	98.7635543
Atibaia	10500	5750	5000	3.02E+11	1000	700	600	350	100	250	200	1.00E+05	30000	1	2.5	2.5	0.12232416	1.763698417	5.09E-02	106.716066
Atibaia	10500	5750	5000	3.02E+11	1000	700	600	350	100	250	200	1.00E+06	30000	1	2.5	2.5	1.22324159	3.136348581	1.81E-02	189.770984
Atibaia	10500	5750	5000	3.02E+11	1000	700	600	350	100	250	200	1.00E+07	30000	1	2.5	2.5	12.2324159	5.577304105	5.09E-03	337.465833
Atibaia	10500	5750	5000	3.02E+11	1000	700	600	350	100	250	200	1.00E+08	30000	1	2.5	2.5	122.324159	9.918005053	1.81E-03	600.108542
Atibaia	10500	5750	5000	3.02E+11	1000	700	550	350												

Imbiricu	8250	4500	5000	1.86E+11	8250	900	700	350	200	350	200	1.00E+08	30000	0.71428571	1.25	2.45	1223.24159	17.37176245	4.93E-04	83.2389337
Imbiricu	8250	4500	5000	1.86E+11	8250	900	650	350	250	300	200	1.00E+04	30000	0.83333333	1	1.44	0.12232416	1.166114479	2.22E-02	27.5191231
Imbiricu	8250	4500	5000	1.86E+11	8250	900	650	350	250	300	200	1.00E+05	30000	0.83333333	1	1.44	1.22324159	2.073677368	7.03E-03	48.93669
Imbiricu	8250	4500	5000	1.86E+11	8250	900	650	350	250	300	200	1.00E+06	30000	0.83333333	1	1.44	12.2324159	3.687577766	2.22E-03	87.0231082
Imbiricu	8250	4500	5000	1.86E+11	8250	900	650	350	250	300	200	1.00E+07	30000	0.83333333	1	1.44	122.324159	6.557543615	7.03E-04	154.751401
Imbiricu	8250	4500	5000	1.86E+11	8250	900	650	350	250	300	200	1.00E+08	30000	0.83333333	1	1.44	1223.24159	11.66114479	2.22E-04	275.191231
Imbiricu	8250	4500	5000	1.86E+11	8250	900	600	350	250	300	200	1.00E+04	30000	1	0.83333333	0.83333333	0.12232416	0.773719218	9.79E-03	94.2123858
Imbiricu	8250	4500	5000	1.86E+11	8250	900	600	350	250	300	200	1.00E+05	30000	1	0.83333333	0.83333333	1.22324159	1.375888954	3.10E-03	167.535946
Imbiricu	8250	4500	5000	1.86E+11	8250	900	600	350	250	300	200	1.00E+06	30000	1	0.83333333	0.83333333	12.2324159	2.446714998	9.79E-04	297.925723
Imbiricu	8250	4500	5000	1.86E+11	8250	900	600	350	250	300	200	1.00E+07	30000	1	0.83333333	0.83333333	122.324159	4.350942904	3.10E-04	528.795179
Imbiricu	8250	4500	5000	1.86E+11	8250	900	600	350	250	300	200	1.00E+08	30000	1	0.83333333	0.83333333	1223.24159	7.73719218	9.79E-05	942.123858
Imbiricu	8250	4500	5000	1.86E+11	8250	900	550	350	250	300	200	1.00E+04	30000	1.25	0.71428571	0.45714286	0.12232416	0.493183198	3.98E-03	363.775408
Imbiricu	8250	4500	5000	1.86E+11	8250	900	550	350	250	300	200	1.00E+05	30000	1.25	0.71428571	0.45714286	1.22324159	0.877017526	1.26E-03	646.894318
Imbiricu	8250	4500	5000	1.86E+11	8250	900	550	350	250	300	200	1.00E+06	30000	1.25	0.71428571	0.45714286	12.2324159	1.55958221	3.98E-04	1150.35885
Imbiricu	8250	4500	5000	1.86E+11	8250	900	550	350	250	300	200	1.00E+07	30000	1.25	0.71428571	0.45714286	122.324159	2.77372931	1.26E-04	2045.65945
Imbiricu	8250	4500	5000	1.86E+11	8250	900	550	350	250	300	200	1.00E+08	30000	1.25	0.71428571	0.45714286	1223.24159	4.93183198	3.98E-05	3637.75408
Imbiricu	8250	4500	5000	1.86E+11	8250	900	550	350	250	400	200	1.00E+04	30000	0.625	5	12.8	0.12232416	6.003116837	5.89E-01	0.20171016
Imbiricu	8250	4500	5000	1.86E+11	8250	800	750	350	50	400	200	1.00E+05	30000	0.625	5	12.8	1.22324159	10.67521907	1.86E-01	0.35669702
Imbiricu	8250	4500	5000	1.86E+11	8250	800	750	350	50	400	200	1.00E+06	30000	0.625	5	12.8	12.2324159	18.98352226	5.89E-02	0.63786352
Imbiricu	8250	4500	5000	1.86E+11	8250	800	750	350	50	400	200	1.00E+07	30000	0.625	5	12.8	122.324159	33.75800677	1.86E-02	1.13429957
Imbiricu	8250	4500	5000	1.86E+11	8250	800	750	350	50	400	200	1.00E+08	30000	0.625	5	12.8	1223.24159	60.03116837	5.89E-03	2.01710156
Imbiricu	8250	4500	5000	1.86E+11	8250	800	700	350	100	350	200	1.00E+04	30000	0.71428571	2.5	4.9	0.12232416	2.921570554	1.40E-01	1.74988302
Imbiricu	8250	4500	5000	1.86E+11	8250	800	700	350	100	350	200	1.00E+05	30000	0.71428571	2.5	4.9	1.22324159	5.195368762	4.41E-02	3.11178095
Imbiricu	8250	4500	5000	1.86E+11	8250	800	700	350	100	350	200	1.00E+06	30000	0.71428571	2.5	4.9	12.2324159	9.238817296	1.40E-02	5.53661599
Imbiricu	8250	4500	5000	1.86E+11	8250	800	700	350	100	350	200	1.00E+07	30000	0.71428571	2.5	4.9	122.324159	16.42919857	4.41E-03	8.84031539
Imbiricu	8250	4500	5000	1.86E+11	8250	800	700	350	100	350	200	1.00E+08	30000	0.71428571	2.5	4.9	1223.24159	29.21570554	1.40E-03	17.4988302
Imbiricu	8250	4500	5000	1.86E+11	8250	800	650	350	150	300	200	1.00E+04	30000	0.83333333	1.66666667	2.4	0.12232416	1.710518399	4.78E-02	87.1916516
Imbiricu	8250	4500	5000	1.86E+11	8250	800	650	350	150	300	200	1.00E+05	30000	0.83333333	1.66666667	2.4	1.22324159	3.04177965	1.51E-02	15.5051119
Imbiricu	8250	4500	5000	1.86E+11	8250	800	650	350	150	300	200	1.00E+06	30000	0.83333333	1.66666667	2.4	12.2324159	5.409134121	4.78E-03	27.5724212
Imbiricu	8250	4500	5000	1.86E+11	8250	800	650	350	150	300	200	1.00E+07	30000	0.83333333	1.66666667	2.4	122.324159	9.618951833	1.51E-03	49.0314689
Imbiricu	8250	4500	5000	1.86E+11	8250	800	650	350	150	300	200	1.00E+08	30000	0.83333333	1.66666667	2.4	1223.24159	17.10518399	4.78E-04	87.1916516
Imbiricu	8250	4500	5000	1.86E+11	8250	800	600	350	200	250	200	1.00E+04	30000	1	1.25	1.25	0.12232416	1.048701353	1.80E-02	37.835778
Imbiricu	8250	4500	5000	1.86E+11	8250	800	600	350	200	250	200	1.00E+05	30000	1	1.25	1.25	1.22324159	1.864884024	5.69E-03	67.282585
Imbiricu	8250	4500	5000	1.86E+11	8250	800	600	350	200	250	200	1.00E+06	30000	1	1.25	1.25	12.2324159	3.316284862	1.80E-03	119.647236
Imbiricu	8250	4500	5000	1.86E+11	8250	800	600	350	200	250	200	1.00E+07	30000	1	1.25	1.25	122.324159	5.897281088	5.69E-04	212.766215
Imbiricu	8250	4500	5000	1.86E+11	8250	800	550	350	250	200	200	1.00E+08	30000	1	1.25	1.25	1223.24159	10.48701353	1.80E-04	378.35778
Imbiricu	8250	4500	5000	1.86E+11	8250	800	550	350	250	200	200	1.00E+04	30000	1.25	1	0.64	0.12232416	0.634752323	6.59E-03	170.626018
Imbiricu	8250	4500	5000	1.86E+11	8250	800	550	350	200	200	200	1.00E+05	30000	1.25	1	0.64	1.22324159	1.128766987	2.08E-03	303.420735
Imbiricu	8250	4500	5000	1.86E+11	8250	800	550	350	200	200	200	1.00E+06	30000	1.25	1	0.64	12.2324159	2.007263092	6.59E-04	539.566846
Imbiricu	8250	4500	5000	1.86E+11	8250	800	550	350	200	200	200	1.00E+07	30000	1.25	1	0.64	122.324159	3.569474627	2.08E-04	959.500613
Imbiricu	8250	4500	5000	1.86E+11	8250	800	550	350	200	200	200	1.00E+08	30000	1.25	1	0.64	1223.24159	6.347523234	6.59E-05	1706.26018
Imbiricu	8250	4500	5000	1.86E+11	8250	700	650	350	50	300	200	1.00E+04	30000	0.83333333	5	7.2	0.12232416	3.899138762	2.49E-01	0.73612587
Imbiricu	8250	4500	5000	1.86E+11	8250	700	650	350	50	300	200	1.00E+05	30000	0.83333333	5	7.2	1.22324159	6.933758177	7.86E-02	1.30903748
Imbiricu	8250	4500	5000	1.86E+11	8250	700	650	350	50	300	200	1.00E+06	30000	0.83333333	5	7.2	12.2324159	12.3301594	2.49E-02	2.3278344
Imbiricu	8250	4500	5000	1.86E+11	8250	700	650	350	50	300	200	1.00E+07	30000	0.83333333	5	7.2	122.324159	21.92646858	7.86E-03	4.13953998
Imbiricu	8250	4500	5000	1.86E+11	8250	700	650	350	50	300	200	1.00E+08	30000	0.83333333	5	7.2	1223.24159	38.99138762	2.49E-03	7.36125871
Imbiricu	8250	4500	5000	1.86E+11	8250	700	600	350	100	250	200	1.00E+04	30000	1	2.5	2.5	0.12232416	1.763698417	5.09E-02	7.95399252
Imbiricu	8250	4500	5000	1.86E+11	8250	700	600	350	100	250	200	1.00E+05	30000	1	2.5	2.5	1.22324159	3.136348581	1.61E-02	14.1444211
Imbiricu	8250	4500	5000	1.86E+11	8250	700	600	350	100	250	200	1.00E+06	30000	1	2.5	2.5	12.2324159	5.577304105	5.09E-03	25.1527329
Imbiricu	8250	4500	5000	1.86E+11	8250	700	600	350	100	250	200	1.00E+07	30000	1	2.5	2.5	122.324159	9.918005053	1.61E-03	44.728587
Imbiricu	8250	4500	5000	1.86E+11	8250	700	600	350	100	250	200	1.00E+08	30000	1	2.5	2.5	1223.24159	17.63698417	5.09E-04	79.5399252
Imbiricu	8250	4500	5000	1.86E+11	8250	700	550	350	150	200	200	1.00E+04	30000	1.25	1.66666667	1.06666667	0.12232416	0.931088283	1.42E-02	54.0611861
Imbiricu	8250	4500	5000	1.86E+11	8250	700	550	350	150	200	200	1.00E+05	30000	1.25	1.66666667	1.06666667	1.22324159	1.655735123	4.48E-03	96.1358941
Imbiricu	8250	4500	5000	1.86E+11	8250	700	550	350	150	200	200	1.00E+06	30000	1.25	1.66666667	1.06666667	12.2324159	2.944359677	1.42E-03	170.956481
Imbiricu	8250	4500	5000	1.86E+11	8250	700	550	350	150	200	200	1.00E+07	30000	1.25	1.66666667	1.06666667	122.324159	5.235894189	4.48E-04	304.00839
Imbiricu	8250	4500	5000	1.86E+11	8250	700	550	350	150	200	200	1.00E+08	30000	1.25	1.66666667	1.06666667	1223.24159	9.31088283</		

Imbiricu	8250	4500	5000	1.86E+11	4000	900	600	350	300	250	200	1.00E+04	30000	1	0.83333333	0.83333333	0.12232416	0.773719218	9.79E-03	194.313046
Imbiricu	8250	4500	5000	1.86E+11	4000	900	600	350	300	250	200	1.00E+05	30000	1	0.83333333	0.83333333	1.22324159	1.375688954	3.10E-03	345.542888
Imbiricu	8250	4500	5000	1.86E+11	4000	900	600	350	300	250	200	1.00E+06	30000	1	0.83333333	0.83333333	12.2324159	2.446714998	9.79E-04	614.471803
Imbiricu	8250	4500	5000	1.86E+11	4000	900	600	350	300	250	200	1.00E+07	30000	1	0.83333333	0.83333333	122.324159	4.350942904	3.10E-04	1092.70256
Imbiricu	8250	4500	5000	1.86E+11	4000	900	600	350	300	250	200	1.00E+08	30000	1	0.83333333	0.83333333	1223.24159	7.73719218	9.79E-05	1943.13046
Imbiricu	8250	4500	5000	1.86E+11	4000	900	600	350	300	250	200	1.00E+04	30000	1.25	0.71428571	0.45714286	0.12232416	0.493183198	3.98E-03	750.28678
Imbiricu	8250	4500	5000	1.86E+11	4000	900	550	350	350	200	200	1.00E+05	30000	1.25	0.71428571	0.45714286	1.22324159	0.877017526	1.26E-03	1334.21953
Imbiricu	8250	4500	5000	1.86E+11	4000	900	550	350	350	200	200	1.00E+06	30000	1.25	0.71428571	0.45714286	12.2324159	1.55958221	3.98E-04	2372.61512
Imbiricu	8250	4500	5000	1.86E+11	4000	900	550	350	350	200	200	1.00E+07	30000	1.25	0.71428571	0.45714286	122.324159	2.773372931	1.26E-04	4219.17262
Imbiricu	8250	4500	5000	1.86E+11	4000	900	550	350	350	200	200	1.00E+08	30000	1.25	0.71428571	0.45714286	1223.24159	4.93183198	3.98E-05	7502.8678
Imbiricu	8250	4500	5000	1.86E+11	4000	800	750	350	50	400	200	1.00E+04	30000	0.625	5	12.8	0.12232416	6.003116837	5.89E-01	0.4160272
Imbiricu	8250	4500	5000	1.86E+11	4000	800	750	350	50	400	200	1.00E+05	30000	0.625	5	12.8	1.22324159	10.67521907	1.86E-01	0.7398126
Imbiricu	8250	4500	5000	1.86E+11	4000	800	750	350	50	400	200	1.00E+06	30000	0.625	5	12.8	12.2324159	18.98352226	5.89E-02	1.31559351
Imbiricu	8250	4500	5000	1.86E+11	4000	800	750	350	50	400	200	1.00E+07	30000	0.625	5	12.8	122.324159	33.75800677	1.86E-02	2.33949286
Imbiricu	8250	4500	5000	1.86E+11	4000	800	750	350	50	400	200	1.00E+08	30000	0.625	5	12.8	1223.24159	60.03116837	5.89E-03	4.16027198
Imbiricu	8250	4500	5000	1.86E+11	4000	800	700	350	100	350	200	1.00E+04	30000	0.71428571	2.5	4.9	0.12232416	2.921570554	1.40E-01	3.60913374
Imbiricu	8250	4500	5000	1.86E+11	4000	800	700	350	100	350	200	1.00E+05	30000	0.71428571	2.5	4.9	1.22324159	5.195368762	4.41E-02	6.41804821
Imbiricu	8250	4500	5000	1.86E+11	4000	800	700	350	100	350	200	1.00E+06	30000	0.71428571	2.5	4.9	12.2324159	9.238817296	1.40E-02	11.413083
Imbiricu	8250	4500	5000	1.86E+11	4000	800	700	350	100	350	200	1.00E+07	30000	0.71428571	2.5	4.9	122.324159	16.42919857	4.41E-03	20.2956505
Imbiricu	8250	4500	5000	1.86E+11	4000	800	700	350	100	350	200	1.00E+08	30000	0.71428571	2.5	4.9	1223.24159	29.21570554	1.40E-03	36.0913374
Imbiricu	8250	4500	5000	1.86E+11	4000	800	650	350	150	300	200	1.00E+04	30000	0.83333333	1.66666667	2.4	0.12232416	1.710518399	4.78E-02	17.9832781
Imbiricu	8250	4500	5000	1.86E+11	4000	800	650	350	150	300	200	1.00E+05	30000	0.83333333	1.66666667	2.4	1.22324159	3.04177965	1.51E-02	31.9792932
Imbiricu	8250	4500	5000	1.86E+11	4000	800	650	350	150	300	200	1.00E+06	30000	0.83333333	1.66666667	2.4	12.2324159	5.409134121	4.78E-03	56.8681187
Imbiricu	8250	4500	5000	1.86E+11	4000	800	650	350	150	300	200	1.00E+07	30000	0.83333333	1.66666667	2.4	122.324159	9.618951833	1.51E-03	101.127405
Imbiricu	8250	4500	5000	1.86E+11	4000	800	650	350	150	300	200	1.00E+08	30000	0.83333333	1.66666667	2.4	1223.24159	17.10518399	4.78E-04	179.832781
Imbiricu	8250	4500	5000	1.86E+11	4000	800	600	350	200	250	200	1.00E+04	30000	1	1.25	1.25	0.12232416	1.048701353	1.80E-02	78.0362922
Imbiricu	8250	4500	5000	1.86E+11	4000	800	600	350	200	250	200	1.00E+05	30000	1	1.25	1.25	1.22324159	1.864684024	5.69E-03	138.770332
Imbiricu	8250	4500	5000	1.86E+11	4000	800	600	350	200	250	200	1.00E+06	30000	1	1.25	1.25	12.2324159	3.316284862	1.80E-03	246.772423
Imbiricu	8250	4500	5000	1.86E+11	4000	800	600	350	200	250	200	1.00E+07	30000	1	1.25	1.25	122.324159	5.897281088	5.69E-04	438.830319
Imbiricu	8250	4500	5000	1.86E+11	4000	800	600	350	200	250	200	1.00E+08	30000	1	1.25	1.25	1223.24159	10.48701353	1.80E-04	780.362922
Imbiricu	8250	4500	5000	1.86E+11	4000	800	550	350	250	200	200	1.00E+04	30000	1.25	1	0.64	0.12232416	0.634752323	6.59E-03	351.916163
Imbiricu	8250	4500	5000	1.86E+11	4000	800	550	350	250	200	200	1.00E+05	30000	1.25	1	0.64	1.22324159	1.128766987	2.08E-03	625.805267
Imbiricu	8250	4500	5000	1.86E+11	4000	800	550	350	250	200	200	1.00E+06	30000	1.25	1	0.64	12.2324159	2.007263092	6.59E-04	1112.85662
Imbiricu	8250	4500	5000	1.86E+11	4000	800	550	350	250	200	200	1.00E+07	30000	1.25	1	0.64	122.324159	3.569474627	2.08E-04	1978.97001
Imbiricu	8250	4500	5000	1.86E+11	4000	800	550	350	250	200	200	1.00E+08	30000	1.25	1	0.64	1223.24159	6.347523234	6.59E-05	3519.16163
Imbiricu	8250	4500	5000	1.86E+11	4000	700	650	350	50	300	200	1.00E+04	30000	0.83333333	5	7.2	0.12232416	3.899138762	2.49E-01	1.51825961
Imbiricu	8250	4500	5000	1.86E+11	4000	700	650	350	50	300	200	1.00E+05	30000	0.83333333	5	7.2	1.22324159	6.933758177	7.89E-02	2.6998898
Imbiricu	8250	4500	5000	1.86E+11	4000	700	650	350	50	300	200	1.00E+06	30000	0.83333333	5	7.2	12.2324159	12.3301594	2.49E-02	4.80115844
Imbiricu	8250	4500	5000	1.86E+11	4000	700	650	350	50	300	200	1.00E+07	30000	0.83333333	5	7.2	122.324159	21.92646858	7.86E-03	8.5378012
Imbiricu	8250	4500	5000	1.86E+11	4000	700	650	350	50	300	200	1.00E+08	30000	0.83333333	5	7.2	1223.24159	38.99138762	2.49E-03	15.1825961
Imbiricu	8250	4500	5000	1.86E+11	4000	700	600	350	100	250	200	1.00E+04	30000	1	2.5	2.5	0.12232416	1.763698417	5.09E-02	16.4051096
Imbiricu	8250	4500	5000	1.86E+11	4000	700	600	350	100	250	200	1.00E+05	30000	1	2.5	2.5	1.22324159	3.136348581	1.61E-02	29.1726886
Imbiricu	8250	4500	5000	1.86E+11	4000	700	600	350	100	250	200	1.00E+06	30000	1	2.5	2.5	12.2324159	5.577304105	5.09E-03	51.8775115
Imbiricu	8250	4500	5000	1.86E+11	4000	700	600	350	100	250	200	1.00E+07	30000	1	2.5	2.5	122.324159	9.918005053	1.61E-03	82.2527106
Imbiricu	8250	4500	5000	1.86E+11	4000	700	600	350	100	250	200	1.00E+08	30000	1	2.5	2.5	1223.24159	17.63698417	5.09E-04	164.051096
Imbiricu	8250	4500	5000	1.86E+11	4000	700	550	350	150	200	200	1.00E+04	30000	1.25	1.66666667	1.06666667	0.12232416	0.931088283	1.42E-02	111.501196
Imbiricu	8250	4500	5000	1.86E+11	4000	700	550	350	150	200	200	1.00E+05	30000	1.25	1.66666667	1.06666667	1.22324159	1.655735123	4.48E-03	198.280282
Imbiricu	8250	4500	5000	1.86E+11	4000	700	550	350	150	200	200	1.00E+06	30000	1.25	1.66666667	1.06666667	12.2324159	2.944359677	1.42E-03	352.597742
Imbiricu	8250	4500	5000	1.86E+11	4000	700	550	350	150	200	200	1.00E+07	30000	1.25	1.66666667	1.06666667	122.324159	5.255894189	4.48E-04	627.017305
Imbiricu	8250	4500	5000	1.86E+11	4000	700	550	350	150	200	200	1.00E+08	30000	1.25	1.66666667	1.06666667	1223.24159	9.31088283	1.42E-04	1115.01196
Imbiricu	8250	4500	5000	1.86E+11	1000	900	750	350	150	400	200	1.00E+04	30000	0.625	1.66666667	4.26666667	0.12232416	2.633515355	1.13E-01	19.710813
Imbiricu	8250	4500	5000	1.86E+11	1000	900	750	350	150	400	200	1.00E+05	30000	0.625	1.66666667	4.26666667	1.22324159	4.683126132	3.59E-02	35.0513329
Imbiricu	8250	4500	5000	1.86E+11	1000	900	750	350	150	400	200	1.00E+06	30000	0.625	1.66666667	4.26666667	12.2324159	8.327906775	1.13E-02	62.3310636
Imbiricu	8250	4500	5000	1.86E+11	1000	900	750	350	150	400	200	1.00E+07	30000	0.625	1.66666667	4.26666667	122.324159	14.80934515	3.59E-03	110.842047
Imbiricu	8250	4500	5000	1.86E+11	1000	900	750	350	150	400	200	1.00E+08	30000	0.625	1.66666667	4.26666667	1223.24159	26.33515355	1.13E-03	197.10813
Imbiricu	8250	4500	5000	1.86E+11	1000	900	700	350	2											

Imbiricu	8250	4500	5000	1.86E+11	1000	900	550	350	350	200	200	1.00E+05	30000	1.25	0.71428571	0.45714286	1.22324159	0.877017526	1.26E-03	5336.87813
Imbiricu	8250	4500	5000	1.86E+11	1000	900	550	350	350	200	200	1.00E+06	30000	1.25	0.71428571	0.45714286	1.22324159	1.55958221	3.98E-04	9490.46049
Imbiricu	8250	4500	5000	1.86E+11	1000	900	550	350	350	200	200	1.00E+07	30000	1.25	0.71428571	0.45714286	1.22324159	2.773372931	1.26E-04	16876.8905
Imbiricu	8250	4500	5000	1.86E+11	1000	900	550	350	350	200	200	1.00E+08	30000	1.25	0.71428571	0.45714286	1.22324159	4.93183198	3.98E-05	30011.4712
Imbiricu	8250	4500	5000	1.86E+11	1000	800	750	350	50	400	200	1.00E+04	30000	0.625	5	12.8	0.12232416	6.003116837	5.89E-01	1.66410879
Imbiricu	8250	4500	5000	1.86E+11	1000	800	750	350	50	400	200	1.00E+05	30000	0.625	5	12.8	0.12232416	10.87521907	1.86E-01	2.9592504
Imbiricu	8250	4500	5000	1.86E+11	1000	800	750	350	50	400	200	1.00E+06	30000	0.625	5	12.8	0.12232416	18.98352226	5.89E-02	5.26237405
Imbiricu	8250	4500	5000	1.86E+11	1000	800	750	350	50	400	200	1.00E+07	30000	0.625	5	12.8	0.12232416	33.75800677	1.86E-02	9.35797143
Imbiricu	8250	4500	5000	1.86E+11	1000	800	750	350	50	400	200	1.00E+08	30000	0.625	5	12.8	0.12232416	60.03116837	5.89E-03	16.6410879
Imbiricu	8250	4500	5000	1.86E+11	1000	800	700	350	100	350	200	1.00E+04	30000	0.71428571	2.5	4.9	0.12232416	2.921570554	1.40E-01	14.4365349
Imbiricu	8250	4500	5000	1.86E+11	1000	800	700	350	100	350	200	1.00E+05	30000	0.71428571	2.5	4.9	0.12232416	5.195368762	4.41E-02	25.6721928
Imbiricu	8250	4500	5000	1.86E+11	1000	800	700	350	100	350	200	1.00E+06	30000	0.71428571	2.5	4.9	0.12232416	9.238817296	1.40E-02	45.652332
Imbiricu	8250	4500	5000	1.86E+11	1000	800	700	350	100	350	200	1.00E+07	30000	0.71428571	2.5	4.9	0.12232416	16.42919857	4.41E-03	81.1826019
Imbiricu	8250	4500	5000	1.86E+11	1000	800	700	350	100	350	200	1.00E+08	30000	0.71428571	2.5	4.9	0.12232416	29.21570554	1.40E-03	144.365349
Imbiricu	8250	4500	5000	1.86E+11	1000	800	650	350	150	300	200	1.00E+04	30000	0.83333333	1.66666667	2.4	0.12232416	1.710518399	4.78E-02	71.9331126
Imbiricu	8250	4500	5000	1.86E+11	1000	800	650	350	150	300	200	1.00E+05	30000	0.83333333	1.66666667	2.4	0.12232416	3.04177965	1.51E-02	127.917173
Imbiricu	8250	4500	5000	1.86E+11	1000	800	650	350	150	300	200	1.00E+06	30000	0.83333333	1.66666667	2.4	0.12232416	5.409134121	4.78E-03	227.472475
Imbiricu	8250	4500	5000	1.86E+11	1000	800	650	350	150	300	200	1.00E+07	30000	0.83333333	1.66666667	2.4	0.12232416	9.618951833	1.51E-03	404.509618
Imbiricu	8250	4500	5000	1.86E+11	1000	800	650	350	150	300	200	1.00E+08	30000	0.83333333	1.66666667	2.4	0.12232416	17.10518399	4.78E-04	719.331126
Imbiricu	8250	4500	5000	1.86E+11	1000	800	600	350	200	250	200	1.00E+04	30000	1	1.25	1.25	0.12232416	1.048701353	1.80E-02	312.145169
Imbiricu	8250	4500	5000	1.86E+11	1000	800	600	350	200	250	200	1.00E+05	30000	1	1.25	1.25	0.12232416	1.864884024	5.69E-03	555.081326
Imbiricu	8250	4500	5000	1.86E+11	1000	800	600	350	200	250	200	1.00E+06	30000	1	1.25	1.25	0.12232416	3.316284862	1.80E-03	887.089693
Imbiricu	8250	4500	5000	1.86E+11	1000	800	600	350	200	250	200	1.00E+07	30000	1	1.25	1.25	0.12232416	5.897281088	5.69E-04	1755.32128
Imbiricu	8250	4500	5000	1.86E+11	1000	800	600	350	200	250	200	1.00E+08	30000	1	1.25	1.25	0.12232416	10.48701353	1.80E-04	3121.45169
Imbiricu	8250	4500	5000	1.86E+11	1000	800	550	350	250	200	200	1.00E+04	30000	1.25	1	0.64	0.12232416	0.634752323	6.59E-03	1407.66465
Imbiricu	8250	4500	5000	1.86E+11	1000	800	550	350	250	200	200	1.00E+05	30000	1.25	1	0.64	0.12232416	1.128766987	2.08E-03	2503.22107
Imbiricu	8250	4500	5000	1.86E+11	1000	800	550	350	250	200	200	1.00E+06	30000	1.25	1	0.64	0.12232416	2.007263092	6.59E-04	4451.42648
Imbiricu	8250	4500	5000	1.86E+11	1000	800	550	350	250	200	200	1.00E+07	30000	1.25	1	0.64	0.12232416	3.569474627	2.08E-04	7915.88006
Imbiricu	8250	4500	5000	1.86E+11	1000	800	550	350	250	200	200	1.00E+08	30000	1.25	1	0.64	0.12232416	6.347523234	6.59E-05	14076.6465
Imbiricu	8250	4500	5000	1.86E+11	1000	700	650	350	50	300	200	1.00E+04	30000	0.83333333	5	7.2	0.12232416	3.899138762	2.49E-01	6.07303843
Imbiricu	8250	4500	5000	1.86E+11	1000	700	650	350	50	300	200	1.00E+05	30000	0.83333333	5	7.2	0.12232416	6.933758177	7.86E-02	10.7995592
Imbiricu	8250	4500	5000	1.86E+11	1000	700	650	350	50	300	200	1.00E+06	30000	0.83333333	5	7.2	0.12232416	12.3301594	2.49E-02	19.2046338
Imbiricu	8250	4500	5000	1.86E+11	1000	700	650	350	50	300	200	1.00E+07	30000	0.83333333	5	7.2	0.12232416	21.92646858	7.86E-03	34.1512048
Imbiricu	8250	4500	5000	1.86E+11	1000	700	650	350	50	300	200	1.00E+08	30000	0.83333333	5	7.2	0.12232416	38.99138762	2.49E-03	60.7303843
Imbiricu	8250	4500	5000	1.86E+11	1000	700	600	350	100	250	200	1.00E+04	30000	1	2.5	2.5	0.12232416	1.763698417	5.09E-02	65.6204383
Imbiricu	8250	4500	5000	1.86E+11	1000	700	600	350	100	250	200	1.00E+05	30000	1	2.5	2.5	0.12232416	3.136348581	1.61E-02	116.691474
Imbiricu	8250	4500	5000	1.86E+11	1000	700	600	350	100	250	200	1.00E+06	30000	1	2.5	2.5	0.12232416	5.577304105	5.09E-03	207.510046
Imbiricu	8250	4500	5000	1.86E+11	1000	700	600	350	100	250	200	1.00E+07	30000	1	2.5	2.5	0.12232416	9.918005053	1.61E-03	369.010842
Imbiricu	8250	4500	5000	1.86E+11	1000	700	600	350	100	250	200	1.00E+08	30000	1	2.5	2.5	0.12232416	17.63698417	5.09E-04	656.204383
Imbiricu	8250	4500	5000	1.86E+11	1000	700	550	350	150	200	200	1.00E+04	30000	1.25	1.66666667	1.06666667	0.12232416	0.931088283	1.42E-02	446.004785
Imbiricu	8250	4500	5000	1.86E+11	1000	700	550	350	150	200	200	1.00E+05	30000	1.25	1.66666667	1.06666667	0.12232416	1.655735123	4.48E-03	793.121127
Imbiricu	8250	4500	5000	1.86E+11	1000	700	550	350	150	200	200	1.00E+06	30000	1.25	1.66666667	1.06666667	0.12232416	2.944359677	1.42E-03	1410.39097
Imbiricu	8250	4500	5000	1.86E+11	1000	700	550	350	150	200	200	1.00E+07	30000	1.25	1.66666667	1.06666667	0.12232416	5.235894189	4.48E-04	2508.06922
Imbiricu	8250	4500	5000	1.86E+11	1000	700	550	350	150	200	200	1.00E+08	30000	1.25	1.66666667	1.06666667	0.12232416	9.31088283	1.42E-04	4460.04785
Pluton	length	width	depth	volume	lateral extent	Tm,initial	Tw,freezing	Tint,far field	Magma superheat	Magma undercooling	Density difference	viscosity	Dyke length	Sinf	Sm	sm/sinf^2	ukH/gp	dyke width	average vel/tr	time taken/yr
Morro Azul	12500	4500	5000	1.41E+11	10000	900	750	350	150	400	200	1.00E+04	30000	0.625	1.66666667	4.26666667	0.12232416	2.633515355	1.13E-01	1.49324341
Morro Azul	12500	4500	5000	1.41E+11	10000	900	750	350	150	400	200	1.00E+05	30000	0.625	1.66666667	4.26666667	0.12232416	4.683126132	3.59E-02	2.65540401
Morro Azul	12500	4500	5000	1.41E+11	10000	900	750	350	150	400	200	1.00E+06	30000	0.625	1.66666667	4.26666667	0.12232416	8.327906775	1.13E-02	4.72205028
Morro Azul	12500	4500	5000	1.41E+11	10000	900	750	350	150	400	200	1.00E+07	30000	0.625	1.66666667	4.26666667	0.12232416	14.80934515	3.59E-03	8.39712478
Morro Azul	12500	4500	5000	1.41E+11	10000	900	750	350	150	400	200	1.00E+08	30000	0.625	1.66666667	4.26666667	0.12232416	26.33515355	1.13E-03	14.9324341
Morro Azul	12500	4500	5000	1.41E+11	10000	900	700	350	200	350	200	1.00E+04	30000	0.71428571	1.25	2.45	0.12232416	1.737176245	4.93E-02	5.20243336
Morro Azul	12500	4500	5000	1.41E+11	10000	900	700	350	200	350	200	1.00E+05	30000	0.71428571	1.25	2.45	0.12232416	3.089184748	1.56E-02	9.25138012
Morro Azul	12500	4500	5000	1.41E+11	10000	900	700	350	200	350	200	1.00E+06	30000	0.71428571	1.25	2.45	0.12232416	5.493433632	4.93E-03	16.4515386
Morro Azul	12500	4500	5000	1.41E+11	10000	900	700	350	200	350	200	1.00E+07	30000	0.71428571	1.25	2.45	0.12232416	9.768859917	1.56E-03	29.2554327
Morro Azul	12500	4500	5000	1.41E+11	10000	900	650	350	250	300	200	1.00E+08	30000	0.71428571	1.25	2.45	0.12232416	17.37176245	4.93E-04	52.0243336
Morro Azul	12500	4500	5000	1.41E+11	10000	900	650	350	250	300	200	1.00E+04	30000	0.83333333	1					

Morro Azul	12500	4500	5000	1.41E+11	10000	800	750	350	50	400	200	1.00E+05	30000	0.625	5	12.8	1.22324159	10.67521907	1.86E-01	0.22418564
Morro Azul	12500	4500	5000	1.41E+11	10000	800	750	350	50	400	200	1.00E+06	30000	0.625	5	12.8	1.22324159	18.98352226	5.89E-02	0.3986647
Morro Azul	12500	4500	5000	1.41E+11	10000	800	750	350	50	400	200	1.00E+07	30000	0.625	5	12.8	1.22324159	33.75800677	1.86E-02	0.70893723
Morro Azul	12500	4500	5000	1.41E+11	10000	800	750	350	50	400	200	1.00E+08	30000	0.625	5	12.8	1.22324159	60.03116837	5.89E-03	1.26068848
Morro Azul	12500	4500	5000	1.41E+11	10000	800	700	350	100	350	200	1.00E+04	30000	0.71428571	2.5	4.9	0.12232416	2.921570554	1.40E-01	1.09367689
Morro Azul	12500	4500	5000	1.41E+11	10000	800	700	350	100	350	200	1.00E+05	30000	0.71428571	2.5	4.9	0.122324159	5.195368762	4.41E-02	1.94486309
Morro Azul	12500	4500	5000	1.41E+11	10000	800	700	350	100	350	200	1.00E+06	30000	0.71428571	2.5	4.9	0.122324159	9.238817296	1.40E-02	3.45951
Morro Azul	12500	4500	5000	1.41E+11	10000	800	700	350	100	350	200	1.00E+07	30000	0.71428571	2.5	4.9	0.122324159	16.42919857	4.41E-03	6.15019712
Morro Azul	12500	4500	5000	1.41E+11	10000	800	650	350	150	300	200	1.00E+08	30000	0.71428571	2.5	4.9	0.122324159	29.21570554	1.40E-03	10.9367689
Morro Azul	12500	4500	5000	1.41E+11	10000	800	650	350	150	300	200	1.00E+04	30000	0.83333333	1.66666667	2.4	0.12232416	1.710518399	4.78E-02	5.44947822
Morro Azul	12500	4500	5000	1.41E+11	10000	800	650	350	150	300	200	1.00E+05	30000	0.83333333	1.66666667	2.4	0.122324159	3.04177965	1.51E-02	9.69069492
Morro Azul	12500	4500	5000	1.41E+11	10000	800	650	350	150	300	200	1.00E+06	30000	0.83333333	1.66666667	2.4	0.122324159	5.409134121	4.78E-03	17.2327632
Morro Azul	12500	4500	5000	1.41E+11	10000	800	650	350	150	300	200	1.00E+07	30000	0.83333333	1.66666667	2.4	0.122324159	9.618951833	1.51E-03	30.6446681
Morro Azul	12500	4500	5000	1.41E+11	10000	800	600	350	200	300	200	1.00E+08	30000	0.83333333	1.66666667	2.4	0.122324159	17.10518399	4.78E-04	54.4947822
Morro Azul	12500	4500	5000	1.41E+11	10000	800	600	350	200	250	200	1.00E+04	30000	1	1.25	1.25	0.12232416	1.048701353	1.80E-02	23.6473613
Morro Azul	12500	4500	5000	1.41E+11	10000	800	600	350	200	250	200	1.00E+05	30000	1	1.25	1.25	0.122324159	1.864884024	5.69E-03	42.0516156
Morro Azul	12500	4500	5000	1.41E+11	10000	800	600	350	200	250	200	1.00E+06	30000	1	1.25	1.25	0.122324159	3.316284862	1.80E-03	74.7795222
Morro Azul	12500	4500	5000	1.41E+11	10000	800	600	350	200	250	200	1.00E+07	30000	1	1.25	1.25	0.122324159	5.897281088	5.69E-04	132.978885
Morro Azul	12500	4500	5000	1.41E+11	10000	800	600	350	200	250	200	1.00E+08	30000	1	1.25	1.25	0.122324159	10.48701353	1.80E-04	236.473613
Morro Azul	12500	4500	5000	1.41E+11	10000	800	550	350	250	200	200	1.00E+04	30000	1.25	1	0.64	0.12232416	0.634752323	6.59E-03	106.641262
Morro Azul	12500	4500	5000	1.41E+11	10000	800	550	350	250	200	200	1.00E+05	30000	1.25	1	0.64	0.122324159	1.128766987	2.08E-03	189.63796
Morro Azul	12500	4500	5000	1.41E+11	10000	800	550	350	250	200	200	1.00E+06	30000	1.25	1	0.64	0.122324159	2.007263092	6.59E-04	337.229279
Morro Azul	12500	4500	5000	1.41E+11	10000	800	550	350	250	200	200	1.00E+07	30000	1.25	1	0.64	0.122324159	3.568474627	2.08E-04	599.687883
Morro Azul	12500	4500	5000	1.41E+11	10000	800	550	350	250	200	200	1.00E+08	30000	1.25	1	0.64	0.122324159	6.347523234	6.59E-05	1086.41262
Morro Azul	12500	4500	5000	1.41E+11	10000	700	650	350	50	300	200	1.00E+04	30000	0.83333333	5	7.2	0.12232416	3.899138762	2.49E-01	0.46007857
Morro Azul	12500	4500	5000	1.41E+11	10000	700	650	350	50	300	200	1.00E+05	30000	0.83333333	5	7.2	0.122324159	6.933758177	7.86E-02	0.81814842
Morro Azul	12500	4500	5000	1.41E+11	10000	700	650	350	50	300	200	1.00E+06	30000	0.83333333	5	7.2	0.122324159	12.3301594	2.49E-02	1.454895
Morro Azul	12500	4500	5000	1.41E+11	10000	700	650	350	50	300	200	1.00E+07	30000	0.83333333	5	7.2	0.122324159	21.92646858	7.86E-03	2.58721249
Morro Azul	12500	4500	5000	1.41E+11	10000	700	600	350	100	300	200	1.00E+08	30000	0.83333333	5	7.2	0.122324159	38.99138762	2.49E-03	4.60078669
Morro Azul	12500	4500	5000	1.41E+11	10000	700	600	350	100	250	200	1.00E+04	30000	1	2.5	2.5	0.12232416	1.763698417	5.09E-02	4.97124533
Morro Azul	12500	4500	5000	1.41E+11	10000	700	600	350	100	250	200	1.00E+05	30000	1	2.5	2.5	0.122324159	3.136348581	1.61E-02	8.84026321
Morro Azul	12500	4500	5000	1.41E+11	10000	700	600	350	100	250	200	1.00E+06	30000	1	2.5	2.5	0.122324159	5.577304105	5.09E-03	15.720458
Morro Azul	12500	4500	5000	1.41E+11	10000	700	600	350	100	250	200	1.00E+07	30000	1	2.5	2.5	0.122324159	9.918005053	1.61E-03	27.9553669
Morro Azul	12500	4500	5000	1.41E+11	10000	700	600	350	100	250	200	1.00E+08	30000	1	2.5	2.5	0.122324159	17.63698417	5.09E-04	49.7124533
Morro Azul	12500	4500	5000	1.41E+11	10000	700	550	350	150	200	200	1.00E+04	30000	1.25	1.06666667	1.06666667	0.12232416	0.931088283	1.42E-02	33.7882413
Morro Azul	12500	4500	5000	1.41E+11	10000	700	550	350	150	200	200	1.00E+05	30000	1.25	1.06666667	1.06666667	0.122324159	1.655735123	4.48E-03	60.0849338
Morro Azul	12500	4500	5000	1.41E+11	10000	700	550	350	150	200	200	1.00E+06	30000	1.25	1.06666667	1.06666667	0.122324159	2.944359677	1.42E-03	106.847801
Morro Azul	12500	4500	5000	1.41E+11	10000	700	550	350	150	200	200	1.00E+07	30000	1.25	1.06666667	1.06666667	0.122324159	5.235894189	4.48E-04	190.005244
Morro Azul	12500	4500	5000	1.41E+11	10000	700	550	350	150	200	200	1.00E+08	30000	1.25	1.06666667	1.06666667	0.122324159	9.31088283	1.42E-04	337.882413
Morro Azul	12500	4500	5000	1.41E+11	4000	900	750	350	150	400	200	1.00E+04	30000	0.625	1.66666667	4.26666667	0.12232416	2.633515355	1.13E-01	3.7310852
Morro Azul	12500	4500	5000	1.41E+11	4000	900	750	350	150	400	200	1.00E+05	30000	0.625	1.66666667	4.26666667	0.122324159	4.683126132	3.59E-02	6.63851003
Morro Azul	12500	4500	5000	1.41E+11	4000	900	750	350	150	400	200	1.00E+06	30000	0.625	1.66666667	4.26666667	0.122324159	8.327906775	1.13E-02	11.8051257
Morro Azul	12500	4500	5000	1.41E+11	4000	900	750	350	150	400	200	1.00E+07	30000	0.625	1.66666667	4.26666667	0.122324159	14.80934515	3.59E-03	20.9928119
Morro Azul	12500	4500	5000	1.41E+11	4000	900	700	350	200	350	200	1.00E+08	30000	0.625	1.66666667	4.26666667	0.122324159	26.33515355	1.13E-03	37.3310852
Morro Azul	12500	4500	5000	1.41E+11	4000	900	700	350	200	350	200	1.00E+04	30000	0.71428571	1.25	2.45	0.12232416	1.737176245	4.93E-02	13.0060834
Morro Azul	12500	4500	5000	1.41E+11	4000	900	700	350	200	350	200	1.00E+05	30000	0.71428571	1.25	2.45	0.122324159	3.089184748	1.56E-02	23.1284503
Morro Azul	12500	4500	5000	1.41E+11	4000	900	700	350	200	350	200	1.00E+06	30000	0.71428571	1.25	2.45	0.122324159	5.493433632	4.93E-03	41.128847
Morro Azul	12500	4500	5000	1.41E+11	4000	900	700	350	200	350	200	1.00E+07	30000	0.71428571	1.25	2.45	0.122324159	9.768859917	1.56E-03	73.1385817
Morro Azul	12500	4500	5000	1.41E+11	4000	900	650	350	250	300	200	1.00E+08	30000	0.71428571	1.25	2.45	0.122324159	17.37176245	4.93E-04	130.060834
Morro Azul	12500	4500	5000	1.41E+11	4000	900	650	350	250	300	200	1.00E+04	30000	0.83333333	1	1.44	0.12232416	1.166114479	2.22E-02	42.9986298
Morro Azul	12500	4500	5000	1.41E+11	4000	900	650	350	250	300	200	1.00E+05	30000	0.83333333	1	1.44	0.122324159	2.073677368	7.03E-03	76.4635781
Morro Azul	12500	4500	5000	1.41E+11	4000	900	650	350	250	300	200	1.00E+06	30000	0.83333333	1	1.44	0.122324159	3.687577766	2.22E-03	135.973607
Morro Azul	12500	4500	5000	1.41E+11	4000	900	650	350	250	300	200	1.00E+07	30000	0.83333333	1	1.44	0.122324159	6.557543615	7.03E-04	241.799065
Morro Azul	12500	4500	5000	1.41E+11	4000	900	650	350	250	300	200	1.00E+08	30000	0.83333333	1	1.44	0.122324159	11.66114479	2.22E-04	429.986298
Morro Azul	12500	4500	5000	1.41E+11	4000	900	600	350	300	250	200	1.00E+04	30000	1	0.83333333	0.83333333	0.12232416	0.773719218	9.79E-03	147.206853
Morro Azul	12500	4500	5000	1.41E+11	4000	900	600	350	300	250	200									

Morro Azul	12500	4500	5000	1.41E+11	4000	800	700	350	100	350	200	1.00E+06	30000	0.71428571	2.5	4.9	12.2324159	9.238817296	1.40E-02	8.64627499
Morro Azul	12500	4500	5000	1.41E+11	4000	800	700	350	100	350	200	1.00E+07	30000	0.71428571	2.5	4.9	122.324159	16.42919857	4.41E-03	15.3754928
Morro Azul	12500	4500	5000	1.41E+11	4000	800	700	350	100	350	200	1.00E+08	30000	0.71428571	2.5	4.9	1223.24159	29.21570554	1.40E-03	27.3419222
Morro Azul	12500	4500	5000	1.41E+11	4000	800	650	350	150	300	200	1.00E+04	30000	0.83333333	1.66666667	2.4	0.12232416	1.710518399	4.78E-02	13.6236956
Morro Azul	12500	4500	5000	1.41E+11	4000	800	650	350	150	300	200	1.00E+05	30000	0.83333333	1.66666667	2.4	1.22324159	3.04177965	1.51E-02	24.2267373
Morro Azul	12500	4500	5000	1.41E+11	4000	800	650	350	150	300	200	1.00E+06	30000	0.83333333	1.66666667	2.4	12.2324159	5.409134121	4.78E-03	43.0819081
Morro Azul	12500	4500	5000	1.41E+11	4000	800	650	350	150	300	200	1.00E+07	30000	0.83333333	1.66666667	2.4	122.324159	9.618951833	1.51E-03	76.6116702
Morro Azul	12500	4500	5000	1.41E+11	4000	800	650	350	150	300	200	1.00E+08	30000	0.83333333	1.66666667	2.4	1223.24159	17.10518399	4.78E-04	136.236956
Morro Azul	12500	4500	5000	1.41E+11	4000	800	600	350	200	250	200	1.00E+04	30000	1	1.25	1.25	0.12232416	1.048701353	1.80E-02	59.1184031
Morro Azul	12500	4500	5000	1.41E+11	4000	800	600	350	200	250	200	1.00E+05	30000	1	1.25	1.25	1.22324159	1.864884024	5.69E-03	105.129039
Morro Azul	12500	4500	5000	1.41E+11	4000	800	600	350	200	250	200	1.00E+06	30000	1	1.25	1.25	12.2324159	3.316284862	1.80E-03	186.948806
Morro Azul	12500	4500	5000	1.41E+11	4000	800	600	350	200	250	200	1.00E+07	30000	1	1.25	1.25	122.324159	5.897281088	5.69E-04	332.447212
Morro Azul	12500	4500	5000	1.41E+11	4000	800	600	350	200	250	200	1.00E+08	30000	1	1.25	1.25	1223.24159	10.48701353	1.80E-04	591.184031
Morro Azul	12500	4500	5000	1.41E+11	4000	800	550	350	250	200	200	1.00E+04	30000	1.25	1	0.64	0.12232416	0.634752323	6.59E-03	266.603154
Morro Azul	12500	4500	5000	1.41E+11	4000	800	550	350	250	200	200	1.00E+05	30000	1.25	1	0.64	1.22324159	1.128766987	2.08E-03	474.094899
Morro Azul	12500	4500	5000	1.41E+11	4000	800	550	350	250	200	200	1.00E+06	30000	1.25	1	0.64	12.2324159	2.007263092	6.59E-04	843.073197
Morro Azul	12500	4500	5000	1.41E+11	4000	800	550	350	250	200	200	1.00E+07	30000	1.25	1	0.64	122.324159	3.569474627	2.08E-04	1499.21971
Morro Azul	12500	4500	5000	1.41E+11	4000	800	550	350	250	200	200	1.00E+08	30000	1.25	1	0.64	1223.24159	6.347523234	6.59E-05	2666.03154
Morro Azul	12500	4500	5000	1.41E+11	4000	700	650	350	50	300	200	1.00E+04	30000	0.83333333	5	7.2	0.12232416	3.899138762	2.49E-01	1.15019667
Morro Azul	12500	4500	5000	1.41E+11	4000	700	650	350	50	300	200	1.00E+05	30000	0.83333333	5	7.2	1.22324159	6.933758177	7.86E-02	2.04537106
Morro Azul	12500	4500	5000	1.41E+11	4000	700	650	350	50	300	200	1.00E+06	30000	0.83333333	5	7.2	12.2324159	12.3301594	2.49E-02	3.63724124
Morro Azul	12500	4500	5000	1.41E+11	4000	700	650	350	50	300	200	1.00E+07	30000	0.83333333	5	7.2	122.324159	21.92646858	7.86E-03	6.46803121
Morro Azul	12500	4500	5000	1.41E+11	4000	700	650	350	50	300	200	1.00E+08	30000	0.83333333	5	7.2	1223.24159	38.99138762	2.49E-03	11.5019667
Morro Azul	12500	4500	5000	1.41E+11	4000	700	600	350	100	250	200	1.00E+04	30000	1	2.5	2.5	0.12232416	1.763698417	5.09E-02	12.4281133
Morro Azul	12500	4500	5000	1.41E+11	4000	700	600	350	100	250	200	1.00E+05	30000	1	2.5	2.5	1.22324159	3.136348581	1.61E-02	22.100658
Morro Azul	12500	4500	5000	1.41E+11	4000	700	600	350	100	250	200	1.00E+06	30000	1	2.5	2.5	12.2324159	5.577304105	5.09E-03	39.3011451
Morro Azul	12500	4500	5000	1.41E+11	4000	700	600	350	100	250	200	1.00E+07	30000	1	2.5	2.5	122.324159	9.918005053	1.61E-03	69.8884171
Morro Azul	12500	4500	5000	1.41E+11	4000	700	600	350	100	250	200	1.00E+08	30000	1	2.5	2.5	1223.24159	17.63698417	5.09E-04	124.281133
Morro Azul	12500	4500	5000	1.41E+11	4000	700	550	350	150	200	200	1.00E+04	30000	1.25	1.66666667	1.06666667	0.12232416	0.931088283	1.42E-02	84.4706033
Morro Azul	12500	4500	5000	1.41E+11	4000	700	550	350	150	200	200	1.00E+05	30000	1.25	1.66666667	1.06666667	1.22324159	1.655735123	4.48E-03	150.212335
Morro Azul	12500	4500	5000	1.41E+11	4000	700	550	350	150	200	200	1.00E+06	30000	1.25	1.66666667	1.06666667	12.2324159	2.944359677	1.42E-03	267.119502
Morro Azul	12500	4500	5000	1.41E+11	4000	700	550	350	150	200	200	1.00E+07	30000	1.25	1.66666667	1.06666667	122.324159	5.235894189	4.48E-04	475.01311
Morro Azul	12500	4500	5000	1.41E+11	1000	900	750	350	150	200	200	1.00E+08	30000	1.25	1.66666667	1.06666667	1223.24159	9.31088283	1.42E-04	844.706033
Morro Azul	12500	4500	5000	1.41E+11	1000	900	750	350	150	400	200	1.00E+04	30000	0.625	1.66666667	4.26666667	0.12232416	2.633515355	1.13E-01	14.9324341
Morro Azul	12500	4500	5000	1.41E+11	1000	900	750	350	150	400	200	1.00E+05	30000	0.625	1.66666667	4.26666667	1.22324159	4.683126132	3.59E-02	26.55040401
Morro Azul	12500	4500	5000	1.41E+11	1000	900	750	350	150	400	200	1.00E+06	30000	0.625	1.66666667	4.26666667	12.2324159	8.327906775	1.13E-02	47.2205028
Morro Azul	12500	4500	5000	1.41E+11	1000	900	750	350	150	400	200	1.00E+07	30000	0.625	1.66666667	4.26666667	122.324159	14.80934515	3.59E-03	83.9712478
Morro Azul	12500	4500	5000	1.41E+11	1000	900	750	350	150	400	200	1.00E+08	30000	0.625	1.66666667	4.26666667	1223.24159	26.33515355	1.13E-03	149.324341
Morro Azul	12500	4500	5000	1.41E+11	1000	900	700	350	200	350	200	1.00E+04	30000	0.71428571	1.25	2.45	0.12232416	1.737176245	4.93E-02	52.0243336
Morro Azul	12500	4500	5000	1.41E+11	1000	900	700	350	200	350	200	1.00E+05	30000	0.71428571	1.25	2.45	1.22324159	3.089184748	1.56E-02	92.5138012
Morro Azul	12500	4500	5000	1.41E+11	1000	900	700	350	200	350	200	1.00E+06	30000	0.71428571	1.25	2.45	12.2324159	5.493433632	4.93E-03	164.515388
Morro Azul	12500	4500	5000	1.41E+11	1000	900	700	350	200	350	200	1.00E+07	30000	0.71428571	1.25	2.45	122.324159	9.768859917	1.56E-03	292.554327
Morro Azul	12500	4500	5000	1.41E+11	1000	900	700	350	200	350	200	1.00E+08	30000	0.71428571	1.25	2.45	1223.24159	17.37176245	4.93E-04	520.243336
Morro Azul	12500	4500	5000	1.41E+11	1000	900	650	350	250	300	200	1.00E+04	30000	0.83333333	1	1.44	0.12232416	1.166114479	2.22E-02	171.994519
Morro Azul	12500	4500	5000	1.41E+11	1000	900	650	350	250	300	200	1.00E+05	30000	0.83333333	1	1.44	1.22324159	2.073677368	7.03E-03	305.854312
Morro Azul	12500	4500	5000	1.41E+11	1000	900	650	350	250	300	200	1.00E+06	30000	0.83333333	1	1.44	12.2324159	3.687577766	2.22E-03	543.894426
Morro Azul	12500	4500	5000	1.41E+11	1000	900	650	350	250	300	200	1.00E+07	30000	0.83333333	1	1.44	122.324159	6.557543615	7.03E-04	967.196259
Morro Azul	12500	4500	5000	1.41E+11	1000	900	650	350	250	300	200	1.00E+08	30000	0.83333333	1	1.44	1223.24159	11.66114479	2.22E-04	1719.94519
Morro Azul	12500	4500	5000	1.41E+11	1000	900	600	350	300	250	200	1.00E+04	30000	1	0.83333333	0.83333333	0.12232416	0.773719218	9.79E-03	588.627411
Morro Azul	12500	4500	5000	1.41E+11	1000	900	600	350	300	250	200	1.00E+05	30000	1	0.83333333	0.83333333	1.22324159	1.375888954	3.10E-03	1047.09966
Morro Azul	12500	4500	5000	1.41E+11	1000	900	600	350	300	250	200	1.00E+06	30000	1	0.83333333	0.83333333	12.2324159	2.446714998	9.79E-04	1852.03577
Morro Azul	12500	4500	5000	1.41E+11	1000	900	600	350	300	250	200	1.00E+07	30000	1	0.83333333	0.83333333	122.324159	4.350942904	3.10E-04	3311.21987
Morro Azul	12500	4500	5000	1.41E+11	1000	900	550	350	350	200	200	1.00E+08	30000	1	0.83333333	0.83333333	1223.24159	7.73719218	9.79E-05	5888.27411
Morro Azul	12500	4500	5000	1.41E+11	1000	900	550	350	350	200	200	1.00E+04	30000	1.25	0.71428571	0.45714286	0.12232416	0.493183198	3.98E-03	2273.5963
Morro Azul	12500	4500	5000	1.41E+11	1000	900	550	350	350	200	200	1.00E+05	30000	1.25	0.71428571	0.45714286	1.22324159	0.877017526	1.26E-03	4043.08949
Morro Azul	12500	4500	5000	1.41E+11	1000															

Morro Azul	12500	4500	5000	1.41E+11	1000	800	650	350	150	300	200	1.00E+07	30000	0.83333333	1.66666667	2.4	122.324159	9.618951833	1.51E-03	306.446681
Morro Azul	12500	4500	5000	1.41E+11	1000	800	650	350	150	300	200	1.00E+08	30000	0.83333333	1.66666667	2.4	1223.24159	17.10518399	4.78E-04	544.947822
Morro Azul	12500	4500	5000	1.41E+11	1000	800	600	350	200	250	200	1.00E+04	30000	1	1.25	1.25	0.12232416	1.048701353	1.80E-02	236.473613
Morro Azul	12500	4500	5000	1.41E+11	1000	800	600	350	200	250	200	1.00E+05	30000	1	1.25	1.25	1.22324159	1.864884024	5.69E-03	420.516156
Morro Azul	12500	4500	5000	1.41E+11	1000	800	600	350	200	250	200	1.00E+06	30000	1	1.25	1.25	12.2324159	3.316284862	1.80E-03	747.759222
Morro Azul	12500	4500	5000	1.41E+11	1000	800	600	350	200	250	200	1.00E+07	30000	1	1.25	1.25	122.324159	5.897281088	5.69E-04	1329.78885
Morro Azul	12500	4500	5000	1.41E+11	1000	800	600	350	200	250	200	1.00E+08	30000	1	1.25	1.25	1223.24159	10.48701353	1.80E-04	2364.73613
Morro Azul	12500	4500	5000	1.41E+11	1000	800	550	350	250	200	200	1.00E+04	30000	1.25	1	0.64	0.12232416	0.634752323	6.59E-03	1066.41262
Morro Azul	12500	4500	5000	1.41E+11	1000	800	550	350	250	200	200	1.00E+05	30000	1.25	1	0.64	1.22324159	1.128766987	2.08E-03	1896.3796
Morro Azul	12500	4500	5000	1.41E+11	1000	800	550	350	250	200	200	1.00E+06	30000	1.25	1	0.64	12.2324159	2.007263092	6.59E-04	3372.29279
Morro Azul	12500	4500	5000	1.41E+11	1000	800	550	350	250	200	200	1.00E+07	30000	1.25	1	0.64	122.324159	3.569474627	2.08E-04	5996.87883
Morro Azul	12500	4500	5000	1.41E+11	1000	800	550	350	250	200	200	1.00E+08	30000	1.25	1	0.64	1223.24159	6.347523234	6.59E-05	10664.1262
Morro Azul	12500	4500	5000	1.41E+11	1000	700	650	350	50	300	200	1.00E+04	30000	0.83333333	5	7.2	0.12232416	3.899138762	2.49E-01	4.60078669
Morro Azul	12500	4500	5000	1.41E+11	1000	700	650	350	50	300	200	1.00E+05	30000	0.83333333	5	7.2	1.22324159	6.933758177	7.86E-02	8.18148424
Morro Azul	12500	4500	5000	1.41E+11	1000	700	650	350	50	300	200	1.00E+06	30000	0.83333333	5	7.2	12.2324159	12.3301594	2.49E-02	14.548965
Morro Azul	12500	4500	5000	1.41E+11	1000	700	650	350	50	300	200	1.00E+07	30000	0.83333333	5	7.2	122.324159	21.92646858	7.86E-03	25.8721249
Morro Azul	12500	4500	5000	1.41E+11	1000	700	650	350	50	300	200	1.00E+08	30000	0.83333333	5	7.2	1223.24159	38.99138762	2.49E-04	46.0078669
Morro Azul	12500	4500	5000	1.41E+11	1000	700	600	350	100	250	200	1.00E+04	30000	1	2.5	2.5	0.12232416	1.763698417	5.09E-02	49.7124533
Morro Azul	12500	4500	5000	1.41E+11	1000	700	600	350	100	250	200	1.00E+05	30000	1	2.5	2.5	1.22324159	3.136348581	1.61E-02	86.4026321
Morro Azul	12500	4500	5000	1.41E+11	1000	700	600	350	100	250	200	1.00E+06	30000	1	2.5	2.5	12.2324159	5.577304105	5.09E-03	157.20458
Morro Azul	12500	4500	5000	1.41E+11	1000	700	600	350	100	250	200	1.00E+07	30000	1	2.5	2.5	122.324159	9.918005053	1.61E-03	279.553669
Morro Azul	12500	4500	5000	1.41E+11	1000	700	600	350	100	250	200	1.00E+08	30000	1	2.5	2.5	1223.24159	17.63698417	5.09E-04	497.124533
Morro Azul	12500	4500	5000	1.41E+11	1000	700	550	350	150	200	200	1.00E+04	30000	1.25	1.66666667	1.06666667	0.12232416	0.931088283	1.42E-02	337.882413
Morro Azul	12500	4500	5000	1.41E+11	1000	700	550	350	150	200	200	1.00E+05	30000	1.25	1.66666667	1.06666667	1.22324159	1.655735123	4.48E-03	600.849338
Morro Azul	12500	4500	5000	1.41E+11	1000	700	550	350	150	200	200	1.00E+06	30000	1.25	1.66666667	1.06666667	12.2324159	2.944359677	1.42E-03	1068.47801
Morro Azul	12500	4500	5000	1.41E+11	1000	700	550	350	150	200	200	1.00E+07	30000	1.25	1.66666667	1.06666667	122.324159	5.235894189	4.48E-04	1900.05244
Morro Azul	12500	4500	5000	1.41E+11	1000	700	550	350	150	200	200	1.00E+08	30000	1.25	1.66666667	1.06666667	1223.24159	9.31088283	1.42E-04	3378.82413
Pluton	length	width	depth	volume	lateral extent	Tm,initial	Tw,freezing	Tinf,lar field	Magma superheat	Magma undercooling	Density difference	viscosity	Dyke length	Sint	Sm	snv/sint^2	ukH/gp	dyke width	average vel/tr	time taken/yr
Itapeti	12500	2000	5000	6.25E+10	10000	900	750	350	150	400	200	1.00E+04	30000	0.625	1.66666667	4.26666667	0.12232416	2.633515355	1.13E-01	0.66366374
Itapeti	12500	2000	5000	6.25E+10	10000	900	750	350	150	400	200	1.00E+05	30000	0.625	1.66666667	4.26666667	1.22324159	4.683126132	3.59E-02	1.18017956
Itapeti	12500	2000	5000	6.25E+10	10000	900	750	350	150	400	200	1.00E+06	30000	0.625	1.66666667	4.26666667	12.2324159	8.327906775	1.13E-02	2.09868901
Itapeti	12500	2000	5000	6.25E+10	10000	900	750	350	150	400	200	1.00E+07	30000	0.625	1.66666667	4.26666667	122.324159	14.80934515	3.59E-03	3.73205546
Itapeti	12500	2000	5000	6.25E+10	10000	900	750	350	150	400	200	1.00E+08	30000	0.625	1.66666667	4.26666667	1223.24159	26.33515355	1.13E-03	6.63663738
Itapeti	12500	2000	5000	6.25E+10	10000	900	700	350	200	350	200	1.00E+04	30000	0.71428571	1.25	2.45	0.12232416	1.737176245	4.93E-02	2.3121926
Itapeti	12500	2000	5000	6.25E+10	10000	900	700	350	200	350	200	1.00E+05	30000	0.71428571	1.25	2.45	1.22324159	3.089184748	1.56E-02	4.1117245
Itapeti	12500	2000	5000	6.25E+10	10000	900	700	350	200	350	200	1.00E+06	30000	0.71428571	1.25	2.45	12.2324159	5.493433632	4.93E-03	7.31179501
Itapeti	12500	2000	5000	6.25E+10	10000	900	700	350	200	350	200	1.00E+07	30000	0.71428571	1.25	2.45	122.324159	9.768859917	1.56E-03	13.0024145
Itapeti	12500	2000	5000	6.25E+10	10000	900	700	350	200	350	200	1.00E+08	30000	0.71428571	1.25	2.45	1223.24159	17.37176245	4.93E-04	23.121926
Itapeti	12500	2000	5000	6.25E+10	10000	900	650	350	250	300	200	1.00E+04	30000	0.83333333	1	1.44	0.12232416	1.166114479	2.22E-02	7.64420086
Itapeti	12500	2000	5000	6.25E+10	10000	900	650	350	250	300	200	1.00E+05	30000	0.83333333	1	1.44	1.22324159	2.073677368	7.03E-03	13.593525
Itapeti	12500	2000	5000	6.25E+10	10000	900	650	350	250	300	200	1.00E+06	30000	0.83333333	1	1.44	12.2324159	3.687577766	2.22E-03	24.1730856
Itapeti	12500	2000	5000	6.25E+10	10000	900	650	350	250	300	200	1.00E+07	30000	0.83333333	1	1.44	122.324159	6.557543615	7.03E-04	42.9865004
Itapeti	12500	2000	5000	6.25E+10	10000	900	650	350	250	300	200	1.00E+08	30000	0.83333333	1	1.44	1223.24159	11.66114479	2.22E-04	76.4420086
Itapeti	12500	2000	5000	6.25E+10	10000	900	600	350	300	250	200	1.00E+04	30000	1	0.83333333	0.83333333	0.12232416	0.773719218	9.79E-03	26.1701072
Itapeti	12500	2000	5000	6.25E+10	10000	900	600	350	300	250	200	1.00E+05	30000	1	0.83333333	0.83333333	1.22324159	1.375888954	3.10E-03	46.5377627
Itapeti	12500	2000	5000	6.25E+10	10000	900	600	350	300	250	200	1.00E+06	30000	1	0.83333333	0.83333333	12.2324159	2.446714998	9.79E-04	82.7571452
Itapeti	12500	2000	5000	6.25E+10	10000	900	600	350	300	250	200	1.00E+07	30000	1	0.83333333	0.83333333	122.324159	4.350942904	3.10E-04	147.165327
Itapeti	12500	2000	5000	6.25E+10	10000	900	600	350	300	250	200	1.00E+08	30000	1	0.83333333	0.83333333	1223.24159	7.73719218	9.79E-05	261.701072
Itapeti	12500	2000	5000	6.25E+10	10000	900	550	350	350	200	200	1.00E+04	30000	1.25	0.71428571	0.45714286	0.12232416	0.493183198	3.98E-03	101.048725
Itapeti	12500	2000	5000	6.25E+10	10000	900	550	350	350	200	200	1.00E+05	30000	1.25	0.71428571	0.45714286	1.22324159	0.877017526	1.26E-03	179.692866
Itapeti	12500	2000	5000	6.25E+10	10000	900	550	350	350	200	200	1.00E+06	30000	1.25	0.71428571	0.45714286	12.2324159	1.55958221	3.98E-04	319.544124
Itapeti	12500	2000	5000	6.25E+10	10000	900	550	350	350	200	200	1.00E+07	30000	1.25	0.71428571	0.45714286	122.324159	2.773372931	1.26E-04	568.238737
Itapeti	12500	2000	5000	6.25E+10	10000	900	550	350	350	200	200	1.00E+08	30000	1.25	0.71428571	0.45714286	1223.24159	4.93183198	3.98E-05	1010.48725
Itapeti	12500	2000	5000	6.25E+10	10000	800	750	350	50	400	200	1.00E+04	30000	0.625	5	12.8	0.12232416	6.003116837	5.89E-01	0.0560306
Itapeti	12500	2000	5000	6.25E+10	10000	800	750	350	50	400	200	1.00E+05	30000	0.625	5	12.8	1.22324159	10.67521907	1.86E-01	0.09963806
Itapeti	12500	2000	5000	6.25E+10	10000	800	750	350	50	400	200	1.00E+06	30000	0.625</						

Itapeti	12500	2000	5000	6.25E+10	10000	800	600	350	200	250	200	1.00E+07	30000	1	1.25	1.25	122.324159	5.897281088	5.69E-04	59.1017265
Itapeti	12500	2000	5000	6.25E+10	10000	800	600	350	200	250	200	1.00E+08	30000	1	1.25	1.25	1223.24159	10.48701353	1.80E-04	105.099383
Itapeti	12500	2000	5000	6.25E+10	10000	800	550	350	250	200	200	1.00E+04	30000	1.25	1	0.64	0.12232416	0.634752323	6.59E-03	47.3961162
Itapeti	12500	2000	5000	6.25E+10	10000	800	550	350	250	200	200	1.00E+05	30000	1.25	1	0.64	1.22324159	1.128766987	2.08E-03	84.2835376
Itapeti	12500	2000	5000	6.25E+10	10000	800	550	350	250	200	200	1.00E+06	30000	1.25	1	0.64	12.2324159	2.007263092	6.59E-04	149.87968
Itapeti	12500	2000	5000	6.25E+10	10000	800	550	350	250	200	200	1.00E+07	30000	1.25	1	0.64	122.324159	3.569474627	2.08E-04	266.527948
Itapeti	12500	2000	5000	6.25E+10	10000	800	550	350	250	200	200	1.00E+08	30000	1.25	1	0.64	1223.24159	6.347523234	6.59E-05	473.961162
Itapeti	12500	2000	5000	6.25E+10	10000	700	650	350	50	300	200	1.00E+04	30000	0.833333333	5	7.2	0.12232416	3.899138762	2.49E-01	0.20447941
Itapeti	12500	2000	5000	6.25E+10	10000	700	650	350	50	300	200	1.00E+05	30000	0.833333333	5	7.2	1.22324159	6.933758177	7.86E-02	0.36362152
Itapeti	12500	2000	5000	6.25E+10	10000	700	650	350	50	300	200	1.00E+06	30000	0.833333333	5	7.2	12.2324159	12.3301594	2.49E-02	0.64662067
Itapeti	12500	2000	5000	6.25E+10	10000	700	650	350	50	300	200	1.00E+07	30000	0.833333333	5	7.2	122.324159	21.92646058	7.86E-03	1.14987222
Itapeti	12500	2000	5000	6.25E+10	10000	700	650	350	50	300	200	1.00E+08	30000	0.833333333	5	7.2	1223.24159	38.99138762	2.49E-03	2.04479409
Itapeti	12500	2000	5000	6.25E+10	10000	700	600	350	100	250	200	1.00E+04	30000	1	2.5	2.5	0.12232416	1.763698417	5.09E-02	2.20944237
Itapeti	12500	2000	5000	6.25E+10	10000	700	600	350	100	250	200	1.00E+05	30000	1	2.5	2.5	1.22324159	3.136348581	1.61E-02	3.92900587
Itapeti	12500	2000	5000	6.25E+10	10000	700	600	350	100	250	200	1.00E+06	30000	1	2.5	2.5	12.2324159	5.577304105	5.09E-03	6.98687024
Itapeti	12500	2000	5000	6.25E+10	10000	700	600	350	100	250	200	1.00E+07	30000	1	2.5	2.5	122.324159	9.918005053	1.61E-03	12.4246075
Itapeti	12500	2000	5000	6.25E+10	10000	700	600	350	100	250	200	1.00E+08	30000	1	2.5	2.5	1223.24159	17.63698417	5.09E-04	22.0944237
Itapeti	12500	2000	5000	6.25E+10	10000	700	550	350	150	200	200	1.00E+04	30000	1.25	1.66666667	1.06666667	0.12232416	0.931088283	1.42E-02	15.0169961
Itapeti	12500	2000	5000	6.25E+10	10000	700	550	350	150	200	200	1.00E+05	30000	1.25	1.66666667	1.06666667	1.22324159	1.655735123	4.48E-03	26.704415
Itapeti	12500	2000	5000	6.25E+10	10000	700	550	350	150	200	200	1.00E+06	30000	1.25	1.66666667	1.06666667	12.2324159	2.944359677	1.42E-03	47.4879114
Itapeti	12500	2000	5000	6.25E+10	10000	700	550	350	150	200	200	1.00E+07	30000	1.25	1.66666667	1.06666667	122.324159	5.235894189	4.48E-04	84.4467751
Itapeti	12500	2000	5000	6.25E+10	10000	700	550	350	150	200	200	1.00E+08	30000	1.25	1.66666667	1.06666667	1223.24159	9.31088283	1.42E-04	150.169961
Itapeti	12500	2000	5000	6.25E+10	4000	900	750	350	150	400	200	1.00E+04	30000	0.625	1.66666667	4.26666667	0.12232416	2.633515355	1.13E-01	1.65915934
Itapeti	12500	2000	5000	6.25E+10	4000	900	750	350	150	400	200	1.00E+05	30000	0.625	1.66666667	4.26666667	1.22324159	4.683126132	3.59E-02	2.9504489
Itapeti	12500	2000	5000	6.25E+10	4000	900	750	350	150	400	200	1.00E+06	30000	0.625	1.66666667	4.26666667	12.2324159	8.327906775	1.13E-02	5.24672253
Itapeti	12500	2000	5000	6.25E+10	4000	900	750	350	150	400	200	1.00E+07	30000	0.625	1.66666667	4.26666667	122.324159	14.80934515	3.59E-03	9.33013864
Itapeti	12500	2000	5000	6.25E+10	4000	900	750	350	150	400	200	1.00E+08	30000	0.625	1.66666667	4.26666667	1223.24159	26.33515355	1.13E-03	16.5915934
Itapeti	12500	2000	5000	6.25E+10	4000	900	700	350	200	350	200	1.00E+04	30000	0.71428571	1.25	2.45	0.12232416	1.737176245	4.93E-02	5.78048151
Itapeti	12500	2000	5000	6.25E+10	4000	900	700	350	200	350	200	1.00E+05	30000	0.71428571	1.25	2.45	1.22324159	3.089184748	1.56E-02	10.2793112
Itapeti	12500	2000	5000	6.25E+10	4000	900	700	350	200	350	200	1.00E+06	30000	0.71428571	1.25	2.45	12.2324159	5.493433632	4.93E-03	18.2794875
Itapeti	12500	2000	5000	6.25E+10	4000	900	700	350	200	350	200	1.00E+07	30000	0.71428571	1.25	2.45	122.324159	9.768859917	1.56E-03	32.5060363
Itapeti	12500	2000	5000	6.25E+10	4000	900	700	350	200	350	200	1.00E+08	30000	0.71428571	1.25	2.45	1223.24159	17.37176245	4.93E-04	57.8048151
Itapeti	12500	2000	5000	6.25E+10	4000	900	650	350	250	300	200	1.00E+04	30000	0.833333333	1	1.44	0.12232416	1.166114479	2.22E-02	19.1105021
Itapeti	12500	2000	5000	6.25E+10	4000	900	650	350	250	300	200	1.00E+05	30000	0.833333333	1	1.44	1.22324159	2.073677368	7.03E-03	33.9838125
Itapeti	12500	2000	5000	6.25E+10	4000	900	650	350	250	300	200	1.00E+06	30000	0.833333333	1	1.44	12.2324159	3.687577766	2.22E-03	60.432714
Itapeti	12500	2000	5000	6.25E+10	4000	900	650	350	250	300	200	1.00E+07	30000	0.833333333	1	1.44	122.324159	6.557543615	7.03E-04	107.466251
Itapeti	12500	2000	5000	6.25E+10	4000	900	600	350	250	300	200	1.00E+08	30000	0.833333333	1	1.44	1223.24159	11.66114479	2.22E-04	191.105021
Itapeti	12500	2000	5000	6.25E+10	4000	900	600	350	250	300	200	1.00E+04	30000	1	0.833333333	0.833333333	0.12232416	0.773719218	9.79E-03	65.4252679
Itapeti	12500	2000	5000	6.25E+10	4000	900	600	350	250	300	200	1.00E+05	30000	1	0.833333333	0.833333333	1.22324159	1.375888954	3.10E-03	116.344407
Itapeti	12500	2000	5000	6.25E+10	4000	900	600	350	250	300	200	1.00E+06	30000	1	0.833333333	0.833333333	12.2324159	2.446714988	9.79E-04	206.892863
Itapeti	12500	2000	5000	6.25E+10	4000	900	600	350	250	300	200	1.00E+07	30000	1	0.833333333	0.833333333	122.324159	4.350942904	3.10E-04	367.913318
Itapeti	12500	2000	5000	6.25E+10	4000	900	600	350	250	300	200	1.00E+08	30000	1	0.833333333	0.833333333	1223.24159	7.73719218	9.79E-05	654.252679
Itapeti	12500	2000	5000	6.25E+10	4000	900	550	350	200	350	200	1.00E+04	30000	1.25	0.71428571	0.45714286	0.12232416	0.493183198	3.98E-03	252.621811
Itapeti	12500	2000	5000	6.25E+10	4000	900	550	350	200	350	200	1.00E+05	30000	1.25	0.71428571	0.45714286	1.22324159	0.877017526	1.26E-03	448.232166
Itapeti	12500	2000	5000	6.25E+10	4000	900	550	350	200	350	200	1.00E+06	30000	1.25	0.71428571	0.45714286	12.2324159	1.55958221	3.98E-04	798.86031
Itapeti	12500	2000	5000	6.25E+10	4000	900	550	350	200	350	200	1.00E+07	30000	1.25	0.71428571	0.45714286	122.324159	2.773372931	1.26E-04	1420.59684
Itapeti	12500	2000	5000	6.25E+10	4000	900	550	350	200	350	200	1.00E+08	30000	1.25	0.71428571	0.45714286	1223.24159	4.93183198	3.98E-05	2526.21811
Itapeti	12500	2000	5000	6.25E+10	4000	800	750	350	50	400	200	1.00E+04	30000	0.625	5	12.8	0.12232416	6.003116637	5.89E-01	0.1400765
Itapeti	12500	2000	5000	6.25E+10	4000	800	750	350	50	400	200	1.00E+05	30000	0.625	5	12.8	1.22324159	10.67521907	1.86E-01	0.24909515
Itapeti	12500	2000	5000	6.25E+10	4000	800	750	350	50	400	200	1.00E+06	30000	0.625	5	12.8	12.2324159	18.98352226	5.89E-02	0.44296078
Itapeti	12500	2000	5000	6.25E+10	4000	800	750	350	50	400	200	1.00E+07	30000	0.625	5	12.8	122.324159	33.75800677	1.86E-02	0.78770803
Itapeti	12500	2000	5000	6.25E+10	4000	800	750	350	50	400	200	1.00E+08	30000	0.625	5	12.8	1223.24159	60.03116637	5.89E-03	1.40076498
Itapeti	12500	2000	5000	6.25E+10	4000	800	700	350	100	350	200	1.00E+04	30000	0.71428571	2.5	4.9	0.12232416	2.921570554	1.40E-01	1.21519654
Itapeti	12500	2000	5000	6.25E+10	4000	800	700	350	100	350	200	1.00E+05	30000	0.71428571	2.5	4.9	1.22324159	5.195368762	4.41E-02	2.16095899
Itapeti	12500	2000	5000	6.25E+10	4000	800	700	350	100	350	200	1.00E+06	30000	0.71428571	2.5	4.9	12.2324159	9.238817296	1.40E-02	3.84276888
Itapeti	12500	2000	5000	6.25E+10																

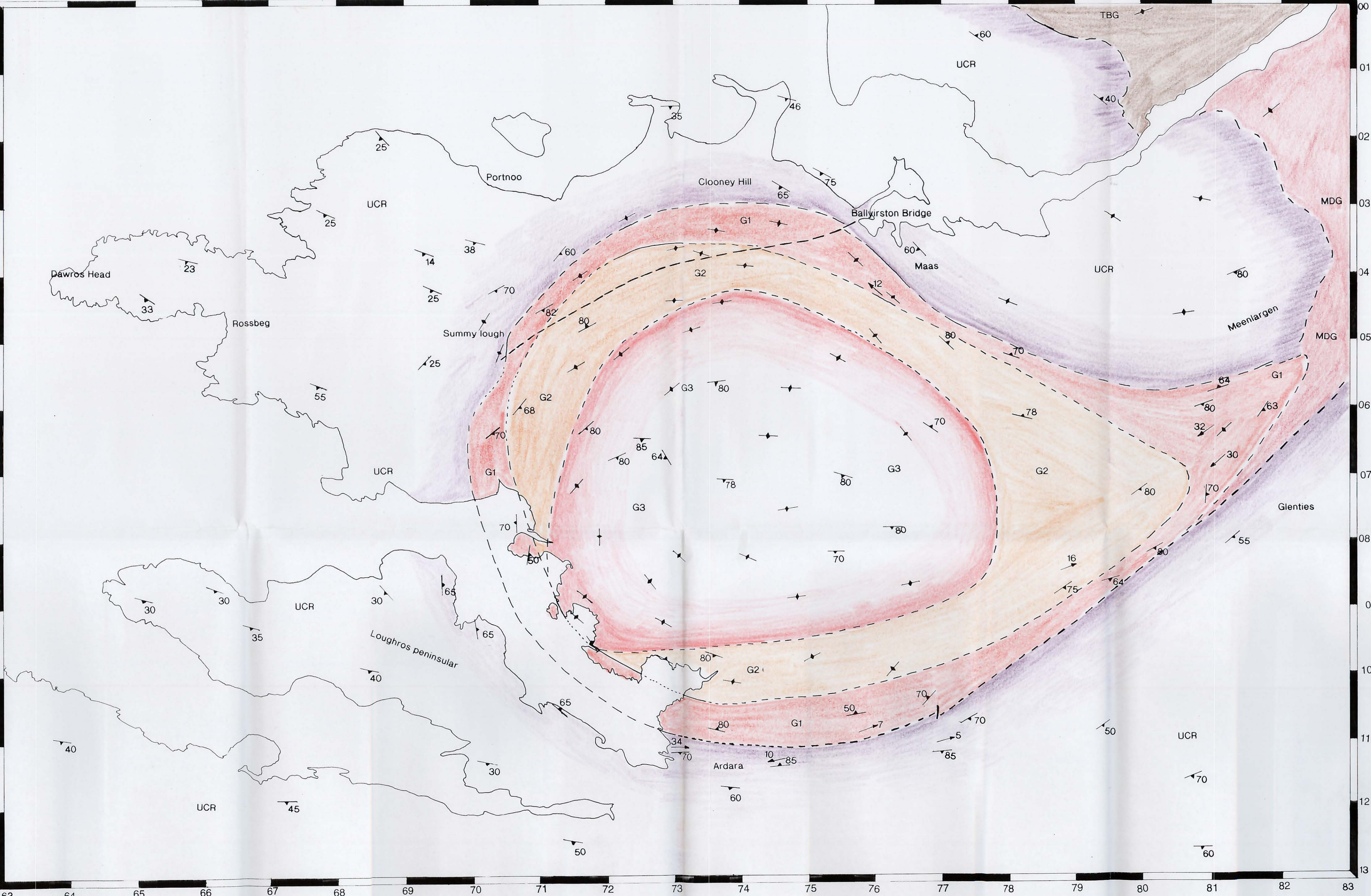
Itapeti	12500	2000	5000	6.25E+10	4000	800	550	350	250	200	1.00E+08	30000	1.25	1	0.64	1223.24159	6.347523234	6.59E-05	1184.90291	
Itapeti	12500	2000	5000	6.25E+10	4000	700	650	350	50	300	200	1.00E+04	30000	0.83333333	5	7.2	0.12232416	3.899138762	2.49E-01	0.51119852
Itapeti	12500	2000	5000	6.25E+10	4000	700	650	350	50	300	200	1.00E+05	30000	0.83333333	5	7.2	1.22324159	6.933758177	7.86E-02	0.9090538
Itapeti	12500	2000	5000	6.25E+10	4000	700	650	350	50	300	200	1.00E+06	30000	0.83333333	5	7.2	12.2324159	12.3301594	2.49E-02	1.61655166
Itapeti	12500	2000	5000	6.25E+10	4000	700	650	350	50	300	200	1.00E+07	30000	0.83333333	5	7.2	122.324159	21.92646858	7.86E-03	2.87468054
Itapeti	12500	2000	5000	6.25E+10	4000	700	650	350	50	300	200	1.00E+08	30000	0.83333333	5	7.2	1223.24159	38.99138762	2.49E-03	5.11198521
Itapeti	12500	2000	5000	6.25E+10	4000	700	600	350	100	250	200	1.00E+04	30000	1	2.5	2.5	0.12232416	1.763698417	5.09E-02	5.52360592
Itapeti	12500	2000	5000	6.25E+10	4000	700	600	350	100	250	200	1.00E+05	30000	1	2.5	2.5	1.22324159	3.136348581	1.61E-02	9.82251468
Itapeti	12500	2000	5000	6.25E+10	4000	700	600	350	100	250	200	1.00E+06	30000	1	2.5	2.5	12.2324159	5.577304105	5.09E-03	17.4671756
Itapeti	12500	2000	5000	6.25E+10	4000	700	600	350	100	250	200	1.00E+07	30000	1	2.5	2.5	122.324159	9.918005053	1.61E-03	31.0615187
Itapeti	12500	2000	5000	6.25E+10	4000	700	600	350	100	250	200	1.00E+08	30000	1	2.5	2.5	1223.24159	17.63698417	5.09E-04	55.2360592
Itapeti	12500	2000	5000	6.25E+10	4000	700	550	350	150	200	200	1.00E+04	30000	1.25	1.66666667	1.06666667	0.12232416	0.931088283	1.42E-02	37.5424904
Itapeti	12500	2000	5000	6.25E+10	4000	700	550	350	150	200	200	1.00E+05	30000	1.25	1.66666667	1.06666667	1.22324159	1.655735123	4.48E-03	66.7610376
Itapeti	12500	2000	5000	6.25E+10	4000	700	550	350	150	200	200	1.00E+06	30000	1.25	1.66666667	1.06666667	12.2324159	2.944359677	1.42E-03	118.719779
Itapeti	12500	2000	5000	6.25E+10	4000	700	550	350	150	200	200	1.00E+07	30000	1.25	1.66666667	1.06666667	122.324159	5.235894189	4.48E-04	211.116938
Itapeti	12500	2000	5000	6.25E+10	4000	700	550	350	150	200	200	1.00E+08	30000	1.25	1.66666667	1.06666667	1223.24159	9.31088283	1.42E-04	375.424904
Itapeti	12500	2000	5000	6.25E+10	1000	800	750	350	150	400	200	1.00E+04	30000	0.625	1.66666667	4.26666667	0.12232416	2.633515355	1.13E-01	6.63663738
Itapeti	12500	2000	5000	6.25E+10	1000	800	750	350	150	400	200	1.00E+05	30000	0.625	1.66666667	4.26666667	1.22324159	4.683126132	3.59E-02	11.8017956
Itapeti	12500	2000	5000	6.25E+10	1000	800	750	350	150	400	200	1.00E+06	30000	0.625	1.66666667	4.26666667	12.2324159	8.327906775	1.13E-02	20.8868901
Itapeti	12500	2000	5000	6.25E+10	1000	800	750	350	150	400	200	1.00E+07	30000	0.625	1.66666667	4.26666667	122.324159	14.80934515	3.59E-03	37.3205546
Itapeti	12500	2000	5000	6.25E+10	1000	800	750	350	150	400	200	1.00E+08	30000	0.625	1.66666667	4.26666667	1223.24159	26.33515355	1.13E-03	66.3663738
Itapeti	12500	2000	5000	6.25E+10	1000	900	700	350	200	350	200	1.00E+04	30000	0.71428571	1.25	2.45	0.12232416	1.737176245	4.93E-02	23.121926
Itapeti	12500	2000	5000	6.25E+10	1000	900	700	350	200	350	200	1.00E+05	30000	0.71428571	1.25	2.45	1.22324159	3.089184748	1.56E-02	41.117245
Itapeti	12500	2000	5000	6.25E+10	1000	900	700	350	200	350	200	1.00E+06	30000	0.71428571	1.25	2.45	12.2324159	5.493433632	4.93E-03	73.1719501
Itapeti	12500	2000	5000	6.25E+10	1000	900	700	350	200	350	200	1.00E+07	30000	0.71428571	1.25	2.45	122.324159	9.768859917	1.56E-03	130.024145
Itapeti	12500	2000	5000	6.25E+10	1000	900	700	350	200	350	200	1.00E+08	30000	0.71428571	1.25	2.45	1223.24159	17.37176245	4.93E-04	231.21926
Itapeti	12500	2000	5000	6.25E+10	1000	900	650	350	250	300	200	1.00E+04	30000	0.83333333	1	1.44	0.12232416	1.166114479	2.22E-02	76.4420086
Itapeti	12500	2000	5000	6.25E+10	1000	900	650	350	250	300	200	1.00E+05	30000	0.83333333	1	1.44	1.22324159	2.073677368	7.03E-03	135.93525
Itapeti	12500	2000	5000	6.25E+10	1000	900	650	350	250	300	200	1.00E+06	30000	0.83333333	1	1.44	12.2324159	3.687577766	2.22E-03	241.730856
Itapeti	12500	2000	5000	6.25E+10	1000	900	650	350	250	300	200	1.00E+07	30000	0.83333333	1	1.44	122.324159	6.557543615	7.03E-04	429.865004
Itapeti	12500	2000	5000	6.25E+10	1000	900	650	350	250	300	200	1.00E+08	30000	0.83333333	1	1.44	1223.24159	11.66114479	2.22E-04	764.420086
Itapeti	12500	2000	5000	6.25E+10	1000	900	600	350	300	250	200	1.00E+04	30000	1	0.83333333	0.83333333	0.12232416	0.773719218	9.79E-03	261.701072
Itapeti	12500	2000	5000	6.25E+10	1000	900	600	350	300	250	200	1.00E+05	30000	1	0.83333333	0.83333333	1.22324159	1.375886954	3.10E-03	465.377627
Itapeti	12500	2000	5000	6.25E+10	1000	900	600	350	300	250	200	1.00E+06	30000	1	0.83333333	0.83333333	12.2324159	2.446714998	9.79E-04	827.571452
Itapeti	12500	2000	5000	6.25E+10	1000	900	600	350	300	250	200	1.00E+07	30000	1	0.83333333	0.83333333	122.324159	4.350942904	9.79E-05	1471.85327
Itapeti	12500	2000	5000	6.25E+10	1000	900	550	350	350	200	200	1.00E+08	30000	1	0.83333333	0.83333333	1223.24159	7.73719218	3.10E-04	2617.01072
Itapeti	12500	2000	5000	6.25E+10	1000	900	550	350	350	200	200	1.00E+04	30000	1.25	0.71428571	0.45714286	0.12232416	0.493183198	3.98E-03	1010.48725
Itapeti	12500	2000	5000	6.25E+10	1000	900	550	350	350	200	200	1.00E+05	30000	1.25	0.71428571	0.45714286	1.22324159	0.877017526	1.26E-03	1796.92866
Itapeti	12500	2000	5000	6.25E+10	1000	900	550	350	350	200	200	1.00E+06	30000	1.25	0.71428571	0.45714286	12.2324159	1.55956221	3.98E-04	3195.44124
Itapeti	12500	2000	5000	6.25E+10	1000	900	550	350	350	200	200	1.00E+07	30000	1.25	0.71428571	0.45714286	122.324159	2.773372931	1.26E-04	5682.38737
Itapeti	12500	2000	5000	6.25E+10	1000	800	750	350	50	400	200	1.00E+08	30000	1.25	0.71428571	0.45714286	1223.24159	4.93183198	3.98E-05	10104.8725
Itapeti	12500	2000	5000	6.25E+10	1000	800	750	350	50	400	200	1.00E+04	30000	0.625	5	12.8	0.12232416	6.003116837	5.89E-01	0.56030599
Itapeti	12500	2000	5000	6.25E+10	1000	800	750	350	50	400	200	1.00E+05	30000	0.625	5	12.8	1.22324159	10.67521907	1.86E-01	0.99638061
Itapeti	12500	2000	5000	6.25E+10	1000	800	750	350	50	400	200	1.00E+06	30000	0.625	5	12.8	12.2324159	18.98352226	5.89E-02	1.77184312
Itapeti	12500	2000	5000	6.25E+10	1000	800	750	350	50	400	200	1.00E+07	30000	0.625	5	12.8	122.324159	33.75800677	1.86E-02	3.15083213
Itapeti	12500	2000	5000	6.25E+10	1000	800	750	350	50	400	200	1.00E+08	30000	0.625	5	12.8	1223.24159	60.03116837	5.89E-03	5.6030599
Itapeti	12500	2000	5000	6.25E+10	1000	800	700	350	100	350	200	1.00E+04	30000	0.71428571	2.5	4.9	0.12232416	2.821570554	1.40E-01	4.86078618
Itapeti	12500	2000	5000	6.25E+10	1000	800	700	350	100	350	200	1.00E+05	30000	0.71428571	2.5	4.9	1.22324159	5.195366762	4.41E-02	8.64383598
Itapeti	12500	2000	5000	6.25E+10	1000	800	700	350	100	350	200	1.00E+06	30000	0.71428571	2.5	4.9	12.2324159	9.238817296	1.40E-02	15.3711555
Itapeti	12500	2000	5000	6.25E+10	1000	800	700	350	100	350	200	1.00E+07	30000	0.71428571	2.5	4.9	122.324159	16.42919857	4.41E-03	27.3342094
Itapeti	12500	2000	5000	6.25E+10	1000	800	700	350	100	350	200	1.00E+08	30000	0.71428571	2.5	4.9	1223.24159	29.21570554	1.40E-03	48.6078618
Itapeti	12500	2000	5000	6.25E+10	1000	800	650	350	150	300	200	1.00E+04	30000	0.83333333	1.66666667	2.4	0.12232416	1.710518399	4.78E-02	24.2199032
Itapeti	12500	2000	5000	6.25E+10	1000	800	650	350	150	300	200	1.00E+05	30000	0.83333333	1.66666667	2.4	1.22324159	3.04177965	1.51E-02	43.0697552
Itapeti	12500	2000	5000	6.25E+10	1000	800	650	350	150	300	200	1.00E+06	30000	0.83333333	1.66666667	2.4	12.2324159	5.409134121	4.78E-03	75.5900589
Itapeti	12500	2000	5000	6.25E+10	1000	800	650	350	150	300	200	1.00E+07	30000	0.83333333	1.66666667	2.4	122.324159	9.618951833	1.51E-03	136.198525
Itapeti	12500	2000	50																	

Itapeti	12500	2000	5000	6.25E+10	1000	700	600	350	100	250	200	1.00E+04	30000	1	2.5	2.5	0.12232416	1.763698417	5.09E-02	22.0944237
Itapeti	12500	2000	5000	6.25E+10	1000	700	600	350	100	250	200	1.00E+05	30000	1	2.5	2.5	1.22324159	3.136348581	1.61E-02	39.2900587
Itapeti	12500	2000	5000	6.25E+10	1000	700	600	350	100	250	200	1.00E+06	30000	1	2.5	2.5	12.2324159	6.577304105	5.09E-03	69.8687024
Itapeti	12500	2000	5000	6.25E+10	1000	700	600	350	100	250	200	1.00E+07	30000	1	2.5	2.5	122.324159	9.918005053	1.61E-03	124.246075
Itapeti	12500	2000	5000	6.25E+10	1000	700	600	350	100	250	200	1.00E+08	30000	1	2.5	2.5	1223.24159	17.63698417	5.09E-04	220.944237
Itapeti	12500	2000	5000	6.25E+10	1000	700	550	350	150	200	200	1.00E+04	30000	1.25	1.66666667	1.06666667	0.12232416	0.931088283	1.42E-02	150.169961
Itapeti	12500	2000	5000	6.25E+10	1000	700	550	350	150	200	200	1.00E+05	30000	1.25	1.66666667	1.06666667	1.22324159	1.655735123	4.48E-03	267.04415
Itapeti	12500	2000	5000	6.25E+10	1000	700	550	350	150	200	200	1.00E+06	30000	1.25	1.66666667	1.06666667	12.2324159	2.944359677	1.42E-03	474.879114
Itapeti	12500	2000	5000	6.25E+10	1000	700	550	350	150	200	200	1.00E+07	30000	1.25	1.66666667	1.06666667	122.324159	5.235894189	4.48E-04	844.467751
Itapeti	12500	2000	5000	6.25E+10	1000	700	550	350	150	200	200	1.00E+08	30000	1.25	1.66666667	1.06666667	1223.24159	9.31088283	1.42E-04	1501.69961



The Ardara pluton and surrounding area

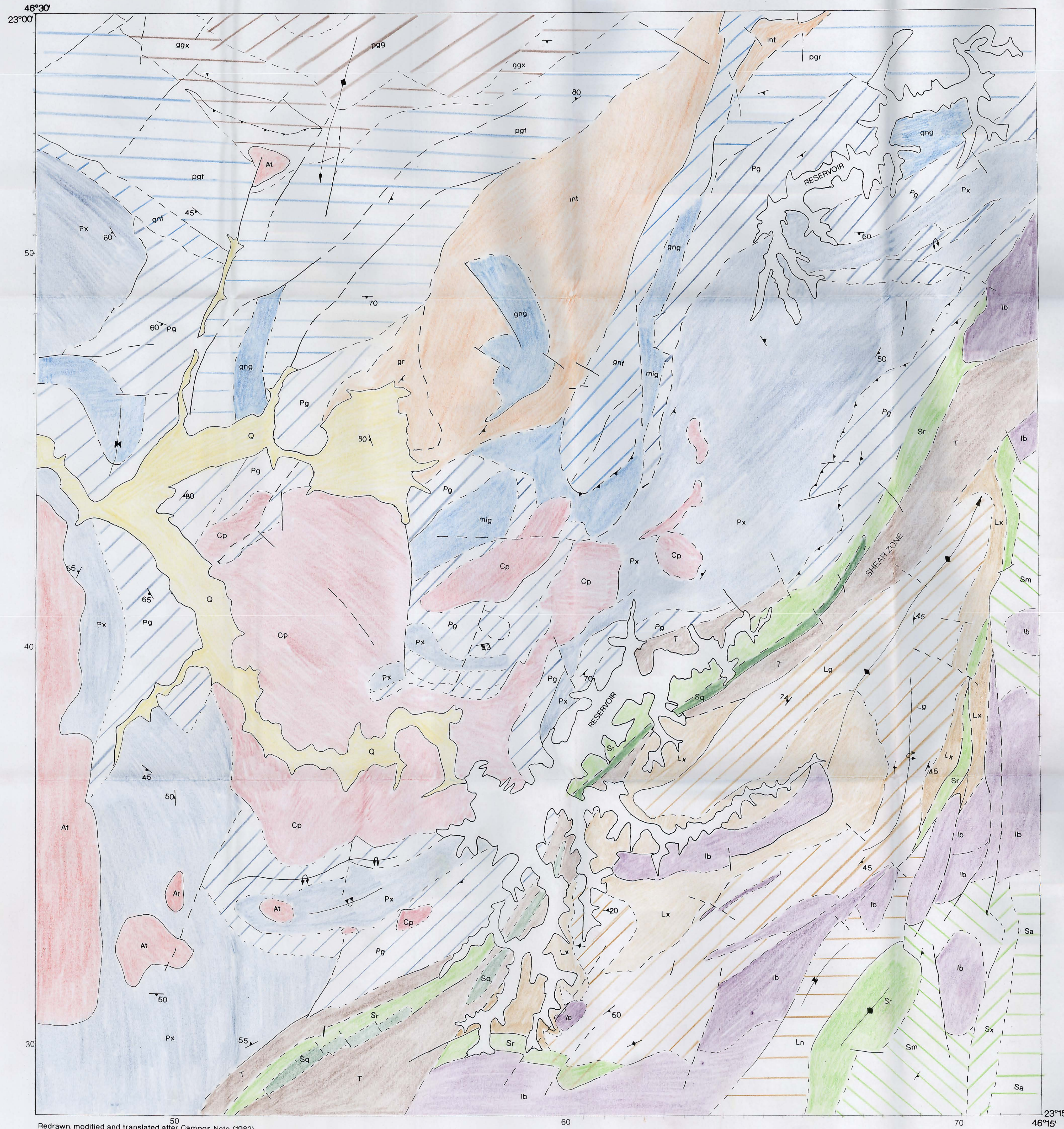
MAP 1



- KEY
- | | | | |
|-------|---|-----|------------------------------|
| MDG - | Main Donegal Granite | / - | Foliation |
| TBG - | Trawenagh Bay Granite | / - | Mineral stretching lineation |
| G3 - | G3, Ardara pluton Granodiorite | / - | Lithological contact |
| G2 - | G2, Ardara pluton Granodiorite | / - | Tectonic contact |
| G1 - | G1, Ardara pluton Plagioclase-rich Granodiorite | | |
| UCR - | Undivided Appin Group meta-sediments and associated metabasites | | |

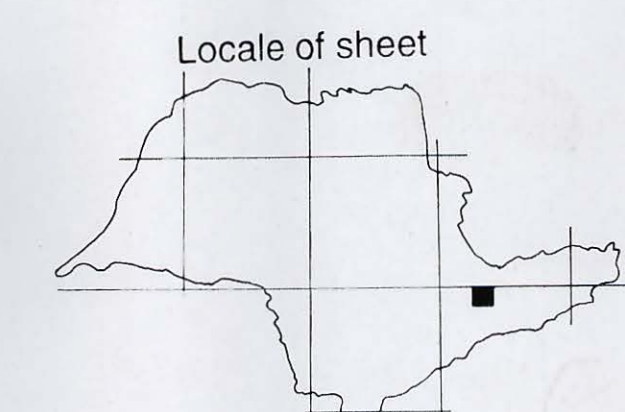
MAP 7

GEOLOGICAL MAP OF PIRACAIA QUADRANGLE



- KEY**
- Q - Quaternary/Tertiary alluvial deposits
 - At - Atibaia granitoid suite
 - Ib - Imbiricu granitoid suite
 - Pg - Piracaia granitoid suite
 - Cp - Nazare Paulista migmatite granitoids
 - T - Cataclastic shear zones
 - Sr - SAO ROQUE DOMAIN Phyllite
 - Sx - Biotite quartz schists
 - Sa - Meta-arenites
 - Sm - Quartz muscovite schists
 - Sq - Quartz amphibolites
 - Lx - Schists
 - Lg - Microcline gneiss
 - Ln - Biotite gneiss
 - Px - PIRACAIA-JUNDIAI DOMAIN Upper schists
 - Pq - Banded gneisses
 - gng - Biotite gneiss
 - gnt - Proto-Blastomylonite gneiss
 - pgt - Basal gneiss
 - ggx - Protomylonite granite gneiss
 - pgg - Homogeneous granite gneiss
 - pgnf - Indivisible basement gneiss

- Foliation
- Mineral stretching lineation
- Lithological contact
- Tectonic contact
- Thrust
- Antiform
- Synform



Redrawn, modified and translated after Campos Neto (1982)

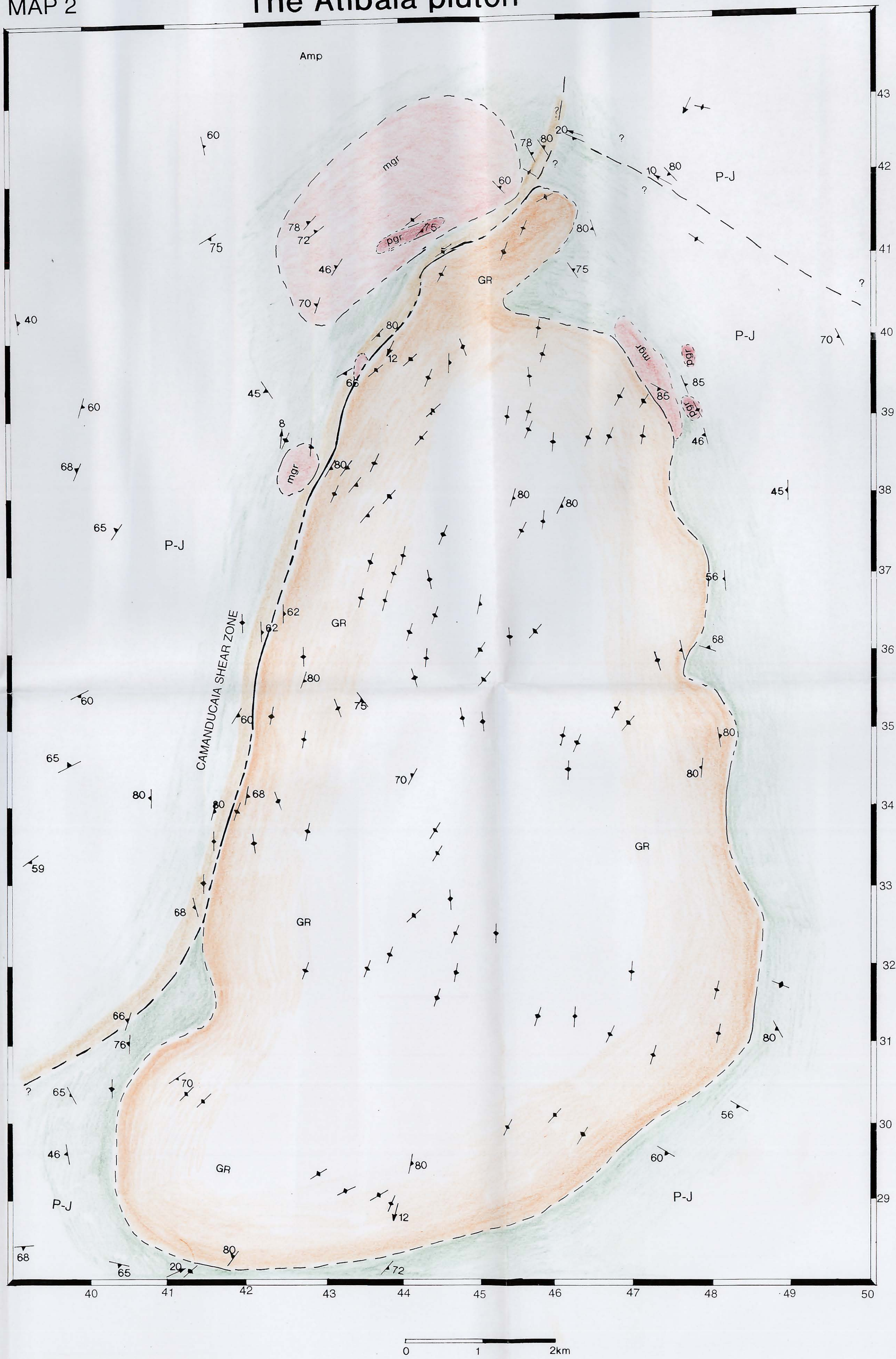
1:50,000

0 1000 2000 3000 4000m

MAP 2

The Atibaia pluton

- KEY**
- GR - Atibaia Granite
 - mgr - White coloured, fine grained microgranite
 - pgr - Porphyroid microgranite
 - P-J - Piracaia-Jundiá domain country rocks
 - / - Lithological contact
 - / - Tectonic contact
 - / - Foliation
 - / - Mineral stretching lineation



135,700

The Imbiricu pluton

MAP 3

- KEY**
- G1 - G1, Imbiricu pluton
K-feldspar rich Alkali Granite
 - G2 - G2, Imbiricu pluton
K-feldspar poor Alkali Granite
 - SZ - Monteiro Lobato shear zone
 - cr - Embu domain country rocks
 - Foliation
 - Mineral stretching lineation
 - Lithological contact
 - Tectonic contact

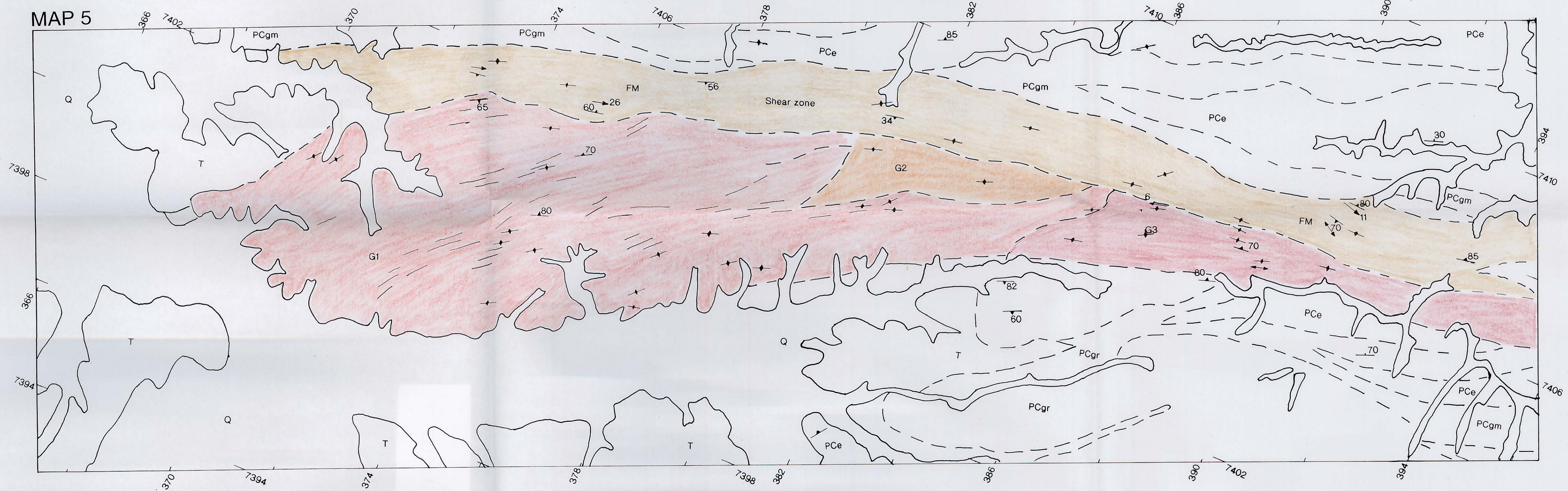


additional country rock data after Campos Neto et al, 1982



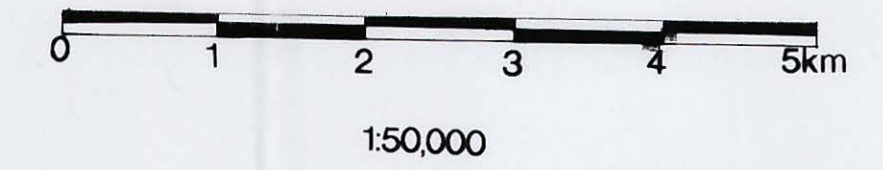
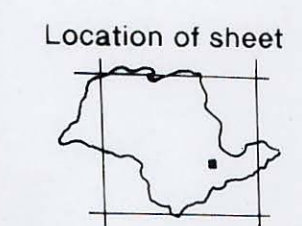
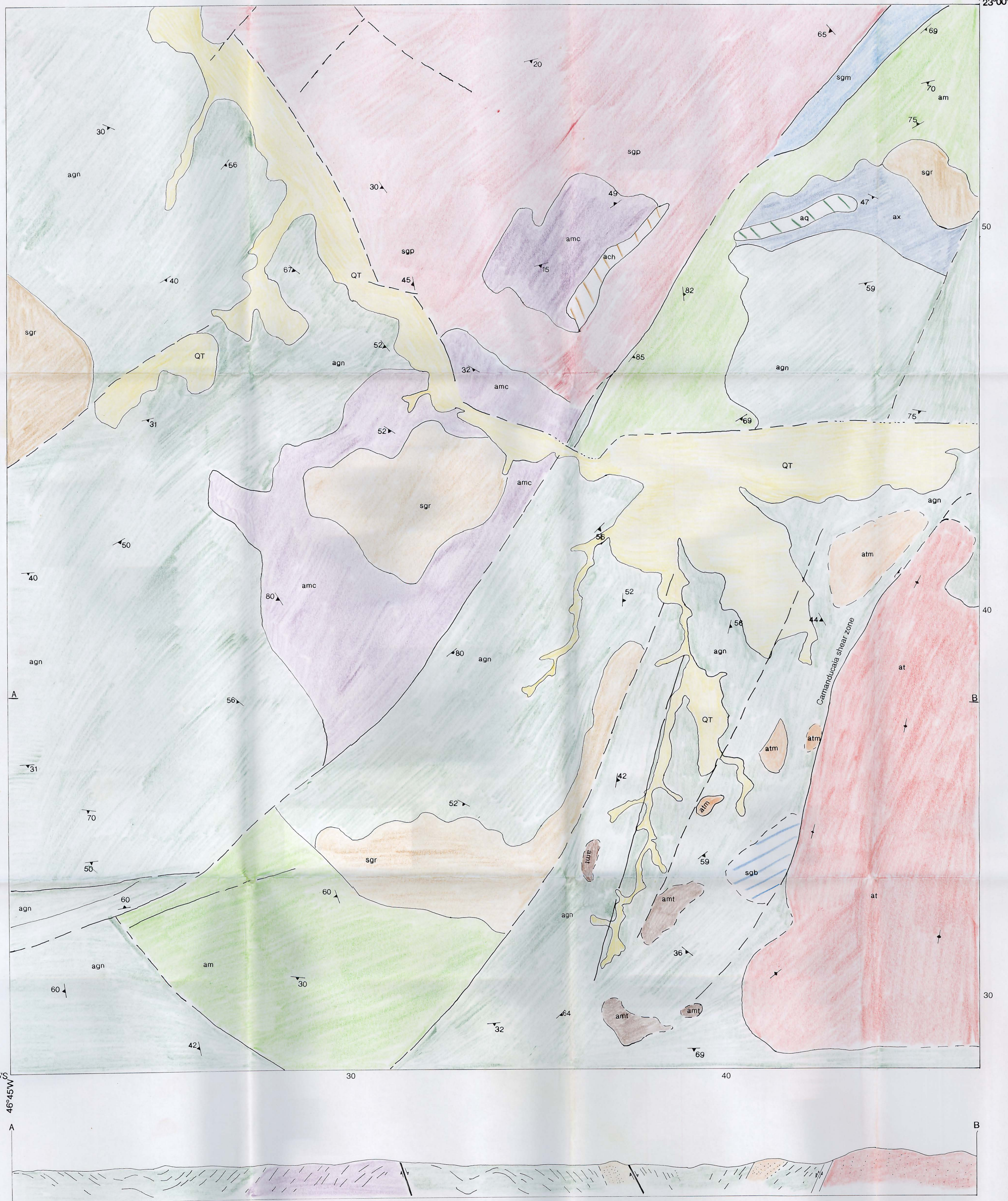
GEOLOGICAL MAP OF ITAPETI GRANITE

MAP 5



MAP 6

Geological Map of the Atibaia quadrangle, SP.



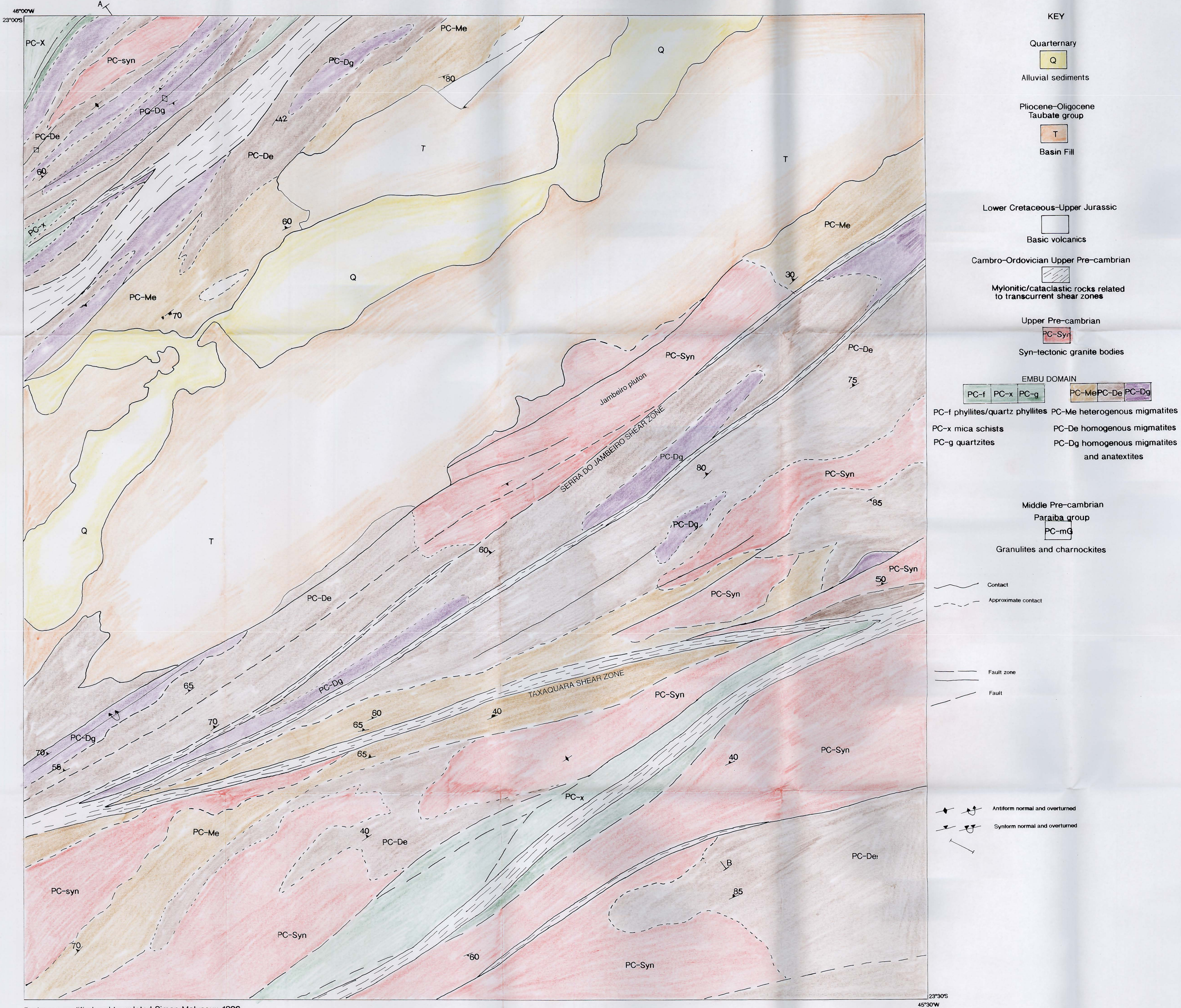
- KEY**
- Quaternary/Tertiary**
- QT
Quaternary/Tertiary sediments and alluvium
- Upper Proterozoic**
Atibaia
- at atm
at-porphyroid Atibaia granite atm-microgranite/microtonalite
- Early, D_{n2} granitoids**
- sgp sgr sgb sgm
sgp-Bragança, pink porphyroid granite sgb-white leucogranite
sgr-fine grained pink granite sgm-strongly deformed porphyroid granite
- Piracaiá-Jundiá domain**
- agn ax am amc ach amt
Garnet-biotite gneisses +/- sillimanite intercalated with schists, quartzites & meta-arkoses
agn-amphibolite amc-garnet migmatites
ax-biotite muscovite schist ach-granulites
aq-quartzites act-metatonalites
am-migmatites

- Lithology contact
- Foliation
- Tectonic contact

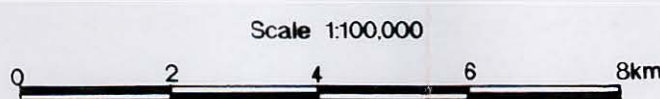
modified, redrawn and translated after Olivera et al (1985)

GEOLOGICAL MAP SÃO JOSE DOS CAMPOS QUADRANGLE

MAP 9



Redrawn, modified and translated Simon Molyneux, 1996
after Hasui et al (1978)



KEY

Quaternary



Alluvial sediments

Pliocene-Oligocene
Taubate group



Basin Fill

Lower Cretaceous-Upper Jurassic



Basic volcanics

Cambro-Ordovician Upper Pre-cambrian



Mylonitic/cataclastic rocks related
to transcurrent shear zones

Upper Pre-cambrian



Syn-tectonic granite bodies

EMBU DOMAIN



PC-f phyllites/quartz phyllites PC-Me heterogenous migmatites

PC-x mica schists

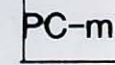
PC-De homogenous migmatites

PC-g quartzites

PC-Dg homogenous migmatites
and anatexites

Middle Pre-cambrian

Paraíba group



Granulites and charnockites

Contact

Approximate contact

Fault zone

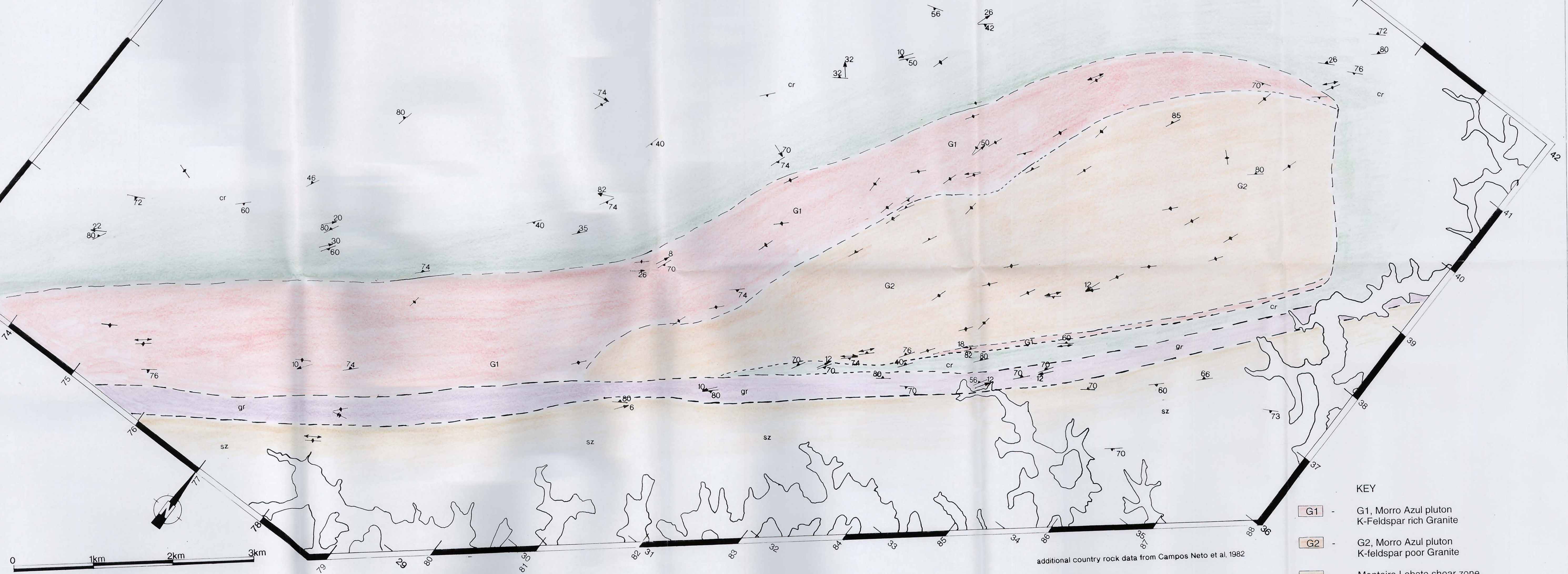
Fault

Antiform normal and overturned

Synform normal and overturned

The Morro Azul pluton

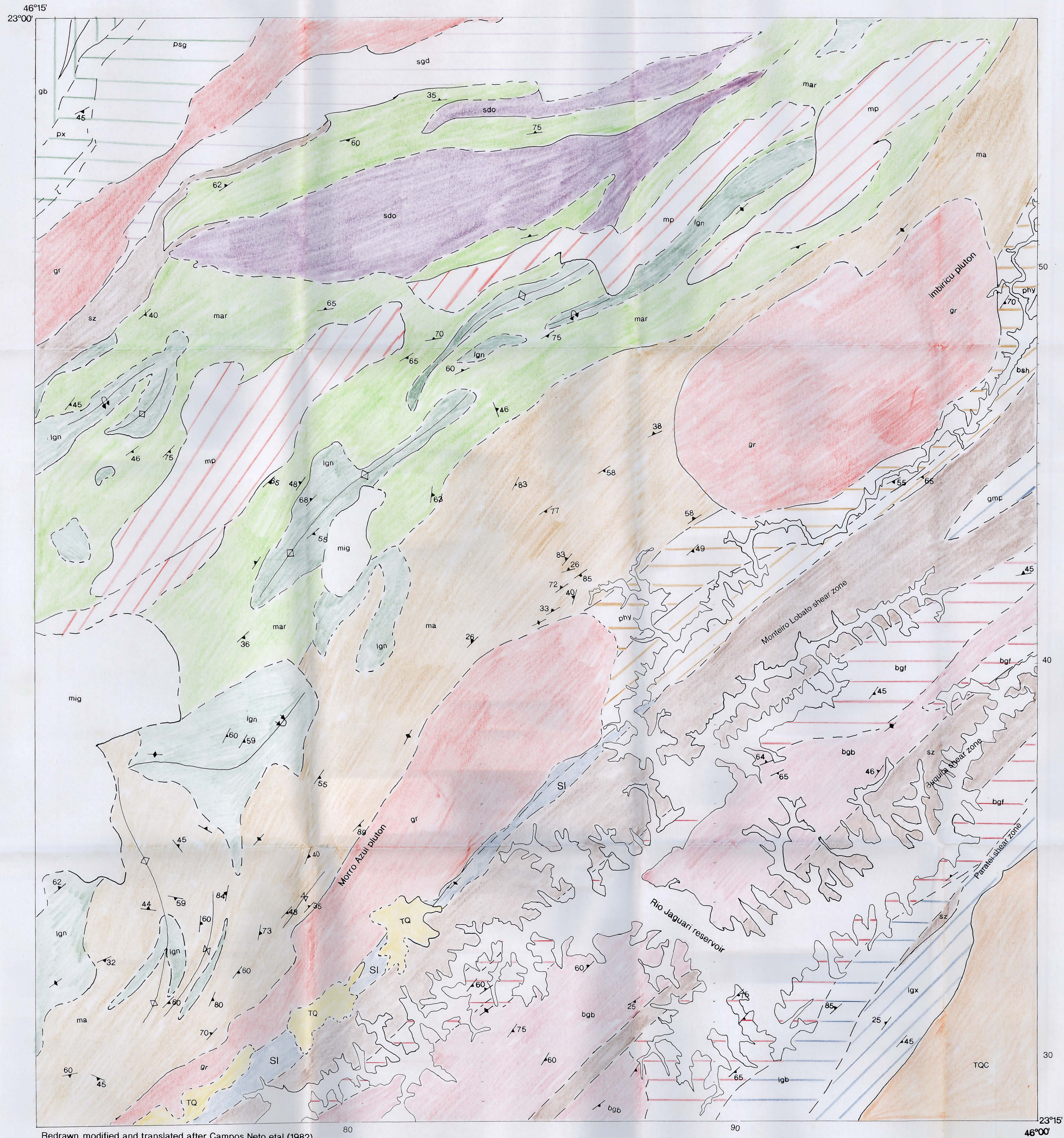
MAP 4



KEY

- G1 - G1, Morro Azul pluton
K-Feldspar rich Granite
- G2 - G2, Morro Azul pluton
K-feldspar poor Granite
- SZ - Monteiro Lobato shear zone
- gr - Santa Isabel gneisses
- cr - Embu domain country rocks
- (with arrow) — Foliation
- (with double arrow) — Mineral stretching lineation
- (dashed) — Lithological contact
- (thick solid) — Tectonic contact

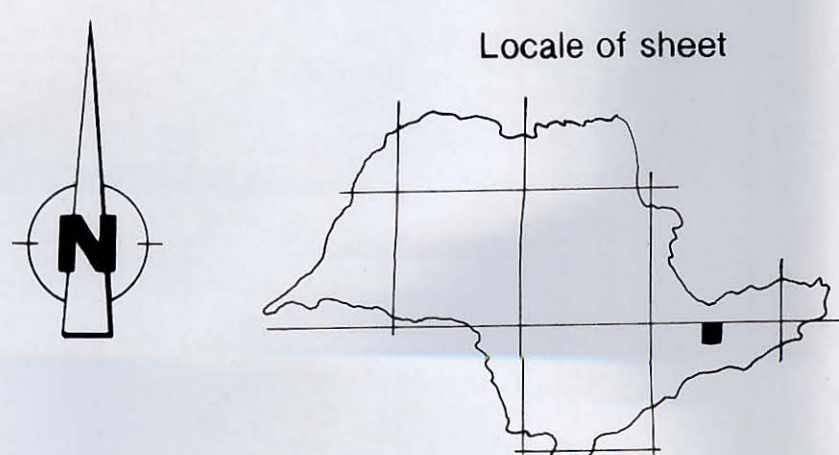
additional country rock data from Campos Neto et al. 1982



- KEY**
- TQ - Quaternary alluvium
 - TQC - Tertiary/Quaternary alluvium
 - BRASILIANO GRANITOIDS**
 - gr - Imbiricu and Morro Azul granitoids
 - mp - Morro do Pao granite suite
 - bgb - Santa Luzia granite
 - bgt - Buquira granite
 - SAO ROQUE DOMAIN**
 - phy - phyllite
 - bsh - biotite schist
 - ma - meta-arenite
 - mar - meta-arkose sandstones
 - sdo - Serra dos Indios granitoids
 - Lgn - Biotite gneiss
 - px - Upper schists
 - gb I - Banded gneiss
 - EMBU DOMAIN**
 - SI - Santa Isabel banded gneisses
 - Lgb - Banded biotite granite gneiss
 - Lgx gmp - Biotite granite gneiss

- Foliation
- Mineral stretching lineation
- Lithological contact
- Tectonic contact

Redrawn, modified and translated after Campos Neto et al (1982)



0 1000 2000 3000 4000m
1:50,000

